

Multiscale prediction of saline-sodic land degradation processes in two South Australian regions

Thesis submitted to The University of Adelaide in fulfilment of the requirements for the degree of
Doctor of Philosophy

by

Mark Thomas

Geology and Geophysics
School of Earth and Environmental Sciences
The University of Adelaide

June, 2007

Dedication

For Paul and Lou, who I have lost. For Ben and William, who I have gained. For Corlia, Mum and Dad, who have always been there.

Table of Contents

Chapter 1.	Introduction	1
Chapter 2.	Review of upland salt-affected soils	6
2.1	Soil layers and morphology	6
2.2	Salts in soils	7
2.3	Sources of salts in Australian landscapes	8
2.4	Dominant ions in salt-affected soils	8
2.5	Measuring and defining soil salinity	8
2.6	Measuring and defining sodic soils	10
2.7	Structural problems associated with sodic soils	11
2.8	Shallow non-groundwater associated salinity	13
2.9	Local terrain and shallow NAS expression	16
2.10	Classification of texture-contrast soils	16
Chapter 3.	Soil-landscape processes and investigation methods	19
3.1	Soil-landscape processes governing soil properties	19
3.2	Morphological indicators of hydropedology	21
3.3	Mapping soil-landscape properties	22
3.4	Digital soil mapping	23
3.5	Terrain analysis in soil-landscape analysis	23
3.6	Geophysical survey methods	24
3.6.1	Electromagnetic induction	24
3.6.2	Magnetic susceptibility	27
3.6.3	Gamma radiometrics	31
Chapter 4.	Research methodology and rationale	33
4.1	Pedological complexity	34
4.2	Soil system scale	34
4.3	Soil modelling support	35
4.4	Linking multiscale investigations	36
4.5	Pedotransfer functions	36
4.6	Conceptual toposequence models	37
4.6.1	Multiscale predictions via conceptual toposequence models	40
4.7	Precision conservation	42
4.8	Study area selections	42
4.8.1	Midnorth study	44
4.8.2	Mount Lofty Ranges study	45

Chapter 5.	Midnorth study area	46
5.1	Regional overview	46
5.2	Climate	46
5.3	Landform	48
5.4	Geology and near-surface geochemistry	53
5.5	Landuse	56
5.6	Soils	57
Chapter 6.	Midnorth fine scale investigation	71
6.1	Plot selection and descriptions	71
6.2	Survey design	71
6.3	Field investigations	72
6.4	Laboratory investigations	73
6.5	Results	74
6.5.1	Field results	74
6.5.2	Laboratory results	78
6.6	Discussion and conclusions	88
6.6.1	Plot interpretations	88
6.6.2	Plot spatial variabilities	90
Chapter 7.	Midnorth medium scale investigation	96
7.1	Intricate soil-landscape patterns	96
7.2	Geophysical ground surveys	96
7.3	Landform, electrical conductivity and κ survey patterns	101
7.3.1	EM31 hillslope patterns	102
7.3.2	EM38 hillslope patterns	104
7.3.3	Volume magnetic susceptibility hillslope patterns	104
7.4	Terrain patterns	104
7.4.1	Slope analysis	105
7.4.2	Terrain wetness index analysis	105
7.5	Airborne gamma radiometrics and mineralogy	105
7.5.1	Airborne K % validation	106
7.5.2	Linking airborne radiometric K % and mineralogy	108
7.6	Descriptive hydropedological model	109
7.7	Conceptual toposequence model	112
Chapter 8.	Midnorth coarse scale investigation	115
8.1	Environmental covariate selection	115
8.2	Soil-landscape function of predictive rules	116
8.3	Upscaling prediction	116
8.4	Validation of upscaling prediction	121
8.5	Regional implications	122

Chapter 9.	Mount Lofty Ranges study area	123
9.1	Regional overview	123
9.2	Climate	125
9.3	Geology	126
9.4	Airborne gamma-radiometric and magnetic coverages	128
9.5	Magnetic susceptibility surveys	130
9.6	Landform	134
9.7	Soil degradation	141
9.8	Soil survey, modelling and mapping	146
9.9	Land use	149
Chapter 10.	Mount Lofty Ranges multi-temporal, fine scale investigation	155
10.1	Survey site selection and soil sampling	155
10.2	Laboratory physicochemical analyses	157
10.3	Multi-temporal solute trends	157
10.4	Conclusions	171
Chapter 11.	Mount Lofty Ranges spatio-temporal, medium scale investigation	172
11.1	Conductivity relationships	173
11.2	Spatio-temporal apparent electrical conductivity patterns	173
11.2.1	Survey methodology	174
11.2.2	Apparent electrical conductivity patterns	175
11.2.3	Inter-seasonal, near-surface conductivity dynamics	179
11.3	Interpretation	187
Chapter 12.	Mount Lofty Ranges regional and coarse scale investigation	191
12.1	Regional soil mapping	191
12.2	Regional prediction of soil salinity	193
12.2.1	Environmental covariate selection	200
12.2.2	Predictive rule functions	202
12.2.3	Assessing upscaling prediction	202
Chapter 13.	Overall conclusions and recommendations	206
13.1	Overall conclusions	206
13.2	Recommendations	209
References		212
Appendix A.	Oral presentations and extended abstracts	239

Appendix B. Midnorth study area profile morphological data	271
Appendix C. Physicochemical data of layers from selected profiles of the Midnorth study area.	298
Appendix D. Midnorth study area plot field data.	303
Appendix E. Midnorth study area plot laboratory data.	307
Appendix F. Midnorth study area X-ray diffraction plots.	314
Appendix G. Mount Lofty Ranges magnetic susceptibility data.	324
Appendix H. Layer physicochemical properties of profiles grouped according to each salinity process model (i.e. Models 1a, 1b, 2a, 2b), featuring winter (W_) and summer (S_) salinity (EC_{se}, dS/m), clay content (%) and concentration of soluble salts (mg/kg⁻¹).	327

Index of Figures

Figure 1.1 Outline of digital soil mapping methodology for regional predictions of saline-sodic soil patterns.....	3
Figure 1.2. Flow diagram that represents the thesis structure according to Chapter numbers and titles, and how Chapters relate to one another.	5
Figure 2.1. Relationship between salt type and concentration (in g l ⁻¹) to resistivity, which is the reciprocal of conductivity (after Keller and Frischknecht 1966).	9
Figure 2.2. Process-based classification scheme for saline soils, including EC _{se} criteria (after Fitzpatrick 2005).....	13
Figure 2.3. Plate (a) shows a shallow NAS-affected area of winter wheat in South Australia's Midnorth region. Shown is a localised area of crop loss, fringed by crops showing salt stress (grey leaf tones, "s"), and nearby patches of shallow NAS crop losses ("p"). Plate (b) shows a close-up view of the affected profile, featuring a shallow, waterlogged A horizon and heavy clay sodic Btn horizon (photographs: DWLBC).	15
Figure 2.4. Conceptualisation of shallow NAS formation processes on hillslopes. Yellow dots indicate relative salt concentrations and blue arrows indicate predominant water movements. Typical scales and horizon textures are indicated in (a).	17
Figure 3.1 Comparison of relative EM38 responses with depth in EC _{ah} and EC _{av} modes (after McNeill 1980b).....	25
Figure 3.2. The Geonics EM38 instrument in use in vertical mode (EC _{av}).....	27
Figure 3.3. EM31 in survey mode (photograph: Rural Solutions SA).....	27
Figure 3.4. Bartington MS2D loop in use taking surface measurements.	28
Figure 3.5. Bartington MS2F probe in action. (a) Being used to take measurements from scuffed soil surfaces, and (b) taking measurements of profile samples.....	29
Figure 4.1. <i>i</i> -level model characteristics based on three characteristics (adapted from: Hoosbeek <i>et al.</i> 2000; Hoosbeek and Bryant 1992).....	35
Figure 4.2. A descriptive conceptual toposequence model of a lateritic-hydromorphic hillslope in the Mount Lofty Ranges (MLR) in South Australia (after Fritsch and Fitzpatrick 1994).	39
Figure 4.3. An explanatory conceptual toposequence model showing biogeochemical and hydraulic condition conditions in a saline-sulfidic environment (after Fitzpatrick <i>et al.</i> 1996).	39
Figure 4.4. A predictive (i.e. "4D") conceptual toposequence model showing biogeochemical and physical changes in a profile over time as conditions change from sulfidic material (i.e. potential acid sulfate soil - PASS) to sulfuric material (i.e. actual acid sulfate soil - ASS) due to increased drainage caused by erosion (after Fitzpatrick and Merry 2002).	40
Figure 4.5. National (inset box) and regional map showing the locations of the Midnorth and Mount Lofty Ranges study areas, elevation classes and rainfall isohyets.....	43
Figure 5.1. Locality map showing the South Australian setting (inset box) for the Midnorth study area, featuring elevation classes (m) and annual rainfall isohyets (mm).	47
Figure 5.2. Mean monthly rainfall (mm) (●), mean monthly daily maximum temperatures (°C) (▲); (iii) mean monthly daily minimum temperatures (°C) (■); and (iv) mean monthly daily 3 pm relative humidity (◆) records for the years 1862 to 1994 for the town of Clare, which is comparable to the Midnorth study area climatic conditions (source: Australian Bureau of Meteorology, ww.bom.gov.au/climate/averages/tables/cw_021014).	48
Figure 5.3. Oblique aerial photographic 3D drape showing the local setting of the Midnorth study area (yellow box, approximately 1,650 by 800 m), which features an east-facing hillslope defined by Ward Hill summit and Freshwater Creek in Belalie Valley.	49
Figure 5.4. Midnorth study area (outlined), featuring a rectified aerial photograph, terrain (2 m contours) and the transect A'-A".....	50

Figure 5.5. Views of transect A'-A", showing (a) the Ward Hill-Freshwater Creek gully edge view of the Belalie Valley, and (b), the opposite view from the gully to Ward Hill, and (c) the study area hillslope in profile.	51
Figure 5.6. Profiles of elevation (m) and slope (°) along the transect A'-A" shown in Figure 5.4. Hillslope profile positions are identified using terminology for hillslope position defined in Schoeneberger <i>et al</i> (2002).	52
Figure 5.7. Freshwater Creek erosional gully east-facing face and gully flat with a saline-sulfidic wetland.	53
Figure 5.8. Midnorth study area (outlined) geology at 1: 100,000 scale, with a hillshade applied to accentuate landform.	54
Figure 5.9. Midnorth study area (outlined) airborne gamma radiometrics coverage, with 2 m contours applied to accentuate landform.	55
Figure 5.10. Yield map of parts of the Midnorth study area, indicating areas that are consistently excellent, good, moderate and poor yielding, based on the farmer's field observations and yield returns.	57
Figure 5.11. Midnorth study area 1988 CSIRO survey site positions (●) and soil cores (★) selected for physicochemical analyses.	59
Figure 5.12. Midnorth study area draft CSIRO soil map of soil mapping unit (SMUs), with a hillshade applied to accentuate local relief.	60
Figure 5.13. Midnorth study area landscape soil unit (LSU) map, with a hillshade applied to accentuate relief. LSUs are defined and summarised in Table 5.2.	69
Figure 5.14. Midnorth study area (1,650 by 800 m) LSU boundaries draped over 3D aerial photograph, featuring selected profiles showing trends in ESP, EC _{se} dS/m and clay % from the 1988 CSIRO soil survey. Note the difference in scales in the LSU 1-type graph.	70
Figure 6.1. Midnorth study area plot locations (P1 and P2), crop yield patterns, 2 m contours and soil landscape units (SLUs).	72
Figure 6.2. Plot survey point marking (pink flags) at 2 m intervals, which are georeferenced using differential geographic information system positioning (photograph of P2 area).	73
Figure 6.3. (a) Gouge auger being hammered into the ground in P1 and (b) the extracted core, which features a loamy A horizon and a heavy clay upper B horizon (Btn), being measured for layer depths. Core sections L1, L2 and L3 are identified.	74
Figure 6.4. Distribution of Plot 1 (18 cores comprising 54 layer samples) and Plot 2 (13 cores comprising 39 later samples) survey point depth section samples used in mid-infrared (MIR) predictions and extractive chemical analyses.	75
Figure 6.5. GIS plot survey patterns for (a) depth to B horizon; (b) EM38 electromagnetic induction EC _{av} (peak response at 0.4 m); and (c) surface κ. Slope direction is shown for each plot.	76
Figure 6.6. Low frequency mass magnetic susceptibility results per layer for Plot 1 (above) and Plot 2 (below). Black bars represent L1 samples, grey bars, L2 samples, and white bars, L3 samples.	81
Figure 6.7. Frequency dependency results per layer for Plot 1 (above) and Plot 2 (below). Black bars represent L1 samples, grey bars, L2 samples, and white bars, L3 samples.	82
Figure 6.8. Cation exchange capacity results per layer for Plot 1 (above) and Plot 2 (below). Black bars represent L1 samples, grey bars, L2 samples, and white bars, L3 samples.	83
Figure 6.9. Soil texture results per layer for Plot 1 (above) and Plot 2 (below). Black bars represent L1 samples, grey bars, L2 samples, and white bars, L3 samples.	84
Figure 6.10. Saturation extract electrical conductivity results per layer for Plot 1 (above) and Plot 2 (below). Black bars represent L1 samples, grey bars, L2 samples, and white bars, L3 samples.	85
Figure 6.11. pH (w) results per layer for Plot 1 (above) and Plot 2 (below). Black bars represent L1 samples, grey bars, L2 samples, and white bars, L3 samples.	86
Figure 6.12. Calcium carbonate results per layer for Plot 1 (above) and Plot 2 (below). Black bars represent L1 samples, grey bars, L2 samples, and white bars, L3 samples.	87

Figure 6.13. Mass magnetic susceptibility (χ) range for the Midnorth study area profiles compared to a selection of other environmental ranges (modified after Dearing 1999b).	90
Figure 6.14. Relationships between soil properties (CEC, clay %, EC_{se} , pH, $CaCO_3$ %, χ_{lf} , χ_{fd} % and soil depth) for Plot 1. Layers have been differentiated (L1: O; L2: □; and L3 △).	91
Figure 6.15. Relationships between soil properties (CEC, clay %, ESP, EC_{se} , pH, $CaCO_3$ %, χ_{lf} , χ_{fd} % and soil depth) for Plot 2. Layers have been differentiated (L1: O; L2: □; and L3 △).	10
Figure 6.16. Conceptual hydro-pedologically-based mechanistic processes models for Plot 1 and Plot 2, showing: (i) layer depths (with positions of reference cores) and shapes (from interpolated coverages), (ii) predominant throughflow direction and strength, (iii) relative calcite, salinity and sodicity distributions, (iv) typical layers, and (v) sketched plot hillslope positions. Note the different horizontal and vertical scales.	94
Figure 7.1. Locations of shared geophysical (EM38, EM31 and Bartington MS2D) survey sites (●) of the Midnorth study area.	97
Figure 7.2. EM31 EC_a (a), EM38 EC_{av} (b) and κ (c) survey patterns of the Midnorth study area, with landscape soil units and two metre contours applied. Coverages are presented with linear, minimum-maximum stretch applied, and showing maximum responses in red and minimum responses in blue.	99
Figure 7.3. Midnorth study area with LSU boundaries overlain on 3D perspective drapes of: (a) aerial photograph (including codes for prominent hillslope features, as described in the text); (b) EM31 EC_a survey; (c) EM38 EC_{av} survey; and (d) κ survey. Each survey is presented using a linear, minimum-maximum stretch (maximum responses = dark red, moderate responses = yellow, and minimum responses = dark blue).	100
Figure 7.4. Profiles of elevation (m) (—) and slope (°) (---) for transect A'-A" in Midnorth study area. The dashed line indicates the hillslope position of the colluvial-alluvial slope, and the LSU 3 and LSU 4 boundary.	101
Figure 7.5. Conceptual model of Midnorth study area showing water flows associated with salt accumulations at LSU3/LSU 4 boundary, and at the erosional gully face. The toposequence shown corresponds to the lower sections of the transect A'-A" shown in Figure 5.4.	103
Figure 7.6. Midnorth study area LSU boundaries overlaying 3D perspective drapes of: (a) slope (0 – 14 ° range, highest gradients = dark blue, moderate gradients = pink, lowest gradients = brightest yellow, shown with minimum-maximum stretch applied) with 2 m contours; (b) TWI (highest values = dark blue, moderate values = white, and lowest values = red).	105
Figure 7.7. Midnorth study area LSU boundaries overlaying 3D perspective drapes of: (a) U ppm (4.0 to 0.0 ppm) (highest values = blue, lowest values = white), (b) Th ppm (15.9 to 6.3 ppm) (highest values = green, lowest values = white), and (c) K % (1.1 to 2.5 %) (highest values = red, lowest values = white). The sampling sites for X-ray diffraction (XRD) analysis (XRD 1 to XRD 6) are identified in (c), and resulting plots for XRD 5 and XRD 6 shown in Appendix F (presented as SPC12 and SPC26, respectively).	107
Figure 7.8. Inset (a) Exploranium GR 320 and (b) locations of GR 320 ground survey sites in the Midnorth study area and surrounding areas.	108
Figure 7.9. Airborne radiometric K % versus field radiometric K % relationship.	108
Figure 7.10. Midnorth study area LSU boundaries and EM38 EC_a survey contours (highest values = red, lowest values = blue) overlaying the TWI coverage. Sites 1, 2 and 3 are referred to in the text as areas that correspond with elevated EM38 EC_a zones and low TWI values.	113
Figure 7.11. Whole-of-landscape 3D process model for Midnorth study area showing (i) 3D aerial photograph drape of study area, overlaid with (ii) a section of EM38 survey (high response: red, low response: blue) (iii) landscape-soil unit (LSU) boundaries, accompanied by (iv) photographs of representative soil profiles for each LSU, (v) underlying geology, (vi) cross-section of typical toposequence showing the main morphological, saline and sodic soil-regolith features/layers and (vii) groundwater and fresh surface water flow paths (after: Fitzpatrick <i>et al.</i> 2003c).	114

Figure 8.1. Upscaling prediction of shallow NAS in the Midnorth study area draped over an aerial photograph, two metre contours, and LSU boundaries. Yellow indicates predictions of LSU 3 areas not effected by shallow NAS, and red indicates predictions of LSU 3 affected by shallow NAS. All other soils remain unclassified.....	118
Figure 8.2. Upscaling prediction of shallow NAS in the east-facing hillslopes of the Midnorth study area (black box) and surrounding (2,275 ha) areas overlaying an aerial photographic drape. Yellow indicates predictions of LSU 3 areas not affected by shallow NAS, and red indicates predictions of LSU 3 affected by shallow NAS. All other soils remain unclassified.	119
Figure 8.3. Upscaling prediction of shallow NAS in plan view of the Midnorth study area (yellow box) and surrounding (2,275 ha) areas overlaying an aerial photograph. Yellow indicates predictions of LSU 3 areas not effected by shallow NAS, and red indicates predictions of LSU 3 affected by shallow NAS. All other soils remain unclassified. Also shown are soil survey sites with accompanying physicochemical data used for upscale prediction validation. The profiles coinciding with predicted shallow NAS-affected areas include 6E, 6B, 10F, 12E and 13D. The profiles coinciding with predicted non-shallow NAS areas include 1B, 2E, 4B, 5C, 7D and 7F.	120
Figure 8.4. Profiles selected from LSU 3 predicted areas shown in Figure 8.3 used validate upscaled predictions of shallow NAS. According to the profile depth distribution of salinity (EC_{se}), five profiles are shallow NAS-affected (solid lines) and six profiles are non-shallow NAS-affected (dotted lines). The profile identities are listed.	121
Figure 9.1. Locality map showing the South Australian setting (inset box) for the Mount Lofty Ranges (MLR) study area, featuring elevation classes (m) and annual rainfall isohyets (mm).....	124
Figure 9.2. Mount Crawford weather station climate trends showing mean monthly (i) rainfall (mm) (●), (ii) daily maximum temperatures (°C) (▲), (iii) daily minimum temperatures (°C) (■), and (iv) mean monthly evaporation (mm) (◆) for the years 1954 to 2004 (source: Australian Bureau of Meteorology, www.bom.gov.au/climate/averages/tables/cw_023763.shtml).....	126
Figure 9.3. Geology of the Mount Lofty Ranges (MLR) study area (outlined) at 1: 100,000 scale (Geological Survey of South Australia 1964a), with a hillshade applied to accentuate local landform.	127
Figure 9.4. Airborne geophysical surveys of the Mount Lofty Ranges (MLR) study area with geological units overlaid, and hillshading applied to accentuate local relief. Plate (a) shows K (range: 0.2 – 1.2 %), plate (b) shows Th (range: 8.4 – 19.3 ppm), plate (c) U (range: 1.0 – 4.9 ppm), and (d) aeromagnetic first vertical derivative.....	130
Figure 9.5. Mount Lofty Ranges (MLR) study area surface volume magnetic susceptibility (κ) survey sites (●) and sites selected for profile (⊙) mass magnetic susceptibility investigations (χ), which are overlaid on an aerial photograph, with 2 m contours applied to show landform.	132
Figure 9.6. Mouth Lofty Ranges (MLR) study area volume magnetic susceptibility (κ) survey patterns with selected profile mass magnetic susceptibility analytic data presented in layer-by-layer graphic form. Two metre contours are overlaid to indicate landform. Regions of interest “a” to “e” are identified.	134
Figure 9.7. Aerial photograph showing the MLR study area (yellow outline), featuring terrain (2 m contours), transect A-A', modelled drainage using GIS, and location and view orientation of the plates shown in Figure 9.9.....	135
Figure 9.8. Profiles of elevation (m) (—) and slope (°) (---) for transect A-A' located in Figure 9.7.....	136
Figure 9.9. Plates showing MLR study area scenes featuring the transect A-A' shown in Figure 9.7 and profiled in Figure 9.8. Plate (a) features a north-easterly view of the south- and north facing hillslopes, and summits (A and A') defining the transect. Plate (b) features an easterly view of the south-facing hillslope. Plate (c) features a westerly view of the north facing hillslope mid and lower slope zones. Plate (d) features an easterly view of the north facing hillslope mid and upper slope zones.....	137

Figure 9.10. Plates showing Mount Lofty Ranges study area views of the Herrmanns Creek terrace. Plate (a) shows a view of the fringing wetland, remnant vegetation and re-vegetation. Plate (b) shows a stand of remnant vegetation in the terrace. Plate (c) shows wetland soil cover adjacent to the creek. Plate (d) is a view of the lower terrace showing eroded creek banks and re-vegetation in the middle distance.....	138
Figure 9.11. Topographic wetness index coverage of the Mount Lofty Ranges study area with a standard deviation stretch applied showing landscape drainage zones, with a hillshade been applied to accentuate local landform.	139
Figure 9.12. Multi-resolution valley bottom flatness (MrVBF) coverage for the Mount Lofty Ranges (MLR) study area with a linear stretch applied for visual consistency. A hillshade has been applied to accentuate local landform differences.....	141
Figure 9.13. Plate (a) showing localised waterlogging and surface ponding in a mid slope zone, and Plate (b) showing ponding in a sloping depression area. Plate (c) shows an example of subsequent erosion, leaving the shallow Btn horizon exposed and showing plough disk grooves. Plate (d) shows an eroded (i.e. “bust”) reverse interceptor drain. All photographs were taken from the north facing slope during June 2005, approximately 24 hours after a prolonged rainfall period.....	143
Figure 9.14. Plate (a) showing eroded surface fissures, which seep saline groundwater under piezometric pressure, in salt encrusted sodic surface clays in scalded lower landscape zones. Plate (b) shows surface salt crusting in highly saline (e.g. $EC_{se} > 30$ dS/m) topsoil. Plate (c) shows salt-iron crusts and exposed mono-sulfidic back ooze in the near-surface, and Plate (d) shows the layering in profile. Plate (e) shows the release of iron-rich gelatinous precipitates (featuring ferrihydrite) to Herrmanns Creek.	144
Figure 9.15. Plates featuring Herrmanns Creek and wetlands in the Mount Lofty Ranges study area. Plate (a) shows the incised creek bed and efforts to re-vegetate in the middle distance stand of remnant vegetation. Plate (b) shows the eroded Herrmanns Creek bed and scalded banks in the lower catchment. The photograph shows exposed saprolite (“sap”) adjacent to a deposit dominated by ferruginised saprolite and quartz. Plate (c) shows magnetic iron gravels. Plate (d) shows a salt encrusted remnant ancient wetland of high bulk density and rich in sulfidic materials. Plate (e) shows the columnar structure of an exposed surface of Btn horizon overlaid by an albic, sandy E horizon.	145
Figure 9.16. EM31 survey points and resulting GIS coverage (linear stretch applied) of deep (~ 6 m) conductivity patterns (linear stretch applied) of the Mount Lofty Ranges study area (source: Fitzpatrick <i>et al.</i> 1999), and a hillshading applied to accentuate local landform. Zones of interest “a” and “b” are identified in the landscape.....	147
Figure 9.17. Plate (a) An aerial photograph of the MLR study area showing survey transects (T-A to T-E) and surveys sites described in Fritsch and Fitzpatrick (1994). The figure (b) shows a descriptive conceptual toposequence model (after Fritsch and Fitzpatrick 1994) (corresponding to transect start and end points “A-B” shown in (a)), features the hillslope profile distribution of mapping units according to (i) drainage, and (ii) top and (iii) bottom soil layers and soil features.	148
Figure 9.18. Soil map of the Mount Lofty Ranges study area (Davies <i>et al.</i> 2002) showing the location of transect “T-A” (•) (Fritsch and Fitzpatrick 1994), which corresponds to the conceptual toposequence model shown in Figure 9.17 (b). A hillshade is applied to accentuate local landform.	150
Figure 9.19. Land tenure in the Mount Lofty Ranges (MLR) study area (boundaries shown as red lines), and land use summarised.....	154
Figure 10.1. Location of survey sites within the Mount Lofty Ranges study area for detailed investigation of seasonal depth solute trends.....	156
Figure 10.2. Upper layer (L1; 0 - 0.1 m) seasonal trends of electrical conductivity (EC_{se}) and concentrations of Na, Cl and S salts in the Mount Lofty Ranges (MLR) study area. Two metre contours indicate local landform.....	158
Figure 10.3. Upper layer (L1; 0. 0.1 m) seasonal trends in comparative concentrations of the soluble salts: Ca, K, Mg, P and S in the Mount Lofty Ranges (MLR) study area. Two metre contours indicate local landform.....	161

Figure 10.4. Conceptual Model 1a for shallow NAS, topographically perched, and in upper hillslopes. The conceptualised contour map that is inset identifies possible affected areas in the landscape, and the indicative location of the transect described in the model.	163
Figure 10.5. Diagnostic down-profile salinity (EC_{se} , dS/m) trends of Model 1a-type soils (profiles: 001, 002, 005, 006, 008 and 010).....	164
Figure 10.6. Diagnostic down-profile salinity (EC_{se} , dS/m) trends of Model 1a-type soils (profiles: 012, 014, 015, 025, 026 and 028).....	165
Figure 10.7. Photograph showing the landscape position of profile 025, and the sharp break of slope (dashed line) that is up slope.	166
Figure 10.8. Conceptual Model 1b for shallow NAS in mid/upper hillslopes, in low-lying areas with partial groundwater influence. The conceptualised contour map that is inset identifies possible affected areas in the landscape, and the indicative location of the transect described in the model.	167
Figure 10.9. Diagnostic down-profile salinity (EC_{se} , dS/m) trends of Model 1b-type soils (profiles: 003 and 009).Table 10.3. Layer physicochemical properties of profiles conforming to Model 1b, featuring winter (W_) and summer (S_) salinity (EC_{se} , dS/m), clay content (%) and concentration of soluble salts (mg/kg^{-1}).....	167
Figure 10.10. Conceptual Model 2a for GAS in upper hillslopes. The conceptualised contour map that is inset identifies possible affected areas in the landscape, and the location of the transect described in the model.....	168
Figure 10.11. Diagnostic down-profile salinity (EC_{se} , dS/m) trends of Model 2a-type soils (profile: 020).Table 10.4. Layer physicochemical properties of profiles conforming to Model 2a, featuring winter (W_) and summer (S_) salinity (EC_{se} , dS/m), clay content (%) and concentration of soluble salts (mg/kg^{-1}).	169
Figure 10.12. Conceptual model of Model 2b GAS, lower hillslopes. The conceptualised contour map that is inset identifies possible affected areas in the landscape, and the indicative location of the transect described in the model.....	170
Figure 10.13. Diagnostic down-profile salinity (EC_{se} , dS/m) trends of Model 2a-type soils (profiles: 011, 018, 027 and 029).	170
Figure 11.1. Relationship between seasonal apparent electrical conductivity (EC_a) and electrical conductivity of the saturated paste extract (EC_{se}) at corresponding depths in the Mount Lofty Ranges study area.	174
Figure 11.2. Mount Lofty Ranges study area winter EM38 EC_{ah} (i.e. surface conductivity) survey patterns with a linear stretch applied for visual consistency. A hillshade has been applied to accentuate local landform. Regions of interest “a” and “e” are identified, along with transect A-A'	175
Figure 11.3. Mount Lofty Ranges study area winter EM38 EC_{av} (subsoil conductivity) survey patterns with a linear stretch applied for visual consistency. A hillshade has been applied to accentuate local landform. Regions of interest “a” to “e” are identified, along with transect A-A'	176
Figure 11.4. Mount Lofty Ranges study area summer EM38 EC_{ah} (surface conductivity) survey patterns with a linear stretch applied for visual consistency. A hillshade has been applied to accentuate local landform. Transect A-A' is identified.	177
Figure 11.5. Mount Lofty Ranges (MLR) study area summer EM38 EC_{av} conductivity (surface conductivity) survey patterns with a linear stretch applied for visual consistency. A hillshade has been applied to accentuate local landform. Transect A-A' is identified. .	178
Figure 11.6. Profiles corresponding to transect A-A', featuring elevation (m), slope ($^{\circ}$) and EM38 winter and summer apparent conductivity (EC_a , mS/m), of surface (EC_{ah}) and subsoil (EC_{av}).	179
Figure 11.7. Summary of seasonal interpretations of GIS analysis of the co-registered seasonal EC_a survey coverages.	180
Figure 11.8. Mount Lofty Ranges study area winter apparent electrical conductivity differences ($EC_{ah} - EC_{av}$) with landform codes (“M” = zone of high volume magnetic susceptibility response; “pl” = perched landform; “bs” = break of slope; “ss” = saline seep;	

“lld” = low lying drainage). A hillshade and two metre contours are applied to accentuate local landform differences.....	181
Figure 11.9. Mount Lofty Ranges study area summer apparent electrical conductivity differences ($EC_{ah} - EC_{av}$) with landform codes (“M” = zone of high volume magnetic susceptibility response; “pl” = perched landform; “bs” = break of slope; “ss” = saline seep; “lld” = low lying drainage). A hillshade and two metre contours are applied to accentuate local landform differences.....	182
Figure 11.10. Mount Lofty Ranges study area apparent electrical conductivity in horizontal mode (EC_{ah}) difference class coverage (i.e. winter $EC_{ah} -$ summer EC_{ah}). A hillshade and two metre contours are applied to accentuate local landform differences.	185
Figure 11.11. Mount Lofty Ranges study area apparent electrical conductivity in vertical mode (EC_{av}) difference class coverage (i.e. winter $EC_{av} -$ summer EC_{av}). A hillshade and two metre contours are applied to accentuate local landform differences.	186
Figure 11.12. Mount Lofty Ranges study area seasonal near-surface salinity vector coverage with a hillshade applied to accentuate local landform variations.....	188
Figure 11.13. Profiles corresponding to transect A-A' in the Mouth Lofty Ranges study area, featuring: elevation (m), slope ($^{\circ}$), apparent electrical conductivity in horizontal mode (EC_{ah}) and apparent electrical conductivity in vertical mode (EC_{av}) differences in units of mS/m.....	190
Figure 12.1. Mount Lofty Ranges study area revised soil units, showing soil core locations (Chapter 10) and a hillshade to accentuate local relief. Soil descriptions for each unit are presented in Table 12.2.	194
Figure 12.2. Mount Lofty Ranges study area refined soil mapping showing 3D oblique views (a) to the southwest, and (b) to the northeast. Two metre contours and hillshading are applied for terrain. Soil descriptions for each unit are presented in Table 12.2.....	199
Figure 12.3. Diagram illustrating the principles behind the moderated terrain difference method.....	201
Figure 12.4. Spatial correspondence of: (i) upscaling-predicted soil salinity classes (solid fill) and (ii) soil salinity classes from the Mount Lofty Ranges refined soil mapping (hatched fill) at 1:5,000 scale. A hillshade has been applied to accentuate local relief....	203
Figure 12.5. Mount Lofty Ranges study area and surrounding area (1,560 ha), featuring salinity process susceptibility classification and the boundary of the Mount Lofty Ranges study area. A hillshade has been applied to accentuate local relief.	205

Index of Tables

Table 2.1. Salinity classification based on EC_{se} (after Soil Survey Staff 1993).	10
Table 3.1. Summary of radiometric elemental abundance, weathering characteristics and pedo-geomorphic expression (multiple sources).	32
Table 4.1. Organisational hierarchy of soil systems with appropriate scales of investigation (adapted from Hoosbeek and Bryant 1992; McKenzie and Cresswell 2002).	36
Table 4.2. Stages of upscaling methodology.	41
Table 5.1. Final Soil Mapping Units (SMUs) classified according to Stace <i>et al.</i> (1968).	61
Table 5.2. Midnorth study area Soil Landscape Unit descriptions (modified from Fitzpatrick <i>et al.</i> 2003c), including topographic location, description, classification according to Australian Soil Classification (Isbell 1998), Soil Taxonomy (Soil Survey Staff 2003) and Great Soil Group (Stace <i>et al.</i> 1968), and typical profile and landscape photographs.	63
Table 6.1. Summary of Plot 1 (18 cores) and Plot 2 (13 cores) field investigations results (complete data presented in Appendix D).	77
Table 6.2. Summary of plot physicochemical data.	79
Table 6.3. Results of ESP analysis for a selection of L3 (upper B horizon) samples.	88
Table 7.1. Statistical review of Midnorth study area geophysical surveys.	98
Table 7.2. Summary of x-ray diffraction (XRD) mineralogical results for the Midnorth study area (incorporating results from Fitzpatrick <i>et al.</i> 2003c), with corresponding clay % values (upper-most layer analysed, and corresponding airborne gamma radiometric K % values.	110
Table 8.1. Environmental covariate thresholds applied in the shallow NAS upscaling methodology used for the Midnorth study area and surrounding areas.	117
Table 9.1. Interpreted relationships between airborne K %, Th ppm, U ppm and aeromagnetic First Vertical Derivative survey coverages and soil, regolith and geology (Figure 9.3) in the Mount Lofty Ranges (MLR) study area.	129
Table 9.2. Layer identification and depth ranges (m).	131
Table 9.3. Interpretation of landform, and drainage and ponding classes according to hillslope position and MrVBF values.	140
Table 9.4. Mount Lofty Ranges study area soil map (shown in Figure 9.18) unit descriptions (according to Davies <i>et al.</i> 2002; Fitzpatrick <i>et al.</i> 1999; Merry <i>et al.</i> 2002).	151
Table 10.1. Layer identification and depth ranges (m).	156
Table 10.2. Typical composition of fertilizers applied in the Mount Lofty Ranges (MLR) study area according to manufacturer information (www.pivot.com.au/ProductInformation.asp).	160
Figure 10.9. Diagnostic down-profile salinity (EC_{se} , dS/m) trends of Model 1b-type soils (profiles: 003 and 009). Table 10.3. Layer physicochemical properties of profiles conforming to Model 1b, featuring winter (W_) and summer (S_) salinity (EC_{se} , dS/m), clay content (%) and concentration of soluble salts (mg/kg^{-1}).	167
Figure 10.11. Diagnostic down-profile salinity (EC_{se} , dS/m) trends of Model 2a-type soils (profile: 020). Table 10.4. Layer physicochemical properties of profiles conforming to Model 2a, featuring winter (W_) and summer (S_) salinity (EC_{se} , dS/m), clay content (%) and concentration of soluble salts (mg/kg^{-1}).	169
Table 12.1. Georeferenced GIS themes, and their thematic mapping support, which were used to refine the Mount Lofty Ranges study area soil map at regional scale.	192
Table 12.2. Mount Lofty Ranges study area revised soil units, with accompanying descriptions of landform elements, soil descriptions, drainage and waterlogging class, acidity/alkalinity class, salinity ranges and depth to saline water, soil salinity type, and model types and associated profile IDs. Refer to Figure 12.1 for map soil units.	195

Table 12.3. Environmental covariate thresholds applied in the GAS, intermediate shallow NAS/GAS soil, shallow NAS soil and soils not susceptible to salinity upscaling methodology used for the Mount Lofty Ranges study area and surrounding areas. 201

Table 13.1. Summary of spatial methods used in an enhanced soil survey (ESS) framework, their scale and mode of application, used in advanced soil survey. 210

List of commonly used abbreviations

AEM	airborne electromagnetic
ASS	acid sulfate soils
CEC	cation exchange capacity
CSIRO	Commonwealth Scientific and Industrial Research Organisation
DAP	di-ammonium phosphate
DDL	double diffuse layer
DEM	digital elevation model
DGPS	differential geographic positioning system
DSM	digital soil mapping
EC _{1:5}	electrical conductivity of 1 soil to 5 water ratio extract
EC _a	apparent electrical conductivity
EC _{ah}	apparent electrical conductivity in horizontal mode using the EM38 instrument
EC _{av}	apparent electrical conductivity in vertical mode using the EM38 instrument
EC _{se}	electrical conductivity of saturated paste extract
EMI	electromagnetic Induction
ESP	exchangeable sodium percentage
ESS	enhanced soil survey
FLAG	Fuzzy Landscape Analysis GIS
GAS	groundwater associated salinity
GIS	geographic information system
GPS	global positioning system
HC	hydraulic conductivity
IAS	irrigation associated salinity
MIR	mid infra-red
MLR	Mount Lofty Ranges
χ	mass magnetic susceptibility
MrVBF	Multi-resolution Valley Bottom Floor index
MTD	moderated terrain difference
NAS	non-groundwater associated salinity
PASS	potential acid sulfate soil
PTF	pedotransfer function
SLU	soil landscape unit
SASMMSP	South Australian Salt Mapping and Management Support Project
SMU	soil mapping unit
TWI	topographic wetness index
κ	volume magnetic susceptibility
$\chi_{fd\%}$	frequency dependency susceptibility
χ_{hf}	high frequency (4.6 kHz) mass magnetic susceptibility
χ_{lf}	low frequency (0.46 kHz) mass magnetic susceptibility
XRD	x-ray diffraction

Statement

This work contains no material which has been accepted for the award of any other degree or diploma in any university or other tertiary institution. To the best of my knowledge and belief, this thesis contains no material previously published or written by another person, except where due reference is made in the text.

I give consent to this copy of my thesis, when deposited in the University library, being available for loan and photocopying.

Mark Thomas

Acknowledgements

I deeply acknowledge my supervisors and mentors, Drs Rob Fitzpatrick (CSIRO Land and Water) and Graham Heinson (Geology and Geophysics, School of Earth and Environmental Sciences, The University of Adelaide). Rob exudes a mix of heady and infectious excitement for the many areas of soil-landscape research that he is master of. Chaos sometimes seems a part of life working with Rob until, that is, it's finally dawned on you where he's going with a concept. Then keeping up is akin to holding on tight to the greased tail of a comet! Graham, on the other hand, applies a more moderated approach to his science, and is an inspirational teacher who, with a refined elegance, makes the complicated look simple. What both have in common is that they are compassionate, serious about their science, deeply committed to education and training, extremely generous with their time and knowledge, and are world leaders in their respective fields. I count myself fortunate to have worked - and grown - under their guidance.

Funding provided by the Cooperative Research Centre for Landscape Environments and Mineral Exploration (CRC-LEME) and the South Australian Department for Water, Land and Biodiversity Conservation (DWLBC) is acknowledged. Of the latter, I am grateful to Andrew Johnson and Russell Flavel who understood the importance of this research for South Australian conditions, and saw to it that additional funding be forthcoming. I have received travel assistance from the South Australian branch of the Australian Soil Science Society Inc. (ASSSI) and Ecophyte Technologies Inc. to present this research internationally, for which I am grateful. Thanks also go to my colleagues at Ecophyte for their

support during the final stages of this research.

I acknowledge the researchers who have gone before me in my study areas, and who's data legacies have unwittingly formed the foundations of my research. These are Mike Cannon and Jim McThompson (Midnorth study area), and Dr Emanuel Fritsch (Mount Lofty Ranges study area). My thanks go the farmers who have generously allowed me to use their land as my "laboratory": the Cootes and Ashby families of the Midnorth, and the Rowan, Wilison, Neumann and Herrmann families of the Mount Lofty Ranges. I am grateful for the field assistance given by Mark Fritz (CSIRO), Tania Dhu, Kate Selby, Tim Raggatt, Layla Tucker and Colin Rivers (University of Adelaide), and John Wilford (Geosciences Australia) - who also threw in a number of "curly" ones to make me think a little harder! I am also grateful to Drs Wayne Meyer and Mike McLaughlin of CSIRO Land and Water, who have supported my stay as a visiting scientist on The Waite Campus, Adelaide, and have ensured that no doors at CSIRO were left unopened.

I have special thanks for Richard Merry (Honourary Fellow, CSIRO Land and Water), a man of great modesty and a deep passion for, and commitment to, both the past and the future of soil science in Australia. He has always been a strong presence during my research, and keen to lend his considerable expertise in soils, whether in the field or laboratory.

Finally, to Corlia my wife, my thanks and love to you for the sacrifices you have had to make, and for keeping us all fed, clean, and happy at home - and for worst job of all over the late nights and weekends: pulling this thesis together! I hope you are proud of it.

Summary

Soil mapping by traditional methods, especially at regional scales, can be prohibitively expensive. Yet these maps are often essential components for making robust agricultural and natural resource management decisions. Digital soil mapping (DSM), which relies on quantitative, computer-based predictions of soil properties, offers promise in addressing problems associated with traditional, qualitative soil mapping approaches. In this thesis, the distribution of saline-sodic properties forming part of a complex pattern of soils in two varied upland agricultural regions in South Australia were predicted at multiple scales (i.e. from hillslopes to regions) using DSM and allied approaches.

The outcomes and advantages of the approaches used are summarised below. Of the regions selected as study areas, the Midnorth receives an annual rainfall of 475 mm, while the Mount Lofty R (MLR) receives an annual rainfall of 680 mm. Combined with the different weathering histories, parent material and land management patterns, these differences give rise to a diverse set of pedogenic conditions, which have a significant bearing on the approaches to predict the distribution of soils in each area.

Chapter 1 introduces the work presented in this thesis, providing an outline of the approaches and methods used. **Chapter 2** presents a review of salt-affected soils, with an emphasis on southern Australian conditions. Saline and sodic soils are defined, and associated soil and land management issues discussed. A new processes-based salinity scheme is presented to classify soil and regolith salinity types. According to this scheme, shallow non-groundwater associated salinity (shallow NAS), which occupies the attention of much of the current

research, is introduced and described. Finally, texture-contrast soils that are most commonly the “host” of shallow NAS are described.

Chapter 3 describes pedogenic processes in relation to hillslopes, with a focus on the movement of matter and solutes, and how these combine to create land degradation issues (e.g. saline and sodic, and waterlogging). DSM is introduced, which involves the combination of soil-landscape models and a geographic information system (GIS). Combined with novel and traditional survey methods (i.e. enhanced soil survey – ESS), these approaches yield quantitative soil predictions and mapping. Following this, a description is given of the novel survey approaches used, which include terrain and geophysical survey methods. The geophysical survey methods used include electromagnetic induction (EMI), mass (χ) and volume (κ) magnetic susceptibility, and gamma-radiometrics. The role of these survey methods in DSM in terms of qualitative (i.e. in developing soil-landscape models) and quantitative (i.e. the role as environmental covariates) approaches are discussed.

Chapter 4 draws the connections between the discussions of the preceding Chapters. Pedological complexity, which is a key feature of the selected study areas, is defined as part of this discussion. The Chapter also describes a DSM approach to predict soil conditions across spatial scales, called “upscaling”. Hydropedology is the branch of soil science concerned with: (i) patterns of water movement in soil-landscapes, and (ii) how these patterns relate to the spatial, profile and temporal distribution of contemporary soil properties. As such, hydropedology is introduced as the scale-linking mechanism used in the upscaling

approach. A discussion is presented in this Chapter concerning “conceptual toposequence models”, which are essentially hydropedologically-based qualitative hillslope models that are used to graphically identify key hillslope processes that govern soil development, and are used to support the formulation of “predictive rules” that are used in the upscaling procedure. Finally, the intellectual rationale for the investigative framework applied during the research programme described in this thesis is presented.

Chapter 5 presents a detailed description of the Midnorth study area, with an emphasis in the discussion on the distribution of soils in the study area hillslope. **Chapter 6** describes fine scale soil investigations of shallow NAS processes and distributions through interpretation of point (profile) and plot (100 m²) physicochemistry. Here, fine scale is consistent with investigation of soil systems operating through the scale range encompassing points (i.e. profile) to polypedons - via pedons that are intermediate. As such, the soil systems involved are best portrayed at mapping scales that are typically finer than approximately 1:1,000. The fine scale investigations were focused on two 100 m² plots established within a texture-contrast soil unit that physicochemistry data indicated to be susceptible to shallow NAS. Using a qualitatively derived map of farm yield of part of the study area, one of the plots was established inside an area of consistently good/reliable farm yields, whereas the other plot was established inside an area of consistently poor farm yields. The detailed investigations applied closely spaced EMI, depth to B horizon, and surface κ surveys, which were interpolated using GIS. When interpreted with reference to laboratory data, the approach yielded limited success in revealing fine scale soil patterns for each plot. However, it was possible to formulate shallow NAS conceptual models for

each plot by considering hillslope position, depth to B horizon, laboratory electrical conductivity, rubbed soil colour, and carbonate presence. The models developed explained the causes of farm yield differences identified for each plot.

The soil system knowledge acquired during the preceding fine scale investigations were used to develop a whole-of-hillslope understanding of pedogenic processes for the study area through medium scale investigations described in **Chapter 7**. Here, medium scale is consistent with soil systems that occur over hillslopes and toposequences, which are typically best captured at mapping scales that range from approximately 1:1,000 through to 1:5,000. Linkages between fine and medium scale investigations were achieved through whole-of-hillslope surveys of EMI, magnetic susceptibility (κ), gamma-radiometrics, and terrain attributes generated from a detailed digital elevation model (DEM). When combined with laboratory data, the spatial patterns generated by these survey approaches were used to interpret whole-of-hillslope soil processes. From this new knowledge, a conceptual toposequence model was developed for the study area hillslope.

Chapter 8 describes coarse scale investigations conducted in the Midnorth study area. Here, coarse scale is consistent with soil systems that span catchments, regions, continents and the globe. As such, these scales are consistent with mapping scales that are coarser than 1:5,000 - typically 1:20,000 scale, and greater. In this Chapter, the multiscale soil knowledge developed through the preceding investigations described in Chapters 6 and 7 helped define the predictive rules applied in an upscaling procedure, which applied the environmental covariates of airborne gamma-radiometrics and terrain attributes. The upscaling method was used to successfully predict the

regional patterns of texture-contrast soils in the region neighbouring the study area hillslope, and within these patterns, the areas affected by shallow NAS.

Chapter 9 provides a detailed description of the Mount Lofty Ranges study area and surrounding region. **Chapter 10** describes fine scale investigations that were conducted over successive seasons (winter 2004, then summer 2005) on selected < 1 m soil profiles from representative soil units identified within the study area. The data generated from these multi-temporal investigations revealed subtle changes in salt distributions in the near-surface (< 1 m) of soil profiles. In conjunction with hillslope position and knowledge of land management practices (e.g. fertilizer applications), the seasonal near-surface salt movements were used to define a number of hydropedological trends, and from these, four generic hydropedological models to describe soil salinisation processes were developed. These models include: (i) Model 1a - for shallow NAS, topographically perched, and in upper hillslopes; (ii) Model 1b - shallow NAS in mid/upper hillslopes, in low-lying areas with partial groundwater influence; (iii) Model 2a - for groundwater associated salinity (GAS) in upper hillslopes; and finally (iv) Model 2b GAS - in lower hillslopes. The seasonal distributions of sulfur salts in the near-surface (< 1 m) of soil profiles indicated the influence of shallow groundwater systems, with the salts transported in groundwater from localised zones of pyritic mineralisation.

Chapter 11 describes medium scale investigations to spatially characterise seasonal salt movements using sequential (i.e. winter 2004, then summer 2005), near-surface (< 1 m) EMI surveys of the whole study area. The seasonal EMI surveys were used to spatially determine the distributions of the hydropedological models that were

developed in Chapter 10, using soil laboratory data for verification. A single κ survey of the whole study area was also conducted, which revealed study areas patterns of near-surface mineralisation, historic burning, erosion/deposition patterns, and near-surface hydromorphic conditions linked to the distribution of the iron oxide, maghemite.

Chapter 12 applies ESS approaches combined with multiscale knowledge from the preceding MLR research Chapters to: (i) refine the legend and soil unit boundaries of a 1:5,000 scale legacy map of the study area, and (ii) upscale the distribution of soils corresponding to the hydropedological salinity models described in Chapter 10. The refinement of the legacy soil map was conducted by combining laboratory data and various spatial datasets coregistered in a 3D GIS. The coregistered datasets used included: (i) gamma-radiometrics, (ii) terrain attributes (e.g. slope, multi-resolution valley bottom floor (MrVBF), topographic wetness index (TWI)), (iii) other soil mapping, (iv) geology, and (v) aerial magnetics. This time, the upscaling approach used was solely reliant on a selection of terrain attributes, which performed successfully as environmental covariates for predicting the regional patterns corresponding to the hydropedological models developed earlier.

Finally, **Chapter 13** presents overall conclusions to the research, and recommendations for further work. The key aspects reported in the conclusions are that the approaches described have revealed shallow NAS to be a highly variable landscape phenomenon in terms of spatial and temporal distribution. Indeed, before the present studies there have been no specific research published that documents these aspects of shallow NAS at scales ranging from medium through to regional.

The methodologies developed here have also revealed that, although occurring in pedologically complex landscapes, the distribution of soil types and shallow NAS within these soil-landscapes is systematic. As such, once revealed using the types of ESS approaches described, qualitative models can be developed to guide the development of quantitative GIS-based methods (e.g. DSM upscaling) to predict the regional distribution of soil types and salinity processes.

The multiscale and multi-temporal approaches described in this thesis have enabled the development soil-landscape process models to a level of spatial and temporal refinement not hitherto achieved. This new knowledge now offers the opportunity for more accurate quantitative soil predictions to be made. The approaches developed have also demonstrated the key role of integrating legacy datasets (e.g. physicochemistry, soil mapping) from previous studies conducted in the study areas. The ability to integrate these data has significantly enhanced the quality of results, widened the scope of the original research, and has provided leverage to ensure that more has been achieved from finite project funding and resources that were originally available.

In conclusion, Chapter 13 contains recommendations that include the need to:

- investigate the role of ground penetrating radar surveys to reveal, in greater detail, subsoil morphology and hydropedology, both spatially and continuously over wider areas than currently feasible with which to refine the quality of qualitative models;
- adapt the generic approaches reported in this thesis to monitor and predict landscape hydromorphological patterns of redox potential (Eh) to manage acid sulfate soil-landscapes and off-site effects; and finally
- couple the approaches of this thesis with emerging spatio-temporal predictive approaches and technologies, including advanced interactive scientific visualisation and virtual reality techniques. Such an approach will lead to the achievement of more refined qualitative soil-landscape models, and with access to advanced computing, achieve faster and more accurate quantitative soil property predictions.

Chapter 1. Introduction

In the recent publication “The Future of Soil Science”, Petersen (2006) appealed for soil scientists to “abandon our current narrow perspective and to become involved in systems-level analysis” and to “start integrating our skills to generate landscape-scale solutions over multiple temporal and spatial scales”. The appeal was made from the imperative that soil science must develop strategies to understand and manage both spatial and temporal soil changes (e.g. Richter and Markewitz 2001), and be able to integrate science at landscape and watershed (catchment) levels. To not do so, Petersen implied, will result in soil science becoming disengaged with the developing needs of broader society.

Why have Petersen and other authors (e.g. Bouma 1989; Dalal-Clayton and Dent 2001; Doran 2002; Webster 1997) implied this? Firstly, they recognise that the spotlight is now firmly on the soil science community to engage concerted effort to integrate and apply the fundamental principles of soil science (under sub-disciplines of mineralogy, biogeochemistry, hydrochemistry, hydrology, and soil physics) - hard won over many years of soil research. This science is required to contribute to solving real global issues (such issues include: rapid population growth and food scarcity; resource conflict and a degraded natural resource base; and global warming and carbon sequestration). Secondly, Petersen (2006) recognises that although many of the challenges are global (or continental or regional) in nature, ultimately solutions will be achieved by a mosaic of countless on-ground activities carried out in a myriad of landscapes distributed throughout the world. Hence, solutions to global soil problems will be tackled at the landscape level, and for this reason, the pressure is on soil science to deliver soil databases (comprising data, maps, and information) consistent with intervention options at this scale. Berry *et al.* (2005) couches such

targeted intervention under the framework of “precision conservation”.

The gathering pace of environmental stresses in the world means the demand for suitable soil-landscape databases are growing rapidly. Soil scientists must anticipate such looming needs by developing methods and approaches to supply soil databases in advance of needs, and in a manner that is cost-effective. Many soil researchers (e.g. Burrough and McDonnell 2000; Grunwald 2006a; McBratney *et al.* 2003; McBratney *et al.* 2000; Webster and Oliver 2001) have identified digital soil mapping (DSM) and allied technologies as a key approaches to satisfying these future needs. DSM represents a shift from qualitative soil mapping that is reliant on labourious field survey and laboratory data (e.g. Gunn *et al.* 1988), to quantitative soil mapping, reliant on modern computing and supported by field and laboratory data.

Grunwald (2006b) identifies four main drivers that have facilitated the shift towards quantitative soil mapping in recent times. These include: (i) *Growth of novel soil mapping tools and sensors*, which provide dense distributions of soil data, rapidly and cost-effectively; (ii) *Data management tools*, e.g. geographic information

systems (GIS) and database management systems; (iii) *Rapid growth in desktop computing power* (simultaneously with falling costs); and (iv) *Methods*, including advanced multivariate and geostatistical techniques, and 3D and 4D scientific visualisation tools. In this thesis, such an integrated approach that incorporates all these components in an advanced soil survey methodological framework (often in conjunction with legacy datasets) is described as “enhanced soil survey” (ESS).

Soil-landscape models are common to both qualitative and quantitative soil mapping techniques. Hudson (1992) described these models as the product of the “soil-landscape paradigm”, and represent abstractions of the real environment contained and communicated through “tacit rules”. Models, whether qualitative or quantitative, represent frameworks that allow systematic translation of knowledge, information, or data across scales via “transfer functions” (Dalal-Clayton and Dent 2001). Pedotransfer functions are specific transfer functions applied in soil modelling, and which correlate to - and are less costly to acquire than - the soil attributes (e.g. texture, hydraulic conductivity) specifically sought to tackle the soil issues in question (Bouma 1989; Hoosbeek *et al.* 2000). As such, pedotransfer functions allow the use of cheaper - or more conveniently acquired - data proxies to be used in soil modelling.

Hydropedology is an approach to link soil-landscape knowledge across data scales (Lin 2003), and novel soil mapping tools and sensors have a role to play in revealing the distribution of hydropedological features in soil-landscapes to develop the models needed. As such, improved soil mapping tools and sensors assist in the formulation of pedotransfer functions.

“Upscaling” (e.g. McBratney 1998) is a quantitative DSM approach that applies GIS to transfer knowledge from local to regional scales for regional soil predictions. Upscaling relies on applying models of soil-landscape properties developed from field investigations conducted in key areas to subsequently predict soil conditions elsewhere in neighbouring regions that exhibit similar soil-landscape conditions. Results are achieved through applying carefully selected combinations of low cost spatial datasets (e.g. digital elevation models) that operate as pedotransfer functions using environmental correlation (McBratney *et al.* 2003; McKenzie and Ryan 1999). Apart from the preliminary work to regionally upscale the distribution of salinity and waterlogging for a small region in the Mount Lofty Ranges (MLR) (Fitzpatrick *et al.* 1999), no soil upscaling studies have since been conducted in South Australia.

In South Australia, the soils in the so-called agricultural areas (nominally > 350 mm rainfall per year, and covering approximately 15 million ha) have been systematically mapped using traditional (qualitative) methods (e.g. Gunn *et al.* 1988) by the Department of Water, Land and Biodiversity Conservation (and predecessors). These maps have been created at scales of either 1:50,000 or 1:100,000, depending on land use intensity and rainfall (Soil and Land Information 2002). Soil landscape units (SLU) represent the fundamental mapping units of the mapping program. These units are principally defined according to parent material and landform. Typically, upland hillslopes with common parent material comprise one or two SLUs. While the South Australian soil mapping arguably ranks amongst the best in the so-called developed world in terms of mapping quality and consistency, the mapping scales are still not suitable for precision conservation. However, in many parts of the developing world,

where the demand for rapid, reliable and low-cost soil maps are all-the-more acute (e.g. the African continent, Bekunda 2006), such data is generally harder to come by at best, and at worst, non-existent.

Anticipating future soil database needs to solve global and regional issues, the objective of this thesis is to describe a combined DSM and field survey approach using ESS to upscale the distribution of soil properties in two regions in South Australia, each with complex soil-landscapes. Specifically, the objective involves developing approaches to predict the spatial distribution of complex saline-sodic soil patterns in the Midnorth and the MLR of South Australia. As such, the research involves refining the preliminary work of Fitzpatrick *et al.* (1999) by developing a more robust upscaling approach for use under South Australian soil conditions. A key

component of the approach involves re-working/accessing, using GIS and statistical analyses, quantities of mostly unpublished legacy soil data from previous studies. Such data prove to be extremely valuable because field and laboratory data are time consuming and expensive to acquire, and would otherwise remain “lost” to research. The proposed new methodology that is summarised in Figure 1.1 features a series of multiscale and multi-temporal, system-level analyses to: (i) develop a detailed and integrated understanding of soil systems at various scales, and (ii) to develop the capability to link the soil processes revealed across various scales. As such, a key aspect of the research is to develop improved soil mapping tools and sensors (e.g. ESS) to determine hydropedological patterns throughout study area soil-landscapes so that scale linkages across soil systems can be achieved.

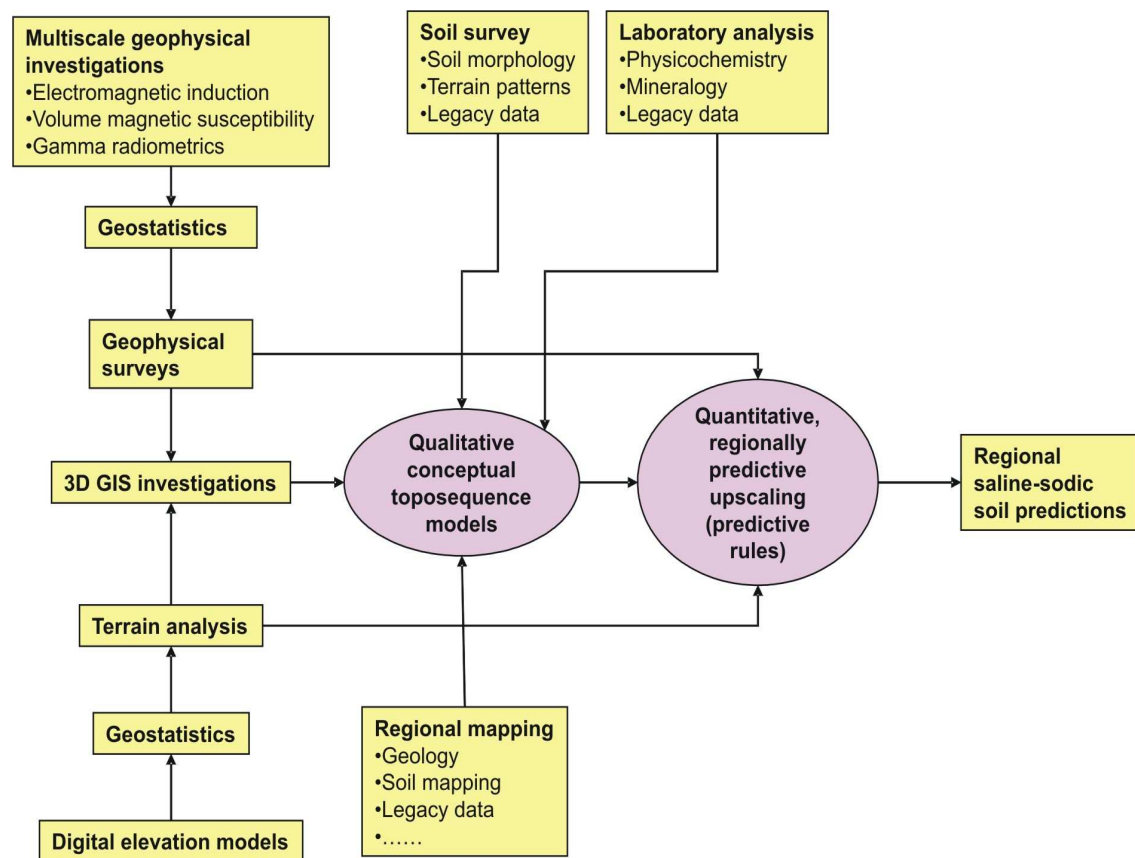


Figure 1.1 Outline of digital soil mapping methodology for regional predictions of saline-sodic soil patterns.

While the current research is focussed on predicting the regional distribution of saline-sodic soils, the generic ESS approaches developed here will also have application in addressing other natural resources and environmental management challenges that rely on a spatial understanding of soil processes (e.g. soil erosion, soil-regolith acidification, and predicting contaminant pathways through soil-landscapes) in Australia and in other parts of the world. As such, this research responds directly to the “call-to-arms” evoked by the previously cited authors (e.g. Bouma 1989; Dalal-Clayton and Dent 2001; Doran 2002; Petersen 2006; Webster 1997) to apply fundamental soil science to solve the present and future spatially-based problems.

Figure 1.2 identifies the flow of tasks conducted as part of the thesis in terms of Chapter sequence. The review Chapters (i.e. Chapters 2 through to 4, shown in green) involve the theoretical components of the thesis, and feature

the outcome of a literature review. Chapters 5 through to 12 (shown in orange) describe the practical, investigative components of the research conducted in the Midnorth study area (Chapters 5 through to 8) and for the MLR study area (Chapters 9 through to 12). The sequences of Chapters for the study areas are governed by the scale of the investigation conducted during the study, i.e. from fine, to medium, to coarse scales. Finally, the remaining Chapters (shown in blue) cover the introduction (this Chapter) and the summary of conclusions and recommendations for further work (Chapter 13).

Finally, the research described in this thesis has yielded a series of presentations and publications (e.g. extended abstracts), which have been presented at various Australian and international scientific fora. A list of these presentations and publications are listed in Appendix A for reference.

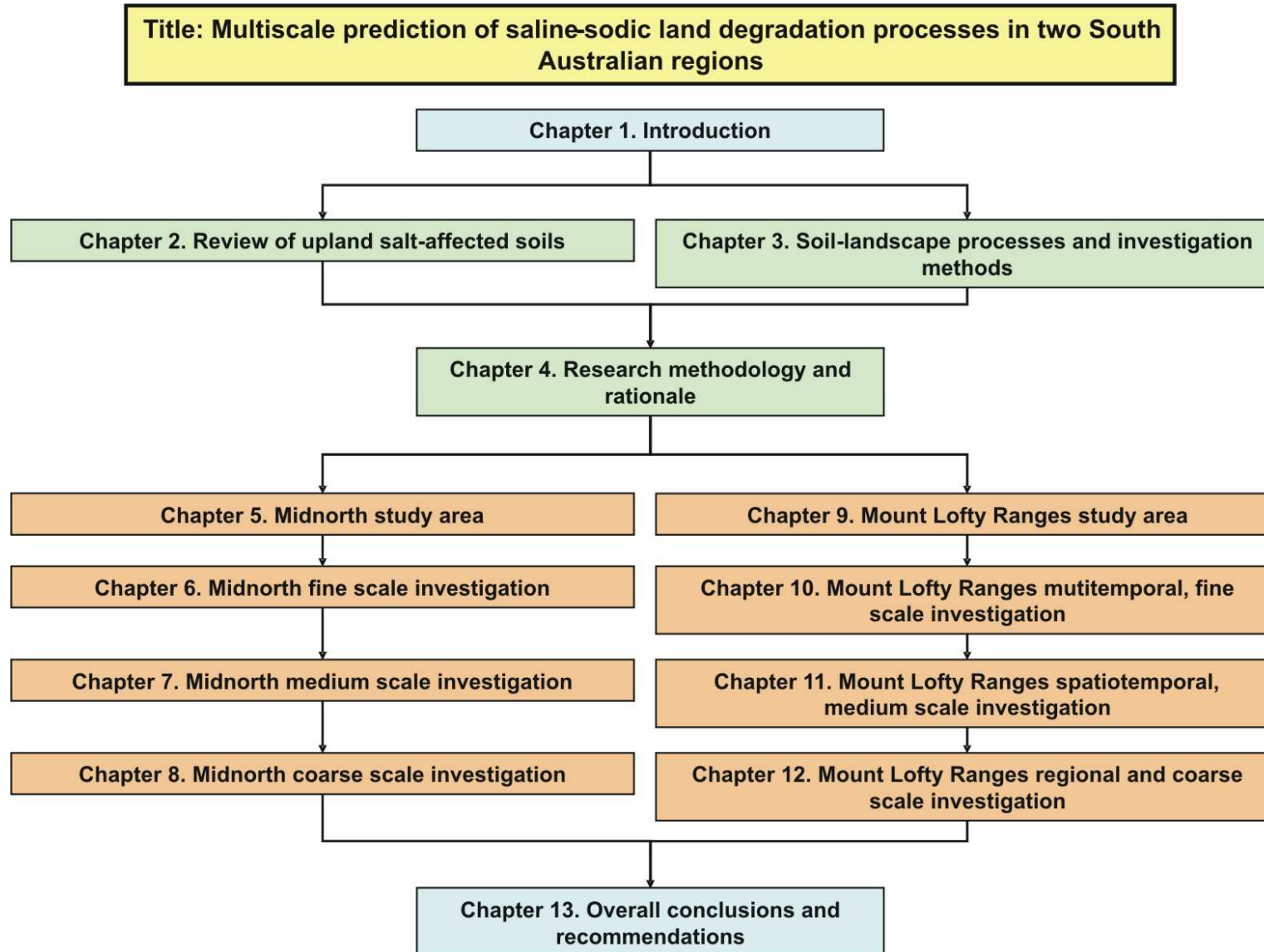


Figure 1.2. Flow diagram that represents the thesis structure according to Chapter numbers and titles, and how Chapters relate to one another.

Chapter 2. Review of upland salt-affected soils

This Chapter reviews the soluble salt composition of salt-affected soils, and the physicochemical effects that these may have on soil properties. Special emphasis is given to salt-affected soils typically found in sloping upland Australian landscapes that have no connection with deep saline groundwater systems. These soils often combine solum (to be discussed) salinity and sodicity in a type of salinity called shallow non-groundwater associated salinity (shallow NAS) (Fitzpatrick 2005; Thomas *et al.* 2005) using a proposed new process-based salinity classification scheme. The scheme is presented in this Chapter.

2.1 Soil layers and morphology

Arable crop roots exist in the soil solum. The solum is generally considered to extend to the depth of maximum perennial plant root penetration, hence all arable crop roots are contained in the solum (Soil Survey Staff 1993). The modern concept of the solum is that it represents the A and B horizons (including all intermediate layers) of the soil profile, all of which have formed under the same generic soil forming conditions (Tandarich *et al.* 2002). The A and B horizons are master horizons that are dominated by weathered mineral material, which may or may not contain fragments of unweathered rock (i.e. parent material).

Although not considered part of the solum, some soil profiles may contain an O horizon, which is characterised by an accumulation of organic matter in various states of decay. Below this layer is the A horizon, which is a mineral layer generally rich in humified organic acids and constitutes the top of the solum. The A horizon is characterised by the accumulation of humified organic matter, and is not dominated by properties characteristics of the E and B horizons.

An E horizon is often present below the A horizon, and is characterised by a loss of silicate clay, iron, aluminium, leaving behind a concentration of sand and silt particles. In Australia, the E horizon is described as the A₂ horizon (McDonald *et*

al. 1998), and henceforth the term E horizon for this particular soil layer is preferred. The E horizon tends to have the lightest colours in the soil profile due to the combination of: (i) the removal of pigmented organic and mineral materials, and (ii) the dominance of the residual bright (i.e. having high Munsell values) quartzite materials. As will be discussed in later Chapters, the E horizon plays an important role in the transport of solutes from up slope areas via focussed soil water flows (i.e. throughflow). The majority of throughflow is conducted through the deepest portion of the E horizon, i.e. at the E/B layer interface. This layer is termed the EB horizon.

Below the A horizon (or E horizon if present) is the B horizon. The B horizon features an accumulation of silicate clays, iron, aluminium, humus, carbonates, gypsum, or silica, either individually, or in combinations thereof. B horizons may also show evidence of removal of carbonates, residual concentration of sesquioxides, coatings of sesquioxides, and may feature a strong, often massive, structure (e.g. blockiness or prismatic structure), and brittleness. Further, B horizons characteristically exhibit stronger colours (e.g. higher chroma, redder hues) than the A and E horizons above.

The subsolum (also termed “substrata” and “parent material” (Wysocki *et al.* 2005)) occurs below the solum. In terms of pedology, the subsolum consists of a C

horizon (if present) and an R layer, which is formed of fresh bedrock. The C horizon is formed from sediment, saprolite and saprock, and unconsolidated bedrock (Soil Survey Staff 1993), which may demonstrate both lithologic and pedologic characteristics (Graham *et al.* 1994), and in places may be > 10 m in depth (Stolt and Baker 1994). The subsolum plays an important role in soil-landscape processes as this is the region of the profile that features the storage and transport of weathered materials (e.g. salts and colloids), groundwater flows and often hosts the redox-dynamic vadose zone. While the C horizon falls within the “regolith” - a term commonly used by quaternary geologists, geomorphologists and hydrologists, and described as “*all surficial material above fresh bedrock*” (Ollier and Pain 1996) - agriculturalists and pedologists differentiate between the solum and subsolum components of the so-called regolith. As such, Taylor and Eggleton (2001) advocate interdisciplinary approaches to regolith research, as promoted by Cremeens *et al.* (1994) through the Soil Science Society of America special publication entitled “*Whole regolith Pedology*”. The term “soil-regolith” as used henceforth combines all of the horizons above the R layer.

In cultivated areas, the A horizon is generally mixed (anthroturbated) and internal layering obliterated, forming an Ap horizon. If shallow enough, the E and material from the upper parts of the B horizon may be combined in the Ap horizon. B horizons that exhibit strong accumulations of silicate clays are given the suffix “t”, while if also possessing a strong accumulation of exchangeable sodium in a natric horizon, are given the suffix “n” (see discussion in Section 2.3). Hence, B horizons combining strong accumulations of silicate clays and an elevated concentration of exchangeable sodium are designated as “Btn horizons” (Soil Survey Staff 1993).

2.2 Salts in soils

Salts are present in almost all soils and are necessary for healthy plant life. However, when critical concentration thresholds are exceeded, plant health is negatively impacted, and the soil deemed salt-affected (Chhabra 2005; Keren 2000; Shaw 1999). Broadly speaking, salt-affected soils fall into two categories: (i) saline soils, and (ii) sodic soils (Ghassemi *et al.* 1995; Northcote and Skene 1972; Sumner 1995b; Szabolcs 1989).

Saline soils are defined by the presence of an excess of salts that are more soluble than gypsum (Soil Survey Staff 1993). Excessive concentrations of salts in the solum create unfavourable conditions for crop growth caused by osmotic gradients (i.e. akin to the effects of droughting caused by a soil moisture deficit) and toxic conditions (Keren 2000; Steppuhn *et al.* 2003). Sodic soils, which are associated with excessive sodium ions (Na⁺) on the positively and negatively charged soil sites (Levy 2000; Soil Survey Staff 1993; Sumner 1995a) that attract free ions of opposite charges (i.e. the soil exchange complex), result in deterioration of the soil structure to become physically hostile to subsoil root development and exploration, and by hampering the movement of water and air through the soil profile (Rengasamy 2002a; Rengasamy and Olsson 1991; So and Aylmore 1995). Because saline soils are often associated with high concentrations of sodium ions in solution, and excessive concentrations of these ions is a key defining feature of sodic soils, the saline condition and the sodic condition often coincide in salt-affected soils (Sumner *et al.* 1998); all sodic soils are saline, whereas many saline soils are not sodic (Northcote and Skene 1972).

Being rich in soluble salts that are easily dissolved under field conditions, localised salt concentrations in the soil profile are strong indicators of prevailing hydro-pedological conditions and equilibria that are detectable through movements of salt-rich wetting fronts and the formation of salt concentration zones

(Shaw 1988). Localised hydrogeological conditions are strongly governed by landform and slope (e.g. Fanning and Fanning 1989; Hall and Olson 1991; Wysocki *et al.* 2000), which are discussed further in Section 2.6 and in Chapter 3.

2.3 Sources of salts in Australian landscapes

Primary salts sources in Australian landscapes include: (i) marine sources and (ii) from mineral weathering of crustal rock (Gunn and Richardson 1979; Isbell *et al.* 1983). Windblown salts from the oceanic sources are of contemporary importance (e.g. Hingston and Gailitis 1976). The processes involved with the release of salts from mineral weathering of bedrock are discussed in Ollier and Pain (1996) and Taylor and Eggleton (2001).

Once released into the soil-regolith, salts may become relocated either by wind as parna (fine aeolian dust) (e.g. Dahlhaus *et al.* 2000; Wilford *et al.* 2001) or in moving groundwaters (e.g. Charman and Wooldridge 2000; Dahlhaus *et al.* 2000; Ghassemi *et al.* 1995; Keren 2000).

2.4 Dominant ions in salt-affected soils

Typically, Australia's crustal rock is rich in soluble salts. For example, sodium, which is one of the most abundant elements in the Earth's crustal rock (Chartres 1995; Taylor and Eggleton 2001) has an average composition of 2.5 % by mass (Isbell *et al.* 1983). Once released from the bedrock through mineral weathering, Na-rich minerals tend to decompose quite readily to yield soluble sodium ions that are easily leached elsewhere in the profile or landscape. These ions remain mobile until either scavenged (e.g. silicate clay formations and alterations), where they become fixed in the soil-regolith matrix, or transported elsewhere, e.g. via groundwater flows (Taylor and Eggleton 2001).

The chloride content of typical Australian crustal rocks is rarely greater than 8 % (Isbell *et al.* 1983). Results of analyses of chloride content of unweathered granitic rock were in the range 0.022 - 0.069 by percent weight. Reported as mean content of chloride by a percent mass basis, the results for unweathered basaltic and metamorphic rocks were 0.016 % and 1.63 %, respectively (Gunn and Richardson 1979).

Sodium chloride commonly dominates saline soils (Gunn and Richardson 1979; Szabolcs 1989). In southern Australia, these halitic salts account for between 50 - 80 % soil salts (Williamson 1990). After chloride (Cl⁻), the most common anionic salts are sulfates (SO₄²⁻) and carbonates (CO₃²⁻) (Cass 1999; Fitzpatrick 2002; Fitzpatrick *et al.* 2001). Sulfates are locally significant in the Mount Lofty Ranges of South Australia (Fitzpatrick 2002). After sodium (Na⁺), the most dominant cations are calcium (Ca²⁺), magnesium (Mg²⁺), and potassium (K⁺) (Sumner *et al.* 1998). Copper (CuCO₃, CuOH⁺), zinc (Zn²⁺, Zn(OH), ZnCO₃) and boron (B(OH)₃, B(OH)₄⁻) ions may be locally significant in some parts of the world (Szabolcs 1979). Fitzpatrick (2005) collates a number of case studies from different saline environments. The author describes the case study saline environments as being predominantly: (i) sodium carbonate-dominant (alkaline), (ii) halitic; gypsum-dominant (gypsic), (iii) pyrite rich (sulfidic), (iv) sulfuric acid-dominant (sulfuric), and (v) high exchangeable sodium percent (ESP) (sodic).

2.5 Measuring and defining soil salinity

Rhoades (1999) presents a comprehensive account of laboratory and field-based methods to determine soil salinity, and Spies and Woodgate (2005) describe salinity mapping and analysis methods in the Australian context. Laboratory methods include measuring the electrical conductivity (EC, preferably in units of dS/m). EC has a near-linear correlation to: (i) salt type and (ii) salt

solution concentration, as shown in Figure 2.1.

Two laboratory methods are commonly used to determine soil salinity. These include determining the EC of: (i) the ratio of 1:5 soil/water extract ($EC_{1:5}$) and (ii) the saturated soil paste extract (EC_{se}). Both methods are fully described in Rayment and Higginson (1992).

The $EC_{1:5}$ method involves mixing a ratio based on mass of one part of soil to five

parts of deionised water, mechanically shaking the mixture for one hour, and then measuring the EC at an extract temperature of 25 °C. Although quick and convenient, the quality of results may be compromised: (i) in the presence of low solubility salts due to the relatively short period of one hour given to reach soil solution equilibrium, and (ii) because the conductivity is measured on a soil solution that is significantly more dilute than field conditions (Shaw 1999).

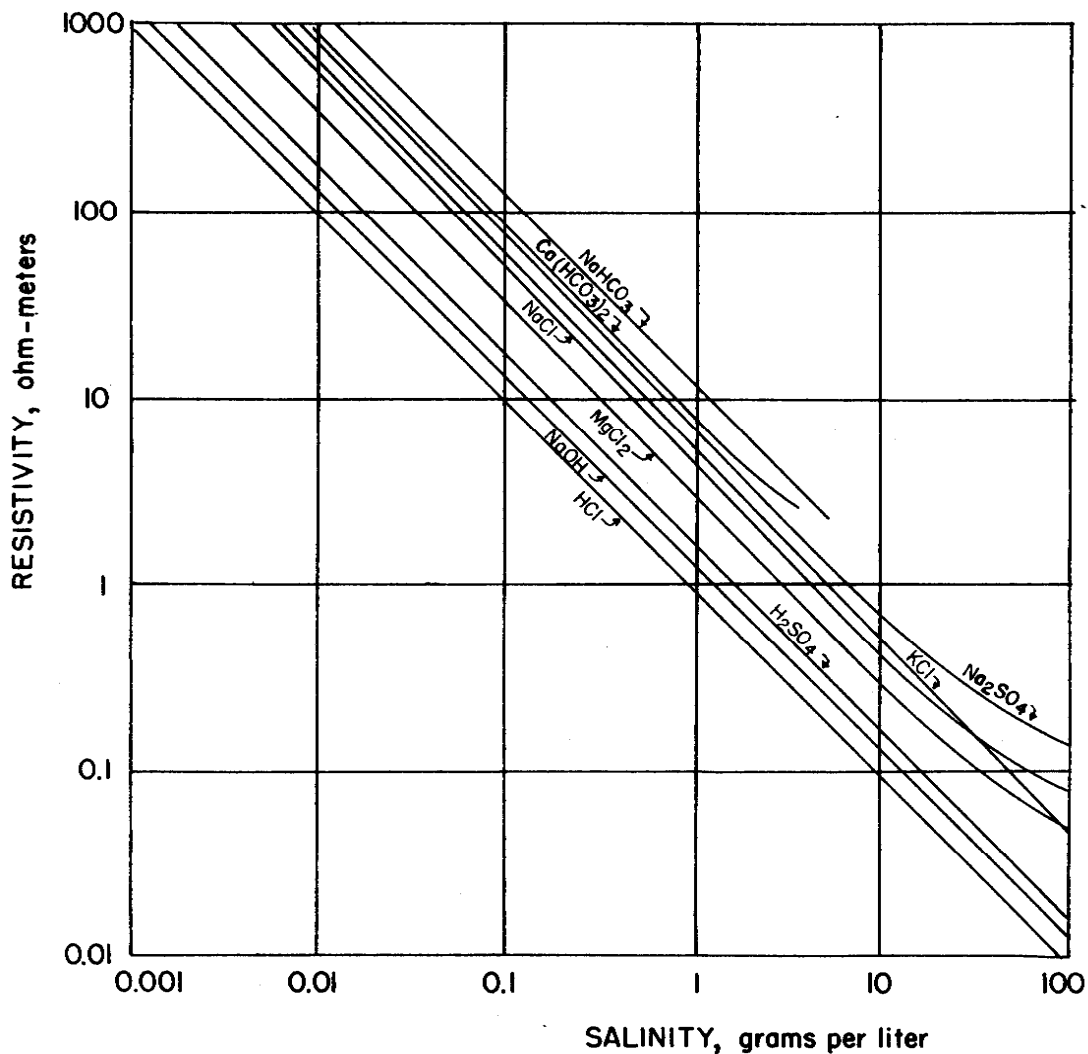


Figure 2.1. Relationship between salt type and concentration (in g l⁻¹) to resistivity, which is the reciprocal of conductivity (after Keller and Frischknecht 1966).

The alternative EC_{se} method gives EC measurements that are more reflective of actual field conditions by performing the EC measurement (at 25 °C) on the liquid extract of a soil/de-ionised water paste, which has been allowed to stand for more than 30 hours, ensuring achievement of a more complete soil/water equilibrium. The EC_{se} method also has the advantage of inherently taking to account the influence of soil texture, related to cation exchange capacity (CEC), on the soil electrical charge (Shaw 1988; 1999). Therefore, being analytically more accurate (albeit more laborious), the EC_{se} technique is recommended for laboratory determinations of soil salinity (Soil Survey Staff 1993).

Various field-based and portable geophysical electromagnetic inductive (EMI) instruments have been designed to measure the EC at various depths through the soil-regolith profile. These EC measurements correlate with salt concentrations, which are given in units of apparent EC (EC_a) in mS/m. Being field portable, the instruments are ideal for spatial investigation of soil-regolith profile conductivity patterns in landscapes. The EM38 (which has an effective to a depth of 1.5 m, and suitable for surface and subsoil applications) and the EM31 (which has an effective to a depth of 8 m, and most suitable for regolith applications) instruments of Geonics Ltd. of Canada are commonly used in soil-landscape conductivity investigations (McNeill 1980b; Rhoades *et al.* 1999). These instruments, and their field operation, are discussed in further detail in Chapter 3.

Soils that have an EC_{se} of greater 2 dS/m are classified as saline (Soil Survey Staff 1993). The salinity classes are presented in Table 2.1. Broadly speaking, these thresholds have their basis in crop responses to soil salinity concentrations.

Table 2.1. Salinity classification based on EC_{se} (after Soil Survey Staff 1993).

Salinity class	EC_{se} (dS/m)
0 Non-saline	0 – 2
1 Very slightly saline	2 – 4
2 Slightly saline	4 – 8
4 Moderately saline	8 – 16
5 Strongly saline	≤16

2.6 Measuring and defining sodic soils

Sodic soils are characterised by an excess of sodium ions in the soil relative to the other soil cations of magnesium, potassium and aluminium. The physicochemical and morphological criteria for sodic soils are presented in further detail below.

Sodic soils have been given various names, including: black alkali sodic soils, non-saline sodic soils, saline sodic soils, and saline alkali sodic soils, and alkali sodic soils (Sumner *et al.* 1998). The variety of names reflects the compositionally diverse nature of these soils as they feature variable concentrations of the ions typically associated with salinity (e.g. Cl, $CaCO_3$, and SO_4) and a variable pH that is typically in the range > pH 7. As discussed in Northcote and Skene (1972), some soils may be simultaneously saline and sodic because of the leaching or non-supply of non-sodic cations. Their absence, and the subsequent dominance of sodium ions, results in the new formation of sodic conditions in the saline environment (Rengasamy and Sumner 1998; So and Aylmore 1995; Sumner *et al.* 1998). However, sodic structural decline is reversible by increasing the electrolytic content of the soil solution by non-sodic salts (Cass 1999; Cass *et al.* 1996; Sumner *et al.* 1998).

The classification of sodic soils can be based on either: (i) physicochemical

laboratory criteria, and/or (ii) soil morphology, including the presence of Btn horizons and associated diagnostic soil structural observations (Bui *et al.* 1998; Northcote and Skene 1972). While laboratory dispersion tests may be used to indicate sodic soil conditions (Emerson 2002; Murphy 1995; Rengasamy 2002a), the measure of ESP is the preferred physicochemical method to define sodic soils (Soil Survey Division Staff 1993; Sumner 1995a).

As referred to earlier, the ESP is the measure of the proportion of sodium ions relative to calcium, potassium, magnesium and aluminium ions attached, through variable strengths, to negatively charged sites within the soil fabric (e.g. including silicate clays, colloids and organic acids) in the electrostatically dynamic soil zone called the “soil exchange complex” (Levy 2000; Rengasamy and Churchman 1999; Sumner 1995a). In effect, the ESP is the measure of the proportion of negatively charged sites on clay platelets that are occupied by sodium ions relative to calcium, magnesium and potassium ions. The ESP is calculated accordingly:

$$ESP = \frac{(100 \times \text{Exchangeable Na})}{CEC}$$

The ESP value ≥ 15 is used to define sodic soils in many parts of the world (Bresler *et al.* 1982; Bui *et al.* 1998). In Australia, however, the ESP value ≥ 6 (Bui *et al.* 1998; Murphy *et al.* 2000; Northcote and Skene 1972; Sumner 1995b; Szabolcs 1989) or less (Rengasamy and Churchman 1999) is used to define sodic soils. The Australian use of lower ESP thresholds reflects the generally higher content of swelling clays in the soils (Chartres 1995; So and Aylmore 1995).

Soil EC (Naidu and Rengasamy 1995), pH (Sumner 1995b), soil texture (Fitzpatrick 2002) and clay mineralogy (Bresler *et al.* 1982) combine to influence the stability of soils with high sodium ionic concentrations. For this reason, relying on fixed ESP thresholds alone to define

sodic soils under typical field electrolytic conditions may be problematic. Instead, some researchers advocate that soils only be defined as sodic once sodic soil structural (e.g. swelling or dispersion) and/or morphological (soil layers) evidence is encountered, irrespective of ESP (Fitzpatrick 2002; Rengasamy 2002b; Rengasamy and Churchman 1999; Sumner 1995b).

Morphologically, sodic soils often exhibit a strong Btn horizon (Bui *et al.* 1998; Fitzpatrick *et al.* 1995), forming a marked increase in texture from the A horizon to the B horizon. In Australia, the term “duplex soils” is sometimes used to describe these soils, whereas the genetic term “texture-contrast” soils is more widely used internationally, and henceforth here is the preferred term. The classification of texture-contrast soils are discussed in further detail in Section 2.10 of this Chapter.

According to Isbell *et al.* (1983) between 190 - 230 M ha (i.e. 25 – 30 %) of the approximate 770 M ha land mass of Australia is mantled by sodic soils, which they define as soils that have an ESP > 6 in the top metre of the profile. While based on less conservative calculations, Rengasamy (2002b) also reports that Australia is mantled by a similarly large area (250 M ha) of sodic soils, and of this area, 20 M ha is either cultivated or under improved grazing. From calculations of potential yields based on rainfall alone, the same researcher shows that crop yields from sodic soils are less than half of those from non-sodic soils. Sodic soils therefore impart a significant impact on economics of the Australian farm sector.

2.7 Structural problems associated with sodic soils

On soil wetting, excessive sodium ions affect the configuration of clay platelets within the soil structure. This in turn leads to problems associated with soil structure and stability, ultimately causing clays to swell and to disperse (Rengasamy and Sumner 1998; So and Aylmore 1995; Soil Survey Division Staff 1993). The

governing factors that determine swelling and dispersive behaviour in soils are the balance between the attractive and repulsive forces that arise from intermolecular electrostatic interactions within the soil particles of the soil exchange complex, and the other charged soil constituents in the soil solution (Rengasamy and Sumner 1998).

Soils often contain a complex mixture of various types of clay minerals, colloids, free ions, sesquioxides, and organic acids. Many of these components exist with either permanent or variable charge polarities on their surfaces. For example, the edges of clay platelets and sesquioxides are either positively or negatively charged. Some of these components have the capacity to switch charge polarity according to prevailing soil pH conditions, although the basal surfaces of clay platelets possess a permanent negative charge. Once in solution, the negatively charged clay surfaces attract the positively charged cations to form a feature known as a “diffuse double layer” (DDL), which determines the width of the gap between clay platelets (Goldberg and Suarez 2000a; Levy 2000; Rengasamy and Sumner 1998; So and Aylmore 1995).

Conceptually, the so-called DDL consists of a swarm of ions in which the cations are strongly drawn towards, and then some become attached to, the negatively charged basal clay sites. The density of the cation swarm reduces exponentially away from the negatively charged clay sites as the attractive forces dissipate with distance. Conversely, the density of anions in solution increases away from the basal clay surfaces. The size of the DDL gap is partially determined by the valency of cations held in the soil solution. For example, divalent-dominated soil solutions (e.g. Ca^{2+} -clays) create strongly attractive cation-to-basal clay platelet forces, resulting in narrow DDL gaps, and consequently closely packed clay platelets. Alternatively, mono-valent Na^+ -clays (i.e. the high ESP, sodic clays) form weaker attractions and hence result in wider DDL gaps. These

soil conditions result in weakly attracted clay platelet-packing that may become easily disrupted leading clay dispersion, which is discussed in further detail below. Ultimately, the DDL gap is determined by the balance between the repulsive and attractive forces at play within the clay-solution complex (Sumner *et al.* 1998).

In addition to the effects of valency, the soil solution ionic concentration (EC_{se}) is also an important factor in determining the DDL dimension. Concentrated solutions increase the overall attractive forces within the clay-solution complex, whereas dilute solutions (e.g. rain water) reduce the overall attractive forces, widening the DDL, and reducing the stability of the complex (Rengasamy and Churchman 1999). Although high concentrations of divalent cations (e.g. Ca^{2+} in gypsum) are the most effective at conferring stability on clay particles, increasing the concentration of sodium ions will also have a positive effect on attractive forces (Cass 1999).

Slaking takes place when DDL gaps become too wide to maintain the integrity of the soil structure. The processes of slaking involves the disaggregation, collapse and dispersion of clay caused by swelling (Emerson 2002). Clay dispersion leads to a decline of hydraulic conductivity and infiltration rates caused by the development of clay cutans in soil voids that affect downward percolation and lateral flows. This sets up waterlogging conditions. Clays in sodic B horizons become hard-setting, especially when dry, severely hampering subsoil root exploration for water and nutrients. Clay dispersion may also lead to sealing of topsoils, creating surface ponding (So and Aylmore 1995). These lead to problems with agricultural workability and trafficability of farm vehicles, and possibly subsurface compaction. The combination of near-surface low HC and high evaporative rates often result in rapid drying and surface crusting. However, loamy sodic soils with moderate hydraulic conductivity (HC) rates have a limited shrinkage capacity when dried. These subsoil conditions

often result in deep, hard-setting soils that limit workability and root penetration, and reduce subsurface recharge, which can result in late-season droughting conditions for crops.

2.8 Shallow non-groundwater associated salinity

Shallow non-groundwater associated salinity (NAS) is a salt-affected soil that combines salinity and sodicity, and is a form of soil salinity that has been described as “dry saline land” (Fitzpatrick *et al.* 2003c; Kennewell 1999; Soil and Land Information 2002) and transient salinity (Rengasamy 2002b). A new and preferred process-based classification scheme for saline soils presented in Figure 2.2 shows shallow NAS in context with other common forms of soil-regolith salinities found in Australia, which include “groundwater associated salinity” (GAS) (commonly termed: “dryland salinity”) and irrigation associated salinity (IAS) (commonly termed “irrigation salinity”).

Importantly, shallow NAS occurs in the upper parts of the landscape that are not influenced by deep saline groundwater (Fitzpatrick *et al.* 2003b; Thomas *et al.* 2004; 2005). This landscape context for shallow NAS is totally unlike that of GAS (or “dryland salinity”), which occurs in low-lying parts of landscapes where saline groundwater tables are close to, or intersect with, the soil surface.

In southern Australia, shallow NAS is generally associated with upland, winter-rainfall areas in the Mediterranean climate zone. With reference to Figure 2.2, shallow NAS is dominated by either one of two forms, which may be used to further define the salinity type:

- Surface NAS, which typically has salinity values on the surface (typically < 0.3 m) in the range EC_{se} 4 - 60 dS/m, and
- Subsoil NAS, which typically has salinity values in the subsoil (typically, 0.3 - 1.0 m) in the range EC_{se} 2 - 8 dS/m in the subsoil form.

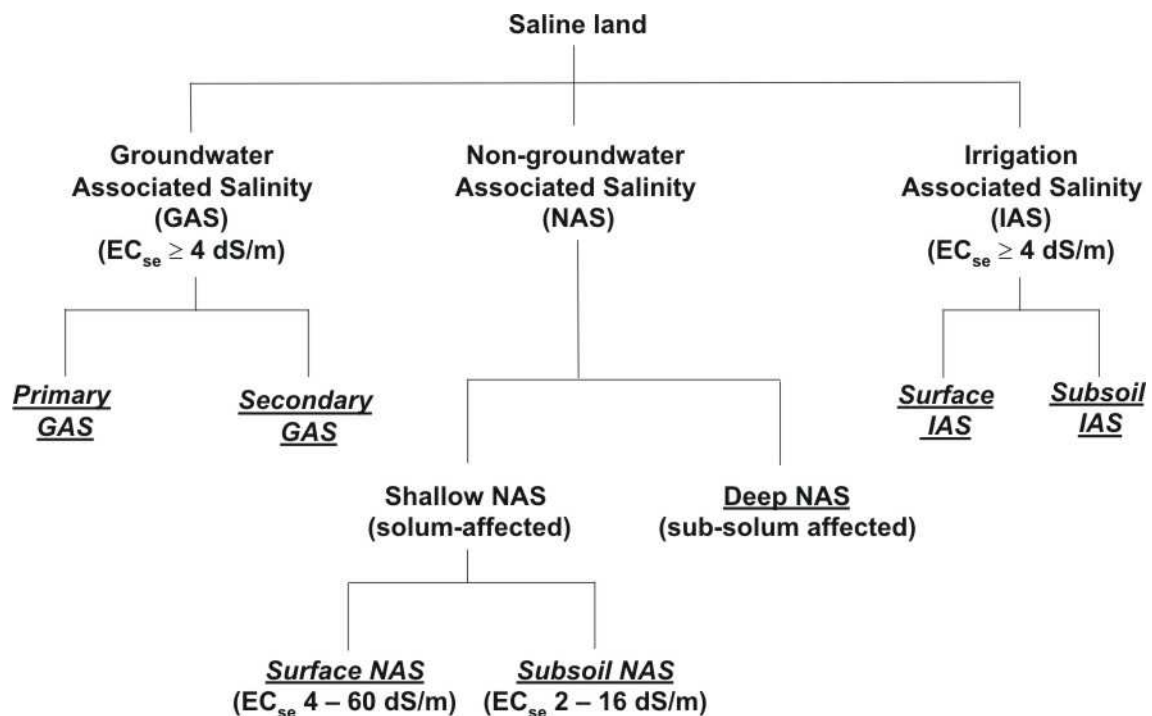


Figure 2.2. Process-based classification scheme for saline soils, including EC_{se} criteria (after Fitzpatrick 2005).

Shallow NAS is strongly associated with texture-contrast soils that feature a sandy/loamy A horizon over a Btn horizon. These soils are agriculturally very important in southern latitudes of Australia, and feature extensive areas of dryland cropping and grazing rotations. French (1981) describes the inherent challenges of farming on these soils. These challenges include poor nitrogen and phosphorous status, periodic growing season water stress, high evaporation during seed filling, and the unpredictable nature of rainfall in the areas that they occupy. These soils also have a propensity to erode as they combine the problems of: (i) occupying sloping areas, and (ii) the surface and subsurface structural problems associated with sodic soils discussed previously. Erosion can often produce a shallow A horizon, which results in a physically reduced water storage capacity. Finally, and adding to the challenge of managing these soils productively, shallow NAS soils are associated with seasonally perched watertables. This often makes shallow NAS difficult to identify because a cursory investigation of the causes of crop losses may indicate waterlogging alone, whereas to be affected by shallow NAS, waterlogging and changing saline conditions are combined (e.g. Eastham *et al.* 2000; Ward *et al.* 1998). Combined, the inherent problems associated with

texture-contrast soils in southern Australia makes the soil processes difficult to conceptualise, document and map using conventional soil survey methods (e.g. Gunn *et al.* 1988; McDonald *et al.* 1998) because they form intricate and complex and patchy landscape patterns that have limited apparent surface field indicators (e.g. colour or texture). The plates in Figure 2.3 show a landscaped view and profile of a winter wheat cropping area in the Midnorth of South Australia affected by shallow NAS. Figure 2.3 (a) features an area of crop loss and a fringing area affected by salinity (“s”), which are identified through stressed blue leaf tones. Nearby patches of shallow NAS affected areas are identifiable (“p”). Figure 2.3 (b) shows an enlargement of the soil profile, which features a shallow (10 cm) loamy A horizon over a sodic heavy clay Btn horizon. Surface water indicates waterlogging conditions.

Sixty seven per cent of agricultural and pastoral land in Australia is estimated to be susceptible to shallow NAS. This figure compares to 16 % for GAS. In terms of economic impact, shallow NAS accounts for a loss of approximately A\$1,330 M of potential earnings for the Australian agricultural economy per annum (Rengasamy 2002b).

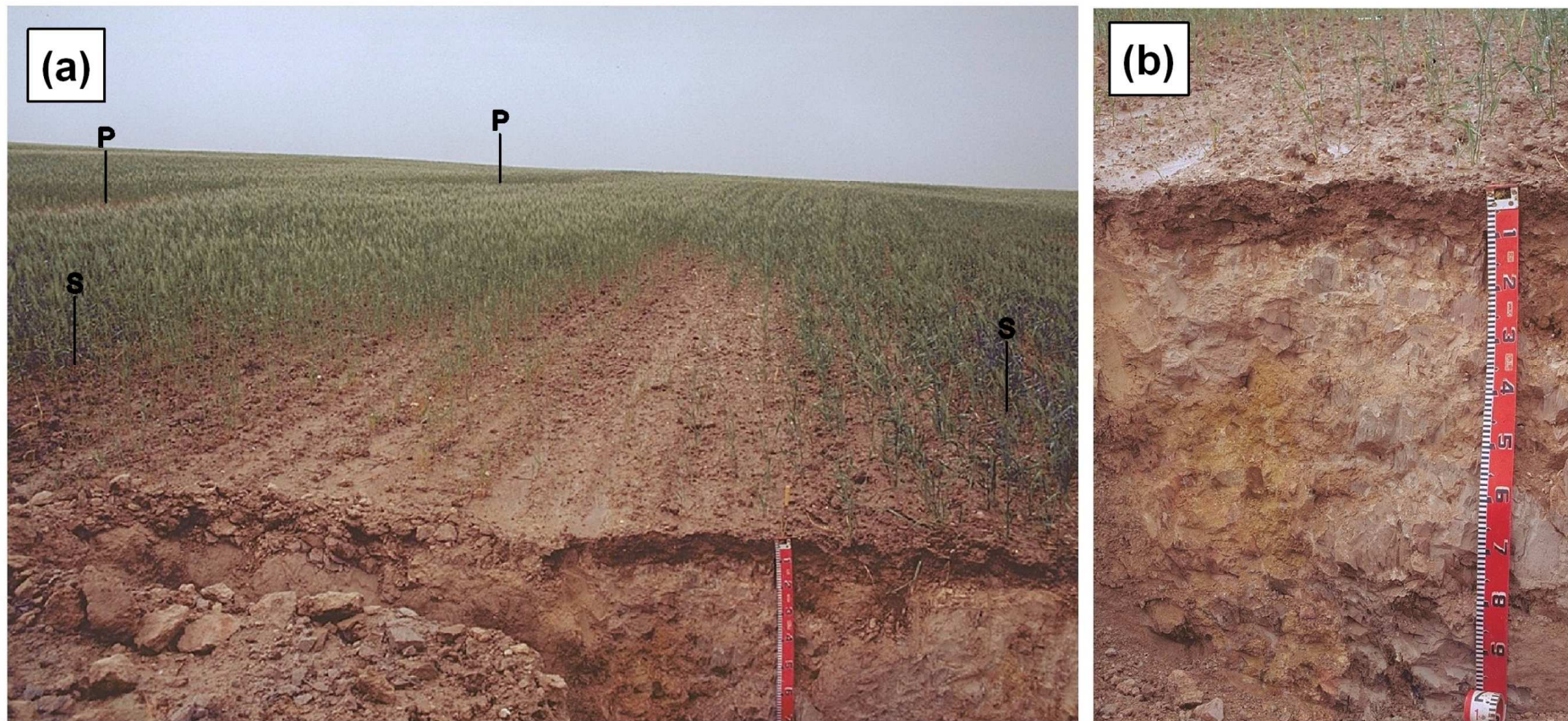


Figure 2.3. Plate (a) shows a shallow NAS-affected area of winter wheat in South Australia's Midnorth region. Shown is a localised area of crop loss, fringed by crops showing salt stress (grey leaf tones, "s"), and nearby patches of shallow NAS crop losses ("p"). Plate (b) shows a close-up view of the affected profile, featuring a shallow, waterlogged A horizon and heavy clay sodic Btn horizon (photographs: DWLBC).

2.9 Local terrain and shallow NAS expression

As discussed, sodic pore clogging in the B horizon of texture-contrast soils creates a layer that is almost impermeable to vertical water movement. Figure 2.4 (a – d) illustrates the conceptualisation of shallow NAS formation processes on hillslope areas. During the time of pre-cultivation (Figure 2.4 (a)) native vegetation creates hydraulic conditions in which salts are held in near-equilibrium throughout the soil-regolith profile. On agricultural land clearance, however, native vegetation is replaced by a matrix of annual vegetation (crops) and shallow rooted grasses, which result in lower water use efficiencies, landscape-wide. Consequently, during winter (Figure 2.4 (b)) when up slope soils are wettest, subsoil water movement is lateral (i.e. down slope), through the coarser textured A horizon. Salts are mobilised in the solum in association with throughflow. Combined, this results in the local formation of dilute saline wet patches (i.e. perched watertables) particularly in the low points of wavy/irregular B horizon boundaries (see Schoeneberger *et al.* 2002), in landform depressions, break of slopes, and where upper layer soil textures become clayier down slope at soil unit transitions. However, where subsoil freshwater flow rates are sufficiently high (e.g. in drainage zones on steep slopes), subsoil salts are washed out to down slope areas. Over time, the perched watertables accumulate salts, which become increasingly concentrated (Figure 2.4 (c)). Subsequently, during warm dry summer periods, the combination of surface evaporation and subsoil evapotranspiration creates dynamic

moisture conditions in the subsoil profile. These conditions cause dissolved salts to mobilise through the subsoil profile in the wetting front, and concentrate in topsoil and subsoil layers as they dry (Rengasamy 2002b) (Figure 2.4 (d)).

The seasonal changes salt concentrations in these layers – both temporally and spatially - pose a considerable farming challenge, often compounded by the associated problems of waterlogging and/or sodic structural decline in the soil. In summary, areas affected by shallow NAS are difficult to farm because they combine the soil problems of: (i) salinity, (ii) sodicity, (iii) seasonal waterlogging during crop establishment, (iv) seasonal water supply limitations during crop maturation, (v) poor nutrient availability, (vi) erosion risk, and finally (vii) a high degree of spatial and temporal variability in soil conditions.

2.10 Classification of texture-contrast soils

Typically, the so-called texture-contrast soils are strongly associated with Australian Soil Classification's Sodosol order described by Isbell (1998). The defining features of Sodosols is that they possess an abrupt or clear increase in texture in the B horizon (i.e. texture-contrast soils), and a major portion of the B horizon that is not strongly acidic (\geq pH 5.5) and is sodic ($ESP \geq 6$). Northcote (1992) applies only morphological criteria to define the so-called duplex soils. The criteria includes a distinct boundary between the A and B horizons, and an increase in texture class (see Northcote 1992) of at least one and a half texture groups between the A to B horizons.

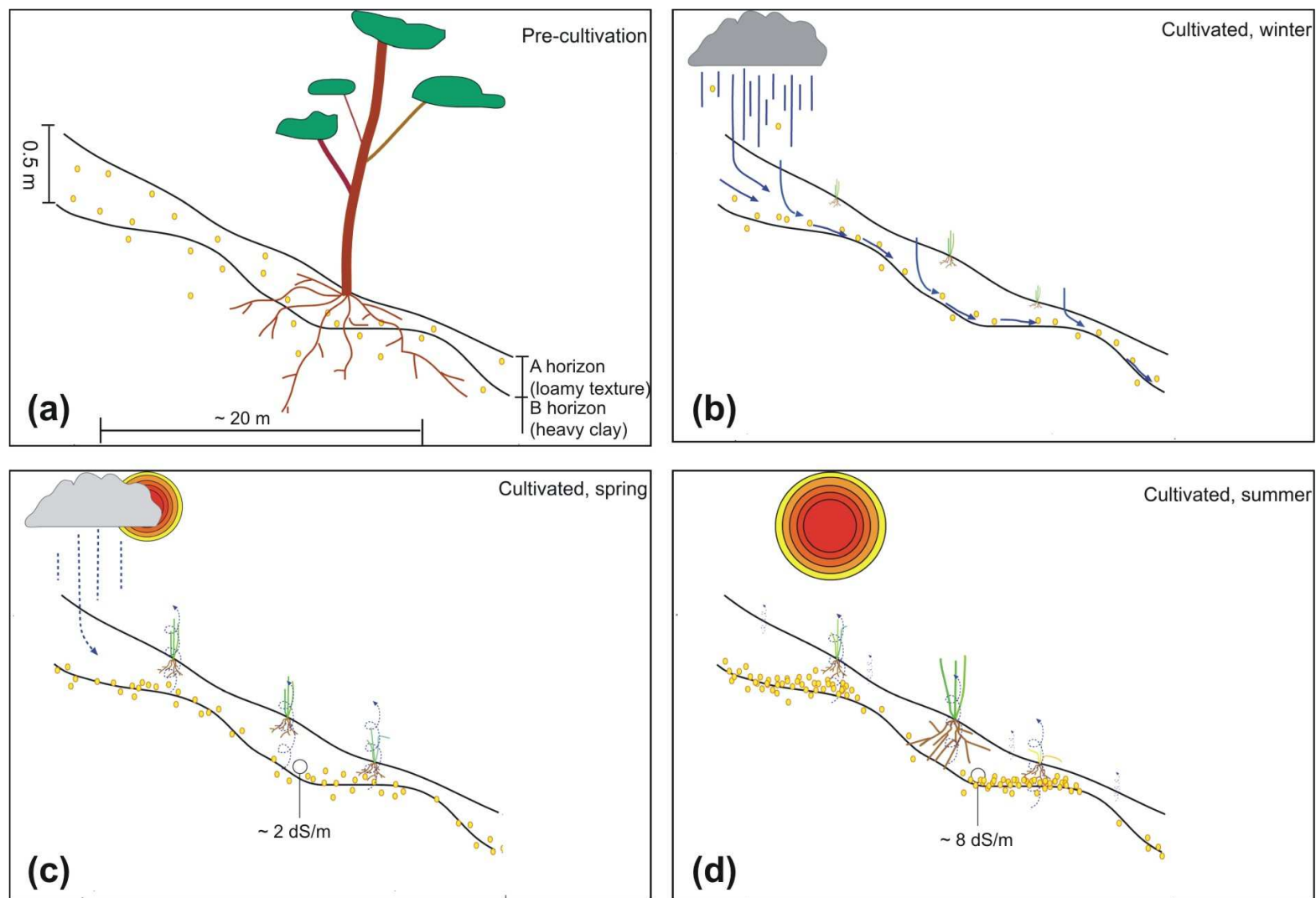


Figure 2.4. Conceptualisation of shallow NAS formation processes on hillslopes. Yellow dots indicate relative salt concentrations and blue arrows indicate predominant water movements. Typical scales and horizon textures are indicated in (a).

In terms of other soil classification systems that might be applied in Australia, Sodosols have equivalence to: (i) solodized solonetz and sodic soils, some soloths and red-brown earths and desert loams of Great Soil Group (Stace *et al.* 1968), (ii) duplex (D) soils of Factual Key (Northcote 1992), (iii) the Solonetz of World Reference Base for Soil Resources

(FAO 2006), and (iv) the Alfisols of Soil Taxonomy (Soil Survey Staff 1999). The central concept of Alfisols is that they possess: (i) a generally thin, mineral-rich A horizon that is often leached (i.e. light coloured, high chroma), (ii) a clay-rich B horizon (Btn), (iii) a moderate to high base saturation, and (iv) seasonally wetting and drying conditions.

Chapter 3. Soil-landscape processes and investigation methods

This Chapter provides an overview of soil-landscape forming processes on hillslopes from a hydrogeological perspective, and explains how this knowledge may be applied in understanding contemporary, hydrogeologically-based degradation processes in soils typically found in southern Australian catchments. The exploitation of the knowledge that soil-landscape forming processes on hillslopes is non-random and forms a systematic soil mapping framework is discussed. Attention is specifically given to quantitative digital soil mapping options (i.e. DSM) based on the use of environmental covariates, which are environmental datasets that spatially correlate with specific soil properties (e.g. terrain and soil wetness). An examination is made of the environmental covariates of digital elevation models (DEMs) used in terrain analysis, and the following geophysical techniques: (i) electromagnetic induction (EMI); (ii) volume magnetic susceptibility (κ); and (iii) gamma-ray surveys (or radiometrics). These survey methods are strongly suited to spatial interpretations of soil-landscape properties, particularly when they are combined. Overlapping with the discussion of κ survey methods, mass magnetic susceptibility (χ) methods are also discussed. As for EMI techniques, interpretations of χ data may also be powerful techniques to aid in understating the stratigraphy of soil layers, and hence useful in resolving spatially detailed pedogenic processes.

3.1 Soil-landscape processes governing soil properties

Soils and landscapes of typical interfluvial-valley bottom catchments can be considered as open systems that continuously gain and lose both material and energy across their boundaries (Gerrard 1992). Gravity, a function of slope and governed by landform, has a fundamental influence on the rate and the direction of material and energy flows in these systems. Broadly speaking, matter is transferred through landscapes under gravity, “whether dissolved, suspended, dragged or rolled” (Conacher 2002).

These processes can be summarised according to: (i) mass wasting or (ii) hydraulic transfer processes. Mass wasting, a physically-based process in which coarser materials move down slope (Daniels and Hammer 1992; Strahler 1975), has the strongest influence on geomorphic processes that dominate the processes that physically shape landforms. These include the processes of colluviation and erosional surface wash. The hydraulic transfer of materials in hillslopes generally takes place via: (i) throughflow (i.e. lateral down slope water flows in the shallow zones above the groundwater surface (Daniels and Hammer 1992)), or (ii) groundwaters that are likely to have little impact on soil properties outside low lying

landscape zones that are not directly influenced by groundwater (e.g. GAS, which was introduced in Chapter 2). Therefore, from the pedologist's perspective, throughflow is considered to be an important hydro-pedological process in shallow soil-regolith profiles, and has an overwhelming influence on soil morphology (e.g. Fritsch and Fitzpatrick 1994). Soil materials that are transported via throughflow are either: (i) salts and organic acids that are held in solution, or are (ii) fine particulate matter (i.e. < 0.02 μm) that are leached and then held in suspension, which, for example, results in the redistribution of clay particles through the soil profile (Fanning and Fanning 1989).

Soils occupying Mediterranean climate zones in sloping areas, and which have significant texture-contrasts between A and B horizons (e.g. Alfisols, Soil Survey Staff 2006), often demonstrate well-formed E horizons (and transitional E horizons, including EB-, E/B- and BE- and B/E horizons) (Hallmark and Franzmeier 2000). According to Fanning and Fanning (1989), the E- and transitional horizons are characteristically depleted of soluble and fine particulate materials through many years of repeating seasonal leaching cycles in a process called "lessivage". With only the more resistant soil materials left *in situ* (i.e. often dominated by coarse-grained quartz and Fe-oxides), these horizons possess a significantly higher hydraulic conductivity rate compared to the other soil horizons in the profile, and therefore act to preferentially focus throughflow, down slope through the soil profile.

Each landform in a soil-landscape tends to be dominated by the influence of either geomorphic or pedogenic processes (Wilding 2000). For example, Conacher and Dalrymple (1977) illustrate this through their nine-unit landsurface model that can generally be applied to most drainage basins. Their model is based on the

combined perspectives of landform, and contemporary geomorphological and pedogenetic processes. The model involves partitioning of surface and subsurface water flows to assist in conceptualising the formation of various soil-landscape properties, whether these be geomorphically or pedologically based.

Each of the nine units has distinguishing soil morphological features as a result of the mass wasting and hydraulic processes associated with each slope position. Milne (1936a; 1936b) was an early researcher who, through studies of soil-landscapes in East Africa, identified repeating soil patterns down hillslopes. Milne identified that these repeating soil patterns were systematically linked to relief and changes of slope, which in turn were linked to mass wasting and hydraulic processes. Milne (1936b) stated that the down slope differences in soil properties were "brought about by drainage conditions, differential transport of erosional material, and leaching, translocation, and redeposition of mobile chemical constituents".

From this knowledge Milne developed systematic models that form the basis of catenary concept. The so-called catenary concept explained why a continuum of soil properties were linked in a predictable sequence of soils stretching from an interfluvial valley bottom hillslope (Daniels and Hammer 1992; Gerrard 1992; Hall and Olson 1991). Such predictable sequences of hillslope soils are termed "toposequences" (e.g. Fanning and Fanning 1989).

It is now widely accepted that in addition to the influence of relief and changes in slope, there are four additional independent variables that influence soil formation. These include: (i) parent material (i.e. underlying geology), (ii) climate, (iii) organisms, including biological and human activity, and (iv) time, or stage

of development (e.g. Buol *et al.* 1973; Fanning and Fanning 1989; Gray and Murphy 1999). Jenny (1941) combined these variables in what is now commonly known as Jenny's "Fundamental Soil Equation", which is essentially a mechanistic model for soil formation, which is presented as:

$$s = f(cl, o, r, p, t \dots)$$

where s is soil state (soil property), cl factor corresponds to climate, o factor corresponds to organisms, r factor corresponds to relief, p factor corresponds to parent material, and t factor corresponds to time. The dots (...) were included so that other soil-forming factors may be incorporated at a later date if discovered.

Numerous discussions have been published on Jenny's equation and its derivatives, and the relative influences on pedogenic processes of each of the five independent soil forming factors (e.g. Bockheim *et al.* 2005; Brady and Weil 1999; Buol *et al.* 1973; Chapman and Atkinson 2000; Fanning and Fanning 1989; Gerrard 1981; Gray and Murphy 1999; Jenny 1980; Soil Survey Staff 1993; Strahler 1975). Nonetheless, Jenny's work provides an excellent framework to conceptualise soil formation in a systematic manner (Wysocki *et al.* 2000). Indeed, Richards (1985) describes the catenary concept as the two-dimensional quantitative solution of Jenny's equation in the form of a topofunction. In pedogenic terms, a topofunction expresses the influence of relief/changes in slope on the orderly formation of hillslope soils - assuming that all other soil-forming factors remain constant.

Although the terms catena and toposequence do not have the same strict meaning, they are often used synonymously (Wysocki *et al.* 2000). Therefore, modifying Jenny's equation, a topofunction can be

expressed as follows (Fanning and Fanning 1989):

$$s = f(r)_{cl, o, p, t}$$

In this equation the variable r (relief) soil-forming factor is identified as being dominant, while the other factors are subscripted because they are considered as unchanging.

Experienced soil surveyors are aware of the importance that topography plays on soils and their properties. Soil surveyors know that field soil properties tend to change in a systematic and often predictable manner down a toposequence. For example, down hillslopes, waterlogging increases, especially in near-surface horizons where texture often becomes finer and soil colours change from reds to yellows to blues and greys (Richardson and Daniels 1993). The soil changes are expressed through changing patterns in the soil matrix, which are often associated with variable patterns in vegetation and land capability. These changing soil-landscape features are indications of Jenny's concepts in action, and may also be exploited as indicators of soil-landscape degradation.

3.2 Morphological indicators of hydropedology

Modifying the land cover of landscapes (e.g. by converting woodland to farmland) changes the patterns of water use efficiency, which in turn alters hydropedological regimes and throughflow pathways that may ultimately contribute to the degradation of soils and land quality. Hydraulic changes such as these in southern Australia often result in localised expressions of seasonal waterlogging, and the formation of salt-affected soils (e.g. saline, sodic, and sulfidic soils) (e.g. Brouwer and Fitzpatrick 2000; 2002a; e.g. Fritsch and Fitzpatrick 1994). The

redistribution of geochemical species caused by altered soil hydrology is also an issue in these landscapes (Cox *et al.* 2002), and the movement and environmental fate of species including Fe, Pb, Zn and S has been documented (e.g. Baker and Fitzpatrick 2003; Skwarnecki *et al.* 2002b).

Shallow NAS is associated with the development of perched saline watertables in locally low lying upland landscape positions, and similarly GAS within saline groundwater seeps and valley bottoms. Such degraded soils can be reliably detected by combining site observations (e.g. subtle landform differences), crop trends (if cropped), soil survey macromorphological observations (e.g. differences in A horizon thickness, soil matrix colour, and depth and type of B horizon mottle patterning) and physicochemical soil analyses. Brouwer and Fitzpatrick (2002b) note the importance of detecting subsurface layers that cause subtle throughflow restrictions (i.e. throttles) in interpreting hydrological processes that lead to soil and landscape degradation. Consequently, the use of field and morphological hydrological indicators mitigates the costly installation piezometers networks, which are conventionally used to detect and monitor soil-landscape degradation (e.g. Brouwer and Fitzpatrick 2002a; Fitzpatrick *et al.* 2003a; Fritsch and Fitzpatrick 1994).

Soil colour has been used as a reliable indicator of hydrological conditions (e.g. Bingham and Ciolkosz 1993; Brouwer and Fitzpatrick 2002a; Conacher and Dalrymple 1977; Richardson and Daniels 1993; Seelig and Richardson 1994), which is strongly related to the Fe-oxide oxidation state in soils (Fanning and Fanning 1989; Gerrard 1992; Schwertmann 1993). Indeed, the Fe-oxides species found in soils serves as an accurate record of the pedogenic

conditions of their formation (Schwertmann and Fitzpatrick 1992). Redder soil colours (10R – 5YR) indicate an abundance of hematite, whereas the more yellow colours (5 – 7.5YR) are consistent with a higher goethite content (Schwertmann 1993). For example, hematite is associated with freely drained and oxidising soil conditions, whereas goethite and lepidocrocite prevail in less free draining and more reducing conditions.

Subtle seasonal changes in redoximorphic soil conditions due to changes in soil moisture are strongly indicated through mottling patterns in soil profiles (e.g. Brouwer and Fitzpatrick 2000; 2002a; 2002b; Fritsch and Fitzpatrick 1994). Indeed, duration of soil waterlogging can be inferred from mottling patterns (Brouwer and Fitzpatrick 2002b). Richardson and Daniels (1993) offer a systematic five-category mottle scheme for B horizons as a guide to field interpretations of the prevailing hydrological conditions in idealised hillslopes.

These landform and soil morphological indicators of hydrologically-based soil degradation processes are reliable to be used as evidence of current or potential land degradation, which can be applied to support land management decisions (Fitzpatrick *et al.* 2003a; Schwenke *et al.* 2003). The practical field guide of Fitzpatrick *et al.* (1997) is one such example of this approach to integrating field and morphological information to support land use planning.

3.3 Mapping soil-landscape properties

Knowledge of the systematic repeatability of toposequences forms the cornerstone of the soil-landscape paradigm, which is described by Hudson (1992), which offers the traditional framework for soil

surveyors to map soils. This paradigm is based on the concept that the combination of a few carefully-positioned soil samples, along with an understanding of soil-landscape processes, can be integrated in the minds of experienced soil surveyors using empirically-based, tacit rules to map soils in any given landscape formed under conventional pedogenic processes (e.g. Bockheim *et al.* 2005; Hoosbeek *et al.* 2000; Hudson 1992; Miller *et al.* 2002). Here, the soil surveyors' tacit rules are the observable, often qualitative relationships between environmental properties and features (e.g. climate, micro-relief, vegetation types, crop responses and parent material from geology maps) and the soil properties in the soil-landscape (McKenzie and Ryan 1999). These rules are typically developed by systematically combining: (i) field observations and descriptions (e.g. Gunn *et al.* 1988; Soil Survey Staff 1993), (ii) soil morphological descriptions (McDonald *et al.* 1998; Schoeneberger *et al.* 2002), and (iii) laboratory physicochemical data (e.g. McKenzie *et al.* 2002; Peverill *et al.* 1999; Rayment and Higginson 1992).

3.4 Digital soil mapping

McBratney *et al.* (2003) contains a seminal review of digital soil mapping philosophies and techniques. These authors distinguish between spatially-based digital predictive methods using: (i) purely geostatistical, neural network and fuzzy logic-based methods, and (ii) methods that fit quantitative relationships between soil properties and environmental/landscape features. With overt reference to Jenny's five soil-forming factors discussed in Section 1.1 above, McBratney *et al.* (2003) describe these as "scorpan" (i.e. *s*: soil property; *c*: climate; *o*: organisms; *r*: topography; *p*: parent material; *a*: age and *n*: space) digital soil mapping models, whereas McKenzie and Austin (1993) describe

these as environmental correlation-based methods. However described, these digital soil mapping methods involve an element of quantification of erstwhile subjective, mentally-based tacit rules that are core to the soil-landscape paradigm in the design of the mapping framework (e.g. Bui *et al.* 1999; de Bruin *et al.* 1999; McKenzie and Ryan 1999).

Recent advances in computing, along with the routine conversion and availability of increasing numbers of environmental datasets to geographic information system (GIS) formats, has made it technically and financially feasible to develop automated approaches to predict soil-landscape properties using environmental covariate-based methods (e.g. Bui and Moran 2001; Lagacherie and Voltz 2000; McBratney *et al.* 2003; McKenzie and Ryan 1999; Sommer *et al.* 2003). Being computer-based, these methods produce quantitative mapped outcomes. Such environmental covariants may include spatially-based GIS datasets of climate (*cl* factor, e.g. rainfall and temperature surfaces), parent material (*p* factor, e.g. geological maps and radiometrics), terrain (*r* factor, e.g. digital elevation models (DEMs)), and vegetation (*o* factor, e.g. remote sensing and aerial photographs).

3.5 Terrain analysis in soil-landscape analysis

A thorough overview of terrain analysis principles and methods is presented in Wilson and Gallant (2000b). Essentially, terrain analysis in pedological studies involves the use of DEMs to generate local topographic attributes, based on terrain shape, to determine landscape properties like:

- near-surface hydrology (e.g. Chaplot *et al.* 2000b; Roberts *et al.* 1997; Summerell *et al.* 2004), and
- predictions of local soil conditions. (e.g. Gessler *et al.* 2000; e.g. Hoosbeek *et al.* 2000; Lagacherie

and Voltz 2000; McKenzie *et al.* 2000; Moore *et al.* 1993; Park *et al.* 2001).

In terms of topographic attributes, primary attributes are computed directly from a DEM, and include properties of altitude, slope, aspect, as well as curvature (plan and profile) (Burrough and McDonnell 2000). Each has significant value in the interpretation of hillslope properties and hydro-pedological processes. For example, slope can be used to assess slope stability and rates of throughflow, aspect, evaporation fluxes, and throughflow pathways.

Secondary (or compound) attributes are computed from primary attributes, or combinations thereof. These include the powerful soil-landscape processes pertaining to topographic attributes like:

- topographic wetness index (TWI) (Wilson and Gallant 2000a); and
- Multi-resolution Valley Bottom Floor (MrVBF) index (Gallant and Dowling 2003; McKenzie *et al.* 2003).

To summarise these secondary topographic attributes, TWI essentially predicts drainage paths and zones of near-surface water concentration in landscapes as a function of up slope contributing area, soil transmissivity and slope gradient (Wilson and Gallant 2000a). The MrVBF algorithm has been designed to stratify hillslopes into regional accumulation zones (i.e. alluvial valley bottom floors) and colluvial zones, recognising significant differences in hydraulic processes of each hillslope system (Gallant and Dowling 2003). Topographic features derived from terrain analysis are regularly used as environmental covariates in digital soil mapping (e.g. Bui *et al.* 1999; Chaplot *et al.* 2000a; de Bruin *et al.* 1999; McBratney *et al.* 2003; McBratney *et al.* 2000; McKenzie *et al.* 2000; McKenzie and

Ryan 1999; Peng *et al.* 2003; e.g. Ventura and Irvine 2000).

3.6 Geophysical survey methods

The following Sections discuss the use of electromagnetic induction (EMI), magnetic susceptibility and gamma-radiometric surveying. These techniques can have a role:

- by determining spatial and vertical (i.e. profile) distributions of soil properties, and
- as direct inputs as environmental covariates in environmental digital soil mapping exercises.

3.6.1 Electromagnetic induction

Portable field geophysical sensors are increasingly being used to characterise and map soil-regolith landscape property patterns, which include salinity, texture, soil layering and groundwater depth. Their key advantages include robustness and ease of operation under field conditions, the ability to rapidly acquire soil data at survey-specific sampling densities, and their non-destructive sampling methods (e.g. Pozdnyakov and Pozdnyakova 2002; Rhoades *et al.* 1999; Tabbagh *et al.* 1997). Commonly used EMI for determining soil-regolith (i.e. < 6 m depth) properties include the EM38 and EM31 of Geonics Ltd. of Canada (McNeill 1980a; 1980b; 1990).

The designs of the EM38 and EM31 incorporate a transmitting and a receiving coil. These are separated along a bar by a fixed distance. In use, the transmitting coil is energised by an alternating current, which injects a time-varying primary magnetic field through the ground. This magnetic field in turn induces a secondary magnetic field through interactions with the bulk of soil components. The receiving coil measures both primary and secondary magnetic fields, the ratio of which bears an approximately

linear relationship to ground conductivity (McNeill 1980a; Sudduth *et al.* 2001). Measurements are made of apparent electrical conductivity (EC_a) in units of mS/m, which can be converted of required to the preferred dS/m units in Australia. The effective depth measurement is governed by the instrument's intercoil spacing, the frequency of the alternating current, and the orientation of coils. For the EM38, the maximum measurement depth is approximately 1.5 m (Sudduth *et al.* 2001), whereas for the EM31 it is approximately 6 m (McNeill 1980b; Williams and Baker 1982), with ~ 50 % of the measured reading derived from the material below 2.75 m in depth in the soil-regolith profile (Rhoades and Corwin 1981).

The EM38 is conventionally operated in one of two modes. In the vertical mode (EC_{av}) the instrument's coils are placed perpendicular to the soil surface and the instrument measures conductivity to the effective maximum depth (Z) of 1.5 m. In this mode the instrument's response dominated by the conductivity at approximately 0.4 m deep, and 75 % of the instrument's response comes from < 1.9 m in depth. In the horizontal mode (EC_{ah}), the instrument's coils are placed parallel to the soil surface and the instrument's response is dominated by soil surface conductivity, and 75 % of the instrument's response is derived from < 0.9 m in depth (McNeill 1990; Rhoades and Corwin 1981).

As discussed above, the EM38 instrument's sensitivity is non-linear with depth in both EC_{ah} and EC_{av} modes, rather, the measurements are depth-weighted as illustrated in Figure 3.1 (McNeill 1990; Rhoades *et al.* 1999). Rhoades *et al.* (1999) also note that the EM38-derived EC_a/EC_{se} relation becomes non-linear when soil EC_{se} values are greater than 2 dS/m.

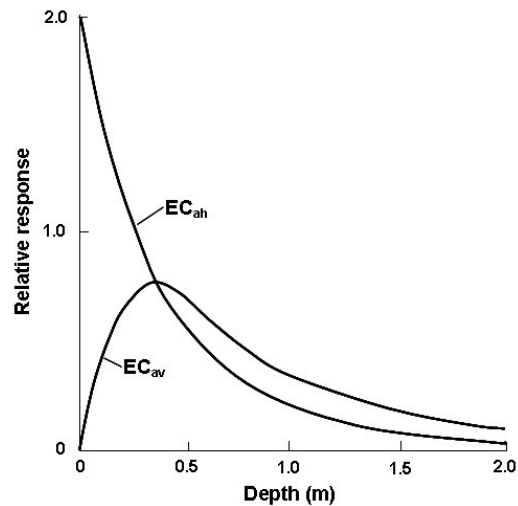


Figure 3.1 Comparison of relative EM38 responses with depth in EC_{ah} and EC_{av} modes (after McNeill 1980b)

The effective width of measurements of the ground volume under the instrument extends to approximately one half of one metre from the sides and ends of the EM38 instrument so that measurements of the ground volume are made within a half-ellipsoid of approximately one by two metres, and to a depth determined by the Z of each measuring mode (Rhoades *et al.* 1999). Therefore, in interpreting the EC_a of the EM38 at a survey point it is necessary to consider that: (i) the measurements taken are the bulked response of the half-ellipsoid volume of soil under the instrument, the volume of which is determined by the Z depth of the measurement mode, that (ii) the bulked responses are depth-weighted, and (iii) caution is required in situations where soil $EC_{se} > 2$ dS/m.

As previously stated, the EC_a ground measurements reflect a bulked EC response of the materials that comprise the soil-regolith profile that is within the EM38 measurement mode's Z depth. Typically, this bulked EC response – or “lumped average” (Acworth 1999) – is dominated by a number of distinct soil properties, comprising: (i) clay content, (ii) clay mineralogy, and strongly related to

this, cation exchange capacity (CEC), (iii) dissolved salts; (iv) moisture content, and (v) temperature (e.g. McNeill 1980b; Pozdnyakov and Pozdnyakova 2002; Sudduth *et al.* 2001).

Electrical conductivity occurs via three alternative pathways within the soil bulk, often occurring simultaneously. The conductivity pathways include:

- liquid soil phase, in which the conductivity is determined by electrolyte type and concentration, pore size and gravimetric soil water content,
- solid soil phase, in which the conductivity is determined by particle mineralogy and particle size, and finally
- alternating conductivity pathways between liquid-solid soil phases (Rhoades *et al.* 1999).

Using an EM31 instrument, Williams and Baker (1982) report that approximately 65 - 70 % of variation of EC_a in saline landscapes is explained by salt content alone.

Clay, salt and water content in soil profiles often correlate in the field. Clay content, and the stratigraphy of clay layers, will have significant influence on upper profile field hydraulics, and the processes involved in salt accumulation. Therefore, EM38-derived EC_a variations influenced by salinity and/or textural differences are useful in interpreting spatial variations in near-surface hydropedological properties and pathways (Slavich and Petterson 1990). EM38 instruments may therefore be used to infer agricultural management zones in landscapes (e.g. Hedley *et al.* 2004).

Portable EMI sensors, usually coupled with global positioning systems (GPS), have been used for assessing and

mapping spatial variability of soil-regolith properties, often at sub-paddock scales¹, which are suitable for supporting land management decisions. Soil-landscape properties mapped in this way include:

- landscape salinity patterns and salt stores (Bennett *et al.* 2000; Broadfoot *et al.* 2002; Corwin *et al.* 2003; Herrero *et al.* 2003; Hopkins and Richardson 1999; McKenzie *et al.* 1997; Nelson and Ham 2000; Williams and Baker 1982);
- topsoil depth and horizonation (e.g. McNeill 1980b; Rhoades *et al.* 1999; Rhoades and Corwin 1981; Sudduth *et al.* 2001; Sudduth *et al.* 1999; Tabbagh *et al.* 1997);
- clay content and soil/agricultural management units (e.g. Earl *et al.* 2003; Hedley *et al.* 2004; Hummel *et al.* 1996; James *et al.* 2003; Taylor *et al.* 2003; Vrindts *et al.* 2003); and
- bedrock topography (e.g. McNeill 1980b).

Researchers have also relied on EC_a coverages as environmental covariates in digital soil mapping exercises (e.g. Greve and Greve 2004; Knotters *et al.* 1996; McBratney *et al.* 2003; McBratney *et al.* 2000; Sommer *et al.* 2003).

The EM38 instrument is operated by allowing the instrument to equilibrate to ambient field temperature, a procedure that takes approximately 10 minutes. During this time, a battery check is made if a new one has not been installed. Next, prior to conducting surveys, the instrument is calibrated for phasing and instrument zero, according to instructions in Geonics Ltd (2003). During the

¹ In Australia, a “paddock” equates to a “field” in many other countries. Australian broadacre paddocks may typically cover 10 – 2,000 ha. Indicatively, “sub-paddock” scale is suitable for managing units within a paddock, perhaps spanning scales of 1: 500 – 1: 5,000.

survey, the operator uses a consistent stance (e.g. kneeling next to the instrument on the ground shown in Figure 3.2) to ensure that any possible interference caused by the operator (negligible if conductive metal objects like coins, buckles and watches have been removed) is negligible. EMI readings are taken after the instrument has been placed firmly on the ground after a very short period of equilibration. Survey sites are chosen away from the cultural electromagnetic interference (e.g. fence lines, buried wires, vehicles, etc.). In the vertical mode (EC_{av}) the instrument is placed vertically on the ground surface, whereas in the horizontal mode (EC_{ah}) the instrument is laid flat on its side on the ground.

An excellent reconnaissance procedure used when walking between survey sites is to sling the instrument using the shoulder strap so that the instrument skims above the ground surface. Through constant observation of the instrument gauge, the technique reveals changing trends in EC_{av} along the walked transect that may highlight soil transitions that are not visible on the ground, which may require subsequent investigation.



Figure 3.2. The Geonics EM38 instrument in use in vertical mode (EC_{av}).

The EM31 instrument is used in survey mode using similar preparation and

survey method as the EM38 instrument (e.g. temperature equilibration to ambient, prescribed calibration method, avoidance of electromagnetic interference). During measurement readings, however, the EM31 instrument is slung above the ground surface (e.g. at knee height), and except for very rare circumstances, the instrument is used horizontal to the ground surface as shown in Figure 3.3. Again, when used in a reconnaissance mode between survey sites, continuous monitoring of the instrument's gauge provides a technique to identify transect trends in EC_a , which may reveal deep profile conductive features for subsequent investigation.



Figure 3.3. EM31 in survey mode (photograph: Rural Solutions SA).

3.6.2 Magnetic susceptibility

The study of soil magnetism is a fast-growing branch of pedological research, and several comprehensive overviews have been published (e.g. Evans and Heller 2003; Mullins 1977; Thompson and Oldfield 1986; Walden *et al.* 1999).

The Bartington loop (MS2D) (Figure 3.4) and probe (MS2F) (Figure 3.5) sensors that are described in Dearing (1999a) are highly portable, field-

based magnetic susceptibility sensors which are commonly used in soil and landscape research. Under field conditions, the MS2D loop provides more of a bulked magnetic susceptibility measurement of the near-surface soil zone due to its larger sensory “footprint” on the ground, whereas the MS2F probe provides more of a spatially precise (i.e. high resolution) near-surface soil zone magnetic susceptibility measurement. Lecoanet *et al.* (1999) compare and contrast the depth and spatial sensory ranges, and their relative sensitivities, of both sensors. Both of these sensors measure volume magnetic susceptibility (κ), which is a magnetic property discussed in the next Section.



Figure 3.4. Bartington MS2D loop in use taking surface measurements.

The field measurement method for the MS2D (loop) (Figure 3.4) and MS2F (probe) (Figure 3.5) sensors is quite similar. Prior to taking the readings with both sensors, the site is scuffed using a boot (or shovel, or other such convenient field tool) to remove loose surface debris (e.g. vegetation and small cobbles) to ensure maximum soil contact for measurements.

The MS2F probe is also suitable for profile readings, which is done in the field by removing augered core

sections or profile face samples, and placing the soil samples in small plastic (i.e. non-magnetic) containers and measuring on flat surfaces of soil aggregates. If however, the structure of the soil sample is blocky and rough, the sample is broken up in the container for maximum contact between the soil sample and probe.

The Bartington MS2B dual frequency sensor (Dearing 1999a) is a laboratory-based instrument that measures mass magnetic susceptibility (χ), a soil magnetic property that is also discussed in the next Section.

Many soil minerals possess diagnostic magnetic properties (Evans and Heller 2003; Mullins 1977; Thompson and Oldfield 1986). The κ property relates to the ratio of amount of magnetisation acquired (M , in A/m units) by a (soil) sample versus the amount of applied magnetising field (H , also in A/m units). The κ is calculated using the following formula:

$$\kappa = M / H$$

Note that κ units are dimensionless because H and M have the same units. The κ of the surface of soils is easily acquired under field conditions using the Bartington ME2F probe (Dearing 1999a; 1999b), making it an ideal instrument for rapid and semi-qualitative, reconnaissance-type field investigations of soils.

The χ property represents the κ property that is normalised by sample bulk density (ρ , in m^3/kg units, giving χ in $\text{m}^3/\text{kg}^{-1}$ units), and is calculated using the following formula:

$$\chi = \kappa / \rho$$



Figure 3.5. Bartington MS2F probe in action. (a) Being used to take measurements from scuffed soil surfaces, and (b) taking measurements of profile samples.

Normalisation by bulk density allows quantitative comparisons to be made between the susceptibilities of soils that have different bulk densities. A Bartington MS2B Dual Frequency system (Dearing 1999a; 1999b) is used to conduct non-destructive measures of χ . Generally these laboratory-based measurements are made on weighed samples that fill purpose-made non-magnetic 10 cm³ pots on the < 2 mm soil fraction. Measurements are made, firstly, in the low frequency mode (χ_{lf} : 0.46 kHz) and then in the high frequency mode (χ_{hf} : 4.6 kHz). Care is taken to align each pot identically to mitigate for χ measurement errors that can be caused by misalignment of the pots. Readings of the Bartington MS2B Dual Frequency system are in $\times 10^{-8}$ SI. Conventionally, of the two frequencies used to measure χ , the χ_{lf} measurement is standard to express the χ property of materials (Dearing 1999b).

The magnetic parameter of percent frequency dependant susceptibility - termed “frequency dependency susceptibility” ($\chi_{fd\%}$) - is derived from routine dual frequency χ measurements using the formula:

$$\chi_{fd\%} = 100 \times ((\chi_{lf} - \chi_{hf}) / \chi_{lf})$$

The $\chi_{fd\%}$ indicates the χ contribution of ultra-fine ($\sim < 0.03 \mu\text{m}$) superparamagnetic ferrimagnetic grains in the sample (Dearing 1999b; Evans and Heller 2003; Oldfield 1991; Thompson and Oldfield 1986). Superparamagnetic behaviour is a property of ultra-fine grains that results in stronger magnetic susceptibility values. This behaviour is caused by the lack of thermodynamic inertia conferred by the small grain size to rapid magnetic alignment in the presence of a field. Thus, a small proportion of superparamagnetic grains in a bulk of soil may have a proportionally large influence on the soil’s magnetic susceptibility (Thompson and Oldfield 1986). The following section discusses the minerals and particle size fractions that are strongly associated with pedogenically formed maghemite.

Importantly, the field-based κ measurements are made on the whole soil texture fraction within the sensitivity range of the sensor. As such, the magnetic response reflects a

bulk texture response, including pedogenetic magnetic gravels, if present. As discussed, the laboratory-based χ measurements are conducted on the < 2 mm soil fraction, in which magnetic gravels have been removed – if originally present. Many southern Australian texture-contrast soils contain significant quantities of magnetic gravels, which often concentrate in the > 2 mm fraction in the A and B horizon interface. They also appear on the surface of Ap horizons, or accumulate colluvially in layers from up slope erosion.

Maghemite (γ Fe_2O_3) is a common soil Fe-oxide that possesses ferrimagnetic properties, which means that it has characteristically high magnetic susceptibilities (Evans and Heller 2003; Thompson and Oldfield 1986). Compositionally, maghemite is identical to hematite (α Fe_2O_3), although they differ in crystal structure (e.g. Schwertmann and Fitzpatrick 1992). This difference in crystalline structure imparts a significantly weaker ferrimagnetic property for hematite compared to maghemite, which can be diagnostic of the two. Magnetite (Fe_3O_4), another Fe-oxide, is less common in soils but has a much higher magnetic susceptibility than maghemite. Maghemite and magnetite, if present, will tend to dominate the bulk magnetic susceptibility of soils. Soil magnetite's origin is often detrital (i.e. in the form of preserved grains released from weathered rock) and is usually present as coarse sand-sized particles (i.e. > 2 mm) (Mullins 1977; Thompson and Oldfield 1986). Maghemite, however, is mainly derived from *in situ* pedogenic conversion of other Fe-oxides via:

- low temperature oxidation;
- firing;
- dehydration of lepidocrocite (γ FeOOH); and/or
- hydromorphic (wetting-drying) redoximorphic processes

(Chadwick and Graham 2000; Mullins 1977).

Firing in the presence of organic matter is probably the most important conversion pathways for the pedogenic creation of maghemite under Australian soil conditions (Taylor and Schwertmann 1974). Pedogenic maghemite is typically in the form of ultra fine-grained ($\sim < 0.03$ μm , Dearing 1999b) superparamagnetic ferrimagnetic grains. Importantly, this means that maghemite tends to dominate the bulk magnetic susceptibility of the finer-than-coarse-sand (< 2 mm) soil fraction. Fine grained hematite (α Fe_2O_3) may also contribute to the magnetic susceptibility in soils.

Interpretation of maghemite and other Fe-oxide patterns, both spatially and down-profile, helps reveal recent and ancient pedogenic conditions (e.g. Taylor and Schwertmann 1974). For example, magnetic methods have been used to demonstrate:

- pedogenic magnetic enhancement/depletion through soil wetting cycle transformations (e.g. Bedard-Haughn and Pennock 2002; de Jong *et al.* 1998; de Jong *et al.* 2000; Evans and Heller 2003; Fine *et al.* 1989; Fontes *et al.* 2000; Grimley and Vepraskas 2000; Williams and Cooper 1990);
- identifying toposequence/catchment scale erosion and deposition processes (e.g. Crockford and Richardson 2004; Crockford and Willett 2001; de Jong *et al.* 1998; Fine *et al.* 1989; Royall 2001);
- forming linkages between soil condition and magnetic biomineralisation (e.g. Mathé and Lévêque 2003); and
- identifying and mapping soil units (e.g. Booth *et al.* 2002; Grimley and Vepraskas 2000; Williams and Cooper 1990).

An additional source of significant environmental magnetic susceptibility activity the soil-landscape is derived from pyrrhotite, particularly in the form Fe_9S_{10} (Evans and Heller 2003; Thompson and Oldfield 1986). According to Evans and Heller (2003), this form of pyrrhotite is created by the firing of soils that are rich in Fe-sulfides at temperatures exceeding 200 °C. Like many Fe-sulfides found in the environment, the occurrence of pedogenic pyrrhotite is associated with the presence of near-surface mineralised zones.

3.6.3 Gamma radiometrics

Gamma-ray spectrometric (often termed “radiometrics”) surveying involves the measurement of radioactive energy in the form of gamma-rays emitted from naturally occurring radioelements found in the landscape (Minty 1997; Wilford 1995). The gamma-rays measured are derived from the decay of potassium (K), thorium (Th) and uranium (U) radioelements. These are measured at diagnostic photo-peaks centred at the following channels: (i) 1.460 MeV (K); (ii) 2.614 MeV (Th); and (iii) 1.765 MeV (U). Another channel (iv) for total count (TC) is measured over the range 0.40 - 2.81 MeV (Minty 1997). Radiometric surveys are conducted from the ground using field portable equipment (e.g. Exploranium GR 320), or using aircraft mounted systems.

Airborne radiometric images are geochemical images of the potassium, thorium and uranium components of the near-surface of landscapes. Due to high level of attenuation of gamma-rays by air, water, soils and geology, approximately 90 % of the measured gamma-rays are derived from the surface 0.3 m (e.g. Dickson and Scott 1997; Minty 1997; e.g. Wilford *et al.* 1997). This means that at locations where rock is exposed the response is dominated by the mineralogy of the geology. However, at locations where overburden exists (i.e. soil-regolith), the gamma-ray response is dominated by parent material mineralogy, although modified to varying degrees by the combined effects of weathering, transportation and pedogenesis (Wilford 1995). For this reason airborne radiometrics have been applied with increasing interest in geomorphological and pedological applications (e.g. Bierwirth 1996; Bierwirth and Walsh 2000; Cook *et al.* 1996; Dickson and Scott 1997; Summerell *et al.* 2000; Taylor *et al.* 2002; Wilford 1995; 2004b; 2004c; Wilford *et al.* 1997; Wilford *et al.* 2001; Wong and Harper 1999).

Table 3.1 on the following page, summarises radiometric elemental abundance, weathering characteristics and pedo-geomorphic expression in landscapes.

Table 3.1. Summary of radiometric elemental abundance, weathering characteristics and pedo-geomorphic expression (multiple sources).

Element	Natural abundance	Weathering characteristics	Pedogeomorphic expression
Potassium (K)	High (approximately 2 % of total elemental occurrence)	Geochemically mobile; soluble under most conditions whereby it is lost in solution (leached) and/or adsorbed to clay minerals	Clay minerals, e.g. illite and montmorillonite. Relatively low concentrations at weathered sites due to depletion. Shallow soils mantled on fresh bedrock rich in K show elevated concentrations.
Thorium (Th)	Low (8.7 ppm)	Geochemically immobile under most weathering conditions	Associated with resistate minerals, hence tends to be concentrated in residual profiles. Adsorbed to Fe-oxides and enrichment associated with deeply weathered profiles.
Uranium (U)	Low (2.7 ppm)	Readily leached and released from soluble minerals under oxidising conditions; precipitates in reducing conditions; groundwater a possible source of enrichment	In surface conditions, may be associated with resistate minerals (e.g. zircon and monazite). As with Th, adsorbed to Fe-oxides. Enrichment associated with deeply weathered profiles.

Chapter 4. Research methodology and rationale

This Chapter broadly defines the research approach of this investigation. It covers a complex set of issues related to the philosophy behind the multiscale approaches adopted in the research. In this the term “pedological complexity”, which was the basis for the selection of the two study area, is explained. The concept of “spatial variability” as it applies to soils is also covered, and explanation is given why the spatial variability of soils is scale-dependant, and has different expression at different “soil system” scales. The concept of the self-organising systems is introduced, as is the way these relate to a “hierarchy of scale levels” comprising “i- levels”, each of which possess their own characteristic set of property patterns. The concept of “upscaling” is presented. Upscaling involves bridging the hierarchy of scale levels to make quantitative predictions of soil properties at higher hierarchical levels from soil data/knowledge from subordinate levels (i.e. finer scale data/knowledge). This Chapter discusses how a framework of hydropedology can be used to conceptually bridge between the different scale levels during upscaling. This is because hydropedology is the sub-discipline that researches soil water flows (i.e. freshwater throughflow and ground flow), and soil water dominates the soil system inter-scale links (e.g. moisture regimes) and soil system intra-scale links (i.e. freshwater throughflows), especially in hillslopes. Many of the hydropedologically-related soil properties can be conveniently predicted via pedotransfer functions, which are presented. “Conceptual toposequence models” are discussed. As will be described, these models (which equate to medium scale soil systems) form the hydropedologically-based linkages between (i) the lower level, fine scale soil systems (e.g. soil profiles) and (ii) the and higher level, coarser scale soil systems (e.g. hillslopes and regions). As such, the construction of these models forms an important precursor in the development of upscaling frameworks designed to predict regional soil conditions.

The concept of precision conservation is introduced, which represents a methodological framework for linking soil-landscape investigation methods (Chapter 3) with the soil-landscape modelling and predictive approaches, which are described in this Chapter. The Chapter concludes with: (i) a brief introduction of the study areas selected (detailed descriptions are given in later Chapters), (ii) an overview of

the selection rationale, and finally, (ii) philosophically-based outlines for the methodologies applied.

4.1 Pedological complexity

The term “pedological complexity” as used here is a relative term to compare patterns of soil properties at comparable scales. The term encompasses degrees of inherent: (i) spatial heterogeneity, and (ii) temporal changes of soil properties of a landscape. These properties coalesce to form zones that are spatially distinct, which, characteristically, possess similar physicochemical and temporal change patterns. Invariably, the distinct soil zones form under common soil forming conditions (e.g. slope and parent material), as discussed in Chapter 3. Typically, the soil zones may extend over a range of a few metres to hundreds of metres, and coalesce into a mosaic that extends over the whole landscape in an identifiable, characteristic and regular pattern. Landscapes that contain a high degree of so-called pedological complexity constitute “complex landscapes”.

4.2 Soil system scale

That soils have variable properties that change in often repeatable and scale-dependant patterns has been observed and documented by many researchers (e.g. Gerrard 1992; Hoosbeek *et al.* 2000; Lin 2003; Wysocki *et al.* 2000). The environmental causes for soil variability, i.e. the role of Jenny’s (1941) soil forming factors, have been previously outlined in Chapter 3. However, it is important to emphasise that soil variability occurs in four dimensions, i.e.:

- vertically, with depth through the soil profile (z),
- spatially, in geographic space (x and y), and
- temporally (time), over time.

Soil variability is scale dependant. Scale dependency means that soil patterns have qualities and properties that resonate at, and are intrinsic to, specific scale levels. The continuum of scale levels may range from microscopic to megascopic (Hoosbeek *et al.* 2000). Hoosbeek and Bryant (1992) developed the so-called “*i*-level diagram” of the hierarchy of scale levels that has been widely accepted as a working framework for research in soil modelling (e.g. de Vries *et al.* 1998; Hoosbeek *et al.* 2000; Lin 2003; e.g. McBratney 1998). The hierarchical framework can equally be applied to ordering soil systems in soil mapping exercises. The concept of “soil systems” is introduced below. Some authors have taken Hoosbeek and Bryant’s (1992) template and have modified it by adding higher (e.g. continental) and lower (e.g. mixtures) level soil systems (e.g. Addiscott 1998; Lin 2003; McBratney 1998; McKenzie and Cresswell 2002). In summary, the so-called *i*-level diagram shown in Figure 4.1 identifies:

- scale (organisational) hierarchy (i.e. *i*-level),
- degree of inherent soil complexity translated to model complexity (i.e. qualitative versus quantitative) for the *i*-levels, and
- the degree of computing effort required (i.e. mechanistic versus empirical) for the *i*-levels (Hoosbeek *et al.* 2000).

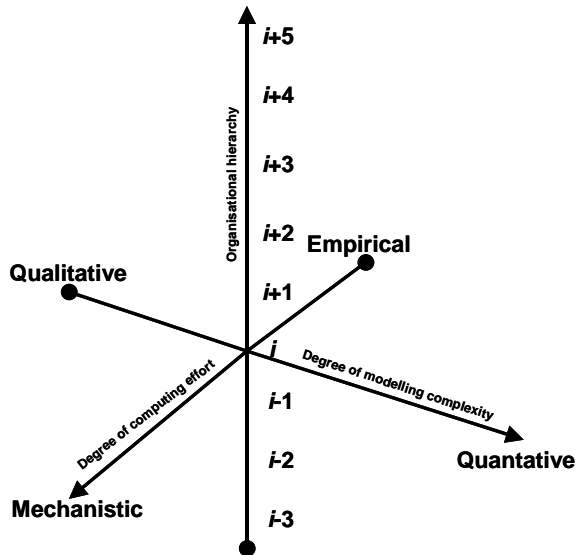


Figure 4.1. *i*-level model characteristics based on three characteristics (adapted from: Hoosbeek *et al.* 2000; Hoosbeek and Bryant 1992).

The framework infers that scale levels have physical dimensions (i.e. the extent of a study area or model), which are implicitly associated with temporal scales (McBratney 1998). For example, lower *i*-levels (e.g. < level *i*) are characterised by smaller aerial extents, in which processes and reactions occur over short distances and generally rapid rates, e.g. the speed and distance that salts might move through a profile on the wetting front. Conversely, higher *i*-levels (e.g. > *i*+2 level) are associated with larger aerial extents and more sluggish landscape-scale processes, e.g. the rate and distance of soil water throughflow and landscape-forming geomorphic and weathering rates.

Hierarchy levels have physical dimensions that are easy to visualise, which helps in defining so-called soil systems (Hoosbeek *et al.* 2000). Each *i*-level can be considered as a single system, each with its own characteristic terminology, and has the capacity to integrate soil subsystems from lower levels in the hierarchy, or combine with others to form higher level soil systems (Hoosbeek and Bryant 1992).

As discussed previously, soil variability is scale dependant. The intrinsic soil system pattern of each hierarchical level reflects the unique distribution, role and relative importance of environmental and landscape properties that govern the soil formation. Soil systems show hierarchical complexity and are recognised as being self-organised (Phillips *et al.* 1999). They are self-organised because their formation is governed by a discrete subset of soil forming factors within the aerial extent of a soil system. However, each soil forming process influences soil variability differently at each hierarchical level. For example, with reference to Table 4.1, climatic factors overwhelmingly influence soil variability over thousands of kilometres at global and continental scale levels (i.e. > level *i*+5), whereas the impact of climate on soil variability is relatively minor at more local scale levels (e.g. over a few metres, i.e. < level *i*+2).

4.3 Soil modelling support

Soil system mapping and soil modelling requires the support of soil survey and laboratory data at so-called “support sizes” (Burrough and McDonnell 2000) that can successfully account for - or “resolve” - the inherent variabilities within the soil systems being investigated (Hoosbeek and Bryant 1992). According to McBratney (1998), in quantitative soil modelling the term “grain size” refers to the physical ground dimension (resolution) of the support size, and the term “extent” refers the ground areal coverage of soil system under investigation. Investigations of soil systems and their processes need to take place at the appropriate scales. For the purposes of the current research, Table 4.1 indicates the investigation scale appropriate for each soil system *i*-level.

Table 4.1. Organisational hierarchy of soil systems with appropriate scales of investigation (adapted from Hoosbeek and Bryant 1992; McKenzie and Cresswell 2002).

Level	Soil system	Examples of types of modelling	Scale of investigation
i+5	World	Global phenomena (e.g. CO ₂ studies)	Course
i+4	Continent	Aeolian dust depositional processes	
i+3	Catchment/ Region	Soil-landscape modelling (e.g. catchment area budget studies)	
i+2	Catena/ toposequence	Erosion studies (e.g. particulate transport); Salinity modelling (e.g. solute transport)	Medium
i+1	Polypedon	Pedological modelling as part of a dynamic ecosystem (e.g. seasonal changes)	Fine
i	Pedon	Dynamics of genetic processes (e.g. mass flow models; eluviation → illuviation)	
i-1	Horizon	Dynamics of horizonation (e.g. mineral stability and weathering; organic matter accumulation)	
i-2	Peds, aggregates	Macromorphological studies (e.g. formation or degradation of cutans; aggregate stability)	Ultra-fine
i-3	Molecular interaction	Ion exchange phenomena; complexation of metal ions by organic matter	Ultra-fine

4.4 Linking multiscale investigations

The challenge of transferring fine scale (i.e. fine grained) soil data and observations, via intermediate scales, to achieve regional scale predictions has been discussed (e.g. Lin 2003). This procedure is called upscaling (McBratney 1998), and requires a system to bridge the hierarchical levels in making the scale linkages. Understanding the movement of water through soils and landscapes offers the conceptual framework to make these linkages because water movement is the common thread that influences the majority of processes that occur within soil systems and catchments (Conacher 2002), especially those in the range of level $i-1$ (horizon level) to $i+2$ (catena/toposequence level) (Table 4.2). Hydropedology is the sub-discipline that researches the near-

surface movement of water, particularly through soils, and makes the connections between: (i) pedology, (ii) soil physics, and (iii) hydrology (Lin 2003).

4.5 Pedotransfer functions

Lin (2003) emphasises that an important component of hydropedology is the development and application of pedotransfer functions (PTFs). PTFs are essentially indirect measures of soil properties, often hydraulic, via more readily available (and less costly) soil data from soil survey investigations (e.g. Bouma 1989; Hoosbeek *et al.* 2000; McKenzie and Cresswell 2002). These relationships can be based on either: (i) empirical, (ii) regression or (iii) functional relationships between the measured soil properties and the inferred soil hydraulic characteristic

under estimation (Lin *et al.* 1999). Examples of PTFs include using soil colour to infer drainage conditions and waterlogging intervals along toposequences (e.g. Richardson and Daniels 1993), the use of particle size distribution to infer hydraulic conductivity (e.g. Chaudhari and Batta 2003) and moisture retention (e.g. Cornelis *et al.* 2001), the determination of bulk density (Kaur *et al.* 2002), and soil layer morphology to infer hydraulic conditions and preferential throughflow pathways (e.g. Brouwer and Fitzpatrick 2002a; Fitzpatrick *et al.* 2003a; Fritsch and Fitzpatrick 1994; Lin *et al.* 1999).

4.6 Conceptual toposequence models

Conceptual toposequence models enable soil-landscape researchers to develop, refine and present mechanistic understanding of vertical (i.e. down profile) and lateral (i.e. down slope) linkages between hillslope soil-regolith, geology and hydrology using a systematic structural approach (Fritsch and Fitzpatrick 1994). Firstly, the models identify and describe, by depth interval, all similar soil-regolith features. Such features include layers that share consistent properties (e.g. colour, texture and structural patterns, physico-chemistry and mineralogy), and separate A horizon matrices (e.g. loamy layers) from B horizon matrices (e.g. clay layers) from C horizon matrices (e.g. silty saprolite). Secondly, similar soil-regolith features are arranged into fewer domains (according to concordant relationships, e.g. mottling patterns), or separated into new domains (according to discordant relationships). In this way, for example, grey/greenish-blue, leached hydromorphic domains are separated from red lateritic domains in the hillslope. Boundaries are drawn to define the various domains juxtaposed in the toposequence, which then may be graphically presented in cross-

section in the conceptual toposequence model.

Each soil-regolith feature displayed are linked to soil-regolith and/or hydrological processes (e.g. water flow paths, salinisation and sodification). The processes links are made either tacitly (i.e. through the interpretive skills of the model user) or actually (e.g. through arrows in the affected regions of the graphic model). Soil-regolith colour (together with other morphological, chemical and mineralogical indicators) and geology are relied on strongly to construct down slope linkages that describe water flow paths (e.g. describing the development of salinity). Such soil-regolith information reveal ancient soil-landscape processes (e.g. hydromorphic and lateritic domains), whereas physicochemical (e.g. EC_{se}, ESP, pH) and hydraulic (e.g. piezometric, mottling patterns and other PTFs) data and field observations (e.g. the emergence of recent scalds, changing patterns in plant species) reveal contemporary and degrading processes. Some field indicators of these processes are obvious (e.g. occurrences of salt crusting soil surfaces), whereas some are more subtle (e.g. subsoil mottling patterns).

Three categories of conceptual toposequence models have been described (Fitzpatrick and Merry 2002; Fitzpatrick and Skwarnecki 2003), which include:

Descriptive models, which, as described above and shown in Figure 4.2, systematically incorporate information of hillslope pedogenesis from both past (e.g. soil colour, layer morphology) and contemporary processes (e.g. salinisation, present water flows). Descriptive models are appropriate for developing and communicating farm-scale management solutions to landscape degradation processes.

Explanatory models, which, taking the descriptive models as the starting point, incorporate mechanistic understanding of specific degradation processes to explain the detail of the major processes at play in typical landscapes, e.g. the landscape development of saline-sulfidic conditions, and resulting formation of various acid sulfate soil (ASS) conditions shown in Figure 4.3. In this case, such detail is generally directed towards the hillslope distribution of applied hydrological conditions (i.e. redox conditions, partitioned to aerobic and anaerobic soil environments) and geochemical environments (e.g. the development of secondary sulfides and associated Fe-oxides).

Predictive models, which like the model shown in Figure 4.4 details the mechanistic processes presented in explanatory models in a temporally predictive way (also known as “4D” models). Taking the acid sulfate soil conceptual model discussed above, the predictive model counterpart illustrates the profile changes in one profile position over time as sulfidic material (i.e. potential acid sulfate soils, or PASS) transform to form sulfuric conditions (i.e. actual acid sulfate soils – or ASS). Staged over time, the model predictively and graphically displays the biogeochemical (i.e. changing mineralogy, redox and pH conditions) and hydraulic changes in the soil profile, and the resultant land cover changes, to finally graphically display the soil profile conditions of a remnant ASS soil, including scalding.

Importantly, conceptual toposequence models are not quantitative mathematical models *per se*. However, the models may be used as a precursor to the development of deterministic models (Fritsch and Fitzpatrick 1994). Conceptual toposequence models are graphic, cross-sectional representations of the soil-regolith-bedrock profile continuum along the

length of a hillslope. These models illustrate the vertical and lateral changes that occur down the toposequence, with an emphasis on highlighting pedohydrological, physicochemical and biogeochemical processes (Fitzpatrick and Merry 2002). These models are a powerful aid for illustrating the “interconnectedness” of soil water-flow systems (e.g. hydromorphic subsoil systems, freely drained red soil systems) and soil processes (e.g. eluviation/illuviation, saprolisation, and salinisation/solonization). Combined, soil water-flow systems and soil processes are described as macromorphological features (Fritsch and Fitzpatrick 1994).

Conceptual toposequence models serve the key functions of:

- providing a framework for soil-landscape researchers to forge the conceptual links between a hillslope series of detailed (fine grained) observations (e.g. soil survey and laboratory data, equating to levels $i-1$ (soil horizon) and i (pedon)). The framework supports understanding of functions and processes of the more extensive soil systems, i.e. equating to levels $i+1$ (polypedon) and $i+2$ (toposequence),
- giving a conceptual framework to guide the development of upscaling predictive methodologies,
- serving as a graphic form (cartoon) to illustrate and communicate often highly complex soil-landscape information and knowledge to other researchers and the broader community, e.g. land management options (Fitzpatrick *et al.* 2003a).

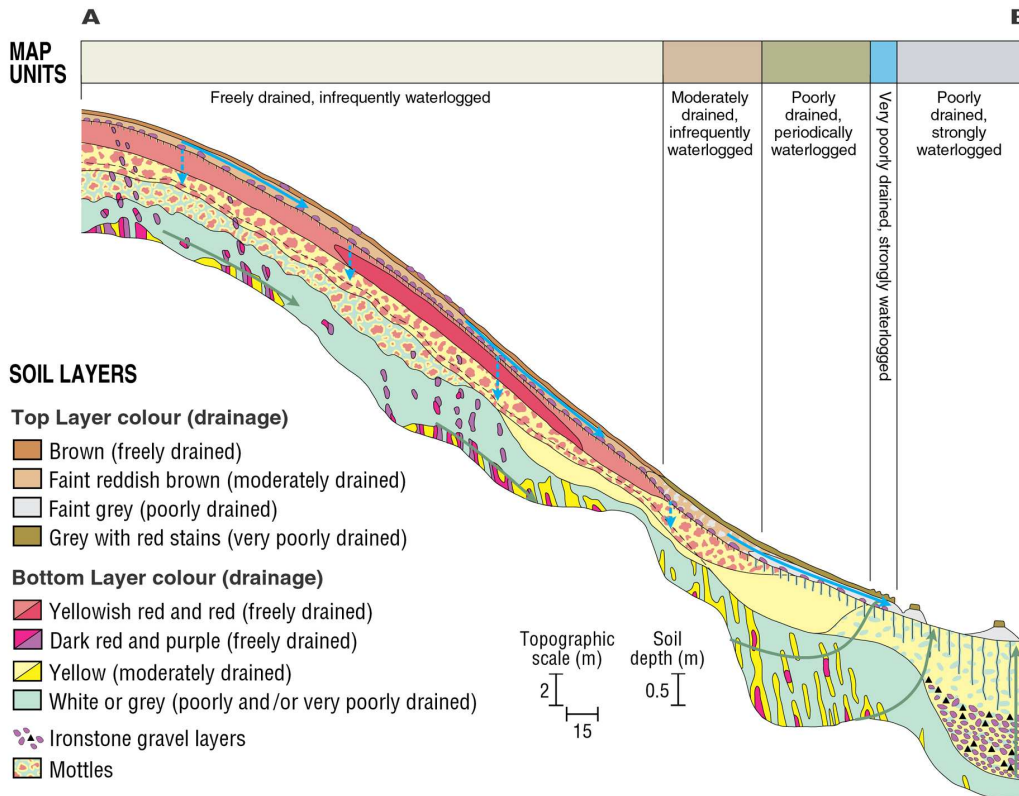


Figure 4.2. A descriptive conceptual toposequence model of a lateritic-hydromorphic hillslope in the Mount Lofty Ranges (MLR) in South Australia (after Fritsch and Fitzpatrick 1994).

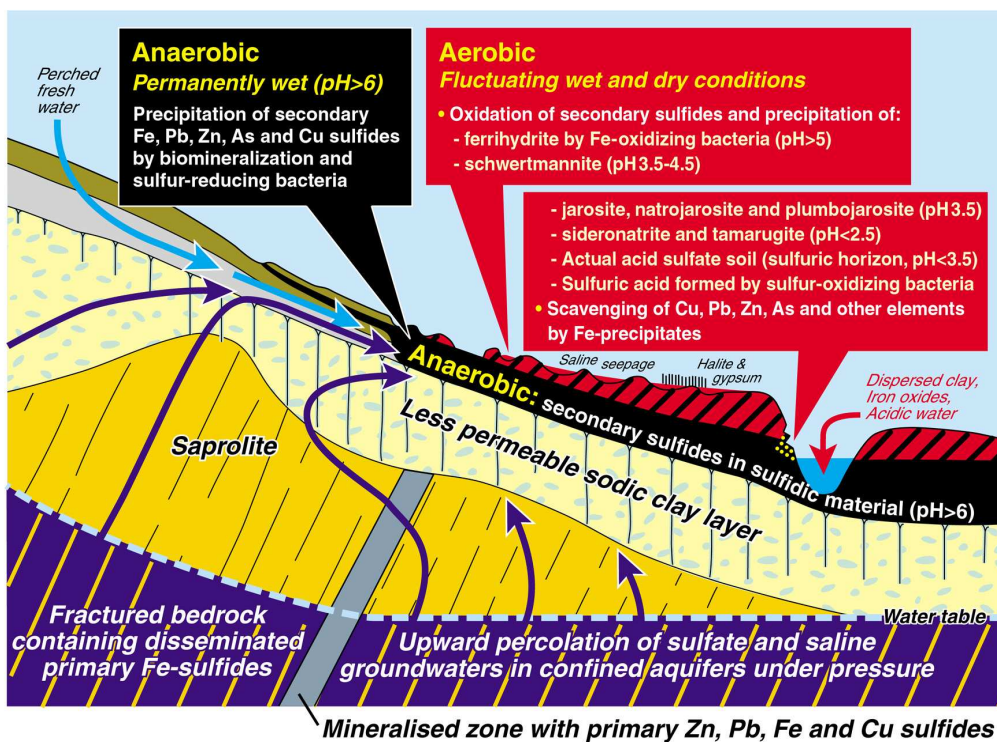


Figure 4.3. An explanatory conceptual toposequence model showing biogeochemical and hydraulic condition conditions in a saline-sulfidic environment (after Fitzpatrick *et al.* 1996).

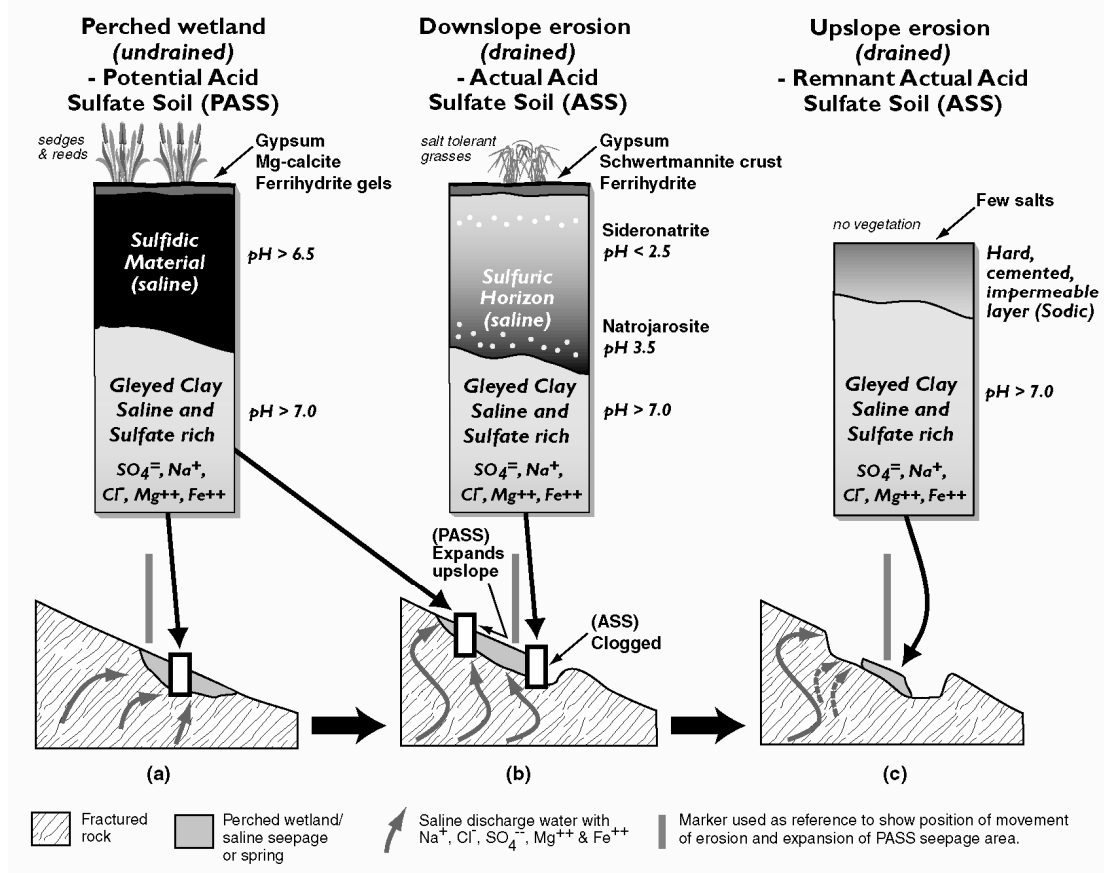


Figure 4.4. A predictive (i.e. “4D”) conceptual toposequence model showing biogeochemical and physical changes in a profile over time as conditions change from sulfidic material (i.e. potential acid sulfate soil - PASS) to sulfuric material (i.e. actual acid sulfate soil - ASS) due to increased drainage caused by erosion (after Fitzpatrick and Merry 2002).

4.6.1 Multiscale predictions via conceptual toposequence models

As discussed in the previous Section, toposequence models provide a powerful framework for researchers to make conceptual links between fine grained soil survey and laboratory data, and the soil-water processes at polypedon ($i+1$) and toposequence ($i+2$) levels. They also offer a conceptual framework to guide the development of predictive upscaling methodologies.

Conceptual toposequence models, which are most relevant and applicable to the polypedon and toposequence soil systems (i.e. levels $i+1$ and $i+2$),

provide the bridging link between the fine grained soil horizon and pedon soil systems (i.e. levels $i-1$ and i), and the catchment and watershed soil systems (i.e. levels $i+3$ and $i+4$, respectively). In essence, the conceptual toposequence model is strongly associated with “hydropedological principles” and serve as the “bridging layer” between the information gleaned from conventional soil survey methods (e.g. Gunn *et al.* 1988; McDonald *et al.* 1998; Schoeneberger *et al.* 2002; Soil Survey Staff 1993), PTFs (e.g. McKenzie and Cresswell 2002), and the catchments/regions requiring strategies to predict soil degradation processes.

A method was successfully developed to upscale several soil attributes such

as drainage/waterlogging, salinity and acidity/alkalinity in a 80 km² area in the Mount Lofty Ranges in South Australia (Davies *et al.* 2002; Fitzpatrick *et al.* 1999; Merry *et al.* 2002). This methodology used field pedology and multiple scale hydrology, vegetation, topography and remotely sensed data to act as checks and for refinement tools. Recognition of soil process patterns at toposequence scale (i.e. a hillslope of 400 m within a 0.2 km² key area) followed by controlled extrapolation of these patterns to catchments (2 km²) and the region (80 km²) is the approach adopted by these workers. The stages of the methodology are summarised in Table 4.2.

To summarise, toposequence models incorporate the catenary concept. In so doing, they emphasise the role of the drainage and mass wasting

topofunctions to serve as important tools in identification and understanding of pedogenic processes and soil degradation. Importantly, in interpreting and graphically representing these models, the location and characterisation of soil macromorphological features and functional groups is made. The function and location (i.e. spatially and down-profile) of many of these features are determined by the location of soil layers, which is based on soil textural, structure and/or colour differences. The presence and location of these layers is especially important in determining hydromorphic domains that are critical to the saline-sodic salt cycles in salt-affected soils and in determining and characterising the redoximorphic conditions, which strongly control the formation of Fe-oxide minerals in specific soil layers.

Table 4.2. Stages of upscaling methodology.

Stage	Task description
1	Conduct point sampling (soil pits, auger samples, geophysical measurements, etc., equating to levels i-1 and i) along reference toposequences, which are representative of the landscape (i.e. in landscapes with similar geological and climatic characteristics) to describe soil profiles and hydrological processes. Hydropedological processes are inferred and domains determined from macromorphological measurements/determinations using the data collected (i.e. via suitable PTFs). Individual site and profile descriptions are made using standard soil survey methods (e.g. Gunn <i>et al.</i> 1988; McDonald <i>et al.</i> 1998; Schoeneberger <i>et al.</i> 2002; Soil Survey Staff 1993).
2	Toposequence models are conceptualised and drafted based on the knowledge of soil macromorphological/functional groups identified through the field sampling and laboratory analyses (Brouwer and Fitzpatrick 2000; Fitzpatrick 2005; Fitzpatrick <i>et al.</i> 1994; Fitzpatrick <i>et al.</i> 2003a; Fritsch and Fitzpatrick 1994).
3	Finally, soil-regolith models are developed through extrapolating the knowledge gained from the toposequence modelling to predict soil properties and associations at landscape/regional scales for land systems in similar geological and climatic zones. This is performed in association with ancillary spatial datasets (e.g. digital elevation models, remote sensing, available soil mapping, geophysical data) using geographic information system-based spatial techniques (Davies <i>et al.</i> 2002).

4.7 Precision conservation

With reference to the discussions in Chapter 3 (principally Sections 3.4, 3.5, and 3.6), next generation, enhanced soil survey (ESS) methods have been developed to supply soil-landscape researchers with soil data of high accuracy, reliability and thematic content, rapidly and relatively low costs compared to conventional soil survey. Typically, these methods combine:

- soil-landscape data collection methods, including soil description, terrain analysis, geophysical survey methods, remote sensing, *in situ* soil-regolith logging and reporting devices;
- laboratory physicochemical analyses;
- field data collection and positioning (e.g. GPS/field logging devices); and
- GIS-based geostatistical interpolation/modelling (e.g. kriging).

ESS products (i.e. typically GIS coverages of soil-landscape attributes) combine with GIS predictive approaches (e.g. deterministic, knowledge-based decision trees) to create digital soil mapping (DSM) frameworks. DSM offers the prospect of soil mapping products that are more reliable, rapid and cost-effective than via conventional, non-computerised soil mapping methods.

Through analysing spatial relationships in mapped products, methods have been developed to apply ESS methods to link (soil) systems from a site specific location to a field, to a set of fields (e.g. farm or catchment), and then to regions to reduce the impacts of environmental degradation in soil-landscapes. Such an approach has been termed “precision conservation” (Berry *et al.* 2005). Precision conservation shares similarities with “precision agriculture” (e.g. Bramley and

Hamilton 2004), which applies similar approaches to increase crop yields. Key to the implementation of precision conservation-type approaches are the development of the understanding of “the interconnectedness of cycles and flows of energy, material, chemicals and water to reduce environmental impacts, off-site transport, and water pollution” (Berry *et al.* 2005). As such, it is evident that precision conservation encompass soil-landscape process and investigation methods described in Chapter 3 with the hydrogeological modelling (e.g. conceptual toposequence models) approaches and predictive (e.g. upscaling) methods described in Chapter 4.

4.8 Study area selections

Two study areas in South Australia were selected for the current research. The first is the Midnorth study area, and the second is the Mount Lofty Ranges (MLR) study area. Their locations are shown in Figure 4.5. Both study areas are described in detail, with the Midnorth study area in Chapter 5 and the MLR study area in Chapter 9.

In addition to occupying upland dryland farming areas, the study areas have in common: (i) texture-contrast soils, especially in mid slope zones, and (ii) a high degree of pedological complexity, which has been described previously in Section 4.1. Furthermore, each study area has been subject to recent (i.e. 2002) airborne geophysical survey campaigns, comprising regional airborne electromagnetic induction (AEM), aeromagnetism and airborne gamma-radiometrics acquisitions. These have been collected under the auspices of the National Action Plan for Salinity and Water Quality, and described in Munday *et al.* (2003). The valuable geophysical datasets have been released for research purposes. The gamma-radiometric and aeromagnetic coverages are selectively applied in the current research at the

regional scale, contributing to the feasibility of bridging the hierarchy of soil system scales discussed previously.

The main causes of the pedological complexity found in the Midnorth study area lie in the combination of the following hillslope conditions and

properties: (i) variable parent material, comprising a down slope sequence of interbedded rock types, and (ii) differences - often subtle - in localised topography and landform, and (iii) paleodrainage systems (e.g. Cresswell and Herczeg 2004).

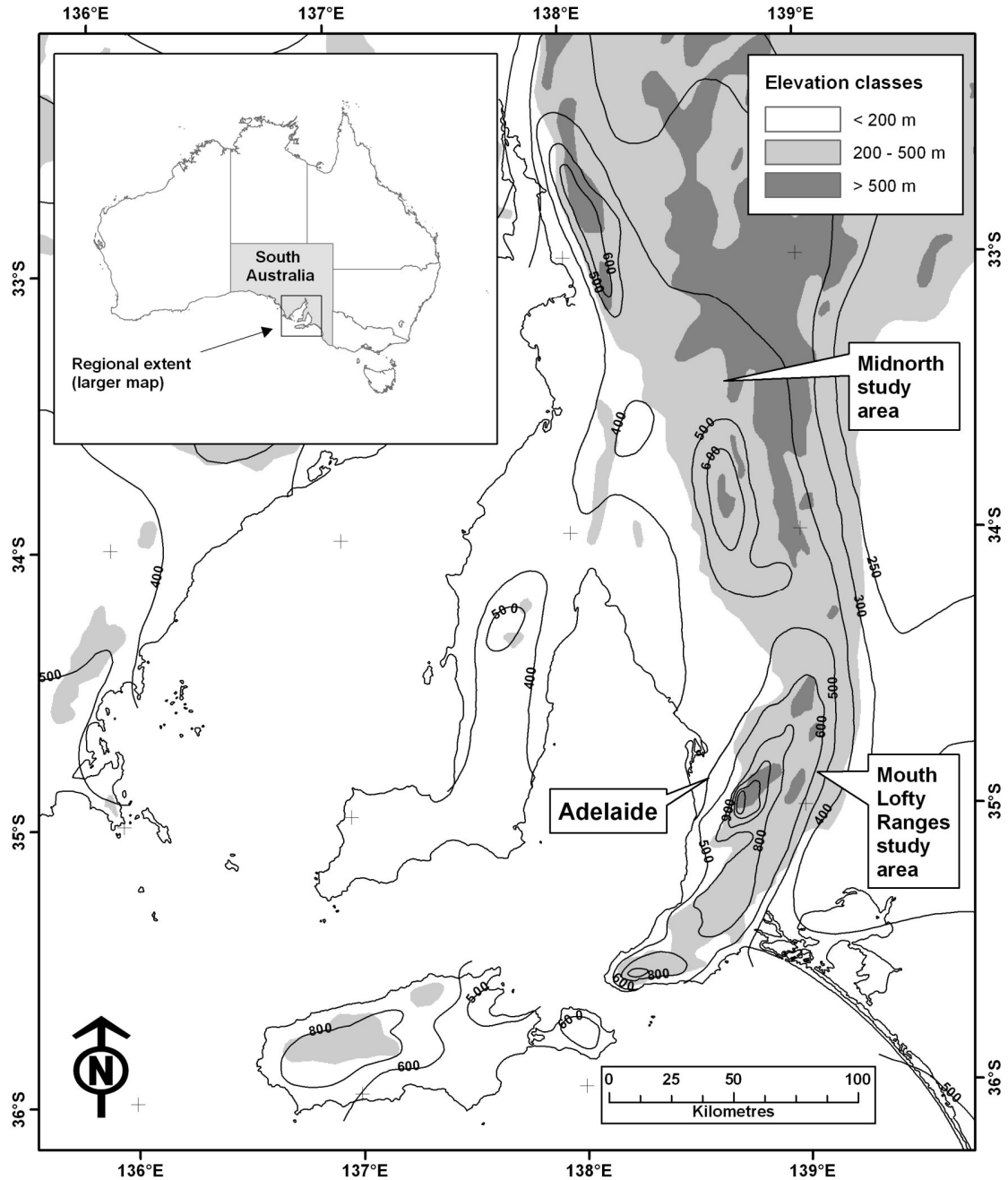


Figure 4.5. National (inset box) and regional map showing the locations of the Midnorth and Mount Lofty Ranges study areas, elevation classes and rainfall isohyets.

In the case of the MLR study area, however, the pedological complexity is in the main a consequence of the combination of the following hillslope conditions and properties: (i) strong topographic and landform variability, (ii) variable aspect orientations, hence variable soil moisture regimes, (iii) strong variations in weathering histories, including contemporary and ancient (Tertiary), (iv) geochemically varied parent material, and (v) differences in agricultural management practices, including areas of remnant vegetation, and cultivated and pasture paddocks.

The current research program builds on the legacies of a number of key research projects that were precursors to the current research program conducted in the Midnorth and MLR study areas. These precursor projects and the research rationale for the current research program are outlined below.

4.8.1 Midnorth study

Two key projects have provided important legacies on which the current Midnorth study area research has built upon. The first of these projects was conducted in 1988 (Fitzpatrick *et al.* in prep.). This project involved a detailed soil investigation to determine the causes of patchy yield problems in the study area, thought to be a root disease issue. The key legacies of this project were: (i) detailed field survey and morphological descriptions, and a large volume of physicochemical data, which were combined to create a (draft) soil series map extending to beyond the Midnorth study area. The second legacy project (in which the author participated) is described in Fitzpatrick *et al.* (2003c). That project featured a qualitatively-based investigation of combined terrain and geophysical survey methods (i.e. electromagnetic induction (EM31, EM38) and volume magnetic susceptibility) to resolve soil-

landscape patterns associated with the formation of shallow NAS and GAS. Key outputs of that project included: (i) refinement of the previously produced soil series map to create a new landscape soil unit (LSU) map, (ii) the interpretation of toposequence-based soil-landscape patterns implicated in the formation of shallow NAS, and (iii) the construction of a conceptual toposequence model for the Midnorth study area hillslope highlighting soil-water and morphological relationships resulting in the formation of shallow NAS and GAS in the landscape. Fitzpatrick *et al.* (2003c) concluded that to confirm the interpretations of saline forming processes, more quantitative work would be required, e.g. via geomorphologic mineralogical and geochemical characterisation. Further work should involve exploiting the regional perspective offered by linking the ground-based data with available airborne geophysics and other regional scale data sets (soil mapping, terrain and geology) to extrapolate the established patterns of shallow NAS in the study area.

The current Midnorth study area research program applies multiscale techniques to address the two concluding remarks presented above. These investigations are described in detail in Chapters 6, 7 and 8, and have been conveniently characterised according to soil system investigation scale (see Table 4.1). Chapter 6 describes fine scale, polypedon-based investigations in selected 100 m² plots. Chapter 7 follows on from Chapter 6 and describes a medium scale toposequence-based investigation of the study area hillslope, including a discussion on the construction of a conceptual toposequence model. Chapter 8 describes the integration of the mechanistic knowledge gained through Chapters 6 and 7, and legacy and newly acquired data to develop a regional upscaling methodology (i.e. coarse scale of investigation) to regionally predict the spatial

distribution of shallow NAS in hillslopes locally surrounding Midnorth study area.

4.8.2 Mount Lofty Ranges study

The current MLR research program also builds on a legacy of earlier research in the study area. Fritsch and Fitzpatrick (1994) describe soil-water flow systems and soil-forming/soil-change processes using hillslope-based field survey and morphological descriptions, piezometric, mineralogical and physicochemical data. These data were combined to: (i) construct a conceptual toposequence model and (ii) create a topsoil and subsoil feature maps within a key area of the MLR study area. Fitzpatrick *et al.* (1996) builds on the earlier research and refines understanding of saline-sulfidic degradation processes in lower landscape seepage zones of the study area using detailed pedological, mineralogical, hydrological and physicochemical investigations. The research created: (i) a second conceptual toposequence model for a second key area confined to the lower landscape (i.e. lower terraces to the wetland), (ii) new soil feature maps for both key areas (i.e. from Fritsch and Fitzpatrick 1994), and (iii) the development of a conceptual mechanistic model to simulate saline-sulfidic degradation processes identified in the conceptual toposequence model.

Several studies (e.g. Davies *et al.* 2002; Fitzpatrick *et al.* 1999; Merry *et al.* 2002) extended the key area soil mapping to create a 1:5,000 scale soil unit map (with soil unit descriptions) for the remaining MLR study area using conventional soil mapping methodology, and served as a

precursor to an upscaling methodology to predict regional patterns of waterlogging /drainage, and salinity and acidity due to de-nitrification.

Based on the outcomes of these previous studies that were conducted in the MLR study area, the current research addresses two key objectives related to pedological complexity. These objectives include, firstly, through the use of more refined survey methods (i.e. ESS) than previously used, improve existing 1:5,000 scale soil mapping of the study area by refining soil unit boundaries and unit descriptions. Secondly, based on the interpretation of hydropedological patterns, to develop a regional upscaling methodology to predict the occurrence of shallow NAS- and GAS-prone landscape zones.

The current MLR investigations are described in detail in Chapters 10, 11 and 12, and have been conveniently characterised according to soil system investigation scale described in Section 4.2. Chapter 10 describes fine scale, multi-temporal investigations at selected profiles to investigate the seasonal dynamics attributed to salt movements in the near-surface profile. Chapter 11 follows on from Chapter 12 and describes a multi-temporal medium scale toposequence-based investigation of the study area near-surface solute hillslope. Chapter 12 describes the integration of the mechanistic knowledge gained through Chapters 10 and 11, and legacy and newly acquired data to develop a regional upscaling methodology (i.e. coarse scale of investigation) to regionally predict the spatial distribution of shallow NAS and GAS in hillslopes locally surrounding MLR study area.

Chapter 5. Midnorth study area

The Midnorth study area, which is identified in Figure 5.1, is centred on the coordinates 138°37'37" E, 33°24'2" S. The study area is 23 km south of the regional centre of Jamestown, and 18 km north of the town of Spalding. A description of the climate, landform, geology and geochemistry, landuse and soils of the Midnorth study area are presented in the Sections that follow.

5.1 Regional overview

The Midnorth defines the geographic region of South Australia that lies between the Barossa Valley in the south, the Yorke Peninsula to the west, and the semi-arid pastoral areas to the north and east. In the context of much of South Australia's agricultural land, the Midnorth is an important dryland broadacre agricultural region that features soils with high agricultural potential, especially under favourable seasonal and management conditions. The highest agricultural land capability is associated with the soils on the mid and lower hillslopes, where deeper soils tend to coincide with good drainage. The dominant agricultural land use of the Midnorth involves winter cropping (e.g. wheat, barley, canola and peas), often in rotation with sheep grazing, which is sometimes supplemented by growing lucerne and hay.

Stephens et al. (1945) reported that by 1945, most of the land had been cleared of native vegetation since the region had been opened up to farming during the 1870s. Nowadays, the farmland has almost replaced the original open savannah cover of the region. Native grasses, such as wallaby grass (*Darthonia semi-annularis*), iron grass (*Lomandra dura*) and *Themeda triandra* dominated the low-lying valley areas, while woody species occupied the elevated, better drained areas. These woody species included sheoak (*Casuarina stricta*), wattles

(*Acacia* spp.) and Mallee habit (*Eucalyptus odorata*).

5.2 Climate

The average annual rainfall of the Midnorth study area is approximately 450 mm, of which approximately 75 % falls during the winter, between April to September. Figure 5.2 shows: (i) the mean monthly rainfall, (ii) mean monthly daily maximum temperatures, (iii) mean monthly daily minimum temperatures, and (iv) mean monthly daily 3 pm relative humidity records for the years 1862 to 1994 for the township of Clare. Clare's elevation is 585 m, and at 50 km south of the Midnorth study area, represents the nearest Australian Bureau of Meteorology weather station with longterm rainfall and temperature records. Although differences do exist in absolute climatic conditions between Clare and the Midnorth study area by virtue of their separation and elevation differences, the climate trends nevertheless remain similar.

Figure 5.2 indicates that the winters are cool and summers are hot, giving rise to a temperate, Mediterranean-type climate. According to Soil Survey Staff (2003) these conditions result in a soil temperature regime that is mesic, and a soil moisture regime that is xeric. The differentiation of seasons is strong. Henschke *et al.* (1994) report that annually, regional potential evaporation exceeds rainfall, resulting in a soil moisture deficit. Comparisons of the monthly mean rainfall and

relative 3 pm humidity trends indicate the climatic reasons for this deficit. As presented in Chittleborough (1981), a seasonal moisture deficit that results

in xeric conditions is a pre-requisite for the genesis of texture-contrast soils.

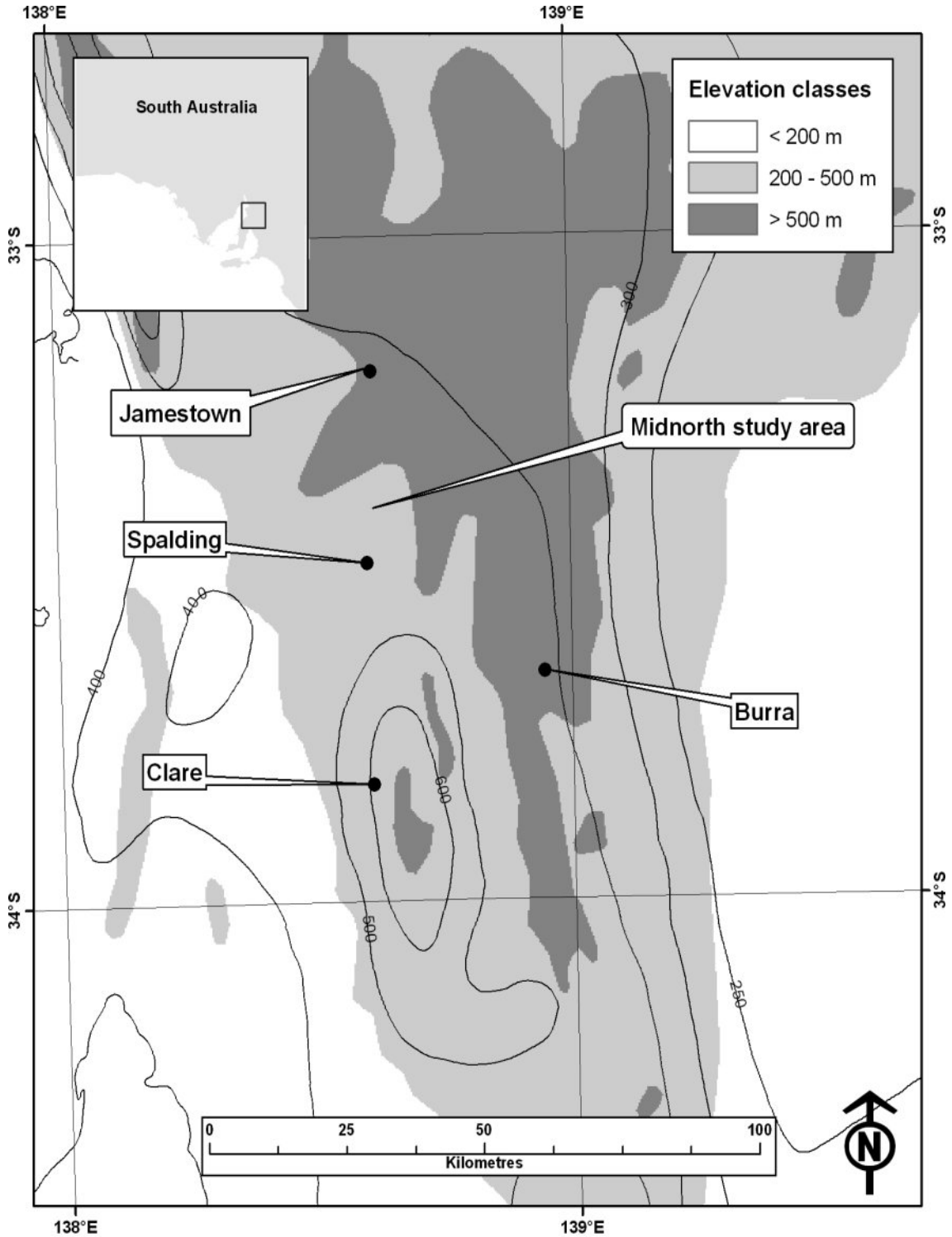


Figure 5.1. Locality map showing the South Australian setting (inset box) for the Midnorth study area, featuring elevation classes (m) and annual rainfall isohyets (mm).

5.3 Landform

The oblique aerial photographic view shown in Figure 5.3 identifies the local setting for the Midnorth study area. The study area occupies an east-facing hillslope defined by the Ward Hill summit and Freshwater Creek below in Belalie Valley. The boundary of the study area is approximately 1,650 m long by 800 m wide, and covers an area of approximately 140 ha. Figure 5.4 gives a plan view of the study area and features the transect A'-A'', which is used for reference in the discussions that follow. The transect defines a west to east toposequence. Field views of the toposequence are shown in Figure 5.5, and from the figure featuring (a) of the downhill view of the of the transect from Ward Hill (i.e. A' to A''), and (b) of the opposite, uphill view (i.e. A'' to A') from the edge of Freshwater Creek.

The hillslope topography is identified through the two metre interval contours shown in Figure 5.4 The contours shown were generated

photogrammetrically from a stereo pair of 1:40,000 scale aerial photographs. The process also produced a GIS dataset comprising a regular array of precisely georeferenced elevation data points with a spatial interval of three metres, and precise to within sub-metre elevation accuracy. These elevation data points were then subsequently interpolated using GIS by means of ordinary kriging geostatistics (Burrough and McDonnell 2000) to create a GIS raster format elevation (DEM) coverage with a data cell (pixel) resolution of 3 m².

Figure 5.6 shows the change in elevation along the transect A'-A''. This indicates a fall in elevation of 75 m, i.e. A' at 470 m to A'' at 395 m. In cross-section, the elevation profile is in shape hyperbolic concave, which is geomorphically consistent with a typical colluviated-alluviated hillslope. Slope gradients in the hillslope vary from approximately 14° (shoulderslope) to flat (toeslope).

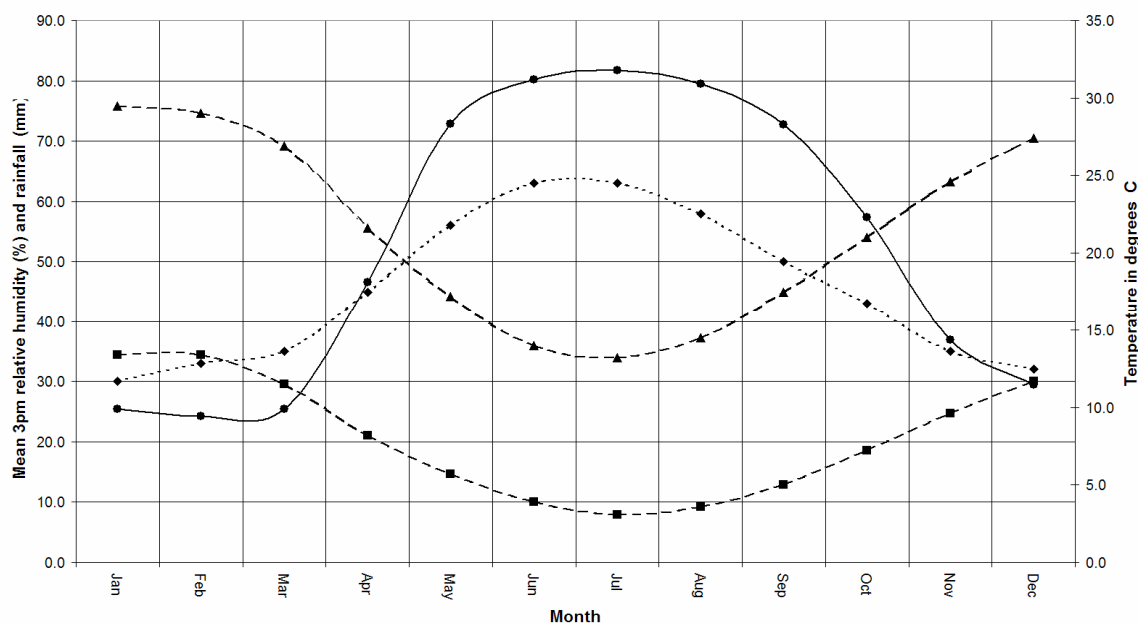


Figure 5.2. Mean monthly rainfall (mm) (●), mean monthly daily maximum temperatures (°C) (▲); (iii) mean monthly daily minimum temperatures (°C) (■); and (iv) mean monthly daily 3 pm relative humidity (◆) records for the years 1862 to 1994 for the town of Clare, which is comparable to the Midnorth study area climatic conditions (source: Australian Bureau of Meteorology, www.bom.gov.au/climate/averages/tables/cw_021014).

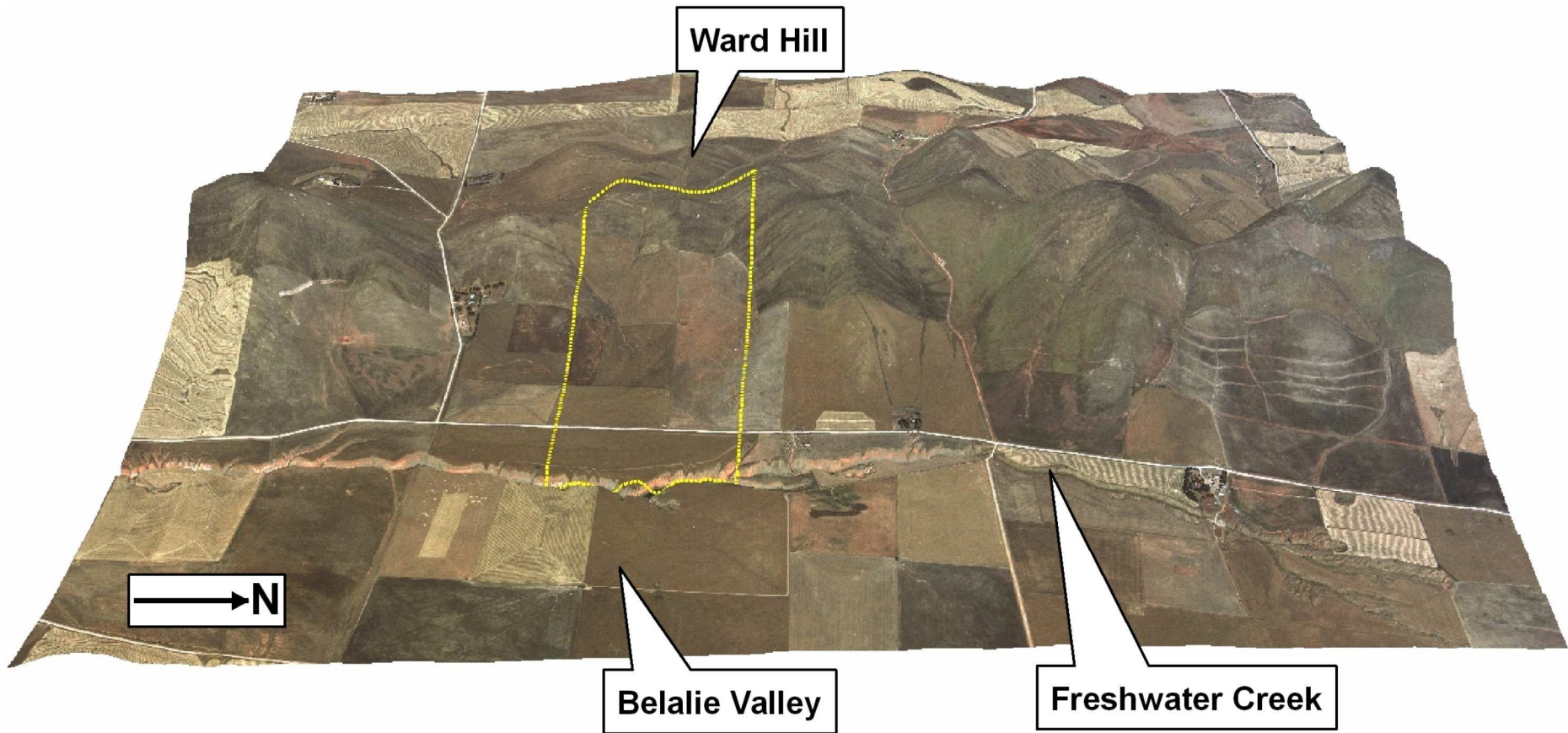


Figure 5.3. Oblique aerial photographic 3D drape showing the local setting of the Midnorth study area (yellow box, approximately 1,650 by 800 m), which features an east-facing hillslope defined by Ward Hill summit and Freshwater Creek in Belalie Valley.

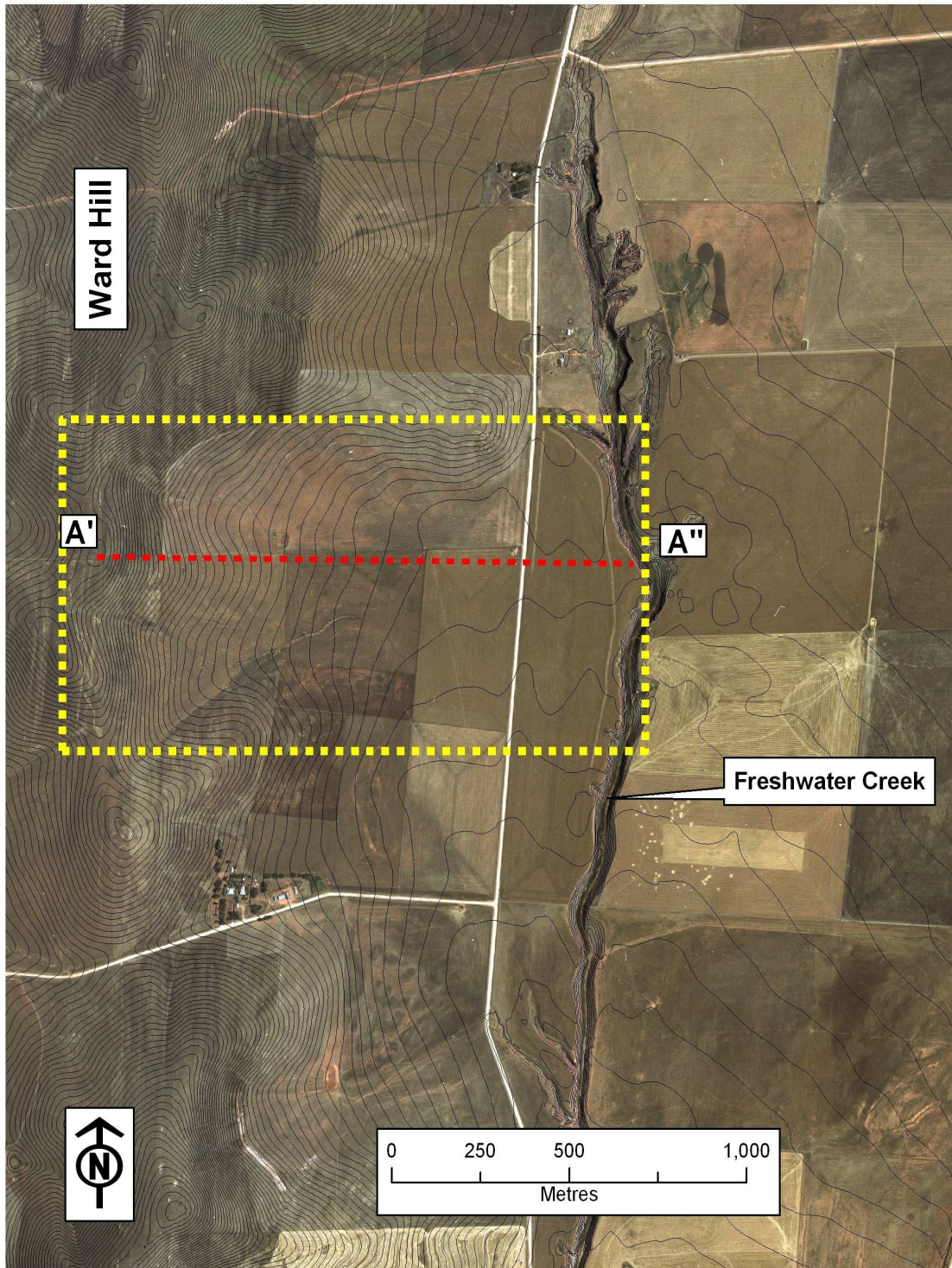


Figure 5.4. Midnorth study area (outlined), featuring a rectified aerial photograph, terrain (2 m contours) and the transect A'-A''.

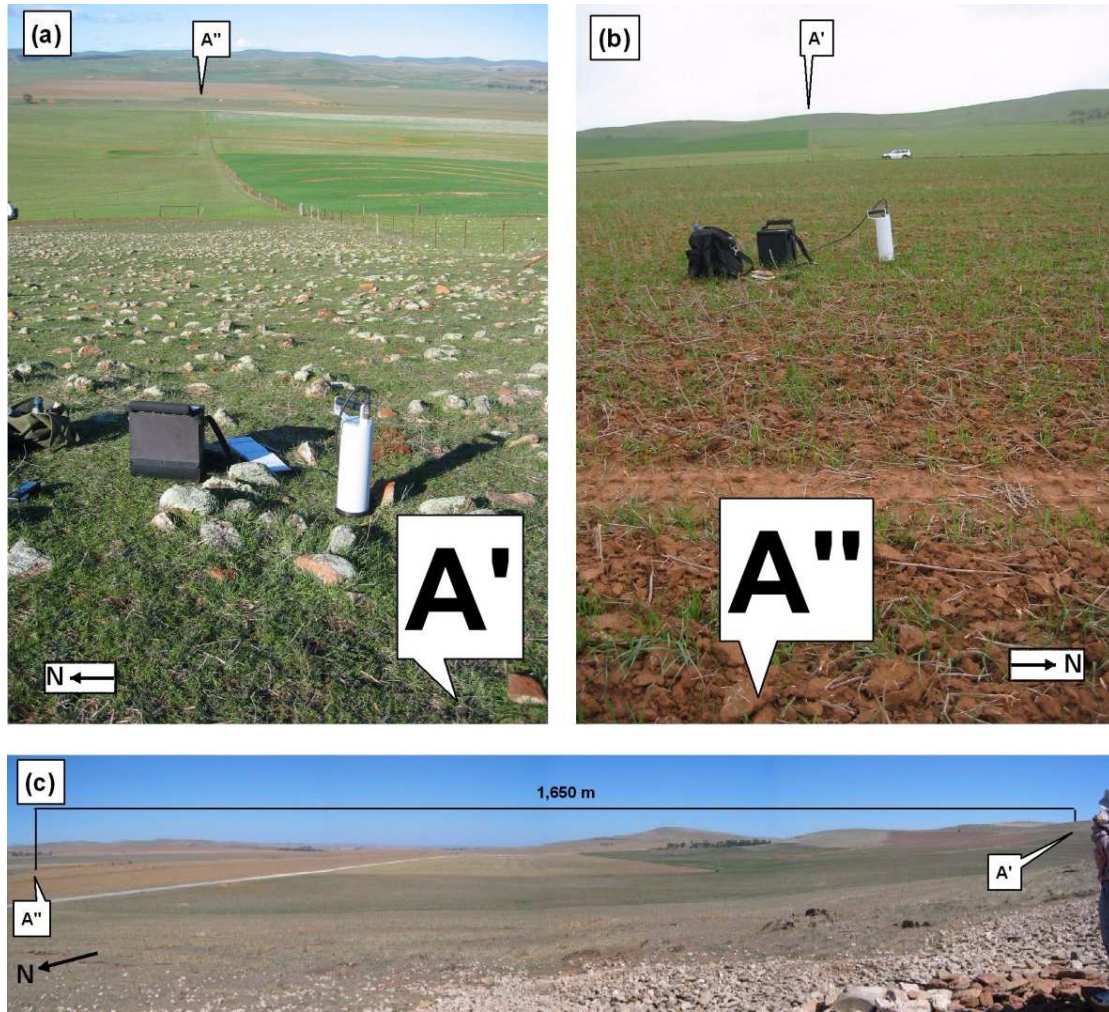


Figure 5.5. Views of transect A'-A'', showing (a) the Ward Hill-Freshwater Creek gully edge view of the Belalie Valley, and (b), the opposite view from the gully to Ward Hill, and (c) the study area hillslope in profile.

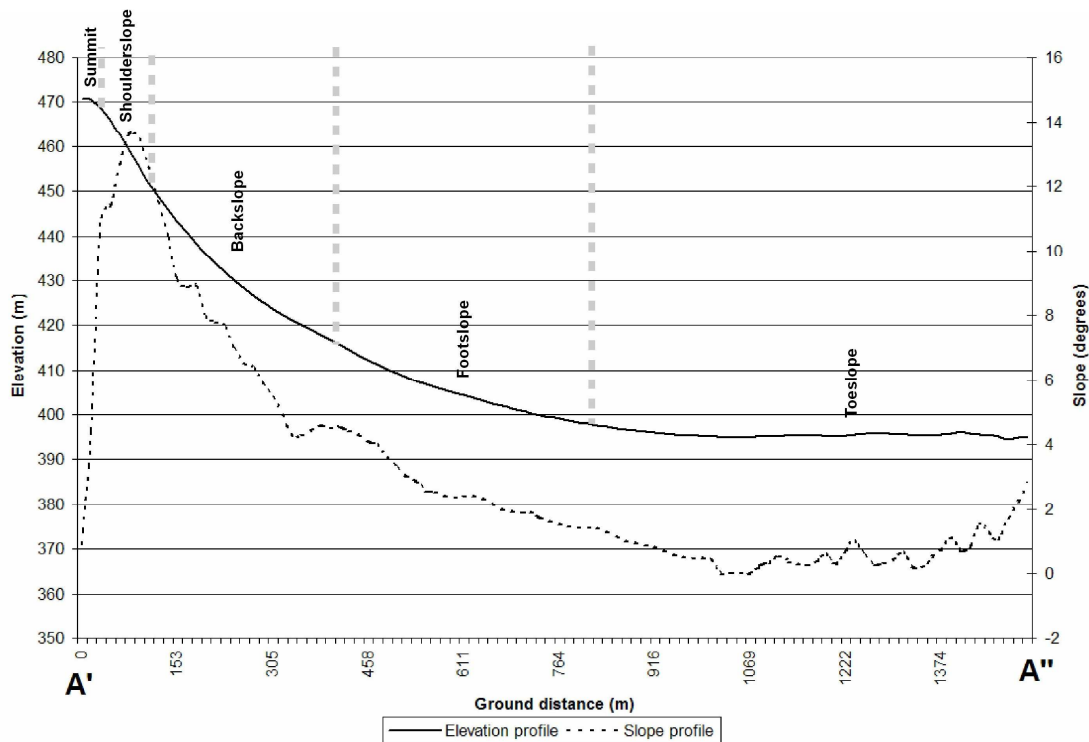


Figure 5.6. Profiles of elevation (m) and slope (°) along the transect A'-A'' shown in Figure 5.4. Hillslope profile positions are identified using terminology for hillslope position defined in Schoeneberger *et al* (2002).

The study area landscape features a series of “nose slopes” that jut eastwards from the flanks of Ward Hill ridge, and act as local hillslope drainage divides, or interfluves. The lower slope zones exhibit colluviated-alluviated soil inter-fingering, evidenced from subtle landforms as observed in the field, non-continuous layers of fine gravels in the upper soil profile (< 1 m), and the existence of buried soils.

Freshwater Creek is an ephemeral watercourse that drains southwards to the Broughton River, and ultimately to the Spencer Gulf. The creek itself features a series of saline groundwater-sustained pools and saline-sulfidic wetlands (Fitzpatrick *et al.* 2003c), and for much of its course runs at the base of a deep erosional gully that was formed during an extreme summer rainfall event in 1941 (reported in Cresswell and Liddicoat 2004). This rainfall event coincided with a period of regionally high erosion caused by poor land

management that involved paddocks that were either over grazed or left bare after cultivation. The section of the gully coinciding with the study area is approximately 12 m deep, and features near-vertical and poorly consolidated walls interspersed with wide, moderate-gradient ramps that were formed by the channelling of overland flow from the paddocks at the base of the valley into the gully (Figure 5.7).

The 12 m Freshwater Creek gully side features many discrete layers of different thicknesses, which indicate the chronology of the sequence of reddish alluvial deposits in the lower valley areas and paleodrainage features. These layers also exhibit weakly formed calcrete pans, and layers with salt effervescences dominated by gypsum and halite salts that have crystallised on wicking from the gully face. The lack of any materials with textures greater than gravels observed in the gully face layers indicates that alluvial deposition



Figure 5.7. Freshwater Creek erosional gully east-facing face and gully flat with a saline-sulfidic wetland.

of layers visible in the gully sides took place under moderately sedate conditions.

The subdued terrain of the low-lying alluvial areas of the Belalie Valley belies a complicated subterranean drainage system that has been recently identified using airborne magnetic survey data (Munday *et al.* 2003). These ancient channels (paleochannels) have been identified as a network of linear, interlaced, magnetically-lined fluvial deposits at various depths within the approximate 40 m valley infill profile that overlays the basement rock for much of the valley. The paleochannels provide important hydrological conduits for deep salt movements in the valley (i.e. acting as “internal plumbing”) due to their higher hydraulic conductivity compared to the alluvial infill that surrounds the paleochannels (Cresswell and Herczeg 2004; Wilford 2004a).

5.4 Geology and near-surface geochemistry

The geology of the Midnorth study area is available from the Burra 1: 250,000 scale geology map sheet (Geological Survey of South Australia 1964b). The geology is also available in GIS format at a scale equivalent to 1: 100,000, and the area corresponding to the Midnorth study area is presented in Figure 5.8. More detailed

geological descriptions of the study area region are presented in Wilford (2004a).

The geology of the study area features a linear north-south oriented sequence of resistant interbedded metamorphic rock types, which includes tillites, quartzite shales and massive quartzites of the Appila Formation that form the resistant spine of Ward Hill. On the east-facing flank of the Ward Hill ridge, and progressing down the hillslope, there occurs an interbedded sequence of less resistant, fine grained siltstone, mudstones and shales associated with the Tindelpina Shales.

Tapley Hill slates and siltstones underlie the generally deep alluvium of lower hillslope areas, although there is some localised outcropping. Where outcropping occurs, the rock tends to be mantled by carbonate, which is likely to be either of fine aeolian origin or as a bi-product of local rock weathering. The weathering of these rocks is also likely to contribute as a source of sulfuric compounds, giving rise to the formation of gypsum crystals observed wicking from the Freshwater Creek erosional gully face, and the sulfidic environment in the wetlands in the creek bed, which is described in more detail in the next Section.

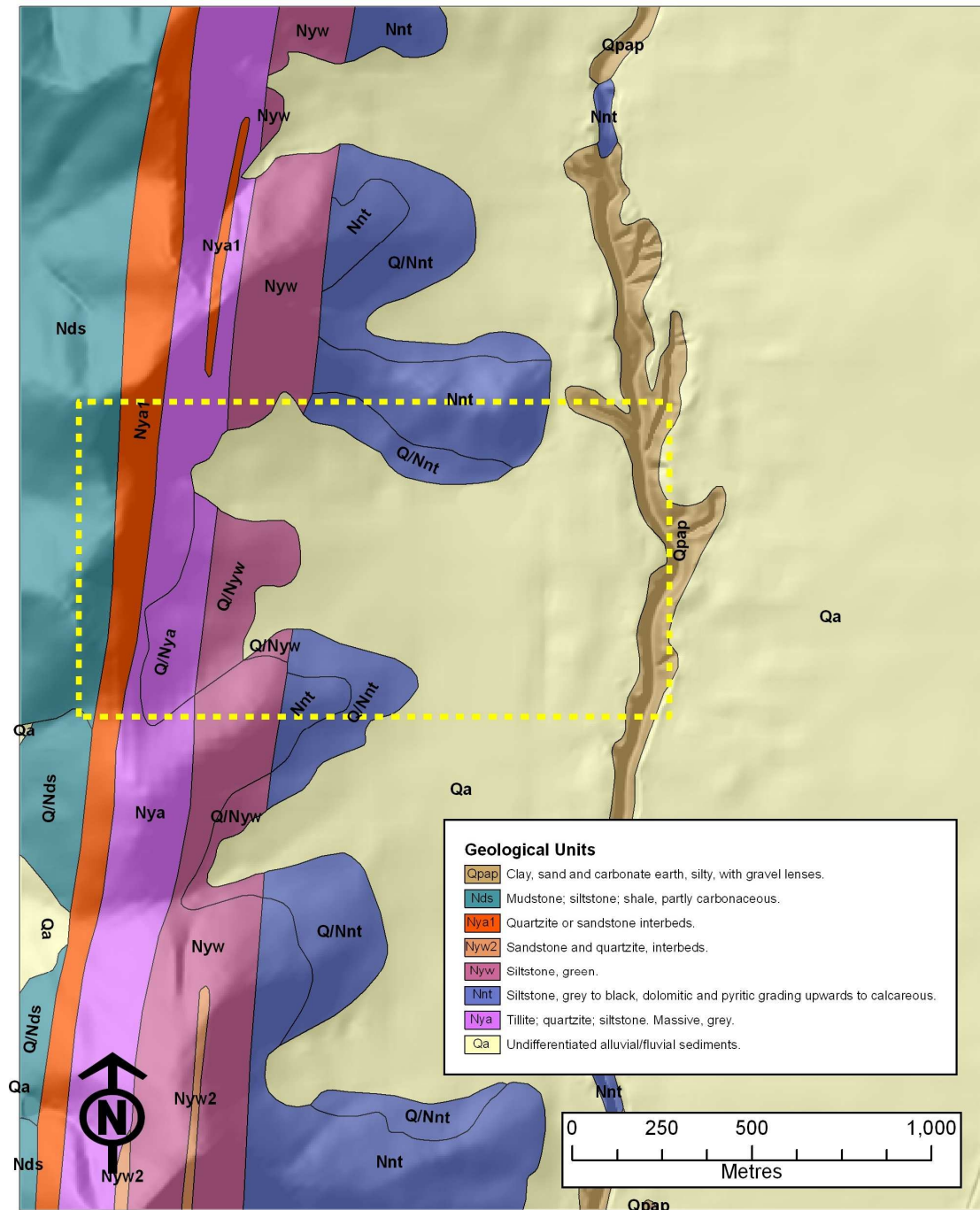


Figure 5.8. Midnorth study area (outlined) geology at 1: 100,000 scale, with a hillshade applied to accentuate landform.

A regional airborne radiometric survey was acquired in September 2003 for the South Australian Salt Mapping and Management Support Project (SA SMMSP) (Cresswell and Liddicoat 2004; Munday *et al.* 2003). The airborne radiometric survey was flown on an east-west orientation, perpendicular to the obvious regional topographic trends. The airborne

survey line spacing used was 100 m, and the survey was conducted at a flying height of 60 m above ground level. The combination of flying height and air speed resulted an flightline sampling rate of approximately one survey point per 7 m. On board, the acquisition system precisely georeferenced the radiometric readings. As is typical with radiometric

surveys, the data acquired consisted of four channels per radiometric survey point on the ground, comprising: (i) potassium (K) %; (ii) thorium (Th) ppm; (iii) uranium (U) ppm; and (iv) total count (TC) ppm.

The radiometric survey data was supplied pre-processed and calibrated (e.g. Minty *et al.* 1997), and interpolated into a four band (i.e. K %, and Th, U and TC ppm) GIS coverage of the whole survey area, and issued at

a ground resolution of 20 m. The study area coverage is shown in Figure 5.9. The coverage shows a speckled pattern of radiometric geochemistry of the upper 0.3 m soil layers (Dickson and Scott 1997; Minty 1997). Reference to the airborne gamma-radiometric coverage shows that the upper slope (colluvial) soils of the study area are co-dominated by a speckled pattern of thorium and uranium geochemistry, whereas the lower slope (alluvial) soils are dominated by potassium geochemistry.

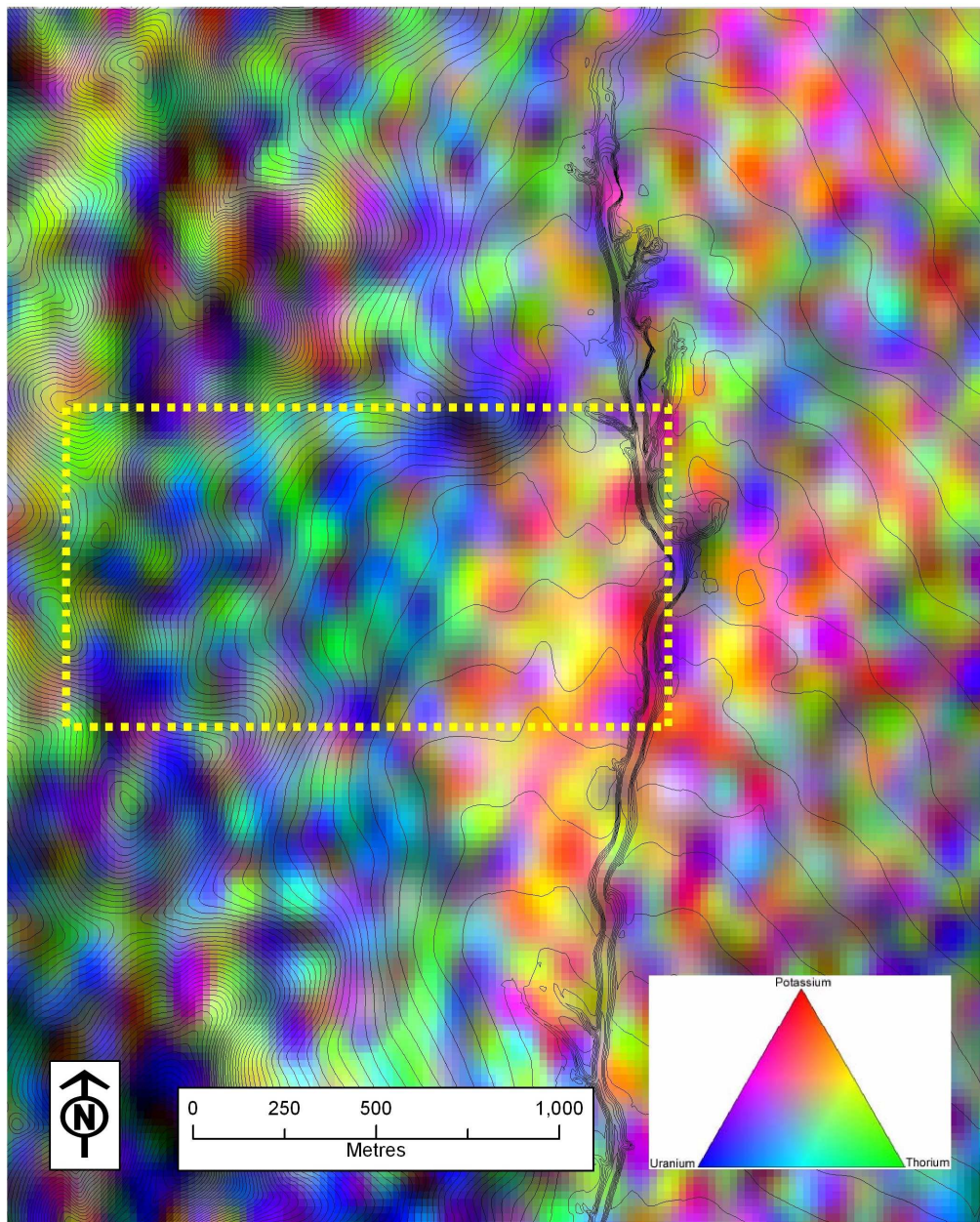


Figure 5.9. Midnorth study area (outlined) airborne gamma radiometrics coverage, with 2 m contours applied to accentuate landform.

5.5 Landuse

The Midnorth study area is farmed by two families. The Cootes family farm, which covers approximately 80 per cent of the Midnorth study area, occupies the sloping areas to the west of the north-south road (Figure 5.4). The Ashby family farms the toeslope paddock to the east of the road. The summit and steepest backslopes are used for sheep grazing on unimproved pasture. In areas of gentle slope and little outcrop (e.g. lower shoulderslope-toeslope), the land has been cleared for dryland cultivation. Here, the farming practice involves annual rotations of winter cereal crops (e.g. wheat and barley), canola and pasture. Pasture is sometimes improved by growing lucerne, depending on the rotation cycle. The pasture is grazed for lamb and wool production.

Soil acidification caused by the leaching and removal of nitrogenous compounds (e.g. in harvested biomass and livestock excreta) results in the need to top-dress with lime on a regular annual basis. In addition, regular annual applications of top-dressed fertilizers like diammonium phosphate (DAP) are also required. DAP contains ammonia (nitrates), phosphorous and sulfur.

Contour banks have been formed in the higher gradient slopes (i.e. upper mid slopes and backslopes) to halt erosive sheet wash, and to promote water interception. Two impoundment dams in the mid slope have been created for livestock use. The impoundments intercept groundwater and the sporadic stream flows.

The study area has a legacy of unpublished CSIRO research

conducted since the late 1980's. Research started when Mr Cootes reported localised and ephemeral patterns of crop yield loss on his land. At the time the cause of the losses was suspected to be a root disease. However, after thorough investigation of the soils, the losses were attributed to ephemeral patterns of near-surface salinisation, i.e. shallow NAS. The investigation involved conducting a soil survey in 1988, which consisted of a comprehensive field survey (involving detailed layer-by-layer soil morphological descriptions) and supplemented by detailed laboratory physicochemical investigations on selected cores. The field and laboratory investigations were combined to generate a soil series map (unpublished) and are discussed in the following Section.

As part of the current investigation, Mr Cootes assisted in the compilation of a map of yield patterns in his farmed area. His qualitative assistance benefited the map production through his more than 25 years of field observations and yield returns. The final yield map is presented in Figure 5.10. In this map, the so-called "poor yield" areas feature usually depressed yields compared to other areas on the farm, even under favourable growing conditions (e.g. timely and consistent soaking winter, spring and early summer rainfall). The so-called "excellent yield" areas usually return the best yields on the farm, even under difficult growing conditions. The so-called "good yield" and "moderate yield" areas take their place within the above range. Gaps are evident in the cropped areas of the map. These areas correspond to areas that Mr Cootes did not report as being noteworthy in their yield consistency, hence probably fall within the "good yield" and "moderate yield" classes.

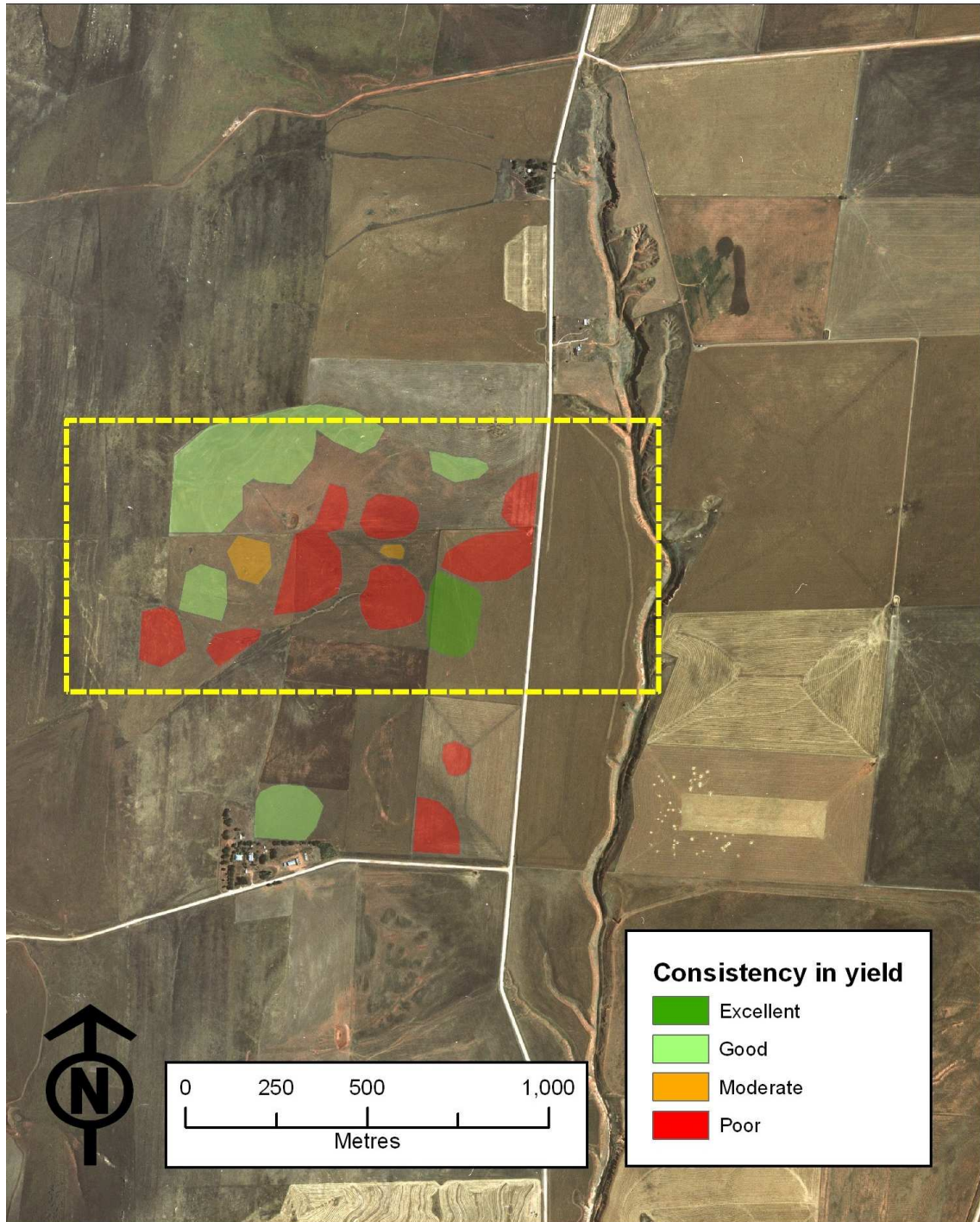


Figure 5.10. Yield map of parts of the Midnorth study area, indicating areas that are consistently excellent, good, moderate and poor yielding, based on the farmer's field observations and yield returns.

5.6 Soils

The soils in the study area have been systematically mapped on a number of occasions. These maps have been created at different scales, and the various soil attributes mapped in each

reflect their specific purpose. The most important maps in terms of scale and soil attributes coinciding with the Midnorth study area are:

- Part of the County of Victoria 1: 63,360 scale soil series map (Stephens *et al.* 1945);
- Statewide soil landscape unit (SLU) 1: 100,000 scale map (Soil and Land Information 2002); and
- draft CSIRO soil mapping unit (SMU) 1: 10,000 scale map (Fitzpatrick *et al.* in prep.)

The SMU map was surveyed by a CSIRO team in 1988. The soil survey was conducted on a semi-rigid design along a series of toposequence-based transects shown in Figure 5.11. The field component of the survey involved identifying and recording significant morphological properties from complete two metre soil cores (unless bedrock was encountered) that were obtained using a vehicle-mounted drilling rig. The first metre section of each core was extracted using a 75 mm tube, and the subsequent core section extracted using a 50 mm tube. The key morphological characteristics described from the intact soil cores included the presence of surface rock, soil horizon depths, designation and hand texture (McDonald *et al.* 1998), Munsell soil colour, carbonate accumulation (consistency and structure), and other significant morphological features (e.g. soil structure, gravel layers and mottling and bleaching patterns). Appendix B presents profile layer morphology described during the survey.

Following the field component, as shown in Figure 5.11, 18 of the soil cores were selected for subsequent laboratory analysis (Rayment and Higginson 1992) for $EC_{1:5}$, pH (H_2O and $CaCl$), chloride content; total and organic carbon content, nitrogen content, exchangeable cations (Ca, Mg, Na and K), CEC (sum of cations), ESP, and texture. Appendix C presents the derived laboratory data.

The combination of the field observations and laboratory analyses (not previously published) enabled the seven SMUs (SMU A-G) to be

classified according to Great Soil Groups (Stace *et al.* 1968) and Factual Key (Northcote 1992). As part of the work of Fitzpatrick *et al.* (2003c), the SMU boundaries were digitised using GIS (shown in Figure 5.12), with the addition of an undescribed “GULLY” unit). The SMU descriptions were also finalised with reference to the: (i) the original 1988 soil survey data and (ii) follow-up field investigation. The refined version resulted in nine SMUs with the addition of the new SMUs of “Gully edge” and “Gully flat”. The unit descriptions are presented in Table 5.1.

The map SMU map (Figure 5.12) cross-references with the SMU descriptions given in Table 5.1. Each indicate the existence of class variants within the soil types. Typically, type variants feature differences in morphological properties including texture, structure and A horizon colour, levels of free carbonate, presence/absence of an E horizon, and in the chemical properties of the subsoils (e.g. neutral and alkaline pH and sodium levels). The “b” variant of the map (e.g. Cb and Ab) denotes the presence of a pale E horizon, while the “s” variant denotes a shallower A horizon (e.g. Fs and Es), while the Table identifies SMU D as a variant of SMU E. Also, both the map and Table feature transitional soils. For example, the map features SMU E-G, which is a transition between SMU E and SMU G, while the table describes SMU E as a transitional soil (between SMU A and SMU B).

As part of the work described in Fitzpatrick *et al.* (2003c), based on the SMU mapping, the study area was divided to create five landscape soil units (LSUs). These new units were based on similarities in: topography, soil-regolith morphology (soil texture, structure), zones of salt accumulation, and hydrology (i.e. groundwater and freshwater flows). The LSU mapping is shown in Figure 5.13, and defined and summarised in Table 5.2.

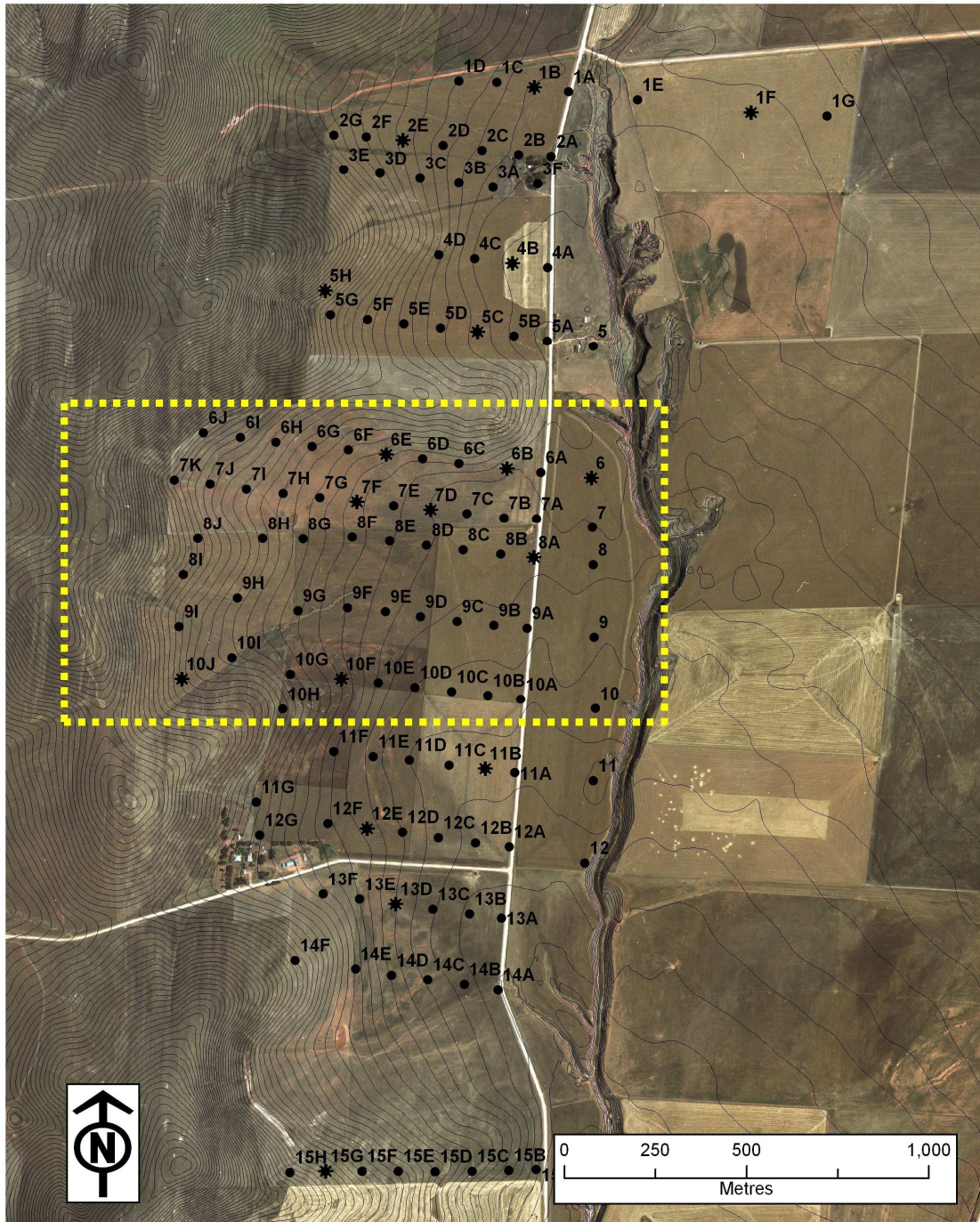


Figure 5.11. Midnorth study area 1988 CSIRO survey site positions (●) and soil cores (*) selected for physicochemical analyses.

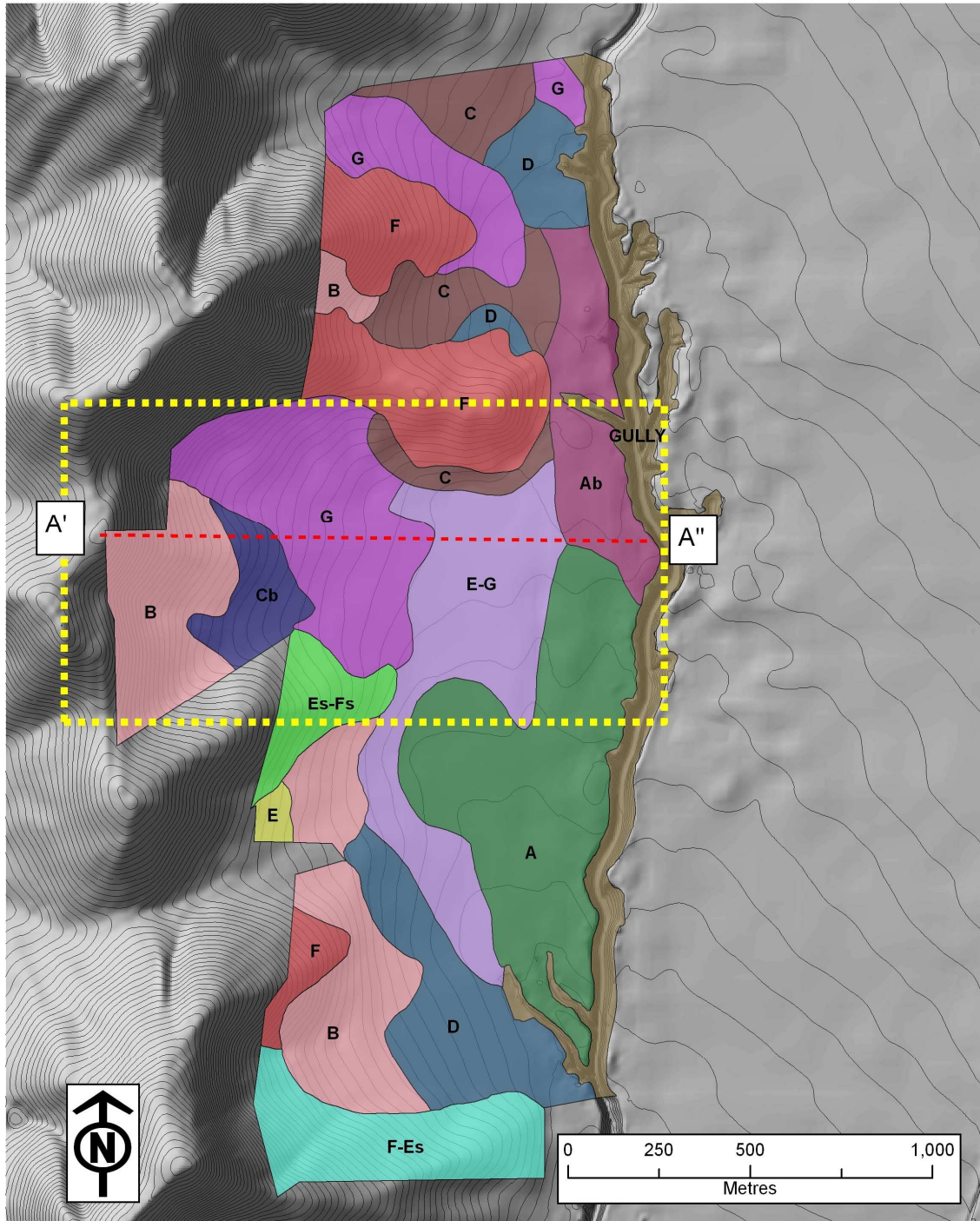




Figure 5.12. Midnorth study area draft CSIRO soil map of soil mapping unit (SMUs), with a hillshade applied to accentuate local relief.

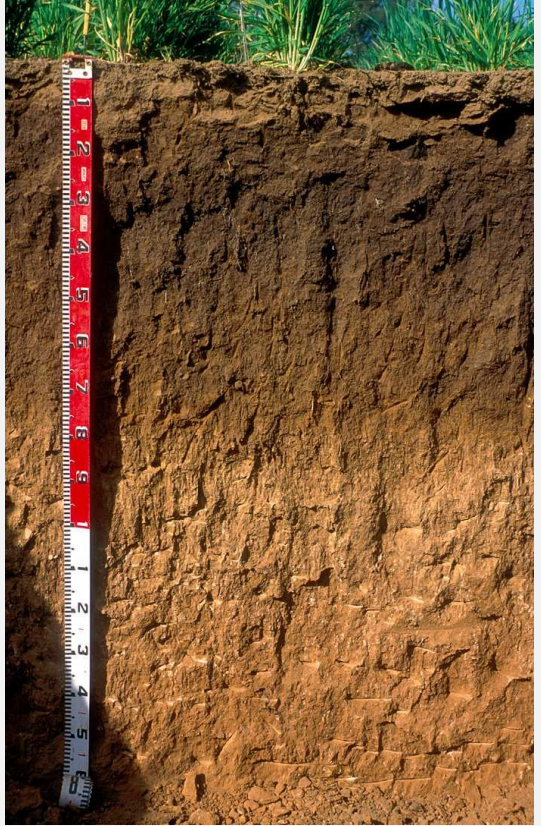

Table 5.1. Final Soil Mapping Units (SMUs) classified according to Stace *et al.* (1968).

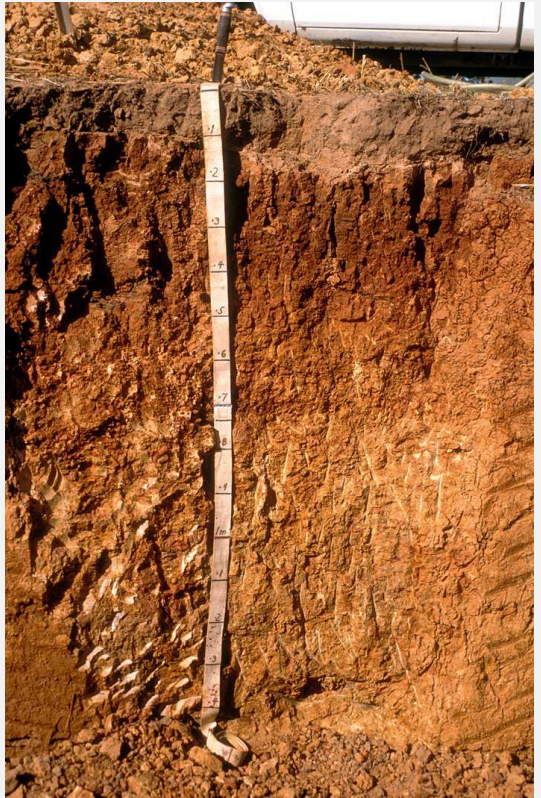

Soil Mapping Unit (SMU)	Great Soil Group (Stace <i>et al.</i> 1968)	Description
A	Brown Clay	These soils are a moderate to strongly structured brown clay soil with field textures dominated by silt in the upper horizons. The soil is deep with what appears to be buried soils of generally redder colour (than the overlying brown clay) at depths of 1 m or more; sodic subsoils with a pale E horizon variant (Ab) may occur. This SMU occurs on the flat, overlying deep alluvium. Sometimes with subsoil expressed sodicity and salinity
B	Sodic Brown Clay	These soils are a clay that may have a weak self-mulching surface and a gradational texture profile that may extend beyond 2.0 m, but the underlying calcareous shales are at a mean depth of 1.6 m and a range of 0.7 m to 2.0 m. These soils are restricted to the very gently inclined to moderately inclined slopes emanating from the low hills and rises overlying colluvium.
C	Red Brown Earth	These soils have a hard setting A horizon of light sandy clay loam to clay loam texture and a clear to sharp change to a dark reddish brown, strongly structured, medium to heavy clay B horizon. The solum is usually greater than 2 m deep. A shallow variant (C-s) has been recognised for those profiles that are less than 0.5 m to the C horizon. The majority of profiles are calcareous although there is considerable variation in depth to the calcareous layer(s), which may be soft, hard and nodular. This SMU occurs in the flat, overlying colluvium. Sometimes with subsoil expressed sodicity and salinity.
D	Red Brown Earth (Similar profile characteristics to SMU C.)	These soils differ from SMU C soils in that they have a sporadic bleach of varying thickness and prominence. This SMU occurs on sloping to flat areas overlying colluvium/alluvium.
E	Transitional to the Brown Clays of SMU A and SMU B (with a gradational texture).	These soils have colours of the major horizons that are generally less red than the Red Brown Earths. The landscape position of soils of this SMU is generally near the transition from uniform profile forms to duplex (Northcote 1992). The gradational features in SMU E may have been enhanced by the cultivation practices resorting surface horizons.
F	Rendzina and Terra Rossa	These soils comprise mainly shallow calcareous loams with calcrete fragments overlying mainly calcareous weathering siltstone with some very shallow, loamy topsoils (<0.1 m) overlying massive calcrete. These shallow soils occur mainly on the crest and upper slopes, and contain outcrops

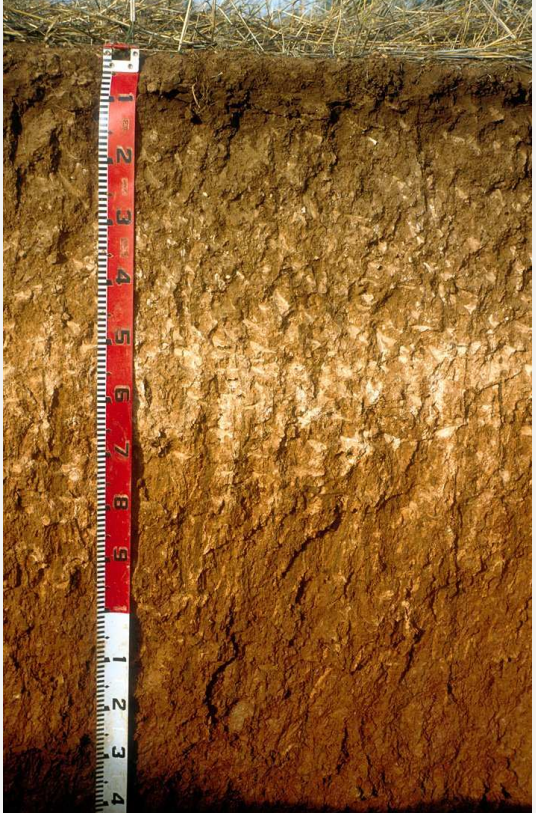

Soil Mapping Unit (SMU)	Great Soil Group (Stace <i>et al.</i> 1968)	Description
		(40 %) of mudstone, siltstone and partly carbonaceous shale. These soils have formed in situ from fine sedimentary rocks (mudstones, siltstones and partly carbonaceous shales). The dominant vegetation is pasture. These soils are darker and browner than SMUs C, D, E and G. Soils with low levels of salinity and sodicity.
G	Red Brown Earth	The main morphological feature distinguishing these soils from the other Red Brown Earths is a lighter surface texture with accompanying poorer structure; the B horizons are strongly structured and medium to heavy clay texture; free lime is evident in the majority of profiles. Mostly with subsoil expressed sodicity and salinity.
Gully edge	Highly saline, sodic Red Brown Earths	The exposed soils at the gully's edge (12 m deep) are highly saline (EC _{se} 360 dS/m), gypsiferous, salic and sodic soils in some layers. Some carbonate-rich gravel bedding layers indicate the presence of alluvial fans in the profile.
Gully flat	Highly saline hydromorphic soils	These soils are highly saline (EC _{se} 4-140 dS/m) sulfidic hydrosols.


Table 5.2. Midnorth study area Soil Landscape Unit descriptions (modified from Fitzpatrick *et al.* 2003c), including topographic location, description, classification according to Australian Soil Classification (Isbell 1998), Soil Taxonomy (Soil Survey Staff 2003) and Great Soil Group (Stace *et al.* 1968), and typical profile and landscape photographs.



Landscape Soil Unit	Topographic location	Description	Australian Soil Classification	Soil Taxonomy	Great Soil Group	Profile photograph	Landscape photograph
LSU 1	Summit	Shallow calcareous loams with very low salinity and sodicity (Rendzina and Terra Rossa soils) interspersed with outcropping (i.e. 5-50% surface cover) shales and siltstones.	Ceteric, Lithic, Lithocalcic, Calcarosol, thin, slightly gravelly, loamy, clay loamy, shallow	Lithic Calcixercept	Brown Clay		

Landscape Soil Unit	Topographic location	Description	Australian Soil Classification	Soil Taxonomy	Great Soil Group	Profile photograph	Landscape photograph
LSU 2	Shoulder/backslope	Saline/sodic clay soils with gradational texture profile and weak self mulching surface.	Lithocalcic Subnatric, Brown, Sodosol, thin (eroded), slightly gravelly, clay loamy, clayey, moderate	Natric Palexeralf	Brown clay		

Landscape Soil Unit	Topographic location	Description	Australian Soil Classification	Soil Taxonomy	Great Soil Group	Profile photograph	Landscape photograph
LSU 3	Footslope	Soils with subsoil expressed sodicity and salinity; strong texture-contrasts between leached upper layer loams above sodic clay layers. B horizons are strongly structured and medium to heavy	Lithocalcic Subnatric, Red, Sodosol, medium, slightly gravelly, loamy, clayey, very deep	Typic Natrixeralf	Red Brown Earth		

Landscape Soil Unit	Topographic location	Description	Australian Soil Classification	Soil Taxonomy	Great Soil Group	Profile photograph	Landscape photograph
LSU 4	Toeslope	Deep moderate to strongly structured sodic clays (sometimes with subsoil expressed sodicity and salinity) with thin leached A horizons; field textures dominated by silt.	Brown, Sodosol, medium, slightly gravelly, loamy, clayey, giant	Vertic Natrixeralfs – (dominant) with some interspersed Typic Natrixeralfs	Brown Clay		

Landscape Soil Unit	Topographic location	Description	Australian Soil Classification	Soil Taxonomy	Great Soil Group	Profile photograph	Landscape photograph
LSU 5	Gully face	Highly saline (EC _{se} 360 dS/m), gypsiferous and sodic soils on steeply inclined slopes with some carbonate-rich bedding	Supracalcic, Subnatric, Red, Sodosol, medium, slightly gravelly, loamy, clayey, giant	Typic Natrixeralf (possible new salidic subgroup)			

Landscape Soil Unit	Topographic location	Description	Australian Soil Classification	Soil Taxonomy	Great Soil Group	Profile photograph	Landscape photograph
LSU 6	Gully flat	Highly saline (EC _{se} 4-140 dS/m) sulfidic hydrosols.	Natric, Sulfidic Salic, Hydrosol; medium, slightly gravelly, clay loamy, deep	Typic Sulfaquent			

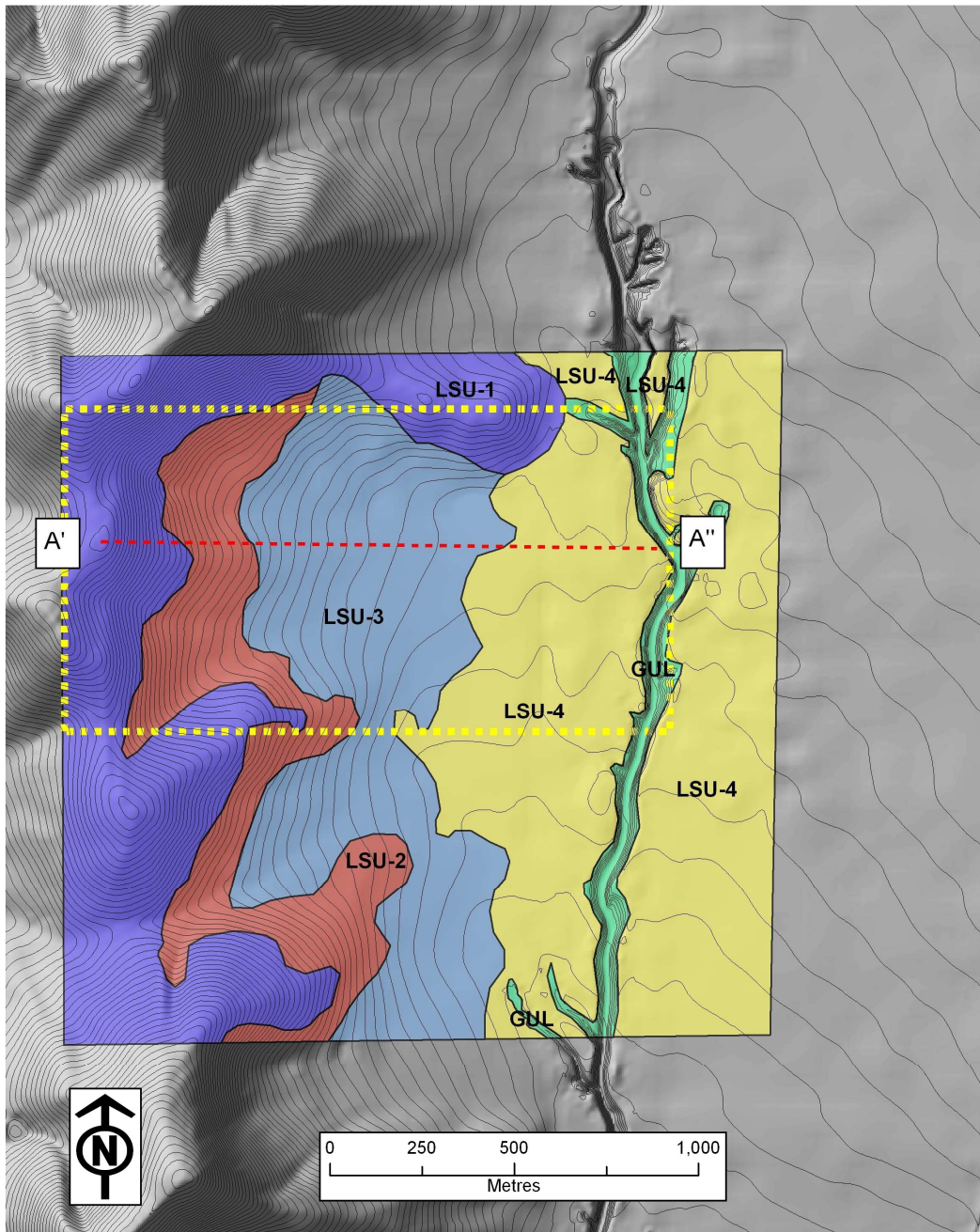


Figure 5.13. Midnorth study area landscape soil unit (LSU) map, with a hillshade applied to accentuate relief. LSUs are defined and summarised in Table 5.2.

With reference to the physicochemistry of selected profiles shown in Figure 5.14, LSUs 3 and 4 are texture-contrast soils (A horizons of < 20 % clay, grading to B horizons of 40 – 60 % clay) with sodic B horizons (ESP 20 – 30 %). However, only the LSU 3 soils show significant salinity ($EC_{se} \sim 3 - 7$ dS/m) within the upper one metre, suggesting that these soils

are effected by shallow NAS according to the criteria presented in Chapter 2. While the LSU 2 soil profile indicates saline conditions in the solum ($EC_{se} \sim 8$ dS/m), the lack of a significant texture-contrast between the A and B horizons (45 % grading to 60 % clay) identifies the lack of requisite texture morphology for shallow NAS conditions.

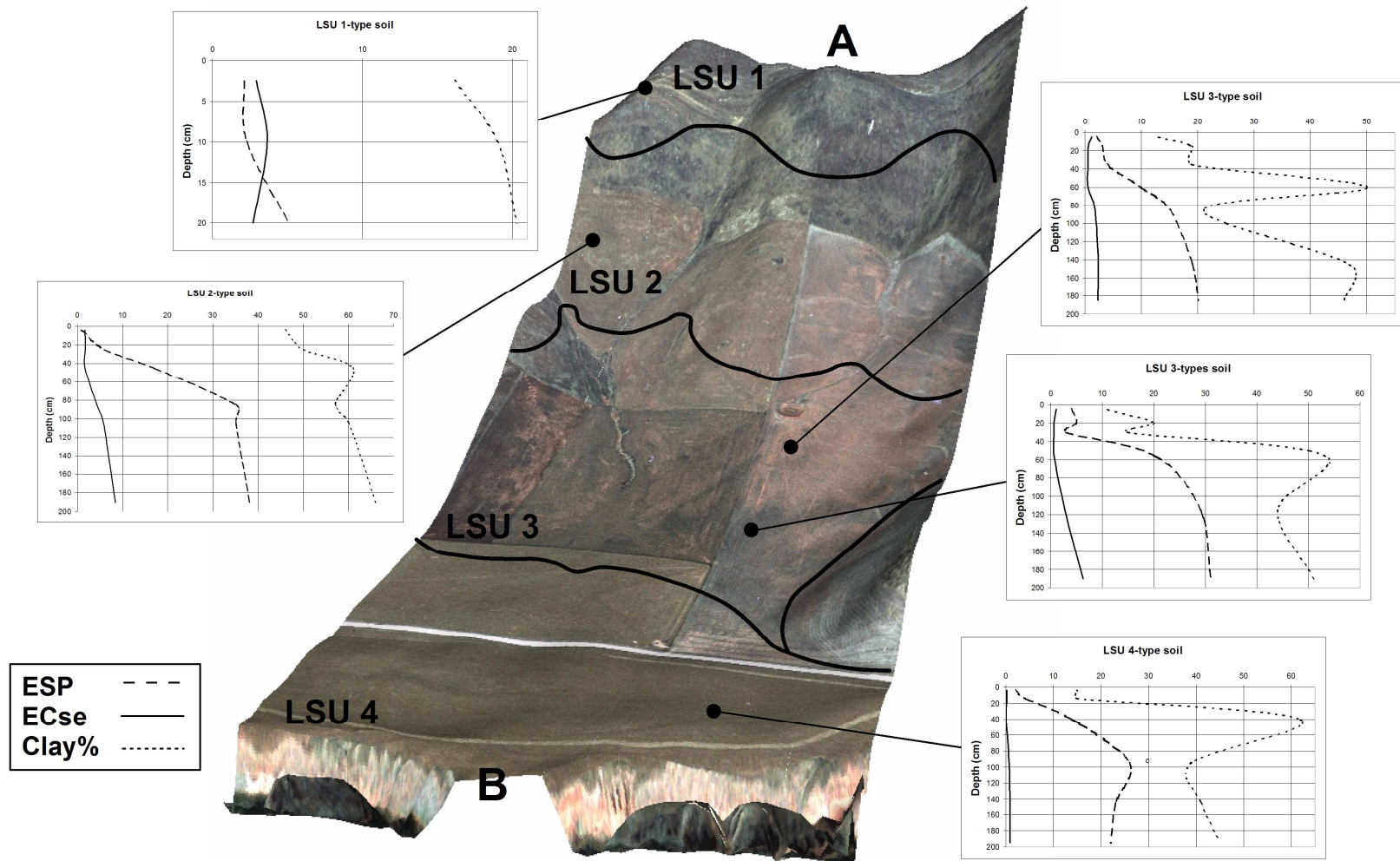


Figure 5.14. Midnorth study area (1,650 by 800 m) LSU boundaries draped over 3D aerial photograph, featuring selected profiles showing trends in ESP, EC_{se} dS/m and clay % from the 1988 CSIRO soil survey. Note the difference in scales in the LSU 1-type graph.

Chapter 6. Midnorth fine scale investigation

This Chapter discusses the interpretation of spatially detailed, fine scale (as defined in Chapter 1) geophysical, morphological and physicochemical investigations of multiple near-surface profiles from two plots (each 10 by 10 m) in the LSU 3 zone of the Midnorth study area. With reference to Chapter 4, the investigations are consistent with the polypedon soil system scale (i.e. $i+1$) (Table 4.1). The soils in each plot feature pedogenic variation caused by differences in hillslope position. Descriptive conceptual mechanistic models are presented for each plot to explain the hydrogeological heterogeneity, and explain how these differences relate to the salt distribution (i.e. shallow NAS) and the variable yield trends from the yield mapping shown in Figure 6.1.

6.1 Plot selection and descriptions

Based on a combined geomorphic and yield pattern investigation of the Midnorth study area to identify end-member variants of LSU 3 soils, two 10 by 10 m plots shown in Figure 6.1 were identified for detailed investigation. Plot areas of 100 m² were deemed sufficient in the Midnorth study area landscape to feature multiple hydrogeologically connected systems (i.e. pedons) (Soil Survey Staff 1993).

The two plots were investigated during November (early summer). Plot 1 (P1) was located in a consistently good yielding area, while Plot 2 (P2) was located in a consistently poor yielding area, shown in Figure 6.1. In terms of local terrain, both plots are located on footslope areas. The elevation of P1 at 398 m and the elevation of P2 is 404 m. The surface gradient of Plot 1 is 6 ° and Plot 2 is 3 °. Both plots are in areas that show little expression of surface relief, nor significant features on the ground (e.g. changes in surface soils colour, vegetation patterns and

outcropping etc.). At time of survey, P1 featured a predominant cover of grasses undergoing senescence, interspersed by dispersed lucerne plantings, while P2 featured a predominant cover of senescing grasses. Field observations and computerised terrain analysis indicate that the landform at Plot 1 is concave linear and Plot 2, subtly convex in plan and profile curvature.

6.2 Survey design

A rigid grid of 6 by 6 survey points at two metre intervals (i.e. giving 36 survey points) was marked out on the ground using brightly coloured markers to define each plot Figure 6.2. The survey points were then accurately georeferenced using a differential GPS (DGPS) to supply sub-metre positional accuracy for subsequent incorporation into a GIS.

The plot investigation were essentially split into a field and a laboratory component, which are discussed in the following Sections.

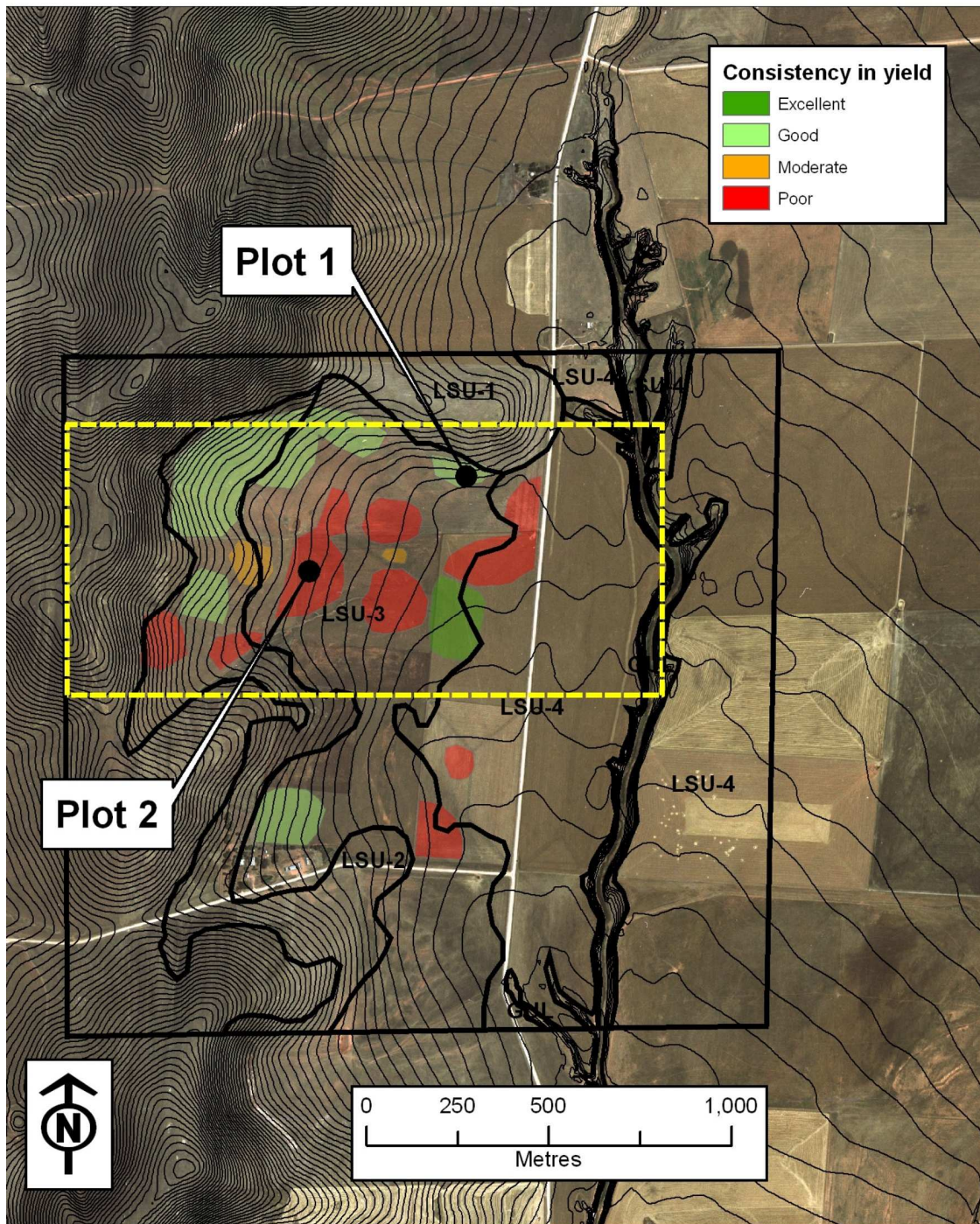


Figure 6.1. Midnorth study area plot locations (P1 and P2), crop yield patterns, 2 m contours and soil landscape units (SLUs).

6.3 Field investigations

The field investigations comprised a field survey component followed by a spatially-based investigation of the field data using a GIS. At every survey point in each plot, the following measurements were taken:

- EM38 apparent ground electrical conductivity readings in both horizontal mode (EC_{ah}) and vertical mode (EC_{av}) (see Chapter 3); and
- the mean of 10 Bartington MS2F probe surface volume magnetic susceptibility (κ) readings (see Chapter 3).



Figure 6.2. Plot survey point marking (pink flags) at 2 m intervals, which are georeferenced using differential geographic information system positioning (photograph of P2 area).

In addition to these readings, a gouge auger was hammered into the ground to extract a complete soil core extending more than a few centimetres into the clay upper B horizon at every survey point in each plot (Figure 6.3 (a)). In this way 108 layers were collected per plot. As shown in Figure 6.3 (b), on extraction each core was split into three layers, comprising:

- upper half of the A horizon (i.e. layer 1: L1);
- lower half of the A horizon (i.e. layer 2: L2); and
- the B1 horizon (i.e. layer 3: L3).

In this manner, 108 layer samples were collected in each plot. All layer depth ranges were measured and recorded. Rubbed dry soil colours were recorded for each layer according to Munsell colour notation, and the layers were hand textured according to McDonald *et al.* (1998).

The georeferenced field data were transferred to GIS, and 0.1 m resolution coverages for each plot survey created using a spline interpolation method (Burrough and McDonnell 2000). Identical input parameters for each survey method were applied in each GIS interpolation to ensure consistency in the way results were generated. In this way, the following GIS coverages were generated per each of the layers:

- depth to B horizon;
- EC_{av} ; and
- surface κ .

6.4 Laboratory investigations

Laboratory investigations were conducted on the samples taken from the selected cores. For each core sample, the investigations included χ and mass magnetic susceptibility

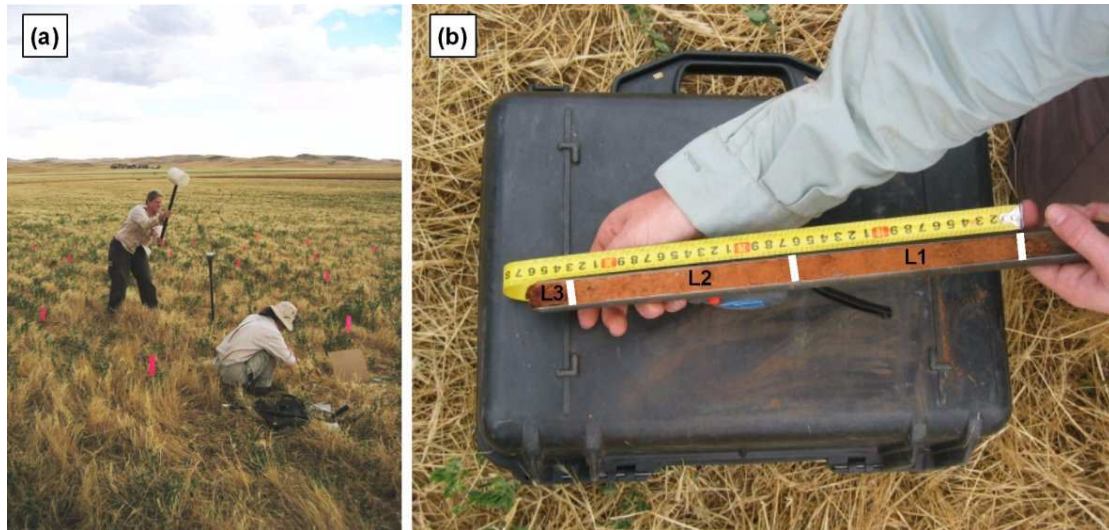


Figure 6.3. (a) Gouge auger being hammered into the ground in P1 and (b) the extracted core, which features a loamy A horizon and a heavy clay upper B horizon (Btn), being measured for layer depths. Core sections L1, L2 and L3 are identified.

frequency dependency (χ_{fd} %) measurements (see methods described in Chapter 3). In addition to these measurements, a suite of physicochemical investigations described below were made on a subset of plot cores in response to project resource limitations. In general, sub-set selection was achieved by choosing every second core. Deviation from this sequence was made when there was insufficient bulk of sample for multiple analyses. Figure 6.4 shows the resulting distribution of 18 cores (comprising 54 layer samples) for Plot 1, and 13 cores (comprising 39 layer samples) for Plot 2.

Each layer sample was dried and sieved, and the < 2 mm fraction analysed using a combination of: (i) mid-infrared (MIR) diffuse reflectance analysis predictions (Forrester *et al.* 2003; Janik *et al.* 1998), and (ii) conventional extractive chemical methods (Rayment and Higginson 1992).

To prepare for the MIR predictions, samples were ground for one minute in a vibrating steel puck mill to attain a particle size of approximately < 100

μm . Predictions were made of the following soil properties: (i) CEC; (ii) clay %; and (iii) CaCO_3 %. Extractive chemical methods (Rayment and Higginson 1992) were used to determine pH (w), $\text{EC}_{1:5}$, and a sub-selection of six L3 samples for ESP once it was revealed that the MIR predictions were unreliable. The electrical conductivity of saturated paste extract (EC_{se}) was predicted using a methodology combining $\text{EC}_{1:5}$ and soil texture (Cass *et al.* 1996). Soil texture was derived from the MIR-predicted clay %, which was used to convert Shaw's (1988) soil texture classes used in the $\text{EC}_{1:5}/\text{EC}_{\text{se}}$ conversion methodology.

6.5 Results

The data acquired from the field investigations are presented in Appendix D and the suite of laboratory χ and physicochemical data are presented in Appendix E.

6.5.1 Field results

The GIS coverages of the plot field surveys are displayed in Figure 6.5, and the data summarised in Table 6.1.

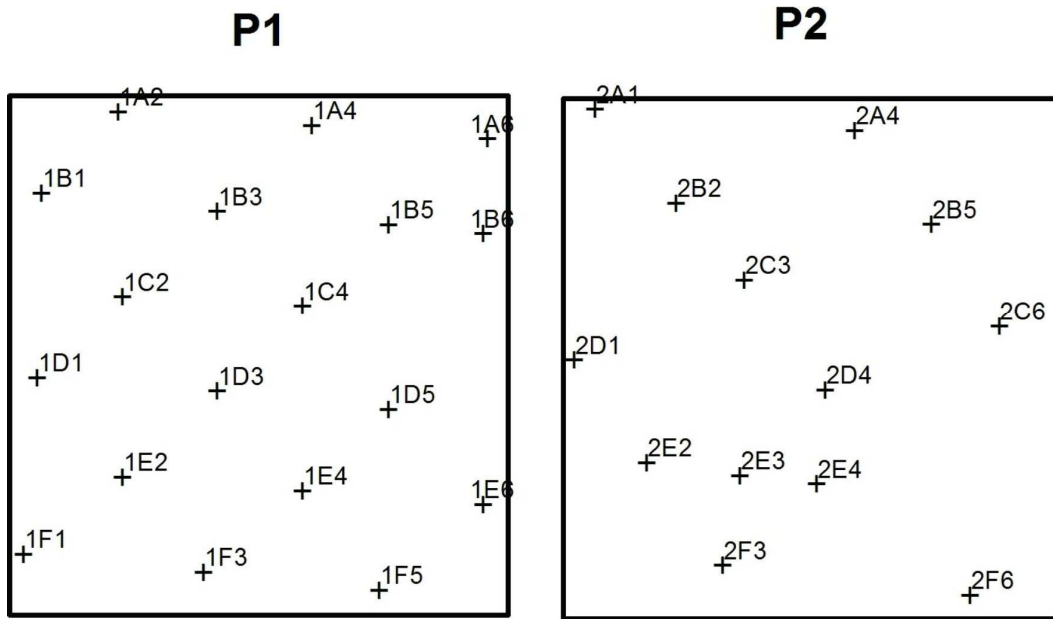


Figure 6.4. Distribution of Plot 1 (18 cores comprising 54 layer samples) and Plot 2 (13 cores comprising 39 later samples) survey point depth section samples used in mid-infrared (MIR) predictions and extractive chemical analyses.

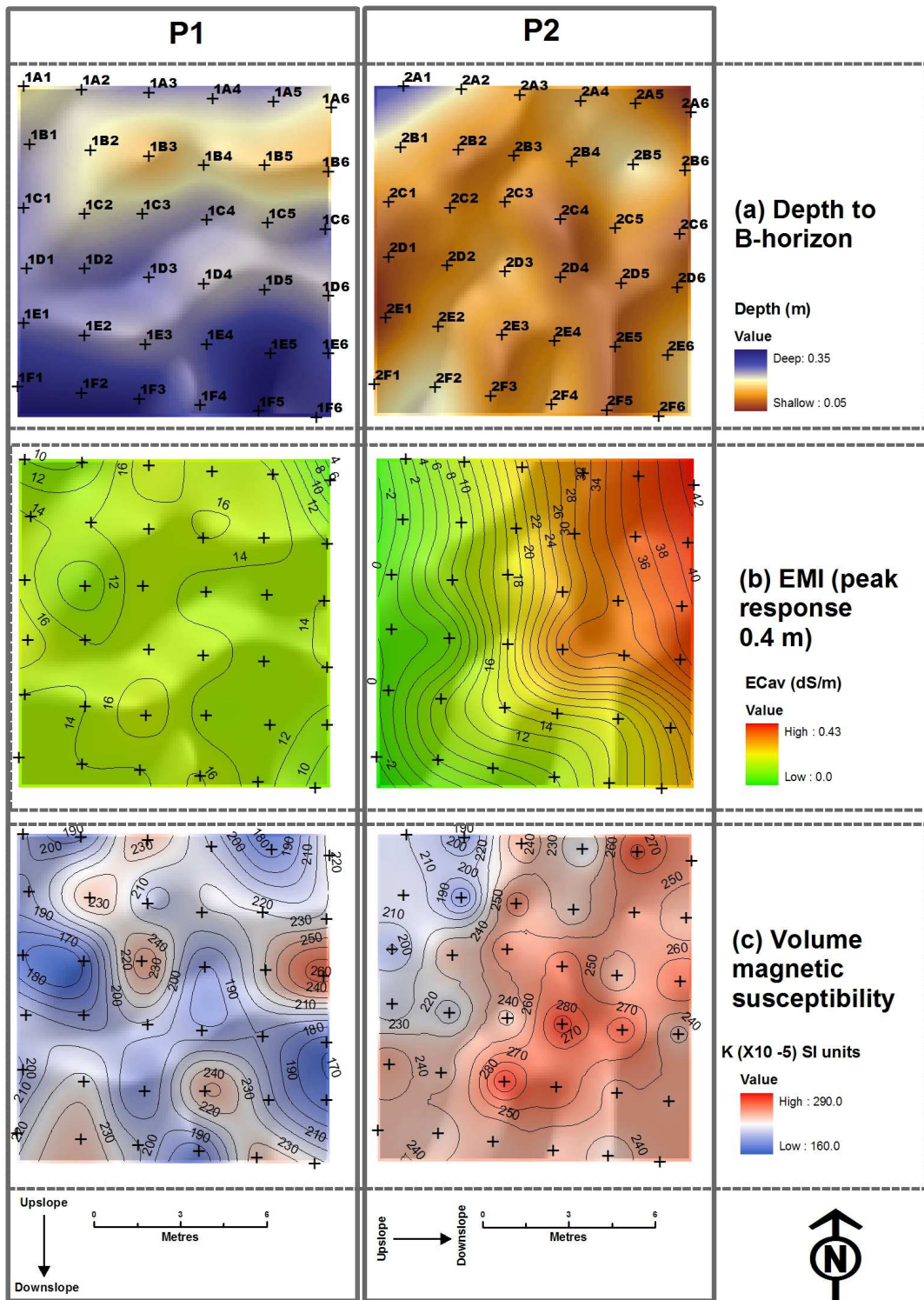


Figure 6.5. GIS plot survey patterns for (a) depth to B horizon; (b) EM38 electromagnetic induction ECav (peak response at 0.4 m); and (c) surface κ . Slope direction is shown for each plot.

Table 6.1. Summary of Plot 1 (18 cores) and Plot 2 (13 cores) field investigations results (complete data presented in Appendix D).

	EC _{av} (mS/m)	EC _{ah} (mS/m)	Depth to B horizon (m)	Surface κ ($\times 10^{-8}$ SI)
Plot 1				
Mean	0.14	0.33	0.24	209.06
Standard deviation	0.02	0.02	0.05	22.87
Range	0.07	0.08	0.19	92.00
Minimum	0.10	0.29	0.16	170.70
Maximum	0.17	0.37	0.35	262.70
Plot 2				
Mean	0.20	0.40	0.13	241.52
Standard deviation	0.13	0.09	0.03	24.70
Range	0.40	0.34	0.12	104.60
Minimum	0.01	0.23	0.08	182.90
Maximum	0.41	0.57	0.20	287.50

Rubbed soil colour and texture

The rubbed dry Plot 1 layers generally have redder hues than the rubbed dry Plot 2 layers, which are more yellow-brown. For example, the core 1C4 is morphologically typical of Plot 1, and has the Munsell colour notation 5YR 4/6 for L1, 5YR 5/4 for L2, and 10R 3/6 for L3. Core 2C6 is morphologically typical of Plot 2. This core has the Munsell colour notation 7.5YR 5/6 in L1, 7.5YR 5/4 in L2, and 5YR 3/4 in L3. All Plot 1 layer hues span the range 5YR - 10R, while Plot 2 layer hues are in the range 7.5YR - 5YR. In both plots the subtle and characteristic reduction in value and chroma between the L1 and L2 layers distinguishes the presence of an EB horizon in each profile, which is mixed with the bulk of the L2 sample.

The textures of the A horizons in each plot were consistently sandy loams, with L2 (featuring the E horizon) often containing fine (< 5 mm) gravels, some of which were magnetic. Magnetic gravels were also often observed on the soil surface of each plot, particularly Plot 2. The B horizons of both plots were dominantly heavy clays, often containing calcrete mottles and weathered chips (< 20 mm) of parent material.

GIS plot patterns

Figure 6.5 shows the interpolated plot GIS coverages showing field survey spatial trends of: (a) depth to B horizon; (b) EC_{av}; and (c) surface κ . Standardised legends were applied for each paired plot survey to assist in visual comparisons. Overlays of pseudo-hillshades derived from depth to B horizon (i.e. the 3D contact shape

of the A and B horizons) have been applied to support visualisation and interpretation of the shape, and to indicate the role that the shape might play in the surveyed property distributions. Contours have been included with the EC_{av} and κ plot GIS coverages to help highlight patterns of distribution.

The depth to B horizon GIS coverages shown in Figure 6.5 for each of the plots indicate the presence of variability over a distance of less than two metres (i.e. significant patterns revealed at the survey interval).

With reference to Plot 1 (Figure 6.5 (a)), the topography of the upper B horizon surface is “wavy” in the notation of Schoeneberger *et al.* (2002), and features two distinct ridges that are oriented east-west, and are tangential to the prevailing ground surface slope. The up slope ridge crest is closer to the surface than the second down slope ridge. The average depth to the B horizon of Plot 1 is 0.24 m, with a B horizon depth range of 0.15 - 0.24 m.

With reference to Plot 2 (Figure 6.5 (a)), the topography of the upper B horizon boundary is also “wavy”. However, the B horizon surface shape is more complex and it exhibits a more haphazard arrangement of undulations that show no strong relationship to prevailing slope. On average the Plot 2

A horizon is shallower (mean: 0.13 m), and the B horizon depth range is wider (0.05 - 0.30 m).

Figure 6.5 (b) shows the EC_{av} (peak soil electrical conductivity at ~ 0.4 m) plot patterns. These show that Plot 1 (EC_a range: 0.03 – 0.17 dS/m; mean: 0.14 dS/m; SD: 0.16 dS/m) shows consistently lower EC_a values compared to P 2 (EC_a range: 0.0 – 0.43 dS/m; mean: 0.19 dS/m; SD: 0.12 dS/m). Little spatial variability is apparent in Plot 1, while Plot 2 shows a strong pattern of increasing EC_a towards the northeast.

Figure 6.5 (c) shows the surface κ plot patterns. The Plot 2 κ values (range: 183.0 – 290 $\times 10^{-8}$ SI; mean: 243 $\times 10^{-8}$ SI; SD: 17.9 $\times 10^{-8}$ SI) trend higher than those of Plot 1 (range: 160 – 263 $\times 10^{-8}$ SI; mean: 209 $\times 10^{-8}$ SI; SD: 18.3 $\times 10^{-8}$ SI). Plot 2 shows strong trend of increasing κ from the northwest to southeast region with a peak towards the central region of the plot, while Plot 1 shows a strong pattern of nucleated high values distributed around the plot. In both cases κ meso-variability (i.e. significant variability in values within a distance of two metres) is evident in the plots.

6.5.2 Laboratory results

The laboratory data are summarised in Table 6.2.

Table 6.2. Summary of plot physicochemical data.

	χ_f (x 10 ⁻⁸ SI)	X _{fd} %	CEC	Clay %	EC _{se} (dS/m)	pH (w)	CaCO ₃ %
Plot 1, L1							
Mean	840.62	8.06	10.10	25.51	0.62	6.88	0.79
Standard Deviation	67.29	0.73	1.36	1.83	0.13	0.17	0.11
Range	287.40	2.96	4.43	7.34	0.42	0.64	0.43
Minimum	646.30	6.42	8.34	22.02	0.45	6.60	0.64
Maximum	933.70	9.38	12.76	29.35	0.87	7.24	1.07
Plot 1, L2							
Mean	856.22	7.45	7.90	25.18	0.49	7.74	0.68
Standard Deviation	149.16	0.67	1.37	2.26	0.11	0.12	0.06
Range	680.10	2.37	5.69	9.46	0.42	0.37	0.25
Minimum	372.90	6.72	6.21	21.82	0.37	7.61	0.56
Maximum	1053.00	9.09	11.90	31.29	0.80	7.98	0.81
Plot 1, L3							
Mean	987.42	13.11	28.53	54.49	0.58	7.98	1.16
Standard Deviation	87.64	1.26	6.87	7.20	0.10	0.11	0.34
Range	324.00	4.19	23.25	22.52	0.44	0.38	1.18
Minimum	849.00	10.88	17.12	42.43	0.40	7.78	0.57
Maximum	1173.00	15.07	40.38	64.95	0.84	8.16	1.75

	χ_f (x 10 ⁻⁸ SI)	X _{fd} %	CEC	Clay %	EC _{se} (dS/m)	pH (w)	CaCO ₃ %
Mean for Plot	894.75	9.54	15.51	35.06	0.56	7.54	0.88
Plot 2, L1							
Mean	765.88	6.98	7.17	18.04	1.07	6.70	0.63
Standard Deviation	69.36	0.46	0.91	1.87	0.25	0.21	0.12
Range	240.40	1.42	3.22	5.59	0.82	0.66	0.35
Minimum	680.70	6.34	5.86	14.50	0.67	6.35	0.40
Maximum	921.10	7.76	9.09	20.08	1.49	7.01	0.75
Plot 2, L2							
Mean	776.40	8.08	8.12	22.90	0.66	7.05	0.56
Standard Deviation	88.82	1.24	1.21	3.29	0.12	0.21	0.05
Range	301.00	4.62	4.70	12.93	0.38	0.67	0.21
Minimum	642.00	6.61	6.31	16.94	0.49	6.75	0.41
Maximum	943.00	11.23	11.01	29.86	0.87	7.42	0.62
Plot 2, L3							
Mean	859.15	13.08	27.97	52.33	0.64	7.67	1.10
Standard Deviation	72.64	2.17	9.89	13.26	0.22	0.30	0.40
Range	265.70	7.42	31.82	45.81	0.56	1.10	1.15
Minimum	677.80	7.97	7.06	20.16	0.34	6.92	0.52
Maximum	943.50	15.39	38.89	65.97	0.90	8.02	1.67
Mean for Plot	800.48	9.38	14.42	31.09	0.79	7.14	0.76

Low frequency mass magnetic susceptibility (χ_{lf})

As discussed in Chapter 3, the χ_{lf} measurement is standard for reporting the χ parameter in soils. Plot χ_{lf} results for each layer are presented in Figure 6.6, and summarised in. Although not shown here, the χ_{lf} and χ_{hf} values correlate (Plot 1: $r^2 = 0.94$; Plot 2 $r^2 = 0.89$). Table 6.2 also shows that the

mean Plot 1 χ_{hf} value of $894 \times 10^{-8} \text{ m}^3/\text{kg}$ is marginally higher than that of Plot 2, which is $800 \times 10^{-8} \text{ m}^3/\text{kg}$. Both plots demonstrate a trend of increasing core layer χ_{lf} values down the profiles, and small but abrupt increase in these values in L3 is evident in the data and graphs.

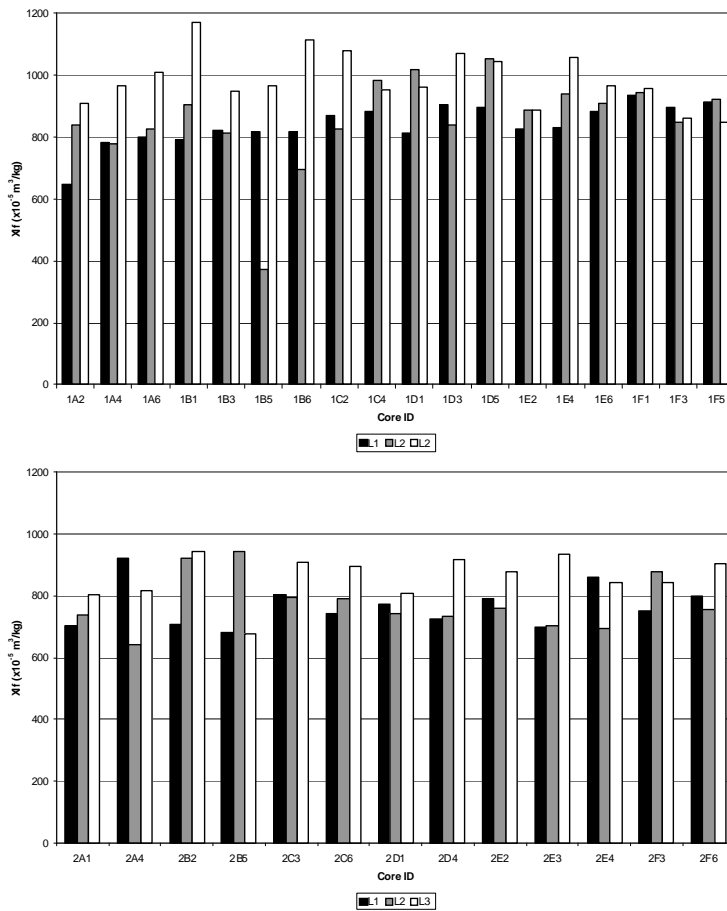


Figure 6.6. Low frequency mass magnetic susceptibility results per layer for Plot 1 (above) and Plot 2 (below). Black bars represent L1 samples, grey bars, L2 samples, and white bars, L3 samples.

Frequency dependency ($\chi_{fd}\%$)

As discussed in Chapter 3, the measure of $\chi_{fd}\%$ indicates the χ contribution of ultra-fine ($\sim < 0.03 \mu\text{m}$) superparamagnetic, pedogenically derived ferrimagnetic grains in the sample. The $\chi_{fd}\%$ results for the layers are presented in Figure 6.7 and summarised in Table 6.2. The summary data shows the mean values

for the plots to be alike (Plot 1: 9.54 %; Plot 2: 9.38 %). However, small differences in the L1 (Plot 1: 8.06 %; Plot 2: 6.98 %) and L2 (Plot 1: 7.45 %; Plot 2: 8.08 %) values are evident, while L3 values similar (Plot 1: 13.11 %; Plot 2: 13.08 %). The down-profile results for the plots show a strong trend of an almost-doubling of B horizon (L3) values compared to the A horizon (i.e. L1 and L2 combined).

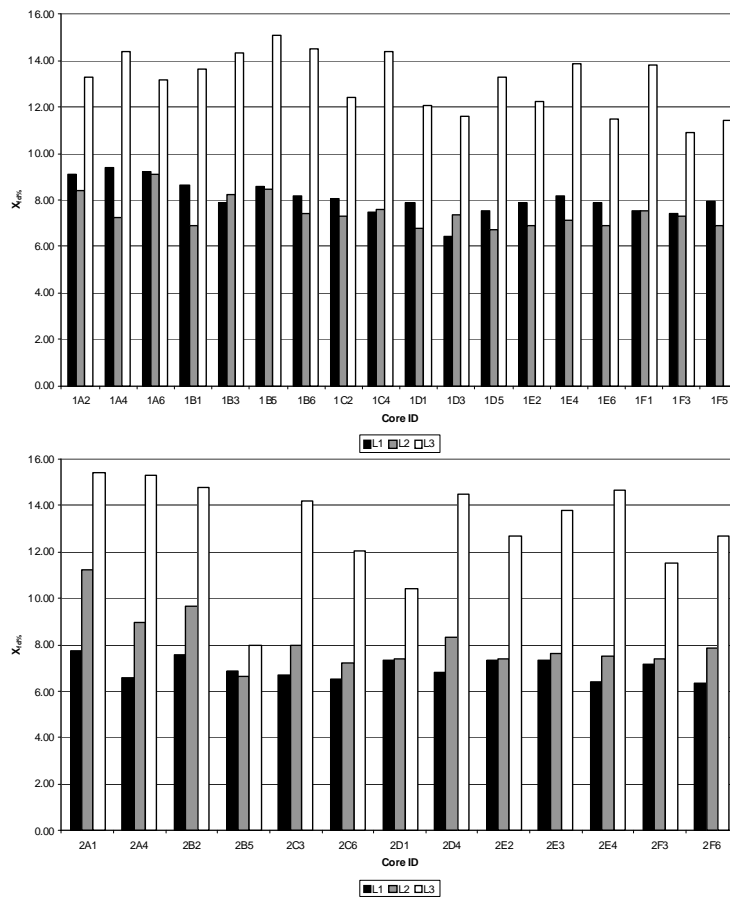


Figure 6.7. Frequency dependency results per layer for Plot 1 (above) and Plot 2 (below). Black bars represent L1 samples, grey bars, L2 samples, and white bars, L3 samples.

Cation exchange capacity

The plot CEC results for each layer are presented in Figure 6.8, and summarised in Table 6.2. There exists a very strong trend of high CEC values in the B horizon compared to those in the A horizon layers (L1 and L2) of both plots. In both plots this increase

is almost a factor of four. When the plots are compared, the mean layer values are similar; L1 values for Plot 1 and Plot 2 are 10.10 and 7.17 respectively, L2 values for Plot 1 and Plot 2 are 7.90 and 8.12 respectively, and finally, L3 values for Plot 1 and Plot 2 are 28.53 and 27.97 respectively. Consequently, the mean plot values are similar (Plot 1: 15.51; Plot 2 : 14.42).

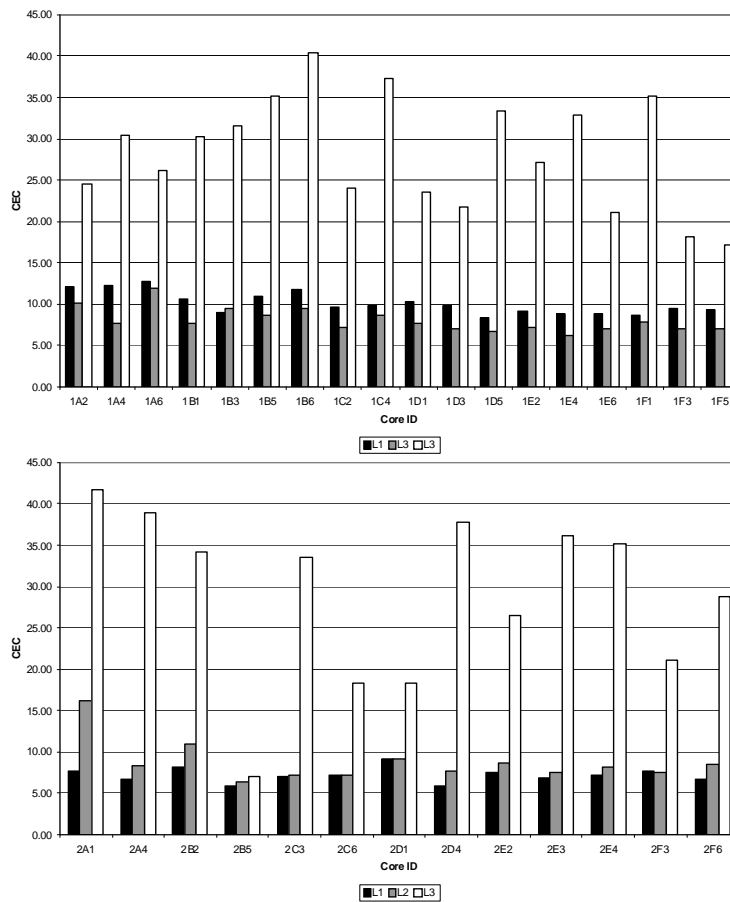


Figure 6.8. Cation exchange capacity results per layer for Plot 1 (above) and Plot 2 (below). Black bars represent L1 samples, grey bars, L2 samples, and white bars, L3 samples.

Soil texture

The plot clay % results for each layer are presented in Figure 6.9, and summarised in Table 6.2. The down-profile trends in clay % in the cores from both plots are similar and strong. In both cases the A horizons (L1 and L2) show clay % values of almost half those of the B horizon. In Plot 1, L1 and L2 show similar values (25.5 %

and 25.2 % respectively) and L3 shows a value of 45.5 %. Plot 2 shows a discernable difference in mean values for L1 (18.04 %) compared to L2 (22.9 %), and 52.3 % for L3. Mean plot values show slight differences (Plot 1: 35.1 %; Plot 2 : 31.1 %). Both plots show significant ranges in their L3 values (Plot 1: 22.5 %; Plot 2 : 45.8%), which are not matched in the other layers.

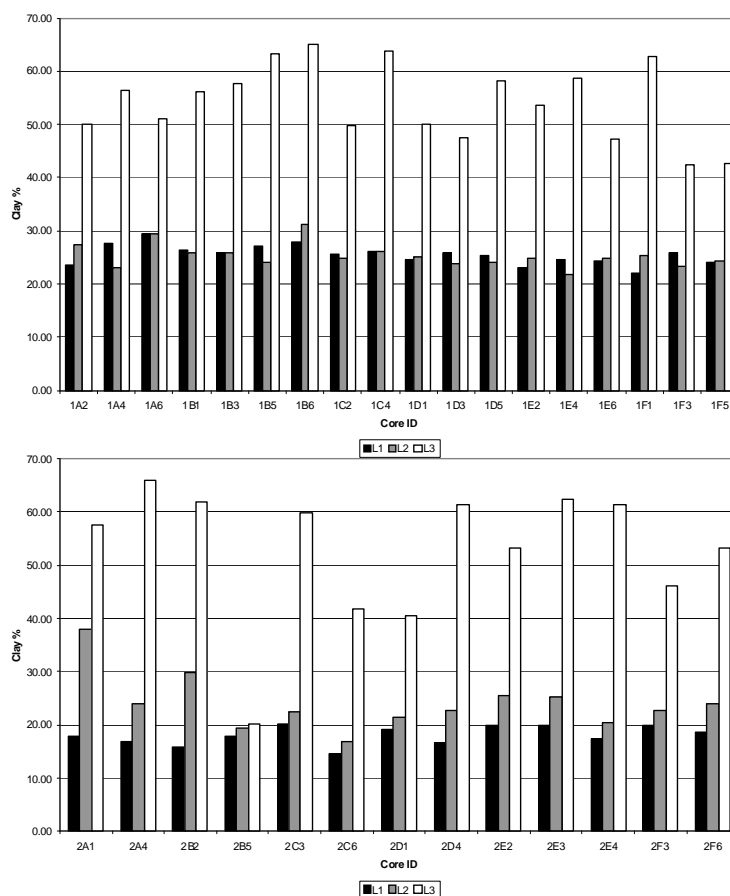


Figure 6.9. Soil texture results per layer for Plot 1 (above) and Plot 2 (below). Black bars represent L1 samples, grey bars, L2 samples, and white bars, L3 samples.

Saturation extract electrical conductivity (EC_{se})

The plot EC_{se} results for each layer are presented in Figure 6.10, and summarised in Table 6.2. This Table shows that Plot 2 (plot mean EC_{se} : 0.79 dS/m) is more saline than Plot 1 (plot mean EC_{se} : 0.56 dS/m), and that in both plots salinity values tend to peak in the upper A horizon (L1). In the case

of Plot 1, L3 (mean EC_{se} : 0.58 dS/m) is more saline than L2 (mean EC_{se} : 0.49 dS/m), whereas for Plot 2, both layers have very similar salinity values (L2 mean EC_{se} : 0.66 dS/m; L3 mean EC_{se} : 0.64 dS/m). Reference to Figure 6.10 shows that the salinity intra-core values tend to be similar in Plot 1, whereas in Plot 2 there is a trend of highest salinity values in the upper A horizon (L1), and progressive reduction in salinity values with depth.

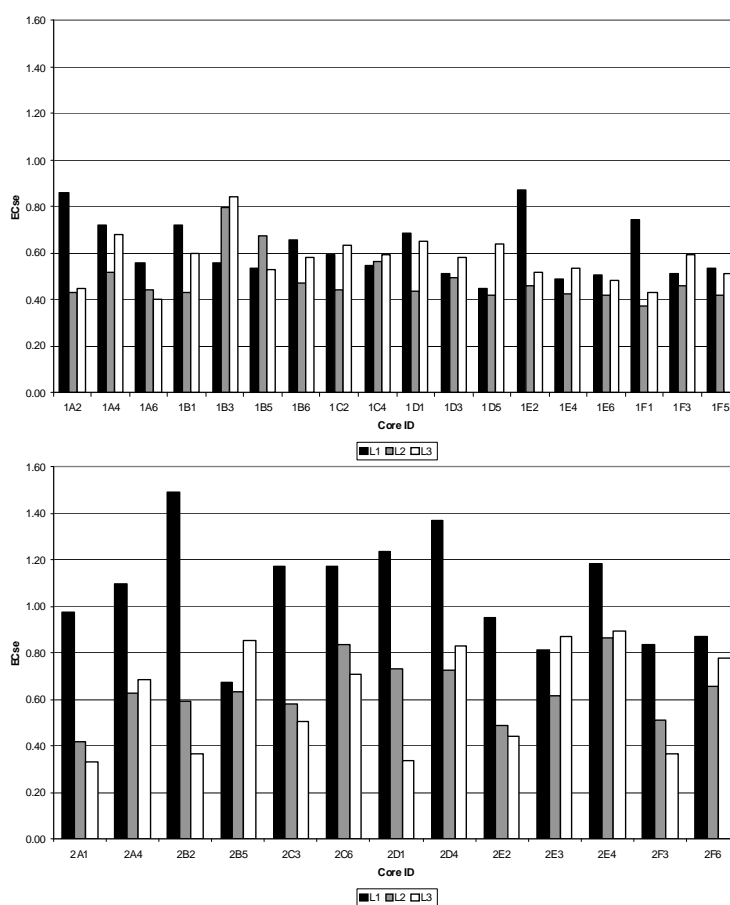


Figure 6.10. Saturation extract electrical conductivity results per layer for Plot 1 (above) and Plot 2 (below). Black bars represent L1 samples, grey bars, L2 samples, and white bars, L3 samples.

pH (w)

The plot pH (w) results for each layer are presented in Figure 6.11, and summarised in Table 6.2. In both plot

cases there is a strong trend in the layers visible of increasing alkalinity with depth (Plot 1, L1: pH 6.88; Plot 1, L2: pH 7.74; Plot 1, L3: pH 7.98; Plot 2 , L1: pH 6.70; Plot 2 , L2: pH 7.05; Plot 2 , L3: pH 7.67).

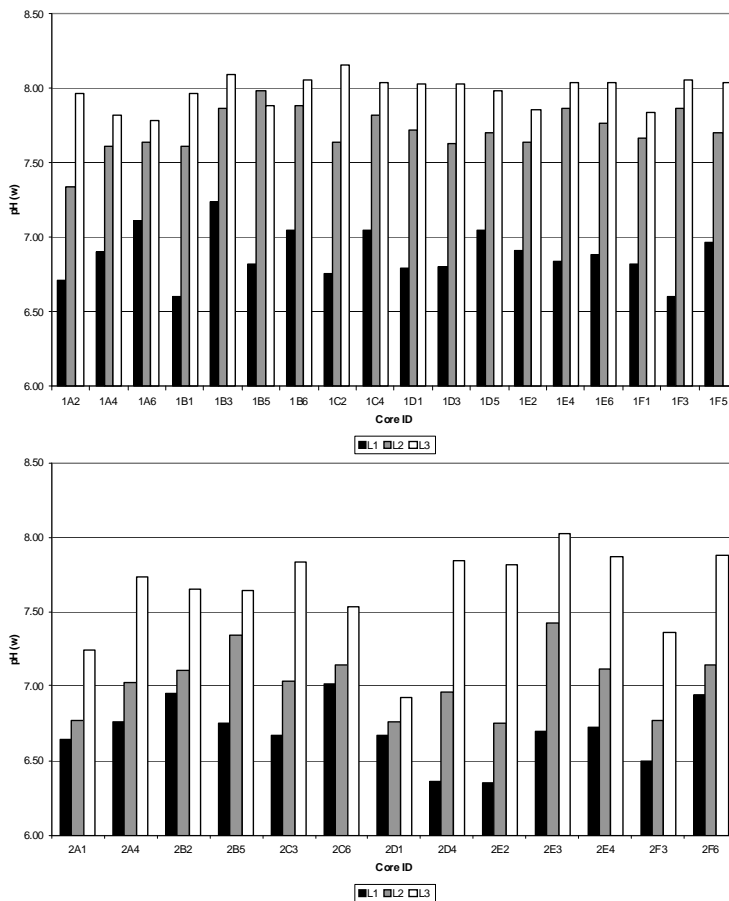


Figure 6.11, pH (w) results per layer for Plot 1 (above) and Plot 2 (below). Black bars represent L1 samples, grey bars, L2 samples, and white bars, L3 samples.

Calcium carbonate

The plot CaCO_3 % results for each layer are presented in Figure 6.12, and summarised in Table 6.2. Overall, Plot 1 has a higher CaCO_3 content (mean for plot: 0.88 %) compared to Plot 2 (mean for plot: 0.76 %). Both plots show a trend of mean CaCO_3 % values that reduce from L1 (Plot 1: 0.79 %; Plot 2 : 0.63 %) to L2 (Plot 1: 0.68 %; Plot 2 : 0.56 %), then increase in L3 (Plot 1: 1.16 %; Plot 2 : 1.10 %). The

summarised data for both plots in shows that L3 values are significantly higher than the L1 ones. The absolute accuracy of calcium carbonate results are drawn into focus, however, particularly given the values plot L1 values, which are slightly acidic (see previous Section). If in error, this is attributed to the quality of calibration data used in the MIR predictions. However, it is anticipated that the calcium carbonate layer trends are correct, and hence informative.

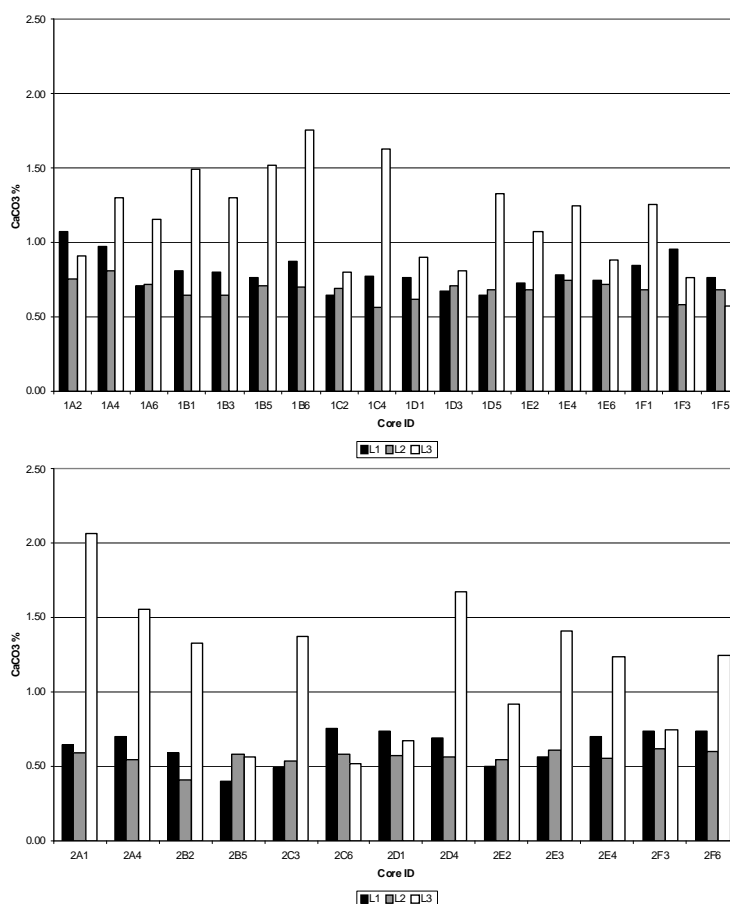


Figure 6.12. Calcium carbonate results per layer for Plot 1 (above) and Plot 2 (below). Black bars represent L1 samples, grey bars, L2 samples, and white bars, L3 samples.

Exchangeable sodium percentage

As discussed earlier, it was revealed that the MIR predictions for ESP appeared to be unreliable due to an inconsistent pattern of results. As a fall-back, and with limited resources available, a selection of three L3 (upper B horizon samples) were selected from each plot for analysis by extractive means (Rayment and Higginson 1992), and the results presented in Table 6.3.

Table 6.3. Results of ESP analysis for a selection of L3 (upper B horizon) samples.

L3 core sample	ESP (%)
1B 6	15
1D 5	18
1A 6	8.3
2E 3	15
2D 4	16
2D 1	1.0

Apart from the result from the sample 2D₁, all of the results shown in Table 6.3 indicate the upper B horizon soils are strongly sodic, and provides a reliable indication that the B horizon soils in each plot are also likely to be moderately to strongly sodic.

6.6 Discussion and conclusions

6.6.1 Plot interpretations

Both plots are located in paddocks actively managed under mixed farming systems. This has important implications for the interpretation of profile data, principally taking into account: (i) soil layer mixing by periodic cultivation (soil mixing) giving rise to an Ap horizon, and (ii) the application of soil conditioners like gypsum and fertilisers. These effects are highlighted in the Figure 6.14 and Figure 6.15 scatter plots in which

certain Ap horizon property combinations feature poor correlations (i.e. “buckshot” scatter), whereas the same combinations in the B horizon show strong correlations via linear data spreads. These data are interpreted to show that the B horizons are generally below the depth of cultivation, leaving the structure of the B horizons ostensibly intact and in a state of near-physico chemical equilibrium. In contrast, the Ap horizon soils exist in a state of near-flux due to pedoturbation and/or variable stages of downward leaching of soil conditioners. For this reason it is sometimes difficult to distinguish between the inherent depth variability of the A horizon soils from the overprint that is management and cultivation-induced.

Positive correlation relationships between clay % and CEC shown in the data from both plots (Figure 6.14 and Figure 6.15). The mean CEC values (range for both plots: 7 - 30 cmol(+)/kg) from Table 6.2. Such values are consistent with soils dominated by the chlorite mineralogy (Goldberg and Suarez 2000b; Rengasamy and Churchman 1999), which links with the findings described in Chapter 7.

The profile soil texture distributions of both plots (Table 6.2, Figure 6.9) show increasing soil texture between the A (sandy loams) and B horizons (heavy clays), which is a key diagnostic feature of texture-contrast soils (Hubble *et al.* 1983; Northcote 1992). The E horizon often found in texture-contrast soils are also evident in the plot soils. The data presented in Table 6.3 indicate the subsoils of the plots to be sodic (Sumner 1993), and hence be classified as a sodic Btn horizon. Sodic structural decline in the Btn horizon of duplex soils results in: (i) reduced hydraulic conductivity in the B horizon and the potential for seasonal water perching in the A horizon (Greacen and Williams 1983), and (ii) physically

hostile conditions for plant root development (Rengasamy 2002b).

The morphological and profile data provide evidence of a Btn horizon throughout both plots. This horizon impairs the downward infiltration of soil water to result in periodic A horizon waterlogging. Evidence for this includes:

- presence of an EB horizon that channels water infiltrated through permeable surface layers and collected from up slope areas laterally over the slightly pervious Btn horizon;
- CaCO₃ accumulation in the B horizon;
- magnetic susceptibility enhancement in profiles; and
- soil colour.

Calcite is a soluble mineral in soils under suitable pH and CO₂ partial pressure conditions (Chadwick and Graham 2000). Once in solution, calcite is readily leached through the soil profile on the seasonal wetting front. Over many years, especially in low rainfall zones, the mineral becomes concentrated in the profile where seasonal downward progress of the wetting front is arrested, e.g. in the less permeable Btn horizon. Where this occurs, secondary calcite is precipitated (appearing as white powdery mottles in the soil matrix) through seasonal de-watering via surface evaporation and/or plant root extraction (Chadwick and Graham 2000). The data from Table 6.2 and Figure 6.12 confirms that calcite is concentrated in the Btn horizons (Plot 1 CaCO₃ %: 1.16; Plot 2 CaCO₃ %: 1.10), indicating the existence of a significant permeability transition between the A and B horizon. Fine grained secondary calcite precipitated in the soil matrix acts to further reduce permeability in the profile.

The χ data range encountered in the study area are enhanced compared to a

selection of environmental conditions, shown in Figure 6.13. The bulk χ responses of the samples (< 2 mm) are dominated by pedogenic maghemite due to the removal by sieving of the > 2 mm detrital magnetite grains of weathered rock origin (Mullins 1977; Thompson and Oldfield 1986). Table 6.2 indicates a general trend of down-profile magnetic enhancement (χ_{lf}) in the < 2 mm fraction in both plots, while the overall χ contribution from ultra-fine ($\sim < 0.03 \mu\text{m}$) superparamagnetic grains is significantly greater in the B horizon of each plot from the χ_{lf} data. However, that χ enhancement in the B horizons relative to the A horizons is not strong in each plot (Figure 6.6) indicates that the overall χ contribution from ultra-fine superparamagnetic grains is not strong. A degree of layer mixing via pedoturbation has taken place from evidence of the χ_{lf} profile trends shown in Figure 6.6. Historic firing (e.g. Mullins 1977) is likely to have contributed to the high levels of magnetic activity of these soils with reference to Dearing's (1999b) collation of environmental χ_{lf} ranges. With reference to the data trends presented in Figure 6.6 and Figure 6.7, magnetic susceptibility depletion of pedogenic ultra-fine superparamagnetic grains of maghemite in the A horizon in comparison to the B horizon is attributed to historic patterns of waterlogging through water perching in the A horizon. The large surface area/volume ratio of such fine grains confers a vulnerability to dissolving - even under moderate waterlogging/reducing conditions.

Munsell colours of the rubbed dry soils were in the ranges 10R – 5YR (Plot 1) and 5 – 7.5YR (Plot 2). Soil colours are strongly related to the occurrence of specific or mixtures of mineral Fe-oxides, and are powerful field indicators of prevailing soil conditions

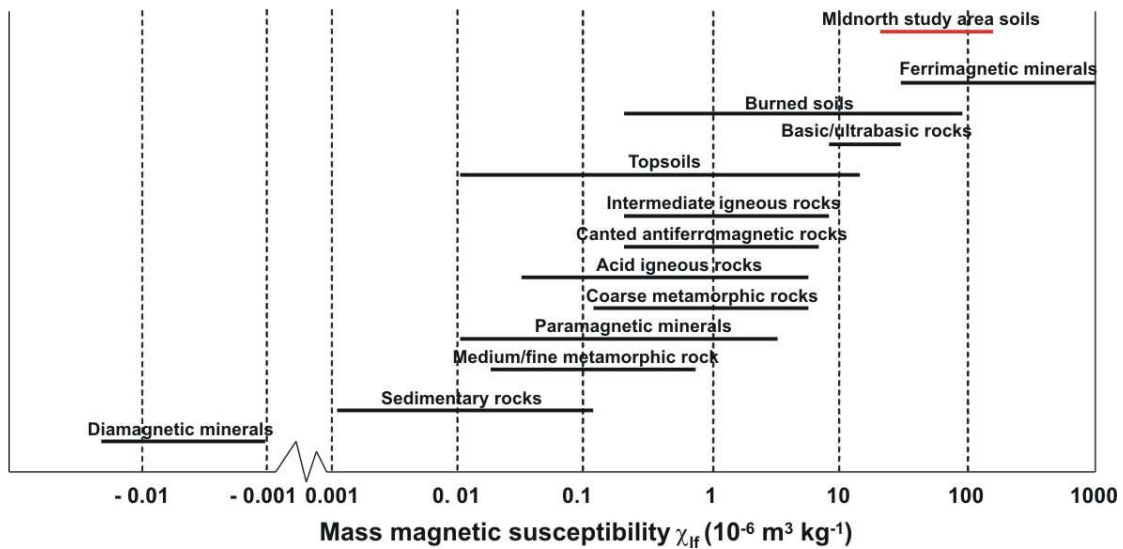


Figure 6.13. Mass magnetic susceptibility (χ) range for the Midnorth study area profiles compared to a selection of other environmental ranges (modified after Dearing 1999b).

(Bingham and Ciolkosz 1993; Richardson and Daniels 1993). The redder soil colours associated with Plot 1 (10R – 5YR) indicate an abundance of hematite, whereas the more yellow colour range of Plot 2 (5 – 7.5YR) is consistent with a higher goethite content (Schwertmann 1993). Hematite (Plot 1) is more associated with freer draining and oxidising soil conditions, while goethite (Plot 2) prevails in less free draining and more reducing conditions. The differences in the rubbed dry soil colours therefore indicate that Plot 1 is more freely draining than Plot 2, a finding also consistent with a comparison of plot EC_{se} values, which are lower in Plot 1 discussed in Section 6.5.2 above.

6.6.2 Plot spatial variabilities

Both plots show fine scale (i.e. < 2 m) spatial variability in a number of properties, with the most striking being the depth to B horizon of both plots though the strong and consistent patterns of Btn horizon undulations (Figure 6.5 (a)). Similarly, non-random patterns in EC_{av} (Figure 6.5(b)) and surface κ (Figure 6.5 (c)) in both plots have been detected. Given the role the movement of water and solute over soil layers have in the

spatial distribution of soil properties, a stronger relationship between depth to B horizon and the observed soil properties in Figure 6.14 and Figure 6.15 was expected, as B horizon form acts to channel throughflow. For example, coherent correlation patterns with soil properties governed by soluble soil chemistry, e.g. $CaCO_3$ %, pH, EC_{se} and ESP were expected. Explanations based on geomorphology and whole-of-landscape processes will be presented for the distribution of salinity at the landscape scale in Chapters 7 and 8.

As both $CaCO_3$ % and $\chi_{fd\%}$ are hydromorphically-derived soil properties, it is not surprising that these properties correlate in Plot 1 ($r^2 = 0.68$) (Figure 6.14) and Plot 2 ($r^2 = 0.68$) (Figure 6.15). In turn, the same properties also correlate with clay %, a key soil property of which spatial and depth distributions determine water and solute movement patterns in soils, and pedogenic accumulation of $CaCO_3$ % and ultra fine superparamagnetic grains ($\chi_{fd\%}$). For example, the Plot 1 and Plot 2 $CaCO_3$ %/clay % correlations are $r^2 = 0.68$ and $r^2 = 0.68$ respectively, while Plot 1 and Plot 2 the $\chi_{fd\%}$ /clay % correlations are $r^2 = 0.94$ and $r^2 = 0.97$, respectively.

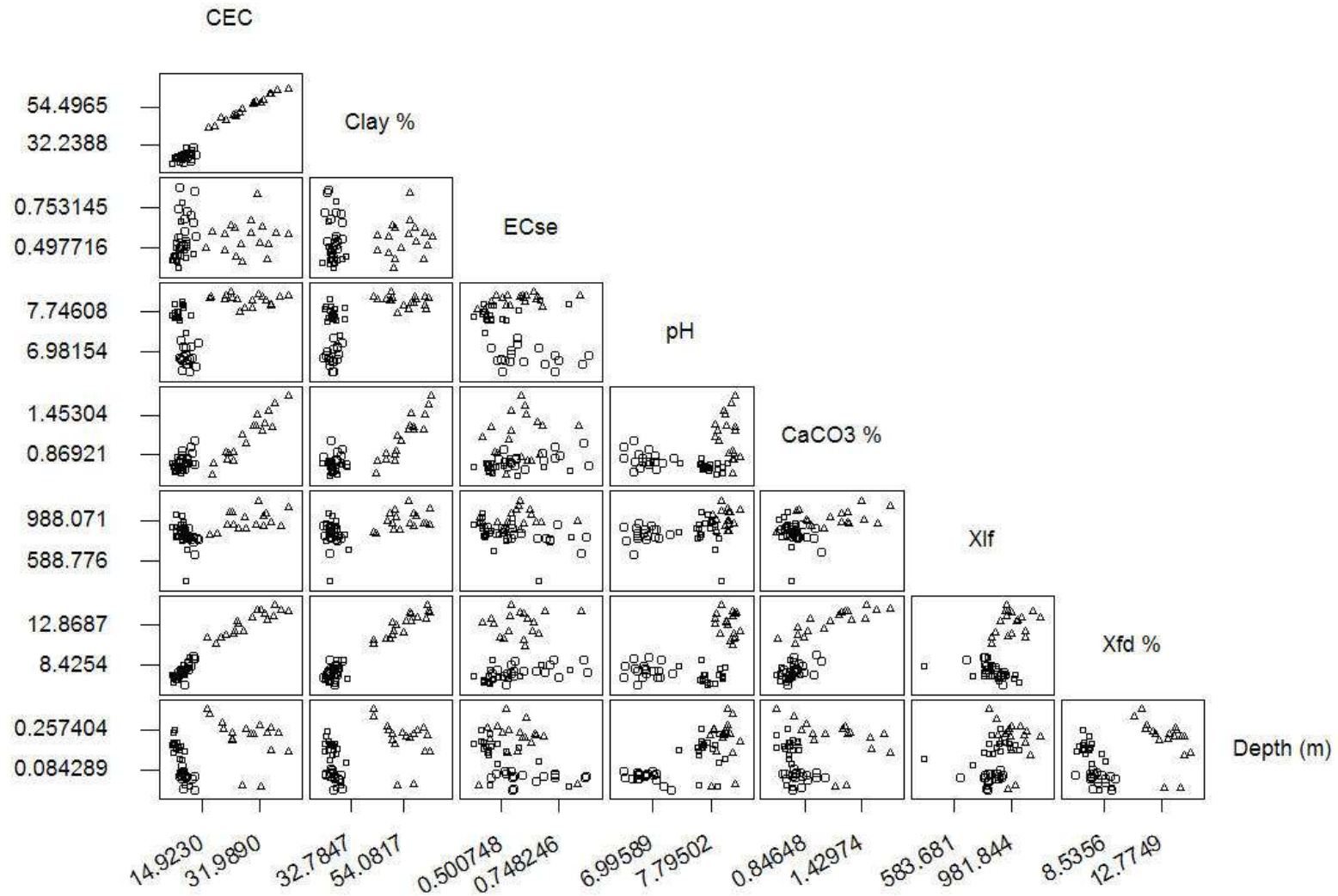


Figure 6.14. Relationships between soil properties (CEC, clay %, EC_{se} , pH, $CaCO_3$ %, χ_{lf} , χ_{fd} % and soil depth) for Plot 1. Layers have been differentiated (L1: O; L2: □; and L3 △).

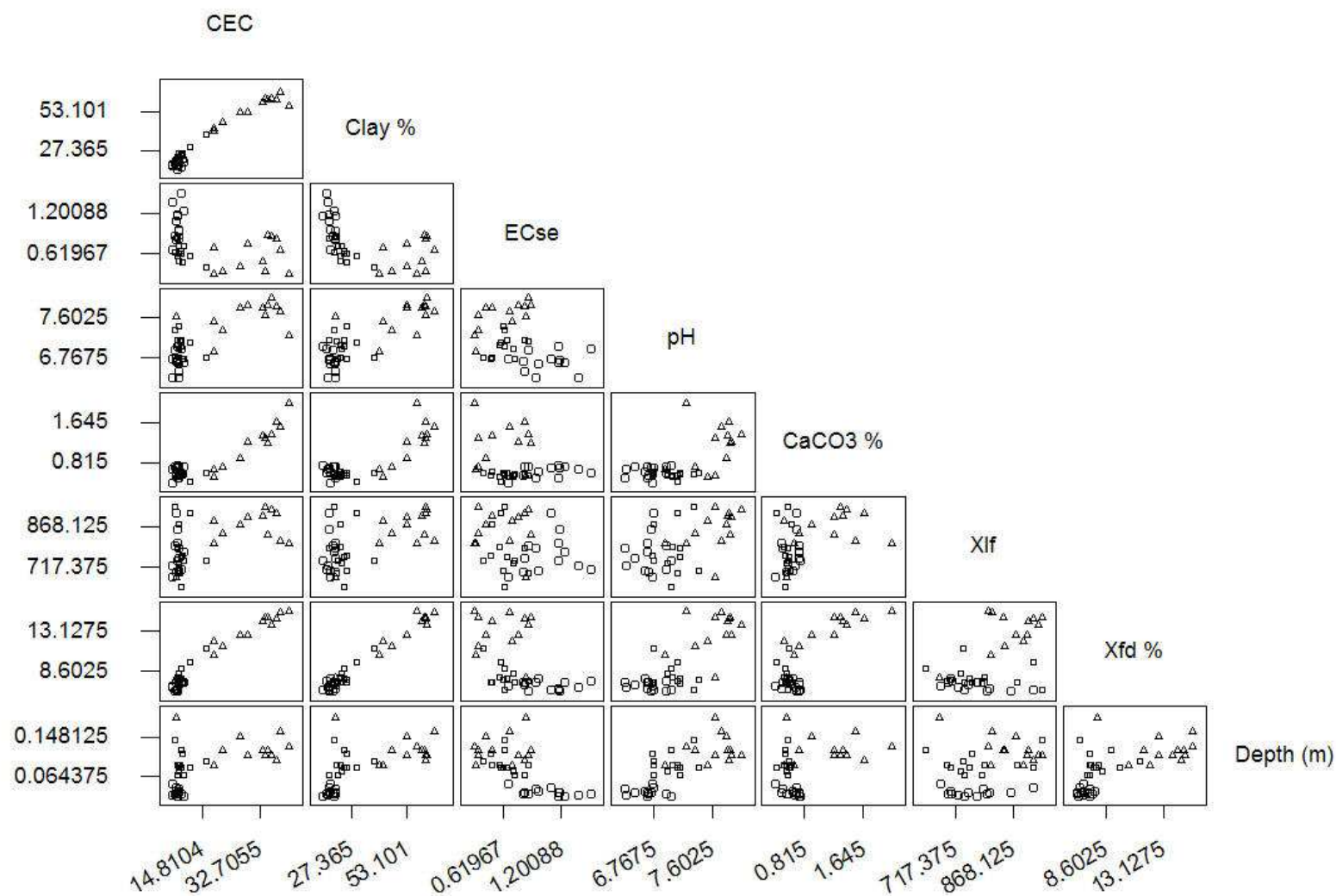


Figure 6.15. Relationships between soil properties (CEC, clay %, ESP, EC_{se}, pH, CaCO₃ %, χ_{if} , χ_{fd} and soil depth) for Plot 2. Layers have been differentiated (L1: O; L2: □; and L3 △).10 by 10 m conceptual mechanistic process models

The data for each plot presented in Table 6.2 and Figure 6.10 indicate that the salinity levels are generally low, and, on their own, are unlikely to cause problems for crop yields (Soil Survey Division Staff 1993; Steppuhn *et al.* 2003). Plot 2 has an average salinity of EC_{se} 0.79 dS/m, which is higher than the average of Plot 1 (EC_{se} 0.56 dS/m). Given the prevalence of similar pedogenic (e.g. parent material) and environmental (e.g. rainfall) conditions at the plot sites by virtue of their proximity, these differences are explained through geomorphic setting, and its influence on solute movement in the landscape. As has been discussed previously, Plot 1 is located on a slope angle of 6 ° and lies in a concave linear landform. Plot 2 is located on a 3 ° slope angle and in a convex (plan and profile) landform shown in Figure 6.1. The combination of local landform, slope angle and soil morphology enables pedogenic interpretation and the development of descriptive conceptual models that explain the different salinity levels of each plot.

In Plot 1, with generally lower salinity levels, the Btn horizon has low hydraulic permeability. During periods of maximum seasonal soil wetness, the Btn horizon focuses subsurface soil water throughflow laterally and down slope through the EB horizon. The combination of a higher-angle slope and the concave linear landform signifies relatively unimpaired down slope soil water movement, which flushes salts down slope and out of the system.

The convexity (plan and profile) of Plot 2 results in a dispersed pattern of soil

water flows (Hall and Olson 1991; Wilding 2000). This combined with lower-angle slope results in lower rates of A horizon flushing, and higher salt concentrations left *in situ*. The hydraulic conditions necessary for this are confirmed by the soil colours in Plot 2, which indicate periodic waterlogging by the dominance of goethitic soil colours in the profile. Therefore, Plot 2 occupies a “perched” landform, and in a landscape position that is bypassed by any significant up slope subsoil flushing, which results in the accumulation of salts. The identification of these hillslope drainage patterns feature in the discussion of medium (toposequence scale) hillslope processes presented in Chapter 7.

Local landform and morphological differences also explain the differences in Ap horizon depths of the two plots. As discussed, Plot 1 is located in a backslope position occupying a concave linear landform on a slope angle of 6 °. This landscape context indicates a colluvial zone in which the rate of up slope matter deposition exceeds the rate of removal by erosion. In this manner periodic up slope surface wash events add to the Ap horizon depth. Plot 2, however, being located on a “perched” landform, experiences rates of deposition and erosion that are either in balance or slightly dominated by erosion, hence the relatively shallower A horizons.

The descriptive conceptual models for each of the plots are presented Figure 6.16. These highlight the influence of landform and morphological differences in the processes that are taking place in the plot soils.

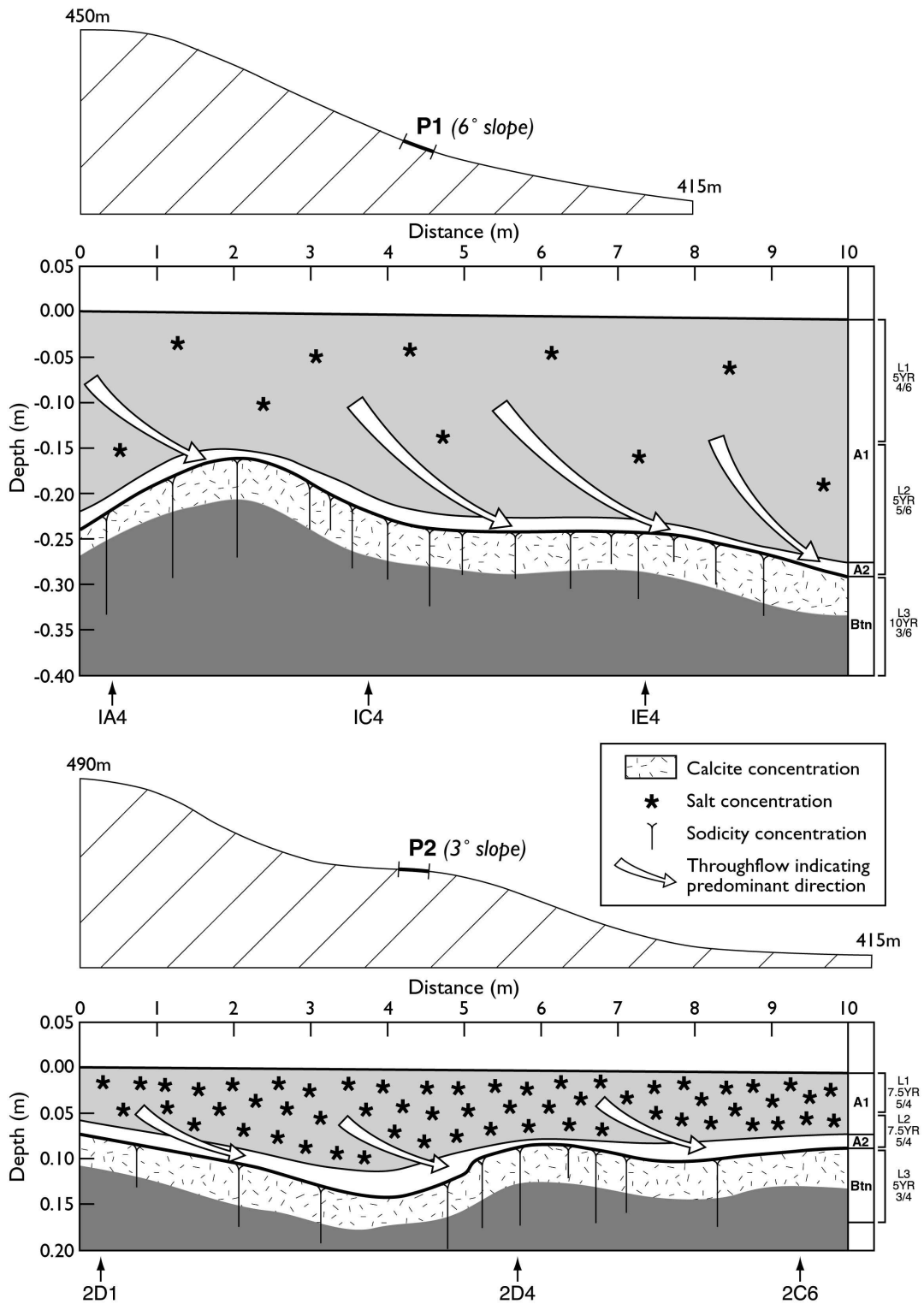


Figure 6.16. Conceptual hydropedologically-based mechanistic processes models for Plot 1 and Plot 2, showing: (i) layer depths (with positions of reference cores) and shapes (from interpolated coverages), (ii) predominant throughflow direction and strength, (iii) relative calcite, salinity and sodicity distributions, (iv) typical layers, and (v) sketched plot hillslope positions. Note the different horizontal and vertical scales.

Given the over all similarities in physicochemical composition of both soils, the variations in crop yields between Plots 1 and 2 are principally caused by differences in A horizon depths. This is compounded by the increased salt concentrations in Plot 2. The A horizon depth is a critical resource of these soils due to the presence of the Btn horizon that acts as a physical barrier to crop root

exploration (and significant surface recharge). This means that the bulk of soil moisture required for crop development can only be accessed from the A horizon as Btn horizon water stores are effectively unavailable to the developing crop. A shallow Ap horizon therefore results in a restricted reservoir of water available to the crop that may deplete before full crop potential is realised.

Chapter 7. Midnorth medium scale investigation

This Chapter discusses the interpretation of spatially detailed, medium scale geophysical, morphological and physicochemical investigations of the hillslope that comprises the Midnorth study area. With reference to the discussion regarding soil system scales presented in Chapter 4, the investigations discussed are most consistent with the toposequence soil system scale (i.e. $i+2$) shown in Table 4.1 of Chapter 4. The focus of the work was to interrogate soil-landscape patterns to:

- investigate and explain intricate soil-landscape patterns linked to shallow NAS distribution; and
- with the support of the fine scale investigations discussed in Chapter 6, describe the construction of a Midnorth study area conceptual toposequence model with emphasis on hillslope hydrogeological patterns.

7.1 Intricate soil-landscape patterns

Typically, the 3D GIS techniques involved spatial coregistration of the geophysical surveys and terrain attributes, often in the form of semi-transparent raster GIS coverage overlays, or “drapes”, placed either over the aerial photograph of the Midnorth study area to give spatial context, or over a land surface relief base derived from the three metre resolution DEM described in Chapter 5. A semi-transparent hillshade display was applied in conjunction with the survey data or aerial photograph in the GIS, which had the effect of accentuating local relief and landform patterns in coregistration with the survey patterns. The 3D GIS visualisation provided a powerful means to display a more integrated, whole-of-landscape, hydrogeologically-based view of the Midnorth study area landscape.

7.2 Geophysical ground surveys

The following three geophysical survey techniques described in Chapter 3 were used to conduct surveys of the Midnorth study area:

- EM38 sensor (in vertical dipole mode apparent electrical conductivity (EC_{av}), with maximum sensitivity at approximately 0.4 m in depth) to identify near-surface conductivity patterns;
- EM31 sensor (apparent electrical conductivity (EC_a), with maximum sensitivity at approximately 6 m in depth) to identify deep conductivity patterns; and
- Bartington MS2D search loop sensor to identify surface volume magnetic susceptibility (κ) patterns.

The three surveys were conducted in succession, and on foot during late summer (March 2003), which is the

time of year when the near-surface soil profiles are driest. As shown in Figure 7.1, the surveys were conducted on a semi-rigid survey design, with transects on an east-west bearing (up and down the toposequence). The along-transect sampling interval was 20 m, and the transects were separated by 50 m, accounting for traversability issues and avoiding likely

electromagnetic interference caused by wire fences. An interval of 100 m was used in the most easterly paddock between the road and the edge of Freshwater Creek gully due to the flat, more uniform nature of this area. All 979 of the survey points were georeferenced in the field using a global positioning system (GPS).



Figure 7.1. Locations of shared geophysical (EM38, EM31 and Bartington MS2D) survey sites (●) of the Midnorth study area.

On completion of the field survey, the georeferenced survey points for each of the surveys (i.e. EM38, EM31 and χ) were transferred to a GIS and geostatistically interpolated using ordinary kriging (Brooker 1991; Burrough and McDonnell 2000; Webster and Oliver 2001) using consistent predictive parameter settings for each survey. In this way, 20 m resolution GIS coverages of each of the survey methods were created. The images shown in Figure 7.2 are displayed with a minimum-maximum stretch so that the relationship between the GIS display colour and the survey values are linear, and cover the whole colour range. The data characteristics from each of the GIS survey coverages are presented in Table 7.1. In the northwest sector of the survey area (Figure 7.2) there is the appearance of “blocky” or “streaky” patterns in the GIS coverages. These patterns are the consequence of GIS interpolations made outside the area covered on foot during the field survey shown in Figure 7.1, and indicate unreliable GIS predictions.

Figure 7.2 shows the relationship between survey patterns and the local

landform via the incorporation of two metre contours. Figure 7.3 shows the survey coverages draped over the study area landscape to give a 3D perspective view, which strongly assists in the interpretation of the survey patterns in the context of local landform. The 3D perspective view shown is one of many possible views of the study area landscape using an interactive capability of 3D GIS. The capability allows multiple 3D perspectives of the landscape to be viewed on-the-fly, and with various combinations of co-registered GIS overlays (e.g. soil, geology, soil surveys, interpolated survey patterns, and aerial photographs) that can be “blended” by changing the transparency setting of the upper-most GIS display layer. In essence, the methodology duplicates, using the convenience of modern GIS technology, the traditional “art” of the soil surveyor, who integrates various soil-landscape patterns (e.g. terrain, drainage, vegetation, soil survey, etc.) to develop a tacit soil-landscape model, which forms the basis for soil mapping using the soil-landscape paradigm described in Hudson (1992).

Table 7.1. Statistical review of Midnorth study area geophysical surveys.

Survey method	Response range	Mean	Standard deviation
EM38 (ECav)	0.14 – 2.5 dS/m	76.7 dS/m	27.7
EM38 (EC _a)	0.05 – 1.1 dS/m	59.3 dS/m	22.6
Bartington MS2D (κ)	94.5 – 791.0 SI (10^{-5})	320.2 (10^{-5})	81.4

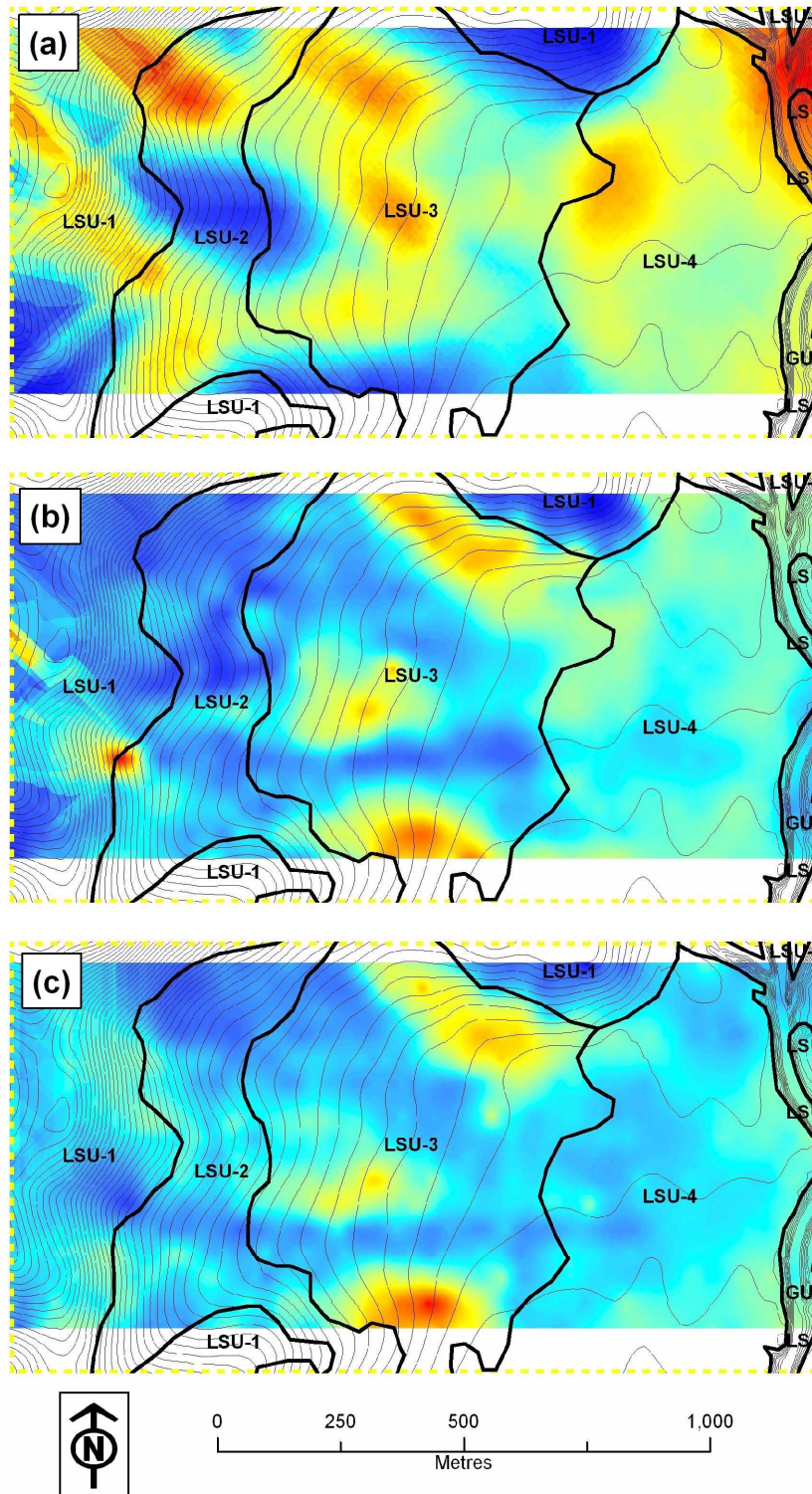


Figure 7.2. EM31 ECa (a), EM38 ECav (b) and κ (c) survey patterns of the Midnorth study area, with landscape soil units and two metre contours applied. Coverages are presented with linear, minimum-maximum stretch applied, and showing maximum responses in red and minimum responses in blue.

The following Section discusses spatial relationships observed between the EMI, κ , slope, topographic wetness index, airborne radiometric K % and

study area hillslope landform patterns, relying strongly on visual interpretation of 3D landscape drapes. When combined with soil

mineralogical and physicochemical data, a whole-of-landscape hydropedologically-based conceptual model is described, with emphasis of near-surface solute movements in the hillslope to explain the local expression of shallow NAS in the landscape. In the Section that follows

the hydropedologically-based conceptual model description, the model is combined with refined soil mapping from Chapter 5 to construct a conceptual toposequence model for the study area landscape, which is also described.

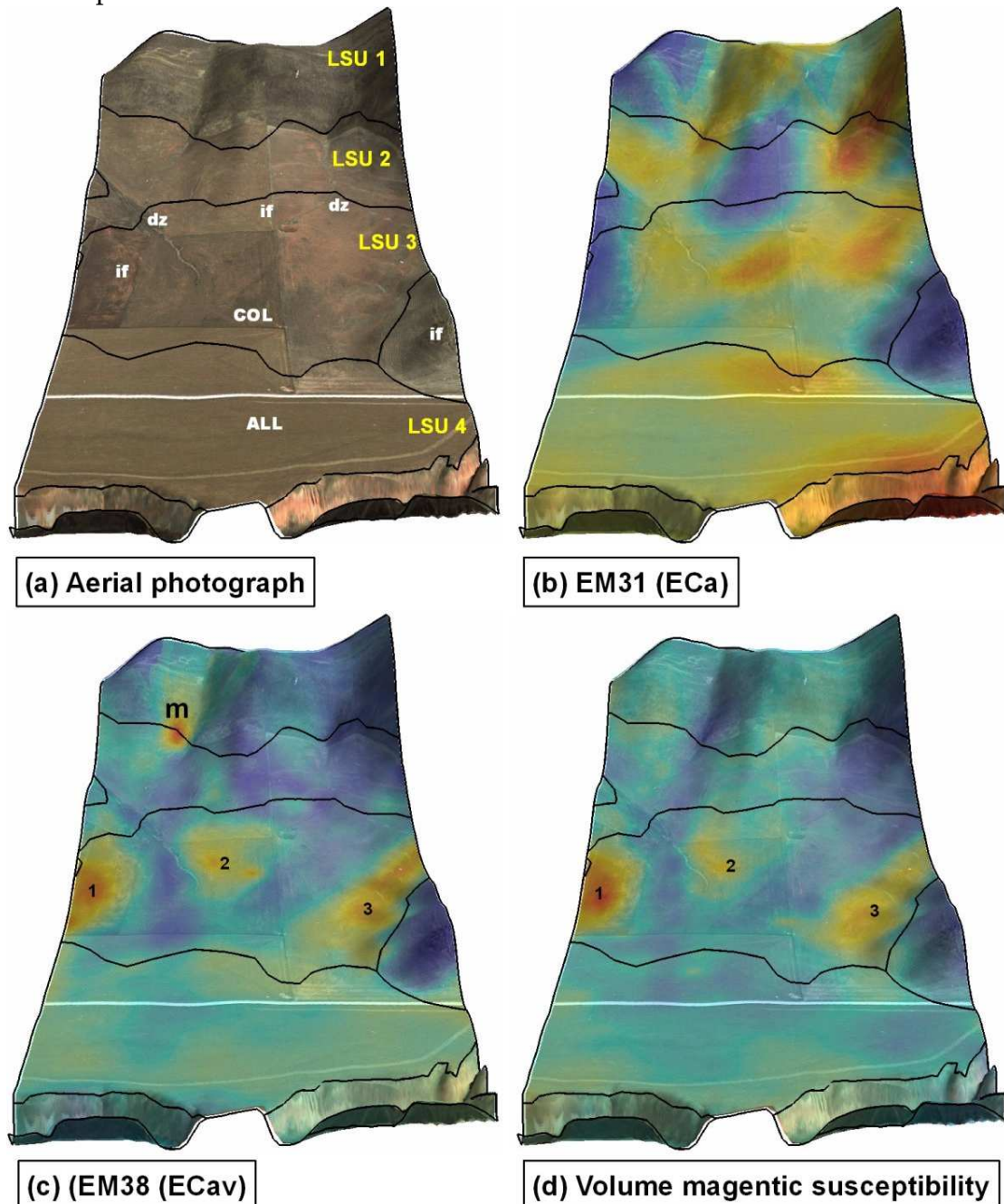


Figure 7.3. Midnorth study area with LSU boundaries overlain on 3D perspective drapes of: (a) aerial photograph (including codes for prominent hillslope features, as described in the text); (b) EM31 EC_a survey; (c) EM38 EC_{av} survey; and (d) κ survey. Each survey is presented using a linear, minimum-maximum stretch (maximum responses = dark red, moderate responses = yellow, and minimum responses = dark blue).

7.3 Landform, electrical conductivity and κ survey patterns

A number of prominent hillslope landform features are identifiable from the 3D perspective view of the aerial photograph shown in Figure 7.3 (a), which when combined help interpret the medium scale hydopedological patterns in the study area landscape. The hillslope features identified include:

- two prominent drainage zones (“dz”), which are bound by three nose slope interfluves (“if”); and

- the break of slope, which coincides with the boundary between the colluviated footslope soils (“COL”) and the alluviated toeslope soils (“ALL”).

Figure 7.4 shows the elevation and slope profile defined by the transect A'-A". The transects show the position (i.e. the vertical dashed line in Figure 7.4) of that boundary between the colluvial and alluvial soils along the hillslope profile. Field investigations (soil morphology and physicochemical data) confirm that the colluvial-alluvial boundary corresponds with the LSU 3 and LSU 4 boundary.

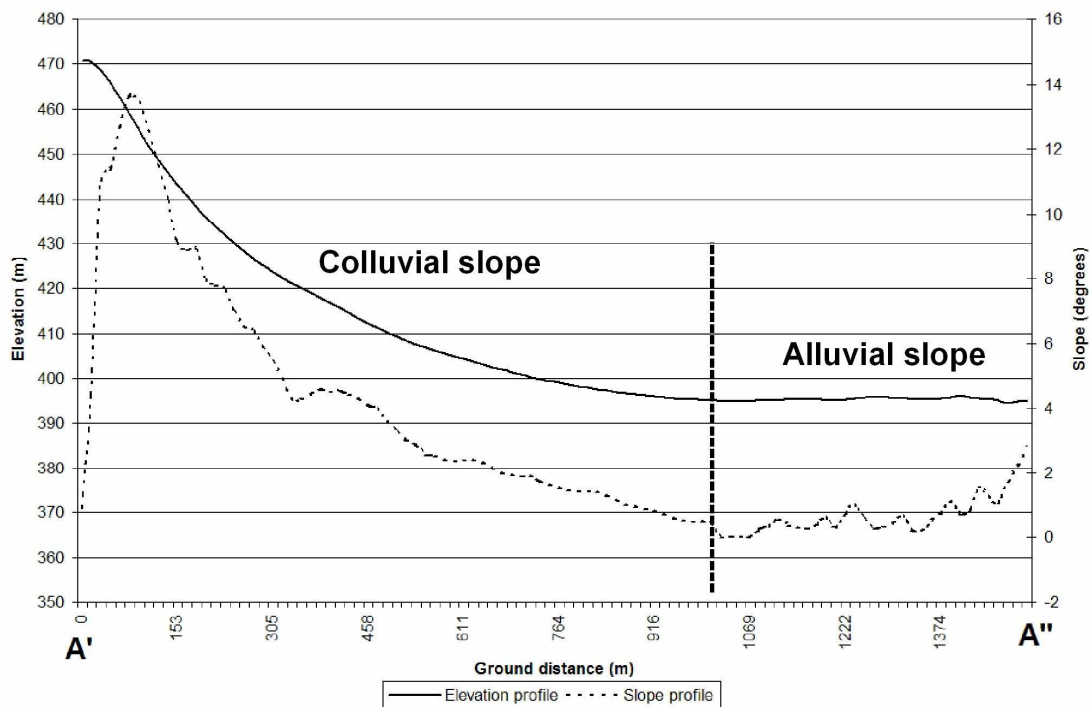


Figure 7.4. Profiles of elevation (m) (—) and slope (°) (---) for transect A'-A'' in Midnorth study area. The dashed line indicates the hillslope position of the colluvial-alluvial slope, and the LSU 3 and LSU 4 boundary.

7.3.1 EM31 hillslope patterns

EM31 EC_a deep profile (~ 6 m) conductivity patterns in the study area hillslope are shown in Figure 7.3 (b). These hillslope patterns feature several high conductivity responses in the study area (i.e. dark red areas). In the upper and mid slope zones of the landscape (i.e. LSUs 1 – 3) the highest EC_a responses are associated with the locally low-lying drainage areas (“dz”), while the lowest responses tend to be associated with the locally elevated areas, i.e. on interfluvial areas (“if”). According to the conceptual drainage and salt accumulation model presented in Figure 7.5, the relatively high EC_a responses in mid slope areas are attributed to the combination of the accumulation of deep profile salts and the presence of conductive basement rock. The contribution of conductive Fe-gravels that have collected in colluvial layers are also speculated to contribute to the high conductivity, although no deep profile data is available to support this. Salts present are likely to have collected and concentrated in the drainage zones from up slope areas, or preferentially seeped from below in saline groundwaters under the influence of piezometric pressure of a confined aquifer.

The transition between the footslope and toeslope areas, which corresponds

strongly with the colluvially-dominated (LSU 3) and alluvial (LSU 4) boundary, forms a prominent contrasting conductivity feature in the hillslope profile. The relatively high electrical conductivity of much of the toeslope zone (LSU 3) is likely to be related to the combination of clay content and salt accumulation. It is possible the salt accumulation in this zone is caused by a hydraulic barrier at the contact between the LSU 3 and LSU 4 soils. Such a hydraulic barrier is caused by the moderately shallow, coarser textured topsoil of the up slope LSU 3 soils that abut generally finer soil textures at the corresponding depths in the LSU 4 soil profile. The sodic clay associated with the LSU 4 B horizon imparts a sluggish rate of throughflow in the deep profile, causing salts originally from up slope positions to be concentrated deep in the LSU 4 profile. The salts that have concentrated deep in the LSU 4 profile seep out of the gully face after slow seepage. Evidence for this process comes from the highest EM31 EC_a values encountered in the study area at the gully face, and the salts (halitic and gypsiferous) observed wicking from the gully face. The rate of salt transport through the LSU 4 profile has increased during the past 50 years, caused by the changed hydraulic properties by the formation of the 12 m erosional gully during 1941, which has been discussed in Chapter 5.

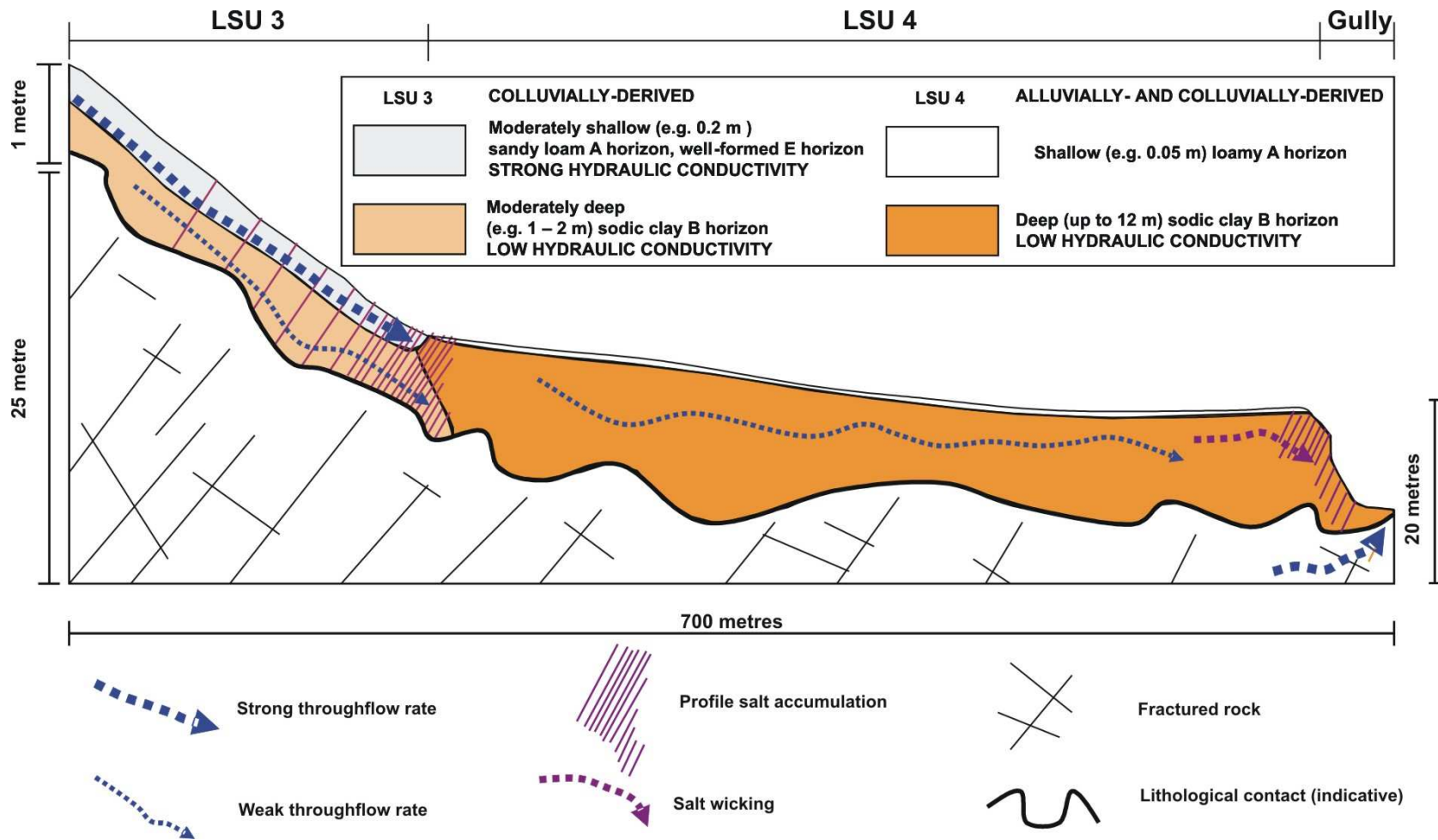


Figure 7.5. Conceptual model of Midnorth study area showing water flows associated with salt accumulations at LSU3/LSU 4 boundary, and at the erosional gully face. The toposequence shown corresponds to the lower sections of the transect A'-A'' shown in Figure 5.4.

7.3.2 EM38 hillslope patterns

When visually compared, the EM31 (Figure 7.3 (b)) and EM38 (Figure 7.3 (c)) study area patterns are reversed in many locations of the hillslope. For example, in areas where the EM31 survey coverage shows high EC_a responses, the corresponding areas of the EM38 survey coverage generally show low EC_{av} responses.

The EM38 EC_{av} survey shows a strongly conductive feature “m” in the shoulderslope, on the boundary of the LSU 1 and LSU 2 soils. This feature corresponds to a near-surface mineralised zone due to the strong and localised intensity of the conductive response. The lack of any significant strong conductive connectivity from the corresponding area in the EM31 survey coverage (Figure 7.3 (b)) confirms that the mineralised feature is restricted to the near-surface zone. Beyond the near-surface mineralised zone, the areas of highest EC_{av} response in the study area hillslope occupy the LSU 3 zone. Within this soil unit, the EC_{av} patterns correspond to the drainage zones and interfluves, with the interfluves featuring relatively high conductivity patterns (sites 1, 2 and 3 in Figure 7.3 (c)) while the drainage zones feature the relatively low EC_{av} responses. Site 1 in the south of the study area occupies a prominent nose slope interfluve, site 2 occupies relatively elevated land juxtaposed between the two prominent drainage zones of the hillslope (where P2 is located, described in Chapter 6), while site 3 in the north occupies the lower fringe of a saddle landform, adjacent to one of the prominent hillslope drainage zones.

The alluvial footslope zone features a region of relatively moderate near-surface conductivity. This conductivity pattern is likely to correspond to soils that contain moderate salt

concentration in combination with a higher clay content (see Appendix C). As for the EM31 survey, the EM38 survey shows a pattern that corresponds to the LSU 3 – LSU 4 boundary.

7.3.3 Volume magnetic susceptibility hillslope patterns

Table 7.1, which presents the data range for the κ survey for the Midnorth study area, shows a range of $94.5 - 791.0 \times 10^{-8}$ SI and a mean of 320.2×10^{-8} SI. While comparisons of κ parameters in different environments are difficult to make given the lack of correction for mass in the magnetic susceptibility measure (i.e. χ), the range for the study area is high (e.g. Table 6.1) compared to many other landscapes (e.g. Figure 6.13) from Chapter 6.

The κ (Figure 7.3 (d)) and EM38 survey patterns (Figure 7.3 (c)) show strong consistency in many zones of the study area, but most significantly in the LSU 3 zone. Here, the EM38 and κ responses are strongest in the locally elevated interfluve zones, whereas they are both weakest in the drainage zones. However, there is a lack of similarity in the κ and EM38 patterns in: (i) the near-surface mineralised zone (“m”, Figure 7.3 (c)), (ii) at the colluvial-alluvial (LSU 3 – LSU 4) boundary, and (iii) in the upper slope zones (LSU 1 and LSU 2), where the κ survey responses are generally of lower values.

7.4 Terrain patterns

Terrain analyses were conducted using a GIS to derive study area coverages of slope Figure 7.6 (a) and topographic wetness index (TWI) Figure 7.6 (b) using the three metre DEM of the study area.

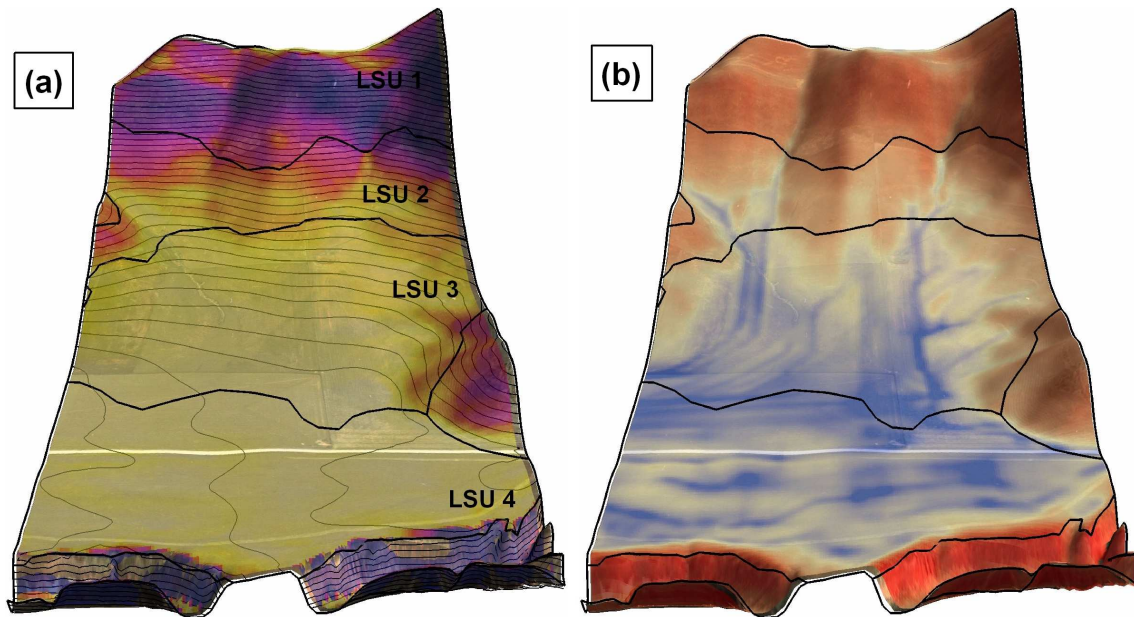


Figure 7.6. Midnorth study area LSU boundaries overlaying 3D perspective drapes of: (a) slope (0 – 14 ° range, highest gradients = dark blue, moderate gradients = pink, lowest gradients = brightest yellow, shown with minimum-maximum stretch applied) with 2 m contours; (b) TWI (highest values = dark blue, moderate values = white, and lowest values = red).

7.4.1 Slope analysis

Reference to Figure 7.6 (a) shows that the steepest slope angles (14 °) are located on the shoulderslope of the hillslope, and the slope angle gradually reduces at a regular rate down slope, reaching near-flat gradients in the toeslope areas. The drainage zones that have been previously identified are locally expressed in the coverage by the patterns of lower gradient zones that finger up slope in the higher elevation backslope zones.

7.4.2 Terrain wetness index analysis

The interpretation of the TWI patterns Figure 7.6 (b) can be stratified according to hillslope position. In the upper and mid slope areas of the landscape, the high TWI values correspond to the drainage zones discussed earlier. The TWI coverage indicates that these are water accumulation zones, which in conjunction with the steeper slope gradients, means that the zones feature focused surface- and

throughflow rates. With reference to Figure 7.6 (b), patterns of high TWI values (i.e. through flow zones) can be clearly seen to finger up slope, corresponding to the drainage zones. The low TWI values in upper and mid slope areas correspond to zones of water dispersion, and the interfluvies are conspicuously defined.

In the lower areas of the landscape where the gradient is flatter, TWI zones correspond to areas where water is likely to accumulate, resulting in reduced drainage and infrequent waterlogging at times.

7.5 Airborne radiometrics gamma and mineralogy

This Section describes an investigation involving a study of airborne gamma radiometrics (described in Chapter 5) geochemical patterns, and the relationship of the patterns to study area landform. An investigation that explains the links between geochemical patterns and near-surface

soil surface mineralogy that was conducted is also explained.

Each of the three 20 m ground resolution radiometric images bands (i.e. K %, Th ppm and U ppm) was individually draped over the hillslope shown in Figure 7.7, and visually evaluated to identify relationships with landform. Visual inspections of the U ppm (Figure 7.7 (a)) and the Th ppm (Figure 7.7 (b)) image bands revealed “incoherent” and “speckly” imagery that had little correlation to landform, hillslope position, nor soil type. This is often the case with the U ppm image band in particular due to the characteristically poor signal/noise ratio (Milligan and Gunn 1997). For the reasons stated, no further use was made of U and Th ppm image bands. However, visual inspection the remaining K % image band (Figure 7.7 (b)) revealed a particularly strong visual relationship with the LSU 3 – LSU 4 boundary. The relationship was regionally repeated in the hillslopes adjacent to the Midnorth study area, making the K % image band potentially useful in a regional upscaling methodology. For this reason, an investigation was conducted to validate the K % image band, and to link the airborne radiometric K % patterns to hillslope mineralogy. These investigations are discussed further in the following Sections.

7.5.1 Airborne K % validation

Given the potential significance of the relationship between the boundary of the LSU 3 and LSU 4 soil units in the regional landscape for upscaling methodology discussed previously, field validation was conducted of the airborne K % image band. This involved using a hand held Exploranium GR 320 gamma

radiometer (Figure 7.8 (a)) to acquire 53 GPS georeferenced gamma radiometric ground readings (K %, Th ppm, and U ppm) both within that study areas, and nearby (Figure 7.8 (b)). The study area survey featured the transect A'-A", which was sampled at a ground interval of 30 m. GR 320 readings were taken over a period of 250 seconds to acquire sufficient time to obtain a statistically significant number of counts (pers coms, Dr Alan Minty at Gamma-ray Spectroscopy Workshop, Adelaide, 20 February 2003).

The GPS-referenced GR 320 K % ground measurements were co-registered with the airborne K % image band using a GIS, and the corresponding airborne K % image values determined. A subsequent regression analysis conducted on the paired datasets resulted in $r^2 = 0.7$, which indicates a strong positive correlation between the airborne and ground-based K % measurements. This value indicates that the airborne K % data reliably reflects the true ground emissions, and therefore can be used regionally, with confidence. For this reason, an investigation was made to establish a predictive link between the airborne-based K % geochemistry and the near-surface mineralogy of the study and surrounding areas.

A key factor in understanding the variation between the airborne and ground-based radiometric K % datasets is explained by the relatively large ground “footprint” of the airborne sensor (i.e. 1,000's m²) - a function of airborne detector field of view and flying height (Minty 1997) - compared to the relatively small ground “footprint” sensed using the ground-based sensor (i.e. a few m²).

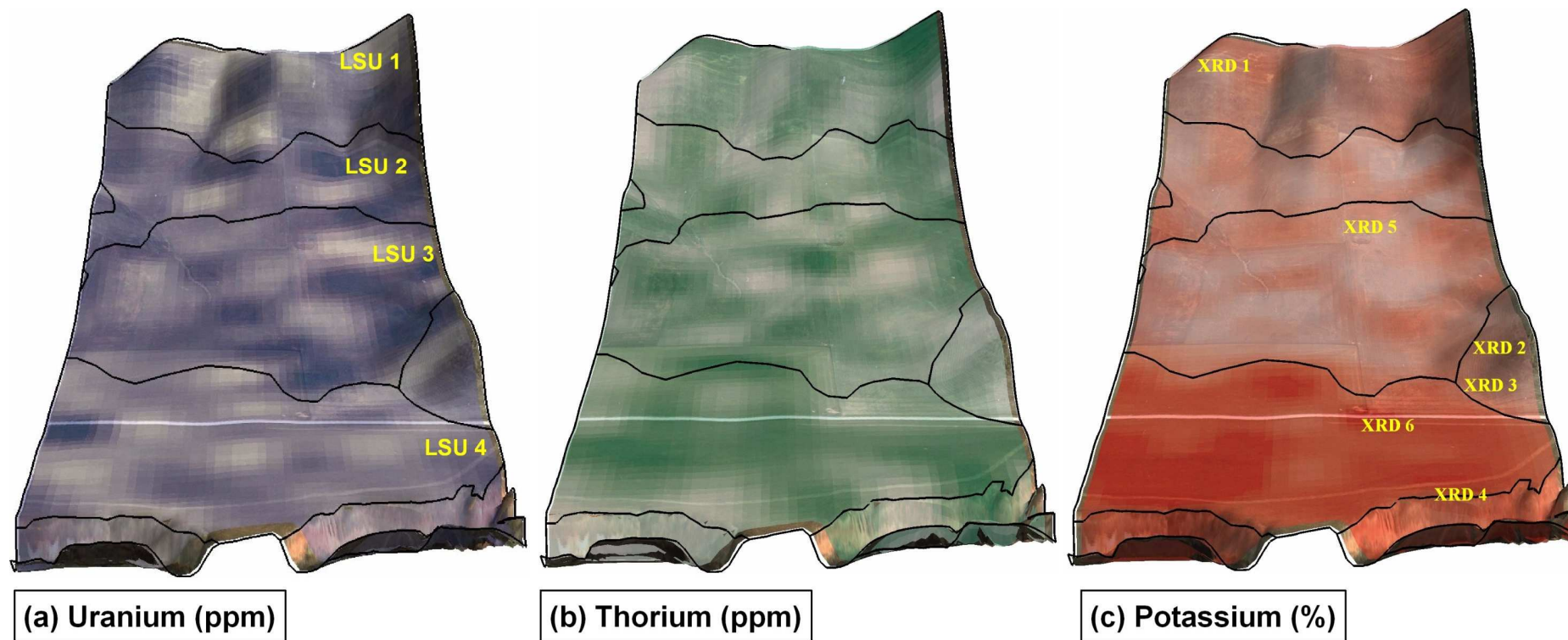


Figure 7.7. Midnorth study area LSU boundaries overlaying 3D perspective drapes of: (a) U ppm (4.0 to 0.0 ppm) (highest values = blue, lowest values = white), (b) Th ppm (15.9 to 6.3 ppm) (highest values = green, lowest values = white), and (c) K % (1.1 to 2.5 %) (highest values = red, lowest values = white). The sampling sites for X-ray diffraction (XRD) analysis (XRD 1 to XRD 6) are identified in (c), and resulting plots for XRD 5 and XRD 6 shown in Appendix F (presented as SPC12 and SPC26, respectively).

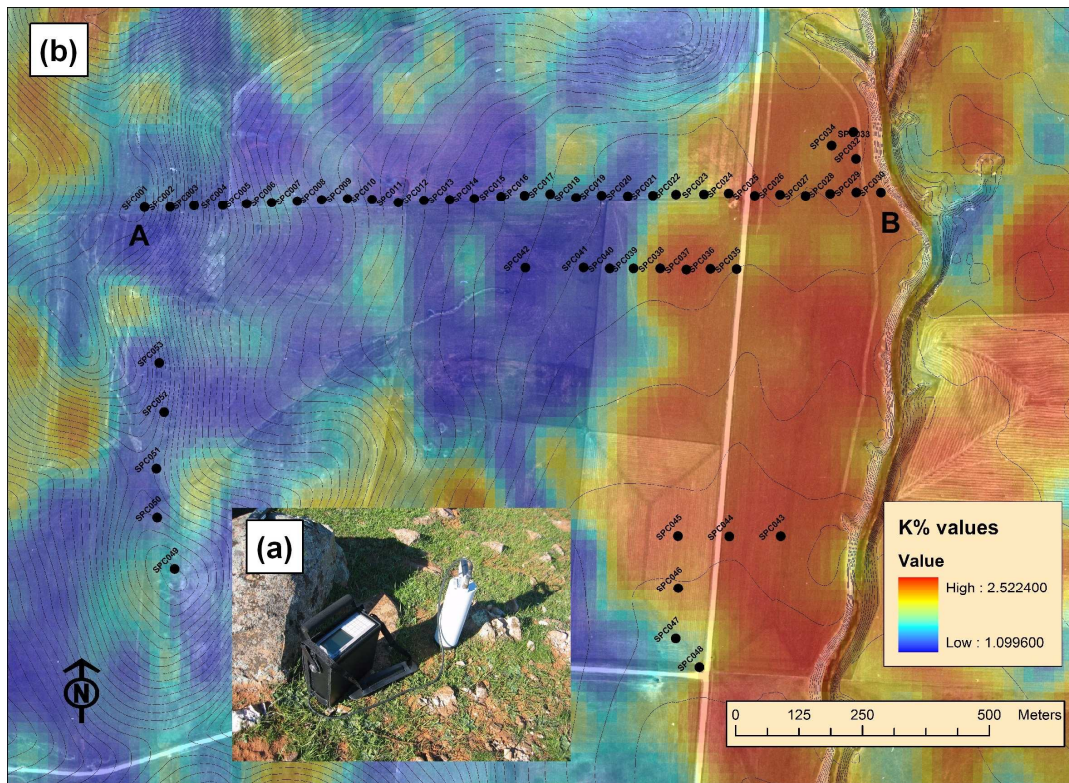


Figure 7.8. Inset (a) Exploranium GR 320 and (b) locations of GR 320 ground survey sites in the Midnorth study area and surrounding areas.

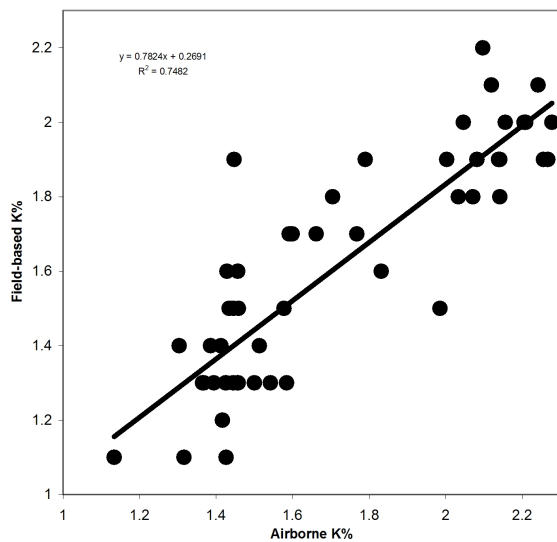


Figure 7.9. Airborne radiometric K % versus field radiometric K % relationship.

7.5.2 Linking airborne radiometric K % and mineralogy

Six topsoil samples were collected in the study area from the locations

shown in Figure 7.7 (c) from the sites labelled “XRD 1” through to “XRD 6”. The samples from XRD 1 and XRD 2 were taken from the upper 0.3 m, the sample from XRD 3 was taken from the top layer of the gully face (< 1 m, bulked), and samples from XRD 4 to XRD 6 were taken from the upper soil layers (< 0.1 m).

Qualitative x-ray diffraction (XRD) analysis (Olson *et al.* 2000; Velde 1992) was conducted on the clay fraction of the samples described above. XRD analysis was also undertaken on a rock fragment taken close to the site XRD 1, to reference the dominant soil mineralogy against the bedrock source. The XRD qualitative interpretations are summarised in Table 7.2, with accompanying clay content and corresponding airborne gamma radiometric K %. The analysis for the sites XRD 1, XRD 2, XRD 3 and XRD 4 were undertaken as part of the investigation by Fitzpatrick *et al.* (2003c). That investigation involved disoriented XRD analyses of the < 2

μm clay fraction prepared using Ca-saturation. Furthermore, detailed qualitative XRD analysis were conducted on the 0 – 0.30 m layers from the sites XRD 5 and XRD 6. The sample depth range was selected to specifically correspond to the effective depth of gamma radiometric sensing sensitivity (e.g. Minty 1997). The analyses were conducted on: (i) the sand and silt fraction (2 mm – 2 μm), (ii) the coarse clay fraction (2 – 0.2 μm), and (iii) the fine clay (< 0.2 μm) fraction, which were separated through centrifugation. Each fraction was analysed as follows: (i) unprepared (pressed powder, disoriented analysis) and (ii) glycerol-solvated glycerol and Ca-saturated (oriented analysis). All XRD traces are presented in Appendix F.

Mica, smectite and chlorite are soil-clay fraction layer silicates. Both mica, illite and smectite have a high K content, while chlorite and kaolinite have a low K content (Taylor and Eggleton 2001). By combining the results of the XRD analysis, soils data, and airborne K % distribution, the following study area patterns are revealed: mica and smectite dominate areas that spatially coincide with: (i) high airborne K % areas, and (ii) LSU 4-type soils. Chlorite dominated areas spatially coincide with (i) low airborne K % areas, and (ii) LSU 1, 2 and 3-type soils.

The clays of XRD 5 and XRD 6, which received detailed XRD and textural analyses, show identical mineralogy, and the clay-rich clays are concentrated in the < 0.2 μm soil fraction (Appendix F). By mass, approximately 3 % of XRD 5 (upper 0.3 m of LSU 3 soil) versus ~ 5 % (upper 0.3 m of LSU 4 soil) topsoil is comprised of the < 0.2 μm clay fraction. XRD 5 shows nearly half the airborne K % response than that of XRD 6 (i.e. 1.3 versus 2 %).

In combination, this information is indicative of a subtle hillslope hydro-pedological process, which involves the selective down slope transfer of K-rich material from the < 0.2 μm soil fraction of LSU 3 soils (XRD 5) via either: (i) a K-rich solution derived from dissolved K-rich clays, or (ii) as intact fine particulate matter leached and then held in suspension during erosion or in throughflow (e.g. Fanning and Fanning 1989). The result of these down slope transfers of K-rich material is to enhance (i.e. via neogenetic or depositional processes) K-mineral concentrations in the LSU 4 soils (samples 2 and 3). However, it is also possible that K-rich mineralogical enhancement in the LSU 4 soils may also have taken place through alluvial processes sourced from higher reaches of the Belalie Valley. If so, the identical clay fraction mineralogy of the LSU 3 soil (XRD 5) and LSU 4 soil (XRD 6) means that the alluvial source shares identical mineralogy to the parent material of the study area.

7.6 Descriptive hydro-pedological model

With reference to the discussions of Chapters 3 and 4, the following qualitative discussion communicates mentally-based tacit rules (i.e. the “descriptive hydro-pedological model”) (Hudson 1992) that are ultimately applied in the quantitative soil mapping framework (Bui *et al.* 1999; de Bruin *et al.* 1999; McKenzie and Ryan 1999) described in Chapter 8 to predict the regional distribution of shallow NAS. The descriptive hydro-pedological model described in the current Section stratifies the study area to two distinct landscape zones based on hillslope position (i.e. upper and mid slopes, and lower slopes), each with distinct hydro-pedological regimes.

Table 7.2. Summary of x-ray diffraction (XRD) mineralogical results for the Midnorth study area (incorporating results from Fitzpatrick *et al.* 2003c), with corresponding clay % values (upper-most layer analysed, and corresponding airborne gamma radiometric K % values.

Site ID - see (Figure 7.7 (c))	Locality / Soil Map Unit	Layer depth (m)	Layer silicate minerals (D = dominant; CD = co-dominant; M = minor; T = trace)	Clay content (%) (upper-most layer analysed)	Airborne gamma radiometric K %
XRD 1	Crest (LSU 1)	0 – 0.05	Chlorite (T), Mica (D), Smectite (T), and Kaolinite (M)	18	1.8
		0.05 – 0.2	Chlorite (D), Vermiculite (T), Mica (M), Kaolinite (M)		
		0.2 – 0.35	Chlorite (D), Vermiculite (T), Mica (M), Kaolinite (M)		
XRD 2	"F block" (upper)	0 – 0.05	Chlorite (T), Mica (D)	19	1.4
		0.05 – 0.2	Chlorite/Mica (CD)		
		0.2 – 0.35	Chlorite/Mica (CD)		
XRD 3	"F block" (lower)	0 – 0.05	Chlorite (T), Vermiculite (T), Mica (D), Kaolinite (M)	21	2.1
		0.05 – 0.2	Chlorite (M), Vermiculite (T), Mica (M), Kaolinite (M)		
		0.2 – 0.35	Chlorite (M), Vermiculite (T), Mica (M), Kaolinite (M)		

Site ID - see (Figure 7.7 (c))	Locality / Soil Map Unit	Layer depth (m)	Layer silicate minerals (D = dominant; CD = co-dominant; M = minor; T = trace)	Clay content (%) (upper-most layer analysed)	Airborne gamma radiometric K %
XRD 4	LSU 4 (Gully face)	1.0	Mica (D), Smectite (M), and Kaolinite (M)	35	2.1
		3.0	Mica (D), Smectite (M), and Kaolinite (M)		
		6.0	Mica (D), Smectite (M), and Kaolinite (M)		
XRD 5	LSU 3	0 – 0.3	Mica/illite/smectite (CD), Kaolinite (M)	13 (comprising: 2 – 0.2 μm , 10 %; < 0.2 μm , 3 %)	1.3
XRD 6	LSU 4	0 – 0.3	Mica/illite/smectite (CD), Kaolinite (M)	18 (comprising: 2 – 0.2 μm , 14 %; < 0.2 μm , 5 %)	2.0

The electromagnetic induction surveys (EM38 and EM31) have revealed conductivity patterns that are dominated by the 3D distribution of salts and clays (type and content), with an additional contribution of deep profile magnetic gravels (i.e. Fe-oxides) to the EM31 survey patterns. The EM38 patterns correlate with the κ patterns, especially in the sloping LSU 3 soil zone. The similarity in these patterns can be hydrogeologically explained, particularly when interpreted in combination with throughflow and water accumulation patterns identified in the TWI coverage. For example, in the LSU 3 soil locations where correlation between the EM38 and κ survey patterns is greatest, these areas tend correspond to perched landforms that receive lower rates of solum flushing (described in Chapter 6), making these zones comparatively drier than other parts of the landscape. These areas of LSU 3 have been highlighted in Figure 7.10 (sites 1 – 3), in which the EM38 contours correspond strongly to the TWI landscape “flushing” patterns from the TWI 3D backdrop. Under these moisture conditions the near-surface layers experience:

- less leaching, resulting in higher residual salt concentrations and higher EM38 conductivity patterns;
- relatively stronger oxidising conditions, favouring pedogenic magnetic enhancement through the formation of maghemite (e.g. Mullins 1977; e.g. Taylor and Schwertmann 1974; Thompson and Oldfield 1986); and
- the EM38 and κ patterns in the sloping LSU 3 soils are therefore the pedogenic expression of near-surface freshwater flushing rates and patterns.

In the lower slope areas, the investigation of the airborne radiometric K % patterns, and the links to soil type and landscape

position has demonstrated that near-surface down slope flushing rates are not equal, and that an illuvial enhancement of the fine clay fraction has taken place in upper profiles of the toeslopes soils (i.e. LSU 4 soils). The illuvial enhancement has created a hydraulic conductivity transition at the contact between the LSU 3 and 4 sola (i.e. from deep loamy A horizons and the thin sodic clay A horizons), causing up slope-derived freshwater soil-water flows that contain salts to become backed-up in the lower LSU 3 zones during winter. During summer when evaporation rates are high, the salts that have accumulated in LSU 3 areas as a consequence of the backed-up seasonal freshwater soil-water flows become more concentrated (i.e. $EC_{se} \geq 2$ dS/m) in the solum, creating the conditions for shallow NAS formation in the LSU 3 soils.

7.7 Conceptual toposequence model

Knowledge accumulated of patterns and soil-regolith processes in the Midnorth study area from combined interpretation of field survey, airborne, terrain and laboratory analyses made it possible to construct a conceptual toposequence model (Fitzpatrick *et al.* 2003c). The systematic structural approach used is described in Fritsch and Fitzpatrick (1994), which is summarised in Chapter 4. However, the methods described in this Section represent an improvement on the methodology previously used because of the combined incorporation of: (i) spatial survey data coverages (i.e. EMI, κ , slope, TWI, gamma radiometric K %), and (ii) 3D GIS techniques to reveal hillslope hydrogeological patterns. The Midnorth study area is characterised by a complex mosaic of soils with shallow NAS conditions - along with associated waterlogging, sodicity and fertility issues. The above investigation has enabled the establishment of relationships between:

- LSUs, and subsoil and regolith salt distributions from ground-based EMI, terrain, soil survey and laboratory analysis data
- LSUs and upper layer clay mineralogy; and
- clay mineralogy and airborne K % radiometrics.

Based on the discussions above, the LSU arrangements in the study area landscape are likely precursors to shallow NAS distributions elsewhere in the region. The combination of medium scale (i.e. $i+2$) ground survey (i.e. EMI, κ , and various terrain attributes), laboratory physicochemical data – with support of the findings of Chapter 2 regarding the fine scale investigations (i.e. $i-1$ (soil horizons) – $i+1$ (polypedon)) - have revealed the intricacy of these patterns in the study area landscape.

These patterns have been revealed through the combined investigation of the regionally available datasets of terrain (slope), near-surface throughflow and accumulation (TWI), and airborne radiometric K % (LSU 3 – LSU 4 boundary) patterns.

Chapter 8 that follows describes the combined use of the above datasets in the development of a regional predictive framework using upscaling. The development of the framework is strongly assisted by soil-landscape process knowledge invested in the study area conceptual toposequence model that highlights hillslope hydropedological processes that contribute to the landscape expression of shallow NAS in the study area region.

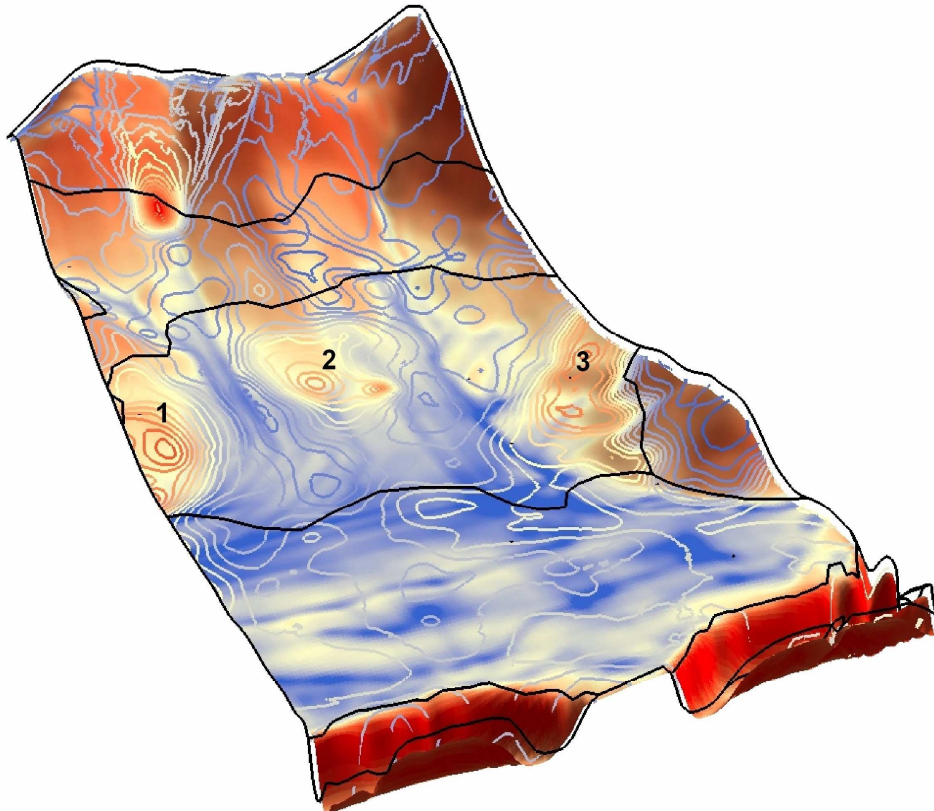


Figure 7.10. Midnorth study area LSU boundaries and EM38 EC_a survey contours (highest values = red, lowest values = blue) overlaying the TWI coverage. Sites 1, 2 and 3 are referred to in the text as areas that correspond with elevated EM38 EC_a zones and low TWI values.

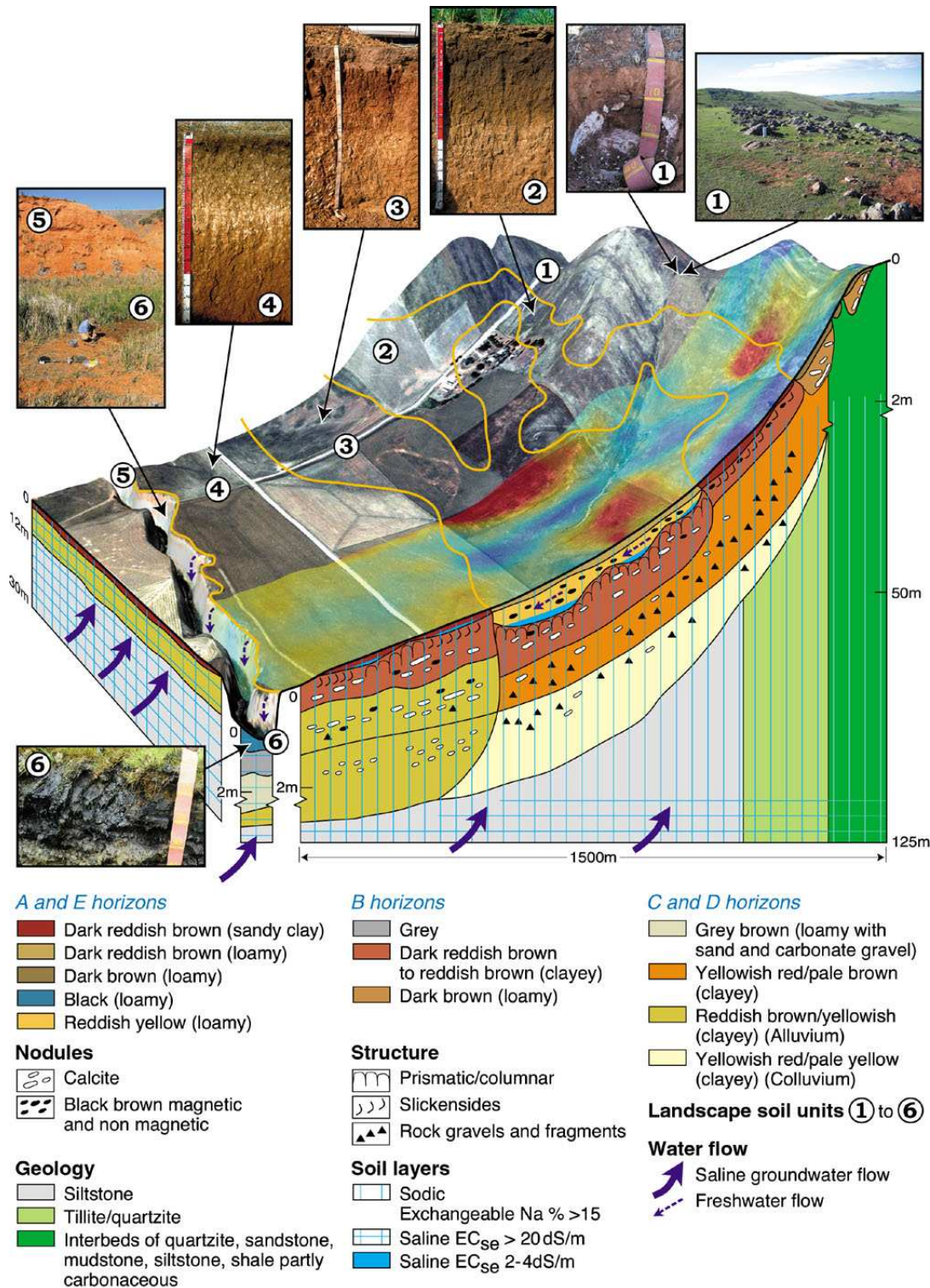


Figure 7.11. Whole-of-landscape 3D process model for Midnorth study area showing (i) 3D aerial photograph drupe of study area, overlaid with (ii) a section of EM38 survey (high response: red, low response: blue) (iii) landscape-soil unit (LSU) boundaries, accompanied by (iv) photographs of representative soil profiles for each LSU, (v) underlying geology, (vi) cross-section of typical toposequence showing the main morphological, saline and sodic soil-regolith features/layers and (vii) groundwater and fresh surface water flow paths (after: Fitzpatrick *et al.* 2003c).

Chapter 8. Midnorth coarse scale investigation

The preceding Chapters have described how the fine scale (Chapter 6) and medium scale (Chapter 7) investigations can be linked to the landscape-wide distribution of shallow NAS in the LSU 3-type soils of the Midnorth study area hillslope. These investigations have shown that local landform is an important factor in determining the local distribution of shallow NAS patterns in the affected soils. The combined application of ground EMI, κ and χ surveys, slope and TWI analyses, airborne gamma radiometric K %, soil survey, and finally laboratory physicochemical investigations, have been used to identify shallow NAS patterns, and to construct an improved conceptual toposequence model of the Midnorth study area. Soil survey data described in Chapter 5, and presented in Appendices 1 and 2.

Therefore, and with consideration to the above, this Chapter describes a coarse scale (i.e. $i+3$, Figure 4.1) investigation to predict the distribution of shallow NAS in the Midnorth study area and surrounding areas (2,275 ha) using an upscaling methodology. The investigation comprised the following components: (i) selection of suitable environmental covariates (see Chapter 3); and (ii) development of a GIS rules-based framework to apply in the upscaling methodology.

In doing so, a shallow NAS upscaling methodology was used to classify the following soil classes in the Midnorth study area and surrounding areas (2,275 ha):

- area of LSU 3 soils that are affected by shallow NAS, and
- area of LSU 3 soils that are not affected by shallow NAS.

The following Sections describe the development and spatial implementation of the rules-based upscaling methodology.

8.1 Environmental covariate selection

The methodology to identify suitable environmental covariates combines: (i) the philosophy that underpins soil-landscape paradigm (Hudson 1992), and (ii) approaches to quantify the subjective, mentally-based tacit rules

to predict soil distribution (Bui *et al.* 1999; de Bruin *et al.* 1999; McKenzie and Ryan 1999). With reference to Chapter 7, the mentally-based, tacit rules have been articulated through the descriptive hydrogeological model (Section 7.6), which describes the mechanistic processes contributing to the occurrence of shallow NAS in

the study area. This, combined with the conceptual toposequence model that visually communicates this information (Section 1.1), assisted in selecting the environmental covariates, and their quantification via the numeric thresholds applied in the upscaling methodology.

The following environmental covariates were selected in the upscaling methodology for the strong visually-based correlation (Section 7.6) between these GIS landscape datasets and the study area patterns identified related to shallow NAS:

- slope (in degrees);
- airborne gamma radiometric K %;
- TWI; and
- curvature (showing localised landform, e.g. rounded summits).

The numeric thresholds applied to the selected environmental covariates in the upscaling framework were determined via an interactive process using the “Knowledge Engineer” module of “ERDAS Imagine 8.4” software (ERDAS 2002). The process took advantage of the capability to semi-interactively use the software to apply a series of environmental covariate threshold permutations, review the results, and apply modifications for new predictions in a rapid manner.

The key method for reviewing predictions was to employ the 3D draping method described in previous Chapters. The predictions were reviewed: (i) quantitatively (e.g. via field observations and accumulated landscape knowledge), and (ii) semi-qualitatively through corresponding predicted classes with soil profile data and the geophysical survey coverages using GIS investigation. The upscaling procedure was halted when it was deemed that the best possible predictive results had been achieved. The final iterative result comprised combination of numeric thresholds presented in Table 8.1.

8.2 Soil-landscape function of predictive rules

Functionally, the predictive framework presented in Table 8.1 applies terrain slope to better discriminate LSU 3 from LSU 2 soils, and airborne radiometric K % to discriminate LSU 3 soils from LSU 4 soils. In the LSU 3 areas, TWI drainage thresholds discriminate between solum salt accumulation and solum salt flushing zones, i.e. the LSU 3 shallow NAS zones from the non-shallow NAS zones. Curvature “filters” out convex (i.e. summits and ridges) landscape positions (e.g. crests and ridges) in the LSU 3 areas.

8.3 Upscaling prediction

The final upscaled prediction for: (i) LSU 3 shallow NAS-affected and (ii) LSU 3 shallow NAS non-affected soils draped over landform for the Midnorth study area is presented in Figure 8.1. The prediction draped over landform for the surrounding area (2,275 ha) is presented in relief in Figure 8.2 and in plan view in Figure 8.3.

The upscaling prediction results show strong spatial consistency with predicted LSU 3 soils and the mapped LSU (Chapter 5) featured in Figure 8.1. However, using the LSU mapping as a guide, the predicted LSU 3 areas appear to encroach significantly into the up slope LSU 2 soils. Much of the encroached areas correspond to the relatively lower elevation drainage areas of LSU 2. The down slope predicted LSU 3 border shows strong correspondence with the mapped LSU 3 / LSU 4 boundary. Within the predicted LSU 3 areas, the non-shallow NAS areas correspond clearly to the locally low elevation drainage zones of the

hillslope, whereas the shallow NAS-prone areas correspond to the other locally elevated (and perched) areas of the landscape.

Given the establishment of visually strong correspondence between the predicted LSU 3 patterns in the Midnorth study area and the LSU mapping, the predicted patterns extending to the surrounding 2,275 ha area shown in Figure 8.2 feature a strong regional repetition of the Midnorth study area patterns. Again,

regionally, the LSU 3 soils predictions dominate the mid slope zones, and within these, the non-shallow NAS areas are consistently occupy the locally lower elevation drainage areas, while the shallow-NAS prone soils occupy the locally higher elevation areas.

Table 8.1. Environmental covariate thresholds applied in the shallow NAS upscaling methodology used for the Midnorth study area and surrounding areas.

Class	Rules			
	Slope in degrees	Airborne radiometric K %	Topographic wetness index	Curvature
LSU 3: not affected by shallow NAS	> 0.6 to < 8.0	< 1.8	< 7.4	< 0.1
LSU 3: affected by shallow NAS	> 0.6 to < 8.0	< 1.8		< 0.1
All other areas	< 0.6 and > 8.0	> 1.8		

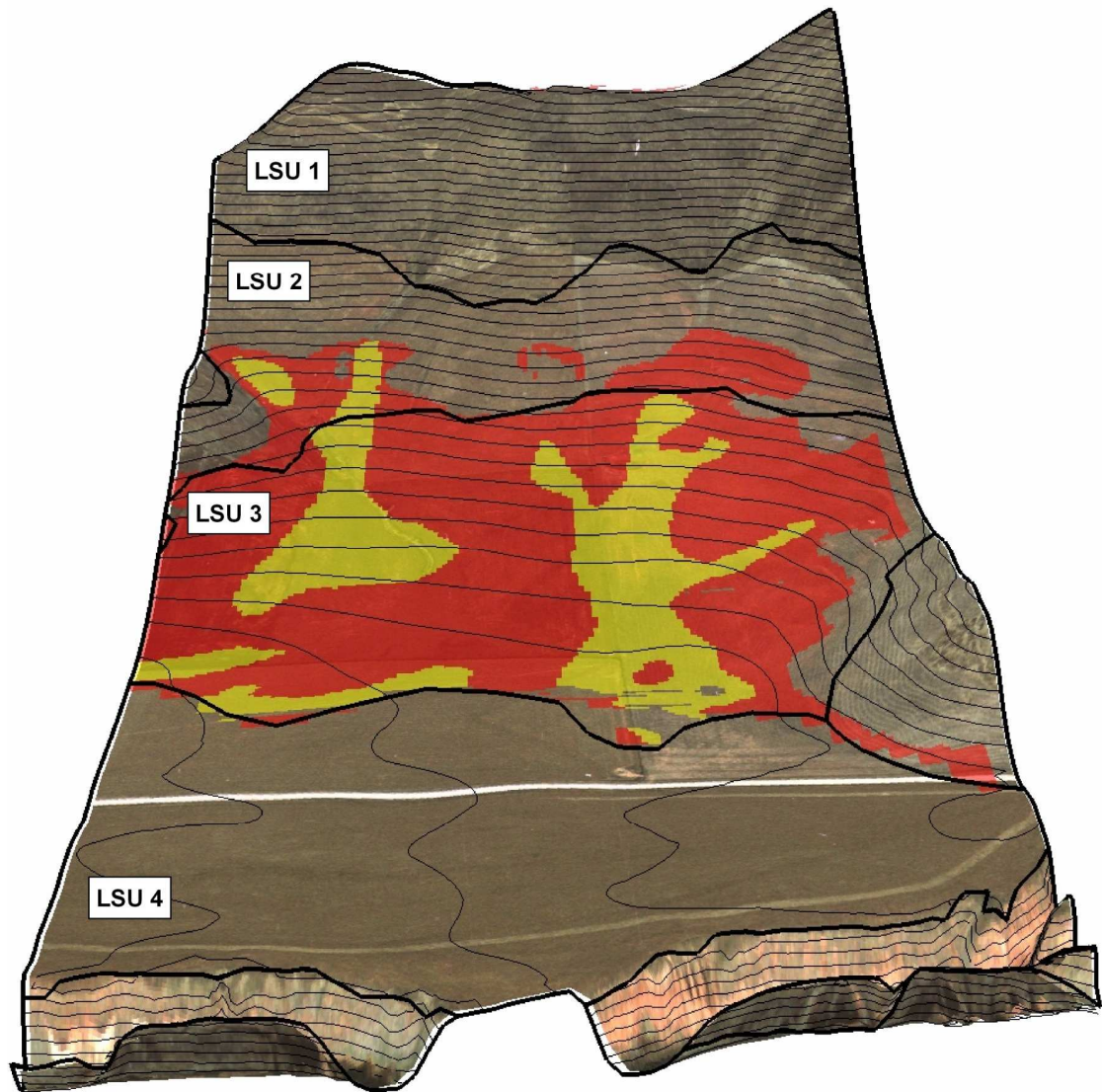


Figure 8.1. Upscaling prediction of shallow NAS in the Midnorth study area draped over an aerial photograph, two metre contours, and LSU boundaries. Yellow indicates predictions of LSU 3 areas not effected by shallow NAS, and red indicates predictions of LSU 3 affected by shallow NAS. All other soils remain unclassified.

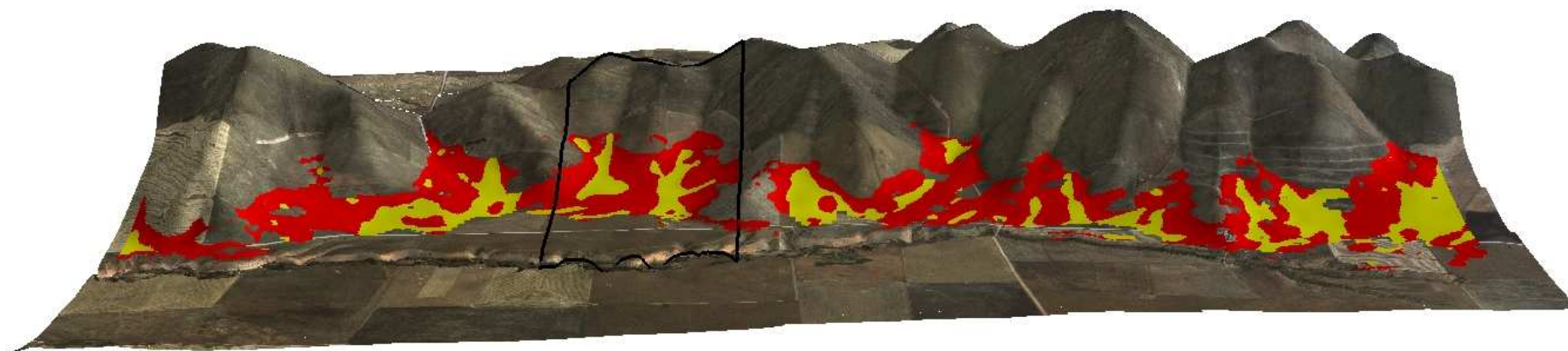


Figure 8.2. Upscaling prediction of shallow NAS in the east-facing hillslopes of the Midnorth study area (black box) and surrounding (2,275 ha) areas overlaying an aerial photographic drape. Yellow indicates predictions of LSU 3 areas not affected by shallow NAS, and red indicates predictions of LSU 3 affected by shallow NAS. All other soils remain unclassified.

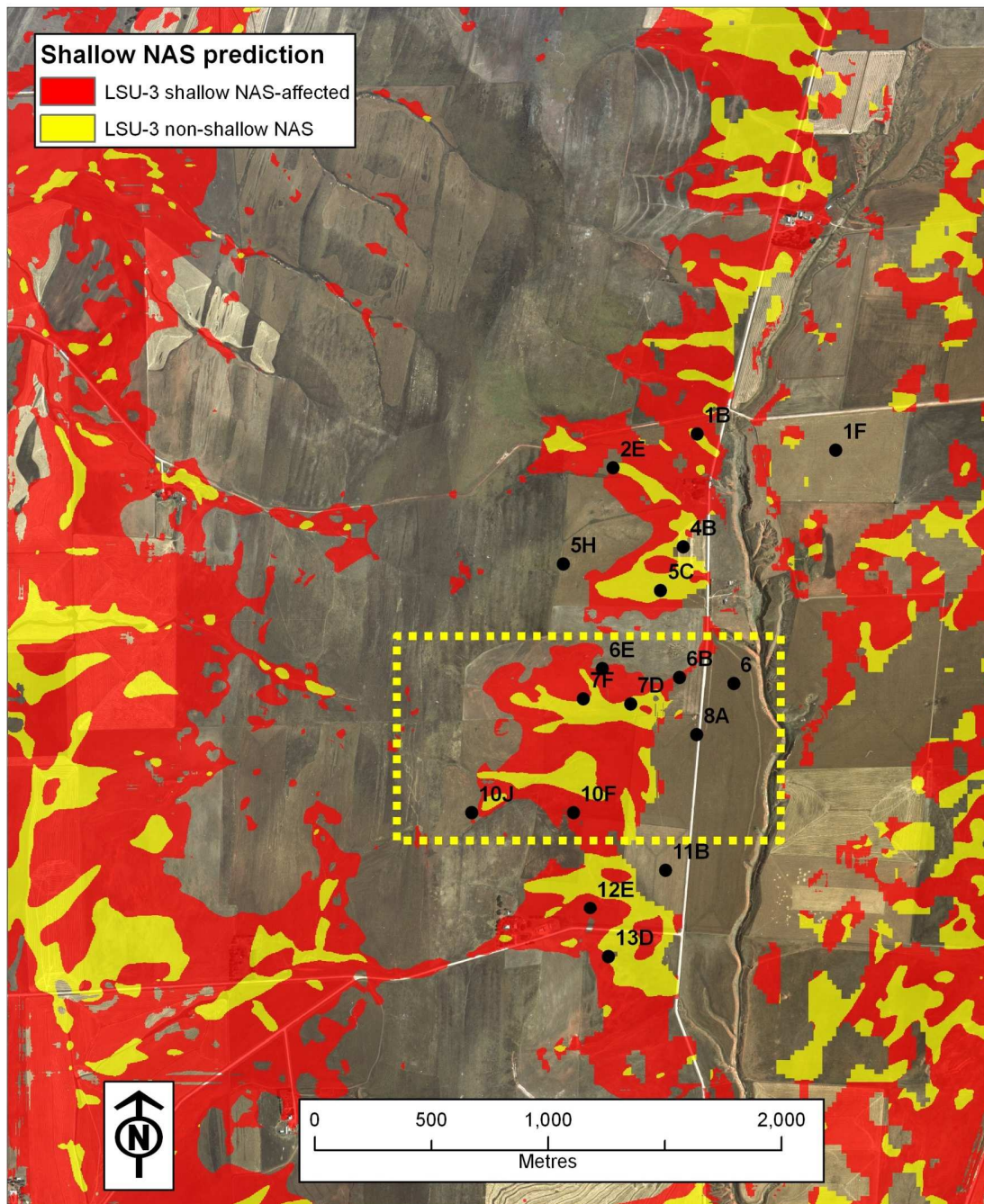


Figure 8.3. Upscaling prediction of shallow NAS in plan view of the Midnorth study area (yellow box) and surrounding (2,275 ha) areas overlaying an aerial photograph. Yellow indicates predictions of LSU 3 areas not effected by shallow NAS, and red indicates predictions of LSU 3 affected by shallow NAS. All other soils remain unclassified. Also shown are soil survey sites with accompanying physicochemical data used for upscale prediction validation. The profiles coinciding with predicted shallow NAS-affected areas include 6E, 6B, 10F, 12E and 13D. The profiles coinciding with predicted non-shallow NAS areas include 1B, 2E, 4B, 5C, 7D and 7F.

8.4 Validation of upscaling prediction

The soil profile physicochemical data collected during CSIRO's 1988 soil survey (Appendices B and C) shown in Figure 8.3 were applied to validate the shallow NAS upscaled predictions. A GIS was used to select the georeferenced soil profiles that fell inside the predicted LSU 3 area. A subset of the profiles was then made according to whether the profiles coincided with either: (i) shallow NAS predicted areas; or (ii) non-shallow NAS predicted areas, which are identified in Figure 8.3.

Figure 8.4 shows the EC_{se} values from the selected profiles plotted according to depth. The box inside the graph ("NAS-affected soil profile zone") is a representation of the graphically-

defined "profile depth / salinity concentration "space" occupied by shallow NAS-affected soils according to the criteria defined in Section VVV of Chapter 2. According to this criteria, the profiles that intersect the shallow NAS box are therefore classified as shallow NAS soils, and used here to validate the predictions.

Figure 8.4 shows that all profiles from shallow NAS predicted areas (solid lines) intersect with the box, thus all have been correctly classified. All except for one profile from non-shallow NAS predicted areas (5C) do not intersect with the box. Therefore, by the preliminary validation method described, 10 of 11 sites selected show the correct predicted classification according to the profile salinity characteristics. This indicated confidence in the upscaling methodology.

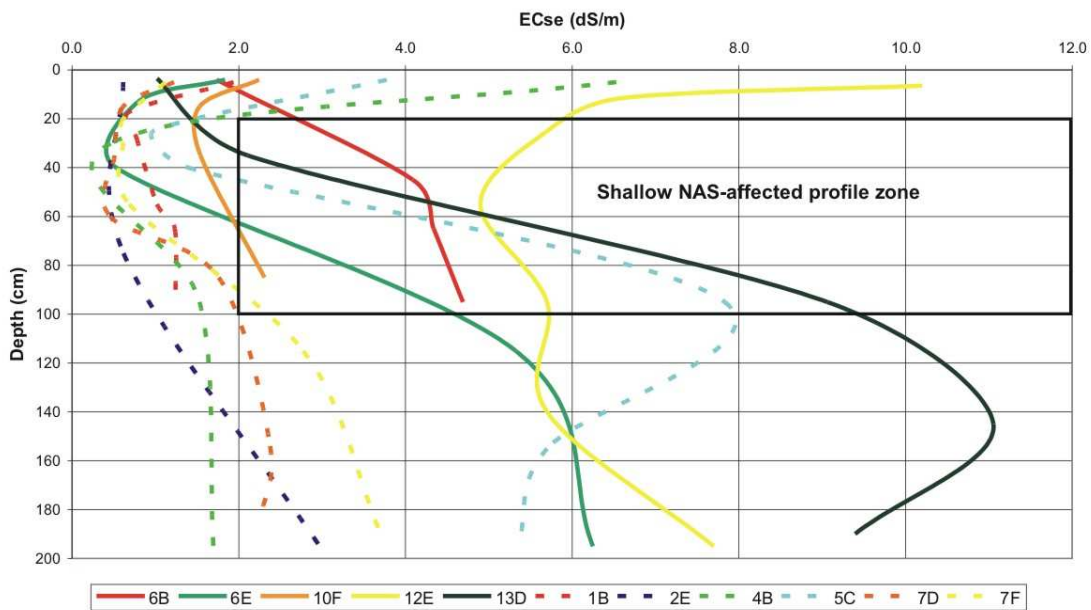


Figure 8.4. Profiles selected from LSU 3 predicted areas shown in Figure 8.3 used validate upscaled predictions of shallow NAS. According to the profile depth distribution of salinity (EC_{se}), five profiles are shallow NAS-affected (solid lines) and six profiles are non-shallow NAS-affected (dotted lines). The profile identities are listed.

8.5 Regional implications

Of the 2,275 ha surrounding the Midnorth study area, the upscaling methodology classified 40 % of the total area (i.e. 910 ha) as being LSU 3 soils. Of this area, 75 % of the area (i.e. 682.5 ha) was classified as shallow NAS, and 25 % (i.e. 227.5 ha) as being

non-shallow NAS-affected. Given that the area surrounding the Midnorth study area features soil-landscape properties that are regionally repeating, it is likely that these ratios (i.e. LSU non-shallow NAS affected/LSU shallow NAS-affected/other soils) would also be regionally repeated.

Chapter 9. Mount Lofty Ranges study area

The Mount Lofty Ranges (MLR) study area is centred on the coordinates 139°0'50" E, 34°53'44" S, and is located 40 km to the east of Adelaide, and 5.5 km southwest of the township of Mount Torrens, shown in Figure 9.1. The study area itself comprises a sub-catchment - locally known as "Herrmann's Catchment" - which covers an area of 130 ha. The following Sections describe the climate, geology and airborne geophysics, landform, soils and landuse of the study area in further detail. The Chapter ends with a discussion of the rationale for the series of multiscale investigations that were conducted in the study area.

9.1 Regional overview

The MLR study area (Figure 9.1) falls within the upland region of the same name, which stretches for approximately 120 km from the Barossa Valley in the north, to Cape Jervis in the south. The Ranges feature a series of mainly north-south orientated ridges and hilltops. Between these, the landscape is generally composed of low rolling hills that typically have a local relief difference of between 30 to 50 m. This landscape has complex topography that features valleys and sub-valleys with variable slope angles and aspects, which combine to make the region rich in meso-climatic variation. At 790 m on the western flank of the Ranges directly east of Adelaide, Mount Lofty is the highest peak in the MLR, and is also one of the highest peaks in South Australia.

The MLR region features some of the most productive agricultural and economically valuable land uses in

South Australia. The region is where early European settlers first started clearing land in the mid-1800's for timber and market gardening. Nowadays, the relatively cool and high rainfall climate combine to make the region ideal for high-value agricultural land uses. The key forms of agriculture in the region include: viticulture, commercial forestry, market gardening, horticulture, and sheep and dairy production. Other important land uses include: water conservation catchments and recreational reserves to protect water quality to the reservoirs that supply Adelaide, small holdings, and regional settlements. Some localised areas have been mined for kaolin, gravel, copper, zinc and tin, and quarried for building stone and gravel. The steep and variable slopes, coinciding with the generally wet winters of much of the region ensures that little of the MLR is suitable for extensive cropping, e.g. growing cereals and canola. The region is also susceptible to various land degradation issues, which include waterlogging, salinity and erosion.

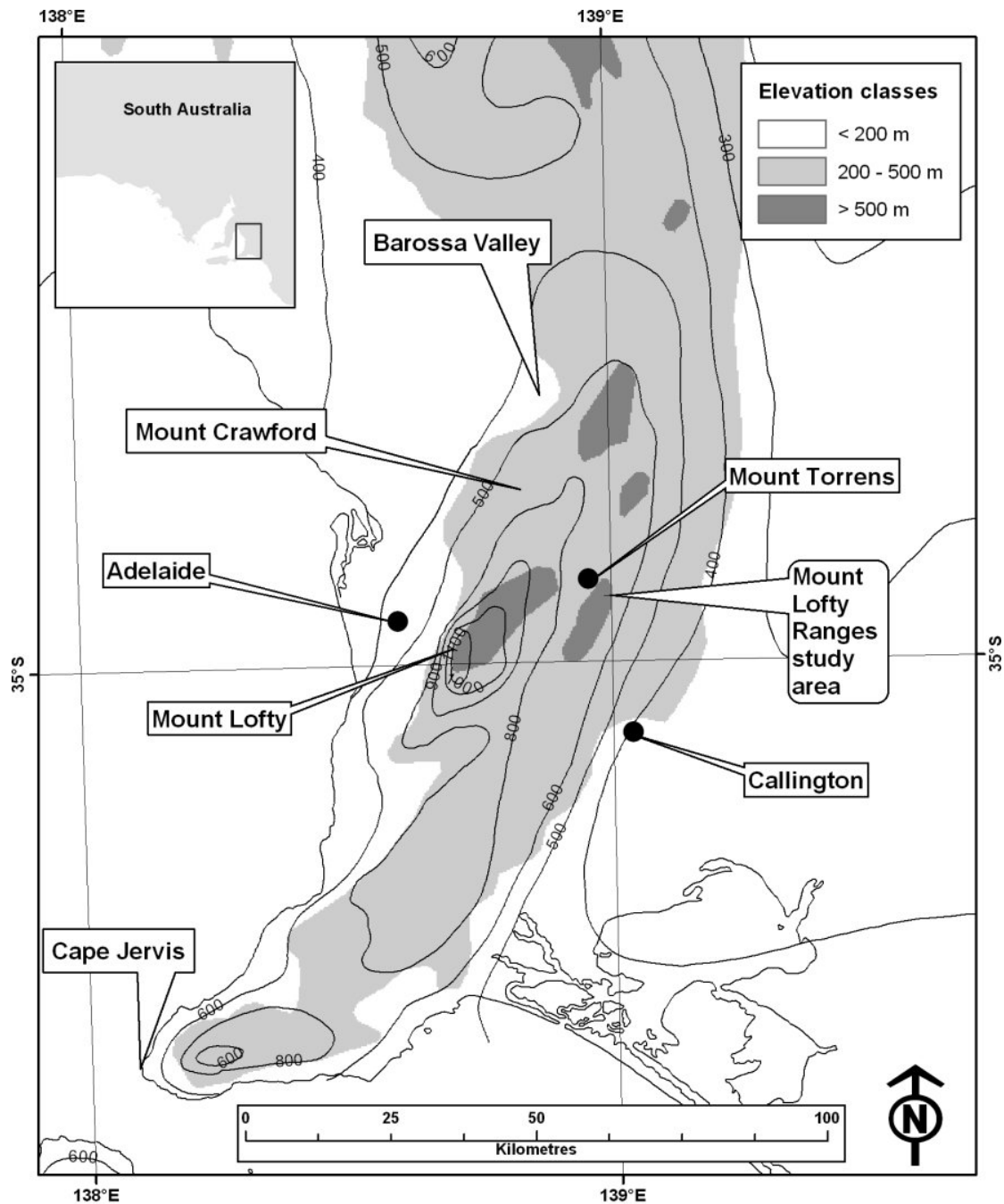


Figure 9.1. Locality map showing the South Australian setting (inset box) for the Mount Lofty Ranges (MLR) study area, featuring elevation classes (m) and annual rainfall isohyets (mm).

The soil-landscapes of the MLR are extremely complex due to the variable geology of the region, and variable weathering histories and development stages of the soils. Generally, the soils are ancient and have undergone prolonged periods of tectonic stability, resulting in preserved soils. Interrupting these periods, there have been times of renewed tectonic

activity. These periods are associated with etching of the preserved soil-regolith profiles, which has led to exposure of fresh bedrock, and new pedogenic cycles. In the modern landscape, ancient soils that mantle deeply weathered regolith (containing deep profile stores of salts, i.e. deep NAS) are juxtaposed with younger, shallower soils that mantle profiles of

actively weathering rocks that are actively releasing salts (e.g. Na, Cl and SO₄) in the landscape. Compounding the complexity of MLR soil-landscapes is the relatively recent imprint of colonial settlement and landuse, and the affect of these on contemporary saline groundwaters and near-surface hydrological patterns. The study area features the juxtaposition of the ancient and contemporary domains discussed above, which has resulted in a diversity of soil-landscape systems, pedology, mineralogy, hydrology and soil degradation processes. It is for this reason that the study area has received considerable research interest within the past 20 years, which has resulted in a strong legacy of data and soil-landscape knowledge.

9.2 Climate

The MLR region has a Mediterranean-type climate, which features cool, wet winters and hot, dry summers. Approximately 65 % of the annual rainfall falls in the winter months (May to September). The topography of the MLR exerts an overriding influence on the regional rainfall distribution. This is because the steeply rising western flanks of the ranges cause the much of the moisture brought in on the westerly-dominated winter weather systems to be shed early, creating a strong rainfall gradient in the leeward, eastern zones of the Ranges. For example, the western flanks of the MLR feature an annual mean rainfall in the range 800 to 1,100 mm, whereas within the relatively short distance of approximately 30 km, the township of Callington (eastern ranges) receives a mean annual rainfall of 380 mm (Figure 9.1).

The study area receives a mean annual rainfall of 680 mm, and has a mean annual evaporation rate of 1,170 mm. This results in a mean annual rainfall deficit of 490 mm (Fritsch and Fitzpatrick 1994). Most of the annual rainfall occurs in the winter months of April to October, which is the growing season for crops. Rainfall beyond this period tends to be sporadic and intense, occurring during thunderstorms (Fitzpatrick *et al.* 1993).

Approximately 18 km northwest of the study area, the Mount Crawford weather station (Figure 9.1) provides longterm weather records (1954 to present day). Although the distance between Mount Crawford and the study area results in an absolute difference in climate, the broad trends nevertheless are comparable. Figure 9.2 shows the monthly climate data for the Mount Crawford weather station for the years 1954 to 2004, and shows the monthly means for: (i) rainfall, (ii) daily maximum temperatures, (iii) daily minimum temperatures, and (iv) evaporation records. These show a peak rainfall in the winter months (approximately 100 mm per month, May–August), and less rainfall in summer months (approximately 30 mm, November–March). Summer rainfall is generally characterised by intense, short-lived events, which may result in water erosion. In the summer months the mean daily maximum temperatures exceed 25 °C, and temperatures may exceed 40 °C. Mean daily minimum temperatures in the winter may be below 0 °C, with daily minimum temperatures reaching approximately 15 °C during the same period. According to Soil Survey Staff (2003) the study area soil temperature regime is mesic and the soil moisture regime, xeric.

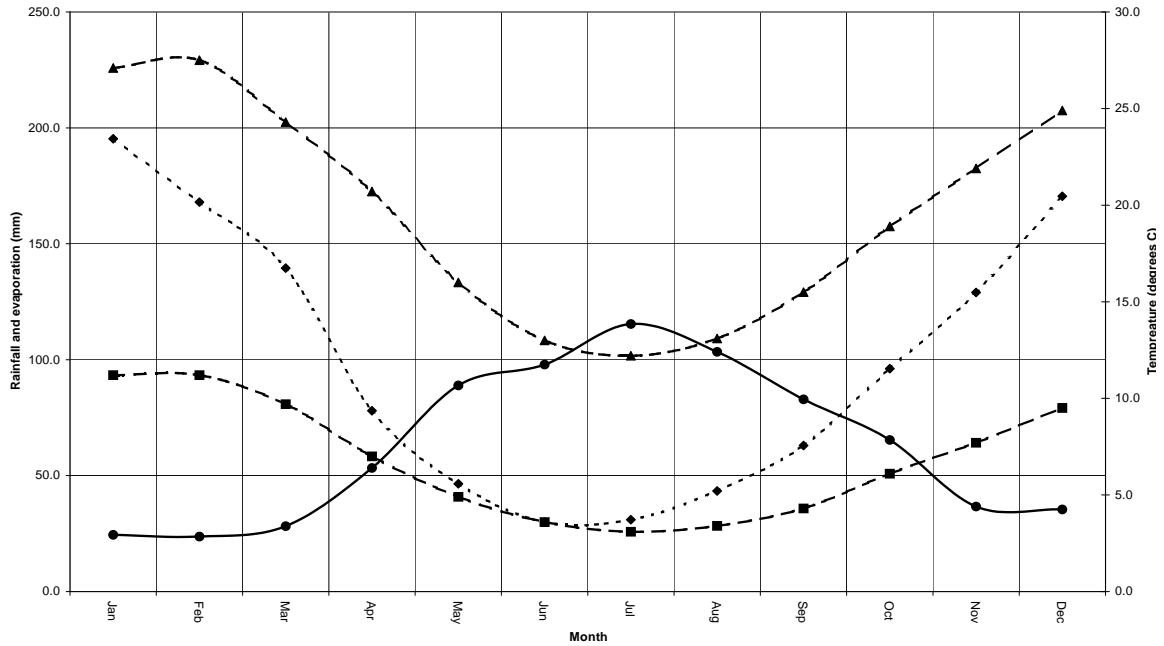


Figure 9.2. Mount Crawford weather station climate trends showing mean monthly (i) rainfall (mm) (●), (ii) daily maximum temperatures (°C) (▲), (iii) daily minimum temperatures (°C) (■), and (iv) mean monthly evaporation (mm) (◆) for the years 1954 to 2004 (source: Australian Bureau of Meteorology, www.bom.gov.au/climate/averages/tables/cw_023763.shtml).

9.3 Geology

The geology of the study area is presented in the Adelaide 1: 250,000 scale sheet (Geological Survey of South Australia 1964a). The mapping is also available in GIS format at a scale equivalent to 1: 100,000, of which a portion corresponding to the study area is presented in Figure 9.3. The regional geology is summarised by Wilford (2004c), while detailed investigations of geology, geochemistry and regolith of the study area are presented in Fitzpatrick and Skwarnecki (2003) and Skwarnecki *et al.* (2002a).

The bedrock geology of the study area is Cambrian in origin and forms part of the Kanmantoo Group, which is part of the Adalaidian Geosyncline. The Kanmantoo Groups, which has an apparent thickness of 15 km, features sandstones, siltstones and phyllites that are interlaced with pelites and minor carbonates. The stratigraphy of the study area strongly features north-

south lineaments, and a strata that dips sub-vertically (Daily and Milnes 1971; 1973; South Australian Geological Survey 1995). The western edge of the study area features laminated metasedimentary sandstones (unit Eeb) of the Backstairs Passage Formation (Figure 9.3). This formation features shallow soils with significant areas of outcropping and subcropping bedrock. A disconformity in the Backstairs Formation occurs in the form of the Tapanappa Formation. On the western boundary of the Tapanappa Formation is a disjointed band of Talisker-Calc siltstones (unit Esa) that forms a regionally significant source of pyritic minerals, and in which gossans are commonly found. To the east of the band of siltstones occurs a unit of fine to coarse grained micaceous sandstones, schists and greywackes (unit Est). Localised areas of siltstones that are rich in pyritic minerals are also found in this unit. East of this unit lies a Quaternary unit of undifferentiated overburden of alluvial

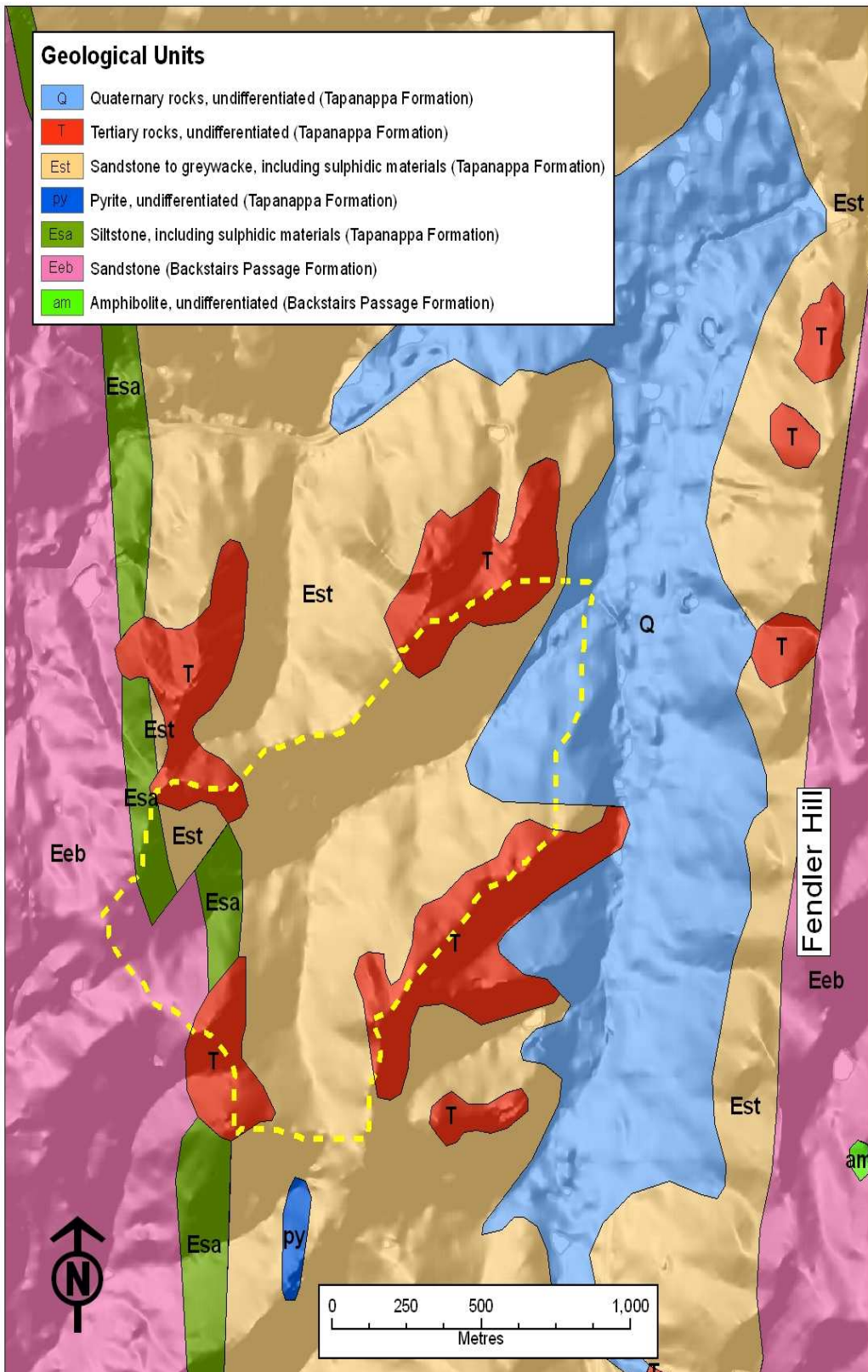


Figure 9.3. Geology of the Mount Lofty Ranges (MLR) study area (outlined) at 1:100,000 scale (Geological Survey of South Australia 1964a), with a hillshade applied to accentuate local landform.

origin (unit Q). This unit borders in the east with another locally high ridge (featuring “Fendler Hill”) comprising sandstones (unit Eeb) at the eastern margin of the Tapanappa Formation disconformity bordering the sandstones of unit Eeb.

9.4 Airborne gamma-radiometric and magnetic coverages

Regional aeromagnetic surveys comprising gamma radiometrics and aeromagnetics (Horsfall 1997) were conducted in the region surrounding the study area during September 2003 (Walker *et al.* 2004). The airborne survey line spacing used was 100 m, and the survey was conducted at a flying height of 60 m above ground level. The combination of flying height and air speed resulted a flightline sampling rate of approximately one survey point per 7 m. On board, the acquisition system precisely georeferenced the radiometric readings and enabled the raw data to be interpolated to create the 20 m

resolution GIS images that were supplied by Geosciences Australia. In terms of gamma radiometric acquisition, the data acquired consisted of four channels comprising: (i) potassium (K) %; (ii) thorium (Th) ppm; (iii) uranium (U) ppm; and (iv) total count (TC) ppm. This information was used to help regional soil-regolith processes (e.g. weathering history) and resulting surface geochemical distribution (e.g. Wilford 2004c). The aeromagnetic survey data is suitable for interpreting regolith and lithological patterns, which includes identification of paleochannels (Cresswell and Liddicoat 2004; Walker *et al.* 2004) and iron-rich (e.g. pyritic) anomalies (Reynolds 2000).

A review of the spatial relationships between the geological units, landform (from hillshade) and the 20 m resolution airborne geophysical survey data shown in Figure 9.4 was conducted visually to enable preliminary understanding of soil-landscape processes relationships. The relationships identified are described in Table 9.1.

Table 9.1. Interpreted relationships between airborne K %, Th ppm, U ppm and aeromagnetic First Vertical Derivative survey coverages and soil, regolith and geology (Figure 9.3) in the Mount Lofty Ranges (MLR) study area.

Airborne geophysical coverage	Soil-regolith-lithological relationship
K (%)	Tertiary units (unit T) are generally associated with areas of lowest relative K % responses in the landscape. These areas are associated with deeply weathered landscape locations in which, over time, the more soluble and mobile K is depleted from soil surface profiles. Higher relative K % responses in the catchment are associated with the western part of the catchment are associated with subcropping or outcropping of: (i) sandstones of the Backstairs Passage Formation (unit Eeb), and (ii) the Talisker-Calc (unit Esa; Tapanappa Formation), which is usually associated with mineralised zones. The quaternary unit (unit Q) in the eastern region of the catchment broadly demonstrates a lower K % response, likely to be associated with residual alluvium.
Th (ppm)	The Th and K patterns are generally inversely related, reflecting the opposite geochemical tendencies that geomorphic and weathering processes have on the environmental concentrations. Tertiary units (unit T) are associated with areas of higher relative Th in the catchment. These areas are associated with deeply weathered landscape positions in which Th, over many years, has been scavenged by Fe-oxides in the soil-regolith, and accumulated in the near-surface of soil profiles. Also, steeper landscape areas that are likely to be less geomorphically stable in relative terms tend to display lower Th concentrations, reflecting the influence of lower concentrations of residual material, which is also associated with areas of the quaternary unit (unit Q) in the eastern catchment zone.
U (ppm)	The U catchment coverage exhibits a speckled pattern, which offers little visual coherency to either landform or the geological units. Indeed, the speckled patterns may be more reflective of the inherently poor signal to noise ratio often associated with airborne radiometric U sampling systems (Minty <i>et al.</i> 1997). However, in the Tapanappa Formation sandstone areas (unit Est), the south-facing slopes show patterns of higher relative U concentrations in mid slope areas, whereas in the north facing slope, the patterns of relatively high U responses are evident in the higher relief interfluvial landforms, and in parts of tertiary (unit T) in the south-west of the catchment. The Tapanappa Formation Talisker-Calc unit (unit Esa) also corresponds with a zone of higher U concentration. The Backstairs Formation sandstone (unit Eeb) is consistent with lower relative U concentrations.
Magnetic First Vertical Derivative (MFVD)	A single high MFVD “hot spot” in the study area corresponds strongly with a section of the southwesterly tertiary unit (unit T) and the Talisker-Calc unit (unit Esa), indicating that these units exhibit a strong and positive magnetic contrast with surrounding geological units. This indicates the existence of a discrete pyritic lithological unit.

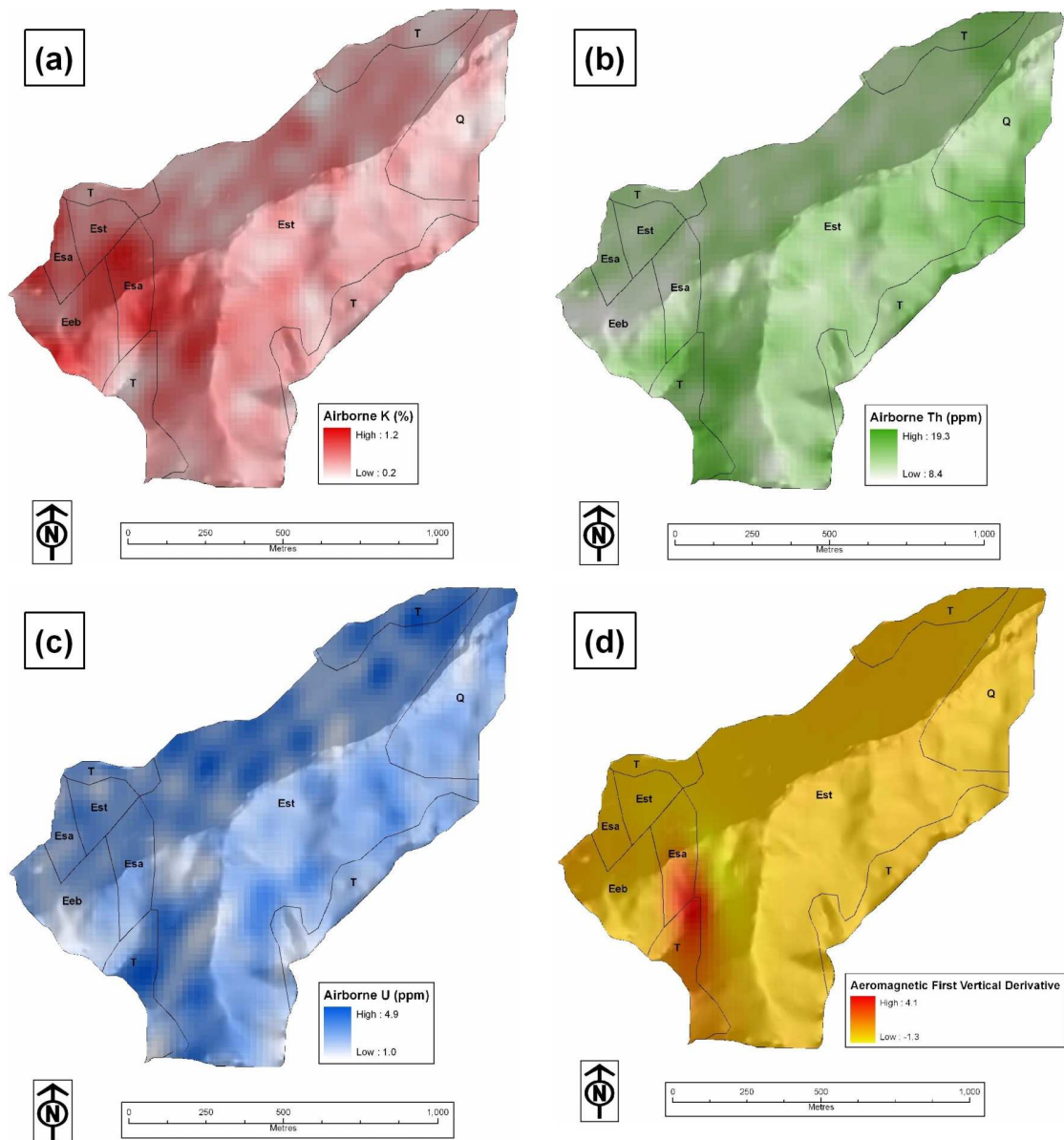


Figure 9.4. Airborne geophysical surveys of the Mount Lofty Ranges (MLR) study area with geological units overlaid, and hillshading applied to accentuate local relief. Plate (a) shows K (range: 0.2 – 1.2 %), plate (b) shows Th (range: 8.4 – 19.3 ppm), plate (c) U (range: 1.0 – 4.9 ppm), and (d) aeromagnetic first vertical derivative.

9.5 Magnetic susceptibility surveys

A surface volume magnetic susceptibility (κ) survey of the whole study area was conducted on foot during September 2005 using a Bartington MS2F probe (e.g. Dearing 1999b). The survey was conducted simultaneously with an EM38 survey using the same survey sites, which are shown in Figure 9.5. The survey was conducted at pre-determined survey

points that were planned using a GIS. The survey was conducted with the aid of a hand held field computer, which integrated the capability to conduct field data entry, GIS display of the survey sites, and real time GPS navigation. The survey design involved traversing the whole catchment on a north-south bearing that essentially crossed the main relief and pedogenic trends of the landscape. Survey lines were separated by 50 m, and a sampling interval of 25 m was used.

Deviations from the planned rigid survey plan were made to: (i) accommodate fence lines to avoid background electromagnetic interference (EM38), and (ii) to collect additional survey data at locations of interest encountered during the surveys. In this way, the catchment survey resulted in 1,085 georeferenced survey sites visited (Figure 9.5).

Once located on the ground, the survey sites were prepared for κ measurements by scuffing the surface of loose debris (e.g. plant material and stones), and noting the average of 10 soil surface κ values made within close proximity of one another. On completion of the survey, the data collected were transferred to a desktop GIS, and the data interpolated using ordinary kriging (Burrough and McDonnell 2000). In this way a five metre GIS coverage of the κ survey was generated, which is displayed in Figure 9.6.

In addition to the κ survey conducted in the study area, 29 sites that are

shown in Figure 9.5 were selected for profile depth-based mass magnetic susceptibility (χ) investigations. Their selection of sites was based on: (i) prior field knowledge of soil types, and (ii) the combined investigation of soil-landscape patterns, including local terrain and drainage. Once the sites were located in the field using a GPS, profile samples were collected according to pre-determined layer depths shown in Table 9.2. The upper layers of the profile (L1 and L2) were collected using a trowel, and the lower layers (L3 and L4) were collected using a gouge auger. The χ measurements were conducted on the < 2 mm fraction of the samples collected, using a Bartington MS2B Dual Frequency sensor in accordance with the methods in Dearing (1999a). The low frequency results (4.6 kHz) for each profile layer are graphically presented in Figure 9.6. The full dataset of χ data, which includes high frequency and the mass magnetic frequency dependency susceptibility ($\chi_{fd\%}$), are shown in Appendix G.

Table 9.2. Layer identification and depth ranges (m).

Layer sample ID	Depth range (m)	Dominant horizon
L1	0 – 0.05	A
L2	0.05 – 0.1	
L3	0.1 – upper B	A/E
L4	Upper B – 0.75	B

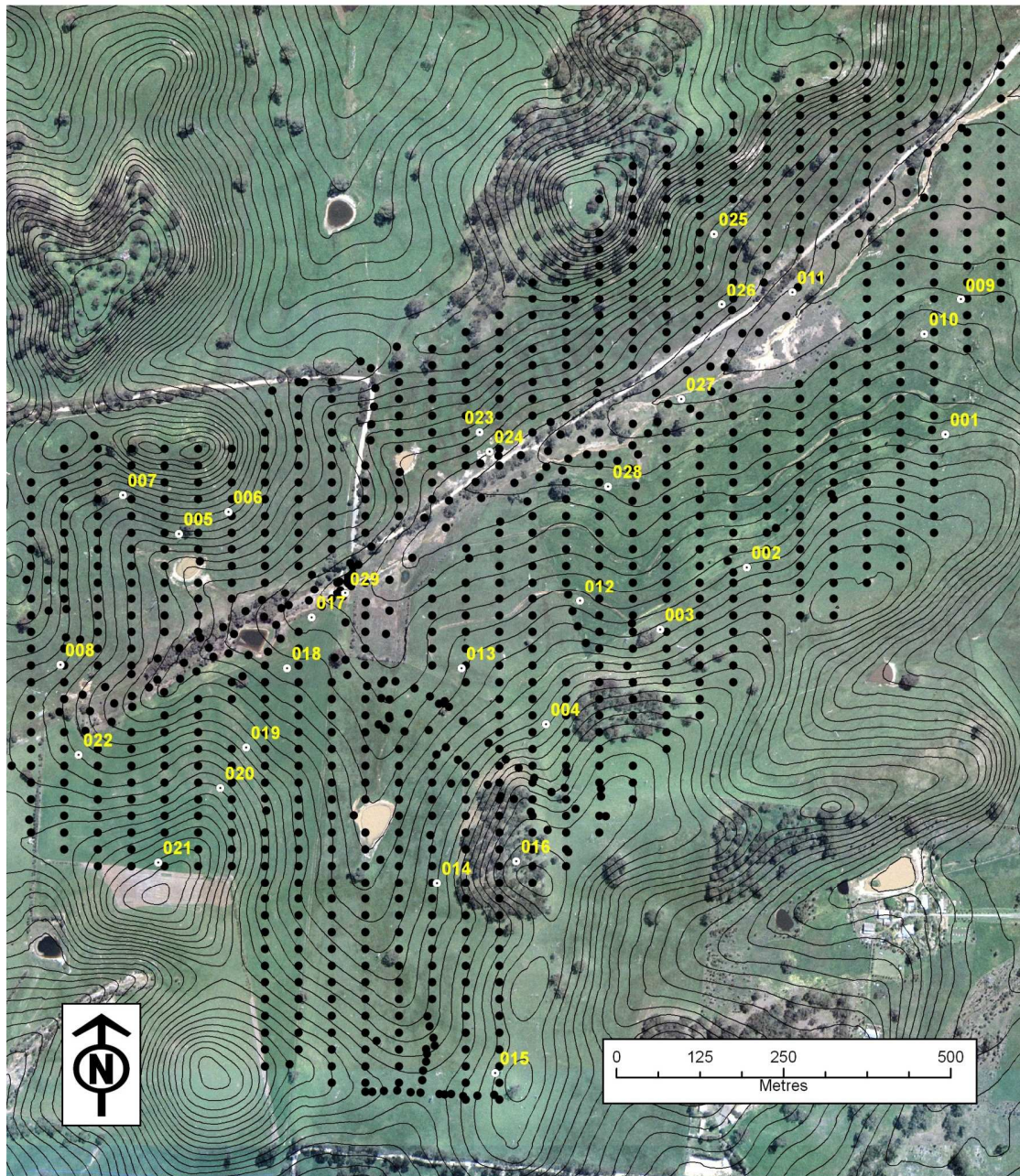


Figure 9.5. Mount Lofty Ranges (MLR) study area surface volume magnetic susceptibility (κ) survey sites (•) and sites selected for profile (⊙) mass magnetic susceptibility investigations (χ), which are overlaid on an aerial photograph, with 2 m contours applied to show landform.

The surface κ survey patterns (range: -8.6 to 500 10^{-8} SI) are shown Figure 9.6, and superimposed on these, the profile layer χ analytical data (range: 0 to 950 10^{-8} SI). Strong surface κ patterns are evident in the study area, particularly on the north facing slopes. The patterns coalesce to form five surface κ value zones of elevated values identified as “a” to “e”. Visually, the surface κ patterns correlate closely

with the profiles that feature in their layers elevated χ values.

The surface κ -elevated value zone identified as “a” in Figure 9.6 spatially corresponds to: (i) the geology of the tertiary (unit T) and the Talisker-Calc siltstone (unit Esa) geological units (Figure 9.3), and (ii) the high MFVD value zone (Figure 9.4). The spatial

coincidence of the high MFVD value response zone with the Talisker-Calc siltstone (unit Esa) confirms the presence of Fe-sulfide (pyritic) materials in the soil-regolith-bedrock profile (Reynolds 2000). With respect to the χ values of the corresponding profiles (18, 19 and 20) in Figure 9.6, the surface κ -elevated value zone identified as “a” features enhanced magnetic susceptibility in the A horizon (L1, L2 and L3), while the upper B horizon features relatively lower values. The elevated magnetic susceptibility (κ and χ) associated with the A horizons of the profiles reflects pedogenic magnetic enhancement caused by firing under bushfire conditions in the upper profile. The burning conditions are attributed to: (i) the formation of maghemite from other Fe-oxides (Mullins 1977; Thompson and Oldfield 1986), and (ii) the Fe_9S_{10} -form of pyrrhotite from other Fe-sulfides from the mineralised zone (Evans and Heller 2003; Thompson and Oldfield 1986). The analysis of the < 2 mm soil fraction makes it likely that sand grain-sized detrital magnetite are no longer present in the soil bulk to contribute to the χ measurement. With reference to Figure 9.6, the shape of the surface κ -elevated value zone identified as “a” features a “fan” shape, in which the apex of the shape is located in the near-summit of the hillslope, and the base of the shape is located at the bottom of the slope. This pattern suggests a down slope colluvial process that re-distributes grains of maghemite and pyrrhotite (and probably magnetite, given the κ measurement on the unsieved surface soil) in the upper profile down slope.

The surface κ -elevated value zones corresponding to “b” to “e” shown in Figure 9.6 are associated with zones of the north facing lower to mid hillslopes. The elevated surface κ responses in these zones are explained by the strong presence of magnetically active ferruginous gravels seen on the soil surface. These presence of the gravels on the soil surface is caused by the action of cultivation by plough disk that takes place on the farmed lower gradient slopes. The action of cultivation has caused the ferruginous gravels that are normally concentrated in the upper later of the B horizon to be brought to the surface. The strongest κ response zones are particularly associated with scalds and depositional accumulations of the ferruginised gravels connected to erosional scars in the low-lying drainage zones of the study area landscape. However, subtle κ patterns particularly associated with mid slope positions on the north facing slope areas are also evident. These κ patterns are likely to reflect κ enhancement of the soil surface due to periodic firing of the drier soils during bushfires before the land was cleared. In general terms, the magnitude of the profile layer χ responses shown in Figure 9.6 match those of the surface κ patterns, i.e. zones of elevated κ responses feature profile χ responses that feature layers with strong responses. Given that the χ analysis of the layers was on the < 2 mm fraction, the χ values received no contribution from the ferruginous gravels that featured so strongly in the surface κ patterns.

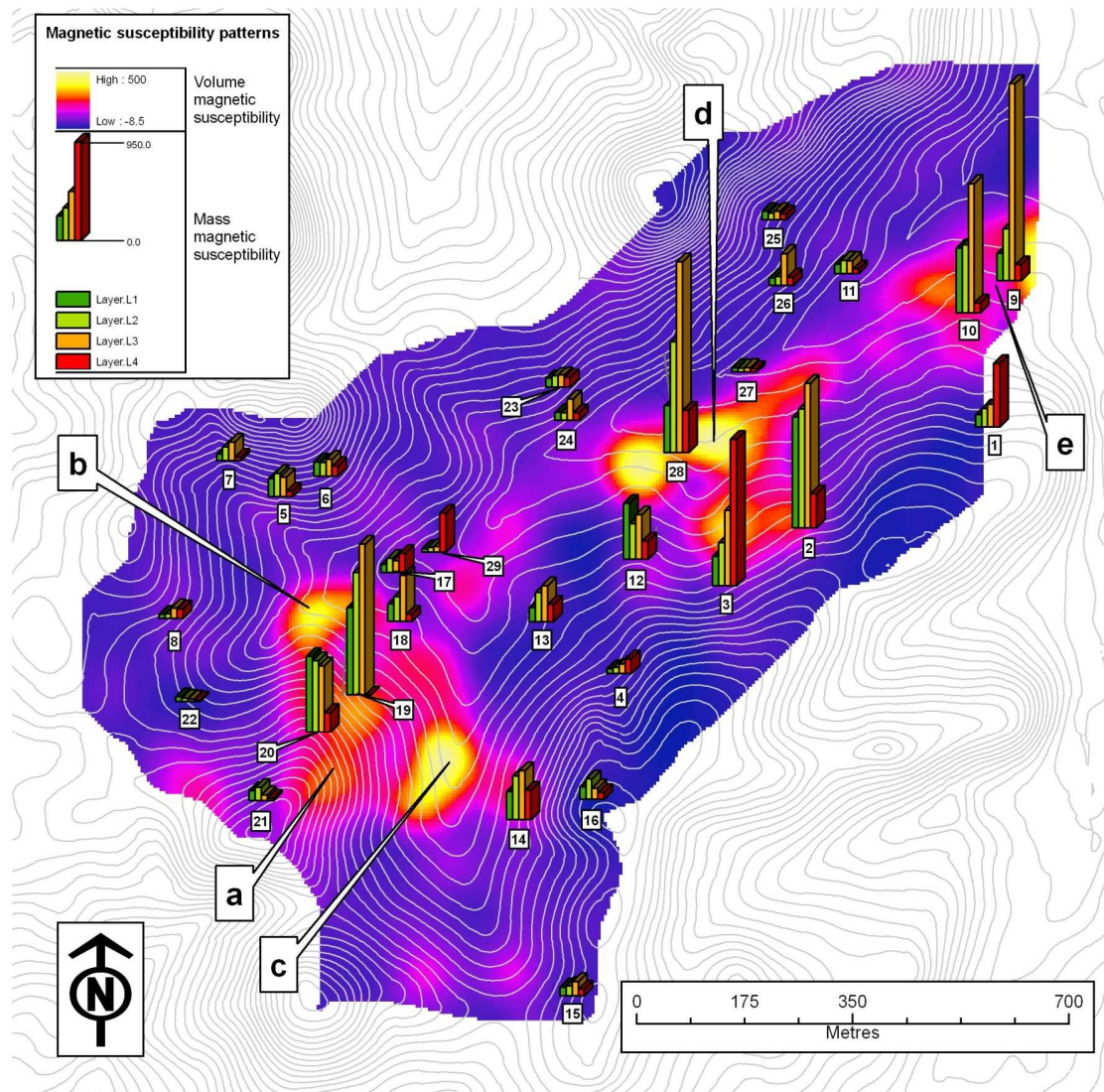


Figure 9.6. Mouth Lofty Ranges (MLR) study area volume magnetic susceptibility (κ) survey patterns with selected profile mass magnetic susceptibility analytic data presented in layer-by-layer graphic form. Two metre contours are overlaid to indicate landform. Regions of interest “a” to “e” are identified.

9.6 Landform

Figure 9.7 shows the landform of the study area, which is highlighted using an overlay of two metre interval contours generated from a DEM that was specifically commissioned of the research. The DEM was generated photogrammetrically from a stereo pair of 1: 40,000 scale aerial photographs, which produced a GIS dataset of a regular array of precisely

georeferenced elevation data points with a spatial interval of three metres, and precise to within sub-metre elevation accuracy. The elevation data points were incorporated into a GIS and interpolated using ordinary kriging (Burrough and McDonnell 2000) to create a GIS raster format with a resolution of three metres. A GIS was used to predict the drainage patterns, as shown in Figure 9.7 from the DEM.

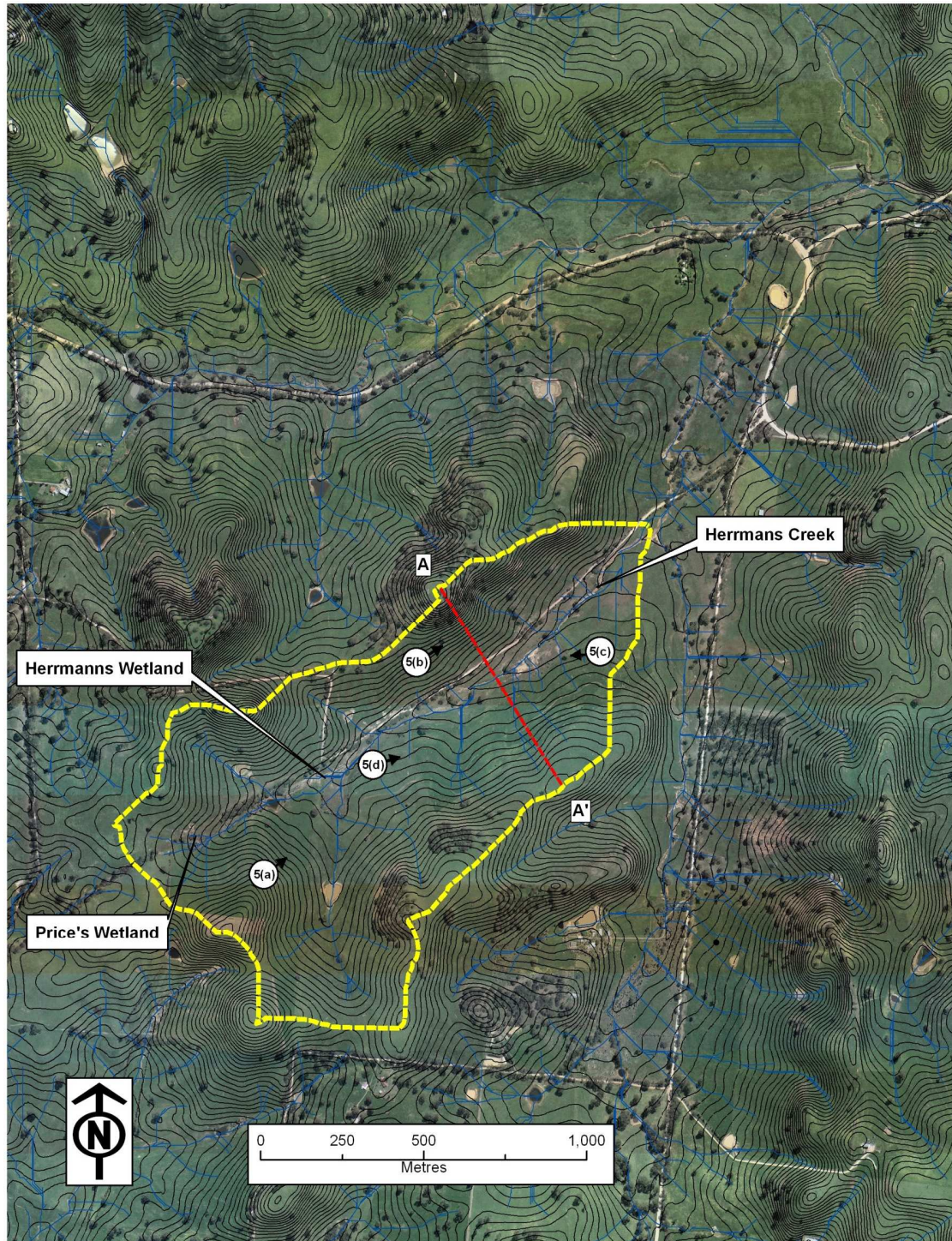


Figure 9.7. Aerial photograph showing the MLR study area (yellow outline), featuring terrain (2 m contours), transect A-A', modelled drainage using GIS, and location and view orientation of the plates shown in Figure 9.9.

The study area comprises a valley floor surrounded by rolling hills that form the watershed. Geomorphically, the study area consists of three units: summits, side slopes and stream terraces. The summit is generally

dominated by Tertiary landforms that feature a mantle of ferruginised saprolite dominated by kaolin formed by strong *in situ* weathering (Mesozoic to present) of very fine-grained feldspar and biotite-rich

metasediments. These form low relief summits that are fringed by often steep shoulderslopes formed by headward erosion etching away at the summits. The side slopes feature less weathered fine-grained metasediments comprising interbedded siltstones and sandstones hosting zones rich in sulfides and pegmatite. Finally, the creek terraces comprise Quaternary deposits of colluvial-alluvial material that have gravel and finer grained textures (Fitzpatrick *et al.* 1993).

The study area has an elevation range of 455 to 385 m and broadly comprises north facing and south-facing

colluviated hillslopes, which are bisected by Herrmanns Creek. Figure 9.7 identifies the 700 m transect A-A' that straddles the main valley of the catchment. The GIS-derived elevation and slope profiles corresponding to the transect are shown in Figure 9.8. These profiles show that the north facing hillslope has a low gradient not exceeding 7 °, and reaches a summit altitude of approximately 420 m. The south-facing slope is steeper (maximum gradient of 20 °) and has a higher summit reaching an elevation of 445 m. Various field views featuring sections of the transects are shown in Figure 9.9.

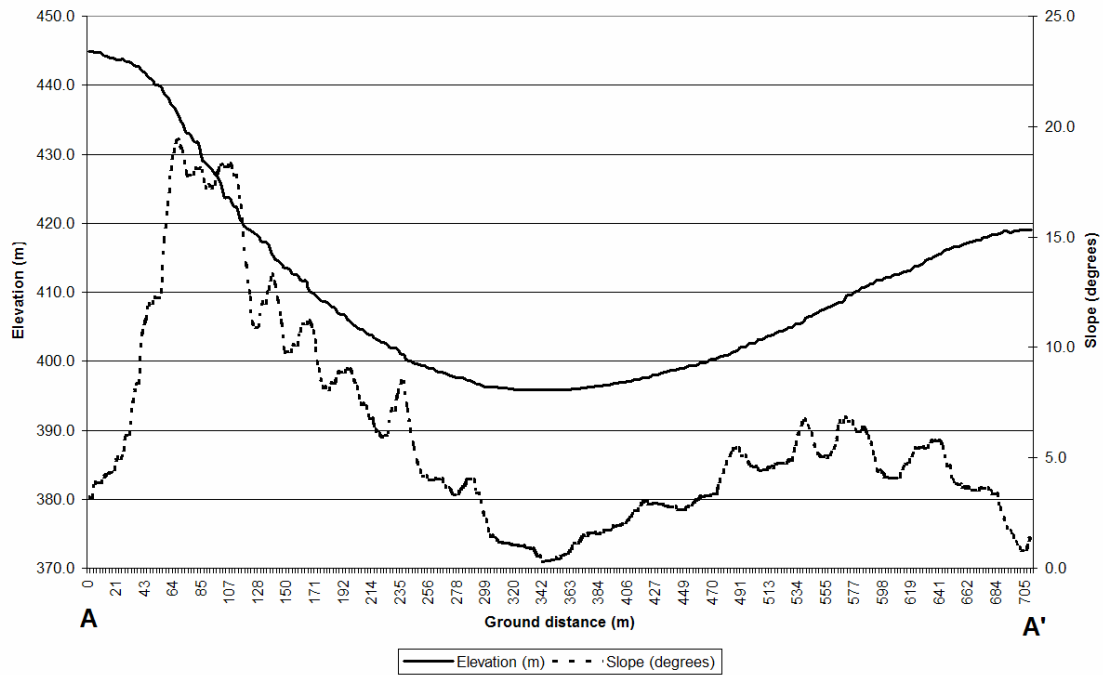


Figure 9.8. Profiles of elevation (m) (—) and slope (°) (---) for transect A-A' located in Figure 9.7.

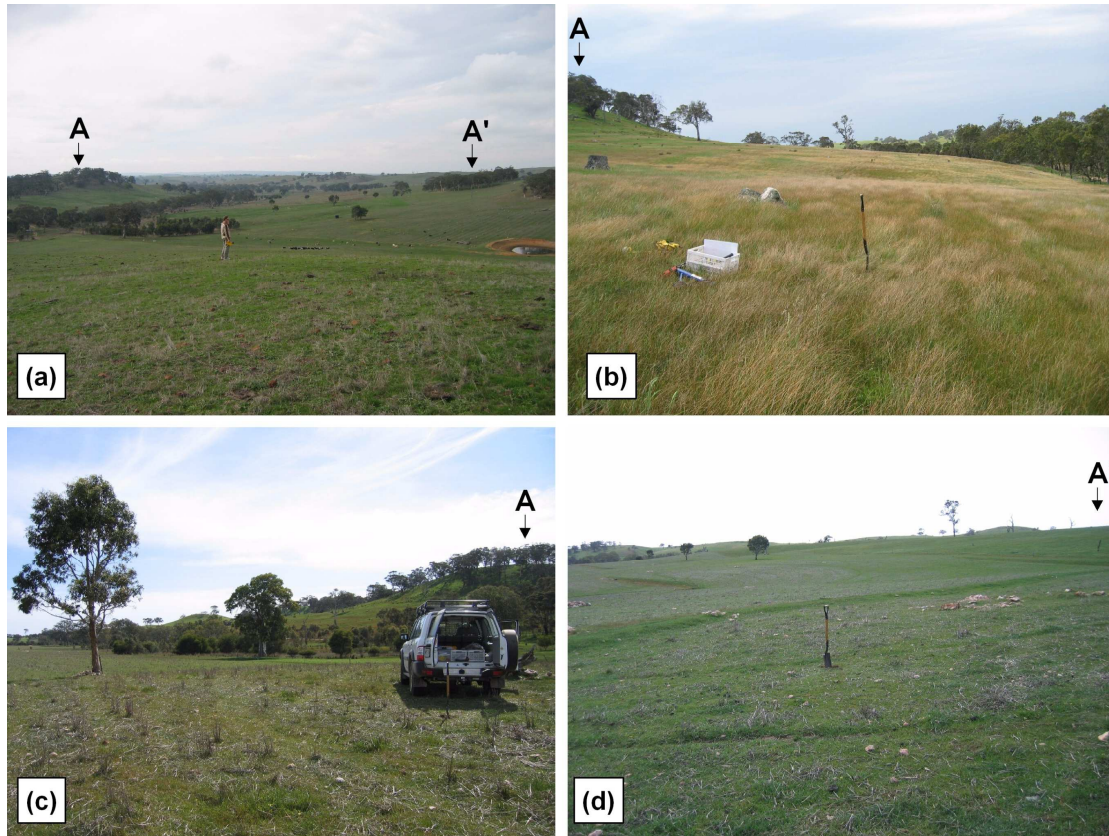


Figure 9.9. Plates showing MLR study area scenes featuring the transect A-A' shown in Figure 9.7 and profiled in Figure 9.8. Plate (a) features a north-easterly view of the south- and north facing hillslopes, and summits (A and A') defining the transect. Plate (b) features an easterly view of the south-facing hillslope. Plate (c) features a westerly view of the north facing hillslope mid and lower slope zones. Plate (d) features an easterly view of the north facing hillslope mid and upper slope zones.

Figure 9.7 shows that the main axis of the study area catchment runs in a southwest-northeast orientation. Herrmanns Creek, which follows the main axis, is a seasonal creek with strongest flows during winter and spring (April to October), and after

significant summer rainfall events. The creek supports a series of fringing wetlands and stands of remnant and re-vegetated woodlands in the stream terraces. Figure 9.10 shows various scenes of the Herrmanns Creek wetland and lower terrace.



Figure 9.10. Plates showing Mount Lofty Ranges study area views of the Herrmanns Creek terrace. Plate (a) shows a view of the fringing wetland, remnant vegetation and re-vegetation. Plate (b) shows a stand of remnant vegetation in the terrace. Plate (c) shows wetland soil cover adjacent to the creek. Plate (d) is a view of the lower terrace showing eroded creek banks and re-vegetation in the middle distance.

At approximately two thirds from the outflow of the catchment, the creek bifurcates at the “Herrmanns Wetland” (1.5 ha). At the point of bifurcation, one of the tributaries continues undeviated (south-westerly) to the “Prices wetland” (Figure 9.7) in the west of the study area. The tributary to Prices Wetland is fringed by wetlands and stands of conserved native vegetation, which help to moderate stream flows. The second tributary that joins the tributary to Prices Wetland branches due south to drain the most southerly region of the study area. The second tributary is fringed by cultivated fields, and flows in a less moderated manner during the wettest times of the year. Both tributaries have been dammed for stock watering.

Using GIS terrain analysis, the three metre DEM of the study area (discussed above) was used to create the topographic wetness index (TWI) (Moore *et al.* 1993; Wilson and Gallant 2000b) coverage shown in Figure 9.11, and the multi-resolution valley bottom floor (MrVBF) (Gallant and Dowling 2003; McKenzie *et al.* 2000) coverage shown in Figure 9.12. (See also discussion in Chapter 3.)

Interpreted in association with local terrain patterns and soil mapping, areas of sloping gradient in upper hillslope zones that have relatively high TWI values identify areas in which local landform acts to concentrate hillslope water flows. Under moderate conditions, the flows are dominated by near-surface water flow pathways (i.e. throughflow).

However, in extremely wet conditions or under intense rainfall, water flows may be overland. Conversely, relatively low TWI values in areas of sloping gradient in upper hillslope zones indicate zones of recharge if no significant impairments to vertical drainage exist. However, if a Btn horizon is present, these areas may be

imperfectly drained and be associated with seasonal watertable perching (i.e. waterlogging). In low gradient areas in lower hillslope zones, high relative TWI values identify areas that accumulate near-surface water. Such areas may become seasonally waterlogged if drainage is impaired.

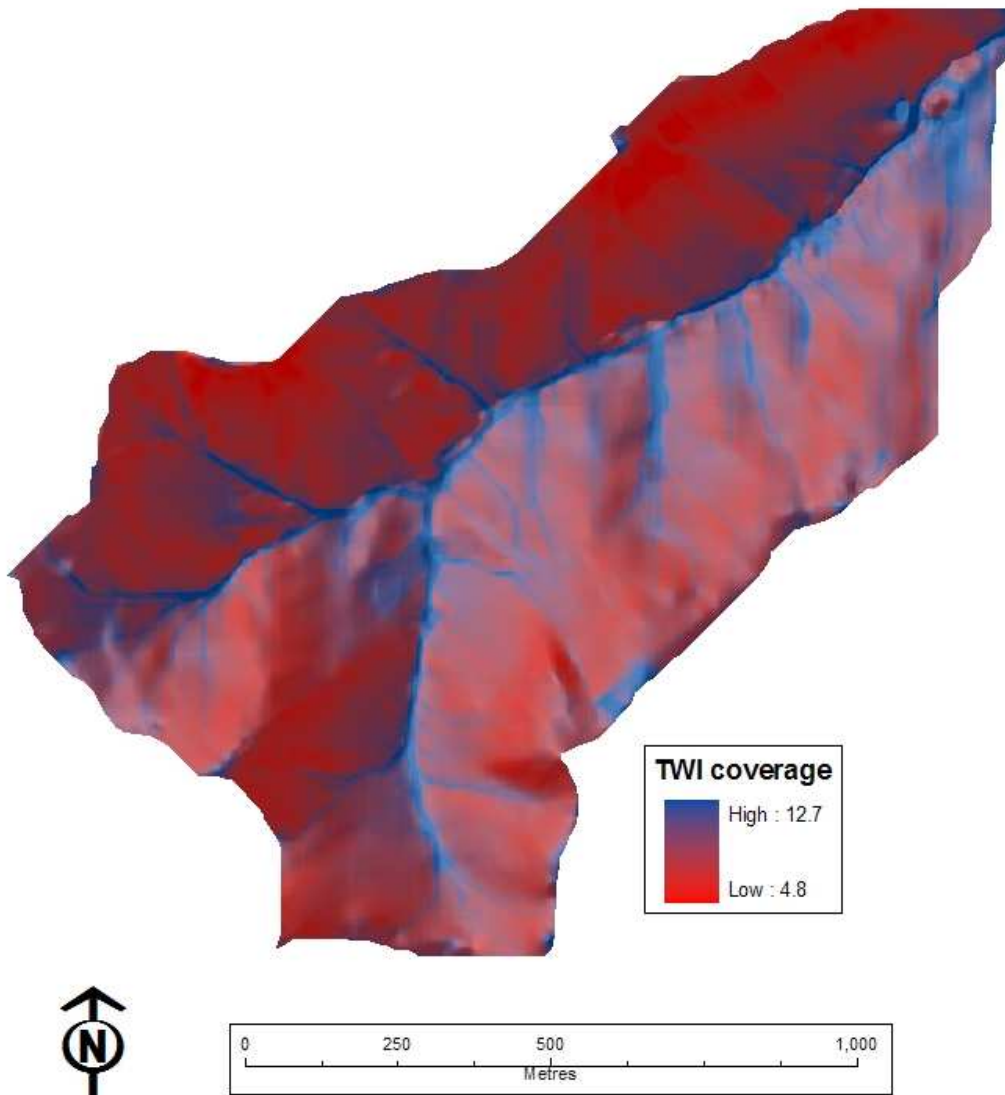


Figure 9.11. Topographic wetness index coverage of the Mount Lofty Ranges study area with a standard deviation stretch applied showing landscape drainage zones, with a hillshade been applied to accentuate local landform.

In conjunction with local landform patterns, TWI patterns and local knowledge of the soils, the MrVBF coverage identifies surface and near-surface hydrology, which may be applied to discriminate zones of erosion from zones of deposition. Areas of high MrVBF values indicate landforms that accumulate water (i.e. depressions), whereas areas of low MrVBF values indicate water-shedding landforms (i.e. summits and ridges).

Interpreted in association with landscape position, high MrVBF value areas in lower slope positions signify

low angle terraces and fluvial zones, while high MrVBF value areas in lower slopes are rarely seen. Low MrVBF value areas in upper slope positions signify high to moderate angle summits and flanks, while high MrVBF values in these areas are rarely seen. High MrVBF value areas in mid slope positions signify drainage zones, while low MrVBF value areas in mid slope areas signify interfluves. Interpretation of landform, and drainage and ponding classes according to hillslope position and MrVBF values are summarised in Table 9.3.

Table 9.3. Interpretation of landform, and drainage and ponding classes according to hillslope position and MrVBF values.

Hillslope and drainage characteristics		High MrVBF values	Low MrVBF values
Upper slope areas	Landform	Rarely seen	High-moderate angle summits and flanks
	Drainage class*		Well drained, and better
	Ponding class*		Occasional, and less frequent
Mid slope areas	Landform	Drainage zones	Interfluves
	Drainage* class	Moderately well drained, and worse	Well drained, and better
	Ponding class*	Occasional, and less frequent	Occasional, and less frequent
Lower slope area	Landform	Low angle terraces and fluvial zones	Rarely seen
	Drainage* class	Moderately well drained, and worse	
	Ponding class*	Frequent	

* Drainage and ponding classes according to Schoeneberger *et al.* (2002).

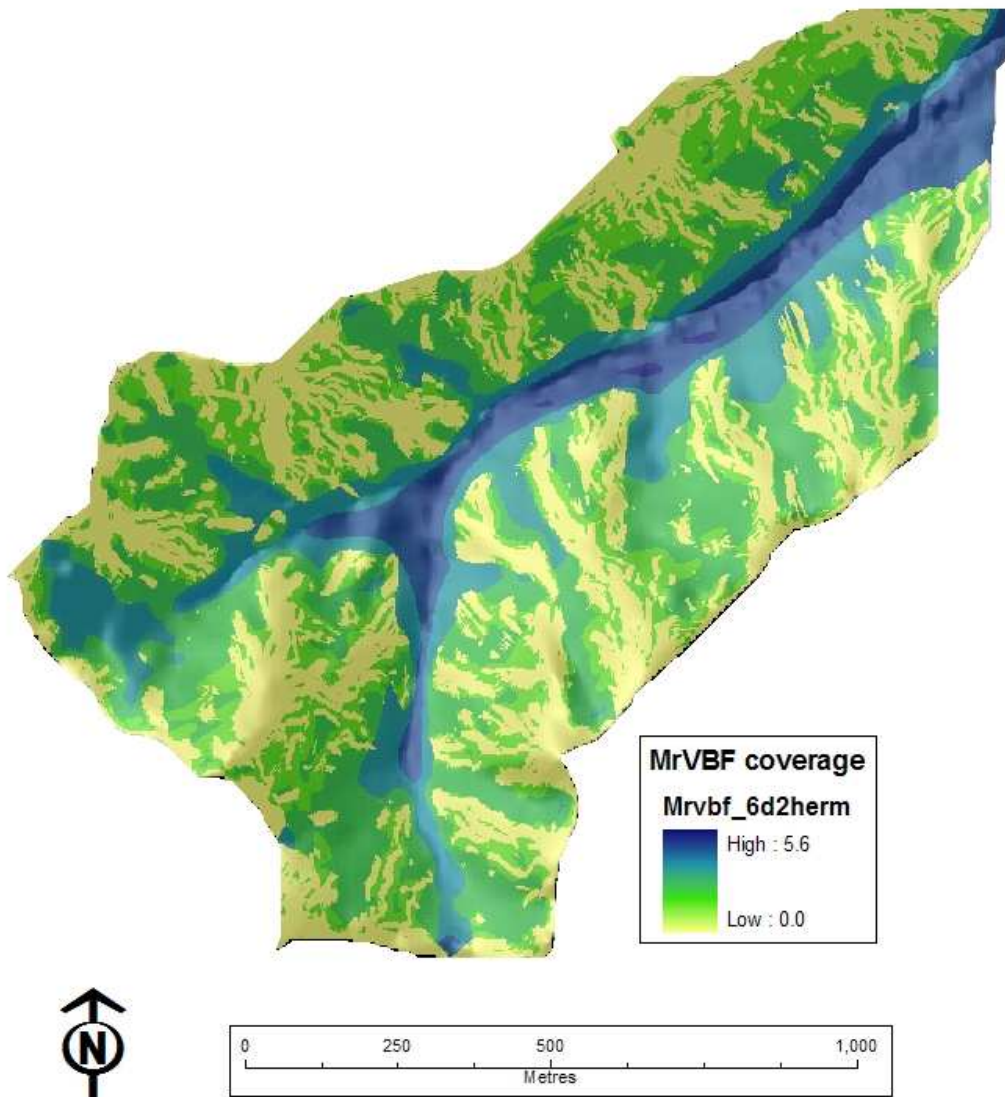


Figure 9.12. Multi-resolution valley bottom flatness (MrVBF) coverage for the Mount Lofty Ranges (MLR) study area with a linear stretch applied for visual consistency. A hillshade has been applied to accentuate local landform differences.

9.7 Soil degradation

The dominant feature of the soil in the study area is the occurrence of a wide range of texture-contrast soils, mostly exhibiting strong development of an E horizon (Fitzpatrick *et al.* 1993). The distribution of the hillslope soils feature a predictable toposequence, with soil properties and morphologies that are strongly consistent with hillslope position and drainage conditions, as discussed in Chapter 3. However, the multifactorial pedogenesis of the study area soil-

landscape (i.e. variable geology, weathering histories, states of preservation and landform) have combined to create a complex arrangement of soils. In addition to the inherent pedogenic complexity described, there is an overprint of post-colonial landuse (e.g. land clearance, circa. 1885 – 1955), which have given rise to contemporary soil degradation patterns. This Section contains an overview of main soil degradation processes affecting the soil-landscape, which is followed with

a general discussion on the soil types of the study area.

Depending on hillslope position, soil degradation in the study area is dominated by processes associated with: (i) perched, near-surface watertables or (ii) deep groundwater watertables. In both cases waterlogging is a major issue in the soil-landscape, and affected areas may also be salt-affected (i.e. saline and sodic) and/or sulfidic (Fitzpatrick *et al.* 1996). Where there is sufficient slope, erosion and scalding may also result.

Waterlogging occurs mostly in the lower gradient slope zones (e.g. at breaks of slope, low in the landscape) during the wettest times of the year (i.e. winter and early spring). Perched watertables that cause waterlogging are the result of impaired drainage because of the presence of less permeable Btn horizons. The waterlogging is confined to the near-surface A and upper Btn horizons in flat and bottomland positions of the landscape. However, waterlogging may also occur on mid- and upper slope positions, especially after periods of intense and prolonged rainfall - even in areas of relatively steep gradients (e.g. slopes greater 8 °). In Figure 9.13 (a) and (b) examples are shown of localised waterlogging and surface ponding in mid slope positions of north facing hillslopes after a period of prolonged rainfall during June 2005. Related to this, the photograph shown in Figure 9.13 (c) was taken on the same day from a similar landscape position in the adjacent depression area in the hillslope. The photograph in Figure 9.13 (c) shows recent erosion of the thin Ap horizon (i.e. < 10 cm) that had exposed the upper layer of the Btn horizon. The grooved appearance of the surface of the Btn horizon was caused by disk cultivation scraping. A series of along-contour reverse interceptor drains were constructed in the hillslope by the farmer to encourage upper slope recharge

(Fitzpatrick *et al.* 1997). The drains failed under the intense rainfall during the June 2005 and caused the erosion previously discussed lower in the slope, as shown in Figure 9.13 (d).

As discussed, the lower hillslope zones (i.e. creek terraces and wetlands) are affected by seasonally fluctuating groundwater watertables that seep upwards under piezometric pressure through the B and C horizons into the surface layers. The saline (e.g. $EC_{se} > 30$ dS/m) groundwater is characteristically rich in salts (e.g. sodium, chloride and sulfate) and iron-rich complexes. Groundwater solutes are derived, in part, from: (i) contemporary weathering of interbedded siltstones and sandstones that host zones rich in sulfides and pegmatite, and (ii) wind blown salts. The seeping groundwaters cause soil surfaces to be crusted by salts and iron-rich evaporites, while the sub-layers feature concentrations of iron- and sulfidic-rich (e.g. mono-sulfides) materials (Fitzpatrick *et al.* 1996). Examples of these are shown in Figure 9.14. Salinity of these soils can become seasonally high (e.g. $EC_{se} > 30$ dS/m) in surface layers due to: (i) summer evaporation or (ii) winter rise of the saline groundwater.

The water quality in the Herrmanns Creek and fringing wetlands is generally in a degraded state, caused by: (i) the concentration of seepage of sodium, chloride and sulfate salts, and precipitation/oxidation of ferrous iron from groundwater, and (ii) consequential erosion and scalding on steeper slopes, as shown in the Figure 9.15 plates. The creek bank is often eroded for much of its course in the catchment. Below nick points the creek bed depth is often incised (e.g. Figure 9.15 (a)), sometimes to a depth of more than two metres. In places saprock is exposed (Figure 9.15 (b)), and in the eroded stream banks deposits of ferricrete lag and magnetic ferruginous gravels Figure 9.15 (c) are evident that have been periodically colluviated

from up slope areas. Discrete exposures of flat, near-horizontal “pavements” in a stepped series are exposed near the creek bed. The so-called pavements comprise preserved ancient wetlands that are characterised by a dark, amorphous organic and mineral-rich grey material of a high bulk density, and contain elevated concentrations of sulfidic materials (Figure 9.15 (d)). Over many years the buried ancient wetlands have been

inundated by groundwaters rich in sodium, chloride and sulfate salts, and have acted as local “sponges”. However, once exposed, the sulfidic material is oxidised and results in water/soil acidification (e.g. < pH 3), and the formation and dispersion of secondary iron gels. The scalding sodic conditions (Figure 9.15 (e)) of the creek banks and fringing zones exacerbate erosion.

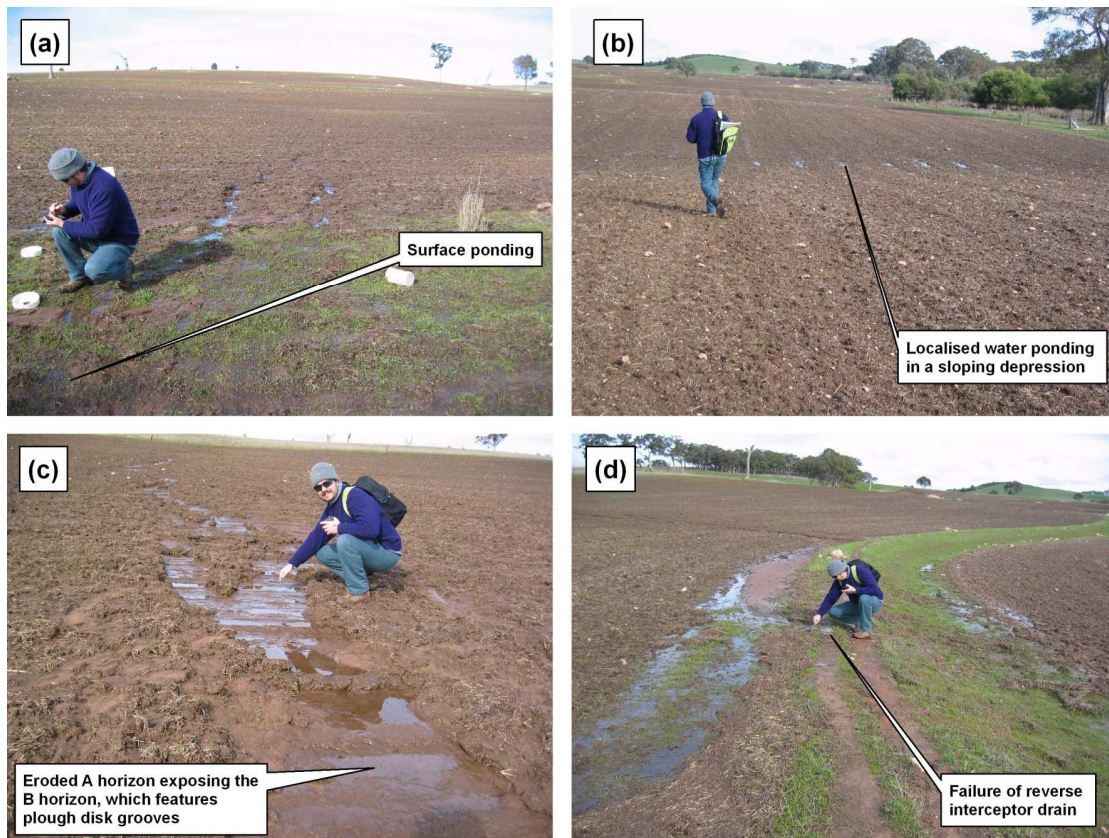


Figure 9.13. Plate (a) showing localised waterlogging and surface ponding in a mid slope zone, and Plate (b) showing ponding in a sloping depression area. Plate (c) shows an example of subsequent erosion, leaving the shallow Btn horizon exposed and showing plough disk grooves. Plate (d) shows an eroded (i.e. “bust”) reverse interceptor drain. All photographs were taken from the north facing slope during June 2005, approximately 24 hours after a prolonged rainfall period.



Figure 9.14. Plate (a) showing eroded surface fissures, which seep saline groundwater under piezometric pressure, in salt encrusted sodic surface clays in scalded lower landscape zones. Plate (b) shows surface salt crusting in highly saline (e.g. $EC_{se} > 30$ dS/m) topsoil. Plate (c) shows salt-iron crusts and exposed mono-sulfidic back ooze in the near-surface, and Plate (d) shows the layering in profile. Plate (e) shows the release of iron-rich gelatinous precipitates (featuring ferrihydrite) to Herrmanns Creek.

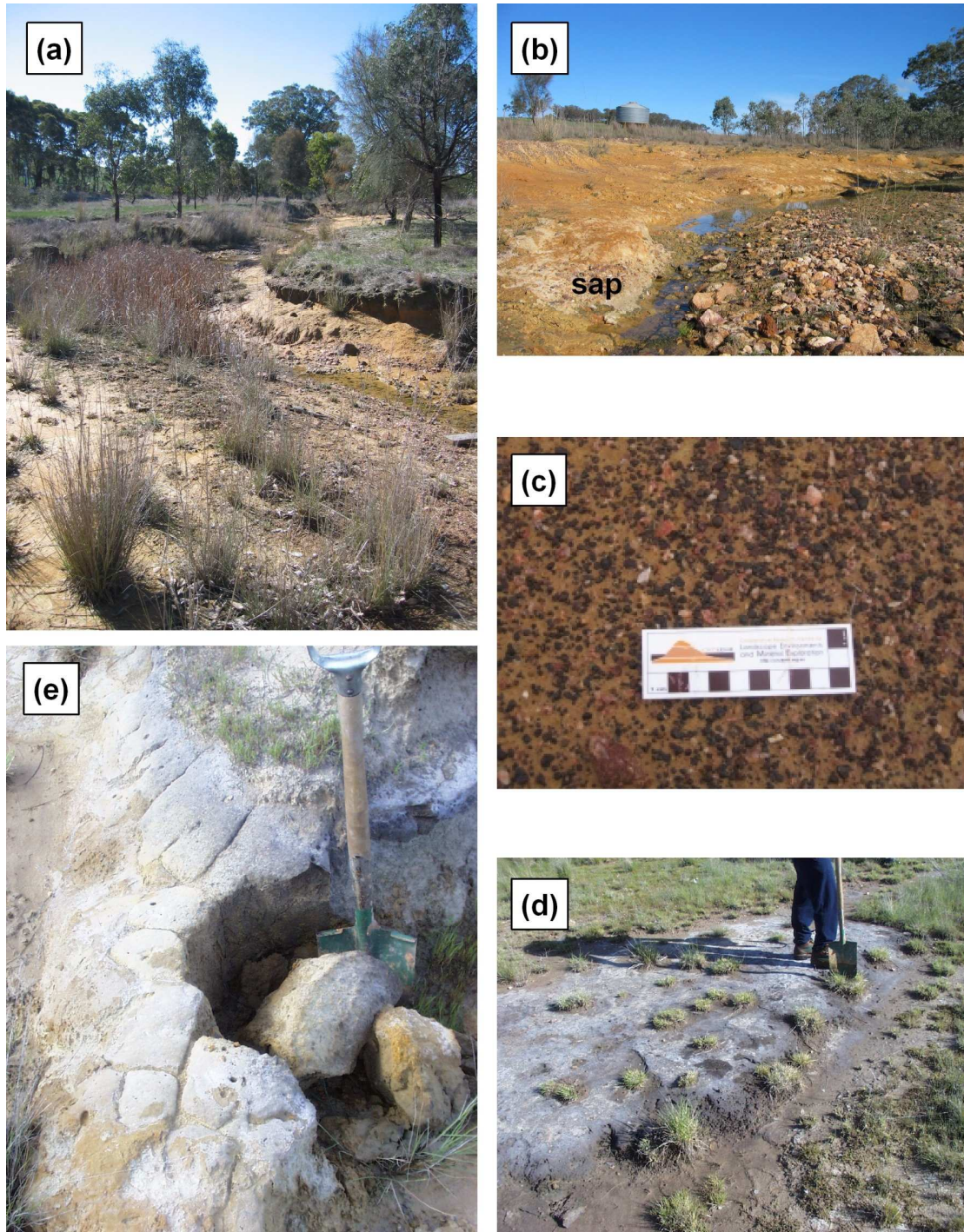


Figure 9.15. Plates featuring Herrmanns Creek and wetlands in the Mount Lofty Ranges study area. Plate (a) shows the incised creek bed and efforts to re-vegetate in the middle distance stand of remnant vegetation. Plate (b) shows the eroded Herrmanns Creek bed and scalded banks in the lower catchment. The photograph shows exposed saprolite (“sap”) adjacent to a deposit dominated by ferruginised saprolite and quartz. Plate (c) shows magnetic iron gravels. Plate (d) shows a salt encrusted remnant ancient wetland of high bulk density and rich in sulfidic materials. Plate (e) shows the columnar structure of an exposed surface of Btn horizon overlaid by an albic, sandy E horizon.

The spatial distribution of the deep (to 6 m) saline groundwaters in the study area were investigated using an EM31 (McNeill 1980b) (see Chapter 3) survey during 1999 (Fitzpatrick *et al.* 1999). The survey involved traversing the study area tangential to the main axis of the creek. An along survey line sampling interval of approximately 20 m was used, and the survey lines separated by approximately 100 m. A free survey was conducted in the steep gradient south-facing slope, north of the creek where the groundwater influence was less due to the gradient. All survey results were recorded and georeferenced in the field using a GPS and integrated in a desktop GIS, which was used to interpolate a five metre resolution GIS coverage using ordinary kriging (Burrough and McDonnell 2000) shown in Figure 9.16.

According to Williams and Baker (1982), the EC_a response is strongly correlated to salt content, and therefore identifies the spatial distribution of the saline groundwaters in the study area. The EC_a patterns indicate that the saline groundwaters are generally restricted to the low-lying terrace areas of the study area, and become more spatially prominent where the valley widens towards the creek outflow. The Prices and Herrmanns Wetlands identified in Figure 9.7 are prominent in the survey. Patterns of higher EC_a responses are also evident in depression areas (e.g. “a”, Figure 9.16) in the north facing slope, indicating the combination of (i) up slope salt accumulation and (ii) the locally lower gradient that causes the EM31 signal to intersect with the upper layers of the deep groundwater. A prominent, localised zone of high conductivity (i.e. “b”, Figure 9.16) identifies a saline groundwater seep emerging from the fractured bedrock under a hydraulic head from the nearby summit to the east.

9.8 Soil survey, modelling and mapping

The investigations described by previous workers (i.e. Davies *et al.* 2002; Fitzpatrick *et al.* 1999; Merry *et al.* 2002) describe the distribution of soils and soil degradation processes, at various scales. Fritsch and Fitzpatrick (1994) describe a series of soil investigations centred on: (i) five toposequence-based transects (“T-A” – “T-E”) and (ii) a 25 ha key area (“Key Area 1”) shown in Figure 9.17 (a). The field component of the investigation involved conducting detailed descriptions on a layer-by-layer basis of soil features (layers, mottles, concretions, colour, etc., according to McDonald *et al.* 1998) at regularly distributed sampling sites (augered or soil pits) along each transect. These workers described each layer taken and analysed in the laboratory for mineralogy (XRD) and a conventional suite of physicochemical analyses (according to Rayment and Higginson 1992). The field and laboratory analyses permitted soil classification according to Soil Taxonomy (Soil Survey Staff 2003) and Factual Key (Northcote 1992).

The toposequence defined by the 400 m transect “T-A” that runs from points A to point B (Figure 9.17 (a)) was identified to be representative in the study area. The toposequence comprised the following down slope sequence of soils: Typic Palexeralfs, Aquic Palexeralfs, then Albic Glossic Natraqualfs, then Typic Natraqualfs (Soil Survey Staff 2003). The toposequence strongly reflects prevailing drainage conditions through the down slope sequence of B horizon colour: yellowish red (summit; freely drained and infrequently waterlogged), then red, then yellowish red, then yellow, then white or grey (lower terrace; poorly drained, strongly waterlogged). The field-based morphological and hydrological interpretations were combined with the laboratory analyses to support the

development of the conceptual toposequence model shown in Figure 9.17 (b) along the transect “T-A” (Figure 9.17 (a)). The conceptual toposequence model incorporates sub-models that feature: (i) soil features (i.e. A and B horizon soil matrices) (ii) soil system domains, and (iii) dominant contemporary water flow systems, i.e. throughflow and recharge flows in upper and mid slope zones, and groundwater (saline sodic-dominated) seepage in the lower landscape, which are associated with degradation. The toposequence-based

investigations described enabled the drafting of two key soil feature maps for the Key Area 1 shown in Figure 9.17 (a). The first key soil feature map showed the distribution of topsoil (i.e. A horizons) features (e.g. pale reddish brown; pale grey; saline and sodic with black sulfidic mottles; and sodic soil layers, modern sandy deposits, and finally eroded soils). The second key soil feature map showed the distribution of uppermost subsoil (i.e. Bt horizon) features (red, yellowish-red; yellow; saline and sodic; and sodic layers, and quaternary deposits).

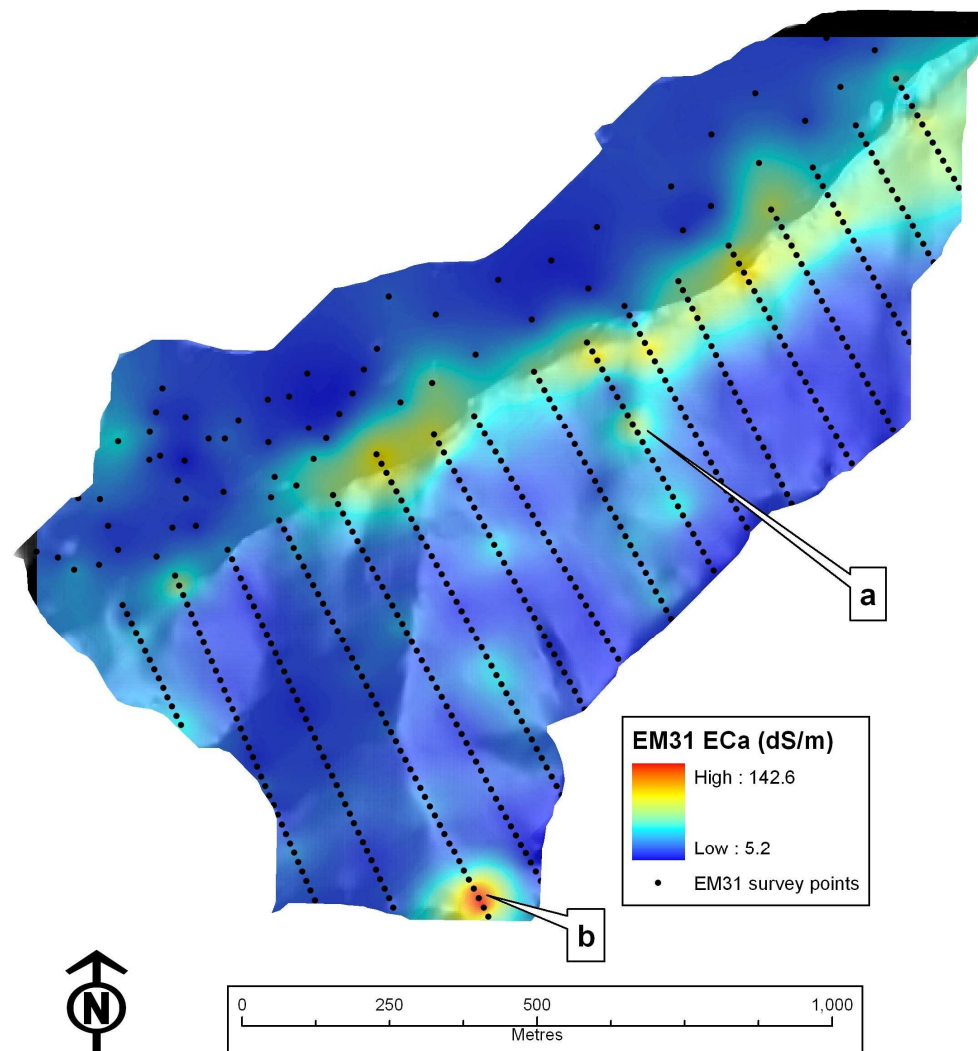


Figure 9.16. EM31 survey points and resulting GIS coverage (linear stretch applied) of deep (~ 6 m) conductivity patterns (linear stretch applied) of the Mount Lofty Ranges study area (source: Fitzpatrick *et al.* 1999), and a hillshading applied to accentuate local landform. Zones of interest “a” and “b” are identified in the landscape.

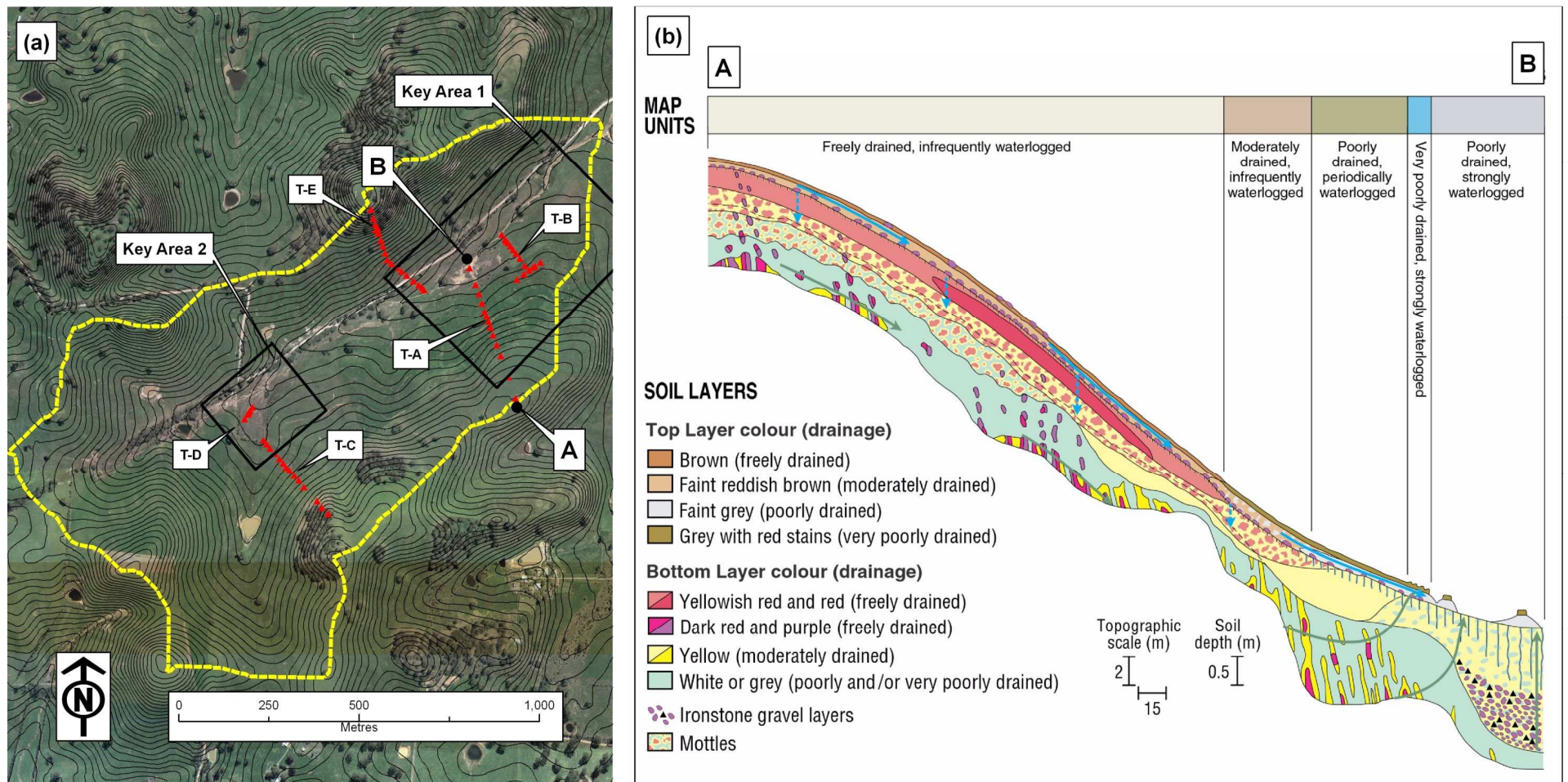


Figure 9.17. Plate (a) An aerial photograph of the MLR study area showing survey transects (T-A to T-E) and surveys sites described in Fritsch and Fitzpatrick (1994). **The figure (b)** shows a descriptive conceptual toposequence model (after Fritsch and Fitzpatrick 1994) (corresponding to transect start and end points “A-B” shown in (a)), features the hillslope profile distribution of mapping units according to (i) drainage, and (ii) top and (iii) bottom soil layers and soil features.

By combining the soil survey, laboratory and mapping described above as a precursor, Fitzpatrick *et al.* (1996) applied a systematic approach to develop conceptual models to explain the development of contemporary degradation systems in the study area soil-landscape. Emphasis in the models was paid towards saline-sulfidic processes caused by perched soil water and groundwater processes. The investigation also involved mapping surface features in an additional lower landscape zone of the study area (i.e. “Key Area 2”, in Figure 9.17 (a)). Finally, field guides were developed to assist in the identification of stages of saline-sodic-sulfidic degradation to support management (e.g. Fitzpatrick *et al.* 1997; Fitzpatrick *et al.* 1994).

The previous studies in the study area (i.e. Davies *et al.* 2002; Fitzpatrick *et al.* 1999; Merry *et al.* 2002) involved extending the soil mapping to the whole study area at a scale 1:5,000 to support a regional soil degradation upscaling methodology to predict waterlogging/drainage, salinity and acidification caused by de-nitrification. The soil map was generated by combining conventional soil mapping and aerial photographic interpretation (e.g. Gunn *et al.* 1988) with remote sensing and terrain attributes (e.g. DEM). The soil map was incorporated in a GIS, and the units (i) classified according to Soil Taxonomy (Soil Survey Staff 2003), and (ii) attributed with map unit codes and degradation classes (i.e. drainage/waterlogging, alkalinity/acidity, and salinity). The study area soil map is shown in Figure 9.18. The soil unit codes shown are referenced to the soil-landscape descriptions presented in Table 9.4.

9.9 Land use

Much of the study area has been cleared of native vegetation for farming during the period 1885 to 1955. The non-cleared areas feature stands of remnant woodland

dominated by *Eucalyptus camaldulensis* and correspond to either the summit areas or the lower terraces (e.g. Figure 9.10(b)). Generally, the summit areas are mantled by dispersed ferruginous saprolite and quartzite stones, boulders and outcropping that have precluded cultivation. Where the trees have been preserved, the sheltered summits are favoured as sheep encampments at night. As discussed previously, re-vegetation efforts have been made in the lower terraces.

Where gradient allows in the north facing mid slopes, the farming involves broadacre winter cereal cropping (wheat and barley) in rotation with improved pasture (e.g. seedings of rye grass and subclover) for cattle. The improved pasture is used to cut hay in the late winter to early summer and grazing at other times. The south-facing mid slopes areas are grazed by cattle (improved pasture) and sheep (unimproved pasture). Based on discussions with the farmers in the study area, annual topdressings of fertilizers (e.g. “Super Phosphate” or “Di-ammonium Phosphate” (DAP)) are made in the arable areas in preparation for the growing season in May or June at a typical rate of 100 – 150 kg/ha. In improved pasture areas, fertilisers (e.g. “Pasture Prompt”) are topdressed at a rate of 80 kg/ha in advance of the growing season. “Super Phosphate” and “Pasture Prompt” feature formulations dominated by P, S and Ca, while DAP features a formulation dominated by N, P and S. Lime is applied to the cropped and improved pasture areas approximately once every two to three years to combat soil acidification. The high gradient areas of the study area (e.g. shoulderslopes) are left for unimproved pasture, which are generally grazed by sheep. Four families farm the study area. Figure 9.19 identifies the families, their tenure and the farming practices in recent times (i.e. since 2000).

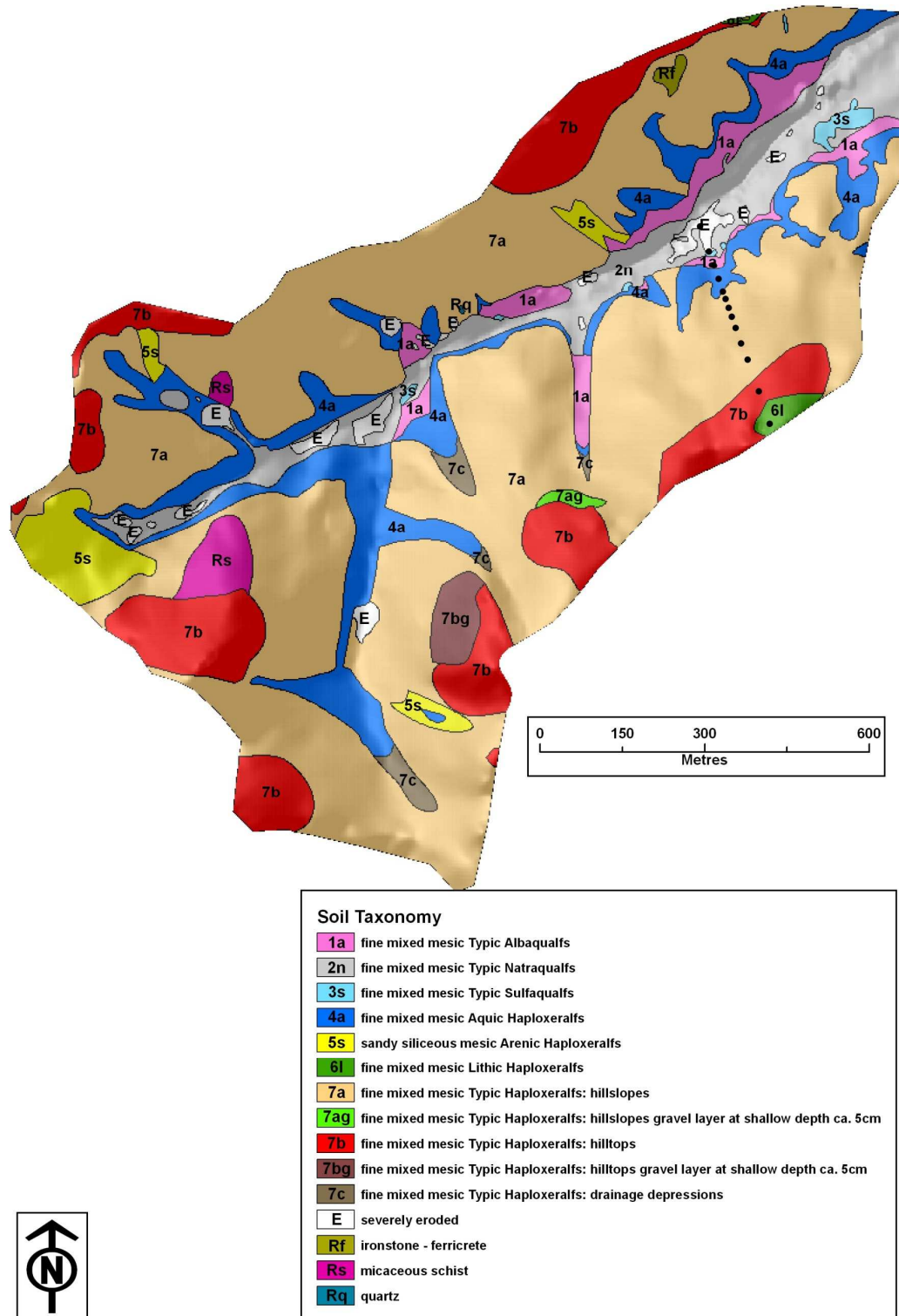


Figure 9.18. Soil map of the Mount Lofty Ranges study area (Davies *et al.* 2002) showing the location of transect “T-A” (●) (Fritsch and Fitzpatrick 1994), which corresponds to the conceptual toposequence model shown in Figure 9.17 (b). A hillshade is applied to accentuate local landform.

Table 9.4. Mount Lofty Ranges study area soil map (shown in Figure 9.18) unit descriptions (according to Davies *et al.* 2002; Fitzpatrick *et al.* 1999; Merry *et al.* 2002).

Map Unit	Landform Elements	Soil Description	Drainage/ Waterlogging	Acidity/Alkalinity ^a	Salinity (ECse)/ depth to saline water(m)
1a	Flat	Grey sandy loam surface layer over yellow-grey mottled clay	Poorly drained Strongly waterlogged	Moderately acidic (pH _w =<6.5) surface, neutral to alkaline at depth	Slightly saline: 1 -4 dS/m; 1 - 1.5 m
2n	Flat	Salt efflorescence (halite & gypsum) on surface with grey sandy loam surface over yellow-grey clay	Poorly drained Strongly waterlogged	Mostly alkaline throughout (pH _w >7.5)	Very saline: >8 - 16 dS/m;< 1 m
3s	Flat/ Lower slope seepages	Salt efflorescences (halite & gypsum) on surface with loamy black sulfidic material over yellow-grey clay	Very poorly drained Strongly waterlogged	Mostly alkaline throughout (pH _w >7.5): sporadic occurrences of highly acidic (pH _w <5.5) near surface layers (<5cm), which develop due to oxidation of sulfidic materials	Extremely saline: >16 dS/m; < 1 m
4a	Lower slope, open depressions	Grey sandy loam surface layer over yellow-red-grey mottled clay	Poorly drained Periodic waterlogging	Neutral throughout (pH _w 6.5-7.5)	Slightly saline: 1 -4 dS/m; 1.5 - 3 m
5s	Lower slope, open depressions	Deep grey sand over yellow-grey mottled clay	Poorly drained Periodic waterlogging	Acidic throughout (pH _w =<6.5) (low buffer capacity)	Non saline: <1 dS/m; 1.5 - 3 m
6l	Crest	Shallow sandy loam over red uniform coloured clay over weathered rock	Freely drained Infrequently waterlogged	Very acidic throughout (pH _w <5.5)	Non saline: <1 dS/m; > 3 m

Map Unit	Landform Elements	Soil Description	Drainage/ Waterlogging	Acidity/Alkalinity ^a	Salinity (ECse)/ depth to saline water(m)
7a	Mid slope	Brown loam over red and yellow uniform coloured clay. Deep	Freely drained Infrequently waterlogged	Moderately acidic (pH _w <6.5) throughout	Non saline: <1 dS/m; > 3 m
7ag	Crest, upper-slope	Deep well drained red and yellow soils	Freely drained Infrequently waterlogged	Moderately acidic (pH _w <6.5) surface, neutral to alkaline at depth	Non saline: <1 dS/m; > 3 m
7b	Crest, upper-slope	Deep well drained red and yellow soils	Freely drained Infrequently waterlogged	Very acidic throughout (pH _w <5.5)	Non saline: <1 dS/m; > 3 m
7bg	Crest, upper-slope	Shallow well drained red yellow soils	Freely drained Infrequently waterlogged	Moderately acidic (pH _w <6.5) throughout	Non saline: <1 dS/m; > 3 m
7c	Lower slope, open depressions	Shallow well drained yellow soils	Moderately drained Infrequently waterlogged	Neutral throughout (pH _w 6.5-7.5)	Non saline: <1 dS/m: 1.5 – 3 m
Rq	Crest, upper-slope	Shallow well drained yellow and red soils with quartz fragments	Freely drained Infrequently waterlogged	Moderately acidic (pH _w <6.5) throughout	Non saline: <1 dS/m; > 3 m
Rf	Crest, upper-slope	Shallow well drained yellow and red soils with ferricrete fragments	Freely drained Infrequently waterlogged	Very acidic throughout (pH _w <5.5)	Non saline: <1 dS/m; > 3 m

Map Unit	Landform Elements	Soil Description	Drainage/ Waterlogging	Acidity/Alkalinity ^a	Salinity (ECse)/ depth to saline water(m)
Rs	Mid slope	Shallow well drained red soils with micaceous rock fragments	Freely drained Infrequently waterlogged	Moderately acidic (pH _w <6.5) surface, neutral at depth, high buffer capacity	Slightly saline: 1 -4 dS/m; > 3 m
E	Flat / stream channel	Gully, tunnel and rill erosion	Very poorly drained Strongly waterlogged	Mostly alkaline throughout (pH _w >7.5)	Extremely saline: >16 dS/m; < 1 m

^a pH_w means that the pH measurement was taken in water

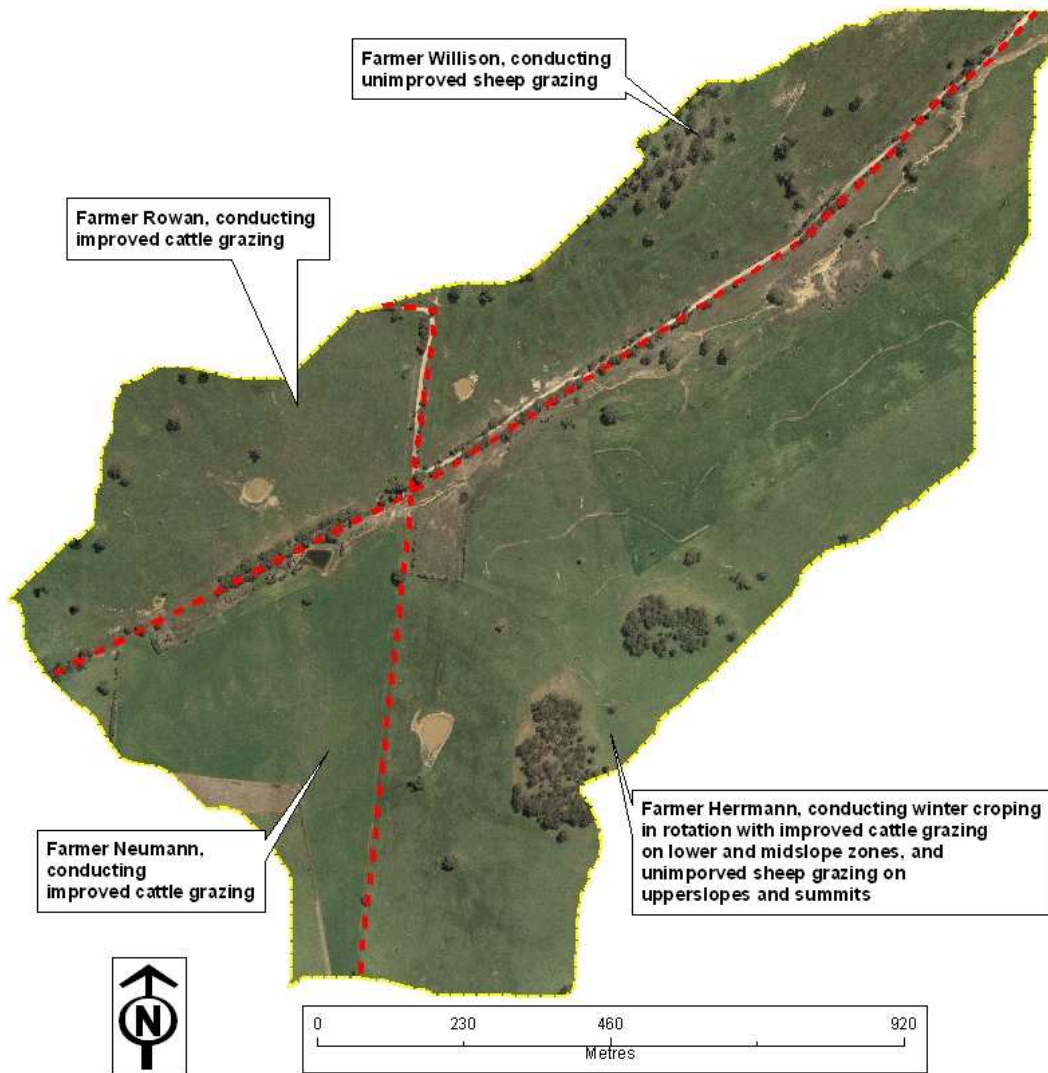


Figure 9.19. Land tenure in the Mount Lofty Ranges (MLR) study area (boundaries shown as red lines), and land use summarised.

Chapter 10. Mount Lofty Ranges multi-temporal, fine scale investigation

This Chapter presents a fine scale investigation (equivalent to level *i* discussed in Chapter 4) of seasonal changes occurring in the solute concentrations (according to electrical conductivity and dominant soluble salts) of the near-surface (< 0.75 m) soil layers from selected sites in the Mount Lofty Ranges study area. Investigations were conducted and compared on soil cores taken during late winter (2004), the time of maximum wetness, and late summer (2005), the time of maximum dryness. The investigative approach applies the principle that in salt-rich environments such as the MLR study area, the profile distribution of soluble salts are pedotransfer functions for hydropedological processes (e.g. Shaw 1988), which allow characterisation of watertable processes, pedogenesis and soil degradation.

10.1 Survey site selection and soil sampling

Nineteen sites were identified in the study area, which are shown in Figure 10.1. Their selection was based on: (i) prior field knowledge of the distribution of soil types described in Chapter 9, and (ii) the combined soil-landscape patterns, including local terrain and drainage (also, Chapter 9). Where possible, combinations of survey points were selected that would form: (i) toposequences (e.g. points 025, 026 and 011; and 020, 018 and 029), and (ii) paired sites from similar hillslope zones, but occupying positions in different local topographic features (e.g. sites 002 and 003; 005 and 006; and 009 and 010).

All sites were located in the field using a GPS. Samples comprising four soil layers were collected at each site during each sampling season, as identified in Table 10.1. The seasonal samples were taken in close proximity

(i.e. no more than one metre apart), with the 2004 summer sample taken from a position up slope of the winter sample site to mitigate local disruption to drainage conditions in the summer profile sample.

During late winter, when the ground was soft, the profile layers L1 and L2 were sampled using a spade and trowel: L3 and L4 were sampled using a gouge auger to the maximum depth of 0.75 m. In this way, four closely separated cores were required to yield sufficient sample for analysis. Due to the hardness of the ground during summer, a vehicle-mounted soil coring rig was required to collect the L3 and L4 samples, using a 50 mm diameter corer. Duplicate cores were required to yield sufficient sample for laboratory analyses. On removal, the cores were sealed in plastic and divided in the laboratory.

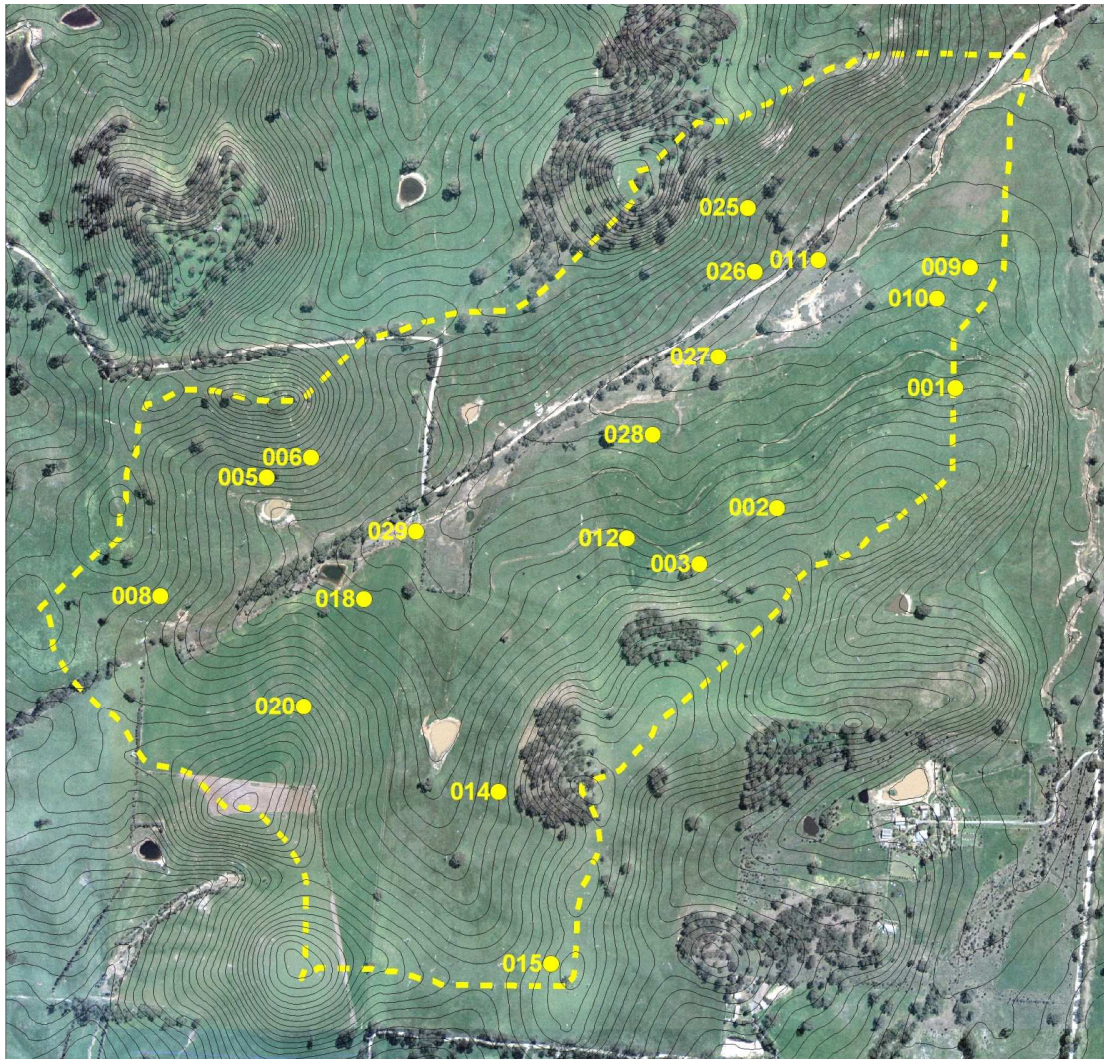


Figure 10.1. Location of survey sites within the Mount Lofty Ranges study area for detailed investigation of seasonal depth solute trends.

Table 10.1. Layer identification and depth ranges (m).

Layer sample ID	Depth range (m)	Dominant horizon
L1	0 – 0.05	A
L2	0.05 – 0.1	
L3	0.1 – upper B	A/E or EB
L4	Upper B – 0.75	B

The winter soil sampling was conducted over two consecutive days during mid September 2004. According to meteorological data from the nearby Mount Crawford weather station shown in Figure 9.2 (source: www.bom.gov.au/climate/dwo/IDCJD/W0503.shtml), the study area received 61 mm of rainfall in the first half of September, of which 53 mm fell in the week prior to sampling. Depending on hillslope position, the field conditions were either wet or damp, and the soil layers collected were either wet or damp to the touch. The late summer sampling was also conducted over two consecutive days, during early April 2005. From meteorological data from the nearby Mount Crawford weather station, the area had approximately 1.8 mm of rainfall during the previous March, and 63.6 mm since the start of the year. Except for the subsoil layers in the lowest terrace position that were damp to the touch, all soil layers sampled during this time were touch dry. Each of the two sampling periods were preceded by rainfall conditions that followed normal seasonal trends .

10.2 Laboratory physicochemical analyses

Laboratory physicochemical analyses were conducted on each of the four soil layers (L1 – L4) acquired during each season using identical preparatory and analytical methods. The analyses of soil layers involved the combination of: (i) traditional 1: 5 soil/water extractive analyses (Rayment and Higginson 1992), and (ii) mid-infrared (MIR) –based particle size analysis predictions (Forrester *et al.* 2003; Janik *et al.* 1998), applying the methods described in Chapter 6. In summary, the laboratory analyses were conducted on the dried < 2 mm soil fraction samples. For the MIR predictions, the samples were ground in a vibrating steel puck mill for one minute to attain a particle size of approximately < 100 μm . The traditional 1: 5 soil/water extractive analyses and the MIR predictive

methods enabled EC_{se} to be estimated using the method described in Chapter 6 that combines laboratory $\text{EC}_{1:5}$ with MIR-derived texture using the R values presented in Cass *et al.* (1996).

10.3 Multi-temporal solute trends

An investigation was conducted to compare seasonal (i.e. winter/summer) changes in solute concentrations occurring in each of the 19 profiles selected for laboratory physicochemical analyses. The investigation was based on the profile trends of a selection of soluble salts, which included: (i) Ca^{2+} , (ii) K^{+} , (iii) Mg^{3+} , (iv) Na^{+} , (v) PO_4^{-} , (vi) Cl^{-} , and finally (vii) SO_4^{-} . In all cases, the concentrations were calculated back to the original soil sample (i.e. mg/kg) from the 1:5 soil/water solution (Rayment and Higginson 1992). In addition to the soluble salt concentrations, electrical conductivity (EC_{se}) as proxy of soil salinity, texture (clay %) and CEC ($\text{cmol}^{+}/\text{kg}$) properties for each layer were also combined in the analysis.

The seasonal solute trends in the selected soil profiles were combined with soil layers (using clay %) and soil morphological features (e.g. soil colour, mottles) to interpret near-surface hydrological properties (e.g. redoximorphic properties/aquic conditions). The hydrological interpretations were assisted by knowledge of local field conditions, recent land management practice (e.g. fertilizer top-dressing history), soil type, and topographic position. The combined interpretations revealed the existence of four generic conceptual hydrogeological models in the study area. Two of the models were dominated by shallow NAS processes, while the other two were dominated by GAS processes. The key diagnostic properties to identify which type of salinisation/near-surface hydrological processes each profile conformed to included seasonal depth trends of: (i)

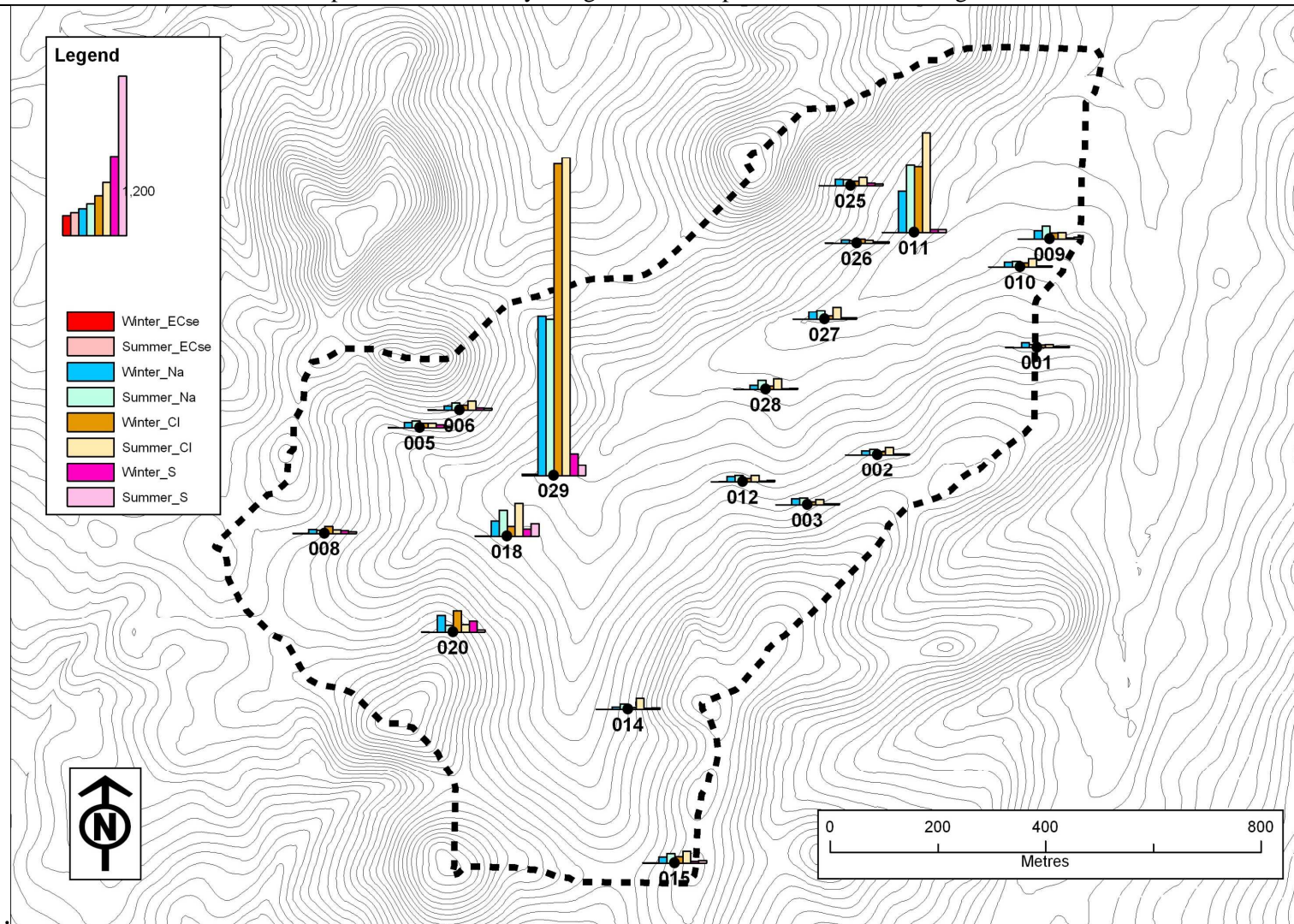


Figure 10.2. Upper layer (L1, 0 - 0.1 m) seasonal trends of electrical conductivity (EC_{se}) and concentrations of Na, Cl and S salts in the Mount Lofty Ranges (MLR) study area. Two metre contours indicate local landform.

salinity (EC_{se}), and (ii) Na, Cl and SO_4 concentrations. Sodium, Cl and SO_4 strongly reflect the influence of groundwater processes in the soil profile because the solutes are characteristic of the composition of local groundwaters (Figure 10.2) (Baker and Fitzpatrick 2003; Fitzpatrick *et al.* 1996; Skwarnecki *et al.* 2002a)

A variant of the models was identified in some of the profiles analysed. The so-called “F-variant” incorporated the seasonal overprint of solutes reflecting the soluble ion composition of annual fertilizer and lime treatments to the land. Based on discussions with the farmers who farm the study area, annual topdressings of fertilizers (diamonium phosphate (DAP)) were made in the cropping areas in preparation for the growing season in May/June each year, at a typical rate of 100 – 150 kg/ha. In improved pasture areas, fertilisers (Pasture Prompt and Super Phosphate – or “Super”) are topdressed at a rate of 80 kg/ha (Pasture Prompt) and 100 – 150 kg/ha (Super) in advance of the growing season. According to manufacturer information (www.pivot.com.au/ProductInformation.asp), the typical composition of each fertiliser is given in Table 10.2.

Treatment to counter soil acidification using lime ($CaCO_3$ - and sometimes dolomite $MgCO_3$) - is applied to the cropped and improved pasture areas approximately once every two to three years. Thus, the various soil improvements that are regularly applied to the surface of the study area provide an anthropogenic source of: (i)

P, (ii) S, (iii) Ca, and (iv) Mg. With the addition of K, the seasonal surface distribution of these salts for each profile are shown in Figure 10.3.

During a field visit in June 2005, recently applied and partially dissolved fertilizer granules were observed and sampled near the surface of survey site “006” (Figure 10.1). Similar looking partially dissolved fertilizer granules were also evident on the surface throughout the remaining area farmed by Rowan, which covers the south-facing, westerly slopes of the study area (Figure 9.19). Subsequent discussion with Rowan confirmed the fertilizer to be Pasture Prompt. The granules were analysed for soluble salts using the solution extract methods described in Rayment and Higginson (1992). The laboratory analyses revealed the fertilizer granule content to include the following soluble components: (i) Al (> 7.5 %), (ii) Ca (19.5 %), (iii) Fe (0.53 %), (iv) K (0.09 %), (v) Mg (0.02 %), (vi) Na (0.14 %), (vii) P (3.6 %), and (viii) S (11.0 %).

The following Sections describe conceptual models that have been developed, which are displayed (Figure 10.4, Figure 10.8, Figure 10.10, and Figure 10.12). The displayed models each contain an inset box that depicts a contour map of an conceptualised summit-to-valley hillslope that is characteristic in landform of the MLR study area. The conceptualised hillslope features a series of interflaves and corresponding slope drainage zones. Also shown in the inset box is the landscape zone in which the model typically occupies, and a transect to indicate the position of the cross-sectional model.

Table 10.2. Typical composition of fertilizers applied in the Mount Lofty Ranges (MLR) study area according to manufacturer information (www.pivot.com.au/ProductInformation.asp).

Fertilizer name	Use and typical application rate in study area	Typical composition (by % mass, according to manufacturer information)			
		P	S	Ca	N
Pasture Prompt	pasture, 80 kg/ha	14.1	13.7	15.0	
“Super” (Super Phosphate)	pasture, 100 – 150 kg/ha	8.8	11.0	20.0	
Diamonium Phosphate (DAP)	cropping, 100 – 150 kg/ha	20.0	1.6		18.0

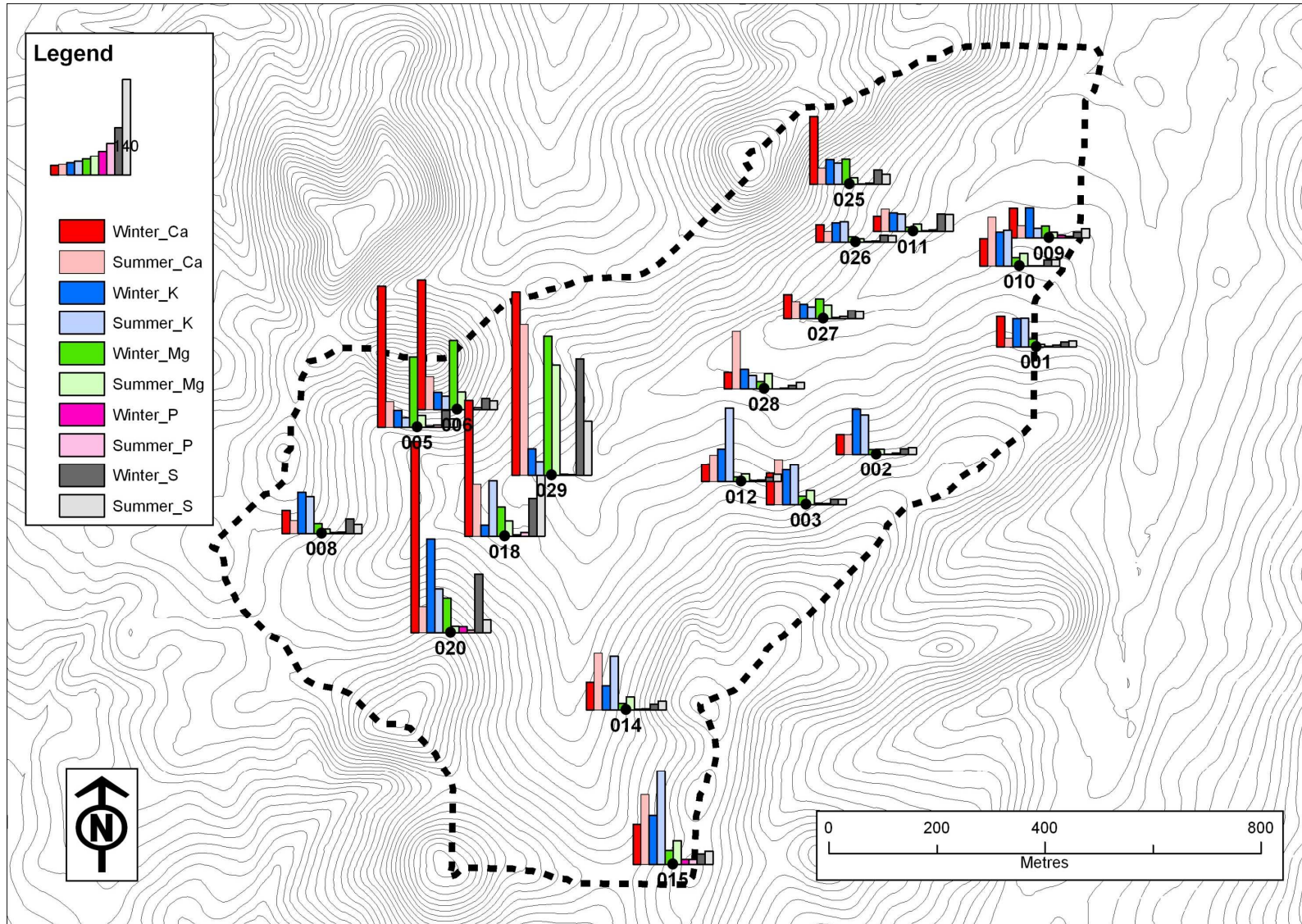


Figure 10.3. Upper layer (L1; 0. 0.1 m) seasonal trends in comparative concentrations of the soluble salts: Ca, K, Mg, P and S in the Mount Lofty Ranges (MLR) study area. Two metre contours indicate local landform.

Model 1a

The soil profiles from the sites 001, 002, 005, 006, 008, 010, 012, 014, 015, 025, 026 and 028 conform to Model 1a, for shallow NAS, topographically perched, and in upper hillslopes, as displayed in Figure 10.4. The salinity depth trends for the profiles are presented in Figure 10.5 and Figure 10.6, and the layer physiochemical data in Appendix H. Typically, the model profiles contain texture-contrast horizons (i.e. the A horizons contain at least half the clay content of the B horizons). In many cases, a bleached E horizon is evident with a lower clay content of L3 compared to the layers above (e.g. 008, 012, 014 and 025). Trends in salinity (EC_{se}) shown in Figure 10.5 and Figure 10.6 show characteristically high values in the surface layers (L1 and L2) compared to layers below, which remain seasonally unchanged. The trends in soluble salt concentration tend to follow the same depth trends as salinity (Appendix H). Model 1a profiles are not hydraulically connected to deep groundwater watertables, which is shown by the lack of seasonal salinity or soluble salt influxes in the deeper layers. The dominant hydrological processes affecting the profiles are therefore confined to surface layers, and are in the form of perched watertables in which salts remain in the A and upper B horizons. Within these layers salts seasonally cycle between the A and B horizons under hydraulic gradients caused by summer capillarity (i.e. via summer evaporation and transpiration), and winter rainfall freshwater infiltration and dilution. In such cases, the summer salinity is greatest on the L1 and L2 layers during summer.

However, variant to the of the Model 1a caused by fertilizer application (a so-called “F-variant”), the most

seasonally elevated concentration (i.e. > 0.75 dS/m) of salts occurs in the L1 and L2 layers during winter, not during summer. The Model 1a F-variants are associated with the profiles 005, 006 and 008 that are located in the area farmed by Rowan. In these profiles, the winter salinity increase is explained by the recent surface application of fertilizer granules that were locally observed on the soil surface. At the time of soil sampling, the granules were in a partially dissolved state, with the dissolved component concentrated in the surface (L1). This explains the elevated EC_{se} and soluble salt concentrations observed (Figure 10.2, Figure 10.3, Figure 10.5, and Appendix H).

Profile 025 (Figure 10.6) shares the depth trends of the other Model 1a F-variants identified, although the seasonal depth trends cannot be explained in the same way because the farmer reported that the unimproved sheep grazing site had not been fertilized in approximately 15 years. The elevated winter salt concentration in the L1 during winter in this profile, therefore, reflects a concentration of pedogenically-derived salts (featuring Ca, K, Mg and S, Figure 10.3) mobilised from up slope positions, and transferred down slope by throughflow in the A horizon (predominantly via the well-developed E horizon (Appendix H)). As shown in Figure 10.7, the location of the profile 025 is just down slope of a prominent break of slope (i.e. backslope: $17 - 20^\circ$ transition to upper footslope: 10°). The sharp gradient transition forms a winter groundwater seep (GAS) that is elevated in salts mobilised during winter from the deep profile (deep NAS) of the deeply weathered Tertiary summit landform. The elevated salinity in the surface L1 compared to the other A horizon layers is due to transpiration and evaporative concentration.

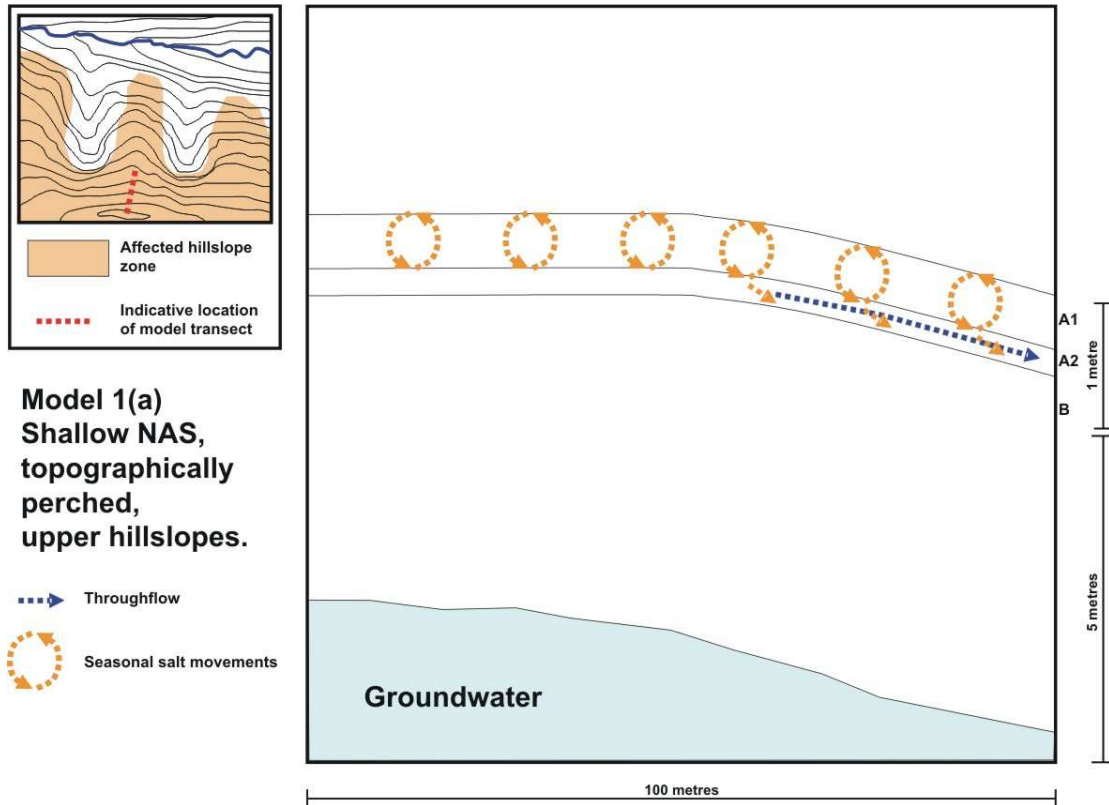


Figure 10.4. Conceptual Model 1a for shallow NAS, topographically perched, and in upper hillslopes. The conceptualised contour map that is inset identifies possible affected areas in the landscape, and the indicative location of the transect described in the model.

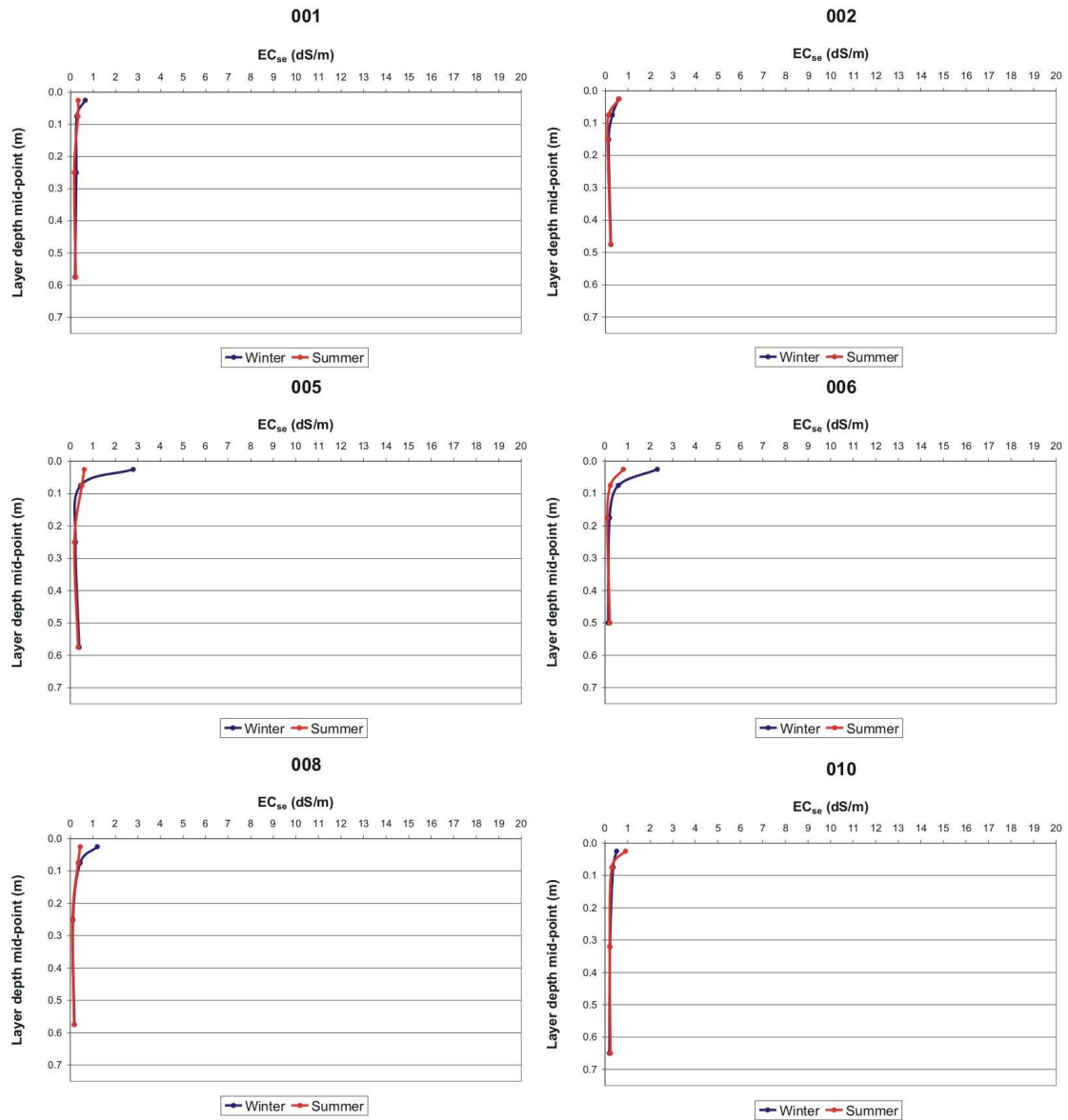


Figure 10.5. Diagnostic down-profile salinity (EC_{se}, dS/m) trends of Model 1a-type soils (profiles: 001, 002, 005, 006, 008 and 010).

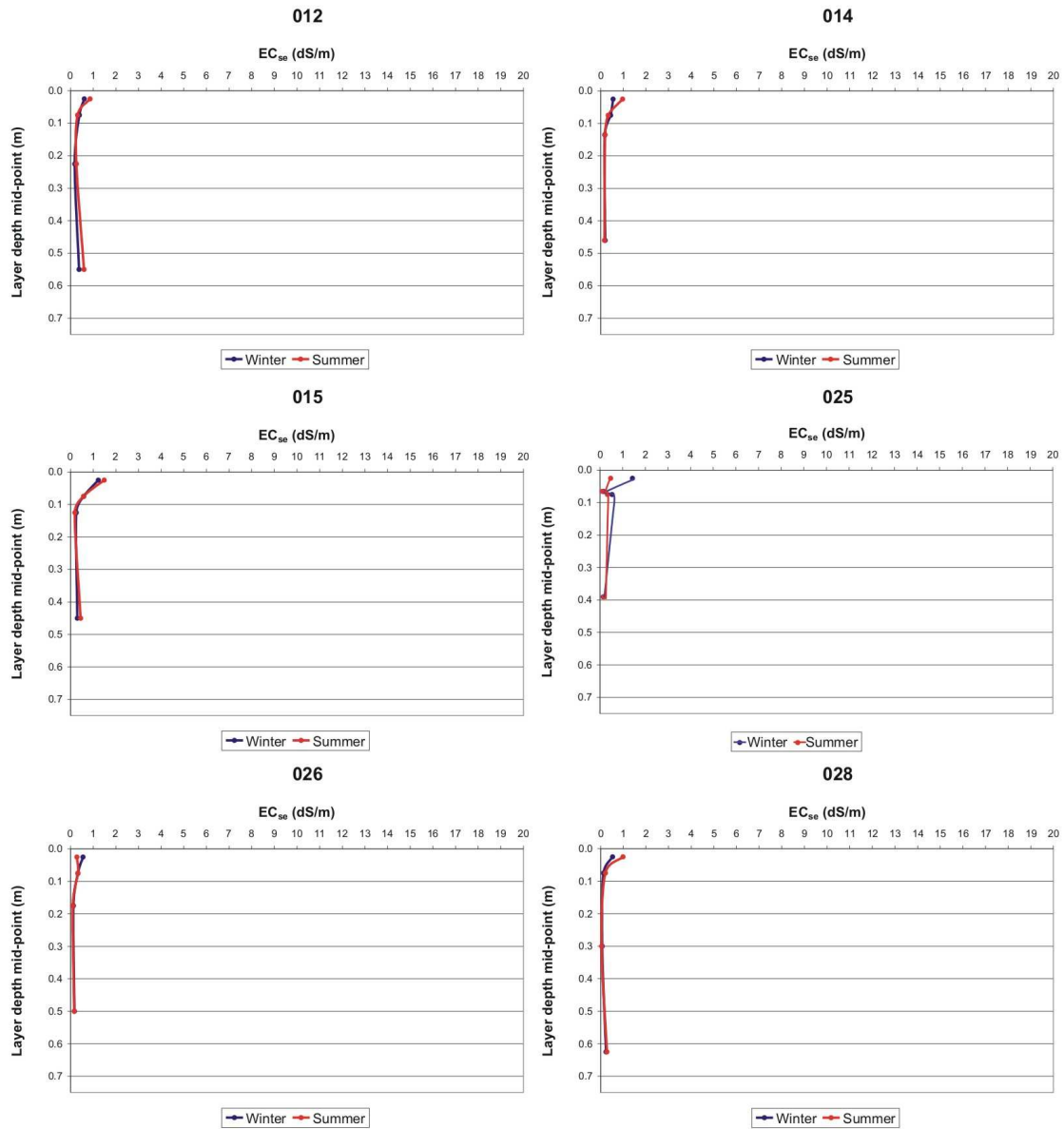


Figure 10.6. Diagnostic down-profile salinity (EC_{se}, dS/m) trends of Model 1a-type soils (profiles: 012, 014, 015, 025, 026 and 028).

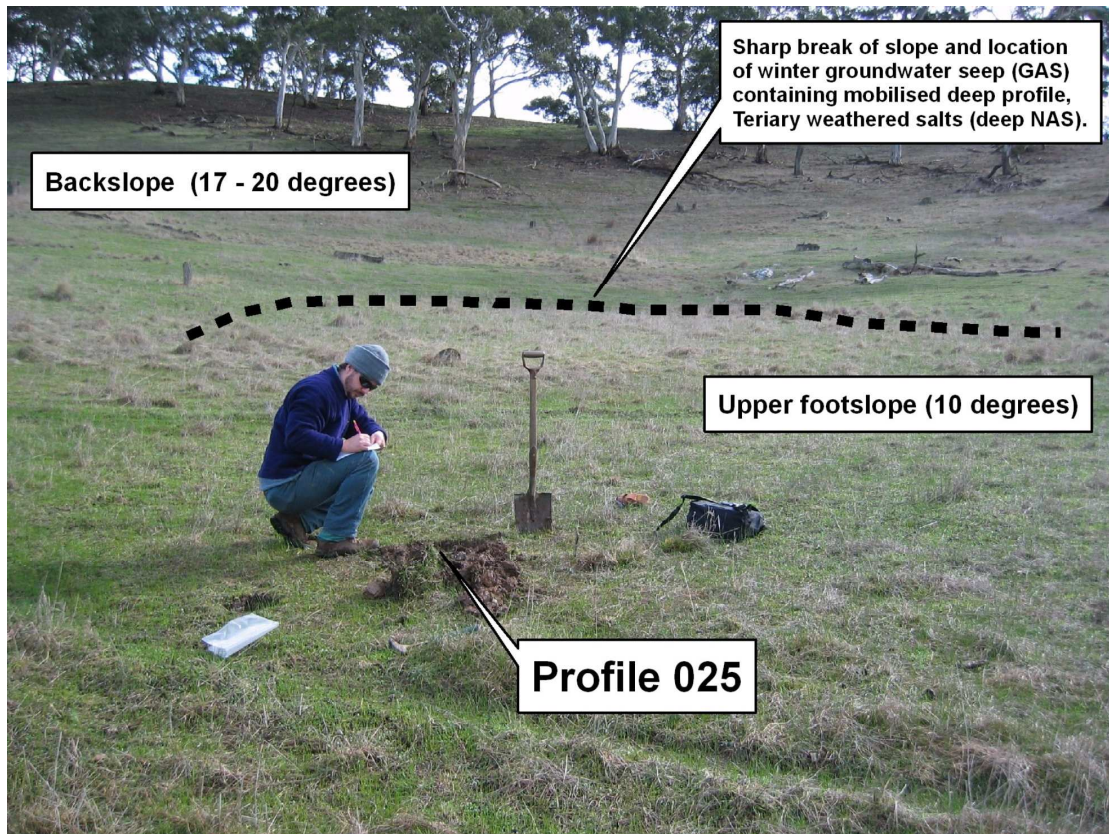


Figure 10.7. Photograph showing the landscape position of profile 025, and the sharp break of slope (dashed line) that is up slope.

Model 1b

The soil profiles from the sites 003 and 009 conform to Model 1b, for shallow NAS in mid/upper hillslopes, in low-lying areas with partial groundwater influence, which is displayed in Figure 10.8. The profile EC_{se} trends are shown in Figure 10.9, and the layer physiochemical data in Appendix H. Both profiles feature texture-contrast soils with either a moderately developed (profile 003) to a well-developed (profile 009) E horizon. Characteristically, these profiles feature elevated EC_{se} values and salt concentrations in the surface and in the upper B horizon. The sloping landscape position and the presence of the relatively coarse textured E horizon creates a hydraulic disconnection between the upper A horizon and the B horizon, leaving

much of the salts perched in the upper layers (L1 and L2) and isolated in the B horizon. The disconnection causes truncation of typical vertical shallow NAS salt cycling between the A and B horizons (see Model 1a) because of the following seasonal influences: (i) rapid rates of down slope, near-horizontal freshwater throughflows during winter and (ii) reduced capillarity due to the coarser textured E horizon during summer. In general terms, the concentrations of Na and Cl are elevated throughout the profiles, with sharp increases in the B horizon during summer. There are also sharp increases in S concentrations in the B horizon during later summer. Together, the increased concentrations during this period indicate the influence of rising groundwater, which intersects with the B horizon in the low-lying areas in the mid/upper hillslope.

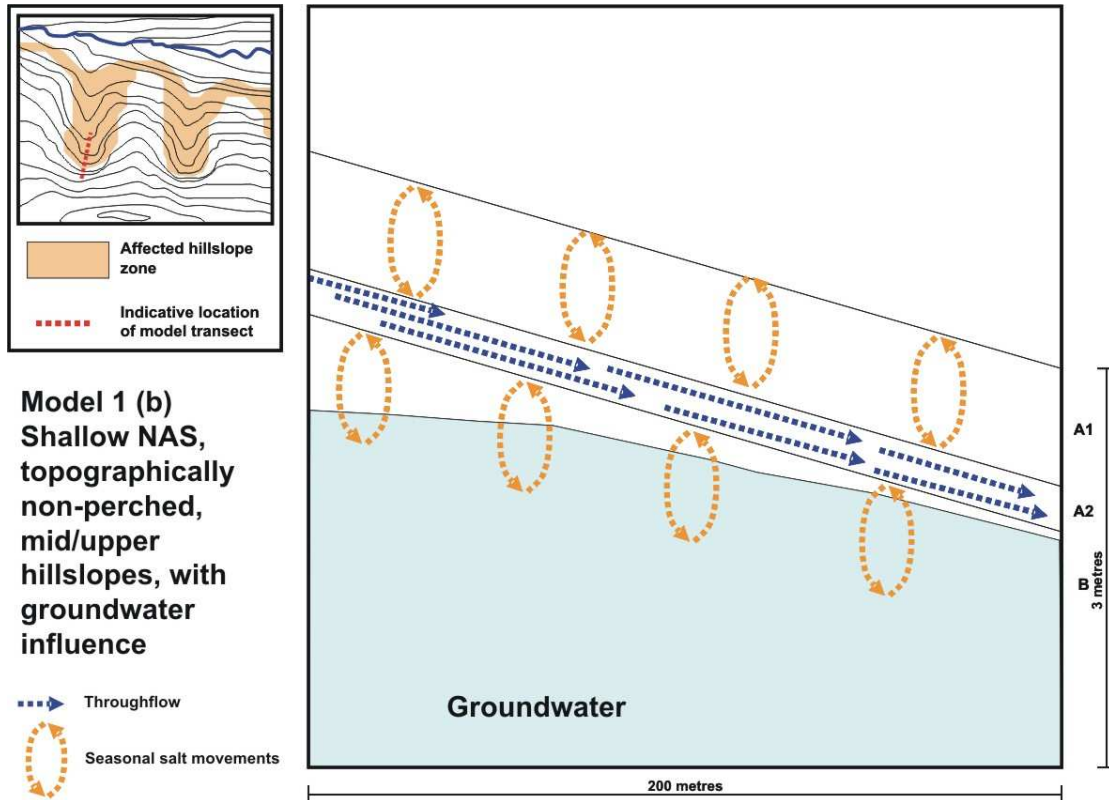


Figure 10.8. Conceptual Model 1b for shallow NAS in mid/upper hillslopes, in low-lying areas with partial groundwater influence. The conceptualised contour map that is inset identifies possible affected areas in the landscape, and the indicative location of the transect described in the model.

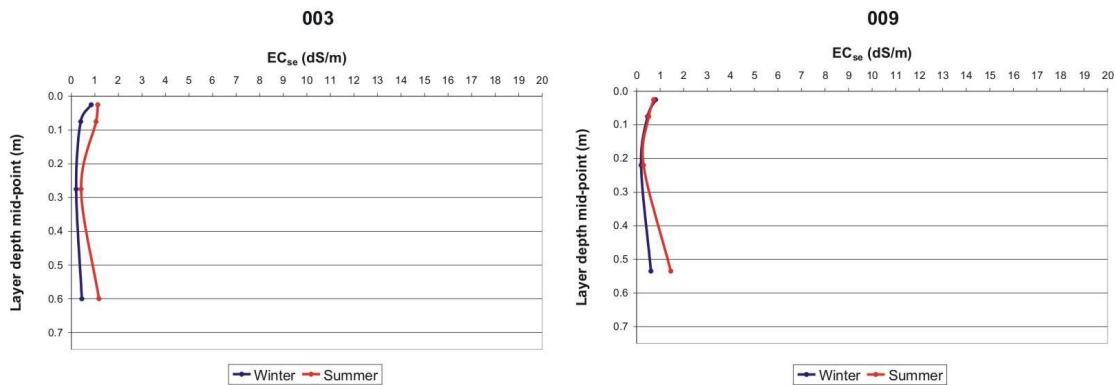


Figure 10.9. Diagnostic down-profile salinity (EC_{se} , dS/m) trends of Model 1b-type soils (profiles: 003 and 009). Table 10.3. Layer physicochemical properties of profiles conforming to Model 1b, featuring winter (W_) and summer (S_) salinity (EC_{se} , dS/m), clay content (%) and concentration of soluble salts (mg/kg^{-1}).

Model 2a

The soil profile from the site 020 conforms to Model 2a for GAS in upper hillslopes, which is displayed in Figure 10.10. The profile EC_{se} trends

are shown in Figure 10.11, and the layer physicochemical data in Appendix H. The profile features a texture-contrast soil. A strong feature of the

profile is the elevated EC_{se} value in the surface layer (L1) during late summer, which corresponds to the late winter trends of elevated concentrations of Ca, K, Mg, Na, P, Cl and S in L1, which are also featured in L2. In most cases the late summer salt concentrations are relatively high compared to other study area values from up slope positions. The elevated salt concentrations identified in the seasonal profile indicates hydraulic connection to a groundwater seep containing elevated concentrations of weathered salts. The location of the profile corresponds closely with the Esa geological unit (Figure 9.3), which features siltstones that contain pyritic mineralised zones. The location of the profile also corresponds with an

anomaly in the first vertical derivative aeromagnetic imagery in (Figure 9.4). According to Reynolds (2000), such anomalies often indicate a concentration pyritic materials in the bedrock. The topographic position of the profile indicates that groundwater seepage occurs under piezometric pressure. The local outcropping and subcropping provides hydraulic connectivity between the pyritic materials in the bedrock and the surface soil layers. Winter salt concentrations imply that the hydraulic gradient is greatest during winter, indicating that the ferruginised zone that exists up slope acts as the local recharge area to the seep (Figure 10.10).

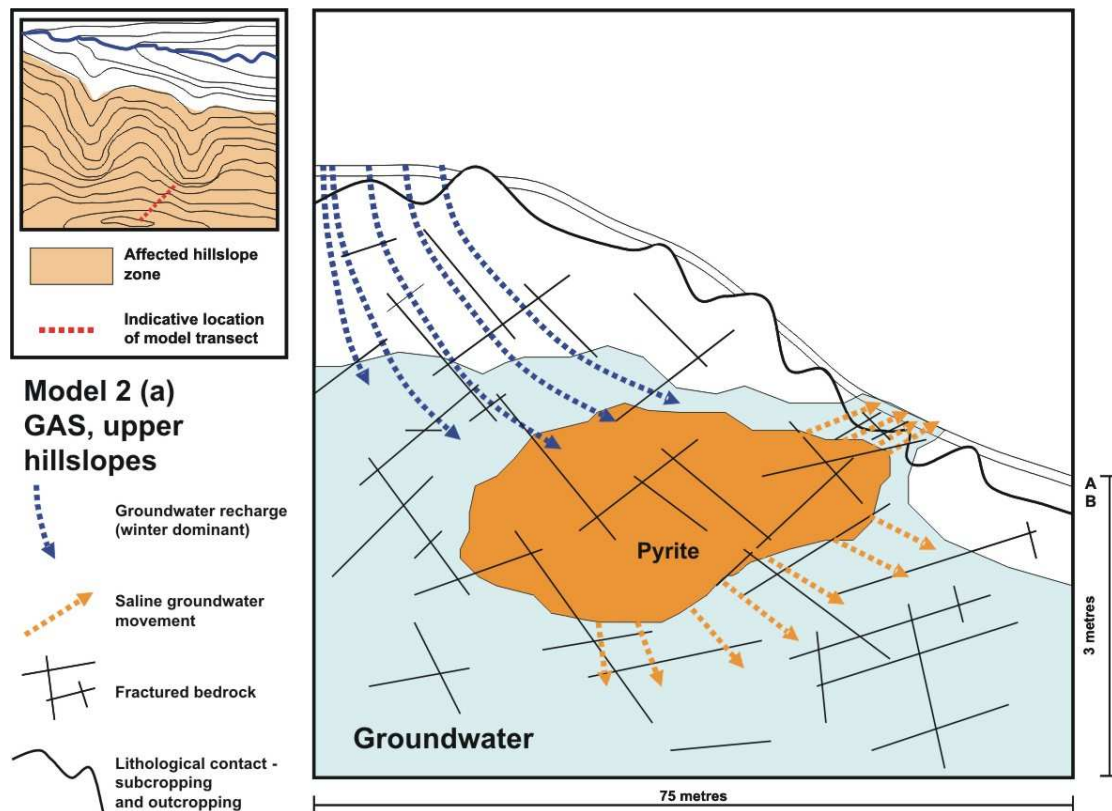


Figure 10.10. Conceptual Model 2a for GAS in upper hillslopes. The conceptualised contour map that is inset identifies possible affected areas in the landscape, and the location of the transect described in the model.

020

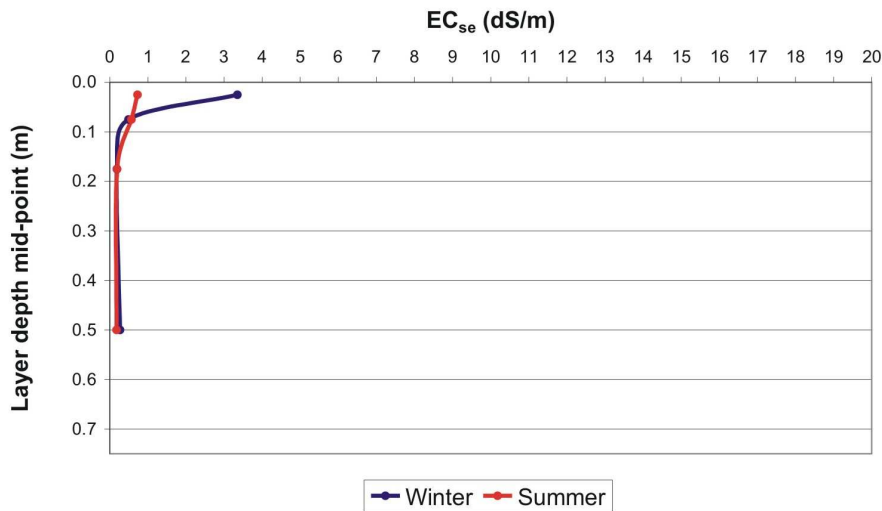


Figure 10.11. Diagnostic down-profile salinity (EC_{se} , dS/m) trends of Model 2a-type soils (profile: 020). Table 10.4. Layer physicochemical properties of profiles conforming to Model 2a, featuring winter (W_) and summer (S_) salinity (EC_{se} , dS/m), clay content (%) and concentration of soluble salts (mg/kg^{-1}).

Model 2b

The soil profiles from the sites 011, 018, 027 and 029 conform to Model 2 (b) for GAS on lower hillslopes, which is displayed in Figure 10.12. The profile EC_{se} trends are shown in Figure 10.13, and the layer physicochemical data in Appendix H. All profiles occupy lower landscape positions adjacent to the creek (profiles 027 and 029) or nearby terraces (profiles 011 and 018).

The key feature of the physicochemistry of this model is the strongly elevated EC_{se} in the B horizon, a reduced EC_{se} in the lower A horizon (L3), and then an increase in EC_{se} in the surface layers (L1 and L2). In all cases, the late summer EC_{se} values below L2 are higher than the late winter values. The profiles also feature highly elevated Na and Cl concentrations, and generally high concentrations of S. Concentrations of salts identified and the profiles signify the influence of groundwater watertable fluctuations.

Salt concentration values in profile 027, which is located a few metres from the creek, indicate lower salt concentrations in comparison to the other Model 2b profiles. This is explained by the presence of the nearby creek that is deeply incised to a depth of approximately 1.5 m, which has caused localised drainage of the profile and the flushing out of salts. The increased salt concentrations measured in the lower profile (L3 and L4) during late summer signify upwardly wicking groundwater salts, which are flushed out of the profile by surface freshwater during winter. Profile 029, which is in the same topographic position as profile 027, is located in the scalded bank of the creek, and features the highest salt concentrations of the study area profiles analysed. Profile trends here indicate little groundwater watertable dynamism in the season, and the seasonal variations in which deeper profile (L2 to L4) EC_{se} values are highest in summer indicate the concentration of salts by wicking in the creek bank.

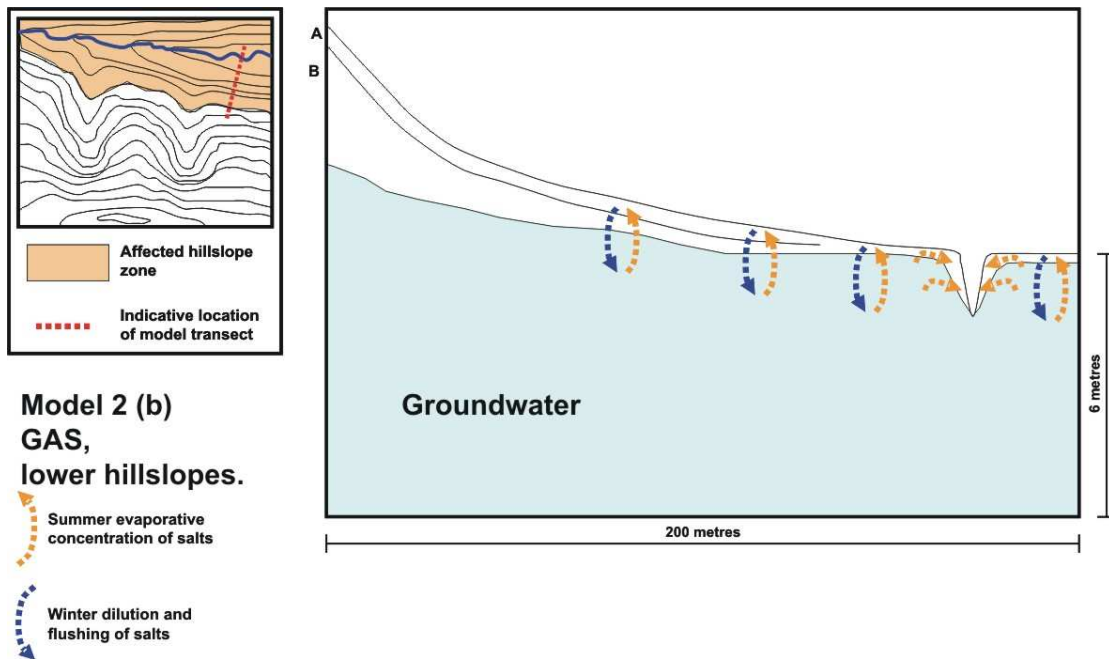


Figure 10.12. Conceptual model of Model 2b GAS, lower hillslopes. The conceptualised contour map that is inset identifies possible affected areas in the landscape, and the indicative location of the transect described in the model.

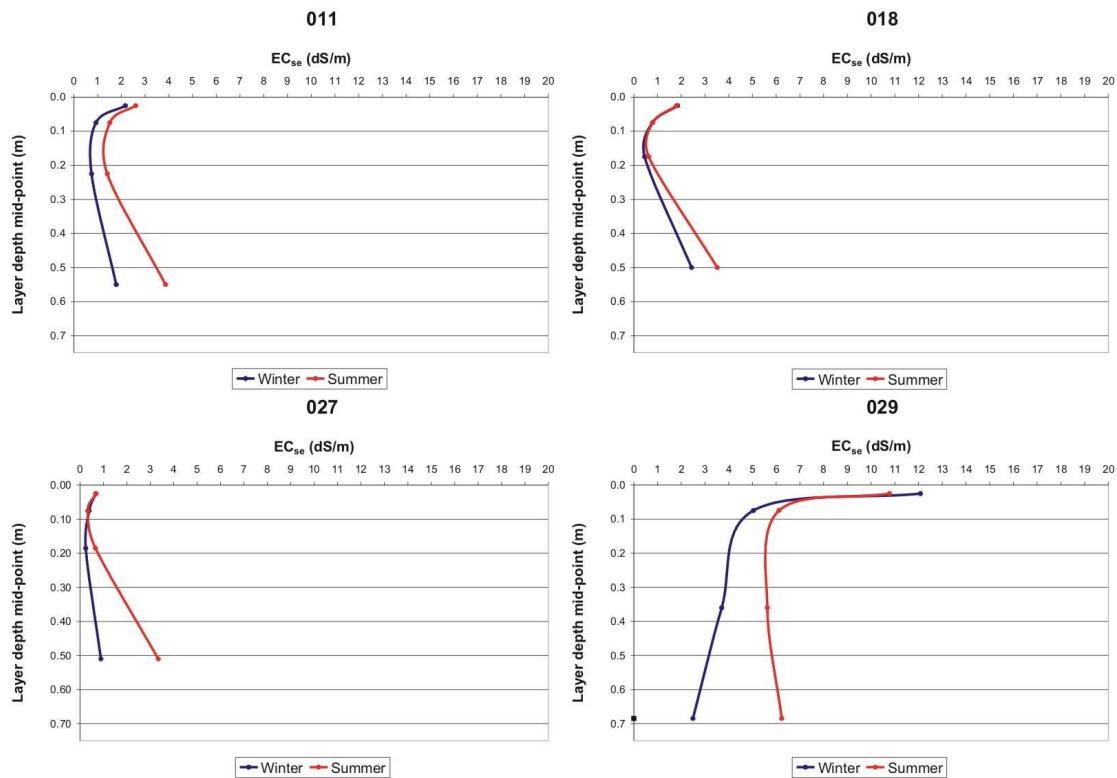


Figure 10.13. Diagnostic down-profile salinity (EC_{se}, dS/m) trends of Model 2a-type soils (profiles: 011, 018, 027 and 029).

10.4 Conclusions

The interpretation of combined site knowledge, soil layer morphology (i.e. soil texture according to clay %), and seasonal soluble salt chemistry (e.g. EC_{se} and selected pedogenic and non-pedogenic salts) at various near-surface profile depths (< 0.75 m) distributed in the MLR study area have revealed the presence of four distinctive hydropedological models. Two of the models are dominated by shallow NAS processes (e.g. Model 1a: Shallow NAS, topographically perched, upper hillslopes; and Model 1b: Shallow NAS, topographically non-perched, mid/upper hillslopes, with groundwater influence). The remaining two models are dominated by GAS processes (i.e. Model 2a: GAS, upper hillslopes; and Model 2b: GAS, lower hillslopes), and are similar to those identified by earlier researchers (i.e. Fitzpatrick *et al.* 1996; i.e. Fritsch and Fitzpatrick 1994). A so-called “F-variant” for Model 1a was also identified, which took into

consideration the seasonal distribution in the soil layers of non-pedogenic salts derived from broadcast fertilisers and lime treatments.

The low-cost investigation methods described shows the importance of seasonal hydropedological changes in the near-surface (< 0.75) of soils in the study area. Such information significantly augments the traditional approaches to interpret pedogenic and degradation processes in soil-landscapes, which include detailed layer morphological description and interpretation (McDonald *et al.* 1998), and the installation of costly nested piezometers (e.g. Fritsch and Fitzpatrick 1994). In the following Chapter, the understanding of the near-surface (< 0.75 m) seasonal hydropedological dynamics in the study at the 19 selected sites (Model 1a, Model 1b, Model 2a, Model 2b), is spatially extended to the whole study area using multi-temporal near-surface (< 1.5 m) survey methods using EM38 (EC_a).

Chapter 11. Mount Lofty Ranges spatio-temporal, medium scale investigation

As described in Chapter 10, from detailed point (pedon) scale investigations of seasonal salt movements in a selection of 19 upper profiles (< 1 m) from Mount Lofty Ranges (MLR) study area, four generic hydro-pedological models were developed. As discussed in Shaw (1988), the development of the models relied on the premise that the seasonal accumulation of soluble salts in the upper 1 m of the soil profile were diagnostic of the prevailing hydro-pedological conditions in a saline soil-landscape. This hydro-pedological knowledge helped to characterise the prevailing salinisation processes in the vicinity of the selected 19 profiles, and enabled the development of four generic conceptual hydro-pedological models for the study area soil-landscape. Two of the models were dominated by shallow NAS processes, and two were dominated by GAS processes.

The work described in Chapter 10 has identified and modelled localised hydro-pedological processes, while previous work (e.g. Fitzpatrick *et al.* 1996; Fritsch and Fitzpatrick 1994) has concentrated on whole hillslope hydro-pedological processes (i.e. conceptual toposquence models) in the degraded study area landscape. In a spatial sense, the investigations eluded to above remain restricted. For example, the investigations described in Chapter 10 are restricted to vertical changes occurring at the selected profile points (i.e. in 1-D), whereas the conceptual toposquence model describe processes along the profile of the hillslope transect (i.e. in 2D). The study described in this Chapter involves a spatially explicit methodology to investigate and describe soil-landscape properties that link hydro-pedological processes for the whole MLR study area. The methodology involves application of multi-temporal, whole-of-study area electromagnetic induction (EMI) survey techniques of the near-surface (< 1 m) using an EM38 sensor (McNeill 1990; Rhoades *et al.* 1999). Combined with other sources of soil-landscape information, the interpretation of the EMI survey data is used to characterise near-surface soil properties (in terms of salt accumulations inferred from EC_a) and understand the spatio-temporal soil processes of the study area in spatially detailed manner, at a scale equivalent to the *i+2* level (catena/toposequence soil system) presented in Table

4.1. As described, access to the spatio-temporally-enhanced soil-landscape information is used to refine existing soil mapping and to support upscaling efforts to predict the occurrences of shallow NAS and GAS-affected areas in the 1,600 ha region that surrounds the study area, as described in Chapter 12.

11.1 Conductivity relationships

At the time of profile sample collection during winter (2004) and summer (2005), an EM38 instrument was used at each profile site to collect soil EC_a readings. At each site, the EM38 was used in both EC_{ah} (maximum surface sensitivity) and EC_{av} (maximum 0.4 m sensitivity) modes, discussed in Chapter 3. The purpose of collecting the EC_a in both modes was to establish the relationship between the field measurements and the laboratory salinity determinations (EC_{se}) from Chapter 10 for each season. With reference to the sensitivity profiles of the EM38 instrument in the EC_{ah} and EC_{av} survey models, the EC_{ah} (surface) readings were compared to the L1 (surface) EC_{se} data. Correspondingly, the EC_{av} (0.4 m) readings were compared to the EC_{se} data for the profile layer that contained a mid-depth that was closest to 0.4 m (i.e. subsoil), which corresponded to either the L3 or L4 layers.

A regression analysis was conducted to investigate the field and laboratory conductivity relationships, shown in Figure 11.1. During winter, a r^2 of 0.53 was achieved for the surface, and a r^2 of 0.63 for the subsoil. During summer, the corresponding values of r^2 of 0.66 and r^2 of 0.87 were achieved. The relationship between the EC_a and EC_{se} was therefore not linear, and was interpreted to indicate that between 47 % ($r^2 = 0.53$) and 13 % ($r^2 = 0.87$) of the EC_a responses are attributed to soil factors other than salt content.

Interpretation of the results is comparable to those of Williams and Baker (1982) in deeper profile investigations using an EM31.

Similar investigations were made for the relationships between EC_a and MIR-predicted clay % and CEC data, which are important soil property contributors to the bulk EC_a response of the soil profile (Rhoades *et al.* 1999). Weak relationships were identified between EC_a and these properties, with r^2 values in the ranges of - 0.20 to 0.02 for clay %, and 0.02 to 0.17 for CEC. Therefore, of the physicochemical properties of each layer analysed in the laboratory, salt content exerted the strongest overall influence on the EC_a values in the soil profiles

11.2 Spatio-temporal apparent electrical conductivity patterns

The purpose of this Section is to describe the investigation of spatio-temporal patterns in study area soils using EM38-derived EC_a changes in the near-surface (< 1 m). As stated in Chapter 3, EC_a ground measurements reflect a bulked EC response in the soil profile, which is governed by clay content; clay mineralogy (CEC), salt content, moisture content, and temperature (McNeill 1980b; Sudduth *et al.* 2001). Of these, salt content dominates the bulked response in saline environments (Williams and Baker 1982).

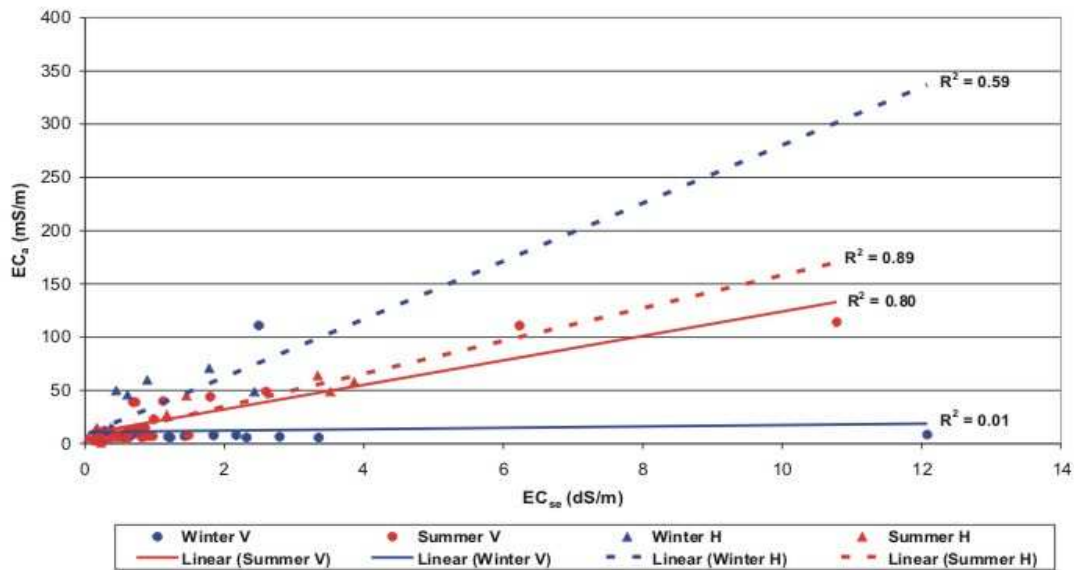


Figure 11.1. Relationship between seasonal apparent electrical conductivity (EC_a) and electrical conductivity of the saturated paste extract (EC_{se}) at corresponding depths in the Mount Lofty Ranges study area.

The investigation described was based on two seasonally consecutive EM38 EC_a surveys conducted in the catchment during late winter (August 2004) and late summer (April 2005). Each survey involved using the EM38 instrument in horizontal mode (EC_{ah}), which provides an EC_a response weighted by depth and dominated by surface conductivity, and in vertical mode (EC_{av}), which provides an EC_a response weighted by depth and dominated by subsoil (~ 0.4 m) conductivity (McNeill 1990; Rhoades *et al.* 1999).

Applied throughout the MLR study area, the seasonal, near-surface EC_a (EM38) survey data were used to develop pedotransfer functions and/or models of near-surface hydro-pedological dynamics. In turn, such models inform spatially-based pedological process, and assist in understanding and predicting soil-landscape degradation patterns (e.g. salinisation and waterlogging). In the first instance, such models are based on a spatial and a depth-based understanding of changes in bulk conductivity patterns interpreted from

contemporaneous EC_{ah} and EC_{av} surveys. This understanding incorporates knowledge that EC_a survey patterns correlate with soil properties under field conditions (Slavich and Petterson 1990). In the second instance, when the spatial EC_a survey data are combined with survey patterns from the successive season, interpretations of seasonal changes in soil profile conductivity (i.e. ΔEC_a) are used to reveal spatio-temporal trends in study area salt concentration patterns (Williams and Baker 1982).

11.2.1 Survey methodology

The winter EC_{ah} and EC_{av} surveys were conducted at the same time as the κ survey described in Chapter 10 at the same 1,085 survey points. This resulted in a survey density of almost 8.4 sites per hectare. The summer survey methodology repeated the survey methodology (i.e. using a combination of rigid and free survey), and took in 1,082 survey points.

As with the κ survey, the field data were recorded on a hand-held computer that operated a GIS, and the

recorded data transferred to a desktop GIS. Field data were then interpolated using ordinary kriging to create survey GIS coverages, each with a five metre ground resolution. The same kriging parameters were applied for each survey to ensure consistency. Coverages were investigated using GIS techniques that are described in the following Sections. A linear contrast enhancement (i.e. minimum-maximum stretch) was applied to each of the resulting GIS survey coverages for visual purposes, which ensures visual consistency in the presentation of intra-coverage data values.

11.2.2 Apparent electrical conductivity patterns

The winter EC_{ah} survey coverage (range: 3.0 to 112.0 mS/m) is shown in Figure 11.2, and the EC_{av} survey coverage (range: 3.0 to 114.0 mS/m) is shown in Figure 11.3. Both Figures show strong similarities in landscape patterns, reflected in the high regression value obtained when the two are compared ($r^2 = 0.95$). Such survey patterns also have strong visual and quantitative similarity to the EM31 EC_a patterns of the study area shown in Chapter 9 (i.e. EM31/ EC_{ah} $r^2 = 0.63$; EM31/ EC_{av} $r^2 = 0.71$).

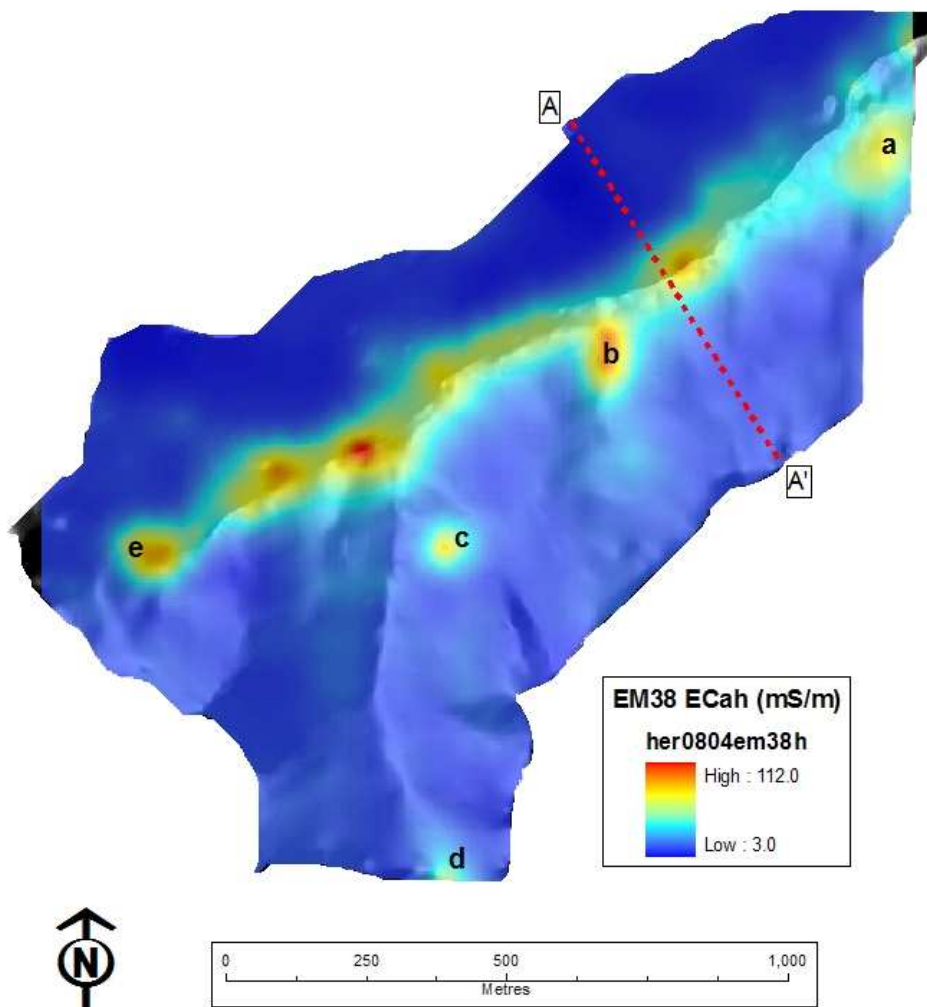


Figure 11.2. Mount Lofty Ranges study area winter EM38 EC_{ah} (i.e. surface conductivity) survey patterns with a linear stretch applied for visual consistency. A hillshade has been applied to accentuate local landform. Regions of interest “a” and “e” are identified, along with transect A-A’.

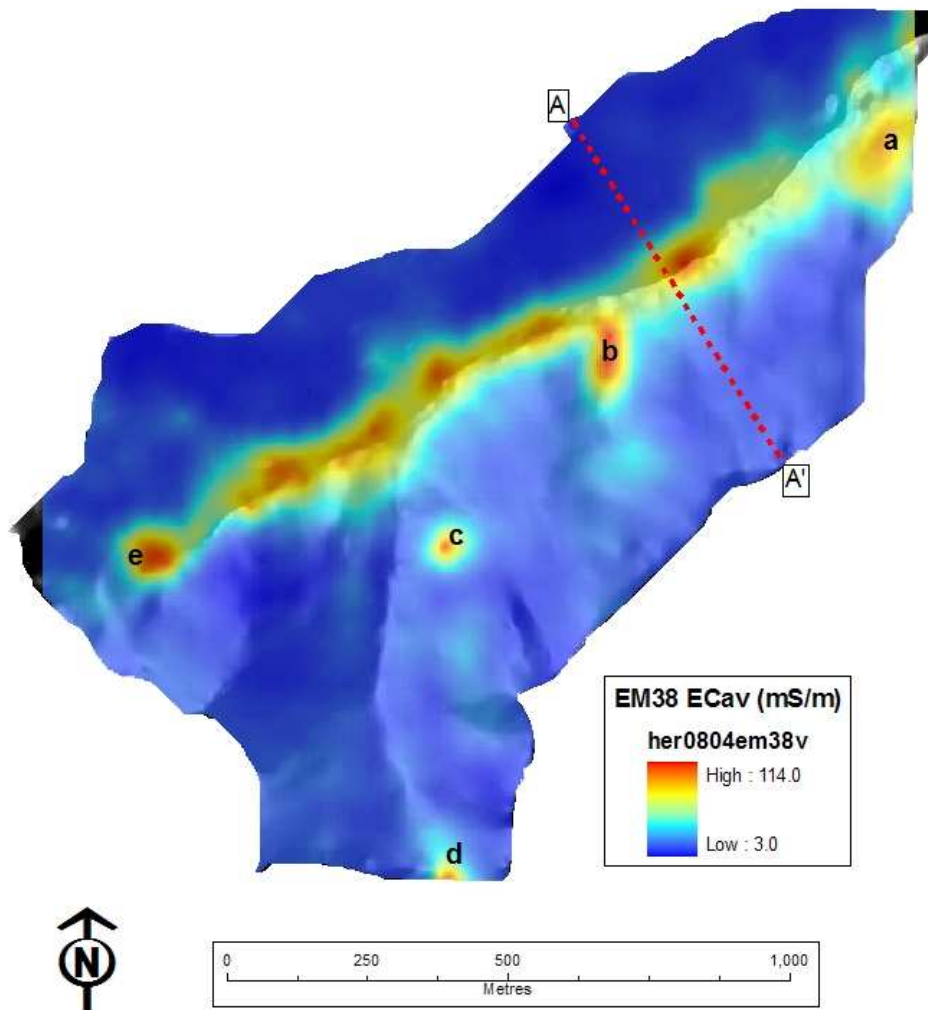


Figure 11.3. Mount Lofty Ranges study area winter EM38 EC_{av} (subsoil conductivity) survey patterns with a linear stretch applied for visual consistency. A hillshade has been applied to accentuate local landform. Regions of interest “a” to “e” are identified, along with transect A-A’.

The patterns are most correlated in the drainage and wetland areas. The strong relationship identified between the EM38 and the EM31 survey in the creek zone indicates the likelihood that deep salts are connected via saline groundwaters to the near-surface areas (i.e. groundwater associated salinity; GAS). Both these coverages also feature an area of elevated EC_a values in the northeast of the north facing slope, identified as “a”. This hillslope zone has relatively low gradients and poorly drained soil, which suggests elevated concentration of salts from lower in the soil profile in the form of GAS. The pattern is consistent with the model described in Chapter 10 as

Model 2b for GAS on lower hillslopes. An area of relatively high EC_{ah} and EC_{av} responses, identified as “b”, on the north facing slope is associated with a drainage area branching from the creek. Again, these responses are likely to represent GAS of Model 2b-type, in which the saline groundwater intersects with the near-surface of the locally low-lying landscape position.

Figure 11.2 and Figure 11.3 indicate high conductivity “hot spots”, identified as “c” in the mid slope of the north facing slope and “d” at the most southern catchment area. These hot spots indicate the presence of saline groundwater seeps (GAS), and

conform to the Model 2a for GAS in upper hillslopes. The saline groundwater seep identified as “c” also features strongly in the EM31 coverage (region “a” in Figure 9.16), whereas “d” in the EM38 coverages is not apparent in the EM31 survey, indicating that this saline groundwater seep is either a near-surface feature (i.e. < 1.0 m), or has recently developed since 1999 when the EM31 survey was conducted.

There is a strong conductive region identified as “e” toward the head of the creek, which is of Model 2b-type. This region represents a saline sulfidic seep associated with a perched wetland, described in Baker and Fitzpatrick (2003).

The summer EC_{ah} survey coverage (range: 1.2 to 140.9 mS/m) is shown in Figure 11.4 and the EC_{av} (subsoil conductivity) survey coverage (range: - 0.4 to 154.9 mS/m) is shown in Figure 11.5.

The summer EC_{ah} and EC_{av} patterns show strong similarities, which is reflected in the high regression value obtained when the two are compared ($r^2 = 0.91$). Visually, the summer EC_a patterns feature similar hillslope and drainage conductivity patterns to the winter EC_a counterparts. However, the saline seeps identified from the winter coverages are poorly defined in the summer counterparts, except for the saline sulfidic seep identified as “e” in Figure 11.2 and Figure 11.3.

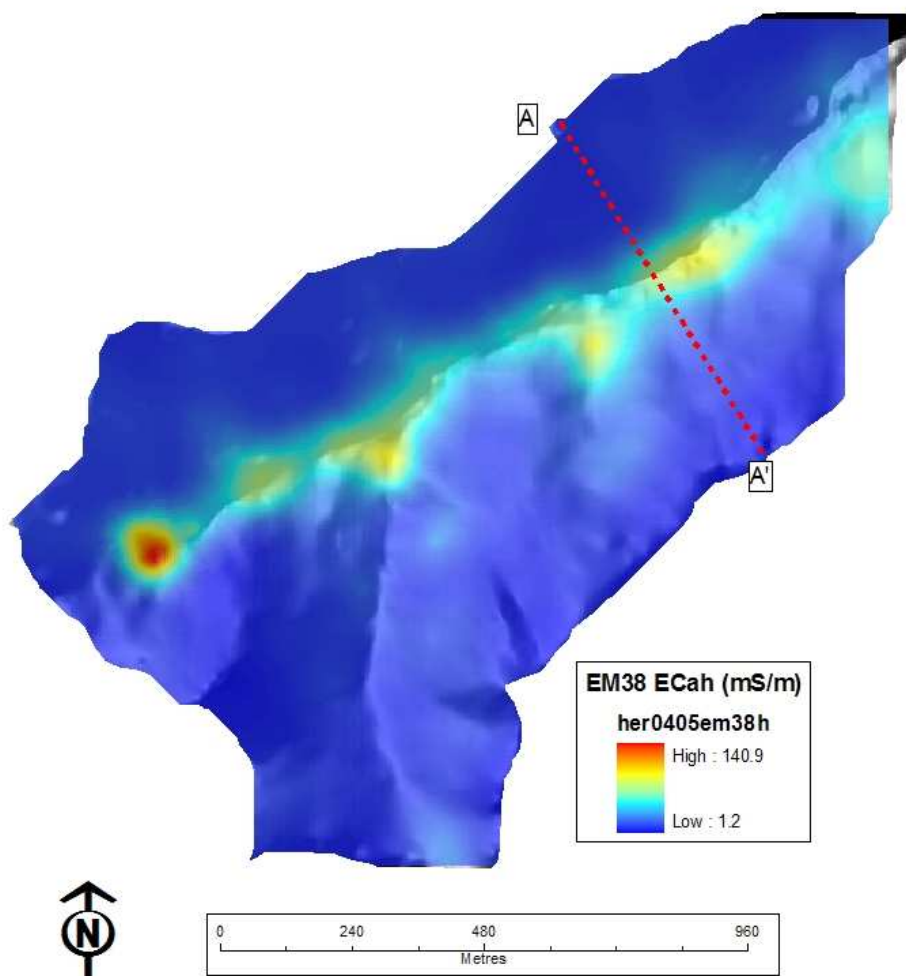


Figure 11.4. Mount Lofty Ranges study area summer EM38 EC_{ah} (surface conductivity) survey patterns with a linear stretch applied for visual consistency. A hillshade has been applied to accentuate local landform. Transect A-A' is identified.

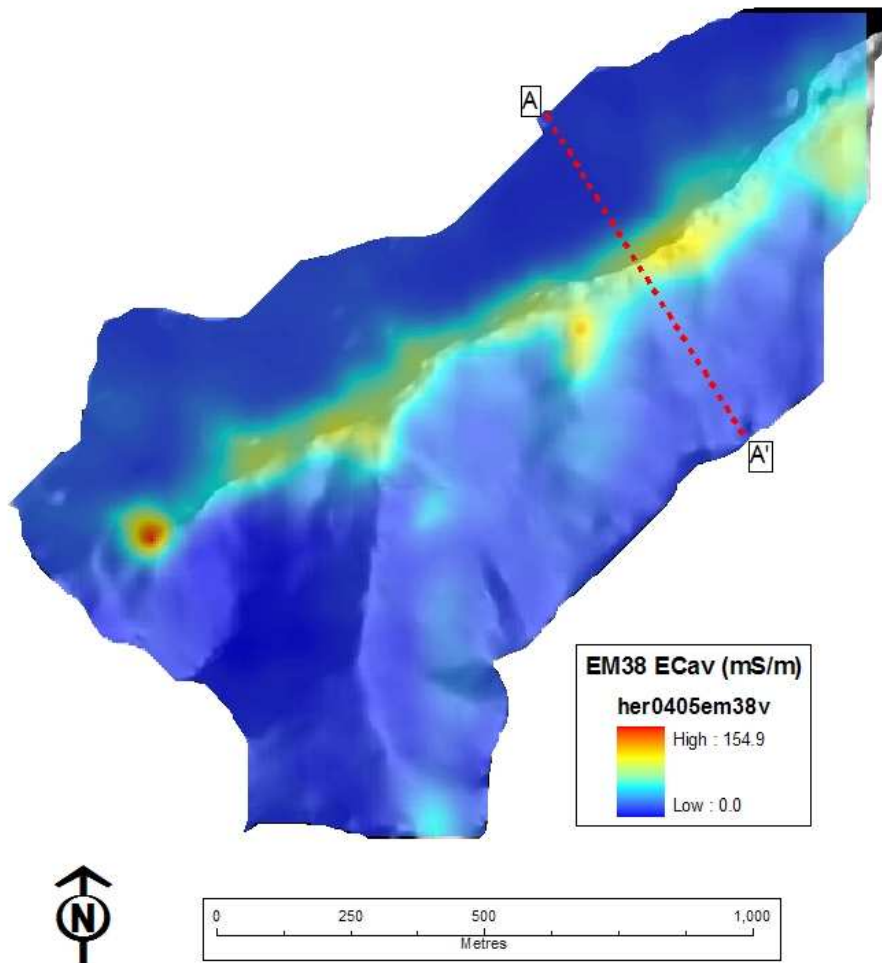


Figure 11.5. Mount Lofty Ranges (MLR) study area summer EM38 EC_{av} conductivity (surface conductivity) survey patterns with a linear stretch applied for visual consistency. A hillshade has been applied to accentuate local landform. Transect A-A' is identified.

Using the transect A-A' as reference, seasonal variations in surface and subsoil conductivity in the hillslopes follow similar trends. These indicate that, in general, subsoil conductivity is greater than surface conductivity during both survey periods, and that the responses are strongly related to hillslope position. All plots in the steep south-facing slope show similar values (within a few mS/m of 10 mS/m), and rise sharply at the break of slope and drainage area. In both seasons, the surface EC_a values are similar (peaking at approximately 70 mS/m), as do the

subsoil EC_a values (peaking at approximately 90 mS/m). The peaks of the summer plots are off-set to the south of the winter plot peaks by approximately 20 m on the ground. Continuing southwards and progressing up the north facing slope, all plots reach their lowest EC_a values on the southern hillslope at the summit. In the summit, the winter subsoil and surface and summer subsoil values are identical (approximately 12 mS/m), whereas the summit surface value is significantly less (approximately 3 mS/m).

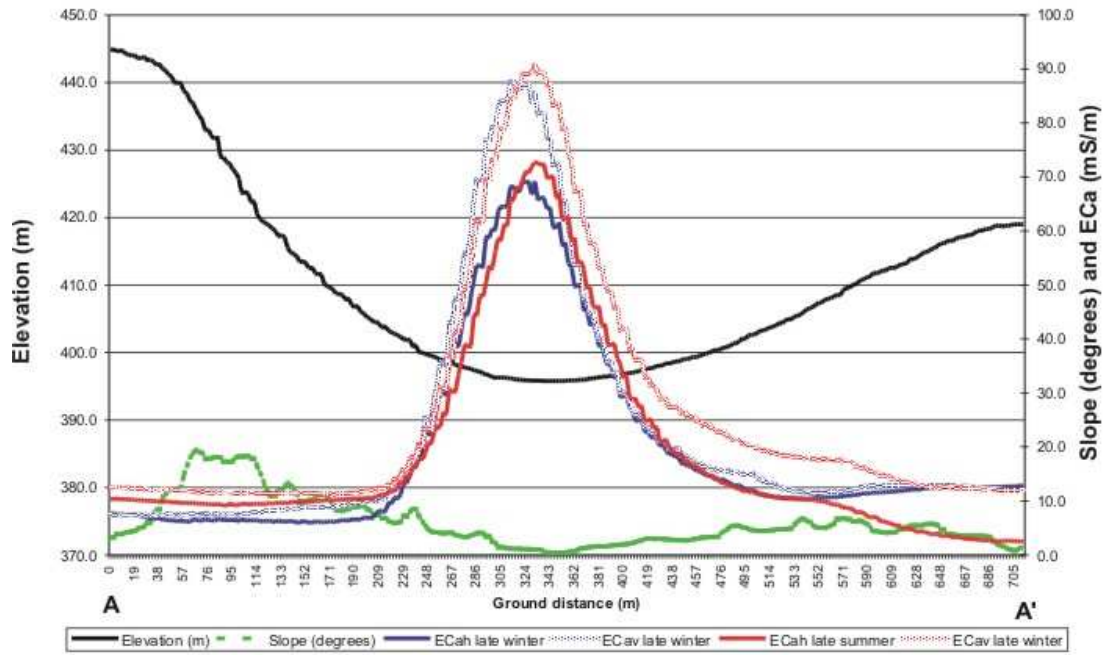


Figure 11.6. Profiles corresponding to transect A-A', featuring elevation (m), slope ($^{\circ}$) and EM38 winter and summer apparent conductivity (EC_a , mS/m), of surface (EC_{ah}) and subsoil (EC_{av}).

Figure 11.6 indicates conceptually strong correlations between landform and the seasonal electrolyte distributions in the soil. The following Sections present investigations and discussions that spatially-relate conductivity patterns with landform to assist in the refinement of our understanding of spatially-based near-surface saline and hydrogeological processes.

11.2.3 Inter-seasonal, near-surface conductivity dynamics

This Section describes a series of near-surface (e.g. < 1 m) depth-based investigations of seasonal conductivity dynamics of the study area soils. These investigations involve the analysis of the results of GIS analysis of the co-registered EC_a survey coverages, and the seasonal result of the GIS investigations, summarised in the schematic presented in Figure 11.7.

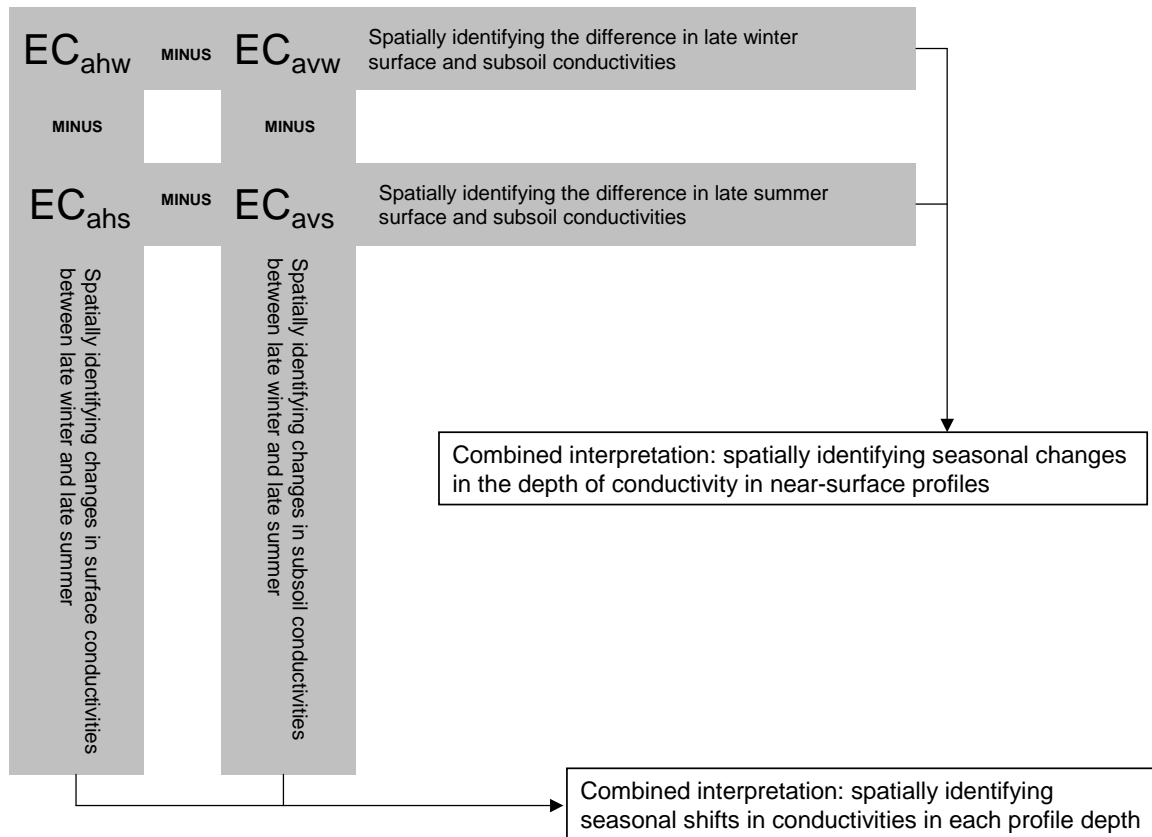


Figure 11.7. Summary of seasonal interpretations of GIS analysis of the co-registered seasonal EC_a survey coverages.

The resulting differences are shown in Figure 11.8 for winter, and Figure 11.9 for summer. Positive values indicate landscape positions in which the surface is more conductive than the subsoil, whereas negative values show where the subsoil is more conductive than the surface. For ease of

interpretation, the Figures have been contoured in increments of $\Delta 10$ mS/m. Strong positive or strong negative Δ conductivity values indicate very different electrolytic conditions in the subsoil and surface, which may be linked to the interpretation of hydrogeological processes.

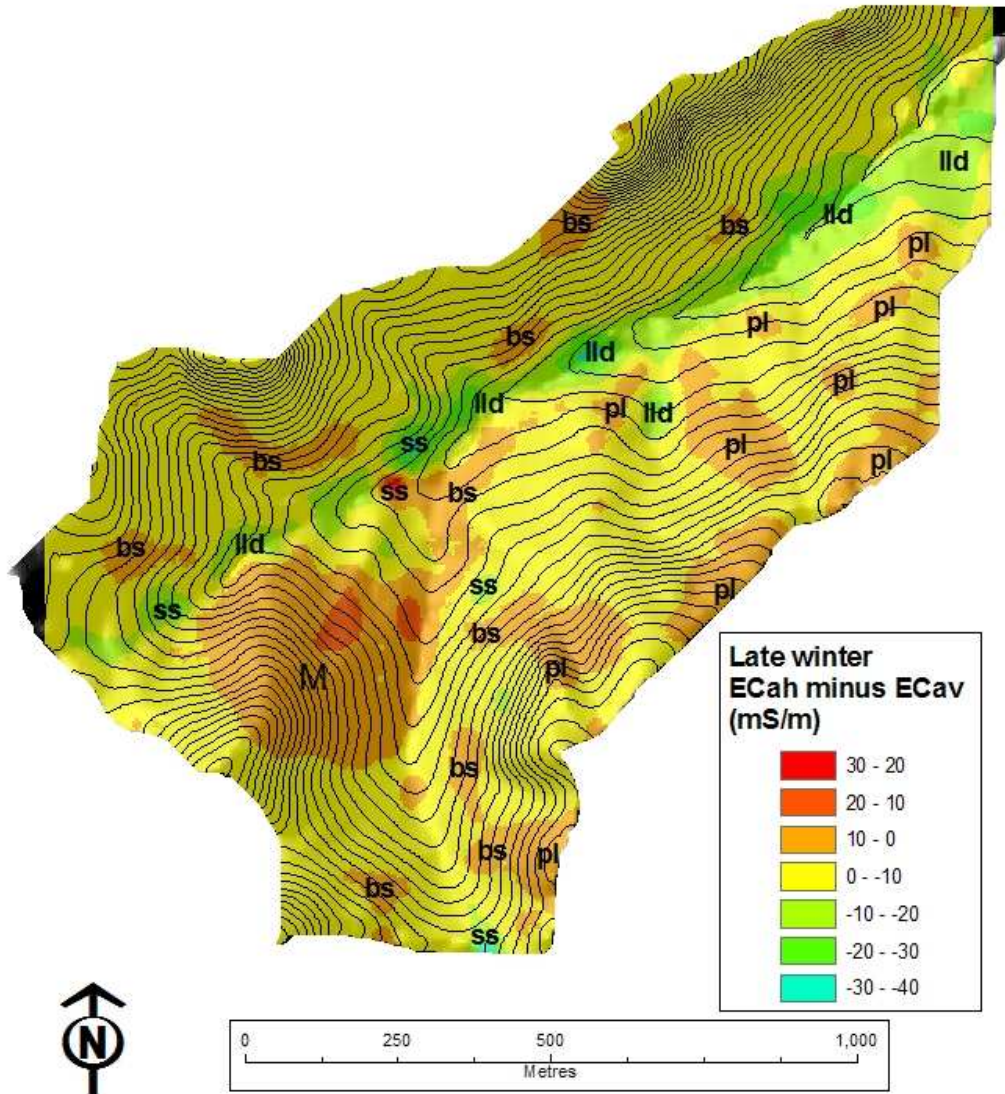


Figure 11.8. Mount Lofty Ranges study area winter apparent electrical conductivity differences ($EC_{ah} - EC_{av}$) with landform codes (“M” = zone of high volume magnetic susceptibility response; “pl” = perched landform; “bs” = break of slope; “ss” = saline seep; “lld” = low lying drainage). A hillshade and two metre contours are applied to accentuate local landform differences.

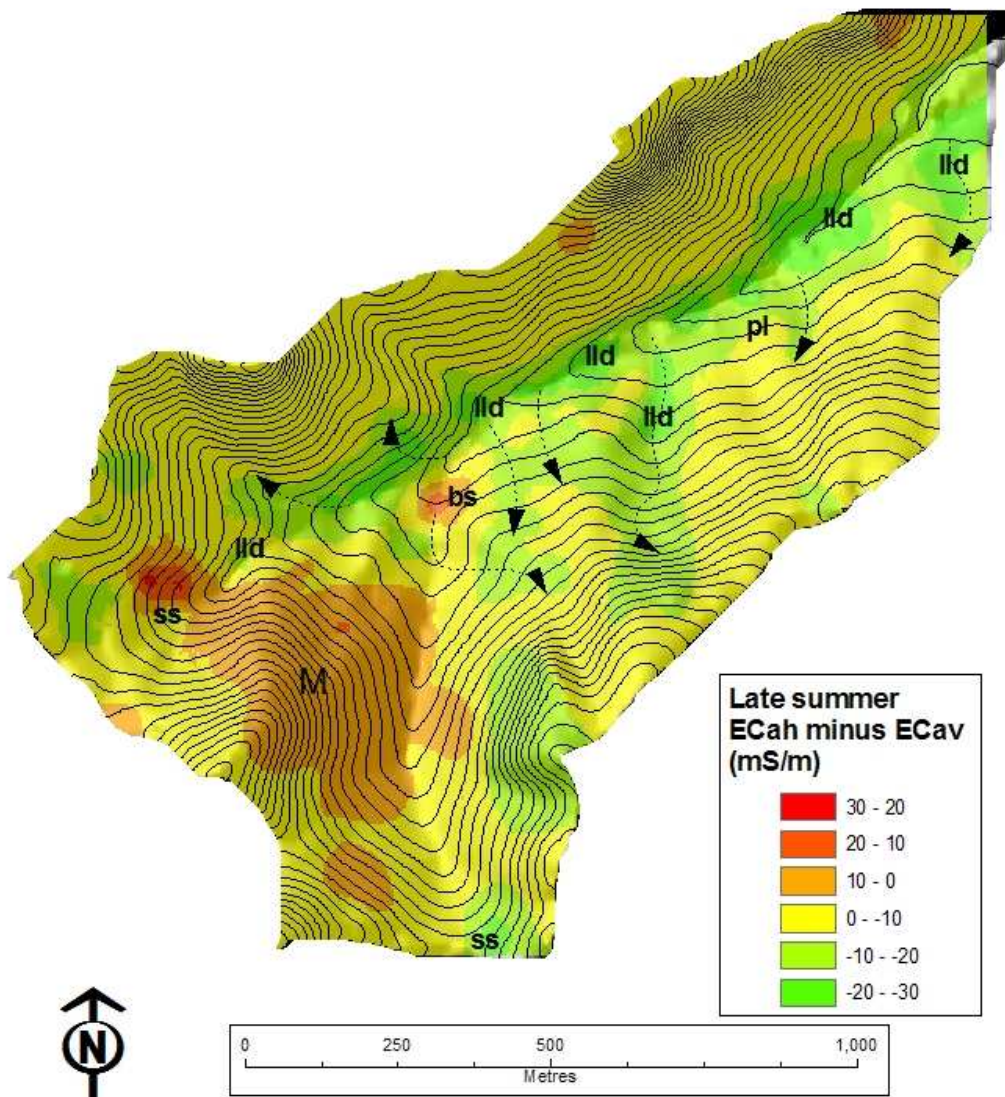


Figure 11.9. Mount Lofty Ranges study area summer apparent electrical conductivity differences ($EC_{ah} - EC_{av}$) with landform codes (“M” = zone of high volume magnetic susceptibility response; “pl” = perched landform; “bs” = break of slope; “ss” = saline seep; “lld” = low lying drainage). A hillshade and two metre contours are applied to accentuate local landform differences.

With reference to Figure 11.8 and Figure 11.9, landscape positions that show positive Δ conductivity values indicate soils that contain the following properties in the near-surface profiles:

- elevated salt concentrations at or near the soil surface;
- texture-contrast soils with thin (i.e. > 0.1 m) A horizons overlying conductive Btn horizons, which may or may not be saline; and/or
- surface concentrations of conductive minerals, e.g. Fe-rich gravels.

The first two of the above scenarios are consistent with break of slope (bs) landforms where A horizons are shallow due to erosion (convex break of slopes), or where salts accumulate through a combination of GAS and NAS processes. In addition, positive Δ conductivity values will also indicate perched (pl) landforms where salts

accumulate near the surface (shallow NAS).

Negative Δ conductivity values indicate landscape situations in which the subsoil is more conductive than the surface layers. Conceptually, a combination of the following soil profile property scenarios are present:

a combination of poorly conductive, coarse textured A horizons (e.g. sands and sandy loams) that overlay moderately deep (> 0.3 m) Btn horizons, which may or may not be saline. In terms of landform position, such soils feature strongly in hillslope zones with moderate gradients; or

saline soils, in which subsoil conductivity dominates in the soil profile. This scenario is consistent with GAS, in which salts intrude the soil profile from below via saline groundwaters. In terms of landform, such profiles are likely to be representative of localised saline seeps and areas of locally low-lying relief connected to low catchment elevations.

Figure 11.8 shows a classified version of the winter Δ conductivity differences. This coverage features a range of 24.9 to -40.0 Δ mS/m, a mean of -3.2 Δ mS/m, and a SD of 5.8. The creek zones show the most negative of the catchment Δ conductivity values, indicating that the subsoil conductivity is much greater than the near-surface. This scenario conforms to the conceptual Δ conductivity profile model associated with GAS. The saline seeps (ss) identified in the north facing slope in Figure 11.2 and Figure 11.3 are also prominent features of locally negative Δ coverage values, again indicating GAS.

The upper hillslope areas are dominated by marginally positive conductivity differences (i.e. the surface is more conductive than the subsoil). This scenario conforms the

model associated with texture-contrast soils, and is in agreement with soil mapping that identified Typic Palexeralf soils as being the aerially dominant in hillslopes soil in the catchment. Zones of larger conductivity differences tend to be locally interspersed in the hillslope areas, especially on the north facing slope. Many of these zones are associated perched landforms. However, a strong positive conductivity difference zone correlates strongly with the zone of high volume magnetic susceptibility response (M) in the north facing slope (e.g. Figure 11.8). Within the magnetic zone there are two zones of stronger positive conductivity differences (> 20 mS/m). The larger of these coincides spatially with the GAS zone described previously (Chapter 9). The second zone, located within feature "M", is located in the lower slope and likely to coincide with a saline seep. North of the feature "M" in the south-facing slope, there is a crescent of positive conductivity differences, which is partially associated with a break of slope landform. The areas of positive Δ conductivity associated with the perched landforms and breaks of slopes are likely to be associated with shallow NAS.

Figure 11.9, which is the summer counterpart of Figure 11.8, features Δ conductivity range of 25.2 to -29.5 mS/m, a mean of -6.9 Δ mS/m, and a SD of 6.7. Compared to the winter counterpart, the summer Δ conductivity value data distribution range have become is broader, and the mean has become more negative (i.e. summer: -6.9 versus winter: -3.2 Δ mS/m).

As for the winter coverage, the summer Δ conductivity differences shows the low lying drainage areas associated with the creek are zones with the most negative conductivity differences in the catchment. Such a pattern shows the predominance of GAS processes in near-surface soil

profiles. However, the summer coverage indicates an up slope progression of higher negative conductivity differences (shown in Figure 11.9 as dotted arrows) predominantly in the north facing slope, and confined to locally low-lying drainage areas. These seasonal changes in near-surface profile conductivities in these low-lying hillslope drainage areas can be explained through either the accumulation of salts in the subsoil from surface flushing, or upward movement of saline groundwater to the subsoil. The up slope expansion of these negative conductivity differences that predominantly occur in the north facing hillslopes is a geomorphic reflection of the lower gradient of the slopes, which result in a larger up slope aerial intersection of shallow saline groundwater/near-surface soil.

Figure 11.9 shows that surface conductivity patterns associated with the locally perched landforms, found predominantly in the north facing slope in the winter (Figure 11.8) are no longer evident in the summer in the Figure. This changing pattern of conductivity in the soil profiles of these landscape zones indicates that surface salts have been leached downwards to the subsoil, and/or salts have been raised from below during summer. The strong positive conductivity difference correlating with the magnetically active zone in the north facing slope ("M"), remains a prominent feature in the summer, although diminished in size compared to winter.

Much of the south-facing slope remains in the same Δ conductivity range (i.e. Δ 0 - -10 mS/m) during both seasons. The most significant change that has occurred in these hillslope areas is the disappearance of the so-called positive Δ conductive crescent north of zone "M" discussed previously. Also, the zone "M" has become larger in the summer survey.

The previous Section presented spatial investigations of inter-layer conductivity differences in the study area, and compared these changing patterns seasonally. Next, inter-seasonal changes in conductivity in the surface and subsoil layers are investigated. Like the previous investigation, the methodology involves the use of a GIS to perform coverage subtractions. The results are shown in Figure 11.10 (EC_{ah}) and Figure 11.11 (EC_{av}). In these, positive Δ conductivity values indicate where winter conductivity dominates the summer conductivity in both the surface and subsoil. Contours showing increments of Δ 20 mS/m conductivity differences have been applied to assist interpretation.

Figure 11.10 shows the surface conductivity (EC_{ah}) Δ conductivity values. This coverage has a Δ conductivity range of between 51.2 and -65.8 mS/m conductivity, with a mean value of 2.1 mS/m and a SD of 7.4 mS/m. Much of the low-lying drainage areas and the north facing slopes feature soil surfaces that are more conductive. However, a significant proportion of the lower and mid slope areas in the northeast of the catchment show higher surface salinity in the summer. In these areas there are local examples in which negative Δ conductivity values finger up slope, associated with perched landforms. Areas of positive Δ conductivity differences in the south-facing slope are confined to the lower-slopes. Where these south-facing slope zones occur, they generally emanate from slope break positions.

Areas of high summer surface salinity show negative differences; i.e. the summer surface salinity is significantly elevated locally in the creek, whereas the up slope saline seeps show locally negative Δ conductivity differences, meaning that these areas are more saline in the surface during summer. Much of the south-facing slope shows higher surface salinity in the summer.

The area identified as a saline seep (see “a” in Figure 11.2 and Figure 11.3) is also clearly apparent in Figure 11.10 (“d”), which shows salinity increase in

summer. Other less significant summer hot spots area also evident in the drainage zone.

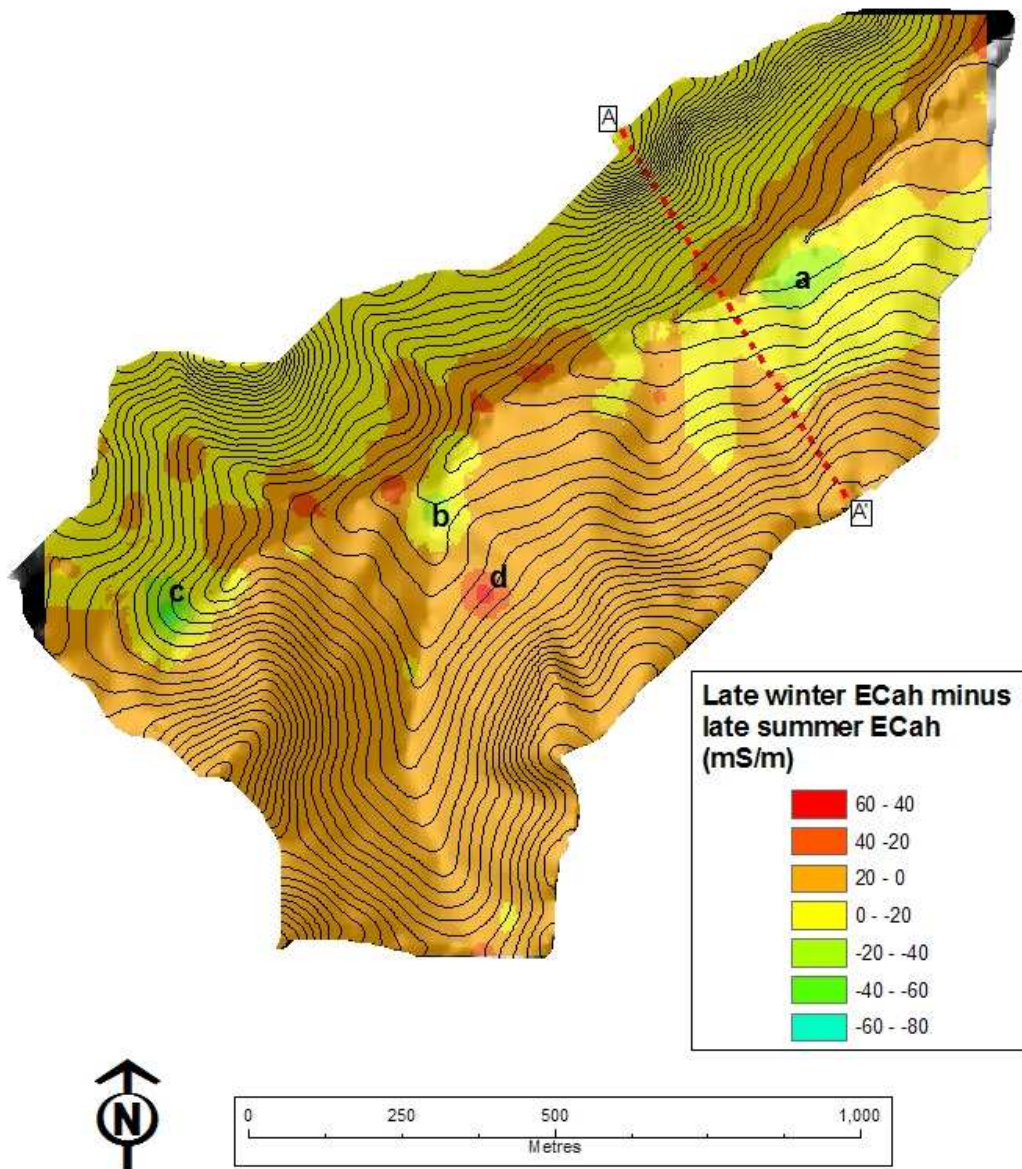


Figure 11.10. Mount Lofty Ranges study area apparent electrical conductivity in horizontal mode (EC_{ah}) difference class coverage (i.e. winter EC_{ah} – summer EC_{ah}). A hillshade and two metre contours are applied to accentuate local landform differences.

The subsoil conductivity (EC_{av}) differences shown in Figure 11.11 have a range of 60.6 and -60.1 mS/m conductivity difference, with a mean value of -1.66 mS/m conductivity difference, and a SD of 8.0 mS/m. A comparison of patterns in Figure 11.11 and Figure 11.10 indicate significantly different conductivity depth patterns in areas of the north facing slope. Whereas much of the catchment shows a winter dominance of Δ conductivity values in the surface (i.e. patterns dominated by positive Δ conductivity differences) in these areas (Figure

11.10), the subsoil (EC_{av}) counterpart (Figure 11.11) indicates a summer dominance of negative subsoil Δ conductivity values. However, comparisons of the statistical distributions of Δ conductivity values of each of the two coverages indicate these differences to be not large, suggesting that the differences are often subtle in much of the catchment. The differences in Δ conductivity values in the north facing slope appear to bear little relationship to landform trends.

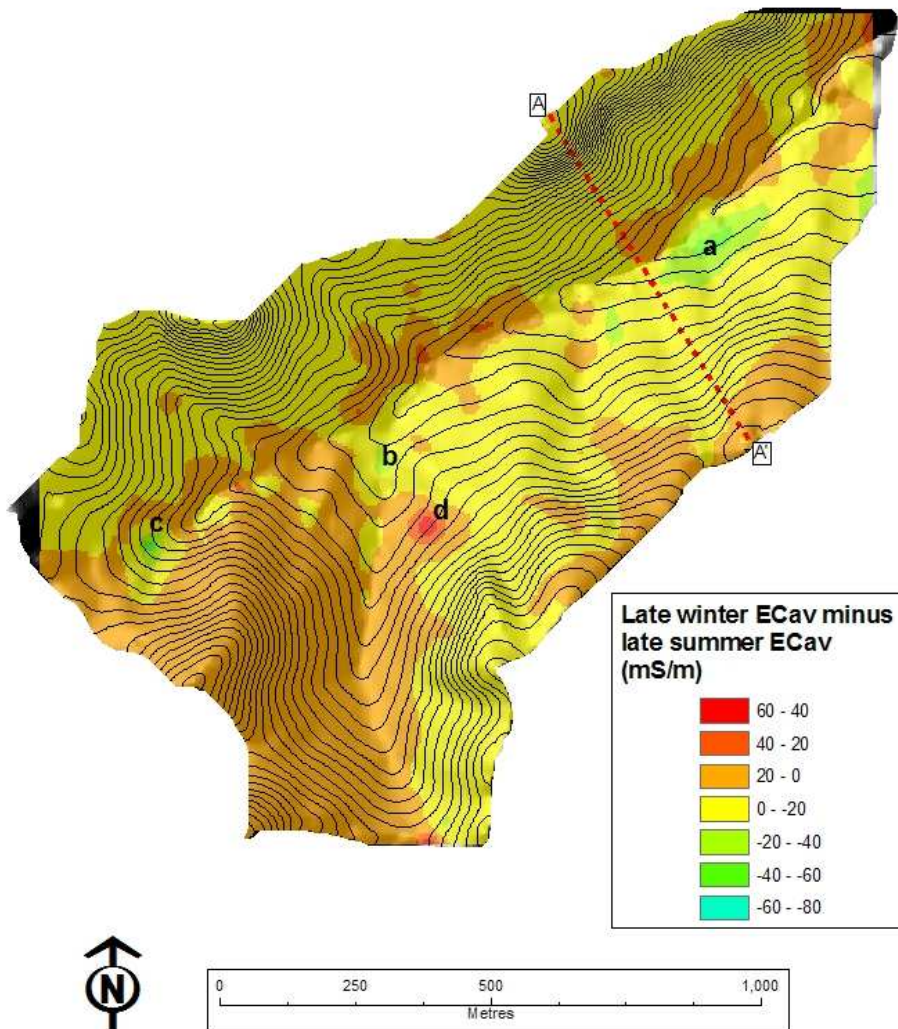


Figure 11.11. Mount Lofty Ranges study area apparent electrical conductivity in vertical mode (EC_{av}) difference class coverage (i.e. winter EC_{av} – summer EC_{av}). A hillshade and two metre contours are applied to accentuate local landform differences.

11.3 Interpretation

The near-surface salinity change map shown in Figure 11.12 represents an analysis of the seasonal dynamics of salt movements between the surface and subsoil layers in the catchment area. The analysis map represents a summary of the + EC_a difference value regions extracted, using a GIS overlaying procedure, from the coverages shown in Figure 11.10 and Figure 11.11. The overlaying procedure results in four classes, each of which represents a unique combination of: (i) higher surface salinity in winter **or** (ii) higher surface salinity summer, **and** (iii) higher subsoil salinity in winter **or** (iv) higher subsoil salinity summer. It is important to emphasise that the analysis method presented here does not take account of the severity of the saline property; it merely separates seasonal near-surface saline soil regimes into classes.

The four possible combinations are summarised in the legend of Figure 11.12. Conceptually, these classes represent the following seasonal saline conditions in the soil profiles:

- **Class 1:** regions in which highest salt concentrations occur in the surface and in the subsoil during summer (shallow NAS/GAS) in red;
- **Class 2:** regions in which highest surface salt concentrations occur during summer and highest salt concentrations in the subsoil occur during winter (GAS) in yellow;
- **Class 3:** regions in which highest surface salt concentrations occur during winter and highest salt concentrations in the subsoil occur

during summer (shallow NAS/GAS) in light blue; and

- **Class 4:** regions in which highest salt concentrations occur in the surface and in the subsoil during winter (shallow NAS/GAS) in dark blue.

Information presented in Figure 11.12 creates a complicated spatial summary of seasonal salt movements in the study area, which is dominated by three of the previously described classes (i.e. Classes 1, 3 and 4 saline conditions) in similar aerial proportions.

In summary, the upper slopes of the south-facing slope and the lower slopes of the eastern end of the north facing slope are dominated by Class 1 saline conditions, in which highest salt concentrations occur at the surface and in the subsoil during summer. Much of the upper slopes of the southern north facing slope and the mid slopes of the central areas of the north facing slope are dominated by Class 3 saline conditions. In these areas, highest surface salt-concentrations occur during winter, and highest salt concentrations in the subsoil occur during summer. Finally, Class 4 saline conditions in which highest salt concentrations occur in the surface and in the subsoil during winter dominate the south western quarter of the of the catchment, the drainage areas (GAS), and the north facing tertiary summit landform (shallow NAS).

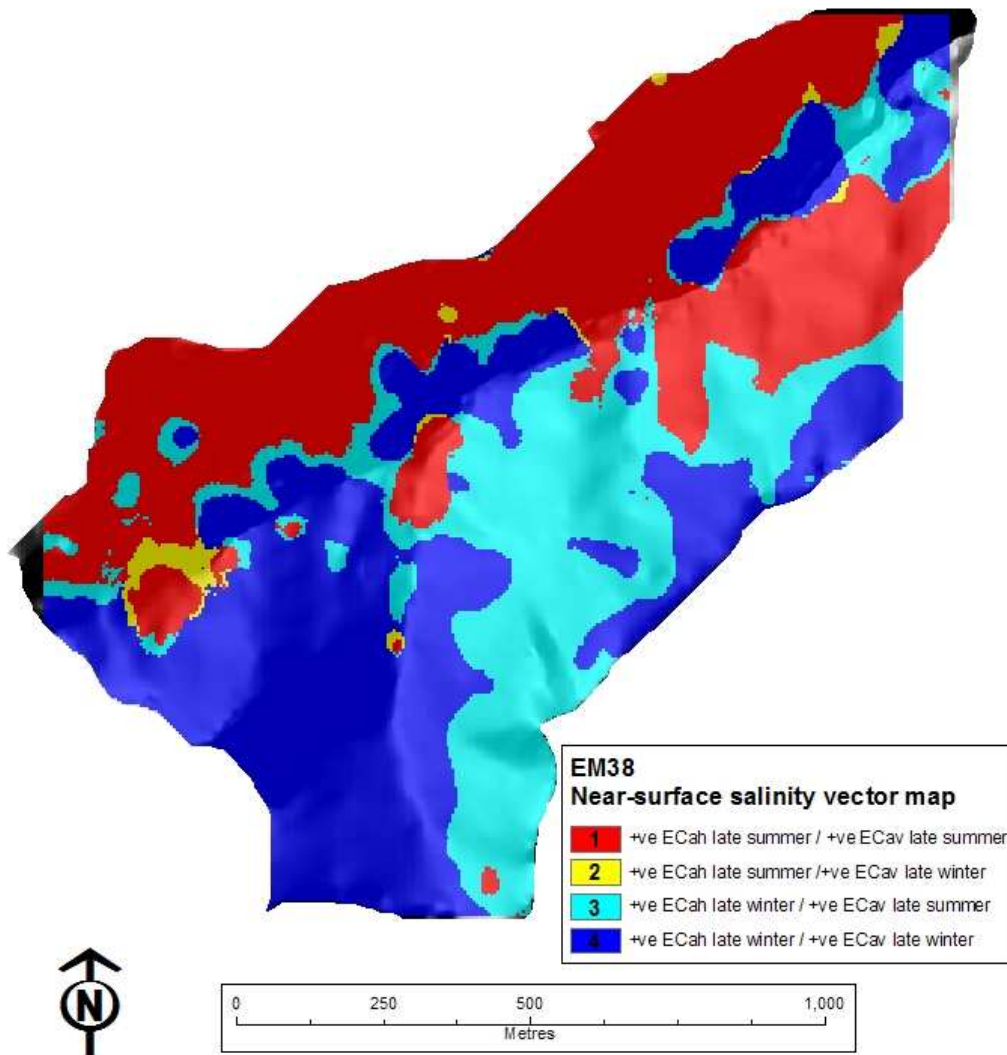


Figure 11.12. Mount Lofty Ranges study area seasonal near-surface salinity vector coverage with a hillshade applied to accentuate local landform variations.

With reference to the profile data corresponding to transect A-A' in Figure 11.3, with the exception of the lower hillslope zones of the south-facing slope (i.e. slope breaks and low-lying drainage areas), much of the slope shows higher surface salinity in the summer, albeit a small value (e.g. ~ 4 mS/m). The south-facing slope break exerts a significant influence on the seasonal surface salinity patterns, resulting in increased salinity in the winter (e.g. ~ 12 mS/m). However, down slope of this in the drainage zone there is a sharp drop in EC_{ah} difference values, indicating a strong boundary between elevated winter- and summer-surface salinity zones. Moving up slope of the drainage area, the difference in surface conductivity becomes progressively more positive towards the summit, crossing over to positive values in the mid slope zone.

Reference to the subsoil salinity profile (EC_{av}) patterns of transect A-A' (Figure 11.13) shows similar hillslope trends to the surface salinity (EC_{ah}) trends in that the south-facing slope shows negative (i.e. higher summer difference) values until the slope break is reached. At the slope break the difference values revert to positive, but

switch sharply again in the drainage area, where summer salinity are highest once again. The EC_{ah} and EC_{av} difference plots almost overlay over the break of slope and the drainage zone. However, the steep trajectory of the EC_{av} difference plot continues to fall to reach a minimum corresponding to the highest summer subsoil difference value for the A-A' transect. The low point corresponds to the southern edge of the drainage area, whereby the plot values track upwards, up slope in the south-facing slope. Moving up slope, the EC_{av} difference values very closely track the EC_{ah} difference values by approximately 10 mS/m. The EC_{av} difference values only become positive within approximately 100 m of the summit zone, the zone tertiary dominated landform.

The following Chapter describes the application of the spatio-temporal soil-landscape data generated through the current investigation in the refinement of existing soil mapping (featured in Chapter 9), and a regional upscaling methodology to predict the occurrences of shallow NAS and GAS-affected areas in the 1,600 ha region that surrounds the MLR study area.

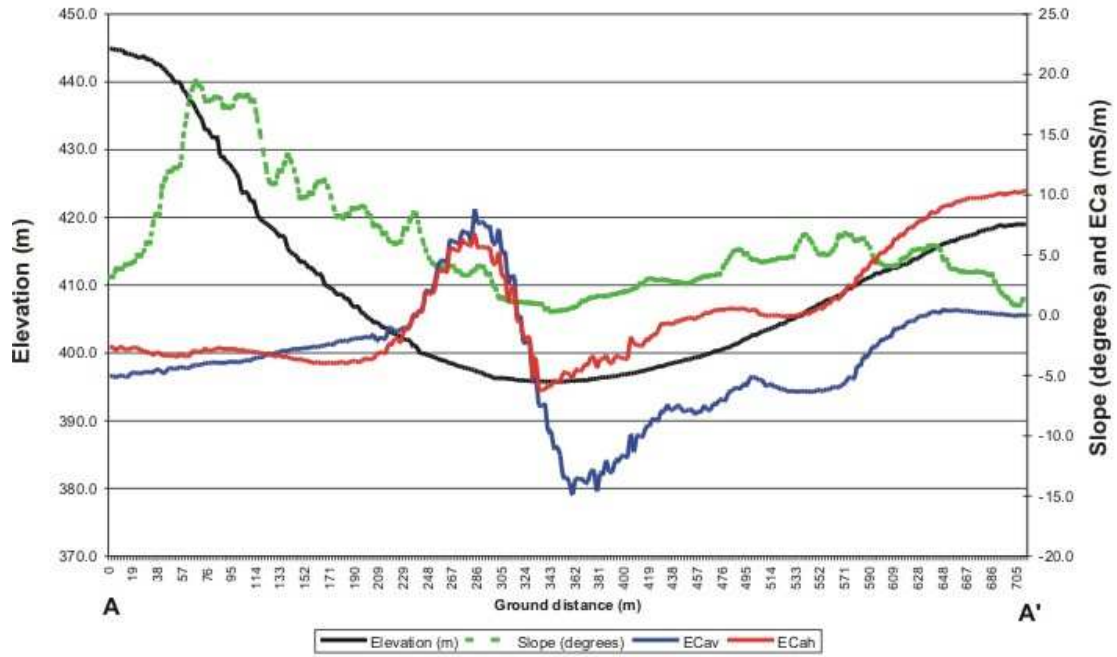


Figure 11.13. Profiles corresponding to transect A-A' in the Mouth Lofty Ranges study area, featuring: elevation (m), slope ($^{\circ}$), apparent electrical conductivity in horizontal mode (EC_{ah}) and apparent electrical conductivity in vertical mode (EC_{av}) differences in units of mS/m.

Chapter 12. Mount Lofty Ranges regional and coarse scale investigation

This Chapter describes research conducted to refine the quality of an existing 1:5,000 scale regional soil map of the MLR study area (equating to $i+3$, Table 4.1). The original soil mapping and accompanying metadata, which featured soil units and associated drainage/waterlogging and salinity and acidity/alkalinity classes, was first presented by Fitzpatrick *et al.* (1999), and later Davies *et al.* (2002) and Merry *et al.* (2002). Refinements made to the original map were in redefining the position of soil unit boundaries, and reviews made to soil unit descriptions *in lieu* of more recent research (e.g. described in previous Chapters). Such refinements were achieved using the qualitative combination of spatially defined soil-landscape datasets, soil process models, and soil data of the study area that have been previously described in Chapters 9, 10 and 11. This Chapter also describes a GIS-based upscaling method developed in this thesis to predict the distribution of shallow NAS and GAS for the region (1,560 ha) that surrounds the study area.

12.1 Regional soil mapping

The original 1:5,000 scale soil map (Davies *et al.* 2002; Fitzpatrick *et al.* 1999) shown in Figure 9.18 was constructed by combining soil physicochemical, morphological, hydrological, terrain analysis (DEM), remote sensing (i.e. aerial photographs and airborne radar), and EM38 electrical conductivity data. However, since publication, systematic inaccuracies have been identified in the original soil map unit boundaries and descriptions since the acquisition of more recent soil-landscape datasets.

In this Section, work is described that addresses the inaccuracies in the original map. This work takes advantage of access to the newly developed/acquired soil-landscape datasets and models from the earlier phases of the MLR study area investigation, which are described in

Chapters 9, 10 and 11. The methods used to refine the original soil unit boundaries rely on qualitative soil mapping techniques (e.g. Gunn *et al.* 1988; Hudson 1992), which apply the newly acquired knowledge of near-surface solute movements, and the resulting interpretations of near-surface hydrology via salt movements.

Refinement of the original soil map was conducted in GIS using interactive digital methods. As with the investigations described in Chapters 6 and 7, the method exploited the capability of 3D GIS to provide an interactive visualisation environment to query multiple, co-registered spatial datasets. Generally, a backdrop of terrain (e.g. hillshade or contours) or aerial photograph was used, providing an interactive proxy for aerial photographic interpretation. The approach assisted in identifying, and then understanding, complex soil-

landscape patterns and their pedogenic origins. As such, the approach enabled mentally-based, tacit soil-landscape models (Hudson 1992) to be developed for the mapping refinement.

Refinement and modification of the original soil map was conducted using GIS editing capabilities. On-screen vector digitising was used to modify the boundaries of existing soil units, or to add new soil units (polygons). Field and laboratory investigations conducted during the investigation revealed one new soil unit featuring saline-sulfidic conditions in mid slope zones. Modifications and edits to soil

unit descriptions were made to the underlying soil map database using GIS tabular editing. Additional soil physicochemical, morphological, hydrological data and soil mapping (e.g. Fitzpatrick *et al.* 1996; Fritsch and Fitzpatrick 1994) and regolith mapping (e.g. Skwarnecki *et al.* 2002a) from the study area assisted in making the modifications to the original soil map.

Table 12.1 presents the spatial datasets that were used during the refinement of the original soil map, and the thematic support that each dataset provided in refining the map boundaries and soil unit descriptions.

Table 12.1. Georeferenced GIS themes, and their thematic mapping support, which were used to refine the Mount Lofty Ranges study area soil map at regional scale.

Theme	Derivative/sub-theme	Thematic mapping support
Detailed (3m) digital elevation model	Contours	Altitude; landform
	Slope	Landform; hillslope characteristics
	Hillshade	Landform
	TWI	Drainage patterns; water accumulation
	MrVBF	Hillslope process
Electromagnetic induction	EM38	Near-surface (< 1.5 m) processes; groundwater depth; soil type; salinity
	EM31	Deep profile processes (< 6 m); groundwater depth; salinity
Volume magnetic susceptibility		Mineralogy; mineralisation; hillslope process
Airborne gamma-radiometrics	K %	Weathering history
	Th (ppm)	Weathering history
Seasonal aerial photographs		Land cover; land use; seasonal patterns
Soil		Point data (field morphology and laboratory physicochemistry); soil units
Geology		Outcropping, landform and soil types

The final soil map of the MLR study area is presented in Figure 12.1, while revised soil descriptions that accompany the soil units are presented in Table 12.2.

With reference to Table 12.1, the DEM (and derivatives) and seasonal aerial photographs proved to be key spatial datasets used in the GIS during the refinements made to the original soil map. The landscape relief information, provided by the hillshade, assisted by offering a whole-of-hillslope perspective to the distribution of terrain patterns. For example, the hillshade backdrop assisted in differentiating between colluvial and alluvial systems, and the demarcation of drainage zones. TWI and MrVBF provided additional information relating to the definition of drainage zones, while MrVBF proved useful in refining the location and nature of the interfluvial zones. However, caution was required in the subdued relief zones in the lower, north facing hillslope when using MrVBF to discriminate between the interfluvial and drainage zones.

12.2 Regional prediction of soil salinity

The preceding Chapters have described how point scale, multi-temporal (Chapter 10) and multi-temporal, toposequence scale (Chapter 11) investigations have been linked to develop a more refined understanding of soil-landscape processes. The investigations lead to the development of soil-landscape models that characterise watertable processes, pedogenesis, and soil degradation –

particularly that of the salinisation of the MLR study area. Such data and models have been used to refine soil mapping at a scale of 1:5,000. This Section describes a coarse scale (*i+3*, Table 4.1) investigation to predict the distribution of shallow NAS, GAS, and intermediate NAS/GAS affected areas in the in the MLR study area and the surrounding regional area, using an upscaling methodology. A similar upscaling methodology was described in Chapter 8 to predict soil patterns in the Midnorth study area. The investigation comprised the key components that included selection of suitable environmental covariates (Chapter 3), and development of a GIS rules-based framework to apply in the upscaling methodology. Upscaling methodology was used to classify the regional study area according to the following classes:

- soils that are predominantly affected by shallow NAS (*shallow NAS* class), i.e. consistent with Model 1a (Chapter 10);
- soils that are predominantly affected by GAS (*GAS* class), i.e. consistent with Model 2b (Chapter 10);
- soils that are affected intermediately by shallow NAS and GAS (*intermediate shallow NAS/GAS* class), i.e. consistent with Model 1b (Chapter 10); and
- soils that are not affected by salinity in summit and crest areas (*summit and crests* class).

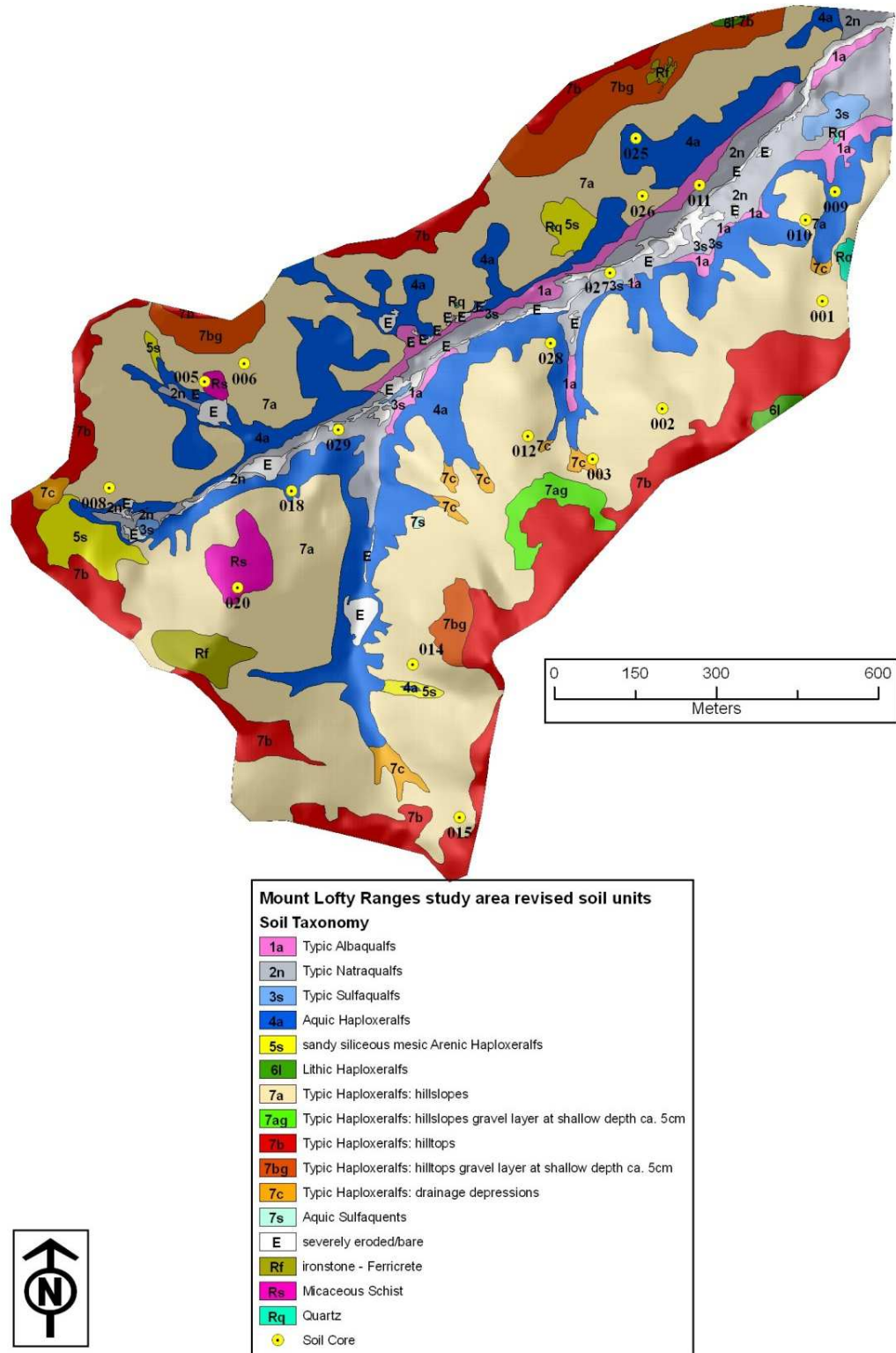


Figure 12.1. Mount Lofty Ranges study area revised soil units, showing soil core locations (Chapter 10) and a hillshade to accentuate local relief. Soil descriptions for each unit are presented in Table 12.2.

Table 12.2. Mount Lofty Ranges study area revised soil units, with accompanying descriptions of landform elements, soil descriptions, drainage and waterlogging class, acidity/alkalinity class, salinity ranges and depth to saline water, soil salinity type, and model types and associated profile IDs. Refer to Figure 12.1 for map soil units.

Soil Unit	Soil taxonomy (Soil Survey Staff 2006)	Landform Element	Soil Description	Drainage/Waterlogging	Acidity/Alkalinity (pHw)*	Salinity (ECse)/depth to saline water (m)	Soil salinity type	Model types/Profile ID**
1a	Typic Albaqualfs	Flat	Grey sandy loam surface layer over yellow-grey mottled clay	Poorly drained Strongly waterlogged	Moderately acidic (pH=<6.5) surface, neutral to alkaline at depth	Slightly saline 1 -4 dS/m; 1 - 1.5 m	GAS	Model 2b: 011
2n	Typic Natraqualfs	Flat	As for 1a, plus salt efflorescence (halite and gypsum) on surface with grey sandy loam surface over yellow-grey clay	Poorly drained Strongly waterlogged	Mostly alkaline throughout (pH >7.5)	Very saline >8 - 16 dS/m < 1 m	GAS	Model 2b: 027, 028
3s	Typic Sulfaqualfs	Flat/ Lower slope seepages	As for 2n, plus black sulfidic material overlying yellow-grey clay	Very poorly drained Strongly waterlogged	Mostly alkaline throughout (pH >7.5): sporadic occurrences of highly acidic (pH <5.5) near surface layers (<5cm), which develop due to oxidation of sulfidic materials	Extremely saline: >16 dS/m; < 1 m	GAS	
4a	Aquic Haploxerafs	Lower slope, open depression	Grey sandy loam surface layer over yellow-red-grey mottled clay	Poorly drained Periodic waterlogging	Neutral throughout (pH 6.5-7.5)	Slightly saline 1 -4 dS/m 1.5 - 3 m	GAS / NAS	Model 1a: 025 Model 1b: 009 Model 2b: 0018

Chapter 12 Mount Lofty Ranges regional and coarse scale investigation

Soil Unit	Soil taxonomy (Soil Survey Staff 2006)	Landform Element	Soil Description	Drainage/Waterlogging	Acidity/Alkalinity (pHw)*	Salinity (ECse)/depth to saline water (m)	Soil salinity type	Model types/Profile ID**
5s	sandy siliceous mesic Arenic Haploxeralfs	Lower slope, open depression	Deep grey sand over yellow-grey mottled clay	Poorly drained Periodic waterlogging	Acidic throughout (pH=<6.5) (low buffer capacity)	Non saline <1 dS/m; 1.5 - 3 m	NAS	
6l	Lithic Haploxeralfs	Summit	Shallow sandy loam over red uniform coloured clay over weathered rock	Freely drained Infrequently waterlogged	Very acidic throughout (pH <5.5)	Non saline <1 dS/m > 3 m	NAS	
7a	Typic Haploxeralfs: hillslopes	Mid slope	Brown loam over red and yellow uniform coloured clay. Deep.	Freely drained Infrequently waterlogged	Moderately acidic (pH <6.5) throughout	Non saline <1 dS/m > 3 m	NAS	Model 1a: 001, 002, 006, 008, 010, 012, 014, 015, 026, 028
7ag	Typic Haploxeralfs: hillslopes gravel layer at shallow depth ca. 5cm	Summit, upper-slope	Deep well drained red-yellow soils	Freely drained Infrequently waterlogged	Moderately acidic (pH <6.5) surface, neutral to alkaline at depth	Non saline <1 dS/m > 3 m	NAS	
7b	Typic Haploxeralfs: hilltops	Summit, upper-slope	Deep well drained red and yellow soils	Freely drained Infrequently waterlogged	Very acidic throughout (pH <5.5)	Non saline <1 dS/m > 3 m	NAS	
7bg	Typic Haploxeralfs: hilltops gravel layer at shallow depth ca. 5cm	Summit, upper-slope	Shallow well drained red and yellow soils	Freely drained Infrequently waterlogged	Moderately acidic (pH <6.5) throughout	Non saline <1 dS/m > 3 m	NAS	

Soil Unit	Soil taxonomy (Soil Survey Staff 2006)	Landform Element	Soil Description	Drainage/Waterlogging	Acidity/Alkalinity (pH _w)*	Salinity (EC _{se})/depth to saline water (m)	Soil salinity type	Model types/Profile ID**
7c	Typic Haploxeralfs: drainage depressions	Lower slope, open depression	Shallow well drained yellow soils	Moderately drained Infrequently waterlogged	Neutral throughout (pH 6.5-7.5)	Non saline <1 dS/m 1.5 – 3 m	NAS	Model 1b: 003
7s	Aquic Sulfaquents	Mid slope	Grey sandy loam surface layer over yellow-grey mottled clay	Poorly drained Strongly waterlogged	Neutral throughout (pH 6.5-7.5)	Extremely saline >16 dS/m < 1 m	GAS	
Rq	Quartz	Summit, upper-slope	Shallow well drained yellow and red soils with quartz fragments	Freely drained Infrequently waterlogged	Moderately acidic (pH <6.5) throughout	Non saline <1 dS/m > 3 m	NAS	
Rf	ironstone - Ferricrete	Summit, upper-slope	Shallow well drained yellow and red soils with ferricrete fragments	Freely drained Infrequently waterlogged	Very acidic throughout (pH <5.5)	Non saline <1 dS/m > 3 m	NAS	
Rs	Micaceous Schist	Mid slope	Shallow sandy loam over gravely sandy clay loam EB horizon on yellow-red-grey mottled clay with abundant micaceous rock fragments	Moderately drained Periodically waterlogged	Moderately acidic (pH <6.5) surface, neutral at depth, high buffer capacity	Saline 1 - 8 dS/m > 3 m	GAS / NAS	Model 1a: 005 Model 2a: 020

Chapter 12 Mount Lofty Ranges regional and coarse scale investigation

Soil Unit	Soil taxonomy (Soil Survey Staff 2006)	Landform Element	Soil Description	Drainage/Waterlogging	Acidity/Alkalinity (pHw)*	Salinity (ECse)/ depth to saline water (m)	Soil salinity type	Model types/ Profile ID**
E	severely eroded/bare	Severely eroded/bare	Gully, tunnel and rill erosion	Very poorly drained Strongly waterlogged	Mostly alkaline throughout (pH >7.5)	Extremely saline >16 dS/m; < 1 m	GAS	

* pHw measured in water

** described in Chapter 10

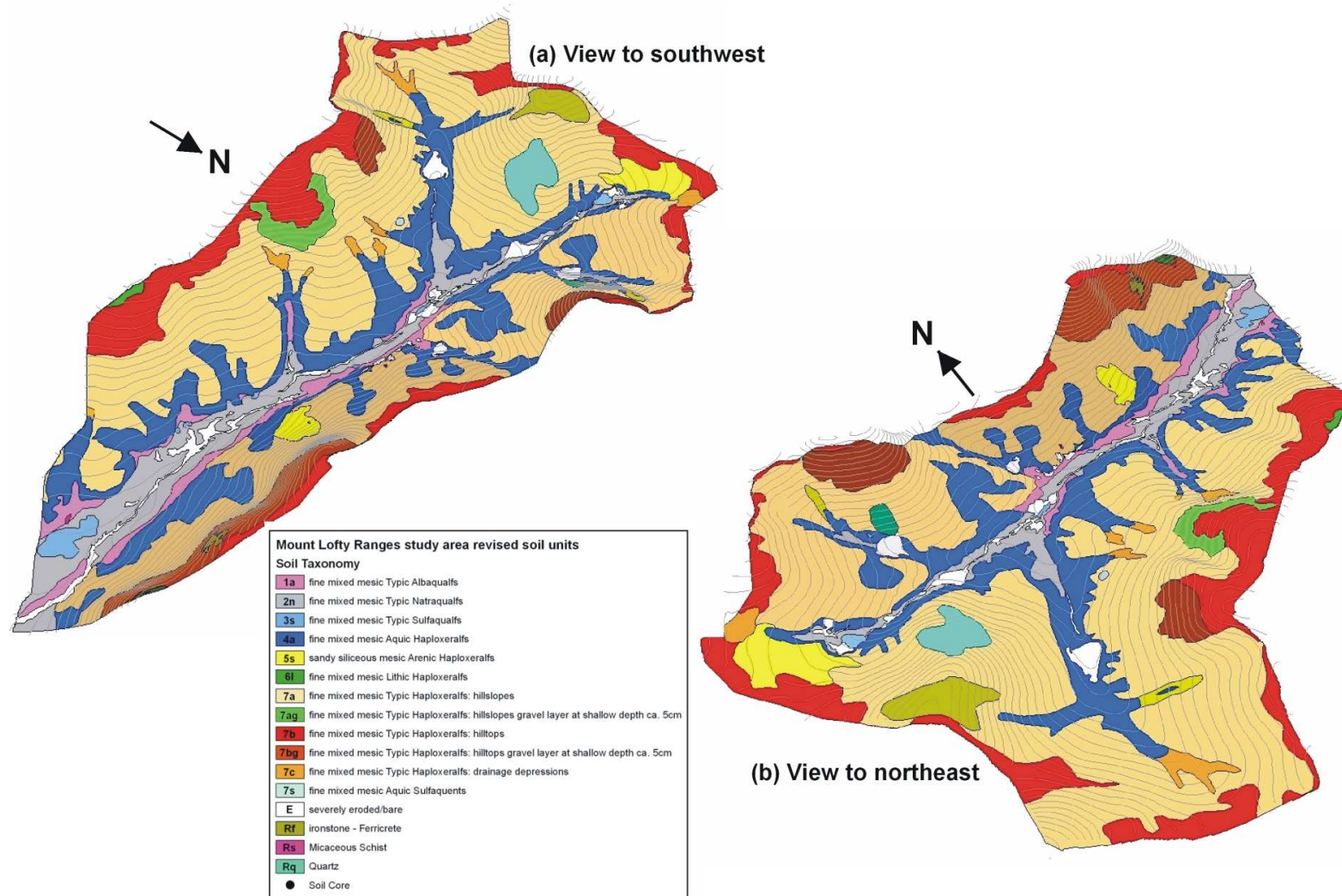


Figure 12.2. Mount Lofty Ranges study area refined soil mapping showing 3D oblique views (a) to the southwest, and (b) to the northeast. Two metre contours and hillshading are applied for terrain. Soil descriptions for each unit are presented in Table 12.2.

12.2.1 Environmental covariate selection

Co-registered GIS coverages, each with ground resolutions of three by three metres, were applied as environmental covariates in the upscaling methodology. These covariates included:

- MrVBF,
- TWI, and
- moderated terrain difference (MTD).

Each covariate was selected because of their strong visual correlation with the study area soil-landscape patterns (i.e. the distributions of shallow NAS and GAS soils, and landforms) identified during previous field and laboratory study area investigations.

The MTD is a computationally efficient terrain analysis method, developed during the current investigation, which is conceptually similar to the fuzzy landscape analysis (FLAG) (Roberts *et al.* 1997). MTD is used to identify topographic summit and depression areas in landscapes, and calculated using a DEM that has had sinks and other surface imperfections removed using GIS methods, thereby ensuring that the modified DEM has surface characteristics that are hydrologically correct. Using a GIS raster-based neighbourhood statistical function, a secondary DEM is generated by determining the mean value of a moving analysis “window” of predetermined raster cell dimensions from the primary DEM. During the current investigation, the primary DEM analysis window dimension was set to 30 by 30 cells, resulting in the cell at the centre of the analysis window returning the mean value of the 900 cell window. In this way, the secondary DEM, which has had the topographic troughs and peaks smoothed out, represents a topographically moderated version of the primary DEM. Using the GIS arithmetic function that is

conceptually illustrated in Figure 12.3, the primary DEM is subtracted from the secondary DEM, creating the MTD coverage. In the MTD coverage, positive DEM values denote topographic depressions (i.e. concave landforms), while negative values denote topographic summits (i.e. convex landforms). The MTD used in the current upscaling method was used to identify summit areas (i.e. negative MTD values), which coincide with areas of the region that are not strongly susceptible to soil salinisation.

As with the upscaling procedure described in Chapter 8, the numeric thresholds applied to the selected environmental covariates in the upscaling framework were determined via an interactive process using the “Knowledge Engineer” module of “ERDAS Imagine 8.4” software (ERDAS 2002). This procedure strongly benefited from the capability to semi-interactively use the software to apply a series of environmental covariate threshold permutations, review the results, and apply modifications for new predictions in a rapid manner.

The key method for reviewing predictions was to employ 3D draping, which has been used and described in previous Chapters. These predictions were reviewed as follows: (i) quantitatively (e.g. via field observations and accumulated landscape knowledge), and (ii) semi-qualitatively through co-registering predicted classes with various soil-landscape datasets (e.g. soil profile data, EMI survey (e.g. EM38 and EM31), and refined 1:5,000 scale soil mapping) using GIS 3D investigative methods.

The iterative upscaling procedure was terminated when it was deemed that the best possible predictive results had been achieved, using the coincidence with the mapped study area soil and salinity patterns from the previous

Section as verification. The final iterative result comprised combination of numeric thresholds of

environmental covariates that are presented in Table 12.3.

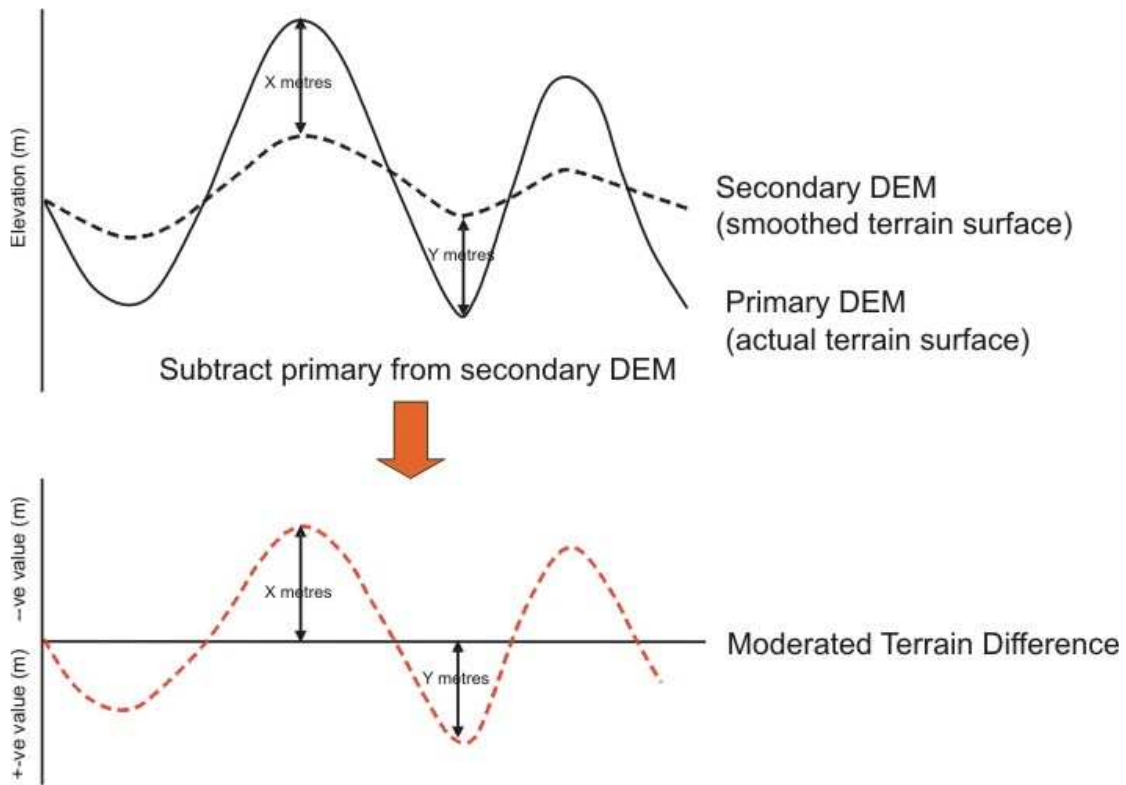


Figure 12.3. Diagram illustrating the principles behind the moderated terrain difference method.

Table 12.3. Environmental covariate thresholds applied in the GAS, intermediate shallow NAS/GAS soil, shallow NAS soil and soils not susceptible to salinity upscaling methodology used for the Mount Lofty Ranges study area and surrounding areas.

Class	Rules		
	MrVBF	TWI	MTD
GAS susceptible soil (Model 2b)	> 3.6		> -1.9
Intermediate shallow NAS/GAS susceptible soil (Model 1b)	< 3.6	> 7.6	> -1.9
Shallow NAS susceptible soil (Model 1a)	< 3.6	< 7.6	> -1.9
Not susceptible to salinity (summits and crests)			< -1/9

12.2.2 Predictive rule functions

Groundwater associated saline soils

Functionally, the predictive framework presented in Table 12.3 applies MrVBF to discriminate broad depressional areas associated with GAS-affected soils. These are areas that are generally low in the landscape (i.e. lower terraces and flats), and which intersect with (saline) groundwaters with a positive piezometric head (Model 2b). The use of “non-summit” MTD in the prediction of GAS soils ensures that no GAS areas are predicted convex (i.e. on local rises) landforms in the broad and flat areas in the lower landscape.

Intermediate shallow non-groundwater associated salinity /groundwater associated saline soils

MrVBF and TWI are combined to predict the intermediate shallow NAS/GAS soils. These soils occupy transitional landscape areas between (lower landscape) GAS and (mid slope) shallow NAS-affected areas (Model 1b). The threshold used for MrVBF ensures that predicted areas are outside the lower terraces and flats, while the TWI threshold ensures that the predicted areas receive moderated solum flushing, which are typically associated with lower landscape positions. The MTD threshold applied in the prediction ensures that convex landforms are not included in the prediction.

Shallow non-groundwater associated saline soils

The shallow NAS-affected soil areas (Model 1a) are predicted using MrVBF, again to locate landscape position outside lower terraces and flats, and the TWI threshold predicts areas of limited solum flushing, which feature soils in areas that receive an accumulation of salts in the solum. The MTD threshold as used ensures that

convex landforms are not included in the prediction.

Summits and crests

Finally, the MTD is used to identify summit areas and crests, which are often associated with deep, tertiary soils that are too elevated in the hillslope to be affected by saline groundwaters (GAS), nor are likely to contain appreciable concentrations of salts in the near-surface soils due to limited salt supplies.

12.2.3 Assessing prediction upscaling

No quantitative validation procedure of predicted results was made of the regional upscaling predictions. The qualitative assessment made was based on strong field knowledge of the soil-landscapes of the region (including the refined 1:5,000 scale soil mapping of the MLR study area, see Figure 12.4), and interpretations from various GIS datasets (e.g. terrain), regional landscape soil unit mapping (1:50,000 scale) (Maschmedt 2000; Soil and Land Information 2002), and remote sensing (e.g. satellite, airborne and aerial photographs).

A strong visual correlation between the refined soil mapping and soil salinity upscaling methodology is shown in Figure 12.4, indicating qualitative strength in the upscaling methodology. For example, GAS susceptible soils (Model 2b) are predicted in positions low in the regional landscape, i.e. in the lower terraces and flats. However, upscaling predictions of GAS susceptible soils have been made in elevated depressions higher in the landscape. Such landscape positions are associated with drainage zones. While these areas are likely to be waterlogged, as confirmed by field investigations and seasonal aerial photographs, their saline status is as not yet determined in the higher elevation zones. However, in the

refined soil mapping, these areas high in the landscape predicted as GAS are more commonly classified as

intermediate shallow NAS/GAS in the refined soil mapping.

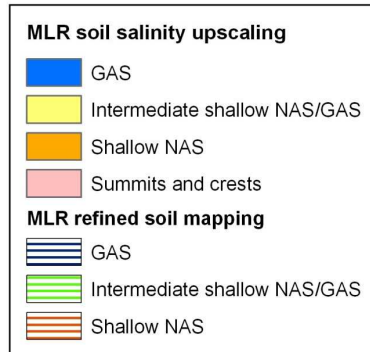
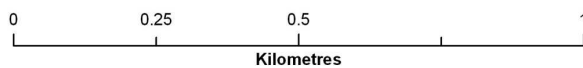
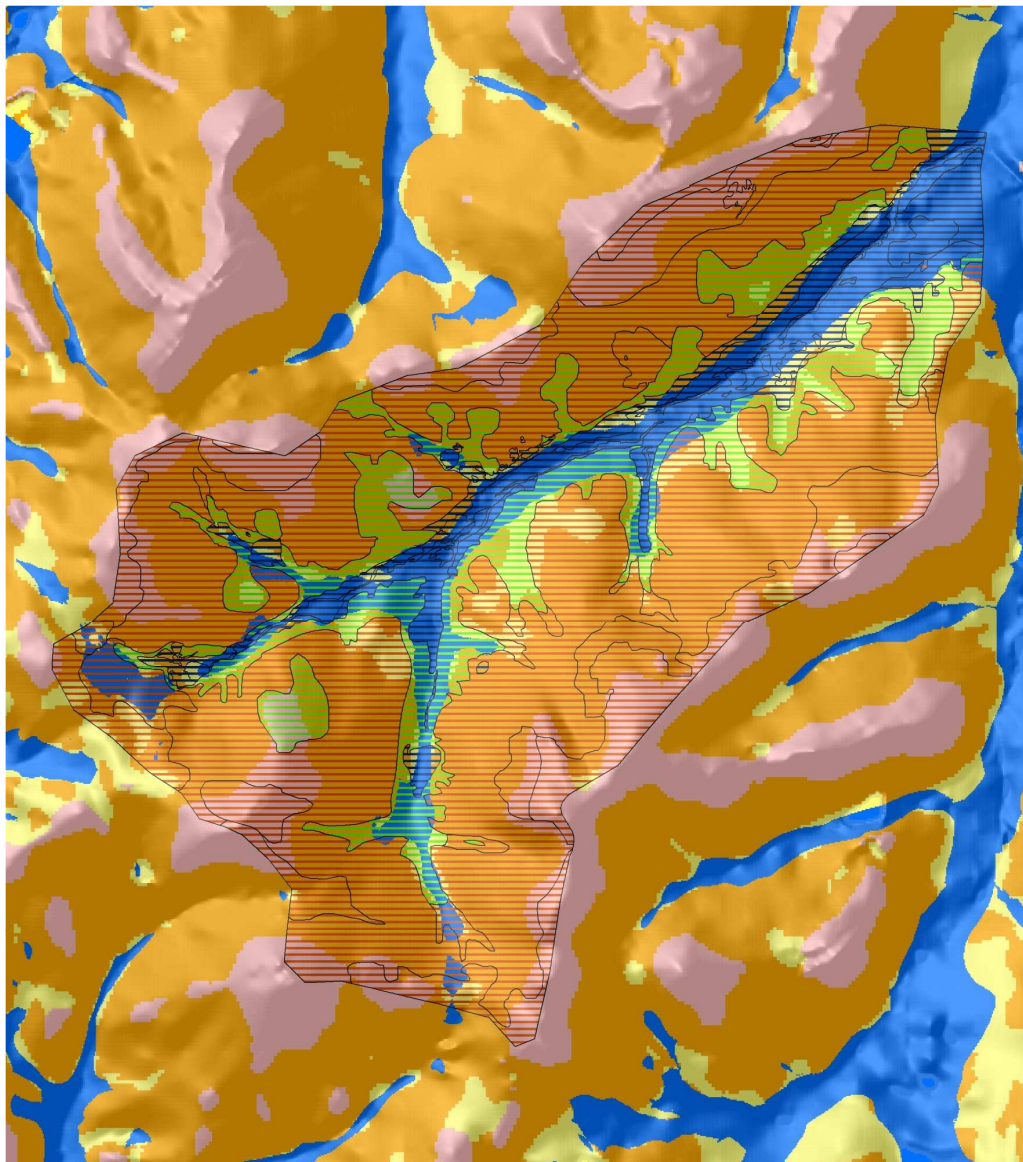


Figure 12.4. Spatial correspondence of: (i) upscaling-predicted soil salinity classes (solid fill) and (ii) soil salinity classes from the Mount Lofty Ranges refined soil mapping (hatched fill) at 1:5,000 scale. A hillshade has been applied to accentuate local relief

The soils predicted to be affected by intermediate shallow NAS/GAS (Model 1b) have generally been predicted in lower hillslope positions, above the valley flat areas. The areas predicted are located on low gradient hillslopes where saline watertables provide a seasonal influence on the near-surface soils. These soils are often where colluvial and alluvial processes co-dominate in the hillslope. However, Figure 12.4 illustrates that the upscaling predictions have been more successful in the lower gradient hillslope of the north facing slope than in the steeper gradient south-facing slope. In the south-facing slopes, the predictions have significantly underestimated the area of intermediate shallow NAS/GAS soils. Areas of limited aerial coverage predicted to be intermediate shallow NAS/GAS soils have also been predicted in upper hillslope positions, particularly on low gradient saddle landforms that are adjacent to summits and ridges. Saline groundwater systems in these upper hillslope position are too deep to influence these soils.

The predictive upscaling methodology has successfully identified mid and upper slope occurrences of soils featuring shallow NAS (Model 1a). The soils occupying these hillslope positions are generally texture-contrast soils, which ensures that salts accumulate in the upper B horizon of the profile, and in which most seasonal salinity changes occur in the overlying A horizon due to the watertable perching that seasonally occurs. As has been discussed, when verified against the refined soil mapping (Figure 12.4), the predictions for shallow NAS areas are underestimated in the north facing slope, whereas these are over-estimated in the south-facing slope.

The soils in summit and crest areas of the landscape are not significantly affected by salinity, and the upscaling methodology has successfully predicted these areas, regionally.

The upscaled prediction of the soil salinity classes for the region surrounding the study area is presented in Figure 12.5. Of the 1,560 ha surrounding the study area, the upscaling methodology classified 18 % of the total area (275 ha) to contain soils susceptible to GAS, 11 % (185 ha) to be susceptible to intermediate shallow NAS/GAS soil, while 54 % (839 ha) is predicted as susceptible to shallow NAS salinisation. Finally, the upscaling methodology predicts that 16 % of the region surrounding the MLR study area features crests and summits that are not affected to any significant degree by salinisation processes.

Given that the upscaling procedure was wholly based on terrain methods, saline soils that have no diagnostic topographic expression cannot be predicted (e.g. mineralised zones). Such soils are associated with saline seeps in upper hillslope positions, consistent with Model 2a salinity type (GAS, upper hillslopes). The other forms of salinity are terrain and rainfall-driven, the terrain-based methodology can be successfully applied to predict the salinity types in the neighbouring valley systems because the landform and climatic patterns are repeated. This is confirmed by reconnaissance work carried out in the neighbouring valleys within the predicted region. However, the upscaling “rules” will fail in areas of the MLR that differ significantly in geology/terrain, and where rainfall patterns are different (e.g. Wilford 2004c).

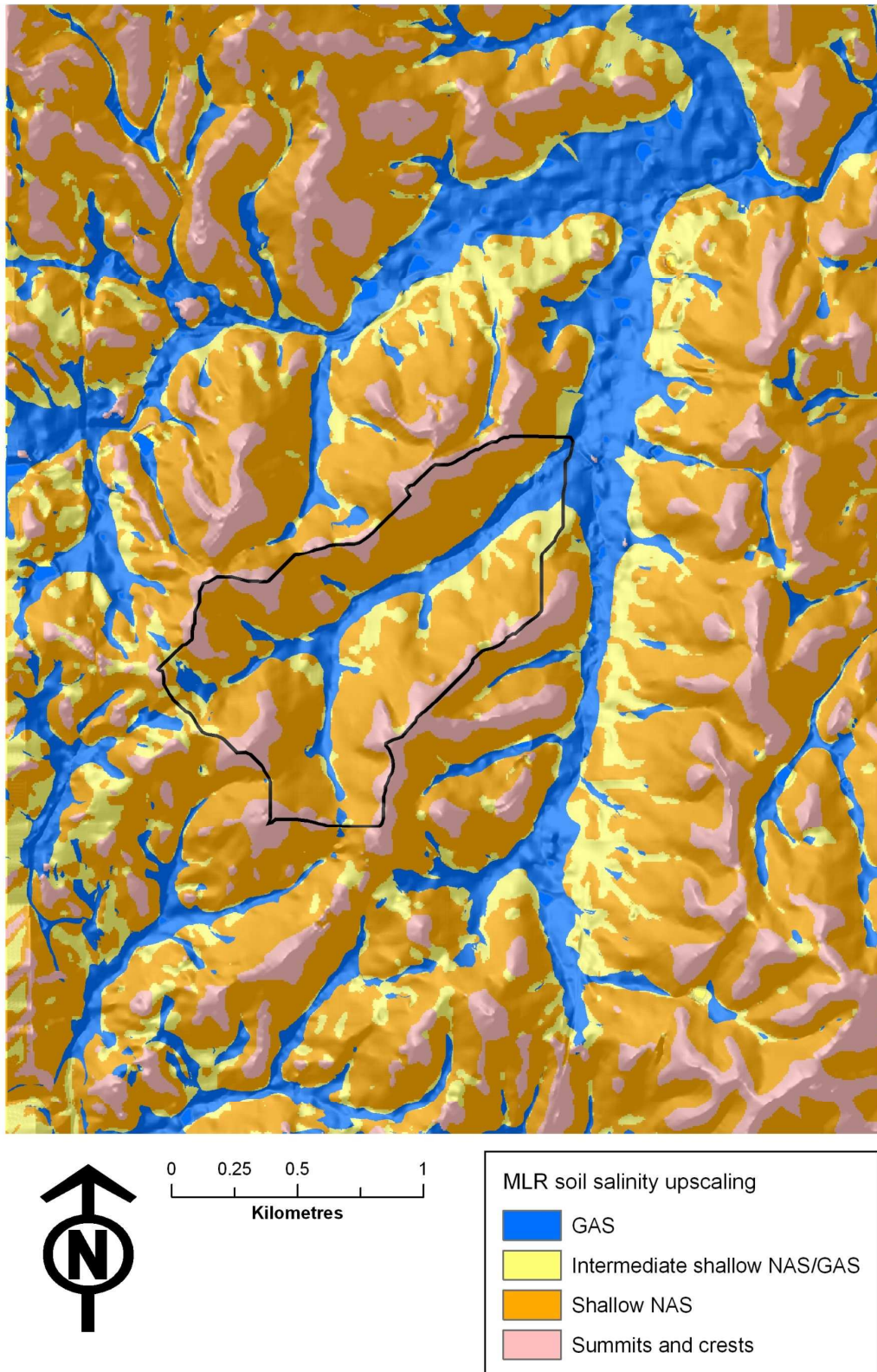


Figure 12.5. Mount Lofty Ranges study area and surrounding area (1,560 ha), featuring salinity process susceptibility classification and the boundary of the Mount Lofty Ranges study area. A hillshade has been applied to accentuate local relief.

Chapter 13. Overall conclusions and recommendations

This, the final Chapter, presents overall conclusions and recommendations that emanate from the research presented in the previous Chapters. This Chapter is divided into a Section of conclusions that address the objectives of the research outlined in Chapter 1. The Chapter ends with a final Section in which recommendations are presented concerning further work to be undertaken in response to the research findings made.

13.1 Overall conclusions

This research has satisfied the prime objective of the thesis to combine ESS and DSM to predict the spatial distribution of complex saline-sodic soil patterns at hillslope and regional scales in the Midnorth and the MLR of South Australia. As such, the objective addresses the scale deficiencies identified in the present South Australian soil mapping that makes it not suitable for precision conservation-type applications for tackling soil issues.

Saline-sodic soils (i.e. NAS soils) have been described in Chapter 2 in terms of their distribution, morphology, classification, and finally, their adverse affects on agricultural production. While the literature (e.g. Rengasamy 2002b) describes “transient salinity” (i.e. shallow NAS) is a dynamic landscape phenomenon featuring significant temporal and spatial variability of salt concentrations in the root zone, no research before now has identified these dynamics at scales ranging from farm to regions. The research has revealed that while the arrangement of soils is complex in the landscapes studied, the distribution of shallow NAS is systematic and predictable, and governed by a number of soil-landscape factors acting together. A generic model for shallow

NAS formation can be summarised involving to the following domains: (i) soil morphology (i.e. texture-contrast); (ii) terrain; and (iii) hillslope soil toposequence.

Morphologically, soils with contrasting textures (i.e. loamy A horizons over clay B horizons) contribute to the formation of shallow NAS. Locally, the sodic Btn horizons result in poor rates of vertical hydraulic conductivity that results in local groundwater perching in the A horizon where slope gradient is insufficient to promote down slope drainage. However, where sufficient slope gradient exists, the soil morphology promotes freshwater throughflow to be transmitted over the Btn horizon to down slope positions. Terrain (i.e. landform) dictates local hydropedological patterns; throughflow rates are high in locally low lying hillslope positions, promoting high throughflow flushing rates and salt being leached down slope. Conversely, throughflow rates are lower in locally elevated hillslope positions, or where down slope soil boundaries are encountered. Salt accumulates in landscapes where throughflow rates are low. Combined, terrain analysis (particularly TWI and MrVBF from DEMs), near-surface EMI (EM38) and volume magnetic susceptibility surveys have been used to successfully discriminate these

hydropedological patterns in the study areas. Terrain analysis correlated with landform and drainage, while the geophysical survey methods indicated certain pedogenic processes (e.g. salt accumulation using EM38 and maghemite persistence and redox conditions using magnetic susceptibility).

Toposequence characteristics are important in shallow NAS formation at the hillslope scale. Shallow NAS formation occurs at soil boundaries that feature a down slope gradation from coarse to heavier A horizon textures. Regionally, such textural boundaries form throttles to throughflow drainage in the A horizon. Under these conditions, waterlogging occurs during the winter, whereas during the summer, increased concentration of accumulated salts occurs as soil water evaporates or is transpired by crops. Such regional soil patterns were discriminated using terrain analysis (principally: slope, TWI, MrVBF), and in the Midnorth, gamma-radiometric K% to discriminate K-rich smectite of pedogenic and alluvial origin.

In this thesis, ESS approaches have been developed that reveal the intricate arrangement of landscape-wide pedogenic patterns. In terms of pedogenic process and history, the patterns can be defined according to whether they are either ancient or contemporary (Fritsch and Fitzpatrick 1994). Ancient patterns relate to soil forming conditions, and thus the properties of soils that are formed. In this research, these patterns were diagnosed best using a combination of terrain analysis and geophysical survey, including EMI (EM31 and EM38) and magnetic susceptibility. Additionally, gamma-radiometrics was found crucial in the Midnorth study area. Once diagnosed, the ancient patterns played a key role in refining soil mapping. Contemporary patterns act as an “over-print” of the ancient patterns, and used to diagnose soil

degradation (e.g. waterlogging, and shallow NAS and GAS formation). As such, the contemporary patterns are strongly related to hydropedological patterns.

While the generic model described above for shallow NAS formation holds in both the study areas, the finer scale and generally more complex pedogenesis of the MLR study area compared with the Midnorth study area has resulted in a more intricate arrangement of soils, soil processes, hydropedology, and saline soils, which are generally expressed at a finer scale. Furthermore, the proximity of the shallow watertable associated with GAS conditions in the MLR study area has resulted in transitional shallow NAS and GAS soil conditions. The transitional soil conditions occur in either locally low-lying upper hillslope locations, or upper slopes of lower terraces and drainage areas. By comparison, the more extensive and open landscape of the Midnorth study area means that for most of the landscape the saline groundwater systems remain deep and beyond the influence of shallow soils. In this landscape, GAS was found to be restricted in the deep (12 m) gully floor.

Multitemporal investigations were conducted in the MLR study area to determine the seasonal dynamics associated with near-surface saline systems. A series of investigations of salt concentration (EC_{se}) and species from shallow (< 1 m) soil cores repeated during the winter of 2004 and then the summer of 2005 revealed sometimes significant changes in salts content and species. These data were used to interpret hydropedological processes and models for soil salinity. Elevated sulfide concentrations in the GAS-affected profiles were found to be diagnostic of GAS conditions, reflecting the elevated sulfate content of groundwater in the study area caused by pyritic weathering. The influence of fertiliser application by

farmers on the soluble salt content in the profiles was also evident from the investigations, which required allowance in interpreting the trends, and developing the models. In summary, the combination of soil morphology, salt concentration and salt species revealed the presence of four models of saline soil formation: (i) two models account for the formation of shallow NAS under perched groundwater situations, (ii) one a model for GAS formation, and (iii) one a model for transitional shallow NAS/GAS systems.

EM38 surveys of apparent conductivity covering the whole study area conducted simultaneously with the detailed soil profile investigations (i.e. winter 2004, summer 2005) revealed the spatial distributions of the four types of salinity for which models were developed.

A key finding of the research was the power of combining multiple co-registered datasets in a 3D GIS (e.g. point soil survey, geophysical survey, terrain and aerial photographic backdrops) as an ESS approach for assisting the interrogation and interpretation of soil-landscape patterns. This approach played a key role in the interpretation of the ancient and contemporary soil-landscape patterns, and served as a strong aid in the construction of the conceptual toposequence models used as the precursor to the quantitative models used in upscaling.

Quantative models have been described in the thesis that were used in the GIS upscaling methodology to predict the regional distributions of soils and soil salinity surrounding the study areas. The accuracy of the predictions made for each study area region have been validated both qualitatively and qualitatively. The ground resolution of the environmental covariates used (i.e. DEMs and gamma-radiometrics) ensured that the resulting soil and

salinity predictions were at scales suitable for supporting targeted, on-ground saline land management typically involved in precision conservation.

The success in the regional upscaling provides the opportunity to address the current limitations of the South Australian soil mapping, which is not suitable for on-ground management decisions. As such, the upscaling methodology developed here is suitable for predicting soils and salinity types in areas of South Australia where: (i) suitable DEMs and gamma-radiometric coverages are available; and (ii) soil-landscape systems are similar to the Midnorth and MLR study areas (i.e. sharing upland, rain fed landscapes of similar terrain, geology and rainfall conditions). DEMs and gamma-radiometric datasets are available in many areas of upland South Australia – and for other regions of Australia. Thus, there is a strong prospect for many areas of South Australia (and nationally) for the capability to conducting cost-effective digital soil mapping soil properties that relate to, or are governed by, hydro-pedological patterns where present day mapping is incomplete or insufficient for effective farm and catchment management decisions to be made.

The research described in this thesis has demonstrated the successful combination of traditional soil survey methods (i.e. field observation, profile morphological descriptions, and laboratory physicochemical and mineralogical analyses) and advanced spatial methods in an ESS framework to analyse and map patterns in finer spatial detail than previously practical using traditional methods alone. These methods are summarised in Table 13.1, which includes the types of soil-landscape attributes that can be interpreted, and the most suitable scale of application in an ESS framework that these may be used in an analytical framework.

Finally, the capability to apply legacy soil data as part of the upscaling approaches described - much of which has remained unpublished - has considerably increased the scope of the research, while at the same time, ensuring more effective use of existing financial resources, which are typically stretched during the course of projects.

13.2 Recommendations

Based on the results from this thesis, the following further work are recommended:

The Midnorth 100 m² plot investigations revealed considerable variability in the depth to B horizon, which were speculated to have a role in shallow NAS formation. It is recommended that this work be conducted more extensively to characterise for larger areas patterns of B horizon depth, and determine the influence that these patterns have on throughflow drainage patterns, shallow NAS, and localised yield patterns. Trials using ground penetrating radar as a possible method to intensively map B horizon depth are recommended.

The research conducted has successfully demonstrated methods to investigate and characterise landscape-wide spatio-temporal hydrogeological patterns. Inland acid sulfate soils are developing as a growing issue in Australia, with implications for local and regional soil and water quality. The conversion of potential to actual acid sulfate conditions are governed by changing

redox conditions (Eh), which in turn are related to soil moisture conditions. It is recommended that based on the methods of this thesis similar hydrogeological survey approaches be applied to monitor and predict landscape-wide Eh conditions. Monitoring efforts could be supported by the installation and trialling arrays of redox probes in the landscape, which are networked wirelessly to GIS to provide regular spatial data of redox dynamics. Such spatio-temporal data will support refined model development, and will validate upscaling efforts.

Virtual reality (VR) technology (Grunwald 2006a; Grunwald and Barak 2001) is emerging as a spatially-based technology showing promise in natural resources management. VR features an advanced computing environment with the combined capabilities of: (i) quantitative environmental modelling (e.g. upscaling); (ii) on-the-fly user interactivity with the modelling; and (iii) superior true 3D visualisation of modelling renditions. Linking to the outcomes of the current thesis, it is recommended that VR be investigated as a method to: (i) refine interrogation and interpretation of soil-landscape patterns from co-registered datasets for the development of refined, 3D conceptual toposequence models; (ii) develop true 3D quantitative modelling for soil-landscape processes; and (iii) use the advanced 3D visualisation capability to communicate complex soil-landscape processes with research peers, land managers and policy-makers.

Table 13.1. Summary of spatial methods used in an enhanced soil survey (ESS) framework, their scale and mode of application, used in advanced soil survey.

Method	Instrument / technique	Application	Potential soil-landscape attributes derived	Units / type	Application scale			
					Point (profile)	Plot (100 m ²)	Hillslope	Regional
Electromagnetic induction (EMI)	EM38	Electromagnetic induction of soil-regolith profile; on foot, field-based	Combined soil profile salinity, texture and moisture; <1.5 m	Apparent EC (EC _a ; dS/m)		•	•	
	EM31		As above, plus including regolith and bedrock >6m				•	
Magnetic susceptibility	Bartington ME2B, dual frequency sensor	Mass magnetic susceptibility of soil layers; laboratory-based	Magnetic iron oxides [magnetite (α - Fe ₂ O ₃) and pedogenic maghemite (γ - Fe ₂ O ₃)]; soil-landscape/pedogenic processes, especially local wetting/drying conditions, leaching, burning	χ		•		
	Bartington ME2E, loop sensor	“Bulked” surface volume magnetic susceptibility (< few cm’s); on foot		κ		•	•	
	Bartington ME2F, probe sensor	High spatial resolution surface volume magnetic susceptibility (< few cm’s); on foot				•		
Gamma radiometrics	Regional airborne survey	Regional geochemical image of topsoil (K, Th, U, total count); GIS	Regional/toposequence soil-landscape process; mineral weathering; mineralogy; soil types	% (K), ppm (Th, U and total count)			•	•

Method	Instrument / technique	Application	Potential soil-landscape attributes derived	Units / type	Application scale			
					Point (profile)	Plot (100 m ²)	Hillslope	Regional
	GR-320 spectral radiometer	High spatial resolution geochemical survey of topsoil (K, Th, U, total count); on foot	Soil-landscape processes; geochemical weathering history; local geochemical patterns				•	
Physico-chemical analysis	Extractive / digestive physico-chemical analysis	Multiple (>30) analyses; accurate	Soil chemistry, soil physical measurements; multiple other attributes	Various	•	•	•	•
	Mid Infrared (MIR) analysis	Multiple (>30) analyses; predictive, low cost, rapid				•		
	X-ray diffraction (XRD)	X-ray diffraction; accurate fine texturing	Clay mineralogy		•		•	
Digital terrain analysis	Aerial photographs; digital elevation models (DEMs)	Terrain attributes; soil-landscape methodology; 3D GIS overlays	Slope; curvature; terrain wetness index (TWI); terrain based 3D renderings	GIS raster	•		•	•
Soil-landscape survey	Yield map	Yield	Soil-landscape processes; farm planning	GIS vector		•	•	
	Soil survey method	Soil classification; soil-landscape methodology; soil mapping	Pedogenic processes; soil hydrology; land capability; soil mapping; multiple soil-landscape properties, field texture, etc...	Models; GIS raster	•	•	•	•

References

Acworth RI (1999) Investigation of dryland salinity using the electrical image method. *Australian Journal of Soil Research* **37**, 623-636.

Addiscott TM (1998) Modelling concepts and their relation to the scale of the problem. *Nutrient Cycling and Agroecosystems* **50**, 239-245.

Baker AKM and Fitzpatrick RW (2003) Lead isotopes for constructing geochemical dispersion models in sulfidic wetlands. In 'Advances in Regolith'. Adelaide. (Ed. Roach I. C.) pp. 2-7. (CRC-LEME).

Bedard-Haughn AK and Pennock DJ (2002) Terrain controls on depressional soil distribution in a hummocky morainal landscape. *Geoderma* **110**, 169-190.

Bekunda M (2006) Managing Africa's agricultural soils: the future of soil science. In 'The Future of Soil Science'. (Ed. AE Hartemink) pp. 13-15. (International Union of Soil Science: Den Haag).

Bennett DL, George RJ and Whitfield B (2000) The use of ground EM systems to accurately assess salt store and help define land management options for salinity management. *Exploration Geophysics* **31**, 249-254.

Berry JA, Delgado JA, Pierce FJ and Kholsa R (2005) Applying spatial analysis for precision conservation across the landscape. *Journal of Soil and Water Conservation* **60**, 363-370.

Bierwirth PN (1996) Investigation of airborne gamma-ray images as a rapid mapping tool for soil and land degradation - Wagga Wagga, NSW. Australian Geological Survey Organisation, Record No. 1996/22, Canberra.

Bierwirth PN and Walsh WD (2000) Delineation of recharge beds in the Great Artesian Basin using airborne gamma-radiometrics and satellite remote sensing. Bureau of Rural Sciences, Canberra.

Bingham JM and Ciolkosz EJ (Eds) (1993) 'Soil Color.' (Soil Science Society of America Inc.: Madison, USA).

Bockheim JG, Gennadiyev AN, Hammer RD and Tandarich JP (2005) Historical development of key concepts in pedology. *Geoderma* **124**, 23-36.

Booth CA, Fullen MA, Smith JP, Hallett MD, Walden J, Harris J and Holland K (2002) Preliminary characterisation of agricultural soil of the Isle of Man by mineral magnetic measurements. In '17th World Congress of Soil Science'. Bangkok, Thailand.

Bouma J (1989) Using soil survey data for quantitative land evaluation. In 'Advances in Soil Science'. (Ed. BA Stewart) pp. 177 - 213. (Springer-Verlag: New York).

Brady NC and Weil RR (1999) 'The nature and properties of soils.' (Prentice-Hall Inc.: Upper Saddle River, New Jersey).

Bramley RGV and Hamilton RP (2004) Understanding variability in winegrape production systems: 1. Within vineyard variation in yield over several vintages. *Australian Journal of Grape and Wine Research* **10**, 32-45.

Bresler E, McNeal BL and Carter DL (1982) 'Saline and sodic soils: principles - dynamics - modelling.' (Springer-Verlag: New York).

Broadfoot K, Morris M, Stevens D and Heuperman A (2002) The role of EM38 in land and water management planning on the Tragowel Plains in Northern Victoria. *Exploration Geophysics* **33**, 90-94.

Brooker PI (1991) 'A Geostatistical Primer.' (World Scientific Publishing Co. Pte. Ltd.: Singapore).

Brouwer J and Fitzpatrick RW (2000) Characterisation of nine soils down a salt-affected toposequence near Gatum on the Dundas Tablelands in south-west Victoria: application of the structural approach for constructing soil-water-landscape models. CSIRO Land and Water, Technical Report No. Technical Report 21/00, Glen Osmond, South Australia.

Brouwer J and Fitzpatrick RW (2002a) Interpretation of morphological features in a salt-affected duplex soil toposequence with an altered soil water regime in western Victoria. *Australian Journal of Soil Research* **40**, 903-926.

Brouwer J and Fitzpatrick RW (2002b) Restricting layers, flow paths, and correlation between duration of soil saturation and soil morphological features along a hillslope with an altered soil water regime in western Victoria. *Australian Journal of Soil Research* **40**, 927-946.

Bui EN, Krogh L, Lavado RS, Nachtergaele FO, Toth T and Fitzpatrick RW (1998) The distribution of sodic soils: the world scene. In 'Sodic soils: distribution, properties, management and environmental consequences'. (Eds ME Sumner and R Naidu) pp. 19 - 33. (Oxford University Press Inc.: New York).

Bui EN, Longhead A and Corner RJ (1999) Extracting soil-landscape rules from previous soil surveys. *Journal of Soil Research* **37**, 495-508.

Bui EN and Moran CJ (2001) Disaggregation of polygons of surficial geology and soil maps using spatial modelling and legacy data. *Geoderma* **103**, 79-94.

Buol SW, Hole FD and McCracken RJ (1973) 'Soil Genesis and Classification.' (The Iowa State University Press: Ames, Iowa).

Burrough PA and McDonnell RA (2000) 'Principles of Geographical Information Systems.' (Oxford University Press Inc.: New York, USA).

Cass A (1999) Interpretation of some soil physical indicators for assessing soil physical fertility. In 'Soil analysis: an interpretation manual'. (Eds KI Peverill, LA Sparrow and DJ Reuter) pp. 95 - 102. (CSIRO Publishing: Collingwood, Victoria).

Cass A, Walker RR and Fitzpatrick RW (1996) Vineyard soil degradation by salt accumulation and the effect on the performance of the vine. In 'Ninth Australian Wine Industry Technical Conference'. Adelaide, South Australia. (Eds CS Stockley, RS Johnstone and TH Lee) pp. 153 - 160.

Chadwick OA and Graham RC (2000) Pedogenic Processes. In 'Handbook of Soil Science'. (Ed. ME Sumner) pp. E41-E75. (CRC Press: Boca Raton, Florida).

Chaplot V, Walter C and Curmi P (2000a) Improving soil hydromorphology prediction according to DEM resolution and available pedological data. *Geoderma* **97**, 405-422.

Chaplot V, Walter C and Curmi P (2000b) Improving soil hydromorphy prediction according to DEM resolution and available pedological data. *Geoderma* **97**, 405-422.

Chapman GA and Atkinson G (2000) Soil survey and mapping. In 'Soils: their properties and management.' (Eds PEV Charman and B Murphy) pp. 106 - 132. (Oxford University Press: Melbourne).

Charman PEV and Wooldridge AC (2000) Soil salinisation. In 'Soils: their properties and management.' (Eds PEV Charman and B Murphy) pp. 237-245. (Oxford University Press: Melbourne).

Chartres CJ (1995) Sodic soils: an introduction to their formation and distribution in Australia. In 'Australian sodic soils: distribution, properties and management'. (Eds R Naidu, ME Sumner and P Rengasamy) pp. 35 - 40. (CSIRO Publications: Melbourne).

Chaudhari SK and Batta RK (2003) Predicting unsaturated hydraulic conductivity functions of three Indian soils from particle size distribution data. *Australian Journal of Soil Research* **41**, 1457-1466.

Chhabra R (2005) Classification of salt-affected soils. *Arid Land Research and Management* **19**, 61-79.

Chittleborough DJ (1981) Genesis. In 'Red-brown Earths of Australia'. (Eds JM Oades, DG Lewis and K Norrish) pp. 29-46. (Waite Agricultural Research Institute, University of Adelaide and CSIRO Division of soils: Adelaide).

Conacher A (2002) A Role for Geomorphology in Integrated Catchment Management. *Australian Geographical Studies* **40**, 179-195.

Conacher AJ and Dalrymple JB (1977) The nine unit landsurface model: an approach to pedogenic research. *Geoderma* **18**, 1-154.

Cook SE, Corner RJ, Groves PR and Grealish GJ (1996) Use of airborne gamma radiometric data for soil mapping. *Australian Journal of Soil Research* **34**, 183 - 194.

Cornelis WM, Ronsyn J, Van Meirvenne M and Hartmann R (2001) Evaluation of Pedotransfer Functions for Predicting the Soil Moisture Retention Curve. *Soil Sci Soc Am J* **65**, 638-648.

Corwin DL, Kaffka SR, Hopmans JW, Mori Y, van Groenigen JW, van Kessel C, Lesch SM and Oster JD (2003) Assessment and field-scale mapping of soil quality properties of a saline-sodic soil. *Geoderma* **114**, 231-259.

Cox JW, Chittleborough DJ, Brown HJ, Pitman A and Varcoe JCR (2002) Seasonal changes in hydrochemistry along a toposequence of texture-contrast soils. *Australian Journal of Soil Research* **40**, 581-605.

Creemeens DL, Brown RB and Huddleston JH (Eds) (1994) 'Whole Regolith Pedology.' (Soil Science Society of America: Madison, WI, USA).

Cresswell R and Liddicoat C (2004) Application of Airborne Geophysical Techniques to Salinity Issues Around Jamestown, South Australia. Department of Water, Land and Biodiversity Conservation, SA-SMMSP Site Summary Report No. Report, DWLBC 2004/37, Adelaide.

Cresswell RG and Herczeg AL (2004) Groundwater Flow Systems and Salinity in the Valleys around Jamestown, South Australia: Geochemical and Isotopic Constraints. CSIRO Land and Water / Bureau of Resource Sciences, SA-SMMSP Jamestown Hydrogeochemistry Report No. CSIRO L&W Report 30/04 / BRS Technical Report, Canberra.

Crockford RH and Richardson DP (2004) The mineral magnetic properties of a multi-layerd soil in the Australian Capital Territory, Australia. CSIRO Technical Report No. 7/04, Canberra.

Crockford RH and Willett IR (2001) Application of mineral magnetism to describe profile development of toposequences of a sedimentary soil in south-eastern Australia. *Australian Journal of Soil Research* **39**, 927-949.

Dahlhaus PG, Nathan EL and Morand VJ (2000) Salinity on the southeastern Dundas Tableland, Victoria. *Australian Journal of Earth Sciences* **47**, 3-11.

Daily B and Milnes AR (1971) Stratigraphic notes on lower Cambrian fossiliferous metasediments between Campbell Creek and Tunkalilla Beach in the type section of the Kanmantoo Group, Fleurieu Peninsula, South Australia. *Transactions of the Royal Society of South Australia* **95**, 199-212.

Daily B and Milnes AR (1973) Stratigraphy, structure and metamorphism of the Kanmantoo Group (Cambrian) in its type section east of Tunkalilla Beach, South Australia. *Transactions of the Royal Society of South Australia* **97**, 213-251.

Dalal-Clayton B and Dent DL (2001) 'Knowledge of the land: land resources information and its use in rural development.' (Oxford University Press: Oxford, UK).

Daniels RB and Hammer RD (1992) 'Soil Geomorphology.' (John Wiley & Sons, Inc.: New York, NY, USA).

Davies PJ, Fitzpatrick RW, Bruce DA, Spouncer LR and Merry RH (2002) Land degradation assessment in the Mount Lofty Ranges: upscaling from points to regions via a toposequence. In 'Regional water and soil assessment for managing sustainable agriculture in China and Australia.' (Eds TR McVicar, L Rui, RW Fitzpatrick and L Changming) pp. 291 - 303. (Australian Centre for International Agricultural Research: Canberra).

de Bruin S, Wielemaker WG and Molenaar M (1999) Formalisation of soil-landscape knowledge through interactive hierarchical disaggregation. *Geoderma* **91**, 151-172.

de Jong E, Nestor PA and Pennock DJ (1998) The use of magnetic susceptibility to measure long-term soil redistribution. *Catena* **32**, 23 - 35.

de Jong E, Pennock DJ and Nestor PA (2000) Magnetic susceptibility in different slope positions in Saskatchewan, Canada. *Catena* **40**, 291 - 305.

de Vries W, Kros J, van der Salm C, Groenenberg JE and Reinds GJ (1998) The use of upscaling procedures in the application of soil acidification models at different spatial scales. *Nutrient Cycling and Agroecosystems* **50**, 223-236.

Dearing JA (1999a) 'Environmental magnetic susceptibility: using the Bartington MS2 system.' (Chi Publishing: Kenilworth, England).

Dearing JA (1999b) Magnetic Susceptibility. In 'Environmental Magnetism; a practical guide'. (Eds J Walden, F Oldfield and J Smith) pp. 35-62. (Quaternary Research Association: London).

Dickson BL and Scott KM (1997) Interpretation of aerial gamma-ray surveys - adding the geochemical factors. *AGSO Journal of Australian Geology & Geophysics* **17**, 187 - 200.

Doran JW (2002) Soil health and global sustainability: translating science into practice. *Agriculture, Ecosystems and Environment* **88**, 119-127.

Earl R, Taylor JC, Wood GA, Bradley I, James IT, Waine T, Welsh JP, Godwin RJ and Knight SM (2003) Soil Factors and their Influence on Within-field Crop Variability, Part I: Field Observation of Soil Variation. *Biosystems Engineering* **84**, 425-440.

Eastham J, Gregory PJ and Williamson DR (2000) A spatial analysis of lateral and vertical fluxes of water associated with a perched watertable in a duplex soil. *Australian Journal of Soil Research* **38**, 879-890.

Emerson WW (2002) Emerson dispersion test. In 'Soil Physical Measurement and Interpretation for Land Evaluation'. (Eds NJ McKenzie, KJ Coughlan and HP Cresswell) pp. 190-199. (CSIRO Publishing: Collingwood, Victoria).

ERDAS (2002) 'ERDAS Field Guide.' (ERDAS LLC: Atlanta, GA, USA).

Evans ME and Heller F (2003) 'Environmental Magnetism: Principles and Applications of Enviromagnetics.' (Academic Press: Burlington, Massachusetts).

Fanning DS and Fanning MCB (1989) 'Soil: morphology, genesis and classification.' (John Wiley & Sons Inc.: New York, NY, USA).

FAO (2006) World reference base for soil resources. FAO, Rome, Italy.

Fine P, Singer MJ, La Ven R, Verosub K and Southland RJ (1989) Role of pedogenesis in distribution of magnetic susceptibility in two California chronosequences. *Geoderma* **44**, 287 - 306.

Fitzpatrick RW (2002) Land degradation processes. In 'Regional water and soil assessment for managing sustainable agriculture in China and Australia.' (Eds TR McVicar, L Rui, RW Fitzpatrick and L Changming) pp. 130 - 138. (Australian Centre for International Agricultural Research: Canberra).

Fitzpatrick RW (2005) Hydro-pedologically based toposequence models as a powerful tool for managing salt-affected landscapes: case studies from geochemically variable saline environments. In 'Extended abstracts for oral presentations, International Salinity Forum. Managing Saline Soils and Water: Science, Technology and Social Issues'. Riverside Convention Center, California, USA pp. 181-184.

Fitzpatrick RW, Boucher SC, Naidu R and Fritsch E (1995) Environmental consequences of soil sodicity. In 'Australian sodic soils: distribution, properties and management'. (Eds R Naidu, ME Sumner and P Rengasamy) pp. 163 - 176. (CSIRO Publications: Melbourne).

Fitzpatrick RW, Bruce DA, Davies PJ, Spouncer LR, Merry RH, Fritsch E and Maschmedt D (1999) Mount Lofty Ranges Pilot Project: Soil Landscape Quality Assessment at Catchment and Regional Scale. CSIRO Land and Water Technical Report 28/99, Technical Report 28/99 No., Adelaide.

Fitzpatrick RW, Cox J and Bourne J (1997) 'Managing waterlogged and saline catchments in the Mt. Lofty Ranges, South Australia.' (CRC for Soil and Land Management / CSIRO: Melbourne).

Fitzpatrick RW, Cox JW, Fritsch E and Hollingsworth ID (1994) A soil-diagnostic key to manage saline and waterlogged catchments in the Mt Lofty Ranges, South Australia. *Soil Use and Management* **10**, 145 - 152.

Fitzpatrick RW, Cox JW, Munday B and Bourne JF (2003a) Development of soil-landscape and vegetation indicators for managing waterlogged and saline catchments. *Australian Journal of Experimental Agriculture* **43**, 245-252.

Fitzpatrick RW, Fritsch E and Self PG (1996) Interpretation of soil features produced by ancient and modern processes in degraded landscapes: V. Development of saline sulfidic features in non-tidal seepage areas. *Geoderma* **69**, 1-29.

Fitzpatrick RW, Fritsch E, Self PG and Cox J (1993) Soil Landscapes in an Adelaide Hills Sub-catchment Undergoing Degradation. In 'Tenth International Clay Conference'. Adelaide. (Eds RW Fitzpatrick, E Fritsch, ID Hollingsworth and J Cox) pp. 3-22.

Fitzpatrick RW and Merry RH (2002) Soil-regolith models of soil-water landscape degradation: development and application. In 'Regional water and soil assessment for managing sustainable agriculture in China and Australia.' (Eds TR McVicar, L Rui, RW Fitzpatrick and L Changming) pp. 130 - 138. (Australian Centre for International Agricultural Research: Canberra).

Fitzpatrick RW, Merry RH, Cox J, Rengasamy P and Davies PJ (2003b) Assessment of physico-chemical changes in dryland saline soils when drained or disturbed for developing management options. CSIRO Land and Water Technical Report 02/03, Technical report 02/03 No. Technical report 02/03, Adelaide.

Fitzpatrick RW, Rengasamy P, Merry RH and Cox J (2001) Is dryland soil salinisation reversible? National Dryland Salinity Program.

Fitzpatrick RW and Skwarnecki MS (Eds) (2003) 'Mount Torrens, eastern Mount Lofty Ranges, South Australia: Regolith Models of Soil-Water Landscape Degradation.' (Cooperative Research Centre for Landscape Environments and Mineral Exploration (CRC LEME) Monograph).

Fitzpatrick RW, Thomas M, Cannon MG and McThompson J (in prep.) Soils and land use of a sub-catchment of Freshwater Creek near Spalding, South Australia. (CSIRO: Adelaide).

Fitzpatrick RW, Thomas M, Davies PJ and Williams BG (2003c) Dry saline land: an investigation using ground-based geophysics, soil survey and spatial methods near Jamestown, South Australia. CSIRO Land and Water, Technical Report No. Technical Report 55/03, Adelaide, South Australia.

Fontes MPF, de Oliveira TS, da Costa LM and Campos AAG (2000) Magnetic separation and evaluation of magnetization of Brazilian soils from different parent materials. *Geoderma* **96**, 81-99.

Forrester S, Janik LJ, Beech A and McLaughlin M (2003) Recent developments in routine soil analyses by mid-infrared: rapid and cost-effective laboratory analysis. In 'Tools for nutrient and pollutant management: Applications to agriculture and environmental quality'. Massey University, New Zealand. (Eds LD Currie and JA Hanly). (Fertilizer and Lime Research Centre, Massey University, New Zealand).

French RJ (1981) Management under low rainfall. In 'Red-brown Earths of Australia'. (Eds JM Oades, DG Lewis and K Norrish) pp. 97-115. (Waite Agricultural Research Institute, University of Adelaide and CSIRO Division of soils: Adelaide).

Fritsch E and Fitzpatrick RW (1994) Interpretation of soil features produced by ancient and modern processes in degraded landscapes. I. A new method for constructing conceptual soil-water-landscape models. *Australian Journal of Soil Research* **32**, 889 - 907.

Gallant JC and Dowling TI (2003) A multiresolution index of valley bottom flatness for mapping depositional areas. *Water Resources Research* **39**, 1347.

Geological Survey of South Australia (1964a) Adelaide Sheet: S.A. Geological Atlas Series Sheet SI 54-9 Zones 5 & 6. (Department of Mines: Adelaide).

Geological Survey of South Australia (1964b) Burra Sheet: S.A. Geological Atlas Series Sheet 1 54-5 Zones 5 & 6. (Department of Mines: Adelaide).

Geonics Ltd (2003) Geonics EM38 ground conductivity meter operating manual. Geonics Limited, Technical Note No., Mississauga, Ontario.

Gerrard AJ (1981) 'Soils and Landform: An Integration of Geomorphology and Pedology.' (George Allen and Unwin: London).

Gerrard J (1992) 'Soil Geomorphology: An Integration of pedology and geomorphology.' (Chapman and Hall: London).

Gessler PE, Chadwick OA, Chamran F, Althouse L and Holmes K (2000) Modelling soil-landscape and ecosystem properties using terrain attributes. *Soil Sci Soc Am J* **64**, 2046-2056.

Ghassemi F, Jakeman AJ and Nix HA (1995) 'Salinisation of Land and Water Resources: Human Causes, Extent, Management and Case Studies.' (University of New South Wales Press Ltd.: Sydney).

Goldberg S and Suarez DL (2000a) Soil Colloidal Behaviour. In 'Handbook of Soil Science'. (Ed. ME Sumner) pp. B195 - B240. (CRC Press: Boca Raton, Florida).

Goldberg S and Suarez DL (2000b) Soil colloidal behaviour. In 'Handbook of Soil Science'. (Ed. ME Sumner) pp. B-195 - B-240. (CRC Press: Boca Raton, Florida).

Graham RC, Tice KR and Guertal WR (1994) The Pedologic Nature of Weathered Rock. In 'Whole Regolith Pedology'. (Eds DL Cremeens, RB Brown and JH Huddleston) pp. 21-40. (Soil Science Society of America: Madison, Wisconsin).

Gray JM and Murphy B (1999) Parent material and soils: A guide to the influence of parent material on soil distribution in Eastern Australia. NSW Department of Land and Water Conservation, Technical Report No. Technical Report No. 45, Sydney.

Greacen EL and Williams J (1983) Physical Properties and Water Relations. In 'Soils: an Australian viewpoint'. (Ed. Division of Soils CSIRO) pp. 499-548. (CSIRO: Melbourne /Academic Press Inc.: London).

Greve MH and Greve MB (2004) Determining and representing width of soil boundaries using electrical conductivity and MultiGrid. *Computers and Geosciences* **30**, 569-578.

Grimley DA and Vepraskas MJ (2000) Magnetic susceptibility for use in delineating Hydric soils. *Soil Science Society of America Journal* **64**, 2174-2180.

Grunwald S (Ed.) (2006a) 'Environmental soil-landscape modeling: geographic information technologies and pedometrics.' (Taylor & Francis Group: Boca Raton, USA).

Grunwald S (2006b) Future of soil science. In 'The Future of Soil Science'. (Ed. AE Hartemink) pp. 51-53. (International Union of Soil Science: Den Haag).

Grunwald S and Barak P (2001) The use of VRML for virtual soil landscape modeling. *Systems Analysis Modelling Simulation* **40**, 755-776.

Gunn RH, Beattie JA, Reid RE and van de Graff RHM (1988) 'Australian Soil and Land Survey Handbook: Guidelines for Conducting Surveys.' (Inkata Press: Melbourne and Sydney).

Gunn RH and Richardson DP (1979) The nature and possible origins of soluble salts in deeply weathered landscapes of eastern Australia. *Australian Journal of Soil Research* **17**, 197 - 215.

Hall GF and Olson CC (1991) Predicting Variability of Soils from Landscape Models. In 'Spatial Variabilities of Soils and Landforms'. (Eds MJ Mausbach and LP Wilding) pp. 9-24. (Soil Science Society of America Inc.: Madison, Wisconsin).

Hallmark CT and Franzmeier DP (2000) Alfisols. In 'Handbook of Soil Science'. (Ed. ME Sumner) pp. E388-E358. (CRC Press: Boca Raton, Florida).

Hedley CB, Yule IJ, Eastwood CR, Sheperd TG and Arnold G (2004) Rapid identification of soil textural and management zones using electromagnetic induction sensing of soils. *Australian Journal of Soil Research* **42**, 389-400.

Henschke CJ, McCarthy DG, Richardson SB and Evans TD (1994) Investigation and management of dryland salinity in a catchment at Jamestown in the Midnorth of South Australia. Primary Industries Primary Industries Technical Paper Number 35.

- Herrero J, Ba AA and Aragüés R (2003) Soil salinity and its distribution determined by soil sampling and electromagnetic techniques. *Soil Use and Management* **19**, 119-126.
- Hingston FJ and Gailitis V (1976) The geographic variation of salt precipitation over Western Australia. *Australian Journal of Soil Research* **14**, 319 - 335.
- Hoosbeek MR, Amundson RG and Bryant RB (2000) Pedological modeling. In 'Handbook of Soil Science'. (Ed. ME Sumner) pp. E77-E116. (CRC Press: Boca Raton, Florida).
- Hoosbeek MR and Bryant RB (1992) Towards the quantitative modeling of pedogenesis: a review. *Geoderma* **55**, 183-210.
- Hopkins DG and Richardson JL (1999) Detecting a salinity plume in an unconfined sandy aquifer and assessing secondary soil salinization using electromagnetic induction techniques, North Dakota, USA. *Hydrogeology Journal* **7**, 380-392.
- Horsfall KR (1997) Airborne magnetic and gamma-ray data acquisition. *AGSO Journal of Australian Geology & Geophysics* **17**, 23 - 30.
- Hubble GD, Isbell RF and Northcote KH (1983) Features of Australian soils. In 'Soils: an Australian viewpoint'. (Ed. Division of Soils CSIRO) pp. 17-47. (CSIRO: Melbourne / Academic Press Inc.: London).
- Hudson BD (1992) The soil survey as a paradigm-based science. *Soil Science Society of America* **56**, 836-841.
- Hummel JW, Gaultney LD and Sudduth KA (1996) Soil property sensing for site-specific crop management. *Computers and Electronics in Agriculture* **14**, 121-136.
- Isbell RF (1998) 'The Australian Soil Classification.' (CSIRO Publishing: Melbourne).
- Isbell RF, Reeve R and Hutton JT (1983) Salt and sodicity. In 'Soils: an Australian viewpoint'. (Ed. C Division of Soils) pp. 107 - 117. (CSIRO: Melbourne / Academic Press: London: Melbourne).

James IT, Waine TW, Bradley RI, Taylor JC and Godwin RJ (2003) Determination of Soil Type Boundaries using Electromagnetic Induction Scanning Techniques. *Biosystems Engineering* **86**, 421-430.

Janik LJ, Merry RH and Skjemstad JO (1998) Can mid infrared diffuse reflectance analysis replace soil extractions? *Australian Journal of Experimental Agriculture* **38**, 681-696.

Jenny H (1941) 'Factors of soil formation, a system of quantitative pedology.' (McGraw-Hill: New York).

Jenny H (1980) 'The soil resource: origin and behaviour.' (Springer-Verlag: New York, NY, USA).

Kaur R, Kumar S and Gurung HP (2002) A pedo-transfer function (PTF) for estimating soil bulk density from basic soil data and its comparison with existing PTFs. *Australian Journal of Soil Research* **40**, 847-857.

Keller GV and Frischknecht FC (1966) 'Electrical Methods in Geophysical Prospecting.' (Pergamon Press: Oxford).

Kennewell BM (1999) Investigations into the management of dry saline land. Primary Industries and Resources South Australia, Technical Report Number 272 No. Report Number 272, Adelaide.

Keren R (2000) Salinity. In 'Handbook of Soil Science'. (Ed. ME Sumner) pp. G3-25. (CRC Press: Boca Raton, Florida).

Knotters M, Brus DJ and Voshaar JHO (1996) A comparison of kriging, co-kriging and kriging combined with regression for spatial interpolation of horizon depth with censored observations. *International Journal of Rock Mechanics and Mining Sciences & Geomechanics Abstracts* **33**, 266A-266A.

Lagacherie P and Voltz M (2000) Predicting soil properties over a region using sample information from a mapped reference area and digital elevation data: a conditional probability approach. *Geoderma* **97**, 187-208.

Lecoanet H, Lévêque F and Segura S (1999) Magnetic susceptibility in environmental applications: comparison of field probes. *Physics of the Earth and Planetary Interiors* **115**, 191-204.

Levy GJ (2000) Sodicity. In 'Handbook of Soil Science'. (Ed. ME Sumner) pp. G27-63. (CRC Press: Boca Raton, Florida).

Lin H (2003) Hydropedology: Bridging Disciplines, Scales, and Data. *Vadose Zone J* **2**, 1-11.

Lin HS, McInnes KJ, Wilding LP and Hallmark CT (1999) Effects of Soil Morphology on Hydraulic Properties: II. Hydraulic Pedotransfer Functions. *Soil Sci Soc Am J* **63**, 955-961.

Maschmedt D (2000) Assessing agricultural land: agricultural land classification standards used in South Australia's land resource mapping program. Primary Industries and Resources South Australia, Adelaide, Australia.

Mathé V and Lévêque F (2003) High resolution magnetic survey for soil monitoring: detection of drainage and soil tillage effects. *Earth and Planetary Science Letters* **212**, 241-251.

McBratney AB (1998) Some considerations on methods for spatially aggregating and disaggregating soil information. *Nutrient Cycling and Agroecosystems* **50**, 51-62.

McBratney AB, Mendonca ML and Minasny B (2003) On digital soil mapping. *Geoderma* **117**, 3-52.

McBratney AB, Odeh IOA, Bishop TFA, Dunbar MS and Shatar TM (2000) An overview of pedometric techniques for use in soil survey. *Geoderma* **97**, 293 - 327.

McDonald RC, Isbell RF, Speight JG, Walker J and Hopkins MS (1998) 'Australian soil and survey handbook.' (Australian Collaborative Land Evaluation Program: Canberra, Australia).

McKenzie N and Austin MP (1993) A quantitative Australian approach to medium and small scale surveys based on soil stratigraphy and environmental correlation. *Geoderma* **57**, 329-355.

McKenzie N and Cresswell H (2002) Estimating soil physical properties using more readily available data. In 'Soil Physical Measurement And Interpretation For Land Evaluation'. (Eds N McKenzie, K Coughlan and H Cresswell). (CSIRO Publishing: Melbourne, Australia).

McKenzie N, Gallant JC and Gregory L (2003) Estimating Water Storage Capacities in Soil at Catchment Scales. Cooperative Research Centre for Catchment Hydrology Technical Report 03/3.

McKenzie NJ, Coughlan K and Cresswell H (2002) 'Soil physical measurement and interpretation for land evaluation.' (CSIRO Publishing: Collingwood, Australia).

McKenzie NJ, Gessler PE, Ryan PJ and O'Connell DA (2000) The role of terrain analysis in soil mapping. In 'Terrain analysis: principles and applications'. (Ed. 2000) pp. 245-265. (John Wiley & Sons: New York).

McKenzie NJ and Ryan PJ (1999) Spatial prediction of soil properties using environmental correlation. *Geoderma* **89**, 67-94.

McKenzie RC, George RJ, Woods SA, Cannon ME and Bennett DL (1997) Use of electromagnetic-induction meter (EM38) as a tool for managing salinisation. *Hydrogeology Journal* **5**, 37-50.

McNeill JD (1980a) Electrical conductivity of soils and rocks. Geonics Ltd. Technical Note TN-5, Ontario, Canada.

McNeill JD (1980b) Electromagnetic terrain conductivity measurement at low induction numbers. Geonics Ltd. Technical Note TN-6, Ontario, Canada.

McNeill JD (1990) Geonics EM38 ground conductivity meter operating instructions and survey interpretation techniques. Geonics Ltd. Technical Note TN-21, Ontario, Canada.

Merry RH, Spouncer LR, Fitzpatrick RW, Davies PJ and Bruce DA (2002) Regional prediction of soil profile acidity and alkalinity. In 'Regional water and soil assessment for managing sustainable agriculture in China and Australia.' (Eds TR McVicar, L Rui, RW Fitzpatrick and L Changming) pp. 155-164. (Australian Centre for International Agricultural Research: Canberra, Australia).

Miller DA, Petersen GW, Kolb PJ and Voortman JJ (2002) The Soil Survey Report: New Forms for the 21st Century. *Journal of Soil and Water Conservation* **57**, 121A-127A.

Milligan PR and Gunn PJ (1997) Enhancement and presentation of airborne geophysical data. *AGSO Journal of Australian Geology & Geophysics* **17**, 63 - 75.

Milne G (1936a) Normal erosion as a factor in soil profile development. *Nature* **138**, 548 - 549.

Milne G (1936b) A provisional soil map of East Africa. East African Research Station Amani Memoirs No. 28, Tanganyika Territory.

Minty BRS (1997) Fundamentals of airborne gamma-ray spectrometry. *AGSO Journal of Australian Geology & Geophysics* **17**, 39 - 50.

Minty BRS, Luyendyk APJ and Brodie RC (1997) Calibration and data processing for airborne gamma-ray spectrometry. *AGSO Journal of Australian Geology & Geophysics* **17**, 51 - 62.

Moore ID, Gessler PE, Nielsen GA and Peterson GA (1993) Soil attribute prediction using terrain analysis. *Soil Science Society of America* **57**, 443-452.

Mullins CE (1977) Magnetic susceptibility of the soil and its significance in soil science. *Journal of Soil Science* **28**, 223 - 246.

Munday T, Walker G, Cresswell R, Wilford JR, Barnett S and Cook P (2003) South Australian Salt Mapping and Management Support Project - An example of the considered application of airborne geophysics in natural resource management. In 'ASEG 16th Geophysical Conference and Exhibition'. Adelaide.

Murphy B (1995) The relationship between the Emerson Aggregate Test and exchangeable sodium percent in some subsoils from Central New South Wales. In 'Australian sodic soils: distribution, properties and management'. (Eds R Naidu, ME Sumner and P Rengasamy) pp. 101-106. (CSIRO Publications: Melbourne).

Murphy BW, Eldridge DJ, Chapman GA and McKane DJ (2000) Soils of New South Wales. In 'Soils: their properties and management'. (Eds PEV Charman and BW Murphy) pp. 133 - 165. (Oxford University Press: Melbourne).

Naidu R and Rengasamy P (1995) Ion interactions and constraints to plant nutrition in Australian sodic soils. In 'Australian sodic soils: distribution, properties and management'. (Eds R Naidu, ME Sumner and P Rengasamy) pp. 127 - 137. (CSIRO Publications: Melbourne).

Nelson PN and Ham GJ (2000) Exploring the response of sugar cane to sodic and saline conditions through natural variation in the field. *Field Crops Research* **66**, 245-255.

Northcote KH (1992) 'A factual key for the recognition of Australian soils.' (Rellim Technical Publications Pty. Ltd.: Coffs Harbour, NSW).

Northcote KH and Skene JKM (1972) Australian soils with saline and sodic properties. CSIRO, Soil Publ. No. 27 No., Melbourne, Victoria.

Oldfield F (1991) Environmental magnetism - a personal perspective. *Quaternary Science Reviews* **10**, 73 - 85.

Ollier C and Pain C (1996) 'Regolith, Soils and Landforms.' (John Wiley & Sons: Chichester).

Olson CG, Thompson ML and Wilson MA (2000) Phyllosilicates. In 'Handbook of Soil Science'. (Ed. ME Sumner) pp. F77-F123. (CRC Press: Boca Raton, Florida).

Park SJ, McSweeney K and Lowery B (2001) Identification of the spatial distribution of soils using a process-based terrain characterization. *Geoderma* **103**, 249-272.

Peng W, Wheeler DB, Bell JC and Krusemark MG (2003) Delineating patterns of soil drainage class on bare soils using remote sensing analyses. *Geoderma* **115**, 26-279.

Petersen GW (2006) Soil science: multiple scales and multiple opportunities. In 'The Future of Soil Science'. (Ed. AE Hartemink) pp. 108-109. (International Union of Soil Science: Den Haag).

Peeverill KI, Sparrow LA and Reuter DJ (Eds) (1999) 'Soil analysis: an interpretation manual.' (CSIRO Publishing: Collingwood, Victoria).

Phillips JD, Gares PA and Slattery MC (1999) Agricultural soil redistribution and landscape complexity. *Landscape Ecology* **14**, 197-211.

Pozdnyakov A and Pozdnyakova L (2002) Electrical fields and soil properties. In '17th World Congress of Soil Science'. Bangkok, Thailand pp. 1558-1551 - 1558-1511.

Rayment GE and Higginson FR (1992) 'Australian laboratory handbook of soil and water chemical methods.' (Inkata Press: Melbourne).

Rengasamy P (2002a) Clay dispersion. In 'Soil Physical Measurement and Interpretation for Land Evaluation'. (Eds NJ McKenzie, KJ Coughlan and HP Cresswell) pp. 200-210. (CSIRO Publishing: Collingwood, Victoria).

Rengasamy P (2002b) Transient salinity and subsoil constraints to dryland farming in Australian sodic soils: an overview. *Australian Journal of Experimental Agriculture* **42**, 351 - 361.

Rengasamy P and Churchman GJ (1999) Cation exchange capacity, exchange cations and sodicity. In 'Soil analysis: an interpretation manual'. (Eds KI Peeverill, LA Sparrow and DJ Reuter) pp. 147 - 157. (CSIRO Publishing: Collingwood, Victoria).

Rengasamy P and Olsson KA (1991) Sodicity and soil structure. *Australian Journal of Soil Research* **29**, 935 - 952.

Rengasamy P and Sumner ME (1998) Processes involved in sodic behaviour. In 'Sodic soils: distribution, properties, management and environmental consequences'. (Eds ME Sumner and R Naidu) pp. 35 - 50. (Oxford University Press Inc.: New York).

Reynolds JM (2000) 'An introduction to applied environmental geophysics.' (John Wiley & Sons Ltd.: London).

Rhoades JD, Chanduvi F and Lesch S (1999) Soil salinity assessment: methods and interpretation of electrical conductivity measurements. FAOPaper 57, Rome.

Rhoades JD and Corwin DL (1981) Determining Soil Electrical Conductivity-Depth Relations Using an Inductive Electromagnetic Soil Conductivity Meter. *Soil Science Society of America Journal* **45**, 255 - 260.

Richards KS, Arnett RR and Ellis S (1985) Introduction. In 'Geomorphology and soils'. (Eds KS Richards, RR Arnett and S Ellis). (George Allen & Unwin Ltd.: London).

Richardson JL and Daniels RB (1993) Stratigraphic and hydraulic influences on soil color development. In 'Soil Color'. (Eds JM Bingham and EJ Ciolkosz) pp. 109-125. (Soil Science Society Inc.: Madison, Wisconsin).

Richter DD and Markewitz D (2001) 'Understanding soil change: soil sustainability over millennia, centuries, and decades.' (Cambridge University Press: Cambridge, UK).

Roberts DW, Dowling TI and Walker J (1997) FLAG: A Fuzzy Landscape Analysis GIS Method for Dryland Salinity Assessment. CSIRO Land and Water Technical Report No. 8/97, Canberra.

Royall D (2001) Use of mineral magnetic measurements to investigate soil erosion and sediment delivery in a small agricultural catchment in limestone terrain. *Catena* **46**, 15-34.

Schoeneberger PJ, Wysocki DA, Benham EC and Broderson WD (2002) 'Fieldbook for describing and sampling soils.' (Natural Resources Conservation Service, National Soil Survey Center: Lincoln, NE., USA).

Schwenke GD, Reuter DJ, Fitzpatrick RW, Walker J and O'Callaghan PO (2003) Soil and catchment health indicators of sustainability: case studies from southern

Australia and possibilities for the northern grains region of Australia. *Australian Journal of Experimental Agriculture* **43**, 205-222.

Schwertmann U (1993) Relationships between iron oxides, soil color, and soil formation. In 'Soil Color'. (Eds JM Bingham and EJ Ciolkosz) pp. 51-70. (Soil Science Society Inc.: Madison, Wisconsin).

Schwertmann U and Fitzpatrick RW (1992) Iron Minerals in Surface Environments. In 'Biomineralization Processes of Iron and Manganese: Modern and Ancient Environments'. (Eds HCW Skinner and RW Fitzpatrick) pp. 7-30. (Catena: Cremlingen).

Seelig BD and Richardson JL (1994) Sodic soil toposequence related to focused water flow. *Soil Science Society of America Journal* **58**, 156-163.

Shaw RJ (1988) Soil salinity and sodicity. In 'Understanding soils and soil data: invited lectures for refresher training course in soil science'. Brisbane. (Ed. IF Fergus) pp. 109-134. (Brisbane Australian Society of Soil Science (Queensland Branch)).

Shaw RJ (1999) Soil salinity - electrical conductivity and chloride. In 'Soil analysis: an interpretation manual'. (Eds KI Peverill, LA Sparrow and DJ Reuter) pp. 129-145. (CSIRO Publishing: Collingwood, Victoria).

Skwarnecki M, Fitzpatrick RW and Davies PJ (2002a) Geochemical dispersion at the Mount Torrens lead-zinc prospect, South Australia, with particular emphasis on acid sulfate soils. CRC-LEMECRC LEME Report 174, Perth.

Skwarnecki M, Fitzpatrick RW and Davies PJ (2002b) Geochemical dispersion at the Mount Torrens lead-zinc prospect, South Australia, with particular emphasis on acid sulfate soils: Volume 1. CRC-LEMERestricted Report 174, Adelaide.

Slavich PG and Petterson GH (1990) Quantifying water movement processes - strategic sampling from EM-38 surveys. In 'Soils and their land use in the 1990s'. Bendigo, Australia pp. 20-26. (Australian Society of Soil Science Inc., Victorian Branch).

So HB and Aylmore LAG (1995) The effects of sodicity on soil behaviour. In 'Australian sodic soils: distribution, properties and management'. (Eds R Naidu, ME Sumner and P Rengasamy) pp. 71 - 87. (CSIRO Publications: Melbourne, Australia).

Soil and Land Information (2002) Atlas of key soil and landscape attributes of the Agricultural Districts of South Australia. (SaLI Group, The Department of Water, Land and Biodiversity Conservation, Adelaide, South Australia: Adelaide, Australia).

Soil Survey Division Staff (1993) 'Soil survey manual.' (U.S. Government Printing Office: Washington).

Soil Survey Staff (1993) 'Soil Survey Manual.' (U.S. Government Printing Office: Washington, USA).

Soil Survey Staff (1999) 'Soil Taxonomy: A Basic System of Soil Classification for Making and Interpreting Soil Surveys.' (U.S. Government Printing Office: Washington).

Soil Survey Staff (2003) 'Keys to Soil Taxonomy.' (United States Department of Agriculture / Natural Resources Conservation Service: Washington, USA).

Soil Survey Staff (2006) 'Keys to Soil Taxonomy.' (U.S. Government Printing Office: Washington, USA).

Sommer M, Wehrhan M, Zipprich M, Weller U, zu Castell W, Ehrich S, Tandler B and Selige T (2003) Hierarchical data fusion for mapping soil units at field scale. *Geoderma* **112**, 179-196.

South Australian Geological Survey (1995) 'The geology of South Australia. Vol. 2, The phanerozoic.' (Adelaide, Australia).

Spies BR and Woodgate P (2005) 'Salinity mapping methods in the Australian context.' (Commonwealth of Australia: Canberra, Australia).

Stace HCT, Hubble GD, Brewer R, Northcote KH, Sleeman JR, Mulchay MJ and Hallsworth EG (1968) 'A Handbook of Australian Soils.' (Rellim: Adelaide).

Stephens CG, Herriot RI, Downes RG, Langford-Smith T and Adcock AM (1945) A Soil, Land-use, and Erosion Survey of Part of County Victoria, South Australia. Council for Scientific and Industrial Research Bulletin No. 188, Melbourne.

Steppuhn H, van Genuchten MTR and Grieve MC (2003) An index for the tolerance of agricultural crops in root-zone salinity. In 'CSAE/SCGR Meeting'. Montreal.

Stolt MH and Baker JC (1994) Strategies for Studying Saprolite and Saprolite Genesis. In 'Whole Regolith Pedology'. (Eds DL Cremeens, RB Brown and JH Huddleston) pp. 1-19. (Soil Science Society of America: Madison, Wisconsin).

Strahler AN (1975) 'Physical geography.' (John Wiley & Sons Inc.: New York).

Sudduth KA, Drummond ST and Kitchen NR (2001) Accuracy issues in electromagnetic induction sensing of soil electrical conductivity for precision agriculture. *Computers and Electronics in Agriculture* **31**, 239-264.

Sudduth KA, Kitchen NR and Drummond ST (1999) Soil conductivity sensing on clay pans: comparison of electromagnetic induction to direct methods. In '4th International Conference on Precision Agriculture'. St. Paul, MN. (Eds PC Robert, RH Rust and WE Larson) pp. 979-990. (ASA-CSSA-SSSA).

Summerell GK, Dowling TI, Richardson DP, Walker J and Lees B (2000) Modelling current parna distribution in a local area. *Australian Journal of Soil Research* **38**, 867-878.

Summerell GK, Dowling TI, Wild JA and Beale G (2004) FLAG UPNESS and its application for mapping seasonally wet to waterlogged soils. *Australian Journal of Soil Research* **42**, 155-162.

Sumner ME (1993) Sodic soils: new perspectives. *Australian Journal of Soil Research* **31**, 683-750.

Sumner ME (1995a) Sodic soils: new perspectives. In 'Australian sodic soils: distribution, properties and management'. (Eds R Naidu, ME Sumner and P Rengasamy) pp. 1 - 34. (CSIRO Publications: Melbourne).

Sumner ME (1995b) Sodic soils: new perspectives. In 'Australian sodic soils: distribution, properties and management'. (Eds R Naidu, ME Sumner and P Rengasamy) pp. 1 - 34. (CSIRO Publications: Melbourne).

Sumner ME, Rengasamy P and Naidu R (1998) Sodic soils: a reappraisal. In 'Sodic soils: distribution, properties, management and environmental consequences'. (Eds ME Sumner and R Naidu) pp. 3 - 17. (Oxford University Press Inc.: New York).

Szabolcs I (1979) 'Review of research on salt-affected soils.' (UNESCO: Paris).

Szabolcs I (1989) 'Salt-affected soils.' (CRC Press Inc.: Boca Raton, Florida).

Tabbagh A, Dabas M, Hesse A and Panissod C (1997) Soil resistivity: a non-invasive tool to map soil structure horizonation. *Geoderma* **97**, 393-404.

Tandarich JP, Darmody RG, Follmer LR and Johnson DL (2002) Historical Development of Soil and Weathering Profile Concepts from Europe to the United States of America. *Soil Sci Soc Am J* **66**, 335-346.

Taylor G and Eggleton RA (2001) 'Regolith geology and geomorphology.' (John Wiley and Sons, Ltd.: Chichester, UK).

Taylor JC, Wood GA, Earl R and Godwin RJ (2003) Soil Factors and their Influence on Within-field Crop Variability, Part II: Spatial Analysis and Determination of Management Zones. *Biosystems Engineering* **84**, 441-453.

Taylor MJ, Smettem K, G. P and Verboom W (2002) Relationships between soil properties and high resolution radiometrics, central Wheatbelt, Western Australia. *Exploration Geophysics* **33**, 95 - 102.

Taylor RM and Schwertmann U (1974) Maghemite in soils and its origin. I. Properties and observations on soil maghemites. *Clay Minerals* **10**, 289-298.

Thomas M, Fitzpatrick RW and Heinson GS (2004) Regional prediction of salt-affected soils in an area of complex soil patterns in South Australia. In 'Regolith 2004'. Canberra. (Ed. Roach I. C.) pp. 355-361. (CRC-LEME).

Thomas M, Fitzpatrick RW and Heinson GS (2005) Intricate salt-affected soil patterns identified and conceptually modelled using soil survey, geophysics and terrain analysis. In 'Extended abstracts for oral presentations, International Salinity Forum. Managing Saline Soils and Water: Science, Technology and Social Issues'. Riverside Convention Center, California, USA pp. 445-448.

Thompson R and Oldfield F (1986) 'Environmental magnetism.' (Allen & Unwin: London).

Velde B (1992) 'Introduction to clay minerals.' (Chapman and Hall: London).

Ventura SJ and Irvine BJ (2000) Automated landform classification methods for soil-landscape studies. In 'Terrain analysis: principles and applications'. (Ed. 2000) pp. 267-294. (John Wiley & Sons: New York).

Vrindts E, Reyniers M, Darius P, De baerdemaeker J, Gilot M, Sadaoui Y, Frankinet M, Hanquet B and Destain MF (2003) Analysis of Soil and Crop Properties for Precision Agriculture for Winter Wheat. *Biosystems Engineering* **85**, 141-152.

Walden J, Oldfield F and Smith JP (1999) 'Environmental magnetism: a practical guide.' (Quaternary Research Association: London).

Walker G, Cox J, Wilford JR, Smitt C and Liddicoat C (2004) Application of Airborne Geophysical Techniques to the Investigation of Salt Stores and Stream Salinity in the Bremer Hills, South Australia. Department of Water, Land and Biodiversity Conservation, SA-SMMSP Site Summary Report No. Report, DWLBC 2004/38, Adelaide.

Ward PR, Dunin FX, Micin SF and Williamson DR (1998) Evaluating drainage responses in duplex soils in a Mediterranean environment. *Australian Journal of Soil Research* **36**, 509-524.

Webster R (1997) Soil resources and their assessment. *Phil. Trans. R. Soc. Lond.* **352**, 963-973.

Webster R and Oliver MA (2001) 'Geostatistics for Environmental Scientists.' (John Wiley & Sons: Chichester, England).

Wilding LP (2000) Pedology. In 'Handbook of Soil Science'. (Ed. ME Sumner) pp. E1-E4. (CRC Press: Boca Raton, FL, USA).

Wilford JR (1995) Airborne gamma-ray spectrometry as a tool for assessing landscape activity and weathering development of regolith, including soils. In 'AGSO Research Newsletter' pp. 12 - 14.

Wilford JR (2004a) 3D regolith architecture of the Jamestown area - implications for salinity. CRC LEME, Open File Report No. CRC LEME Open File Report 178, Bentley, Australia.

Wilford JR (2004b) 3D regolith architecture of the Jamestown area with applications for salinity. CRC LEME, Restricted report No., Canberra.

Wilford JR (2004c) Regolith-landforms and salt stores in the Angas-Bremer Hills. CRC-LEME CRC-LEME Open File Report 177, Canberra, Australia.

Wilford JR, Bierwirth PN and Craig MA (1997) Application of airborne gamma-ray spectrometry in soil/regolith mapping and applied geomorphology. *AGSO Journal of Australian Geology & Geophysics* **17**, 201 - 216.

Wilford JR, Dent DL, Dowling T and Braaten R (2001) Rapid mapping of soils and salt stores. In 'AGSO Research Newsletter' pp. 33 - 40.

Williams BG and Baker GC (1982) An electromagnetic induction technique for reconnaissance surveys of soil salinity hazards. *Australian Journal of Soil Research* **20**, 107-118.

Williams RD and Cooper JR (1990) Locating soil boundaries using magnetic susceptibility. *Soil Science* **150**, 889 - 895.

Williamson DR (1990) Salinity - an old environmental problem. CSIRO Division of Water Resources, Technical Memorandum, 90/7 No.

Wilson JP and Gallant JC (2000a) Digital terrain analysis. In 'Terrain analysis: principles and applications'. (Eds JP Wilson and JC Gallant) pp. 1-27. (John Wiley & Sons Inc.: New York).

Wilson JP and Gallant JC (2000b) 'Terrain Analysis: Principles and Applications.' (John Wiley & Sons Inc.: New York).

Wong MTF and Harper RJ (1999) Use of on-ground gamma-ray spectrometry to measure plant-available potassium and other top soil attributes. *Australian Journal of Soil Research* **37**, 267 - 277.

Wysocki DA, Schoeneberger PJ and LaGarry HA (2000) Geomorphology of soil landscapes. In 'Handbook of Soil Science'. (Ed. ME Sumner) pp. E5-E39. (CRC Press: Boca Raton, FL, USA).

Wysocki DA, Schoeneberger PJ and LaGarry HE (2005) Soil surveys: a window to the subsurface. *Geoderma* **126**, 167-180.

Appendix A. Oral presentations and extended abstracts

Date	Title	Forum, venue
December, 2002	Combining remote sensing and terrain analysis with conceptual toposequence models in two dry saline land affected areas (Jamestown and Mt Lofty Ranges) for upscaling root zone constraints	PhD research proposal, University of Adelaide, Adelaide, Australia
August, 2002	Combining remote sensing and terrain analysis with conceptual toposequence models in two dry saline land affected areas (Jamestown and Mt Lofty Ranges) - leading to land capability mapping	LEME Salinity Workshop, University of Adelaide, Adelaide, Australia
August, 2002	Combining geophysics, geochemistry and spatial methods in dry saline land soil mapping; Jamestown area progress	LEME Salinity Workshop, University of Adelaide, Adelaide, Australia
February, 2003	Predicting regional saline-sodic soil-regolith patterns	Geology and Geophysics seminar, School for Earth and Environmental Sciences, University of Adelaide, Adelaide, Australia
November, 2003	Mapping complex soil-landscape patterns using radiometric K%: a dry saline land farming area case study near Jamestown, SA	LEME Symposium, Adelaide, Australia
March, 2004	Predicting regional saline-sodic soil patterns at management scale	LUAC, Adelaide, Australia
September, 2004	Regional prediction of salt-affected soils in an area of complex soil patterns in South Australia	Global Workshop on Digital Soil Mapping, Montpellier, France
October, 2004	Linking airborne radiometric K, soil mineralogy and terrain to map soil patterns in a salt-affected South Australian toposequence	Clay Mineralogy & Geophysics for Environmental Management and Mineral Exploration, Adelaide, Australia
October, 2004	Regional prediction of salt-affected soils in an area of complex soil patterns in South Australia	LEME Symposium (2004), Canberra, Australia
March, 2005	Intricate salt-affected soil patterns identified and conceptually modelled using soil survey, geophysics and terrain analysis	Royal Society of South Australia, Adelaide, Australia

Date	Title	Forum, venue
April, 2005	Intricate salt-affected soil patterns identified and conceptually modelled using soil survey, geophysics and terrain analysis	First International Salinity Forum, Riverside, USA
March, 2006	Multiscale prediction of saline-sodic degradation processes in upland South Australia	Department of Primary Industries, Victoria, Bendigo, Australia
July, 2006	Predicting regional complex saline-sodic soil patterns using geophysical, hydrogeological and mineralogical approaches that translate across scales	18 th World Congress of Soil Science, Philadelphia, USA
July, 2006	Using gamma-ray spectroscopy in mineralogical and geochemical soil-regolith investigations: Australian case studies in depositional and erosional landscapes	18 th World Congress of Soil Science, Philadelphia, USA

MAPPING COMPLEX SOIL-LANDSCAPE PATTERNS USING RADIOMETRIC K%: A DRY SALINE LAND FARMING AREA CASE STUDY NEAR JAMESTOWN, SA

Mark Thomas¹, Rob W. Fitzpatrick² and Graham S. Heinson³

¹ CRC-LEME/University of Adelaide, PMB 2, Glen Osmond, Adelaide, SA 5064

² CRC-LEME/CSIRO Land and Water, PMB 2, Glen Osmond, Adelaide, SA 5064

³ CRC-LEME/University of Adelaide, North Terrace, Adelaide, SA 5000

INTRODUCTION

Location

The study area ("Cootes' site") straddles two farms in South Australia's NAD, and covers an area of 121 ha. To the north is Jamestown (25 km), and to the south Spalding (20 km) and Adelaide (180 km) (Figure 1a). The study site is on the east flank of a broad north-south valley system (Figure 1b), drained southwards by the "Freshwater Creek". The site is on the east flank of the valley. The crest-to-valley bottom toposequence (A/B) (inset, Figure 1b) length is 1,500 m, and has a relief difference of 100 m, i.e., 470-370 m. A basement of tillites, quartzites, mudstones, siltstones and shales underlies the toposequence. A prominent feature of the landscape is the deeply incised (12 m) erosional gully formed by the creek. 75% of the 450 mm annual rainfall falls in the winter growing season (May to October).

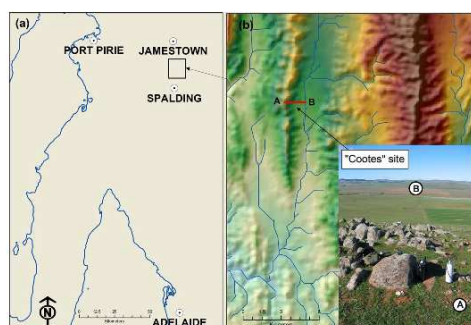


Figure 1: Study area regional context (a), and landscape location with toposequence A/B marked (b). Inset, photo of study area looking from A to B.

Dry saline land forming factors

Dry saline land occurs in the upper parts of the landscape not influenced by deep saline groundwater (Fitzpatrick *et al.* 2003a, b). This landscape context is totally unlike that of "dryland salinity", which occurs in low parts of landscapes where saline groundwater tables are close to or at the surface. Dry saline land is found in upland, winter-rainfall zones in South Australia that are usually semi-arid. Typical salinities on the soil surface range from EC_{se} 4-60 dS/m (surface form) and EC_{se} 2-8 dS/m in the subsoil (i.e., 0.3-1.0 m) (subsoil form), and present a hazard to agriculture in increasing concentrations.

The development of dry saline land salinity is strongly associated with texture-contrast (duplex) soils (e.g., loams over clays) in which key soil-landscape processes include sodification and salinisation. On wetting, sodicity causes general subsoil structural decline as clay aggregates disintegrate, disperse and clog soil pores. Sodic pore clogging in the A-B horizon interface creates a layer that is almost impermeable to vertical water movement. Consequently, during winter when up-slope soils are wettest, subsoil water movement is lateral (i.e., down slope), through the coarser-textured A horizon. Locally, this results in the formation of wet patches (i.e., perched watertables) in depressions, break-of-slopes, and where upper layer soil textures become clayier down-slope at soil unit transitions. However, where subsoil freshwater flow rates are high enough, i.e., in drainage zones on steep slopes, subsoil salts are washed out. Over time the perched watertables accumulate salts. Subsequently, during warm dry summer periods, the combination of surface

evaporation and subsoil evapotranspiration creates dynamic moisture conditions in the subsoil profile. These conditions cause dissolved salts to mobilise through the subsoil profile with the wetting front, and to concentrate in topsoil and subsoil layers as they dry (Rengasamy 2002). The seasonally changing salt concentrations in these layers—both temporally and spatially—pose a considerable farming challenge, often compounded by the associated problems of waterlogging and/or sodic structural decline in the soil.

DATA SETS AND INTERPRETATION

Soil and landscape data

The interpretation of dry saline land soil-landscape processes in the study area is described in Fitzpatrick *et al.* (2003a). This work relied on previous soil mapping and laboratory analysis (Fitzpatrick *et al.* 2003c), geology, a digital elevation model, and volume magnetic susceptibility and electromagnetic (EM) data from labour-intensive ground surveys.

The study area was divided into a number of landscape soil units (LSUs) based on similarities in: morphology (soil texture, layers, structure, etc.); zones of salt accumulation; and hydrology (i.e., groundwater and freshwater flows). These, with the laboratory analysis data (clay %, EC_{se} and ESP), are shown in Figure 2, overlaid on a 3-D aerial photo drape. Also shown are the locations of soils (“a” and “b” from < 0.3 m, and “c” at 1.0 m) and taken for XRD analysis.

Briefly, LSU 1-type soils are shallow loams on the crest, interspersed with outcropping (i.e., 5-50% surface cover) shales and siltstones. LSU 2-type soils are saline/sodic clays on steep upper slopes. LSU 3-type soils are on lower colluvial/alluvial slopes, and demonstrate strong texture contrasts between the leached upper layer loams above sodic clay layers (refer to Figure 2 profile data). LSU 4-type soils are deep alluvial sodic clays with thin leached A horizons.

EM surveys

The EM surveys were conducted using an EM38 (Figure 3a) and an EM31 (Figure 3b) (Fitzpatrick *et al.* 2003a). The EM38 determines subsoil conductivity at approximately 0.75 m deep, and the EM31, the regolith conductivity at approximately 6 m deep. Figure 3 shows high conductivity values in red, medium values in yellow-turquoise, and low values in dark blue. Conductivity values are generally strongly related to salt content (apparent EC).

Salt distribution

Figure 3a (EM38) displays three zones of relatively high subsoil conductivity. Feature “m” in LSU 2 is likely to represent an area of near-surface mineralisation. LSU 3 displays regions of conductivity associated with sloping areas that are not in drainage zones. These regions are likely to represent subsoil salts, and are indicative of the subsoil form of dry saline land discussed earlier. Moderate conductivities are displayed throughout LSU 4 areas, and are likely to be associated with low salt concentrations in the subsoil (ref. Figure 2 profile data).

By contrast, the EM31 plot (Figure 3b) shows regolith (6 m) conductivity in all LSUs, especially in the drainage zones on sloping areas, and throughout LSU 4. A large proportion of high conductivity response on the sloping areas is probably associated with conductive basement rock or the deposition of magnetic colluvial material. In the sloping area drainage zones the highly conductive regolith pattern is likely to reflect magnetic colluvial material and/or salt accumulation. These salts are likely to have been washed down from upper-slope areas, or from below in saline groundwater. The LSU 3/4 boundary forms a prominent contrasting conductivity feature. The high conductivity throughout most of LSU 4 is likely to reflect the hydraulic barrier - caused by the low sodic clay permeability - which traps and concentrates up-slope regolith salts. Perhaps after a considerable time in storage the salts seep out of the gully face, evidenced by high EM31 conductivity zones and laboratory data.

The conductivity patterns from Figure 3, combined with soil profile data (ESP, salinity and clay %) in A and B horizons in Figure 2, suggest that soil-landscape patterns with LSU 3-type soils up-slope of LSU 4-type soil are likely to be indicative of landscapes prone to dry saline land formation and salt entrapment - along with the attendant soil issues discussed earlier. Therefore, this type of soil-landscape pattern expressed in areas with similar environmental conditions (e.g., climate, geology, land use) is likely to be a useful predictor of where these soil issues are likely to occur in the landscape. If so, the ability to predict these patterns will be important in managing these areas more effectively.

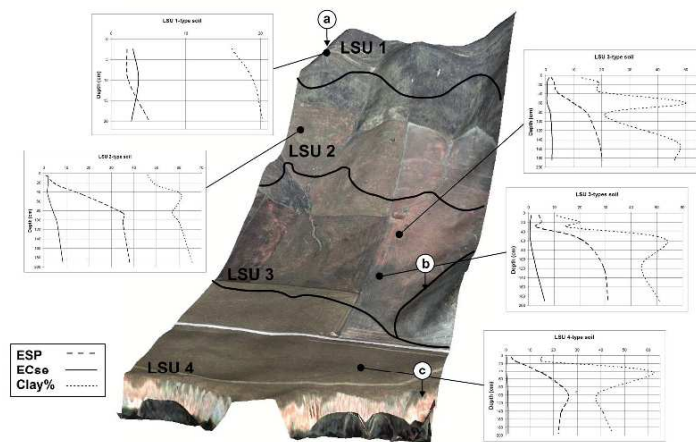


Figure 2: 3-D aerial photo drape of the study area with landscape soil unit boundaries, laboratory data and XRD sampling locations indicated.

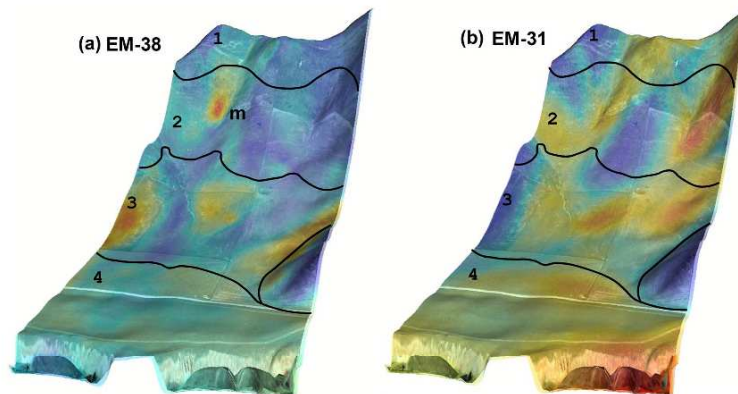


Figure 3: EM38 (a) and EM31 (b) surveys over laid on a 3-D aerial photo drape of the study area. High conductivity values are in red, medium values in yellow-turquoise, and low values in dark blue.

Airborne K% radiometrics

Airborne radiometrics measure the gamma activity released in the radio-decay of K, Th and U in the top 0.35 m of the land surface (Minty 1997). Depending on the specific survey requirements and data application, acquisition costs can be cost-effective, e.g., A\$1.80 per ha or less. The farm scale (i.e., 20 m resolution) airborne radiometrics used in the study was acquired through NAP as part of South Australian Salt Mapping and Management Support Project (Munday *et al.* 2003).

The airborne K% distribution in the study area is shown in Figure 4. The values range from 1.1% to 2.5%. High K% values are shown in red and low values in yellow. Figure 4 shows a strong pattern of high K% values in the LSU 4-type soils, and generally lower values throughout the rest of the landscape soil units in the study area. The LSU 3/4 boundary forms a prominent contrasting K% feature, very similar to the strong contrast seen in the EM31 regolith conductivity (Figure 3b) in the same part of the landscape.

M. Thomas, R.W. Fitzpatrick & G.S. Heinson. *Mapping complex soil-landscape patterns using radiometric K%: a dry saline land farming area case study near Jamestown, SA.*

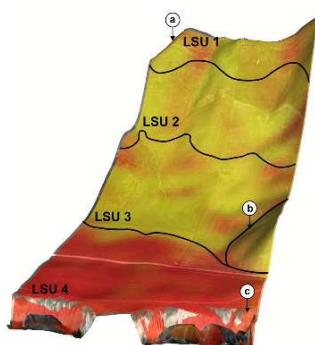


Figure 4: Study area airborne radiometric K% distribution over laid on a 3-D aerial photo drupe. High K% values are in red, low values in yellow. XRD sampling locations (a, b and c) are indicated.

Airborne radiometric K% validation

A regression analysis was conducted to determine airborne K% accuracy. This involved conducting 53 field K% readings using a hand held gamma-ray radiometer (taken over 250 seconds for a sufficient count rate) throughout the study area (Figure 5).

These readings were co-registered to the airborne K% using a geographic information system, and a regression analysis conducted on the paired data. Figure 6 shows a reasonably strong R^2 value of 0.75, initially indicating a useful relationship between airborne and field K%. An important contributor to the variation seen in the two data sets is due to the large ground footprint acquired by the airborne sensor (i.e., mixing the signal from all surface materials in the footprint, e.g., soils, rocks, etc.) compared to the comparatively very small area of soil signal acquired in the field using the hand held radiometer.

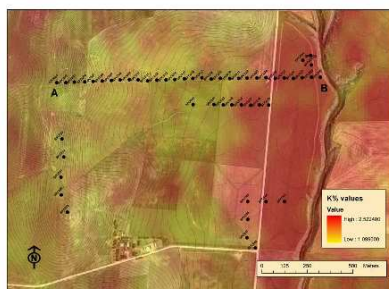


Figure 6: Locations of field hand held gamma-ray spectrometer readings, over laying 2 m contours, airborne K% coverage and aerial photo of the study area.

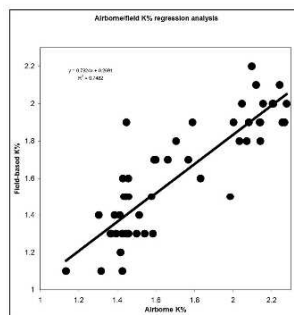


Figure 5: Airborne (X-axis) versus field based (Y-axis) K% radiometric regression plot.

Clay mineralogy

Preliminary XRD analysis on the clay fractions from soil samples “a”, “b” and “c” (Figures 2 and 4) was conducted. The results are shown in Table 1, with airborne K% and soil clay %.

This investigation indicates that chlorite dominates the < 0.25 m depth clay fraction of the crest (LSU 1) and the < 0.35 m depth clay fraction of the sloping area (LSU 3) soils, while mica and smectite co-dominate the clay fraction at 1.0 m in the LSU 4-type soil.

M. Thomas, R.W. Fitzpatrick & G.S. Heinson. *Mapping complex soil-landscape patterns using radiometric K%: a dry saline land farming area case study near Jamestown, SA.*

Table 1. XRD interpretation for soil samples “a”, “b” and “c” with airborne K% and soil clay %.

Site	Depth range (m)	XRD interpretation	Airborne K%	Ave. soil clay content (%)
a	0.0-0.25	Chlorite dominant	1.8	18
b	0.0-0.35	Chlorite dominant	1.5	21
c	1.0	Mica and smectite co-dominant	2.1	35

LINKING CLAY MINERALOGY, DRY SALINE LAND PROCESS AND AIRBORNE RADIOMETRICS

Mica, smectite and chlorite are soil-clay fraction layer silicates. Both mica and smectite have a high K content, while chlorite has a low K content (Taylor and Eggleton 2001). By combining the results of the XRD analysis, soils data, and airborne K% distribution, the following study area patterns are revealed: mica and smectite dominate areas that spatially coincide with (i) high airborne K% areas and (ii) LSU 4-type soils. Chlorite dominated areas spatially coincide with (i) low airborne K% areas, and (ii) LSU 1, 2 and 3-type soils. Soil data from Figure 2 indicates that low airborne K%/LSU 1, 2 and 3 areas have subsoil dry saline land salinity due to maximum salinity values at <1 m depth ranging between EC_{se} 2.5-5.5 dS/m. However, high airborne K%/LSU 4-type soils do not demonstrate dry saline land conditions. The reduced hydraulic permeability in the subsoil of the LSU 4-type soils from the sodic mica/smectite clay dispersion is likely to create the hydraulic conditions for dry saline land formation in the up-slope, LSU 3-type soils, i.e. impeded subsoil freshwater flow, perched watertable formation, and finally subsoil salt accumulation. Therefore, patterns showing low airborne K% areas (LSU 3-type soils) up-slope of high airborne K% areas (LSU 4-type soils) may provide the spatial “clues” for the prediction of dry saline land-prone landscapes in up-slope, LSU 3-type soils.

CONCLUSIONS

This study in an area characterised by a complex mosaic of soils with dry saline land conditions - along with attendant waterlogging, sodicity and fertility issues - has enabled us to establish relationships between (i) landscape soil units, and subsoil and regolith salt distributions from ground-based EM, terrain, soil survey and laboratory analysis data; (ii) landscape soil units and upper layer clay mineralogy; and (iii) clay mineralogy and airborne K% radiometrics. Based on the discussion in previous sections on soil-landscape arrangements being likely precursors to dry saline land conditions, the patterns derived from cost-effective airborne K% imagery are likely to be helpful in the pursuit of an airborne methodology to predict dry saline land soil patterns in landscapes under similar environmental conditions for farming purposes. A regression relationship of R^2 0.75 between airborne and ground based K% initially indicates confidence in the accuracy of the airborne K%.

Future work will focus on quantitative XRD analysis to confirm airborne radiometrics K, Th and U/clay mineral and heavy metal relationships in the landscape from samples acquired during the validation fieldwork (Figure 5). We will also develop a stronger understanding of soil-landscape patterns employing, for example, subsoil B horizon micro-relief analysis, surface terrain analysis, and airborne magnetic imagery acquired through NAP.

REFERENCES

- FITZPATRICK R.W., DAVIES P.J., THOMAS M. & WILLIAMS B. 2003a. *Dry saline land: an investigation using ground-based geophysics, soil survey and spatial methods near Jamestown, South Australia*. CSIRO Land and Water, Adelaide.
- FITZPATRICK R.W., MERRY R.H., COX J., RENGASAMY P. & DAVIES P.J. 2003b. *Assessment of physico-chemical changes in dryland saline soils when drained or disturbed for developing management options*. CSIRO Land and Water, Adelaide, pp. 57.
- FITZPATRICK R.W., THOMAS M., CANNON M.G., McTHOMPSON J. & COOTES T.R. 2003c. *Soils and land use of a sub-catchment of Freshwater Creek near Spalding, South Australia*. CSIRO, Adelaide.
- MINTY B.R.S. 1997. Fundamentals of airborne gamma-ray spectrometry. *AGSO Journal of Australian Geology & Geophysics* 17, 39 - 50.
- MUNDAY T., WALKER G., CRESSWELL R., WILFORD J. R., BARNETT S. & COOK P. 2003. South Australian Salt Mapping and Management Support Project - An example of the considered application of airborne geophysics in natural resource management. *ASEG 16th Geophysical Conference and Exhibition*, Adelaide.

M. Thomas, R.W. Fitzpatrick & G.S. Heinson. *Mapping complex soil-landscape patterns using radiometric K%: a dry saline land farming area case study near Jamestown, SA.*

RENGASAMY P. 2002. Transient salinity and subsoil constraints to dryland farming in Australian sodic soils: an overview. *Australian of Experimental Agriculture* **42**, 351 - 361.

TAYLOR G. & EGGLETON R.A., 2001 *Regolith geology and geomorphology*. John Wiley and Sons, Ltd., Chichester, UK.

Acknowledgements: We acknowledge the Cootes and Ashby families for access to their land, NAP for radiometrics data, Brian Minty (Geosciences Australia) for radiometric advice and equipment loan, and Mark Raven (CSIRO Land and Water) for XRD analyses. Mark Thomas acknowledges CSIRO Land and Water and the Department for Water, Land and Biodiversity Conservation (SA) for their continued support.

M. Thomas, R.W. Fitzpatrick & G.S. Heinson. *Mapping complex soil-landscape patterns using radiometric K%: a dry saline land farming area case study near Jamestown, SA.*

Regional prediction of salt-affected soils in an area of complex soil patterns in South Australia

Mark Thomas¹, Rob W. Fitzpatrick² and Graham S. Heinson³

¹ CRC-LEME/University of Adelaide/South Australian Department for Water, Land and Biodiversity Conservation, PMB 2, Glen Osmond, Adelaide, SA 5064

² CRC-LEME/CSIRO Land and Water, PMB 2, Glen Osmond, Adelaide, SA 5064

³ CRC-LEME/University of Adelaide, North Terrace, Adelaide, SA 5000

Abstract

In this paper we draw together the themes of three papers in preparation, which when combined, document the steps involved in the development of a GIS-based regional methodology to predict a form of salt-affected soils called shallow non-groundwater associated salinity (NAS). We demonstrate how point (profile), plot (100 m²) and toposequence (121 ha) scale investigations are linked to develop the regional scale (2,300 ha) predictive methodology, via multiscale soil-landscape models. The GIS-based regional scale predictions are based on cost-effective terrain and airborne radiometric K% coverages. The methodology offers new perspectives into shallow NAS forming processes, and provides validated maps at a scale suitable for farm management planning.

Keywords: Geophysical survey techniques; Terrain modelling; Soil-landscape modelling; GIS; Salt-affected soils

1. Introduction

Shallow non-groundwater associated salinity (shallow NAS), which is described in Fitzpatrick et al. (in prep.), is found in upland parts of landscapes that have no direct contact with saline groundwater watertables, unlike groundwater associated salinity (GAS). GAS is characterised in terms of catchment-scale hydrological processes, and is managed accordingly. Conversely, shallow NAS is characterised by localised soil patterns, which are governed by soil-landscape processes at various scales.

Shallow NAS soils feature (i) high exchangeable sodium percentage (ESP) (i.e. “sodic” and featuring excessive Na⁺ ions on the exchange complex) and (ii) high soluble salt concentrations (i.e. “saline”, generally featuring Na⁺ and Cl⁻ ions, and measured by EC_{se}) in the solum (i.e. A and B-horizons, typically <1.2 m deep). In Australia, soils with ESP ≥5 are generally considered as being sodic (Rengasamy and Churchman, 1999). These soils show signs of a decline in soil structure due to clay dispersion, which in turn creates waterlogging, hard-setting physical barriers to root growth, and poor gas transfer rates. Elevated EC_{se} values (i.e. ≥2 dS/m) give rise to droughting and toxic conditions in soils, which affect crop growth (Soil Survey Division Staff, 1993). When sodicity and salinity combine through shallow NAS, the harmful affects on crops are magnified. Shallow NAS is strongly associated with texture contrast soils, which feature sandy/loamy A-horizons over sodic clay B-horizons. These are very important agricultural soils in southern Australia.

According to Rengasamy (2002), approximately A\$1,330 million of farm income is lost annually through shallow NAS in Australia. More locally, in the Northern Agricultural District (NAD) (302,000 ha) of South Australia, subsoil (e.g. 0.3 – 1.2 m) salts are a widespread problem. According to 1:100,000 scale State-wide soil

mapping (Soil and Land Information, 2002), >15% of the NAD soils are affected by salinity ($EC_{se} \geq 2$ dS/m) and >60% by sodicity ($ESP \geq 6$). Most of the saline areas spatially overlap with the sodic areas in the mapping, indicating that a significant proportion of the NAD is affected by shallow NAS. However, shallow NAS soils are difficult to map by conventional field-based soil-landscape survey methods (e.g. McDonald et al., 1998) because they form complex patterns with no apparent visual surface clues (e.g. colour, texture) (Thomas et al., 2003). For this reason, shallow NAS has not been mapped in South Australia at scales suitable for farm management planning (e.g. 1:5,000 - or larger).

Our aim is describe a GIS-based regional digital soil mapping methodology to predict shallow NAS for a small regional study area in the NAD.

2. Regional study area

The small regional study area (2,300 ha) is in an upland farming zone of the NAD (Fig. 1). The average annual rainfall is 450 mm, of which approximately 75 % falls during the winter. Winters are cool and summers are hot, giving rise to a temperate, Mediterranean-type climate. The predominant agricultural land use in the area involves wheat, barley, canola and sheep grazing rotations.

The regional study area landscape features a north-south ridge system flanked by broad (>8 km) valleys draining south. From this we selected a regionally representative toposequence area (121 ha) on the east-facing flank of the ridge. The toposequence was 1.5 km long and had a 100 m relief difference. As a consequence of the multi-factorial genesis of the soils reflecting the variable parent material (interbedded tillites, shales, quartzites, mudstones and siltstones), the toposequence can be described as being pedologically complex (Fitzpatrick et al., 2003). Essentially, all land in the toposequence area, and most of the regional area, has been cleared of native vegetation.

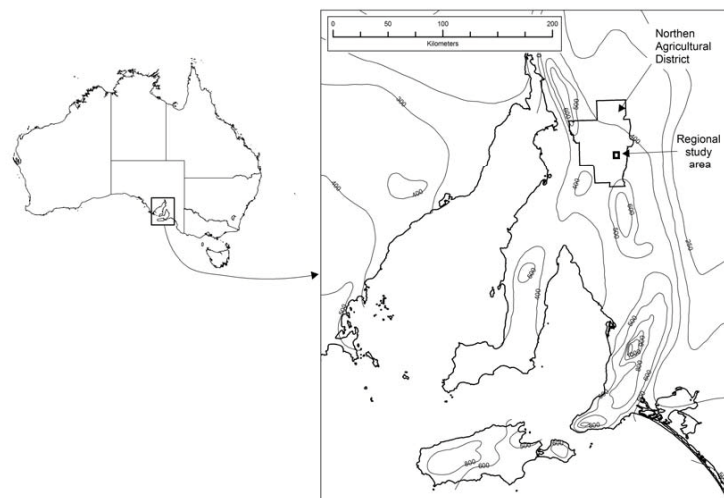


Figure 1. Map showing location of regional study area in Australia, featuring South Australia's Northern Agricultural District and rainfall zones.

3. Methods and materials

Our approach was to combine multiscale soil and hydrological processes models to predict, using a GIS, shallow NAS in the regional study area. The multiscale analyses were undertaken using field survey and laboratory methods, which were conducted at point (profile), plot (100 m²) and toposequence (121 ha) scales. The resulting datasets were used to display the main soil, regolith, geological and hydrological features in the toposequence using a cross-sectional, graphic format called a “conceptual toposequence model” (CTM). At this stage the model was used to assesses/display toposequence-scale soil-landscape variability - i.e. as a *descriptive* CTM (Fitzpatrick and Merry, 2002) - specifically related to shallow NAS toposequence expression. With the introduction of soil-landscape process knowledge from the multiscale investigations (e.g. solute transport pathways, shallow NAS zone processes), the *descriptive* CTM was transformed into an *explanatory* CTM (Fitzpatrick and Merry, 2002). The final stage of the methodology involved spatially implementing the *explanatory* CTM, via a GIS, to make the regional shallow NAS predictions.

As discussed, three papers in preparation combine to fully document the whole regional predictive approach. In the first, Fitzpatrick et al. (in prep.) refine soil salinity concepts and definitions, and propose generic soil-process models. In the second, Thomas et al. (in prep.-a) describe at the point (profile), plot (100 m²) and toposequence (121 ha) scales, soil-landscape investigations to construct the soil and hydrological processes models. They also document the conceptual toposequence modelling in the regionally representative, shallow NAS-affected toposequence. In the third, Thomas et al. (in prep.-b) discuss the development and implementation of the regional predictive framework, via the conceptual toposequence modelling, to achieve the regional shallow NAS predictions.

3.1 Multiscale surveys and analyses

The multiple survey and analytical techniques used, and their scales and modes of application, are summarised in Table 1. Figure 2 is closely linked to Table 1 as it displays conceptually how the multiscale analyses and models connect to construct the *explanatory* CTM via the “model input” arrows and feedback loops. Figure 2 also highlights the links between the *explanatory* CTM and the GIS-based regional predictive framework, and the resulting regional shallow NAS predictions.

We summarise the key outputs from the multiscale analyses, and briefly discuss the models that were developed.

3.1.1 Point scale (profile) investigations

Point scale surveys and analyses were used to determine spatial relationships between soil physico-chemical properties and to map the soils of the regionally representative toposequence area. Four landscape soil units (LSUs) were identified (Figs. 2 and 3) (Thomas et al., 2003). Analysis of profile physico-chemical data showed that shallow NAS was confined to the LSU 3-types of soils on lower colluvial/alluvial slope landscape areas (Fitzpatrick et al., 2003).

3.1.2 Plot scale (100 m²) investigations

At plot scale (100 m²), we focused our investigations on morphological and chemical properties at the contact between the A and B-horizons by incorporating 3D GIS techniques (Fig. 2). These investigations were conducted in two plots inside the LSU

3 soil area; one from a good crop yielding area (P1) and the other from a poor crop yielding area (P2) (Figs. 2-3). The key soil properties investigated included EC_{se} , CEC, ESP and magnetic susceptibility.

No strong relationships were identified between the A and B-horizon contact shape and plot soil patterns. However, P1 (the good crop yielding area) generally had a thicker A-horizon (0.16-0.34 m) and was less saline (EC_{se} 0.4 – 0.7 dS/m), whereas P2 (the poor crop yielding area) generally had a thinner A-horizon (0.10 – 0.18 m), and was more saline (EC_{se} 0.7 – 1.4 dS/m). By taking landform positions into account (Figs 2 and 3) during interpretation of these findings, we were able to determine that P1 was likely to be more agriculturally productive because of the combination of (i) a higher water holding capacity (thicker A-horizon), and (iii) a higher rate of freshwater flushing (leaching salts from the solum into downslope areas) due to the low-lying landscape position.

3.1.3 Toposequence (141 ha) investigations

At toposequence scale (141 ha), investigations focused on the relationships between landform [based on terrain wetness index (TWI) and slope], surface and subsoil salt concentrations/clay distribution (EM38), soil-regolith salinity/clay distribution (EM31), surface volume magnetic susceptibility (κ) and surface mineralogy (airborne radiometric K%) in the toposequence area (Fig. 2). The electromagnetic induction (EMI) techniques (EM38 and EM31) revealed strong soil-landscape patterns, which were visually linked to the landscape-wide distribution of shallow NAS and hydrological patterns (Figs. 2) using 3D GIS techniques and soil data (e.g. Fig. 3). We also found that κ patterns strongly correlated with those of EM38, which in turn linked to landscape drainage patterns. Our interpretation for these observations was that high EM38 values/high κ values corresponded with low solum freshwater flushing zones in the TWI coverage (Table 1). Wetness index patterns and soil data (e.g. Fig.3) confirmed this relationship. Thus, we concluded that EM38 and κ patterns were pedogenic expressions of solum freshwater flushing patterns.

Thomas et al. (2003) demonstrated the link between topsoil clay mineralogy and soil types. In that study they reported that airborne radiometric K% could be used to regionally map the boundary between the LSU 4 and LSU 3 soils (Figs. 2 and 3).

3.2 Conceptual toposequence model construction

Fritsch and Fitzpatrick (1994) and Fitzpatrick and Merry (2002) detail the construction and interpretation of CTMs. Figure 2 illustrates the connections and feedback loops (i.e. multiscale extrapolation/verification sequences) involved in the process of constructing the CTM through the spatial and conceptual integration of the multiscale investigations. In Figure 2, the CTM highlights the connections between: landform; parent material (geology); the four soils (LSUs 1 to 4); their soil morphologies (horizons and structure); and soil-landscape hydrology (structure, nodules and water flow). Salt/solute pathways and processes (saline and sodic), which influence the expression of shallow NAS in the landscape, are also highlighted by the *explanatory* CTM.

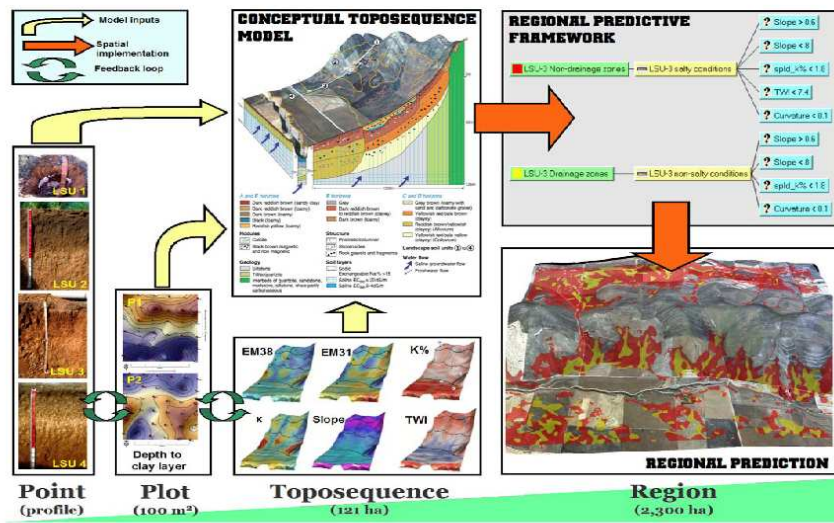


Figure 2. Shown links between point, plot and toposequence scale investigations and the construction of the explanatory conceptual toposequence model. The regional predictive framework shows the numeric thresholds for the GIS prediction. The regional predictions for shallow NAS (red areas)/ non-shallow NAS (yellow areas) in LSU 3 soils is shown, overlaying a draped 3D rendition of the regional aerial photograph.

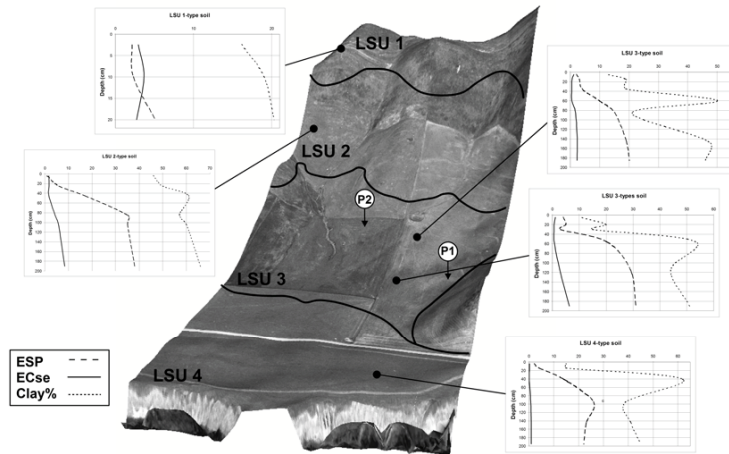


Figure 3. 3D aerial photo drape of the toposequence area with landscape soil unit boundaries, selected profile datasets showing ESP, EC_{se} and clay% by depth, and P1 and P2 sites indicated.

3.3 Regional prediction methodology

Given that we discovered that shallow NAS only featured in LSU 3 soils, and that our multiscale investigations revealed that not all LSU 3 soils were affected by shallow NAS, we focussed on the following two classes in our regional shallow NAS prediction methodology:

- LSU 3, shallow NAS affected; (i.e. “LSU 3 salty conditions”; Fig. 2) and
- LSU 3 (i.e. “LSU 3 non-salty conditions”, Fig 2).

Our approach was to extrapolate soil and hydrological patterns associated with shallow NAS from easily accessible and low-cost regional coverages. The extrapolation of these patterns was achieved through the spatial implementation of regional predictive framework (Fig. 2). This procedure involved:

1. Using soil data and knowledge from the *explanatory* CTM to identify regional coverages that have patterns that spatially corresponded with LSU 3 soils and shallow NAS and hydrological process patterns.
2. Defining threshold values from these coverages that lend numeric expression to the patterns, “captured” in the form of a rules-based regional predicative framework (Fig. 2).
3. Spatially implementing the rules-based regional predicative framework via a GIS.

Table 1. Summary of methods showing survey and analytical techniques used, their scale and mode of application, and key references.

Method	Instrument / technique	Application	Potential soil landscape attributes derived	Units / type	Key references	Application scale			
						Point (0-100 ha)	Plot (100 m ²)	Toposequence (21 ha)	Regional (2,800 ha)
Electromagnetic induction (EMI)	EM38	Electromagnetic induction of soil-regolith profile, on foot, field-based	Combined soil profile salinity, texture and moisture, <1.5 m	Apparent EC (EC _a , dS/m)	(McNeill, 1980, Sudduth et al., 2001)		•	•	
	EM31		As above, plus including regolith and bedrock >6m					•	
Magnetic susceptibility	Bartington ME2B, dual frequency sensor	Mass magnetic susceptibility of soil layers, laboratory-based	Magnetic iron oxides [magnetite (α - Fe ₃ O ₄) and pedogenic magnetite (γ - Fe ₃ O ₄)], soil-landscape/pedogenic processes, especially local wetting/drying conditions, leaching, burning	χ	(Deering, 1999, Evans and Heller, 2003)		•		
	Bartington ME2E, loop sensor	"Bulked" surface volume magnetic susceptibility (< few cm ²), on foot		κ			•	•	
	Bartington ME2F, probe sensor	High spatial resolution surface volume magnetic susceptibility (< few cm ²), on foot						•	
Gamma radiometrics	Regional airborne survey	Regional geochemical image of topsoil (K, Th, U, total count), GIS	Regional toposequence soil-landscape process, mineral weathering, mineralogy, soil types	% (C, ppm (K, Th, U and total count))	(Dickson and Scott, 1997, Minby 1997, Wilford et al., 1997)			•	•
	GR-320 spectral radiometer	High spatial resolution geochemical survey of topsoil (K, Th, U, total count), on foot	Soil-landscape processes, geochemical weathering history, local geochemical patterns					•	
Physico-chemical analysis	Extractive / digestive physico-chemical analysis	Multiple (>30) analyses, accurate	Soil chemistry, soil physical measurements, multiple other attributes	Various	(Rayment and Higginson, 1992)	•	•	•	•
	Mid Infrared (MIR) analysis	Multiple (>30) analyses, reproducible, low cost, rapid			(Janik et al., 1998)		•		
	X ray diffraction (XRD)	X ray diffraction, accurate fine texturing	Clay mineralogy		(Olson et al., 2000)	•		•	
Digital terrain analysis	Aerial photographs, digital elevation models (DEM)	Terrain attributes, soil-landscape methodology, 3D GIS overlays	Slope, curvature, terrain wetness index (TWI), terrain based 3D renderings	GIS raster	(Burrough and McDonnell, 2000, Wilson and Gallant, 2000)	•		•	•
Soil-landscape survey	Yield map	Yield	Soil-landscape processes, farm planning	GIS vector	(McDonald et al., 1998, Schoeneberger et al., 2002)		•	•	
	Soil survey method	Soil classification, soil-landscape methodology, soil mapping	Pedogenic processes, soil hydrology, land capability, soil mapping, multiple soil-landscape properties, field texture, etc.	Models, GIS raster		•	•	•	•

From the multiscale investigations, we identified the following regional coverages that corresponded with shallow NAS soil and hydrological patterns:

- Slope;
- Airborne radiometric K%;
- TWI; and
- Plan curvature.

The final numeric model defining the predictive thresholds is presented in the regional predictive framework in Figure 2. Spatial implementation of the regional predictive framework was achieved using a GIS. The result is presented in the regional prediction in Figure 2.

Functionally, the regional predictive framework (Fig. 2) uses slope to discriminate LSU 3 from LSU 2 soils, and airborne radiometric K% to discriminate LSU 3 from LSU 4 soils. In the LSU 3 areas, TWI drainage thresholds further discriminate between salt accumulation and salt flushing zones (i.e. LSU 3 shallow NAS vs. non-shallow NAS). Profile curvature is used to filter out convex landscape positions (e.g. crests and ridges) in LSU 3 areas.

Validation of the LSU shallow NAS/non-shallow NAS predictions was undertaken using soil profile data from the point (profile) scale investigations from LSU 3 predicted areas. Figure 4 shows these, in which EC_{se} is plotted against depth. Here, 5 profiles from shallow NAS predicted areas (dotted lines), and 6 from non-shallow NAS predicted areas (solid lines) are plotted. The box inside the graph (i.e. “shallow NAS-affected soil profile zone”) defines shallow NAS soils according to soil depth/ EC_{se} thresholds (Fitzpatrick et al., in prep.). All profiles that intersect this box are shallow NAS-affected soils.

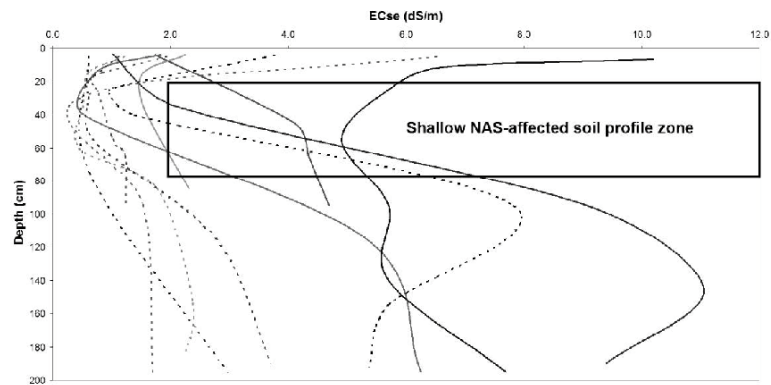


Figure 4. Profiles from plot scale investigations from LSU 3 shallow NAS predicted areas (solid lines) and profiles from LSU 3 non-NAS predicted areas (dotted lines) are plotted.

Figure 4 shows that all profiles from shallow NAS predicted areas (solid lines) intersect with the box, thus all have been correctly classified. All except for one

profile from non- shallow NAS predicted areas (dotted) do not intersect with the box, making all except for one correctly classified as non-shallow NAS.

Of the 2,300 ha regional study area, the regional predictive methodology classified 40% (i.e. 744 ha) as being LSU 3 soils. Of this area, 75% of the area (i.e. 654 ha) was classified as shallow NAS and 25% (i.e. 190 ha) as non-shallow NAS.

4. Conclusions

We have drawn together the themes of three papers in preparation, which when combined, document the steps involved in the development of a GIS based regional methodology to predict shallow NAS. We have demonstrated the links between multiscale investigations to develop an *explanatory* CTM that highlights shallow NAS processes (e.g. salt/solute flows). In turn the *explanatory* CTM was used to develop a GIS-based framework for regional shallow NAS spatial predictions. The regional methodology is based on easy-to-acquire, cost-effective GIS coverages (DEM and regional airborne radiometric K%). Using this predictive methodology we show that, of the selected 2,300 ha high value farming region, approximately 30% (i.e. 75% of LSU 3 soils) is affected by shallow NAS.

New insights have been gained into the role of soil-landscape factors, like regional landform and drainage patterns, in governing the distribution of shallow NAS patterns at the toposequence scale. We have also demonstrated the value of combining, through GIS-based 3D terrain techniques, multiple (i) geophysical surveys (e.g. terrain, EMI and κ), (ii) detailed field and laboratory data, (iii) airborne radiometric K%, and (iv) terrain modelling in developing soil-landscape models that underpin digital soil mapping methods that are likely to support farming decisions in landscapes with complex soil patterns.

Further work will investigate how our regional methodology to predict shallow NAS can be adapted for another high value farming area in a higher rainfall zone in South Australia.

Acknowledgements

We acknowledge the South Australian branch of the Australian Society of Soil Research Inc (ASSSI) for sponsorship to attend the Global Workshop on Digital Soil Mapping, and the Cootes and Ashby families for access to their farm land.

References

- Burrough, P.A. and McDonnell, R.A., 2000. Principles of Geographical Information Systems. Oxford University Press Inc., New York.
- Dearing, J.A., 1999. Magnetic Susceptibility. In: J. Walden, F. Oldfield and J. Smith (Editors), Environmental Magnetism; a practical guide. Technical Guide, No. 6. Quaternary Research Association, London, pp. 35-62.
- Dickson, B.L. and Scott, K.M., 1997. Interpretation of aerial gamma-ray surveys - adding the geochemical factors. AGSO Journal of Australian Geology & Geophysics, 17(2): 187 - 200.
- Evans, M.E. and Heller, F., 2003. Environmental Magnetism: Principles and Applications of Enviromagnetics. Academic Press, Burlington, Massachusetts.

- Fitzpatrick, R.W. and Merry, R.H., 2002. Soil-regolith models of soil-water landscape degradation: development and application. In: T.R. McVicar, L. Rui, R.W. Fitzpatrick and L. Changming (Editors), *Regional water and soil assessment for managing sustainable agriculture in China and Australia*. ACIAR Monograph. Australian Centre for International Agricultural Research, Canberra, pp. 130 - 138.
- Fitzpatrick, R.W., Thomas, M., Davies, P.J. and Williams, B.G., 2003. Dry saline land: an investigation using ground-based geophysics, soil survey and spatial methods near Jamestown, South Australia. 55/03, CSIRO, Adelaide.
- Fitzpatrick, R.W., Thomas, M. and Rengasamy, P., in prep. Non-groundwater associated salinity (NAS) in an area of complex soil patterns in South Australia: Definitions and generic soil-landscape models.
- Fritsch, E. and Fitzpatrick, R.W., 1994. Interpretation of soil features produced by ancient and modern processes in degraded landscapes. I. A new method for constructing conceptual soil-water-landscape models. *Australian Journal of Soil Research*, 32: 889 - 907.
- Janik, L.J., Merry, R.H. and Skjemstad, J.O., 1998. Can mid infrared diffuse reflectance analysis replace soil extractions? *Australian Journal of Experimental Agriculture*, 38: 681-96.
- McDonald, R.C., Isbell, R.F., Speight, J.G., Walker, J. and Hopkins, M.S., 1998. *Australian soil and survey handbook*. Australian Collaborative Land Evaluation Program, Canberra.
- McNeill, J.D., 1980. Electrical conductivity of soils and rocks. Technical Note TN-5, Geonics Ltd., Ontario.
- Minty, B.R.S., 1997. Fundamentals of airborne gamma-ray spectrometry. *AGSO Journal of Australian Geology & Geophysics*, 17(2): 39 - 50.
- Olson, C.G., Thompson, M.L. and Wilson, M.A., 2000. Phyllosilicates. In: M.E. Sumner (Editor), *Handbook of Soil Science*. CRC Press, Boca Raton, Florida, pp. F77-F123.
- Rayment, G.E. and Higginson, F.R., 1992. *Australian laboratory handbook of soil and water chemical methods*. Australian Soil and Land Survey Handbook. Inkata Press, Melbourne.
- Rengasamy, P., 2002. Transient salinity and subsoil constraints to dryland farming in Australian sodic soils: an overview. *Australian Journal of Experimental Agriculture*, 42(3): 351 - 361.
- Rengasamy, P. and Churchman, G.J., 1999. Cation exchange capacity, exchange cations and sodicity. In: K.I. Peverill, L.A. Sparrow and D.J. Reuter (Editors), *Soil analysis: an interpretation manual*. CSIRO Publishing, Collingwood, Victoria, pp. 147 - 157.
- Schoeneberger, P.J., Wysocki, D.A., Benham, E.C. and Broderson, W.D., 2002. *Fieldbook for describing and sampling soils*. Natural Resources Conservation Service, National Soil Survey Center, Lincoln, NE., USA.
- Soil and Land Information, 2002. *Land Resource Information - Northern Agricultural Districts of South Australia*. SaLI Group, The Department of Water, Land and Biodiversity Conservation, Adelaide, South Australia.
- Soil Survey Division Staff, 1993. *Soil survey manual*. U.S. Department of Agriculture Handbook No. 18. U.S. Government Printing Office, Washington.
- Sudduth, K.A., Drummond, S.T. and Kitchen, N.R., 2001. Accuracy issues in electromagnetic induction sensing of soil electrical conductivity for precision agriculture. *Computers and Electronics in Agriculture*, 31: 239-264.

- Thomas, M., Fitzpatrick, R.W. and Heinson, G.S., 2003. Mapping complex soil-landscape patterns using radiometric K%: a dry saline land farming area case study near Jamestown, SA. In: R.I. C. (Editor), *Advances in Regolith*. CRC-LEME, Adelaide, pp. 411-416.
- Thomas, M., Fitzpatrick, R.W. and Heinson, G.S., in prep.-a. Dry saline land in an area of complex soil patterns in South Australia: Identification and variability at plot and toposequence scales.
- Thomas, M., Fitzpatrick, R.W. and Heinson, G.S., in prep.-b. Dry saline land in an area of complex soil patterns in South Australia: Identification and variability at regional scales.
- Wilford, J.R., Bierwirth, P.N. and Craig, M.A., 1997. Application of airborne gamma-ray spectrometry in soil/regolith mapping and applied geomorphology. *AGSO Journal of Australian Geology & Geophysics*, 17(2): 201 - 216.
- Wilson, J.P. and Gallant, J.C., 2000. Digital terrain analysis. In: J.P. Wilson and J.C. Gallant (Editors), *Terrain analysis: principles and applications*. John Wiley & Sons Inc., New York, pp. 1-27.

Linking airborne radiometric K, soil mineralogy and terrain to map soil patterns in a salt-affected South Australian toposequence

Mark Thomas¹, Rob W. Fitzpatrick² and Graham S. Heinson³

¹ CRC-LEME/University of Adelaide/South Australian Department for Water, Land and Biodiversity Conservation, PMB 2, Glen Osmond, Adelaide, SA 5064

² CRC-LEME/CSIRO Land and Water, PMB 2, Glen Osmond, Adelaide, SA 5064

³ CRC-LEME/University of Adelaide, North Terrace, Adelaide, SA 5000

In this study we combine soil data (soil mineralogy, morphology and chemistry), terrain and airborne radiometric K from a representative toposequence in an upland farming area near Spalding in the mid-north of South Australia to characterise and map complex soil-landscape patterns. These patterns, which were aggregated into distinct landscape soil units (LSUs) based on soil and landscape properties, govern the distribution of saline-sodic patterns in the landscape.

X-ray diffraction (XRD) analyses of the clay fraction (< 2 micron fraction) from representative soils from the LSU's indicate that layer silicates are dominated by either (i) co-dominant mica and smectite, or (ii) chlorite. Both mica and smectite are radiometric K-rich minerals, whereas chlorite is not a radiometric K-rich mineral. Airborne-based, high radiometric K response/co-dominant mica-smectite zones were found in toeslope/footslope areas, corresponding to deep alluvial sodic clay soils (LSU 4). Airborne-based, low radiometric K response/co-dominant mica-smectite zones were found in backslope areas, corresponding to leached sodic-saline duplex soils (i.e. loams over clays) (LSU 3). Chlorite dominated the soil-clay fraction higher in the toposequence. In these zones low radiometric K responses on shoulder slopes corresponded to sodic clays (LSU 2), while in crest zones, these radiometric patterns corresponded to shallow clay loams (LSU 1).

Soil data indicated that low radiometric K response soils (LSUs 1-3) were generally saline-sodic (EC_{se} 2.5 - 5.5 dS/m; ESP >5 at <1 m), whereas high radiometric K soils (LSU 4) were non-saline. By linking spatial patterns from soil data and landform, we propose that the reduced subsoil hydraulic conductivity of LSU 4 soils (due to sodic soil-clay fraction dispersion) impedes down-slope subsoil freshwater flows, creating a landscape-wide barrier to subsoil freshwater flushing. This in turn has led to salts being backed up and concentrated in the up-slope soils - particularly in the LSU 3 soils that are immediately up-slope. We conclude that these representative toposequence patterns may be used to predict saline-sodic soils in these types of landscapes.

REGIONAL PREDICTION OF SALT-AFFECTED SOILS IN AN AREA OF COMPLEX SOIL PATTERNS IN SOUTH AUSTRALIA

Mark Thomas¹, Rob W. Fitzpatrick² & Graham S. Heinson³

¹CRC LEME, University of Adelaide and South Australian Department for Water, Land and Biodiversity Conservation, PMB 2, Glen Osmond, SA, 5064

²CRC LEME, CSIRO Land and Water, PMB 2, Glen Osmond, SA, 5064

³CRC LEME, School of Earth and Environmental Sciences, University of Adelaide, SA, 5005

INTRODUCTION

Shallow Non-groundwater Associated Salinity (shallow NAS), which is described in Fitzpatrick *et al.* (in prep.), is found in upland parts of landscapes that have no direct contact with saline groundwater waterbodies, unlike Groundwater Associated Salinity (GAS). GAS is characterised in terms of catchment-scale hydrological processes, and is managed accordingly. Conversely, shallow NAS is characterised by localised soil patterns, which are governed by soil-landscape processes at various scales.

Shallow NAS soils feature: (i) high exchangeable sodium percentage (ESP) (i.e., are "sodic" and feature excessive Na⁺ ions on the exchange complex); and, (ii) high soluble salt concentrations (i.e., are "saline", generally featuring Na⁺ and Cl⁻ ions, and measured by EC_{se}), in the solum (i.e., A and B-horizons, typically < 1.2 m deep). In Australia, soils with ESP ≥ 5 are generally considered as being sodic (Rengasamy & Churchman 1999). These soils show signs of a decline in soil structure due to clay dispersion, which in turn creates waterlogging, hard-setting physical barriers to root growth, and poor gas transfer rates. Elevated EC_{se} values (i.e. ≥ 2 dS/m) give rise to droughting and toxic conditions in soils, which affect crop growth (Soil Survey Division Staff 1993). When sodicity and salinity combine through shallow NAS, the harmful effects on crops are magnified. Shallow NAS is strongly associated with texture contrast soils, which feature sandy/loamy A-horizons over sodic clay B-horizons. These are very important agricultural soils in southern Australia.

According to Rengasamy (2002), approximately A\$1,330 million of farm income is lost annually through shallow NAS in Australia. More locally, in the Northern Agricultural District (NAD) (302,000 ha) of South Australia, subsoil (i.e., 0.3-1.2 m) salts are a widespread problem. According to 1:100,000 scale State-wide soil mapping (Soil and Land Information 2002), > 15% of the NAD soils are affected by salinity (EC_{se} ≥ 2 dS/m) and > 60% by sodicity (ESP ≥ 6). Most of the saline areas spatially overlap with the sodic areas in the mapping, indicating that a significant proportion of the NAD is affected by shallow NAS. However, shallow NAS soils are difficult to map by conventional field-based soil-landscape survey methods (e.g., McDonald *et al.* 1998) because they form complex patterns with no apparent visual surface clues (e.g., colour, texture) (Thomas *et al.* 2003). For this reason, shallow NAS has not been mapped in South Australia at scales suitable for farm management planning (1:5,000 or larger).

Our aim is describe a GIS-based regional digital soil mapping methodology to predict shallow NAS for a small regional study area in the NAD.

REGIONAL STUDY AREA

The small regional study area (2,300 ha) is in an upland farming zone of the NAD (Figure 1). The average annual rainfall is 450 mm, of which approximately 75 % falls during the winter. Winters are cool and summers are hot, giving rise to a temperate, Mediterranean-type climate. The predominant agricultural land use in the area involves wheat, barley, canola and sheep grazing rotations.

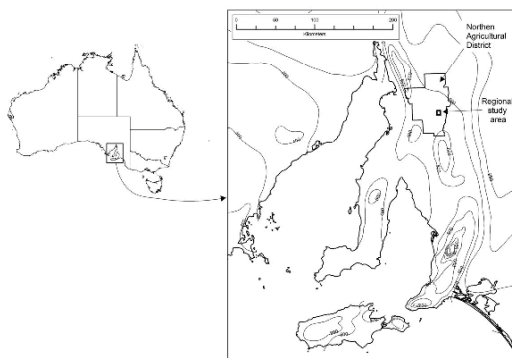


Figure 1: Map showing location of regional study area in Australia, featuring South Australia's Northern Agricultural District and rainfall zones.

The regional study area landscape features a north-south ridge system flanked by broad (> 8 km) valleys draining south. From this we selected a regionally representative toposequence area (121 ha) on the east-facing flank of the ridge. The toposequence was 1.5 km long and had a 100 m relief difference. As a consequence of the multi-factorial genesis of the soils reflecting the variable parent material (interbedded tillites, shales, quartzites, mudstones and siltstones), the toposequence can be described as being pedologically complex (Fitzpatrick *et al.* 2003). Essentially, all land in the toposequence area, and most of the regional area, has been cleared of native vegetation.

METHODS AND MATERIALS

Our approach was to combine multiscale soil and hydrological process models to predict, using a GIS, shallow NAS in the regional study area. The multiscale analyses were undertaken using field survey and laboratory methods, which were conducted at point (profile), plot (100 m²) and toposequence (121 ha) scales. The resulting datasets were used to display the main soil, regolith, geological and hydrological features in the toposequence using a cross-sectional, graphic format called a Conceptual Toposequence Model (CTM). At this stage the model was used to assess/display toposequence-scale soil-landscape variability, i.e., as a *descriptive* CTM (Fitzpatrick & Merry 2002) specifically related to shallow NAS toposequence expression. With the introduction of soil-landscape process knowledge from the multiscale investigations (e.g., solute transport pathways, shallow NAS zone processes), the *descriptive* CTM was transformed into an *explanatory* CTM (Fitzpatrick & Merry 2002). The final stage of the methodology involved spatially implementing the *explanatory* CTM, via a GIS, to make the regional shallow NAS predictions.

As discussed, three papers in preparation combine to fully document the whole regional predictive approach. In the first, Fitzpatrick *et al.* (in prep.) refine soil salinity concepts and definitions, and propose generic soil-process models. In the second, Thomas *et al.* (in prep.-a) describe at the point (profile), plot (100 m²) and toposequence (121 ha) scales, soil-landscape investigations to construct the soil and hydrological processes models. They also document the conceptual toposequence modelling in the regionally representative, shallow NAS-affected toposequence. In the third, Thomas *et al.* (in prep.-b) discuss the development and implementation of the regional predictive framework, via the conceptual toposequence modelling, to achieve the regional shallow NAS predictions.

Multiscale surveys and analyses

The multiple survey and analytical techniques used, and their scales and modes of application, are summarised in Table 1. Figure 2 is closely linked to Table 1 as it displays conceptually how the multiscale analyses and models connect to construct the *explanatory* CTM via the "model input" arrows and feedback loops. Figure 2 also highlights the links between the *explanatory* CTM and the GIS-based regional predictive framework, and the resulting regional shallow NAS predictions. Here we summarise the key outputs from the multiscale analyses, and briefly discuss the models that were developed.

Point scale (profile) investigations

Point scale surveys and analyses were used to determine spatial relationships between soil physico-chemical properties and to map the soils of the regionally representative toposequence area. Four landscape soil units (LSUs) were identified (Figures 2 and 3) (Thomas *et al.* 2003). Analysis of profile physico-chemical data showed that shallow NAS was confined to the LSU 3-types of soils on lower colluvial/alluvial slope landscape areas (Fitzpatrick *et al.* 2003).

Plot scale (100 m²) investigations

At plot scale (100 m²), we focused our investigations on morphological and chemical properties at the contact between the A and B-horizons by incorporating 3D GIS techniques (Figure 2). These investigations were conducted in two plots inside the LSU 3 soil area; one from a good crop yielding area (P1) and the other from a poor crop yielding area (P2) (Figures 2 and 3). The key soil properties investigated included EC_{se}, CEC, ESP and magnetic susceptibility.

No strong relationships were identified between the A and B-horizon contact shape and plot soil patterns. However, P1 (the good crop yielding area) generally had a thicker A-horizon (0.16-0.34 m) and was less saline (EC_{se} 0.4-0.7 dS/m), whereas P2 (the poor crop yielding area) generally had a thinner A-horizon (0.10-0.18 m), and was more saline (EC_{se} 0.7-1.4 dS/m). By taking landform positions into account (Figures 2 and 3) during interpretation of these findings, we were able to determine that P1 was likely to be more agriculturally productive because of the combination of (i) a higher water holding capacity (thicker A-horizon); and, (ii) a higher rate of freshwater flushing (leaching salts from the solum into downslope areas) due to the low-lying landscape position.

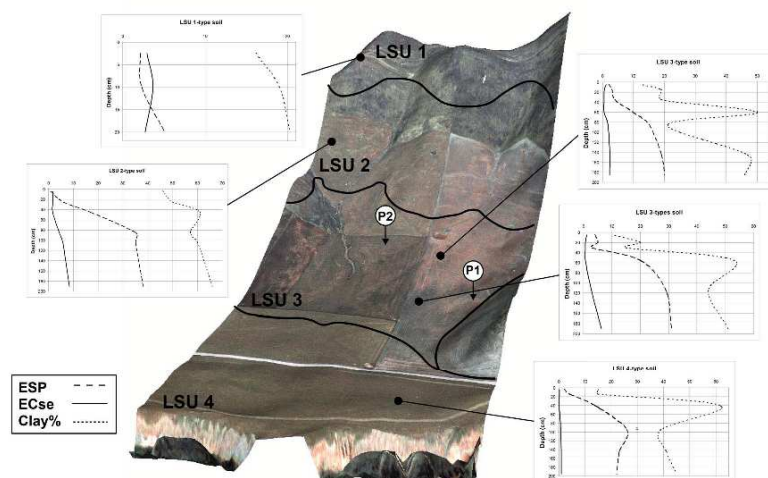


Figure 3: 3D aerial photo drape of the toposquence area with landscape soil unit boundaries, selected profile datasets showing ESP, EC_{se} and clay% by depth, and P1 and P2 sites indicated.

Regional prediction methodology

Given that we discovered that shallow NAS only featured in LSU 3 soils, and that our multiscale investigations revealed that not all LSU 3 soils were affected by shallow NAS, we focussed on the following two classes in our regional shallow NAS prediction methodology: LSU 3, shallow NAS affected; (i.e., "LSU 3 salty conditions"; Figure 2); and LSU 3 (i.e., "LSU 3 non-salty conditions", Figure 2).

Our approach was to extrapolate soil and hydrological patterns associated with shallow NAS from easily accessible and low-cost regional coverages. The extrapolation of these patterns was achieved through the spatial implementation of regional predictive framework (Figure 2). This procedure involved:

- Using soil data and knowledge from the *explanatory* CTM to identify regional coverages that have patterns that spatially corresponded with LSU 3 soils and shallow NAS and hydrological process patterns;
- Defining threshold values from these coverages that lend numeric expression to the patterns, "captured" in the form of a rules-based regional predicative framework (Figure 2); and,
- Spatially implementing the rules-based regional predicative framework via a GIS.

From the multiscale investigations, we identified the following regional coverages that corresponded with shallow NAS soil and hydrological patterns:

- Slope;
- Airborne radiometric K%;
- TWI; and,
- Plan curvature.

The final numeric model defining the predictive thresholds is presented in the regional predictive framework in Figure 2. Spatial implementation of the regional predictive framework was achieved using a GIS. The result is presented in the regional prediction in Figure 2.

Functionally, the regional predictive framework (Figure 2) uses slope to discriminate LSU 3 from LSU 2 soils, and airborne radiometric K% to discriminate LSU 3 from LSU 4 soils. In the LSU 3 areas, TWI drainage thresholds further discriminate between salt accumulation and salt flushing zones (i.e., LSU 3 shallow NAS vs. non-shallow NAS). Profile curvature is used to filter out convex landscape positions (e.g., crests and ridges) in LSU 3 areas.

Toposequence (141 ha) investigations

At toposequence scale (141 ha), investigations focused on the relationships between landform (based on terrain wetness index (TWI) and slope), surface and subsoil salt concentrations/clay distribution (EM38), soil-regolith salinity/clay distribution (EM31), surface volume magnetic susceptibility (κ) and surface mineralogy (airborne radiometric K%) in the toposequence area (Figure 2). The electromagnetic induction (EMI) techniques (EM38 and EM31) revealed strong soil-landscape patterns, which were visually linked to the landscape-wide distribution of shallow NAS and hydrological patterns (Figure 2) using 3D GIS techniques and soil data (e.g., Figure 3). We also found that κ patterns strongly correlated with those of EM38, which in turn linked to landscape drainage patterns. Our interpretation for these observations was that high EM38 values/high κ values corresponded with low solum freshwater flushing zones in the TWI coverage (Table 1). Wetness index patterns and soil data (Figure 3) confirmed this relationship. Thus, we concluded that EM38 and κ patterns were pedogenic expressions of solum freshwater flushing patterns.

Thomas *et al.* (2003) demonstrated the link between topsoil clay mineralogy and soil types. In that study they reported that airborne radiometric K% could be used to regionally map the boundary between the LSU 4 and LSU 3 soils (Figs. 2 and 3).

Conceptual toposequence model construction

Fritsch & Fitzpatrick (1994) and Fitzpatrick & Merry (2002) detail the construction and interpretation of CTMs. Figure 2 illustrates the connections and feedback loops (i.e., multiscale extrapolation/verification sequences) involved in the process of constructing the CTM through the spatial and conceptual integration of the multiscale investigations. In Figure 2, the CTM highlights the connections between: landform; parent material (geology); the four soils (LSUs 1 to 4); soil morphologies (horizons and structure); and soil-landscape hydrology (structure, nodules and water flow). Salt/solute pathways and processes (saline and sodic), which influence the expression of shallow NAS in the landscape, are also highlighted by the *explanatory* CTM.

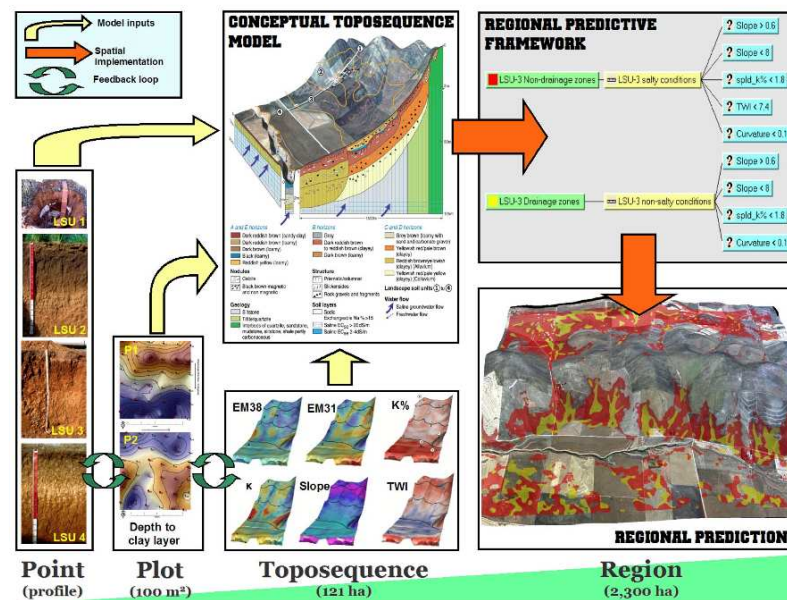


Figure 2: Links between point, plot and toposequence scale investigations and the construction of the *explanatory* CTM. The regional predictive framework shows the numeric thresholds for the GIS prediction. The regional predictions for shallow NAS (red areas)/non-shallow NAS (yellow areas) in LSU 3 soils is shown, overlaying a draped 3D rendition of the regional aerial photograph.

M. Thomas, R.W. Fitzpatrick & G.S. Heinson. *Regional prediction of salt-affected soils in an area of complex soil patterns in South Australia.*

Table 1: Summary of methods showing survey and analytical techniques used, their scale and mode of application, and key references.

Method	Instrument/ technique	Application	Potential soil-landscape attributes derived	Units / type	Key references	Application scale			
						Point (profile)	Plot (100 m ²)	Toposequence (121 ha)	Regional (>300 ha)
Electromagnetic induction (EMI)	EM38	Electromagnetic induction of soil-regolith profile; on foot, field-based	Combined soil profile salinity, texture and moisture; <1.5 m	Apparent EC (EC _a , dS/m)	(Mcneill 1980, Sudduth <i>et al.</i> 2001)		•	•	
	EM31		As above, plus including regolith and bedrock >6m					•	
Magnetic susceptibility	Bartington ME2B, dual frequency sensor	Mass magnetic susceptibility of soil layers; laboratory-based	Magnetic iron oxides [magnetite (α - Fe ₃ O ₄) and pedogenic maghemite (γ - Fe ₃ O ₄)].	χ	(Dearing 1999, Evans and Heller 2003)		•		
	Bartington ME2E, loop sensor	"Bulked" surface volumic magnetic susceptibility (< few cm ³); on foot	landscape/pedogenic processes, especially local wetting/drying conditions, leaching, burning	κ			•	•	
	Bartington ME2F, probe sensor	High spatial resolution surface volumic magnetic susceptibility (< few cm ³); on foot					•		
Gamma radiometrics	Regional airborne survey	Regional geochemical image of topsoil (K, Th, U, total count), GIS	Regional/toposequence soil-landscape process, mineral weathering, mineralogy, soil types	% (K), ppm (Th, U and total count)	(Dickson and Scott 1997, Minty 1997, Wilford <i>et al.</i> 1997)			•	•
	GR-320 spectral radiometer	High spatial resolution geochemical survey of topsoil (K, Th, U, total count), on foot	Soil-landscape processes, geochemical weathering history, local geochemical patterns					•	
Physico-chemical analysis	Extractive / digestive physico-chemical analysis	Multiple (>30) analyses; accurate	Soil chemistry, soil physical measurements; multiple other attributes	Various	(Rayment and Higginson 1992)	•	•	•	•
	Mid infrared (MIR) analysis	Multiple (>30) analyses; predictive, low cost, rapid			(Janik <i>et al.</i> 1998)		•		
	X-ray diffraction (XRD)	X-ray diffraction; accurate fine texturing	Clay mineralogy		(Olson <i>et al.</i> 2000)	•		•	
Digital terrain analysis	Aerial photographs; digital elevation models (DEMs)	Terrain attributes, soil-landscape methodology, 3D GIS overlays	Slope, curvature, terrain wetness index (TWI); terrain based 3D renderings	GIS raster	(Burrough and McDonnell 2000, Wilson and Gallant 2000)	•		•	•
Soil-landscape survey	Yield map	Yield	Soil-landscape processes, farm planning	GIS vector	(McDonald <i>et al.</i> 1998; Schoeneberger <i>et al.</i> 2002)		•	•	
	Soil survey method	Soil classification, soil-landscape methodology, soil mapping	Pedogenic processes, soil hydrology, land capability, soil mapping, multiple soil-landscape properties, field texture, etc...	Models, GIS raster		•	•	•	•

Validation of the LSU shallow NAS/non-shallow NAS predictions was undertaken using soil profile data from the point (profile) scale investigations from LSU 3 predicted areas. Figure 4 shows these, in which EC_{se} is plotted against depth. Here, 5 profiles from shallow NAS predicted areas (dotted lines), and 6 from non-shallow NAS predicted areas (solid lines) are plotted. The box inside the graph ("shallow NAS-affected soil profile zone") defines shallow NAS soils according to soil depth/EC_{se} thresholds (Fitzpatrick *et al.* in prep.). All profiles that intersect this box are shallow NAS-affected soils.

Figure 4 shows that all profiles from shallow NAS predicted areas (solid lines) intersect with the box, thus all have been correctly classified. All except for one profile from non- shallow NAS predicted areas (dotted) do not intersect with the box, making all except for one correctly classified as non-shallow NAS.

M. Thomas, R.W. Fitzpatrick & G.S. Heinson. *Regional prediction of salt-affected soils in an area of complex soil patterns in South Australia.*

Of the 2,300 ha regional study area, the regional predictive methodology classified 40% (744 ha) as being LSU 3 soils. Of this area, 75% of the area (654 ha) was classified as shallow NAS and 25% (190 ha) as non-shallow NAS.

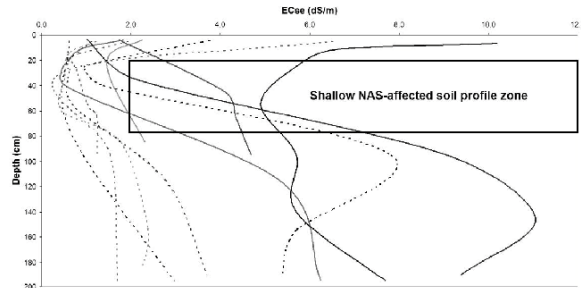


Figure 4: Profiles from plot scale investigations from LSU 3 shallow NAS predicted areas (solid lines) and profiles from LSU 3 non-NAS predicted areas (dotted lines) are plotted.

CONCLUSIONS

We have drawn together the themes of three papers in preparation, which, when combined, document the steps involved in the development of a GIS based regional methodology to predict shallow NAS. We have demonstrated the links between multiscale investigations to develop an *explanatory* CTM that highlights shallow NAS processes (e.g., salt/solute flows). In turn the *explanatory* CTM was used to develop a GIS-based framework for regional shallow NAS spatial predictions. The regional methodology is based on easy-to-acquire, cost-effective GIS coverages (DEM and regional airborne radiometric K%). Using this predictive methodology we show that, of the selected 2,300 ha high value farming region, approximately 30% (i.e., 75% of LSU 3 soils) is affected by shallow NAS.

New insights have been gained into the role of soil-landscape factors, like regional landform and drainage patterns, in governing the distribution of shallow NAS patterns at the toposequence scale. We have also demonstrated the value of combining, through GIS-based 3D terrain techniques, multiple: (i) geophysical surveys (e.g., terrain, EMI and κ); (ii) detailed field and laboratory data; (iii) airborne radiometric K% and, (iv) terrain modelling in developing soil-landscape models that underpin digital soil mapping methods that are likely to support farming decisions in landscapes with complex soil patterns.

Further work will investigate how our regional methodology to predict shallow NAS can be adapted for another high value farming area in a higher rainfall zone in South Australia.

Acknowledgements: We acknowledge the Cootes and Ashby families for access to their farmland.

REFERENCES

- BURROUGH P.A. & McDONNELL R.A. 2000. *Principles of Geographical Information Systems*. Oxford University Press Inc., New York.
- DEARING J.A. 1999. Magnetic Susceptibility. In: WALDEN J., OLDFIELD F. & SMITH J. eds. *Environmental Magnetism; a practical guide*. Quaternary Research Association, London, pp. 35-62.
- DICKSON B.L. & SCOTT K.M. 1997. Interpretation of aerial gamma-ray surveys - adding the geochemical factors. *AGSO Journal of Australian Geology & Geophysics* 17, 187-200.
- EVANS M.E. & HELLER F. 2003. *Environmental Magnetism: Principles and Applications of Enviromagnetics*. Academic Press, Burlington, Massachusetts.
- FITZPATRICK R.W. & MERRY R.H. 2002. Soil-regolith models of soil-water landscape degradation: development and application. In: MCVICAR T.R., RUI L., FITZPATRICK R.W. & CHANGMING L. eds. *Regional water and soil assessment for managing sustainable agriculture in China and Australia*. Australian Centre for International Agricultural Research, Canberra, pp. 130-138.
- FITZPATRICK R.W., THOMAS M., DAVIES P.J. & WILLIAMS B.G. 2003. Dry saline land: an investigation using ground-based geophysics, soil survey and spatial methods near Jamestown, South Australia.

- CSIRO, Adelaide.
- FITZPATRICK R.W., THOMAS M. & RENGASAMY P. in prep. Non-groundwater associated salinity (NAS) in an area of complex soil patterns in South Australia: Definitions and generic soil-landscape models.
- FRITTSCH E. & FITZPATRICK R.W. 1994. Interpretation of soil features produced by ancient and modern processes in degraded landscapes. I. A new method for constructing conceptual soil-water-landscape models. *Australian Journal of Soil Research* **32**, 889-907.
- JANIK L.J., MERRY R.H. & SKJEMSTAD J.O. 1998. Can mid infrared diffuse reflectance analysis replace soil extractions? *Australian Journal of Experimental Agriculture* **38**, 681-696.
- MCDONALD R.C., ISBELL R.F., SPEIGHT J.G., WALKER J. & HOPKINS M.S. 1998. *Australian soil and survey handbook*. Australian Collaborative Land Evaluation Program, Canberra.
- MCNEILL J.D. 1980. *Electrical conductivity of soils and rocks*. Geonics Ltd., Ontario, pp. 22.
- MINTY B.R.S. 1997. Fundamentals of airborne gamma-ray spectrometry. *AGSO Journal of Australian Geology & Geophysics* **17**, 39-50.
- OLSON C.G., THOMPSON M.L. & WILSON M.A. 2000. Phyllosilicates. In: SUMNER M.E. ed. *Handbook of Soil Science*. CRC Press, Boca Raton, Florida, pp. F77-F123.
- RAYMENT G.E. & HIGGINSON F.R. 1992. *Australian laboratory handbook of soil and water chemical methods*. Inkata Press, Melbourne.
- RENGASAMY P. 2002. Transient salinity and subsoil constraints to dryland farming in Australian sodic soils: an overview. *Australian Journal of Experimental Agriculture* **42**, 351 - 361.
- RENGASAMY P. & CHURCHMAN G.J. 1999. Cation exchange capacity, exchange cations and sodicity. In: PEVERILL K.I., SPARROW L.A. & REUTER D.J. eds. *Soil analysis: an interpretation manual*. CSIRO Publishing, Collingwood, Victoria, pp. 147157.
- SCHOENEBERGER P.J., WYSOCKI D.A., BENHAM E.C. & BRODERSON W.D. 2002. *Fieldbook for describing and sampling soils*. Natural Resources Conservation Service, National Soil Survey Center, Lincoln, NE, USA.
- SOIL AND LAND INFORMATION 2002. *Land Resource Information - Northern Agricultural Districts of South Australia*. SaLI Group, The Department of Water, Land and Biodiversity Conservation, Adelaide, South Australia.
- SOIL SURVEY DIVISION STAFF 1993. *Soil survey manual*. U.S. Government Printing Office, Washington.
- SUDDUTH K.A., DRUMMOND S.T. & KITCHEN N.R. 2001. Accuracy issues in electromagnetic induction sensing of soil electrical conductivity for precision agriculture. *Computers and Electronics in Agriculture* **31**, 239-264.
- THOMAS M., FITZPATRICK R.W. & HEINSON G.S. 2003. Mapping complex soil-landscape patterns using radiometric K₉₀: a dry saline land farming area case study near Jamestown, SA. In: ROACH I.C. ed. *Advances in Regolith*. CRC LEME, pp. 411-416.
- THOMAS M., FITZPATRICK R.W. & HEINSON G.S. in prep.-a. *Dry saline land in an area of complex soil patterns in South Australia: Identification and variability at plot and toposequence scales*.
- THOMAS M., FITZPATRICK R.W. & HEINSON G.S. in prep.-b. *Dry saline land in an area of complex soil patterns in South Australia: Identification and variability at regional scales*.
- WILFORD J.R., BIERWIRTH P.N. & CRAIG M.A. 1997. Application of airborne gamma-ray spectrometry in soil/regolith mapping and applied geomorphology. *AGSO Journal of Australian Geology & Geophysics* **17**, 201 - 216.
- WILSON J.P. & GALLANT J.C. 2000. Digital terrain analysis. In: WILSON J.P. & GALLANT J.C. eds. *Terrain analysis: principles and applications*. John Wiley & Sons Inc., New York, pp. 1-27.

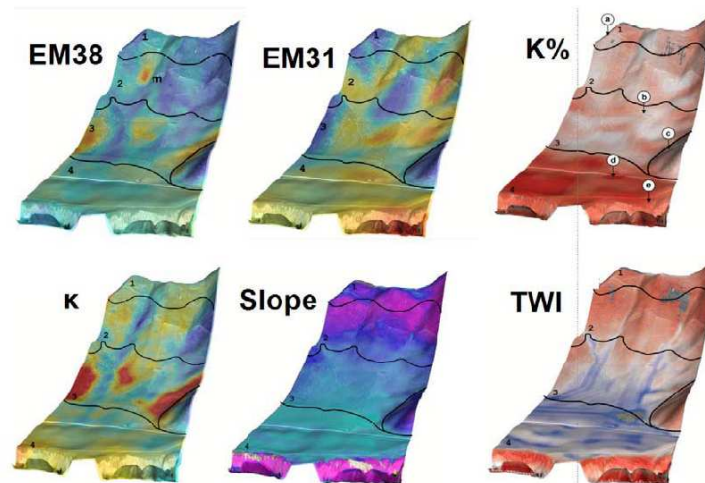


Figure 1 The 1.5 by 0.8 km study area toposequence with 3D overlays of geophysical survey and landform coverages with accompanying landscape soil units (LSUs). Coverages include: EM38 (peak EC_a at 0.75 m) and EM31 (peak EC_a at ~6 m), conductivity range from red (maximum) to blue (minimum); K%, concentration range from red (maximum) to white (minimum), including sample sites for mineralogy-XRD investigations (a-e); κ , susceptibility range from red (maximum) to blue (minimum); slope, angle range from magenta (steepest) to turquoise (flattest); and topographic wetness index (TWI), index range from blue (maximum downslope drainage/accumulation) to red (minimum downslope drainage/accumulation). The “m” in the EM38 coverage indicates likely near-surface mineralisation.

3 METHODS AND MATERIALS

3.1 Non-groundwater associated salinity, geophysical and terrain pattern relationships

Thomas *et al.* (2003) demonstrated the link between topsoil clay mineralogy and soil types, proposing that near-surface K % could be used to map the LSU 3 and 4 boundary. Furthermore, the authors conceptualised that the hydraulic conductivity change at the contact between the LSU 3 and 4 sola (i.e. the deep loamy A-horizons and the thin sodic clay A-horizons) results in freshwater soil-water flows, which contain salts leached from upslope areas, perennially backing-up into LSU 3 areas in winter. During summer when evaporation rates are high, the salts that have accumulated in LSU 3 areas as a consequence of the backed-up seasonal freshwater soil-water flows become more concentrated (i.e. $EC_{se} \geq 2$ dS/m) in the solum, creating the conditions for NAS.

The geophysical survey methods are reported elsewhere (e.g. Fitzpatrick *et al.*, 2003; Thomas *et al.*, 2003). These investigations focused on relationships in LSU 3 areas between (i) solum and regolith salt distributions from EC_a surveys (using, respectively, EM38 and EM31 ground conductivity meters), (ii) κ distributions, (iii) slope, and (iv) topographic wetness index (Figure 1). The topographic wetness index is a terrain analysis method that combines slope gradient, soil transmissivity and upslope contributing area to locate near-

surface saturation zones (Wilson and Gallant, 2000), which are indicative of surface and near-surface freshwater drainage and water accumulation zones. Hence low lying landscape positions with large contributing areas have large topographic wetness indices.

The physicochemical data showed strong correlation between NAS distribution, EM38 EC_a and κ survey patterns, and landform derived from slope and topographic wetness indices. With reference to Figure 1 we noted that low EM38 EC_a and low κ response patterns coincided with the distribution of large topographic wetness indices. In the case of EM38 EC_a , this relationship is explained through salts being leached out of the freshwater drainage zone sola, resulting in patterns of locally low EC_a values. For κ , the low response patterns in the drainage zones relates to the presence of hydromorphic conditions that dissolve ferromagnetic iron oxides, resulting in locally low κ patterns.

We conclude that EM38 EC_a and κ distributions are related to drainage patterns, and that the local concentration of freshwater solum drainage (identified from topographic wetness index patterns) determines the local presence of NAS in LSU 3 areas.

3.2 Conceptual toposequence model

Fritsch and Fitzpatrick (1994) describe methods to construct conceptual toposequence models. Based on these, Fitzpatrick *et al.* (2003) combined (i) physicochemical data, (ii) the geophysical surveys, (iii) the terrain analysis, (iv) geology and finally (v) the conceptualisations of NAS formation from the preceding section to develop the model shown in Figure 2. This model displays linkages between landform, parent material, LSUs, soil morphology (i.e. horizons and structure), and soil-landscape hydrology (structure, nodules and water flow). The model also illustrates salt and solute pathways that govern the expression of NAS.

4 CONCLUSIONS

The combination of (i) near-surface geophysical surveys of potassium concentration, soil apparent ground electrical conductivity, and surface volume magnetic susceptibility, (ii) terrain analysis, (iii) soil survey and physicochemical data, and (iv) the whole-of-landscape conceptual toposequence model have increased understanding of NAS-forming processes and distribution in a South Australian toposequence. We have identified that solum drainage, which is profoundly influenced by topography, governs NAS formation and distribution. In addition to terrain analysis, these patterns are also revealed through EM38 EC_a and volume magnetic susceptibility survey methods. Finally, the conceptual toposequence model gives a framework for collating and integrating multiple soil-landscape datasets, for conceptualising intricate soil-landscape relationships and processes, and for communicating this information to other researchers and land managers.

5 ACKNOWLEDGEMENTS

We acknowledge the kind co-operation of the Cootes and Ashby families who farm the study area, and the South Australian Salt Mapping and Management Support Program (which is part of the National Action Plan for Salinity and Water Quality) for access to airborne gamma radiometrics imagery. Mark Thomas wishes to acknowledge the assistance of the South Australian Department of Water, Land and Biodiversity Conservation for their research support.



18th World Congress of Soil Science
July 9-15, 2006 -
Philadelphia, Pennsylvania, USA



[Main Menu](#) | [Search](#) | [CD Help](#) | [Access the Technical Program](#)

Thursday, 13 July 2006

55-4

This presentation is part of [55: 1.3A New Frontiers in Soil Genesis - Oral](#)

Predicting Regional Complex Saline-Sodic Soil Patterns Using Geophysical, Hydropedological and Mineralogical Approaches That Translate Across Scales.

Mark Thomas, CRC-LEME/CSIRO Land and Water/Univ of Adelaide, Waite Road, Urrbrae, Adelaide, Australia, Robert Fitzpatrick, CRC-LEME/CSIRO Land and Water, Waite Road, Urrbrae, Adelaide, Australia, and Graham S. Heinson, CRC-LEME/Univ of Adelaide, Mawson Labs, North Terrance, Adelaide, Australia.

In this study, we use combined geophysical, mineralogical, terrain, and hydropedological approaches from representative toposequences to assess the scaling behaviour of variability in two saline-sodic soil-landscapes in upland South Australia. The complex patterns of spatial and temporal soil variation observed in these landscapes are the cumulative result of several geomorphological, hydrological and geochemical processes acting together. The soil-landscape process at one scale has a feedback to action at another scale. Consequently, spatial and temporal variations occur over several levels of scale and resolution, principally: (i) molecular (nano-scale), (ii) profile (point scale), (iii) plot (100 m²), (iv) toposequence (50 to 20,000 m), (v) catchment (100 to 500 ha) and (vi) regional scales (100 to 500 km²). In this paper two study areas were selected in a high rainfall zone (680 mm) and a low rainfall zone (475 mm) to study regional digital predictions of land degradation in high value rain fed farming areas via "upscaling" approaches. This approach was used to: (i) refine existing large scale soil maps (e.g. ~ 1: 5,000 scale) and reveal in more detail the distribution of the complex soil-landscape patterns, and (ii) identify near-surface hydropedological patterns featuring preferential water flow pathways within the complex soil-landscape patterns. The multiscale soil investigation approaches applied included: (i) near-surface geophysical surveys of potassium concentration (K %) and thorium (Th ppm) from gamma radiometrics, ground apparent electrical conductivity (ECa), and volume magnetic susceptibility ($\hat{\epsilon}$), (ii) soil survey (e.g. structural morphology) and physicochemical data (e.g. mineralogy, chemistry), and (iii) terrain analysis. The newly acquired hydropedological understanding for each of the study area landscapes underpinned: (i) construction of graphic 3D whole-of-landscape conceptual toposequence models that both highlighted and communicated more widely hillslope processes (e.g. soil types, soil morphological and salt distributions), and (ii) the development of rules-based frameworks to digitally predict (upscale) the distribution of saline-sodic patterns in nearby, regionally repeating toposequences. The application of the newly acquired hydropedological knowledge for each study area landscape played a key role by providing the conceptual link between the various scales of soil investigation that were conducted, allowing, for example, the fine scale soil system patterns to be aggregated to support interpretation of soil processes identified in more coarsely scaled soil system patterns. The application of hydropedological principles were successful in this respect because water movement is the common thread that influences (and links) the majority of processes within the hillslope soil systems investigated.



**18th World Congress of Soil Science
July 9-15, 2006 -
Philadelphia, Pennsylvania, USA**



[Main Menu](#) | [Search](#) | [CD Help](#) | [Access the Technical Program](#)

Thursday, 13 July 2006
74-2

*This presentation is part of 74: 2.4B Soil Mineralogy and Geophysics:
Environmental and Soils Management and Mineral Exploration -
Oral*

**Using Gamma-Ray Spectroscopy in Mineralogical and Geochemical Soil-
Regolith Investigations: Australian Case Studies from Depositional and
Erosional Landscapes.**

John R. Wilford, CRC-LEME/Geosciences Australia, Cnr Jerrabomberra Ave & Hindmarsh Drive, Symonston, Canberra, Australia, Mark Thomas, CRC-LEME/CSIRO Land and Water/Univ of Adelaide, Waite Road, Urrbrae, Adelaide, Australia, and Robert Fitzpatrick, CRC-LEME/CSIRO Land and Water, Waite Road, Urrbrae, Adelaide, Australia.

Gamma-ray spectrometry is a passive remote sensing technique that measures the natural emission of gamma-ray radiation in the upper 0.3 m of the earth's surface. The technique estimates the abundances of potassium (K), thorium (Th) and uranium (U) via the gamma-ray emitting isotopes of the ⁴⁰K, ²³²Th and ²³⁸U decay series, respectively. Conventionally, gamma-ray surveys are conducted using either low flying aircraft (e.g. regional surveys), or on foot/vehicle mounted (e.g. field and catchment surveys). Earth surface gamma-ray emissions relate strongly to the mineralogy and geochemistry of the bedrock and weathered materials (e.g. soils, saprolite, alluvial and colluvial sediments). The imagery generated can thus be regarded as surface geochemical maps of the distribution of rock, regolith and soil radionuclides. Where the bedrock contains K-bearing minerals, the loss of K in the soil can often be used as a surrogate for mapping the degree of surface weathering and leaching. Potassium is also associated with potassic clays such as illite, and in smaller amounts incorporated in the structure of clays (e.g. montmorillonite and kaolinite). In contrast, U and Th are often associated with more stable weathered constituents in the soil profile. Uranium and Th released during weathering are readily adsorbed to clay minerals, oxides (Fe and Al) and soil organic matter. Elevated U and Th can also be associated with resistate minerals. For the reasons discussed, Th and U concentrations often increase as K decreases during bedrock weathering and soil formation. In erosional landscapes the gamma-ray response strongly relates to the bedrock mineralogy and geochemistry, weathering history, and contemporary and ancient landscape processes. Soil gamma-ray responses in depositional landscapes reflect the geochemistry and mineralogy of the source rock (or regolith) from which the sediments are derived, and the post-depositional sorting and weathering processes. In both erosional and depositional landscapes, when the radioelement characteristic of the sources are well understood, gamma-ray data can be used to predict specific soil characteristics and provide information about erosional, depositional and weathering processes. This paper presents Australian case studies that feature the use of regional and field scale gamma-ray surveys as part of investigations to support prudent land use in upland saline landscapes. These case studies highlight the importance of integrating with the gamma-ray imagery auxiliary datasets (e.g. digital elevation models, soil and regolith electromagnetic conductivity, soil and geological mapping) to enhance the quality of soil-regolith information generated as part of the investigations. Soil-regolith information generated through these methods include new knowledge of

weathering histories, soil types and landscape evolution, and the location of deep profile salt stores.

Back to [2.4B Soil Mineralogy and Geophysics: Environmental and Soils Management and Mineral Exploration - Oral](#)
Back to [WCSS](#)

Back to [The 18th World Congress of Soil Science \(July 9-15, 2006\)](#)

Appendix B. Midnorth study area profile morphological data

SPJ_Appendix.txt
Summary of Profile data from Tom Cootes Property between Spalding and Jamestown, South Australia

L3324	13824			24SPME	H	44	Gs	RBEDr2.13SPJ	1A 1SS	TOM COOTES	RBE
Ag	0 14	5YR34	LS+	W2SB		D2	CSPJ	1A 4SS			
B1	14 28	5YR34	SCL	M4SB		D2	21CSPJ	1A 6SS 1			
B21	28 44	5YR34	CL	M5SB		T2	21CSPJ	1A 6SS 2			
BC	44	44RSA			54	KA	T	21A SPJ	1A 6SS 3		
L3324	13824							SPJ	1A 6SS 4		
				13SPME	H	45C	Cs	RBEDr2.13SPJ	1B 1SS	TOM COOTES	
Ag	0 11	5YR33	SCL-	W2SB		D2	MCSPJ	1B 4SS			
B21	11 19	5YR33	SC	M3SB		D2	11CSPJ	1B 6SS 1			
B22	19 33	5YR44	MHC	W5SB		T2	11 SPJ	1B 6SS 2			
B23	33 45	5YR44	MHC	5 SPME	DV	T2	11 SPJ	1B 6SS 3			
C1K	45 60	5Y52	ZL	KA	V	T2	5FN3	11 SPJ	1B 6SS 4		
C2K	60 75	5Y58	ZL	KA	V	T2		SPJ	1B 6SS 5		5S
C3K	75 100	5Y52	ZL	KA	V	T2		SPJ	1B 6SS 6		5S
C2	MAYBE SOIL HORIZON:										
L3324	13824							SPJ	1B 6SS 7		5S
								SPJ	1B 9SS		
				13 UQZ	H		C	RBEDr2.13SPJ	1C 1SS	TOM COOTES	
Ag	0 11	5YR48	SCL-	V		D2	CSPJ	1C 4SS			
A3	11 28	2.5YR36 11F	SCL	W4SB		22D2	1 CSPJ	1C 6SS 1			
B21	28 48	2.5YR34	MHC	S4AB		T3	1 CWSPJ	1C 6SS 2		5YR56	
B22	48 90	5YR48	MHC	S4AB		T3	1 D SPJ	1C 6SS 3			
B23k	90 110	5YR48	MHC	S4AB		T3	1 D SPJ	1C 6SS 4			
B24n	110 160	2.5YR36	MHC	S4AB		T3	D SPJ	1C 6SS 5			2S2
B25k	160 200	5YR48	MHC	S4AB		T3	4FL2	D SPJ	1C 6SS 6		
	196-200CM ACCUMULATION OF CARBONATE:										
L3324	13824							SPJ	1C 6SS 7		
								SPJ	1C 9SS		
				13 UQZ	H		C	RBEDr2.13SPJ	1D 1SS	TOM COOTES	
Ag	0 15	5YR44	SCL-	V		D2	CSPJ	1D 4SS			
A3	15 43	2.5YR36	SCL	W4SB		22D2	11CSPJ	1D 6SS 1			
B21	43 80	2.5YR34	MHC	S4AB		T3	11CSPJ	1D 6SS 2			
B22k	80 95	2.5YR36	MHC	S4AB		T3	11G SPJ	1D 6SS 3			
B25sb	95 120	2.5YR36 11F	MC	M4SB		T3	3FL2	11D SPJ	1D 6SS 4		
B2k	120 200	2.5YR36	MHC	S4AB		T5	3FL2	D SPJ	1D 6SS 5		3S2
	2B ZONE OF INCREASING CARBONATE:										
L3324	13824							3FL2	1D 6SS 6		2S2
								SPJ	1D 6SS 6		2S2
								SPJ	1D 9SS		
								SPJ	1E 1SS		
Ag	0 6	5YR34	SCLFS	0			C	RBEDr2.13SPJ	1E 4SS		
								CSPJ	1E 4SS		
								2G SPJ	1E 6SS 1		

Appendix B – Midnorth study area profile morphological data

SPJ_Appendix.txt													
A3	6	11	5YR33	SCLFS	M4SB	23T3		1G	SPJ	1E	6SS	2	
B1	11	20	5YR33	ZC	M4SB	12T3		1C	SPJ	1E	6SS	3	
B21	20	762.	5YR34	MHC	S3AB	12T6		1C	SPJ	1E	6SS	4	S5PR
B22k	76127		5YR38	MC	M4SB	12T3		D	SPJ	1E	6SS	5	3S2
B23	127200		5YR38	LC	W4SB	12T2			SPJ	1E	6SS	6	3S2
SODIC SUBSOIL ?:									SPJ	1E	9SS		
L3324	13824						A	BC	Uf6.31	SPJ	1F	1SS	
				0		H			CSPJ	1F	4SS		
Ap	0	6	5YR34	ZC	M3SB	22T		G	SPJ	1F	6SS	1	
B1	6	14	5YR33	ZC	M3SB	22T		G	SPJ	1F	6SS	2	
B21	14	64	5YR33	MHC	S3AB	22T		A	SPJ	1F	6SS	3	M5PR
B22k	64	95	5YR56	MHC	S3SB	12T		D	SPJ	1F	6SS	4	4C2
B23	95147		5YR48	MHC	M4SB	12T		D	SPJ	1F	6SS	5	2S2
B24	1471802.		5YR38	LMC	M4SB	12D		D	SPJ	1F	6SS	6	1S1
B25	180200		5YR66	LMC	M4SB	12D	1MS1		SPJ	1F	6SS	7	
SODIC SUBSOIL									SPJ	1F	9SS		
L3324	13824						A	BC	Uf6.31	SPJ	1G	1SS	
				0		H			CSPJ	1G	4SS		
Ap	0	7	5YR34	ZC	M3SB	D2		SPJ	1G	6SS	1		
B11	7	11	5YR33	ZC	M4SB	D4		SPJ	1G	6SS	2		
B21	11	672.	5YR34	MHC	S3AB	T6		SPJ	1G	6SS	3		M5PR
B22k	671072.		5YR46	LC	M4SB	T6	2FN2	SPJ	1G	6SS	4		3C2
B23	1071902.		5YR36	MHC	S3AB	D6	3FN2	SPJ	1G	6SS	5		1S1
L3324	13824						B	BC	Uf6.31	SPJ	1H	1SS	
A	2	6			12SPME	H			CSPJ	1H	4SS		
Ap	0	52.	5YR34	FSC	W2SB	22T2		SPJ	1H	6SS	1		
B1	5	97.	5YR33	FSC	M4SB	22D4		SPJ	1H	6SS	2		
B21	9	732.	5YR34	MHC	S3AB	22D6		SPJ	1H	6SS	3		
B22k	73114		5YR46	MHC	32 RME DM3SB	22D4		SPJ	1H	6SS	4		4S2
D1	114160		5YR46	CLFS	W4SB	22D6	2FN	SPJ	1H	6SS	5		2S1
D2	160200		5YR46	LMC	V4SB	22D6		SPJ	1H	6SS	6		2S1
90-95 & 110-115 HAVE NARROW META GRAVEL LENSES:									SPJ	1H	9SS		
L3324	13824						D	RBEDr2.33	SPJ	2A	1SS	TOM COOTES	
				13SPME	H				CSPJ	2A	4SS		
Ap	0	16	5YR44	SCL-	V	D3		11CS	SPJ	2A	6SS	1	
A2sb	16	50	5YR34	SCL-	V	22D3		11CS	SPJ	2A	6SS	2	
B21	50	822.	5YR34	MHC	S4AB	T4		11G	SPJ	2A	6SS	3	
B22k	821402.		5YR36	MHC	S4AB	T4	3FL2	C	SPJ	2A	6SS	4	2S2
2B	1401722.		5YR34	MC-	M4AB	T5		C	SPJ	2A	6SS	5	2S2
3B	1721902.		5YR36	MHC	S4SB	T5		SPJ	2A	6SS	6		2S2

Appendix B – Midnorth study area profile morphological data

SPJ_Appendix.txt										
4Bk	1902002.5YR34	MC-	M4AB	T5		SPJ	2A	6SS	7	2S2
L3324	13824				D	RBEDr2.33SPJ	2B	1SS	TOM COOTES	
			13SPME	H		CSPJ	2B	4SS		
Ap	0 14 5YR44	SCL-	V	D3		21 SPJ	2B	6SS	1	
A12	14 38 5YR34	SCL	W2SB	22D3		11 SPJ	2B	6SS	2	
A3sb	38 532.5YR36	CLS	W3SB	D5		11 SPJ	2B	6SS	3	
B21	531152.5YR34	MHC	S4AB	T5		11 SPJ	2B	6SS	4	
B22k	1151582.5YR36	MHC	S4AB	T5		11 SPJ	2B	6SS	5	2S2
2Bk	1581802.5YR34	MHC	S4AB	T5		SPJ	2B	6SS	6	2S2
3B	1802002.5YR36	MHC	S4AB	T5		SPJ	2B	6SS	7	2S2
L3324	13824				E	RBEGn3.13SPJ	2C	1SS	TOM COOTES	
			33 UQZ	H		CSPJ	2C	4SS		
Ap	0 15 5YR32	CLFS	W4SB	D3		21G SPJ	2C	6SS	1	
A3	15 232.5YR36	CL	M4SB	22D3		1G SPJ	2C	6SS	2	
B1	23 652.5YR32	LMC	M AB	22T5		1G SPJ	2C	6SS	3	
B21	651402.5YR32	MHC	S3AB	22T5		1G SPJ	2C	6SS	4	
B22k	1401702.5YR34	MHC	S3AB	22T5		G SPJ	2C	6SS	5	2C3
B23	1702002.5YR36	MHC	S3AB	22T5		SPJ	2C	6SS	6	1C3
						SPJ	2C	9SS		
MAYBE	OVERBURDEN FROM EROSION OR FILLED:									
L3324	13824				D	RBEDr2.33SPJ	2D	1SS	TOM COOTES	
			63 UQZ	H		CSPJ	2D	4SS		
Ap	0 127.5YR44	SCL-	W2SB	D4		CSPPJ	2D	6SS	1	
A2sp	12 52 5YR34	21F SCL	V	22D4		G SPJ	2D	6SS	2	5YR64
B21	521002.5YR36	MHC	S3AB	22T4		G SPJ	2D	6SS	3	
B22	1001182.5YR36	MHC	S3AB	22T4	3FN2	G SPJ	2D	6SS	4	2S1
B23	1181582.5YR36	MHC	43SPME DS3AB	22T4		G SPJ	2D	6SS	5	
B24	1581802.5YR36	MHC	23SPME DS3AB	22T4		G SPJ	2D	6SS	6	
B25k	180200 5YR46	MC	M3AB	T4		SPJ	2D	6SS	7	4S
L3324	13824				Gb	RBEDr2.33SPJ	2E	1SS	TOM COOTES	
						SPJ	2E	2SS		
020589			33 UQZ	H		CSPJ	2E	4SS		
Ap	0 10 5YR34	LS	W2SB	D3		22CSPPJ	2E	6SS	1	
A2sb	10 48 5YR42	LFS	V	23D2		11C SPJ	2E	6SS	2	
B21	48 882.5YR32	HC	43SPME DM2AB	23T4		11C SPJ	2E	6SS	3	
B22	881662.5YR46	MHC	V	23T4		11 SPJ	2E	6SS	4	
B23k	1662002.5YR32	MHC	S2AB	T5		SPJ	2E	6SS	5	3S3
L3324	13824				G	RBEDr2.13SPJ	2F	1SS	TOM COOTES	
			33 UQZ	H		CSPJ	2F	4SS		
Ap	0 14 5YR42	SL	W2SB	D3		12CSPPJ	2F	6SS	1	
A12	14 25 5YR46	FSL	V	23D3		11 SPJ	2F	6SS	2	

Appendix B – Midnorth study area profile morphological data

SPJ_Appendix.txt											
B21	25	522.5YR36	LC	32SPME	DW2SB	23T6	11	SPJ	2F	6SS 3	
B22	521102.	5YR36	MHC		M2AB	23T6		SPJ	2F	6SS 4	
B23k	1101832.	5YR46	MHC	12SPME	D	23T6		SPJ	2F	6SS 5	3S2
B24	1832002.	5YR36	MHC			23T6		SPJ	2F	6SS 6	
META ROCK QUARTSITE? AT 52CM 7CM DIAMETER:											
L3324	13824							SPJ	2F	9SS	
				33	UQZ	H		G	RBEDr2.13	SPJ	2G 1SS TOM COOTES
Ap	0	10	5YR42	SL	W2SB	D2		CSPJ	2G	4SS	
A12	10	322.	5YR36	SCL-	W3SB	D2		CSSPJ	2G	6SS 1	
A3	32	452.	5YR34	SCL-	W3SB	T4		G SPJ	2G	6SS 2	
B21	45	702.	5YR36	MHC	43SPME	DS3AB	T4	C SPJ	2G	6SS 3	
B22	70	882.	5YR36	MC	S3SB	T4		SPJ	2G	6SS 4	
B23k	882002.	5YR46	MC	M3SB	T2			SPJ	2G	6SS 5	
L3324	13824							SPJ	2G	6SS 6	4S
								G	RBEDr2.13	SPJ	3A 1SS TOM COOTES
030589								SPJ	3A	2SS	
Ap	0	12	5YR34	FSL	W2SB	22D3		CSPJ	3A	4SS	
A1	12	18	5YR34	SCL	W4SB	22D3	11	SPJ	3A	6SS 1	
A3	18	432.	5YR36	CLS	M4SB	21T5	11	SPJ	3A	6SS 2	
B1	43	622.	5YR36	HC	S4AB	21T5	11	SPJ	3A	6SS 3	
B21	62140	5YR36	HC	S3AB	21T5		11	SPJ	3A	6SS 4	
B22k	1402002.	5YR36	LMC	M3AB	T5			SPJ	3A	6SS 5	
APPEARS MORE LIKE A Gn3:											
L3324	13824							SPJ	3A	6SS 6	2S2
								G	RBEDr2.13	SPJ	3B 1SS TOM COOTES
Ap	0	8	5YR44	FSL	W3SB	22D3		CSPJ	3B	4SS	
A1	8	28	5YR43	SCLFS-	W3SB	21D3		22C SPJ	3B	6SS 1	
A3	28	44	5YR54	CLS	V	21T		11G SPJ	3B	6SS 2	
B21	44	972.	5YR34	MHC	S4AB	21T		11A SPJ	3B	6SS 3	
B22k	972002.	5YR46	MC	22SPME	DM4AB	21T		11G SPJ	3B	6SS 4	
L3324	13824							3FN2	SPJ	3B	6SS 5
								C	RBEDr2.13	SPJ	3C 1SS TOM COOTES
Ap	0	13	5YR42	SCLFS-	M2SB	H 135		CSPJ	3C	4SS	
B21	13	56	5YR34	LMC	S3AB	22		21C SPJ	3C	6SS 1	
B22k	56	82	5YR46	MHC	DS3AB	21		11C SPJ	3C	6SS 2	
BCK	82135	5YR58			DV	21		11C SPJ	3C	6SS 3	3S2
C	135200	2.5Y63	32D		DV			C SPJ	3C	6SS 4	4S2
L3324	13824							SPJ	3C	6SS 5	5S2
A	8	6						C	RBEDr2.13	SPJ	3D 1SS TOM COOTES
Ap	0	87.	5YR32	CL	M3SB	H 66		CSPJ	3D	4SS	
						22D2		21	SPJ	3D	6SS 1

Appendix B – Midnorth study area profile morphological data

SPJ_Appendix.txt										
A31	8 18	5YR34	CL	M3SB	22T4	11	SPJ	3D	GSS 2	
A32	18 28	5YR44	CL+	S4AB	21T4	11	SPJ	3D	GSS 3	
B2	28 57.2	5YR34	MHC	S4AB	21T4	11	SPJ	3D	GSS 4	
BC	57 66		MHC 32SPME	DS4AB	21T4	11	SPJ	3D	GSS 5	2s2
L3324	13824									
				43 UQZ	S 26		Cs L Dd3.13SPJ	3E 1SS	TOM COOTES	
Ap	0 4	5YR32	CL	M3SB	22T3		MECSPJ	3E 4SS		
BC	4 262.	5YR32	MHC 54SPME	DS1AB	22T3		GISPJ	3E 6SS 1		
L3324	13824						SPJ	3E 6SS 2		
1		T8MEUCAMEUCAL					D RBEDr2.33SPJ	3F 1SS	TOM COOTES	
				0	S		SPJ	3F 3SS		
A11	0 5	5YR23	L	S2SB	32M2		CSPJ	3F 4SS		
A12	5 10	5YR36	ZCL	W5SB	32T2		SPJ	3F 6SS 1		
A13	10 222.	5YR36	ZCL	W5SB	21D3		SPJ	3F 6SS 2		
A14	22 34	5YR48	ZCL	M4SB	21D6		SPJ	3F 6SS 3		
A2sb	34 46	5YR48	CLFS	W2SB	21D6		SPJ	3F 6SS 4		
B21	46 772.	5YR36	MHC	S3AB	21D6	2FL1	SPJ	3F 6SS 5	5YR64	
B22	771202.	5YR36	MHC	S3AB	21D6	2FL1	SPJ	3F 6SS 6		S5PR
2Asb	120130	5YR48	CLFS	W5SB	21D6	2FL1	SPJ	3F 6SS 7	5YR44	1S1
2B21	1301672.	5YR34	MHC	S3AB	21D6	2FL1	SPJ	3F 6SS 8	5YR64	1S1
2B22	1671882.	5YR38	MHC	S3AB	21D6	2FL1	SPJ	3F 6SS 9		1S1
2B23	1882002.	5YR36	MHC	S3AB	21D6	2FL1	SPJ	3F 6SS10		1S1
L3324	13824						C RBEDr2.13SPJ	4A 1SS	TOM COOTES	
A <1	6			0	H		CSPJ	4A 4SS		
Ap	0 9	5YR34	CL-	W3SB	22		1CSSPJ	4A 6SS 1		
A1	9 312.	5YR34	CL+	M4SB	22		1G SPJ	4A 6SS 2		
B21	31 772.	5YR34	MHC	S4	21		1G SPJ	4A 6SS 3		
B22k	77190	5YR46	MC	M4	21		D SPJ	4A 6SS 4		2s2
B23	190200	5YR48	MC	M4	21		SPJ	4A 6SS 5		1S1
CALCILICATE ROCK 70MM AT 110CM:										
L3324	13824						SPJ	4A 9SS		
				13 UKA	H		G RBEDr2.13SPJ	4B 1SS	TOM COOTES	
Ap	0 13	5YR43	LS	W4SB	22D2		CSPJ	4B 4SS		
A1	13 23	5YR43	LFS	S4AB	22D5		2G SPJ	4B 6SS 1		
B21	23 732.	5YR34	MHC	S5PR	21T6		1G SPJ	4B 6SS 2		
B22	73 862.	5YR34	MHC	M4AB	22T6		1S SPJ	4B 6SS 3		
B3k	86142	5YR46	SC	W5SB	32T4		C SPJ	4B 6SS 4		3s2
2B	1422002.	5YR34	MHC	S4AB	21T6		SPJ	4B 6SS 5		
CALCILICATE AT 163-166CM:										
L3324	13824						SPJ	4B 9SS		
							Gn Dr2.53SPJ	4C 1SS	TOM COOTES	

Appendix B – Midnorth study area profile morphological data

SPJ_Appendix.txt

Ap	0	87.5YR42	LFS	13 UQZ	H	CSPJ	4C	4SS	
B21	8	15 5YR33	LC	W3SB	22D2	C SPJ	4C	6SS 1	
B22	15	28 5YR34	LC	M4SB	22D3	SPJ	4C	6SS 2	
B23	28100	5YR46	LC 43 SKA	W3SB	21T2	SPJ	4C	6SS 3	
B24k	100200	5YR48	LC 32 SKA	DW3SB	21T2	SPJ	4C	6SS 4	
			LC	V	21T2	SPJ	4C	6SS 5	
CALCILICATE COARSE FRAGMENTS AT 15-28; 85-90; SODIC? :									
L3324	13824					SPJ	4C	9SS	
				13SPSL	SLS 20	F	Um6.41SPJ	4D	1SS TOM COOTES
Ap	0	87.5YR32	ZCL	W3SB	4	KACSPJ	4D	4SS	
A12	8	207.5YR32	ZCL+	W5SB	4	G SPJ	4D	6SS 1	
L3324	13824					SPJ	4D	6SS 2	
						A	BC Uf6.31SPJ	5	1SS
Ap	0	6 5YR36	LC	W3SB	23M3	CSPJ	5	4SS	
B1	6	18 5YR38	LMC	W3SB	23M3	2C SPJ	5	6SS 1	
B21	18	63 5YR34	MHC	S AB	22T6	1G SPJ	5	6SS 2	
B22	631002.	5YR36	MHC	S AB	21D6	1G SPJ	5	6SS 3	S5PR
B23	100158	5YR36	MHC	S AB	21D6	1C SPJ	5	6SS 4	
B24	158166	5YR46	LC	V	21D6	1C SPJ	5	6SS 5	
2B21	1661782.	5YR36	MHC	S AB	21D6	1C SPJ	5	6SS 6	2S1
2B22	1782462.	5YR36	MHC	S AB	21D6	1G SPJ	5	6SS 7	2S1
2B23	246253	5YR46	LC	V	21D6	1C SPJ	5	6SS 8	2S2
3B21	253338	5YR48	MHC	S AB	21D6	1C SPJ	5	6SS 9	3S1
3B22	338370	5YR46	LC	V	21D6	1G SPJ	5	6SS10	3S1
AT 173-178	LARGE	CALCILICATE:				1 SPJ	5	6SS11	3S1
L3324	13824					SPJ	5	9SS	
						C	RBEDr2.13SPJ	5A	1SS TOM COOTES
Ap	0	10 5YR34	CL	M4SB	H	CSPJ	5A	4SS	
A3	10	22 5YR44	CL+	W4SB		21G SPJ	5A	6SS 1	
B21	22	962.5YR34	MHC	S4AB		11C SPJ	5A	6SS 2	
B22	961302.	5YR36	MHC	S4AB		11 SPJ	5A	6SS 3	
B23n	130173	10R36	MHC	S4AB		11 SPJ	5A	6SS 4	3S2
B24k	1732002.	5YR36	MHC	21SPME DS4AB		4FN2 SPJ	5A	6SS 5	
L3324	13824					3FN2 SPJ	5A	6SS 6	4S2
A	4	6				D	RBEDr2.33SPJ	5B	1SS TOM COOTES
Ap	0	8 5YR34	CL	W3SB	H 200	CSPJ	5B	4SS	
A2sb	8	25 5YR34	CLFS	V	22D2	22G SPJ	5B	6SS 1	
B21	23	772.5YR33	MHC	S4AB	22D3	11C SPJ	5B	6SS 2	
B22	771252.	5YR33	MHC	S4AB	21T6	11 SPJ	5B	6SS 3	
B23	125170	5YR58 42D	LMC	12SPME DM4SB	21T3	11 SPJ	5B	6SS 4	3S2
						SPJ	5B	6SS 5	5YR68 3S2

Appendix B – Midnorth study area profile morphological data

Bck		170200		22SPME		D		SPJ_Appendix.txt		SPJ		5B		6SS		6		4s2	
L3324	13824								D	RBEDr2.33	SPJ	5C	1SS	TOM	COOTES				
Ap	0	9	5YR44	CL		W3SB		H	22D2	21C	SPJ	5C	6SS	1					
A2sb	9	30	5YR43	LC-		V			22D3	21C	SPJ	5C	6SS	2					
B21	30	552.	5YR24	MHC		S3AB			21T6	11	SPJ	5C	6SS	3					
B22	55	702.	5YR34	MHC		S3AB			21T5	11	SPJ	5C	6SS	4					
B23k	70110		5YR48	MHC		W3SB			21T3		SPJ	5C	6SS	5					5s2
B24	110162		10R36	MHC		S3AB			T3	3FN2	SPJ	5C	6SS	6					4s2
B31	1621672.		5YR24	LMC	33SPME	DV			T3		SPJ	5C	6SS	7					5s2
B32	167200		5YR48	LMC		W3SB			T3		SPJ	5C	6SS	8					5s2
L3324	13824									C	RBEDr2.13	SPJ	5D	1SS	TOM	COOTES			
Ap	0	10	5YR34	SCL		W3SB	13	H	22D2	2	SPJ	5D	6SS	1					
A1	10	242.	5YR36	CLS		W4SB			22D3	1	SPJ	5D	6SS	2					
A3	24	392.	5YR36	CLS		W4SB			22D3	1	SPJ	5D	6SS	3					
B21	39	742.	5YR34	MHC		S3SB			21T6	1	SPJ	5D	6SS	4					
B22	741152.		5YR36	MHC		S3SB			21T6		SPJ	5D	6SS	5					3s2
B23	1151182.		5YR36	MHC	23SPME	DS3SB			21T6		SPJ	5D	6SS	6					2s2
B24n	118152		10R36	MC		S3SB			21T5	2FN2	SPJ	5D	6SS	7					2s2
B25k	1522002.		5YR36	LMC		W3AB			T2	4FN2	SPJ	5D	6SS	8					4s2
WEAK SPORADIC BLEACHING ON TOP OF B2:																			
L3324	13824									C	RBEDr2.13	SPJ	5E	1SS	TOM	COOTES			
A	6						13	H			CSPJ	5E	4SS						
Ap	0	8	5YR34	SCL-		W3SB			22D2	2C	SPJ	5E	6SS	1					
A31	8	33	5YR34	CLS		W4SB			22D4	1	SPJ	5E	6SS	2					
A32	33	502.	5YR36	CLS+22	SME	DW3SB			21T4	1	SPJ	5E	6SS	3					
B21	50	872.	5YR34	MHC		S3AB			21T6	1	SPJ	5E	6SS	4					
B22	871142.		5YR34	MHC	42SPME	DS3AB			21T6		SPJ	5E	6SS	5					2s2
B23	1141442.		5YR36	MHC		S3AB			21T6		SPJ	5E	6SS	6					2s2
B24n	1401602.		5YR36	MHC		S3AB			T6	3FN2	SPJ	5E	6SS	7					2s2
B25k	1602002.		5YR46	MC		M3SB			T3		SPJ	5E	6SS	8					5s2
WEAK SPORADIC BLEACHING ON TOP OF B2:																			
L3324	13824									C	RBEDr2.13	SPJ	5F	1SS	TOM	COOTES			
A	8						13	H			CSPJ	5F	4SS						
Ap	0	10	5YR34	SCL		M3SB			23D2	2	SPJ	5F	6SS	1					
B11	10	36	5YR33	LMC		V			23D3	1	SPJ	5F	6SS	2					
B12	36	522.	5YR36	SC		V			22T6	1	SPJ	5F	6SS	3					
B21	52	732.	5YR34	MHC	22	AQZ	DS3AB		21T6	1	SPJ	5F	6SS	4					
B22	73	82		MHC	32SPME	DM3AB			21T6	1	SPJ	5F	6SS	5					

Appendix B – Midnorth study area profile morphological data

SPJ_Appendix.txt										
B23	82	892.5	YR36	MHC	S3AB	21T6	1	SPJ	5F 6SS 6	2s2
B24	891132.	5YR36		MHC	M2SB	21T2		SPJ	5F 6SS 7	4s2
B25k	1132002.	5YR68		MHC	M2SB	T2		SPJ	5F 6SS 8	5s2
L3324	13824							C	RBEDr2.13SPJ	5G 1SS TOM COOTES
14	6				13SPME	H 175		CSPJ	5G 4SS	
Ap	0	8	5YR42	SCL-	W2SB	22D2		SPJ	5G 6SS 1	
A1	8	302.	5YR44	SCL	21 AQZ DV	22D3		SPJ	5G 6SS 2	
B21	30	432.	5YR34	HC	V	22T5		SPJ	5G 6SS 3	
B22	43	662.	5YR46	HC	S3AB	21T5		SPJ	5G 6SS 4	
B23	661162.	5YR33		HC	S3AB	21T5		SPJ	5G 6SS 5	2s2
B24	1161412.	5YR33		HC	S3AB	21T5	4FN2	SPJ	5G 6SS 6	1s2
B25k	141175	5YR46		LC	W3SB	21T2		SPJ	5G 6SS 7	4s2
C	175200	5Y63		LC	V	T2		SPJ	5G 6SS 8	4s2
SHALE	GRAVEL	AT 116-119	:							
L3324	13824							B	Uf6.32SPJ	5H 1SS TOM COOTES
A 19	6				0	S 98		ME	SPJ 5H 4SS	R
Ap	0	87.	5YR32	MC	S2AB	23T3		G	SPJ 5H 6SS 1	
B21	8	16	10YR22	MC	M4AB	23T3		SPJ	5H 6SS 2	
B22	16	63	5YR33	MHC	S4AB	22T3		SPJ	5H 6SS 3	
B23	67	78	5YR46	MHC	S4AB	22T4		SPJ	5H 6SS 4	2s2
Bck	78	98	5YR58		M	T4		SPJ	5H 6SS 5	3s2
ck	98105				32SPME D			SPJ	5H 6SS 6	4s2
L3324	13824							Ab	Uf4.41SPJ	6 1SS
<1	6				0	H		CSPJ	6 4SS	
Ap	0	8	5YR44	ZC	M3SB	32M1		2C	SPJ 6 6SS 1	
A2	8	19	5YR38	LC	M4SB	32D6		1C	SPJ 6 6SS 2	5YR88
B21	19	662.	5YR35	MHC	S3AB	21T6		1G	SPJ 6 6SS 3	S4PR
B22k	66	85	5YR46	MHC	S3AB	21T4		1	SPJ 6 6SS 4	4s2
B23	85158	5YR33	22D	MHC	S3AB	21T4	2FL1	1	SPJ 6 6SS 5	5YR32
B24	158200	5YR46		LC	23 UKA DS3AB	21T4		1	SPJ 6 6SS 6	3s2
L3324	13824							E	Gn3.13SPJ	6A 1SS TOM COOTES
Ap	0	87.	5YR32	SCLFS	W4SB	32D3		CSPJ	6A 4SS	RBE
B21	8	60	5YR34	LC	S3SB	22D3		22C	SPJ 6A 6SS 1	
B22	60	78	5YR44	CL	W5PR	22D4		11D	SPJ 6A 6SS 2	S4PR
2Bk	78119	5YR54		CL	V	21D4	1FN1	11	SPJ 6A 6SS 3	
2B	119144	5YR46		LC	M4SB	21D4		11	SPJ 6A 6SS 4	4s3
3A	144176	5YR48		CS	V	21D4	2MS2		SPJ 6A 6SS 5	2s3
3B	1762002.	5YR36		CLS	W4SB	21D4			SPJ 6A 6SS 6	1s3
APPEARS TO BE LAYERED SOIL:										
									SPJ	6A 9SS

Appendix B – Midnorth study area profile morphological data

```

L3324 13824
Ap 0 117.5YR32 CL 1 UKA H C 60 Um6.41SPJ 6B 1SS TOM COOTES R
A1 11 227.5YR32 CL- KA M3SB 22D2 MECSPJ 6B 4SS
B3k 22 607.5YR74 SCLKS 32 SH V 21D2 C SPJ 6B 6SS 1
C11 60 732.5YR44 SCLKS 32 SH V 21D2 A SPJ 6B 6SS 2 4S4
C12 731007.5YR76 SCLKS 32 SH V D2 A SPJ 6B 6SS 3 5S4
L3324 13824 SPJ 6B 6SS 47.5YR74 4S4
A 12 6 33SPKA H C 30 Um6.41SPJ 6C 1SS TOM COOTES R
Ap 0 127.5YR32 CL M3SB 22D1 SHCSPJ 6C 4SS
A 12 217.5YR32 CL- W3SB 22D1 2C SPJ 6C 6SS 1 2S3
B3k 21 30 32 KA DV 21D2 1C SPJ 6C 6SS 2 2S3
C 30 62 32SPSH DV D2 C SPJ 6C 6SS 3 3C3
CALCAREOUS THROUGHOUT: SPJ 6C 6SS 4 5S2
L3324 13824 E RBEGn3.13SPJ 6D 1SS TOM COOTES
A 8 6 13 UKA H C 60 KACSPJ 6D 4SS
Ap 0 8 5YR34 CL W3SB 22D3 2C SPJ 6D 6SS 1
A1 8 172.5YR34 CL+ W3SB 22D3 2C SPJ 6D 6SS 2
B21 17 482.5YR34 LMC S3AB 21T3 1D SPJ 6D 6SS 3 5 54PR
B22k 48 602.5YR34 S3AB T3 SPJ 6D 6SS 4
CARBONATE STOPPED PENETRATION (52-60): SPJ 6D 9SS
L3324 13824 E RBEGn3.13SPJ 6E 1SS TOM COOTES
A 7.5 6 0 H 22D4 CSPJ 6E 4SS
Ap 0 8 5YR34 CL W4SB 22D4 22C SPJ 6E 6SS 1
B1 8 18 5YR34 LC M5SB 22D4 11D SPJ 6E 6SS 2
B21 18 58 5YR33 MHC 12 AQZ D 21D4 11D SPJ 6E 6SS 3 5 55PR
B2k 58200 5YR48 LC 12 AQZ D 21D2 2FN2 SPJ 6E 6SS 4 4S3
L3324 13824 Gb RBEDr2.33SPJ 6F 1SS TOM COOTES
A 5 6 0 H 22M2 CSPJ 6F 4SS
Ap 0 10 5YR34 SL M3SB 22D2 22C SPJ 6F 6SS 1
A3 10 31 5YR34 CLS W5AB 22D2 11C SPJ 6F 6SS 2
B21 31 69 5YR32 MHC 22SPSH DS3AB 21T6 11 SPJ 6F 6SS 3 5 55PR
B22 69110 5YR34 MHC 22SPSH DS3AB 11T6 SPJ 6F 6SS 4 2S2
B23 1101402.5YR36 MHC S3AB 11T6 2FN2 SPJ 6F 6SS 5 4S2
B24n 1401682.5YR36 MHC S3AB 11T6 4FN2 SPJ 6F 6SS 6 3S2
B25k 1682002.5YR36 MHC S3AB 11T6 SPJ 6F 6SS 7 4S2
50MM QUARTZITE GRAVEL AT 27-31;WEAK BLEACH ON BOTTOM OF A;168-200 LENSESPJ 6F 9SSS OF META GRAVELS:
L3324 13824 G RBEDr2.13SPJ 6G 1SS TOM COOTES
A 9 6 13 SQZ H 33D2 CSPJ 6G 4SS
Ap 0 8 5YR34 SL W3SB 33D2 2C SPJ 6G 6SS 1

```

Appendix B – Midnorth study area profile morphological data

SPJ_Appendix.txt

A12	8	17	5YR56	FSL		W4SB	33D3		2D	SPJ	6G	6SS	2				
A13	17	37	5YR56	FSL	21	AQZ	DW4SB	22D6	2FN	1C	SPJ	6G	6SS	3			
B21	37	522.	5YR32	MHC		S3AB	21D6				SPJ	6G	6SS	4	2.5YR36	S5PR	
B22	52	752.	5YR36	MHC		S3AB	21T6				SPJ	6G	6SS	5			
B23	75100		5YR46	MHC	31	SPME	DW4SB	21T6	3FN2		SPJ	6G	6SS	6		3S2	
B24	1001232.		5YR36	MHC		S3AB	21T6				SPJ	6G	6SS	7		2S2	
B25	1231582.		5YR36	MHC		S3AB	21T6				SPJ	6G	6SS	8		2S2	
B26	1581672.		5YR36	MHC	21	AQZ	DS3AB	21T6			SPJ	6G	6SS	9		1S2	
B27k	1672002.		5YR36	MHC		S3AB	21T6				SPJ	6G	6SS	10		3S2	
120-123 QUARTZITE GRAVELS; SHALE AT 153-158; 167-200 LAYERS OF IRONSTONE												SPJ	6G	9SS	GRAVEL AND SHALE:		
L3324	13824								C	RBEDr2.13	SPJ	6H	1SS	TOM	COOTES		
A	9	6					13SPSL		H		CSPJ	6H	4SS				
Ap	0	8	5YR34	SCL-12	AQZ	DM3SB	22T2			22C	SPJ	6H	6SS	1			
A3	8	14	5YR44	CLFS	22	AQZ	DW4SB	22D3		22C	SPJ	6H	6SS	2			
B21	14	47	5YR34	MHC	2		S3AB	21T6		11	SPJ	6H	6SS	3		S3PR	
B22	471502.		5YR46	MHC	12	UQZ	DS3AB	21T6		11	SPJ	6H	6SS	4		2S2	
B23	1501582.		5YR46	MHC			S3AB	21T6			SPJ	6H	6SS	5			
B24	1581702.		5YR46	MHC			S3AB	21T6			SPJ	6H	6SS	6		1S2	
B25k	1702002.		5YR48	MHC	22	UQZ	DS3AB	21T6			SPJ	6H	6SS	7		4S2	
ODD QUARTZITE GRAVEL THROUGH B22; 147-157 IRONSTONE AND QUARTZ GRAVELS;												SPJ	6H	9SS	WEAK SPORADIC BLEACH:		
L3324	13824								Gg	RBEGn3.19	SPJ	6I	1SS	TOM	COOTES		
A	11	6					13SPSL		H		CSPJ	6I	4SS				
Ap	0	10	5YR34	SL			W3SB	22T2		2C	SPJ	6I	6SS	1			
A3	10	35	5YR46	SCL			W4SB	22D2		1D	SPJ	6I	6SS	2			
B1sb	35	50	5YR46	32D	SC		W4SB	21	4	2D	SPJ	6I	6SS	3	5YR52		
B21	501002.		5YR36	MHC			S3AB	21	6	2FS2	G	SPJ	6I	6SS	4		S5PR
B22k	1001482.		5YR36	MHC			S3AB	21	6	2FS2	G	SPJ	6I	6SS	5		4S2
B23	1482002.		5YR36	LMC			M4AB	31	4	2FS2		SPJ	6I	6SS	6		2S2
98-100 QUARTZITE 50MM GRAVEL:												SPJ	6I	9SS			
L3324	13824								G	RBEDr2.12	SPJ	6J	1SS	TOM	COOTES		
A	14	6					35	SQU	H		CSPJ	6J	4SS				
Ap	0	87.	5YR34	LFS			M4SB	22T2	1FN2	22C	SPJ	6J	6SS	1			
A1	8	23	5YR34	CLFS			W4SB	22D4	1FN2	21D	SPJ	6J	6SS	2			
A2sb	23	34	5YR36	SCL			W4SB	21D4	1FN2	11C	SPJ	6J	6SS	3	5YR64		
B21	34	60	5YR33	MHC			S3AB	21T6	1FN2	11	SPJ	6J	6SS	4		S5PR	
LARGE QUARTZ GRAVEL - LIME FREE PROFILE:												SPJ	6J	9SS			
L3324	13824								Ab	BC	Uf4.41	SPJ	7	1SS		BC	
<1	6							0	H	60		CSPJ	7	4SS			
Ap	0	8	5YR44	ZC			W3SB	22M1			3G	SPJ	7	6SS	1		
A2	8	18	5YR36	ZC			M4SB	22D2			2	SPJ	7	6SS	2		

Appendix B – Midnorth study area profile morphological data

SPJ_Appendix.txt															
B21	18	852.	5YR34	MHC		S3AB	21T5		1	SPJ	7	GSS	3		S4PR
B22k	85128		5YR36	MHC	32 UKA	DS3AB	21T5		1	SPJ	7	GSS	4	4S2	
B23	1281732.		5YR36	MHC		S3AB	21T6			SPJ	7	GSS	5	1S2	
B24n	173195		5YR48	MHC		V	21T5	3FN2		SPJ	7	GSS	6	4S2	
B25	195200		5YR36	LC			21	4FN2		SPJ	7	GSS	7	2S2	
L3324	13824							G	RBEDr2.13	SPJ	7A	1SS	TOM	COOTES	
					0		H			CSPJ	7A	4SS			
Ap	0	8	5YR46	LFS		w4SB	22T2			22C	SPJ	7A	GSS	1	
A1	8	13	5YR46	ZL		V	11D4			11	SPJ	7A	GSS	2	
A3	13	202.	5YR46	CL		V	11D4			11	SPJ	7A	GSS	3	
B21	20	73	5YR33	MHC		S3AB	11T6			11	SPJ	7A	GSS	4	
B22k	73124		5YR44	MHC		S AB	11T6			11	SPJ	7A	GSS	5	4S2
B23	1241652.		5YR46	MHC		S AB	11T6				SPJ	7A	GSS	6	5S2
B24	165200		5YR46	LC		w4SB	11D2				SPJ	7A	GSS	7	4S2
L3324	13824							C	RBEDr2.13	SPJ	7B	1SS	TOM	COOTES	
					0		H			CSPJ	7B	4SS			
Ap1	0	6	5YR36	ZCL		w4SB	22T3			2	SPJ	7B	GSS	1	
Ap2	6	12	5YR44	ZCL+		w4SB	21D4			2	SPJ	7B	GSS	2	
B21	12	62	5YR33	MHC		S3AB	11T6				SPJ	7B	GSS	3	S5PR
B22	62	78	5YR36	MHC		S3AB	11T6				SPJ	7B	GSS	4	
2Bk	78110		5YR34	22D		S3AB	11T6				SPJ	7B	GSS	5	10YR31
2B	110150		5YR44	22D	MC 21	KA	S3AB	11T6			SPJ	7B	GSS	6	10YR31
2B	150200		5YR46	MC 21	KA	M4SB	11D5				SPJ	7B	GSS	7	4S2
L3324	13824							C	RBEDr2.13	SPJ	7C	1SS	TOM	COOTES	3S2
					0		H			CSPJ	7C	4SS			
Ap	0	8	5YR36	ZL		w4SB	D2			C	SPJ	7C	GSS	1	
A1	8	18	5YR34	ZCL		w4SB	D4			G	SPJ	7C	GSS	2	
A3	18	282.	5YR36	ZCL		M3AB	T6			D	SPJ	7C	GSS	3	
B21	28	712.	5YR34	MHC		S3AB	T6			A	SPJ	7C	GSS	4	
B22k	711002.		5YR36	MHC		S3AB	T6				SPJ	7C	GSS	5	4S2
B23	1001542.		5YR36	MHC		V	T3				SPJ	7C	GSS	6	
B24	1541852.		5YR38	MC		V	T3	3FN2			SPJ	7C	GSS	7	
											SPJ	7C	9SS		
CORE STUCK IN TUBE B23 APPROXIMATE DEPTH:								Cn	RBEDr2.12	SPJ	7D	1SS	TOM	COOTES	
L3324	13824									CSPJ	7D	4SS			
A	2	6					H								
Ap	0	10	5YR34	SCLFS-		V	22T2			C	SPJ	7D	GSS	1	
B1	10	242.	5YR36	CLS		w4SB	22D4			G	SPJ	7D	GSS	2	
Bsb	24	462.	5YR36	CLS		w4SB	21D5			C	SPJ	7D	GSS	3	
2B21	46	652.	5YR24	CLS		S AB	21D5			G	SPJ	7D	GSS	4	S5PR
2B22	65	882.	5YR38	MHC		S AB	21T5			G	SPJ	7D	GSS	5	

Appendix B – Midnorth study area profile morphological data

SPJ_Appendix.txt

2B23	881562.5YR36	MHC	S AB	21T5	2FN2	G SPJ	7D	6SS	6		
2B24	1561902.5YR36	MHC	S AB	21T5	3FN2	G SPJ	7D	6SS	7	1s1	S5PR
LIME FREE:											
L3324	13824					Gn	RBEDr2.12	SPJ	7E	1SS	TOM COOTES
A	1.5		0					CSPJ	7E	4SS	
Ap	0 8	5YR43	LS	V	22T2		22C	SPJ	7E	6SS	1
B21	8 25	5YR46	LC	W4SB	22D4		11G	SPJ	7E	6SS	2
B22	25 432	5YR46	LC	W4SB	21D4		11C	SPJ	7E	6SS	3
2Asb	43 512	5YR46	LC	W4SB	21D4		11C	SPJ	7E	6SS	4
2B21	51123	10R36	MHC	S3AB	21T5	2FS1	11G	SPJ	7E	6SS	5
2B22	123200	10R36	MHC	12 AQZ DS3AB	21T5	3FN2		SPJ	7E	6SS	6
NO CARBONATE;PHOTO TAKEN OF PLOUGH LAYER:											
L3324	13824					G	RBEDr2.13	SPJ	7F	1SS	TOM COOTES
A	<4			13SPSL				CSPJ	7F	4SS	
Ap	0 10	5YR34	LS	V	22T2			SPJ	7F	6SS	1
A12	10 262	5YR34	SCL-	W4SB	22D4			SPJ	7F	6SS	2
A13	26 342	5YR36	SCL-	W4SB	21D4			SPJ	7F	6SS	3
B21	34 842	5YR34	MHC	S3AB	21T6			SPJ	7F	6SS	4
B22	84 912	5YR36	MHC	S3AB	21T6			SPJ	7F	6SS	5
B23n	911862	5YR36	MHC	S3AB	21T6	2FL2		SPJ	7F	6SS	6
B24	1862002	5YR36	MHC	S3AB	21T6	2FL2		SPJ	7F	6SS	7
ALMOST IDENTICAL TO 7G:											
L3324	13824					G	RBEDr2.13	SPJ	7G	1SS	TOM COOTES
A	<4			0				CSPJ	7G	4SS	
Ap	0 10	5YR36	LS	V	22T2		22C	SPJ	7G	6SS	1
A1	10 312	5YR36	SCL-	W4SB	22D4		11C	SPJ	7G	6SS	2
B21	31 70	10R34	MHC	S3AB	21D6		11G	SPJ	7G	6SS	3
B22	701102	5YR36	MHC	S3AB	21T6	2FN2	11	SPJ	7G	6SS	4
B23	1101502	5YR36	MHC	S3AB	21T6	2FN2		SPJ	7G	6SS	5
B24n	1501872	5YR36	MHC	S3AB	21T6	3FN2		SPJ	7G	6SS	6
B25	1872002	5YR36	MHC	22 SME DS3AB	21T6			SPJ	7G	6SS	7
50MM QUARTZITE AT 157;CLOSE TO BLEACH ON TOP OF B:											
L3324	13824					G	RBEDr2.13	SPJ	7H	1SS	TOM COOTES
A	6			13 SQU				CSPJ	7H	4SS	
Ap	0 8	5YR54	LS	V	22T2		11C	SPJ	7H	6SS	1
A3	8 27	5YR44	ZL	W4SB	22D5		11C	SPJ	7H	6SS	2
B21	27 66	5YR33	MHC	S3AB	21 6		11G	SPJ	7H	6SS	3
B22	661202	5YR34	MHC	S3AB	21 6	2FN2		G SPJ	7H	6SS	4
B23n	1201472	5YR36	MHC	22 SQZ DS3AB	21 6	4FN2		G SPJ	7H	6SS	5
B24	147200	5YR56	MHC	22 SME DS3AB	21 6	4FN2		SPJ	7H	6SS	6

Appendix B – Midnorth study area profile morphological data

										SPJ_Appendix.txt											
VERY WEAK BLEACHING ON TOP OF B:																					
L3324	13824											G	RBEDr2.13SPJ	7I	1SS	TOM	COOTES				
A	7	6								13	SQU	H		CSPJ	7I	4SS					
Ap	0	82	5YR44	LS							22T2	22C	SPJ	7I	6SS	1					
A3	8	282	5YR46	CLFS							22D4	11D	SPJ	7I	6SS	2					
B21	28	562	5YR42	MHC							21T5	11G	SPJ	7I	6SS	3	S5PR				
B22k	561	102	5YR36	MHC							21T6	11G	SPJ	7I	6SS	4	2S2				
B23n	1101	502	5YR36	MHC							21T6	2FN2	D	SPJ	7I	6SS	5	1S2			
B24	1502	002	5YR46	MHC							T6	2FN2		SPJ	7I	6SS	6				
60MM QUARTZITE AT 28CM:																					
L3324	13824											G	RBEDr2.13SPJ	7J	1SS	TOM	COOTES				
A	10	6								13	SQU	H		CSPJ	7J	4SS					
Ap	0	10	5YR43	SL							22T2	C	SPJ	7J	6SS	1					
A1	10	34	5YR46	FSL							22D2	C	SPJ	7J	6SS	2					
B21	34	105	10R32	MHC							21T4	G	SPJ	7J	6SS	3	S5PR				
B22	1051	282	5YR46	MHC							21T4	D	SPJ	7J	6SS	4					
B23k	1281	952	5YR46	MHC							21T4		SPJ	7J	6SS	5	3S2				
95-105 QUARTZ GRAVELS TO 60MM:																					
L3324	13824											E	RBEGn3.13SPJ	7K	1SS	TOM	COOTES				
A	16	6								13	SQU	H	190	MECSPJ	7K	4SS					
Ap	0	8	5YR33	CLFS							22T2	22G	SPJ	7K	6SS	1					
B11	8	162	5YR36	LC							22D6	11C	SPJ	7K	6SS	2					
B12	16	332	5YR36	LC							21D6	11C	SPJ	7K	6SS	3					
B21	33	78	10R32	MHC							21T3	1G	SPJ	7K	6SS	4	S5PR				
B22	78	145	10R32	MHC							21T3	G	SPJ	7K	6SS	5	2S2				
B23k	145	190	10R33	MHC							21T3	C	SPJ	7K	6SS	6	4S2				
Ck	190	200		LMC							T2		SPJ	7K	6SS	7	2S2				
50MM QUARTZITE GRAVEL AT 30CM:																					
L3324	13824											A	BC Uf6.31SPJ	8	1SS						
	110589									0		H		SPJ	8	2SS					
Ap	0	8	5YR44	ZC							22M2	CSPJ	8	4SS							
B1	8	16	5YR34	LC							22T2	C	SPJ	8	6SS	2					
B21	16	71	5YR34	MHC							21T6	G	SPJ	8	6SS	3	S4PR				
B22k	71	165	5YR38	MHC	32	UKA	DS3AB				23T6	3FL1	D	SPJ	8	6SS	4	4S2			
B23	165	2002	5YR36	MHC							21T5	3FL1		SPJ	8	6SS	5	1S2			
L3324	13824											D	RBEDr2.33SPJ	8A	1SS	TOM	COOTES				
<1	6								0		H		CSPJ	8A	4SS						
Ap	0	8	5YR34	ZL							22T2	C	SPJ	8A	6SS	1					
A2sb	8	20	5YR46	CL							22T2		SPJ	8A	6SS	2					

Appendix B – Midnorth study area profile morphological data

SPJ_Appendix.txt												
B21	20	702.5YR36	MHC		S3AB	21T5		SPJ	8A	6SS	3	
B22k	70108	5YR36	MHC	12 UKA	S3AB	21T5	2FN2	SPJ	8A	6SS	4	2S2
B23	1081702.	5YR36	MHC		S3AB	21T5		SPJ	8A	6SS	5	1S2
B24	170200	5YR48	LC		W4SB	21T3		SPJ	8A	6SS	6	1S2
L3324	13824						C	RBEDr2.13SPJ	8B	1SS	TOM COOTES	
<1	6			0		H		CSPJ	8B	4SS		
Ap	0	8 5YR36	ZCL+		M4SB	23T2		C SPJ	8B	6SS	1	
B1	8	14 10YR38	ZC		M4SB	23T2		C SPJ	8B	6SS	2	
B21	14	622.5YR34	MHC		S3AB	21T6		C SPJ	8B	6SS	3	S5
B22k	62	81 5YR36	MHC		S3AB	21T6		G SPJ	8B	6SS	4	3S2 S5
B23	81	952.5YR36	MHC		S3AB	21T6		G SPJ	8B	6SS	5	1S2
2B21	95126	10YR31	MHC		S3AB	21T6		G SPJ	8B	6SS	6	1S2
2B22	126166	5YR36	MHC		S3AB	21T6		D SPJ	8B	6SS	7	1S2
2B23k	166182	5YR36	MHC		S3AB	21T6		G SPJ	8B	6SS	8	4S2
2B24	1822002.	5YR36	MC		M4SB	21T6		SPJ	8B	6SS	9	1S2
PIPING BELOW 126CM OF RED MATERIAL:												
L3324	13824			0		H		SPJ	8B	9SS		
							C	RBEDr2.13SPJ	8C	1SS	TOM COOTES	
Ap	0	87.5YR32	LFSY		W3SB	22T2		C SPJ	8C	6SS	1	
A31	8	167.5YR34	CL+		W3SB	22T2		G SPJ	8C	6SS	2	
A32	16	30 5YR36	CL+		M4SB	21T5		SPJ	8C	6SS	3	
B21	30	842.5YR36	MHC		S4AB	21T5		SPJ	8C	6SS	4	5YR64
B22k	84100	5YR36	MHC		S3AB	21T53FDV		SPJ	8C	6SS	5	2S2
B23	1001632.	5YR36	MHC		S3AB	21T5		SPJ	8C	6SS	6	
B24	1631902.	5YR34	MHC		S3	21T5	3FN2	SPJ	8C	6SS	7	
L3324	13824						G	RBEDr2.13SPJ	8D	1SS		
Ap	0	22.5YR36	LS		M4SB	M3		SPJ	8D	6SS	1	
A1	2	132.5YR34	FSL		W4SB	M3		SPJ	8D	6SS	2	
A3	13	392.5YR34	SCL+		V4SB	T5		SPJ	8D	6SS	3	
B21	39	702.5YR36	MHC		S3AB	T5		SPJ	8D	6SS	4	
B22	701002.	5YR36	MHC		S3AB	T6		SPJ	8D	6SS	5	1S2
B23	1001662.	5YR46	MHC		S3AB	T6		SPJ	8D	6SS	6	1S2
B24	1662002.	5YR46	MHC		S3AB	T5		SPJ	8D	6SS	7	
L3324	13824						G	RBEDr2.13SPJ	8E	1SS	TOM COOTES	
Ap	0	10 5YR44	LS	0	W4SB	22T1		CSPJ	8E	4SS		
A31	10	222.5YR36	CLS		M4SB	22T1		12C SPJ	8E	6SS	1	
A32	22	292.5YR36	CLKS		M4SB	21T3		11C SPJ	8E	6SS	2	
B21	291152.	5YR34	MHC		S3	21T4	1FN3	11G SPJ	8E	6SS	4	S5PR
B22k	1151502.	5YR46	MHC		S3	21T4		11G SPJ	8E	6SS	5	3C2

Appendix B – Midnorth study area profile morphological data

SPJ_Appendix.txt										
B23	1501762.5YR46	MHC	S3	21T4	1FN2	SPJ	8E	6SS	62.5YR48	
B24	1762002.5YR46	MHC	S3	21T4	2FN2	SPJ	8E	6SS	7	
CALCILICATE AT 89CM; QUARTZITE AT 150-157CM:										
L3324	13824				G	RBEDr2.13SPJ	8F	1SS	TOM COOTES	
			0			CSPJ	8F	4SS		
Ap	0 9 5YR36	LS	W4SB	H	D2	D SPJ	8F	6SS	1	
A3	9 172.5YR36	SCLKS-	M4SB		D5	C SPJ	8F	6SS	2	
B21	17 512.5YR34	MHC	S3AB		M4	2FN1	8F	6SS	3	S5PR
B22k	511002.5YR36	MHC	S3AB		M4	2FN1	8F	6SS	4	2S2
SANDSTONE - QUARTZITE AT 100 PROBABLY GRAVEL:										
L3324	13824				Gb	RBEDr2.33SPJ	8G	1SS	TOM COOTES	
A	2 6		0			CSPJ	8G	4SS		
Ap	0 72.5YR36	SL	W3SB	H	32T1	2C SPJ	8G	6SS	1	
A1	7 282.5YR34	CLS	M4SB		32T1	1G SPJ	8G	6SS	2	
A2sb	28 342.5YR36	SCLKS-	W SB		21T3	1A SPJ	8G	6SS	3	5YR73
B21	34 532.5YR36	MHC	S AB		21T6	1G SPJ	8G	6SS	4	S4PR
B22	53 762.5YR36	MHC	S AB		21T6	D SPJ	8G	6SS	5	S4PR
B23	761342.5YR36	MHC	S AB		21T5	2FL2	8G	6SS	6	3S2
B24	1341652.5YR38	MHC	22SPSA DM SB		21T3	3FL2	8G	6SS	7	3S2
QUARTZITE GRAVEL AT TOP OF B2:										
L3324	13824				Cs	Dr2.13SPJ	8H	1SS	TOM COOTES	RBE
A	5 6		12SPSH	H	C 30	SHCSPJ	8H	4SS		
Ap	0 3 5YR34	SCL-	W3SB		22T1	2C SPJ	8H	6SS	1	
B2	3 10 5YR34	LC-22SPME	DM4SB		21T3	1C SPJ	8H	6SS	2	2C2
Bck	10 30	LC	V		21T63KCV	C SPJ	8H	6SS	3	5C
C	30 40		42SPSA DM3PL		T6	SPJ	8H	6SS	4	3S2
L3324	13824				B	BC Uf6.31SPJ	8I	1SS	TOM COOTES	
A	18 6		12 UQZ	S		CSPJ	8I	4SS		
Ap	0 5 5YR33	MC	S3SB		11T2	2 SPJ	8I	6SS	1	
B1	5 10 5YR33	MHC	S3AB		11T2	1 SPJ	8I	6SS	2	
B21	10 24 5YR33	MHC	S3AB		11T4	1 SPJ	8I	6SS	3	S4PR
B22	24 592.5YR32	MHC	S3AB		11T6	1 SPJ	8I	6SS	4	1S1
B23	591002.5YR34	MHC	S3AB		11T6	1 SPJ	8I	6SS	5	3S2
QUARTZ GRAVELS 40-44CM:										
L3324	13824				B	BC Uf6.31SPJ	8J	1SS	TOM COOTES	
A	7 6		22SPSI	S	C 143	SHCSPJ	8J	4SS		
Ap	0 5 5YR33	LC	M3SB		T3	2C SPJ	8J	6SS	1	
B1	5 182.5YR34	LC	M3SB		T3	1 SPJ	8J	6SS	2	
B21	18 612.5YR26	MHC	S3AB		T6	1 SPJ	8J	6SS	3	

Appendix B – Midnorth study area profile morphological data

SPJ_Appendix.txt														
B22	61	922.5	YR36	MHC	S3AB	T6	1	SPJ	8J	6SS	4	3S2		
B23k	92128	5	YR88	LMC	22SPSI	DS3AB	T2	1	SPJ	8J	6SS	5	4S2	
BC	128143	10	YR63	LMC	32SPSI	DM4AB	D4		SPJ	8J	6SS	6	4S	
C	143200	2.5	Y62		42SPSI	D	D4		SPJ	8J	6SS	7	5S	
50MM QUARTZITE GRAVEL AT 10CM:														
L3324	13824								SPJ	8J	9SS			
	110589								A	BC	Uf6.31	SPJ	9	1SS
	<1											SPJ	9	2SS
Ap	0	8	5YR34	LC		M4SB	H	22M2		CSPJ		9	4SS	
AB	8	13	5YR34	LC		M4SB		22T2		2C	SPJ	9	6SS	1
B21	13	72	5YR34	MHC		S3AB		21T4		1C	SPJ	9	6SS	2
B22k	72165	5	YR36	MHC		S3AB		21T4		1G	SPJ	9	6SS	3
B23	165177	5	YR44	MHC		S3AB		21T4	FL2	1G	SPJ	9	6SS	4
B24	1772002.	5	YR36	LMC		M4SB		21T3	3FL2	G	SPJ	9	6SS	5
CONCENTRIC EARTHY SECTION AT 170-175:														
L3324	13824											SPJ	9	9SS
									C	RBEDr2.13	SPJ	9A	1SS	TOM COOTES
												CSPJ	9A	4SS
Ap1	0	87.	5YR34	ZL		W3SB	H	22T1		22C	SPJ	9A	6SS	1
A3	8	16	5YR36	ZCL		W4SB		22T3		11D	SPJ	9A	6SS	2
B21	16	78	5YR34	MHC		S3AB		21T6	1FS2	11D	SPJ	9A	6SS	3
B22	781202.	5	YR36	MHC	22D	S3AB		21T6	1FS2	11D	SPJ	9A	6SS	4
B23k	1201672.	5	YR36	MHC		S3AB		21T6		D	SPJ	9A	6SS	5
B24	1671902.	5	YR36	MHC		S3		21T6		D	SPJ	9A	6SS	6
B25	190200	5	YR46	LC		V4		21T4	1MS1	SPJ	9A	6SS	7	
L3324	13824								C	RBEDr2.13	SPJ	9B	1SS	TOM COOTES
A	<2											SPJ	9B	4SS
Ap	0	67.	5YR32	CL		M4SB		22T2		2C	SPJ	9B	6SS	1
B1	6	14	5YR23	LC		M4SB		22T2		1C	SPJ	9B	6SS	2
B21	14	42	5YR23	LMC		S4AB		21T4		1D	SPJ	9B	6SS	3
B22k	45110	5	YR36	MC		M4SB		21T4		D	SPJ	9B	6SS	4
2B21	1101377.	5	YR33	MC		S3AB		21T6		D	SPJ	9B	6SS	5
2B22	137176	5	YR36	LC		M4SB		32T6			SPJ	9B	6SS	6
2B23	176200	5	YR36	LC		M4		21T5			SPJ	9B	6SS	7
VERY CLOSE TO Gn SOIL:														
L3324	13824											SPJ	9B	9SS
									C	RBEDr2.13	SPJ	9C	1SS	TOM COOTES
												CSPJ	9C	4SS
Ap	0	6	5YR34	ZL		W3SB	H	22T1		2C	SPJ	9C	6SS	1
A3	6	18	5YR34	CL+		M4SB		22T2		2G	SPJ	9C	6SS	2
B21	18	25	5YR33	MHC		S3AB		21T6		1G	SPJ	9C	6SS	3
B22	25	432.	5YR33	MHC		S3AB		21T6		1D	SPJ	9C	6SS	4

Appendix B – Midnorth study area profile morphological data

SPJ_Appendix.txt

B23	431392.5YR33	MHC	S3AB	21T6	1D SPJ	9C 6SS 5		
B24k	1391502.5YR34	MHC	S3AB	31T6	2FN2	1D SPJ	9C 6SS 6	5YR48
B25	1502002.5YR36	MHC	S3AB	31T6	3FN2	SPJ	9C 6SS 7	
LIME FREE TO 140CM:								
L3324	13824				Cn	RBEDr2.12SPJ	9D 1SS	TOM COOTES
A <2	6		0	L		CSPJ	9D 4SS	
Ap	0 10	5YR36	SCLFS-	W4SB	22M1	2C SPJ	9D 6SS 1	
A3/A2	10 232.	5YR36	SCLFS	W4SB	22M1	1 SPJ	9D 6SS 2	
B21	23 68	5YR34	MHC	S3AB	11M4	1 SPJ	9D 6SS 3	S5PR
B22	68145	5YR36	MHC	S3AB	11T4	2FN2	1 SPJ	9D 6SS 4
B23	145200	5YR34	MHC	S3AB	11T6	3FN2	SPJ	9D 6SS 5
LIME FREE:								
L3324	13824				G	RBEDr2.13SPJ	9E 1SS	TOM COOTES
A 3.5	6		0	H		CSPJ	9E 4SS	
Ap	0 92.	5YR36	LS	M SB	22T1	C SPJ	9E 6SS 1	
A1	9 302.	5YR36	FSL	M SB	22T1	C SPJ	9E 6SS 2	
B21	30 742.	5YR34	MHC	S3AB	21T6	D SPJ	9E 6SS 3	S5PR
B22	741442.	5YR36	MHC	S3AB	21T5	3FL1	D SPJ	9E 6SS 4
B23	1441852.	5YR36	MHC	S3AB	21T5	3FL1	SPJ	9E 6SS 5
QUARTZITE AT 75-80CM:								
L3324	13824				G	RBEDr2.12SPJ	9F 1SS	TOM COOTES
A 5	6		0	H		CSPJ	9F 4SS	
Ap	0 9	5YR44	SL	M4SB	22T3	2C SPJ	9F 6SS 1	
B21	9 22	5YR34	SC	W3SB	22T3	1D SPJ	9F 6SS 2	
B22	22 352.	5YR34	SC	M4SB	21T3	1D SPJ	9F 6SS 3	
B2A	35 52	5YR44	SCL-	4SB	21T6	1C SPJ	9F 6SS 4	
2B21	521102.	5YR34	MHC	S3AB	21T6	1D SPJ	9F 6SS 5	
2B22	1101452.	5YR36	MHC 11	AQZ DS3AB	21D6	2FL1	D SPJ	9F 6SS 6
2B23	1452002.	5YR36	MHC 31	ASH DS3AB	21D6	2FL1	SPJ	9F 6SS 7
100 QUARTZITE GRAVEL - LIME FREE PROFILE:								
L3324	13824				C	RBEDr2.13SPJ	9G 1SS	TOM COOTES
A <1	6		22	UME	H	CSPJ	9G 4SS	
Ap	0 9	5YR34	CLFS	M4SB	22T2	2C SPJ	9G 6SS 1	
B1	9 222.	5YR34	LC	M4SB	22T2	1C SPJ	9G 6SS 2	
B21	22 662.	5YR34	MHC	S3AB	21T6	1D SPJ	9G 6SS 3	
B22k	661202.	5YR36	MHC	S3AB	21T6	D SPJ	9G 6SS 4	S5PR
B23	1201852.	5YR34	MHC	S3AB	21T6	3FL1	SPJ	9G 6SS 5
L3324	13824				C	RBEDr2.13SPJ	9H 1SS	TOM COOTES
Ag	0 8	5YR33	CLFS	12 UME	H	CSPJ	9H 4SS	
				W3SB	32M2	2C SPJ	9H 6SS 1	

Appendix B – Midnorth study area profile morphological data

SPJ_Appendix.txt												
A3	8	12	5YR33	CLFS+	M4SB	21M2	1G	SPJ	9H	6SS	2	
B21	12	342.	5YR24	MHC	S3AB	21M4	1D	SPJ	9H	6SS	3	
B22	34	822.	5YR34	MHC	S3AB	21M4	1D	SPJ	9H	6SS	4	2S1
B23k	811282.		5YR36	MHC	22 AQZ DS3AB	21M6	1D	SPJ	9H	6SS	5	4S2
B24	1281642.		5YR46	LC	W3SB	32T5	D	SPJ	9H	6SS	6	4S2
B25	1642002.		5YR46	MHC	22SPME DS3AB	21T6	2FL1	SPJ	9H	6SS	7	2S2
SODIC? :												
L3324	13824						C	RBEDr2.13	SPJ	9I	1SS	TOM COOTES
A	7	6			12	USH	H		CSPJ	9I	4SS	
Ap	0	32.	5YR38	CLFS	V	33T3	C	SPJ	9I	6SS	1	
A1	3	92.	5YR36	CLFS	21 UQZ DV	33T3	G	SPJ	9I	6SS	2	
A3	9	152.	5YR34	SCL	W4SB	22T3	A	SPJ	9I	6SS	3	
B21	15	432.	5YR34	MHC	S3AB	21T5	SPJ	9I	6SS	4		S5PR
B22	43	522.	5YR34	MHC	S3AB	21T5	SPJ	9I	6SS	5		1S1
B23k	521362.		5YR36	MHC	S3AB	21T6	SPJ	9I	6SS	6		3S2
B24	1361752.		5YR38	MHC	S3AB	21T6	SPJ	9I	6SS	7		2S2
B25	1752002.		5YR38	MHC	S3AB	21T6	SPJ	9I	6SS	8		1S1
L3324	13824						A	BC Uf6.31	SPJ	10	1SS	
110589												
<1	0	6			0		H		SPJ	10	2SS	
Ap	0	5	5YR34	LC-	M4SB	22M2	CSPJ	10	4SS			
B1	5	13	5YR34	MC	M4SB	22M2	2C	SPJ	10	6SS	1	
B21	13	62	5YR34	MHC	S3AB	21T4	1G	SPJ	10	6SS	2	
B22k	62132		5YR36	MHC	S3AB	21T4	1G	SPJ	10	6SS	3	S5PR
B23	132170		5YR36	MHC	S3AB	21T6	1G	SPJ	10	6SS	4	3S2
B24	1702002.		5YR36	MHC	M5SB	21T6	1G	SPJ	10	6SS	5	2S2
L3324	13824						C	RBEDr2.13	SPJ	10	6SS	6
110589												
<1	0	6			0		H		CSPJ	10A	1SS	TOM COOTES
Ap	0	5	5YR34	CL	M3SB	22T2	C	SPJ	10A	4SS		
B1	5	12	5YR34	LC	M4SB	22T3	C	SPJ	10A	6SS	1	
B21	12	64	5YR34	MHC	S3AB	21T6	1MS1	D	SPJ	10A	6SS	2
B22k	64119		5YR44	MHC	S3AB	21T6	1MS1	C	SPJ	10A	6SS	3
2B21	119160		5YR34	22D	MHC	S3AB	21T6	D	SPJ	10A	6SS	4
2B22	160180		5YR36	MHC	S3AB	21T6	2FN2	D	SPJ	10A	6SS	5
2B23	1802002.		5YR36	22D	MHC	S3AB	21T6	2FN2	D	SPJ	10A	6SS
CALCILICATE IN B22:												
L3324	13824						C	RBEDr2.13	SPJ	10A	6SS	6
110589												
Ap	0	6	5YR34	CL	M3SB	22T3	CSPJ	10B	1SS	TOM	COOTES	
B1	6	11	5YR34	LC	M4SB	22T3	22	SPJ	10B	4SS		
							22	SPJ	10B	6SS	1	
												10YR41
												4S3
												3S3
												2S2
												1S2
												10YR42

Appendix B – Midnorth study area profile morphological data

SPJ_Appendix.txt

Profile	Horizon	Depth	Soil	Material	SPJ	Horizon	SPJ	Material	Soil	Horizon	SPJ	Material	Notes
B21	11 67	5YR34	MHC	S3AB	21T6	11	SPJ	10B	GSS 3				S5PR
B22	67 88	5YR36	MHC	S3AB	21T6	11	SPJ	10B	GSS 4				S5PR
B23k	88116	5YR48	MHC	S3AB	21T6		SPJ	10B	GSS 5				4S3
2B21	116150	10YR31 32P	MHC	S3AB	21T6		SPJ	10B	GSS 6		5YR46		4S3
2B22	1502002	5YR36 32	MHC	S3AB	21T6		SPJ	10B	GSS 7		5YR48		4S3
L3324	13824									A	BC Uf6.31	SPJ 10C 1SS TOM COOTES	
				0	H								
Ap	0 8	5YR36	ZC	W4SB	32T2		G	SPJ	10C	GSS 1			
B1	8 15	5YR34	ZLC	M4SB	32T2		D	SPJ	10C	GSS 2			
B21	15 80	5YR34	MHC	S3AB	21T5			SPJ	10C	GSS 3			
B22	80130	5YR36	MHC	S3AB	21T5			SPJ	10C	GSS 4			2S2
B23	130150	5YR48	MHC	S3AB	21T5			SPJ	10C	GSS 5			4S2
B24	150178	5YR36	MC	S3AB	21T4			SPJ	10C	GSS 6			4S2
B25	178200	5YR48	MC	M4SB	T4			SPJ	10C	GSS 7			4S2
		FAINT BURIED SOIL APPEARANCE AT 110-120CM:											
L3324	13824									C	RBEDr2.13	SPJ 10D 1SS TOM COOTES	
A <2	6			23SPME	H 90C	90							
Ap	0 8	5YR34	SCL-	W4SB	22M3			C	SPJ	10D	GSS 1		
A1	8 17	5YR33	SCLFS	M4SB	21M3			C	SPJ	10D	GSS 2		
B21	17 32	10R36	LMC	S3AB	21M3				SPJ	10D	GSS 3		
B22	32 50	10R36	MHC	S3AB	M3				SPJ	10D	GSS 4		
B23k	50 90	5YR46	MC	M4SB					SPJ	10D	GSS 5		5C2
C	90150								SPJ	10D	GSS 6		5C2
L3324	13824			SL									
A 6	6			22 UKA	H 50C	50		F	Um6.41	SPJ 10E 1SS TOM COOTES			R
Ap	0 8	5YR34	SCLFS	M3SB	22T1				SPJ	10E	GSS 1		
A31	8 17	5YR32	CLFS	M3SB	21T1				SPJ	10E	GSS 2		
A32	17 30	5YR32	CLFS	M3SB	21T1				SPJ	10E	GSS 3		
k	30 50	5YR44			21				SPJ	10E	GSS 4		5S3
C11	50 72	2.5Y74	KSL	M3PL	T1				SPJ	10E	GSS 5		2S2
C12k	72 78	10YR64	KSL	M3PL	T1				SPJ	10E	GSS 6		5S2
CB	78160	2.5Y62	KSL	M3PL	T1				SPJ	10E	GSS 7		2S2
		17-30CM CARBONATE RUBBLE LAYER:											
L3324	13824							Es	Gn3.13	SPJ 10F 1SS TOM COOTES			BC
A 7	6			32SPME	H 42C	42							
Ap	0 8	5YR34	ZCL	M3SB	22T2			G	SPJ	10F	GSS 1		1S1
B2	8 21	5YR33	LC	M4SB	21T2			G	SPJ	10F	GSS 2		2S1
BC	21 42	5YR36	LC	M4SB	21T2			G	SPJ	10F	GSS 3		5S
C	42 92		43SPSH	DS3PL					SPJ	10F	GSS 4		5S
L3324	13824							Cs	RBEDr2.13	SPJ 10G 1SS TOM COOTES			

Appendix B – Midnorth study area profile morphological data

SPJ_Appendix.txt

A	5	6		12	ASH	H	52C	52	SACSPJ	10G	4SS		
Ap		0 7	5YR34	SCLFS	M3SB		M2		C SPJ	10G	6SS	1	
B1		7 10	5YR36	LC	M3AB		M2		G SPJ	10G	6SS	2	
B2		10 292.	5YR34	MHC	S3AB		M4		G SPJ	10G	6SS	3	M5PR
BC		29 522.	5YR34	32SPSH	DS3PL		4		G SPJ	10G	6SS	4	3S2
L3324		13824						F	Um6.43SPJ	10H	1SS	TOM COOTES	R
A	6				23SPSH	H	8C	8	SH SPJ	10H	4SS		
Ap		0 82.	5YR36	CLS	w4SB		T2		C SPJ	10H	6SS	1	
BC		8 10	5YR33	CLS	22SPSH D				SPJ	10H	6SS	2	
C48SPJ		10G20SS		52SPSH	D				SPJ	10H	6SS	3	
CARBONATE FREE:													
L3324		13824						C	RBEDr2.13SPJ	10I	1SS	TOM COOTES	
A	4	6			12SPSH	H			CSPJ	10I	4SS		
Ap		0 5	5YR36	SCLFS	w4SB		32M1		C SPJ	10I	6SS	1	
A3		5 10	5YR36	CLFS	w4SB		32T1		C SPJ	10I	6SS	2	
B11		10 302.	5YR34	SC	w3AB		32T2		D SPJ	10I	6SS	3	
B12		30 332.	5YR34	MHC	M3AB		21M4		G SPJ	10I	6SS	4	M5PR
B21		33 462.	5YR36	MHC	S3AB		21M4	2FL1	D SPJ	10I	6SS	5	M5PR
B22		46 562.	5YR36	MHC	32 UQZ DS3AB		21M4	2FL1	D SPJ	10I	6SS	6	
B23		561002.	5YR34	MHC	S3AB		21M4	2FL1	D SPJ	10I	6SS	7	
B24k		1001562.	5YR36	MHC	S3AB		21M4	3FL1	SPJ	10I	6SS	8	3S2
B25		1562002.	5YR38	MC	S3AB		21M4	3FL1	SPJ	10I	6SS	9	1S1
L3324		13824						B	BC Uf6.31SPJ	10J	1SS	TOM COOTES	
A	5	6			12SPME	C			CSPJ	10J	4SS		
Ap		0 8	5YR33	LMC	S3SB		12M2		2C SPJ	10J	6SS	1	
B21		8 31	5YR33	MHC	21 UQZ DS3AB		12M3		1D SPJ	10J	6SS	2	1S1
B22		31 422.	5YR34	MHC	S3AB		11M3		1D SPJ	10J	6SS	3	3S2
B23k		42 932.	5YR36	MHC	S3AB		11M4		1D SPJ	10J	6SS	4	4S2
B24		931682.	5YR36	MHC	S3AB		11M4		D SPJ	10J	6SS	5	3S2
B25g		168200 10YR53	43D	MHC	S3AB		11w4		SPJ	10J	6SS	6	2S1
L3324		13824						A	BC Uf6.31SPJ	11	1SS		
<1		6			0	H			CSPJ	11	4SS		
Ap		0 8	5YR34	ZLC	M2SB		22M2		C SPJ	11	6SS	1	
B1		8 16	5YR44	ZMC	w4SB		22D6		C SPJ	11	6SS	2	
B21		16 68	5YR34	MHC	S3AB		21T4		G SPJ	11	6SS	3	S4PR
B22		68190	5YR36	MHC	S3AB		21T3	2FL2	D SPJ	11	6SS	4	4S2
B23		1902002.	5YR36	MHC	S3AB		21T3	3FL2	SPJ	11	6SS	5	1S2
L3324		13824						A	BC Uf6.31SPJ	11A	1SS	TOM COOTES	
110589									SPJ	11A	2SS		

Appendix B – Midnorth study area profile morphological data

SPJ_Appendix.txt									
Ap	0	8	5YR33	ZC	0	M3SB	H	22M2	CSPJ 11A 4SS
B1	8	23	5YR33	LC		M4SB		22M2	SPJ 11A 6SS 1
B21	23	60	5YR23	MHC		S3AB		21T3	SPJ 11A 6SS 2
B22k	60138	5YR34	MHC			S3AB		21T6	SPJ 11A 6SS 3
B23	138173	5YR46	MHC			S3AB		21T6	SPJ 11A 6SS 4
B24	1732002.	5YR36	MHC			S3AB		21T6	SPJ 11A 6SS 5
L3324	13824								SPJ 11A 6SS 6
									2FL1
									A BC Uf6.31SPJ 11B 1SS TOM COOTES
Ap	0	9	5YR33	MC	0	S3SB	H	22T2	CSPJ 11B 4SS
B21	9	48	5YR33	MHC		M4SB		22T2	C SPJ 11B 6SS 1
B22	48	51	5YR33	MHC		S		21T3	G SPJ 11B 6SS 2
B23	51	65	5YR36	MC		S		21T3	G SPJ 11B 6SS 3
B24	65129	5YR34	22D	MC		M		21D4	G SPJ 11B 6SS 4
B25k	129157	5YR36	MC			S		21D4	G SPJ 11B 6SS 5
B26	1571902.	5YR38	MC			M		21D3	G SPJ 11B 6SS 6
65CM+	MAYBE BURIED SOIL:								G SPJ 11B 6SS 7
L3324	13824								SPJ 11B 9SS
									A BC Uf6.31SPJ 11C 1SS TOM COOTES
Ap	0	8	5YR33	ZC	0	M3SB	H	M2	CSPJ 11C 4SS
B21	8	30	5YR33	MHC		S3AB		M2	2C SPJ 11C 6SS 1
B22k	30	51	5YR33	MC		S3AB		T4	1G SPJ 11C 6SS 2
2Bk1	51	80	5YR34	MC		S3AB		T4	1G SPJ 11C 6SS 3
2Bk2	80100	5YR44	22D	MC		S3AB		T4	1G SPJ 11C 6SS 4
2B	1001242.	5YR46	SC	12 UKA	Dw4SB	S3AB		T4	1G SPJ 11C 6SS 5
3B21	1241622.	5YR36	MC		S3AB	S3AB		T4	G SPJ 11C 6SS 6
3B22	1622002.	5YR38	MC		S3AB	S3AB		D6	G SPJ 11C 6SS 7
CALCILIGATE PAN AT 100CM:									SPJ 11C 6SS 8
L3324	13824								SPJ 11C 9SS
A <2									SPJ 11D 1SS TOM COOTES
Ap	0	6	5YR36	SCLFS	0	w4SB	H	22T2	C SPJ 11D 4SS
A1	6	12	5YR34	SCLFS		M4SB		22T2	C SPJ 11D 6SS 1
A3	12	402.	5YR38	SCL		M3AB		21M3	G SPJ 11D 6SS 2
B12	60	80	5YR36	SCL		M3AB		21M3	G SPJ 11D 6SS 3
B21	80150	10R36	MC			S3AB		21M5	D SPJ 11D 6SS 4
B22n	150200	10R36	MC			S3AB		21M5	D SPJ 11D 6SS 5
L3324	13824								SPJ 11D 6SS 6
A 5	6								2FN2
Ap	0	72.	5YR36	FSL		w4SB	H	22T2	3FN2
A3	7	152.	5YR35	SCL+12 AQZ		Dw4SB		22T2	G RBEDr2.13SPJ 11E 1SS TOM COOTES
									CSPJ 11E 4SS
									2C SPJ 11E 6SS 1
									1C SPJ 11E 6SS 2

Appendix B – Midnorth study area profile morphological data

SPJ_Appendix.txt														
B21	15	602.5	YR34	MHC	S3AB	21T4		1G	SPJ	11E	6SS	3		M5PR
B22		601332.	5YR38	MHC	S3AB	21T4		1G	SPJ	11E	6SS	4	1S2	
B23	1331482.	5YR48		MHC	S3AB	21T4	2FN2	G	SPJ	11E	6SS	5	3S2	
BCK	1482002.	5YR48		LMC	32SPME	DS3AB	21T3	2FN2	SPJ	11E	6SS	6	5N2	
L3324	13824							B	BC	Uf6.31SPJ	11F	1SS	TOM COOTES	
A	8	6			12SPME	H	145	145	SACSPJ	11F	4SS			
Ap1	0	2	5YR33	LC	M3SB	32M2			C	SPJ	11F	6SS	1	
Ap2	2	12	5YR33	LC	M3SB	32M2			SPJ	11F	6SS	2		
B21	12	252.	5YR34	MHC	S3AB	21M2			SPJ	11F	6SS	3		
B22	25	282.	5YR36	MHC	32SPSH	DS3AB	21T3		SPJ	11F	6SS	4		
B23	28	392.	5YR34	MHC	S3AB	21T3			SPJ	11F	6SS	5		S4PR
B24	39	602.	5YR36	MC	S4SB	21T3	2FN2		SPJ	11F	6SS	6	1S1	
B25k	601052.	5YR38			M4SB	21T3			SPJ	11F	6SS	7	5S2	
BCK	105145	5YR48			32SPSH	DM4PL	21T4		SPJ	11F	6SS	8	10YR58	5S2
L3324	13824							E	Gn3.13SPJ	11G	1SS	TOM COOTES	RBE	
A	5	6			0	0	H		CSPJ	11G	4SS			
Ap	0	8	5YR23	CLFS	M3SB	32T2			SPJ	11G	6SS	1		
B1	8	27	5YR33	LC	M4SB	32T2			C	SPJ	11G	6SS	2	
B21	27	502.	5YR34	MHC	S3AB	21M3			SPJ	11G	6SS	3		M5PR
B22	50	712.	5YR36	MHC	23 UQZ	DS3AB	21M3		SPJ	11G	6SS	4	2S2	M5PR
B23k	711222.	5YR36		MHC	S3AB	21M3			SPJ	11G	6SS	5	4S2	
B24	1221762.	5YR38		MHC	S3AB	21T6	3FL2		SPJ	11G	6SS	6	4S2	
B25	176200	5YR36		MHC	32SPME	DS3AB	21T4	3FN2	SPJ	11G	6SS	7	4S2	
50MM QUARTZITE GRAVEL AT 50CM; META GRAVELS AT 127CM:														
L3324	13824							A	BC	Uf6.31SPJ	12	1SS		
<1	6				0	H			CSPJ	12	4SS			
Ap	0	8	5YR33	ZC	M4SB	22M2			2C	SPJ	12	6SS	1	
B1	8	12	5YR34	LC	M4SB	22M2			1C	SPJ	12	6SS	2	
B21	12	57	5YR34	MHC	S3AB	21T4			1G	SPJ	12	6SS	3	
B22k	57165	5YR36		MHC	S3AB	21T4			1D	SPJ	12	6SS	4	4C2
B23	1652002.	5YR36		LC	S3AB	21T3	3FN2		SPJ	12	6SS	5	2S2	
L3324	13824				0	H		A	BC	Uf6.31SPJ	12A	1SS	TOM COOTES	
									CSPJ	12A	4SS			
Ap	0	7	5YR33	ZC	M3SB	22M2			2G	SPJ	12A	6SS	1	
B1	7	29	5YR33	LC	M4SB	22T3			1G	SPJ	12A	6SS	2	
B21	19	58	5YR23	MHC	S4AB	21T4			1G	SPJ	12A	6SS	3	
B22k	58	91	5YR34	22D	MHC	S3AB	21T4		1D	SPJ	12A	6SS	4	5YR84
B23	91112	5YR46		MHC	S3AB	21T5	2FN2		D	SPJ	12A	6SS	5	4S2
B24	1121452.	5YR36		MC	S3AB	21T6	3FN2		SPJ	12A	6SS	6	3S2	
L3324	13824							A	BC	Uf6.31SPJ	12B	1SS	TOM COOTES	2S2

Appendix B – Midnorth study area profile morphological data

SPJ_Appendix.txt																			
Ap	0	3	5YR34	ZC	22	UME	L	W2SB	32M2	CSPJ	12B	4SS							
B1	3	242.	5YR34	LMC				M4SB	32	2	C	SPJ	12B	6SS	1				
B21	24	572.	5YR34	MC				M4SB	21	4	D	SPJ	12B	6SS	2				
B22	57154		5YR34	MHC				S3	21	4	D	SPJ	12B	6SS	3				
B23	1542002.		5YR38	MHC				S3	21	4	D	SPJ	12B	6SS	4			1N5	S4PR
LIME FREE GENERALLY:																			
L3324	13824																		
<2	6																		
Ap	0	7	5YR34	SCL	22	UME	C	W3SB	22M2	C	RBEDr2.13	SPJ	12C	1SS	TOM	COOTES			BC
B11	7	202.	5YR34	LMC				M4SB	22M2			CSPJ	12C	4SS					
B12	20	302.	5YR36	SC-				W4SB	21T6			1C	SPJ	12C	6SS	1			
B21	30	782.	5YR34	MHC				S3AB	21T6			1	SPJ	12C	6SS	2			
B22	78169		10R36	MHC				S3AB	21T6			1	SPJ	12C	6SS	3			
B23k	1692002.		5YR38	MHC				S3AB	21T6	2FN1		1	SPJ	12C	6SS	4			
L3324	13824			MHC				S3AB	21T6	4FN1			SPJ	12C	6SS	5			2S2
A	3	6																	4S2
Ap	0	5	5YR33	CL+	0		L	W4SB	T2	E	RBEGn3.13	SPJ	12D	1SS	TOM	COOTES			
AB	5	10	5YR33	SC-				M4SB	T2			CSPJ	12D	4SS					
B21	10	65	10R34	MHC				S3AB	T4			SPJ	12D	6SS	1				
B22	65120		5YR36	MHC				S3AB	T4	1FN2		SPJ	12D	6SS	2				S5PR
B23k	120180		5YR36	MHC				S3AB	6	3FN2		SPJ	12D	6SS	3				3S2
B24	180200		5YR36	MHC	22SPME	D		S3AB	6	4FN2		SPJ	12D	6SS	4				5S2
L3324	13824																		4S2
A	5									C	RBEDr2.13	SPJ	12E	1SS	TOM	COOTES			
Ap1	0	4	5YR34	SCL-	22	AME	2ME	W4SB	22T2			SPJ	12E	4SS					
Ap2	4	9	5YR33	SCL				W4SB	22T2			2C	SPJ	12E	6SS	1			
Ap3	9	142.	5YR36	SCL				M3SB	21T4			2C	SPJ	12E	6SS	2			
B21	14	402.	5YR34	MHC				M3AB	21T4			1G	SPJ	12E	6SS	3			
B22k	40	652.	5YR36	MHC				S3AB	21T3	1FL1		1	SPJ	12E	6SS	4			
B23	651052.		5YR36	MHC				S3AB	21T5	1FL1		1	SPJ	12E	6SS	5			
B24	105152		10R36	MHC				S3AB	21T5	2FL1			SPJ	12E	6SS	6			2S2
B25k	1522002.		5YR38	LC				S3AB	11T5	2FL1			SPJ	12E	6SS	7			1S2
L3324	13824									1FL1			SPJ	12E	6SS	8			4S2
A	5	6																	
Ap	0	8	5YR34	ZC	0		H	M3	22M2	B	BC	Uf6.32	SPJ	12F	1SS	TOM	COOTES		
B21	8	522.	5YR32	MHC				S3	22M2			CSPJ	12F	4SS					
B22	52	882.	5YR36	MHC	23	AQZ		DS3	21M3			2C	SPJ	12F	6SS	1			
2B2	881382.		5YR38	MHC				S3	21T4			1D	SPJ	12F	6SS	2			
2B2k	1382002.		5YR38	MHC				S3	21T6	2FL1		1D	SPJ	12F	6SS	3			2S2
													SPJ	12F	6SS	4			S5PR
																			5C2

Appendix B – Midnorth study area profile morphological data

SPJ_Appendix.txt												
L3324	13824											
A	5	6		12	AQZ	H	E	BC Gn3.13	SPJ 12G 1SS	TOM COOTES		
Ap	0	5	5YR23		W3SB				CSPJ 12G 4SS			
B1	5	14	5YR33		S2AB	32M2			SPJ 12G 6SS 1			
B21	14	39	5YR23		MHC	S2AB			SPJ 12G 6SS 2			
B22k	39	60	5YR36		MHC	V			SPJ 12G 6SS 3			
B23	60	752	5YR36		MHC	V			SPJ 12G 6SS 4	3s1		
									SPJ 12G 6SS 5	2s1		
STUCK IN TUBE:												
L3324	13824											
<1	6											
Ap	0	10	5YR34		ZC	W3SB		A	BC Uf6.31	SPJ 13A 1SS	TOM COOTES	
B1	10	16	5YR36		LC	M5SB	22M2		CSPJ 13A 4SS			
B21	16	78	5YR34		MHC	S3AB	21T6		2G SPJ 13A 6SS 1			
B22k	78	132	5YR48		MC	S3AB	21T6	2FN2	1G SPJ 13A 6SS 2			
B23n	132	2002	5YR36		MHC	S3AB	11T6	3FN2	1C SPJ 13A 6SS 3	3s2		
									SPJ 13A 6SS 4	1s2		
									SPJ 13A 6SS 5			
BROWN SUBSOIL:												
L3324	13824											
2	6											
Ap	0	10	5YR34		CLFS	M3SB	32M2		E	RBEGn3.13	SPJ 13B 1SS	TOM COOTES
B11	10	222	5YR36		LC	W5SB	32T2		CSPJ 13B 4SS			
B12	22	552	5YR36		SC	V	21T4		SPJ 13B 6SS 1			
B21	55	702	5YR36		MHC	S3AB	21T6	2FL1	SPJ 13B 6SS 2			
B22k	70	752	5YR36		MHC	S3AB	21T6	3KCV	SPJ 13B 6SS 3	1s2		
B23	75	1442	5YR36		MHC	S3AB	21T6	2FL1	SPJ 13B 6SS 4	4s2		
B24k	144	1502	5YR36		MHC	S3AB	21T6	2KCV2FL1	SPJ 13B 6SS 5	1s2		
B25	150	1802	5YR36		MHC	S3AB	21T6	3FL1	SPJ 13B 6SS 6	4s2		
									SPJ 13B 6SS 7	1N2		
									SPJ 13B 6SS 8			
L3324	13824											
4	6											
Ap	0	10	5YR36		SCL	M4SB	22M		C	RBEDr2.13	SPJ 13C 1SS	TOM COOTES
A31	10	242	5YR36		SCLKS	M5SB	22T		CSPJ 13C 4SS			
A32	24	332	5YR36		SCLKS	22 RME	DM5SB	21T 1FCS	3C SPJ 13C 6SS 1			
B21	33	772	5YR34		MHC	S3AB	21T		1C SPJ 13C 6SS 2			
B22k	77	1652	5YR38		MHC	22 RQZ	DS3AB	21T	1G SPJ 13C 6SS 3			
B23	165	2002	5YR38		MHC	S3AB	21T	3FL1	1C SPJ 13C 6SS 4	5PR		
									C SPJ 13C 6SS 5	4N2		
									SPJ 13C 6SS 6	4N2		
L3324	13824											
4	6											
Ap	0	72	5YR38		SCLKS-	W4SB	12T3		D	RBEDr2.33	SPJ 13D 1SS	TOM COOTES
A2sb	7	122	5YR36		SCLFS	22SPME	DM4SB	12T3	CSPJ 13D 4SS			
B21	12	482	5YR34		MHC	S3AB	11T6		2 SPJ 13D 6SS 1	5YR64		
B22	48	932	5YR36		MHC	12 AQZ	DS3AB	11T6	1C SPJ 13D 6SS 2			
									1D SPJ 13D 6SS 3	5PR		
									1D SPJ 13D 6SS 4	2s		

Appendix B – Midnorth study area profile morphological data

SPJ_Appendix.txt

B23	931172.5YR36	MHC	22SPME	DS3AB	11T6	2FN2	D SPJ	13D	GSS	5		2s	
B24	1171652.5YR38	MHC		M4SB	11T6		D SPJ	13D	GSS	6		4s	
B25	1651762.5YR38	LMC	32SPME	DM4SB	11T4		D SPJ	13D	GSS	7		4s	
B26k	176200.5YR56	LMC		M4	11T4		SPJ	13D	GSS	8		5s	
L3324	13824					Bs	R	Uf6.31SPJ	13E	1SS	TOM COOTES		
A	11			22 AME	L	38C		38	SHCSPJ	13E	4SS		
Ap	0 10	5YR34	LC	M4SB	T2			2C	SPJ	13E	GSS	1	1s1
B2	10 177	5YR32	LC	M4SB	T2			1G	SPJ	13E	GSS	2	2s1
Bck	17 387	5YR32		33SPSH	M3PL	T5		1A	SPJ	13E	GSS	3	3s2
C	38 55	2.5Y54		53SPSH	S3PL	T5		1	SPJ	13E	GSS	4	
L3324	13824						Bs	R	Uf6.31SPJ	13F	1SS	TOM COOTES	
A	12	6		12 UME	H	90			CSPJ	13F	4SS		
Ap	0 6	5YR34	LC	S3AB	22T			2	SPJ	13F	GSS	1	
A	6 12	5YR34	LMC	S3AB	22T			1	SPJ	13F	GSS	2	
B2k	12 24	5YR33	LMC	S3AB	21T			1	SPJ	13F	GSS	3	3C3
B1	24 38	5YR33	LMC	S3AB	21T			1	SPJ	13F	GSS	4	
Bck	38 90	5YR56	MC		21T			1	SPJ	13F	GSS	5	5s2
C	90100	2.5Y62			21T			1	SPJ	13F	GSS	6	
L3324	13824						C	RBEDr2.13SPJ	14A	1SS	TOM COOTES		
A	2	6		0	S				CSPJ	14A	4SS		
Ap	10 13	5YR34	ZCL	M2SB	22M2			G	SPJ	14A	GSS	1	
A31	13 25	5YR36	KSL	21 AQZ	DM2SB	22T2		G	SPJ	14A	GSS	2	
A32	25 43	5YR48	LFSY	W4SB	22T2			G	SPJ	14A	GSS	3	
2A	43 54	5YR36	SCLKS	M4SB	32T4				SPJ	14A	GSS	4	
2B1	54 892	5YR36	SCLFS	M4SB	21T4				SPJ	14A	GSS	5	
2B21	59133	10R36	MHC	S3AB	21T6		2FL2		SPJ	14A	GSS	6	
2B22k	133200	10R36	MHC	S3AB	21T6		3FL2		SPJ	14A	GSS	7	2s2
CARBONATE ONLY AT 133-136CM:													
L3324	13824						A	Uf/Dr	SPJ	14A	9SS		
A	4	6		12 UME	H				SPJ	14A	9SS		
Ap	0 92	5YR36	SC	M4SB					CSPJ	14B	4SS		
A31	9 20	5YR48	SC	M4SB			2FC1		SPJ	14B	GSS	1	
A32	20 362	5YR38	CLS	W5SB					SPJ	14B	GSS	2	
2Asb	36 502	5YR36	SCL	W5SB					SPJ	14B	GSS	3	
2B2	50 932	5YR34	MHC	S3AB				C	SPJ	14B	GSS	47.5YR64	
2B2	93143	10R36	MHC	S3AB					SPJ	14B	GSS	5	5SPR
2B2	143161	10R36	MHC	S3AB					SPJ	14B	GSS	6	2s1
2B2k	161200	10R38	MHC	22SPME	DS3AB		3FC1		SPJ	14B	GSS	7	1s1
90-93CM	LARGE QUARTZ GRAVELS:								SPJ	14B	GSS	8	5s2
									SPJ	14B	9SS		

Appendix B – Midnorth study area profile morphological data

L3324 13824		SPJ_Appendix.txt		D RBEDr2.33SPJ 14C 1SS TOM COOTES			
5	6		12 UME	H		CSPJ 14C 4SS	
Ap	0 82.5YR36	CLS	M4SB	22T3		2 SPJ 14C 6SS 1	
A2sb	8 232.5YR36	CLS	M4SB	22T3		1 SPJ 14C 6SS 2	5YR74
A3	23 602.5YR24	SCL 22	UQZ DS3AB	21T6		1 SPJ 14C 6SS 3	
B21	60 792.5YR36	MHC 32	SPSH D 3AB	21T6		SPJ 14C 6SS 4	2S1
B22k	79100 5YR48	MHC	3AB	21T6		SPJ 14C 6SS 5	5S2
70-72CM CALCILICATE:							
L3324	13824				B	Uf6.31SPJ 14D 1SS TOM COOTES	R
A 7	6		12 AQZ	H 70		CSPJ 14D 4SS	
Ap	0 88.5YR34	MC	S3AB	22T2		SPJ 14D 6SS 1	
B2	8 382.5YR34	MHC 12	SPSH DS3AB	22T2		D SPJ 14D 6SS 2	2S2
B2k	38 90 5YR66	MHC 22	SPSH DS3AB	21T53K		C SPJ 14D 6SS 3	
BC	90100 10YR74	4	SPSH D	21T5		SPJ 14D 6SS 4	3S2
L3324	13824				B	Uf6.31SPJ 14E 1SS TOM COOTES	R
A 11	6		22 UME	H		CSPJ 14E 4SS	
Ap	0 87.5YR32	LC	S3AB	T2		SPJ 14E 6SS 1	
B2	8 27 5YR34	LMC 22	SPSH DS3AB	T2		SPJ 14E 6SS 2	
BC1k	27 41 5YR48	MHC 22	SPSH DS3AB	T6		SPJ 14E 6SS 3	4S
BC2	41 52 2.5Y74	MHC 42	SPSH DM5SB	T6		SPJ 14E 6SS 4	5YR48
BC3	52 70 5YR36	42	SPSH DM5SB	T6		SPJ 14E 6SS 5	2.5Y74
C	70 75 2.5Y74	52	SPSH DM3PL	T6		SPJ 14E 6SS 6	4S2
L3324	13824				F	Um6.43SPJ 14F 1SS TOM COOTES	R
A 12	6		22 ME	H 43C	43	SLCSPJ 14F 4SS	
Ap	0 6 5YR32	SCL-	w2SB	23T1		2G SPJ 14F 6SS 1	
A3	6 13 5YR44	SCL	M3SB	23T1		1C SPJ 14F 6SS 2	
Bck	13 43 10YR63		V	T		A SPJ 14F 6SS 3	5S
C	43100	54	SPME DS PL	T		SPJ 14F 6SS 4	4S
L3324	13824				F	Um6.24SPJ 15A 1SS TOM COOTES	R
A <5	6		32SPME	L 30	30	SLCSPJ 15A 4SS	
Ap	0 107.5YR32	LFS	w4SB	2 M1		A SPJ 15A 6SS 1	2S1
Bck	10 30		V	3KCV		G SPJ 15A 6SS 2	5C2
C	30 50	SH	S2PL			SPJ 15A 6SS 3	
L3324	13824				Es	Gn3.23SPJ 15B 1SS TOM COOTES	R
A <2	6		32SPME	L 47	47	CSPJ 15B 4SS	
Ap	0 117.5YR32	CL+	M4SB	22M1		2G SPJ 15B 6SS 1	2S1
B21	11 24 10YR23	ZC	M3	22M2		1G SPJ 15B 6SS 2	2S1
B22	24 33 10YR33	ZC	M3	21T2		1C SPJ 15B 6SS 3	2S1
Bck	33 47		V	3KCV		C SPJ 15B 6SS 4	5C5

Appendix B – Midnorth study area profile morphological data

		SPJ_Appendix.txt															
C	47 87		S						SPJ	15B	6SS	5					
L3324	13824								Gn3.23SPJ	15C	1SS	TOM	COOTES				R
A <2	6		32SPME	L	50C	50			SLCSPJ	15C	4SS						
Ap	0 97.5YR22	CL+	W4SB		M1				G SPJ	15C	6SS	1					2S
B	9 18 10YR23	ZC	M3SB		M1				C SPJ	15C	6SS	2					2S
Bck	18 50					3KCV			G SPJ	15C	6SS	3					5C
C	50 70								SPJ	15C	6SS	4					
L3324	13824								Gn3.23SPJ	15D	1SS	TOM	COOTES				R
A 15	6		33SPME	L	30	30			SHCSPJ	15D	4SS						
Ap	0 8 10YR23	CL 13 U C	M4SB		M1				2C SPJ	15D	6SS	1					2S1
B	8 19 10YR33	ZC	M4SB		M1				1C SPJ	15D	6SS	2					2S1
Bck	19 30 10YR33	ZCL-22SPSL	DW5SB						1 SPJ	15D	6SS	3					5S1
L3324	13824								Gn3.23SPJ	15E	1SS	TOM	COOTES				R
A 4	6		24SPSL	3SLL	22	22			SHCSPJ	15E	4SS						
Ap	0 7 10YR33	ZCL	M4SB		M1				2C SPJ	15E	6SS	1					2S1
B	7 14 10YR33	ZC	M4SB		M1				1 SPJ	15E	6SS	2					2S1
Bck	14 22	ZCL	M4SB			3KDV			1 SPJ	15E	6SS	3					5C
L3324	13824								Um6.43SPJ	15F	1SS	TOM	COOTES				R
A <4	6		22SPSL	L	25	25			SHCSPJ	15F	4SS						
Ap	0 77.5YR32	ZCL	M4SB		M2				C SPJ	15F	6SS	1					2S1
B	7 16 10YR33	ZCL	M4SB		M2				SPJ	15F	6SS	2					2S1
Bck	16 25	ZCL	12SPME	DM4SB	M2				SPJ	15F	6SS	3					5S2
BC	25 30		52SPSL	D		3KDV			SPJ	15F	6SS	4					3S1
L3324	13824								Um6.43SPJ	15G	1SS	TOM	COOTES				R
A 20	6		22SPSL	SLH	63C	63			SHCSPJ	15G	4SS						
Ap	0 6 10YR33	CL	M		M2				SPJ	15G	6SS	1					2S1
A3	6 177.5YR34	CL	M		M2				SPJ	15G	6SS	2					2S1
B	17 237.5YR34	CL 22SPME	DW		M2				SPJ	15G	6SS	3					4S1
Bk	23 47 10YR64		V			2KCV			SPJ	15G	6SS	4					5S2
B3	47 63 10YR54		V						SPJ	15G	6SS	5					3S1
CR	63 87		S3PL						SPJ	15G	6SS	6					
L3324	13824								Dr2.52SPJ	15H	1SS	TOM	COOTES				RBE
A 7	6		22SPSL	MEH	24C	24			SHCSPJ	15H	4SS						
Ap	0 15 5YR32	LFSY	W4SB		22M2				C SPJ	15H	6SS	1					
B1	4 10 5YR38	SCLFS	V		22D5				SPJ	15H	6SS	2					
B2	10 24	LC	M4SB		22D5				SPJ	15H	6SS	3					
C	24 +	LC							SPJ	15H	6SS	4					
Z																	

Appendix C. Physicochemical data of layers from selected profiles of the Midnorth study area.

Profile ID	Depth (cm)	Moisture %	E.C. 1:5 dS/m	pH (H ₂ O)	pH (CaCl ₂)	Cl mg/kg	Total C%	Org. C %	Total N %	Exch. Cations Cmol (+)/kg			K Cmol (+)/kg	Total	C.E. C (NH ₄)	pH of Total	ESP	CO ₃ as CaCO ₃ %	Clay %	Silt %	Sand %	Fine sand %	Total %
										Ca Cmol (+)/kg	Mg Cmol (+)/kg	Na Cmol (+)/kg											
11B	0-9	3.87	0.15	6.6	6.5	28	1.9	1.8	0.16	14.7	9.19	0.19	2.24	26	26	7.0	1	-	30	51	16	1	99
	20-30	4.98	0.12	6.9	6.6	29	0.9	0.9	-	17.3	12.8	0.40	1.37	32	31	7.0	1	-	49	41	9	<1	99
	50-60	4.54	0.21	8.0	7.7	62	0.8	0.6	-	14.5	12.3	0.71	1.07	29	28	8.5	3	1.7	32	57	8	1	98
	100-110	3.30	0.27	8.7	8.0	73	5.0	0.2	-	6.09	11.8	1.79	0.99	21	19	8.5	9	38.0	37	32	16	15	99
	130-140	4.10	0.35	8.9	8.3	65	2.3	0.3	-	4.89	16.1	3.64	1.52	26	24	8.5	15	15.8	40	39	10	9	98
	180-190	3.01	0.40	9.0	8.4	88	0.6	0.0	-	3.18	11.3	4.05	1.20	20	19	8.5	22	4.6	37	38	16	7	99
6	0-8	1.60	0.25	5.8	5.5	50	2.5	2.5	0.26	5.64	2.54	0.28	1.74	10	13	7.0	2	-	15	45	34	3	97
	8-19	1.34	0.09	5.8	5.3	57	0.6	0.6	-	3.61	2.13	0.35	0.69	7	9	7.0	4	-	21	45	33	1	99
	35-45	4.84	0.14	7.9	7.1	35	0.6	0.6	-	7.65	14.7	3.87	1.47	28	28	8.5	14	0.1	62	26	14	<1	101
	90-100	3.73	0.72	8.9	8.3	444	0.8	0.3	-	5.89	11.3	5.85	1.30	24	22	8.5	26	3.9	39	38	21	2	99
	140-150	3.74	0.88	8.7	8.2	701	1.0	0.2	-	6.68	11.1	5.22	1.22	24	23	8.5	23	6.4	41	37	16	4	99
	190-200	4.20	0.87	8.6	8.2	705	0.3	0.1	-	7.07	12.2	5.50	1.24	26	25	8.5	22	1.9	45	45	9	2	100
1F	0-6	2.17	0.18	6.2	6.0	88	2.0	2.0	0.21	10.5	3.36	0.12	2.27	16	18	7.0	1	-	19	40	38	3	100
	6-12	2.58	0.13	6.7	6.5	29	1.6	1.6	0.17	13.1	3.76	0.17	1.57	19	18	7.0	1	-	22	42	34	2	100
	70-80	3.06	0.18	8.4	7.9	51	2.7	0.2	-	11.2	6.08	0.70	0.70	19	18	8.5	4	19.4	34	31	24	10	99

Appendix C – Physicochemical data of layers from selected profiles of the Midnorth study area

Profile ID	Depth (cm)	Moisture %	E.C. 1:5 dS/m	pH (H ₂ O)	pH (CaCl ₂)	Cl mg/kg	Total C%	Org. C %	Total N %	Exch. Cations Cmol (+)/kg			K Cmol (+)/kg	Total	C.E.C (NH ₄)	pH of Total	ESP	CO ₃ as CaCO ₃ %	Clay %	Silt %	Sand %	Fine sand %	Total %
										Ca Cmol (+)/kg	Mg Cmol (+)/kg	Na Cmol (+)/kg											
10J	100-110	1.68	0.21	8.8	8.2	50	0.4	0.1	-	4.44	5.46	1.43	0.56	12	12	8.5	12	2.4	21	13	65	1	100
	140-150	2.52	0.37	9.0	8.3	97	1.3	0.2	-	4.26	8.95	3.25	0.87	17	15	8.5	21	8.8	27	42	26	3	98
	190-200	1.87	0.38	8.8	8.2	218	0.2	0.2	-	2.34	6.61	2.53	0.67	12	11	8.5	23	0.2	26	39	33	2	100
	0-8	5.28	0.25	7.8	7.6	100	1.6	1.5	0.14	29.2	5.56	0.48	1.95	37	33	8.5	1	0.3	46	17	28	8	99
	20-30	5.15	0.27	8.2	7.8	66	1.5	1.2	-	25.3	8.91	1.86	1.38	37	33	8.5	6	1.7	50	14	29	6	99
	40-50	5.82	0.34	8.9	8.2	68	1.8	0.4	-	17.8	14.0	5.92	1.16	39	34	8.5	17	10.8	61	15	19	5	100
	80-90	4.73	0.75	9.1	8.4	513	2.3	0.1	-	8.57	12.6	9.31	1.16	32	27	8.5	35	17.7	57	18	20	4	100
	100-110	5.23	1.01	8.9	8.4	846	1.4	0.3	-	9.68	12.4	10.4	1.27	34	30	8.5	35	8.5	60	13	21	6	100
5H	185-195	5.38	1.71	8.1	7.8	2020	<0.1	<0.1	-	8.39	13.6	12.6	1.11	36	33	8.5	38	<0.1	66	11	20	3	100
	0-8	4.59	0.21	7.6	7.4	81	2.2	2.1	0.21	28.0	3.13	0.33	1.61	33	32	8.5	1	0.1	47	20	20	13	100
	30-40	6.40	0.15	7.6	7.2	38	1.2	1.1	-	25.9	12.9	2.16	1.22	42	40	8.5	5	0.1	76	10	10	4	100
	65-75	5.17	0.33	8.5	8.0	64	1.9	0.2	-	15.1	13.8	4.18	0.93	34	31	8.5	13	12.9	68	15	12	5	100
12E	90-98	3.81	0.42	8.8	8.1	134	3.1	0.3	-	10.4	11.4	4.50	0.57	27	24	8.5	19	22.1	59	22	12	6	99
	4-9	1.03	0.08	6.0	5.6	30	0.7	0.6	0.06	4.11	1.88	0.35	0.64	7	9	7.0	4	-	14	17	47	21	99
	9-14	3.47	0.10	7.2	6.4	31	0.6	0.6	-	7.24	8.66	2.69	1.30	20	20	7.0	14	<0.1	48	12	29	12	100
	20-30	4.32	0.15	7.8	7.1	52	0.7	0.7	-	7.89	11.4	4.15	1.57	25	27	8.5	15	0.1	58	11	23	8	100
	50-60	5.28	0.67	8.8	8.3	533	0.4	0.2	-	7.01	15.5	7.76	2.03	32	30	8.5	25	1.5	63	12	18	7	100
	90-100	4.44	1.24	8.6	8.3	1220	0.6	<0.1	-	6.19	13.5	7.66	1.54	29	27	8.5	29	4.3	56	14	22	8	100
	135-145	4.02	1.26	8.5	8.2	1120	0.4	0.3	-	5.11	13.3	7.61	1.36	27	26	8.5	30	0.6	51	11	24	13	100
190-200	2.87	0.88	8.9	8.3	705	1.9	<0.1	-	4.45	7.60	5.57	0.87	18	20	8.5	28	15.1	33	21	30	16	100	

Appendix C – Physicochemical data of layers from selected profiles of the Midnorth study area

Profile ID	Depth (cm)	Moisture %	E.C. 1:5 dS/m	pH (H ₂ O)	pH (CaCl ₂)	Cl mg/kg	Total C%	Org. C %	Total N %	Exch. Cations Cmol (+)/kg			K Cmol (+)/kg	Total	C.E.C (NH ₄)	pH of Total	ESP	CO ₃ as CaCO ₃ %	Clay %	Silt %	Sand %	Fine sand %	Total %
										Ca Cmol (+)/kg	Mg Cmol (+)/kg	Na Cmol (+)/kg											
7D	0-10	1.00	0.12	6.6	6.6	30	1.5	1.4	0.10	5.51	1.57	0.16	0.68	8	8	7.0	2	-	13	23	51	14	101
	10-20	1.03	0.06	6.0	5.6	22	0.7	0.7	-	3.43	1.57	0.19	0.47	6	6	7.0	3	-	19	21	45	14	99
	30-40	1.14	0.05	6.3	5.9	24	0.4	0.4	-	2.34	2.38	0.24	0.35	5	6	7.0	4	-	19	20	47	14	100
	55-65	3.79	0.08	7.6	6.8	32	0.4	0.4	-	5.62	10.7	2.30	1.25	20	24	8.5	10	<0.1	50	15	29	5	99
	80-90	1.48	0.20	8.5	8.2	63	0.4	0.3	-	3.01	5.40	1.59	0.59	11	11	8.5	15	1.3	21	29	41	9	99
	140-150	4.36	0.36	8.6	8.2	178	0.2	0.1	-	5.95	14.4	4.86	1.41	27	26	8.5	19	0.9	47	21	27	4	99
	180-190	3.78	0.34	8.3	7.9	281	0.1	0.1	-	5.10	12.2	4.51	1.53	23	23	8.5	20	0.1	46	18	27	7	99
1B	0-10	2.23	0.19	7.5	7.4	31	1.8	1.7	0.16	13.0	1.66	0.08	1.79	17	18	8.5	0	0.4	17	29	44	10	100
	15-19	3.33	0.09	7.5	7.4	22	1.0	0.9	-	17.5	2.43	0.13	1.31	21	22	8.5	1	0.1	31	29	35	7	101
	25-30	3.41	0.10	7.4	7.3	44	0.8	0.8	-	17.9	2.70	0.14	1.20	22	22	8.5	1	0.1	34	27	34	6	101
	50-60	0.75	0.10	8.4	8.0	33	4.0	0.3	-	4.14	0.74	0.12	0.13	5	4	8.5	3	30.4	11	25	61	4	102
	60-70	2.40	0.14	8.2	7.9	49	4.1	0.2	-	10.9	3.03	0.28	0.40	15	8	8.5	4	31.6	25	30	37	8	100
	90-100	0.71	0.10	8.5	8.1	38	3.6	0.4	-	3.66	1.39	0.15	0.14	5	4	8.5	4	26.8	5	17	57	20	99
13D	0-7	1.07	0.10	6.8	6.7	25	0.9	0.9	0.10	6.29	1.07	0.16	0.96	8	7	7.0	2	-	11	18	53	18	101
	30-40	5.38	0.43	8.3	7.8	164	0.7	0.7	-	7.14	15.9	8.36	2.92	34	31	8.5	27	0.1	70	11	17	3	101
	90-100	4.26	1.59	8.6	8.3	1550	0.4	0.1	-	4.08	13.4	8.60	1.23	27	24	8.5	36	2.6	52	15	25	7	100
	140-150	2.93	1.68	8.7	8.2	1840	2.8	<0.1	-	3.65	8.94	5.97	0.89	19	16	8.5	36	22.1	43	22	28	8	101
	185-195	2.59	1.22	8.8	8.2	1420	3.6	0.2	-	3.35	7.72	4.95	0.96	17	14	8.5	34	28.1	36	27	25	13	101
8A	0-8	1.45	0.26	6.4	6.3	42	1.6	1.6	0.19	7.79	1.99	0.20	1.03	11	11	7.0	2	-	11	38	46	3	98
	10-20	1.39	0.07	6.5	6.2	29	0.5	0.5	-	4.58	2.53	0.35	0.44	8	8	7.0	4	-	22	43	34	1	100

Appendix C – Physicochemical data of layers from selected profiles of the Midnorth study area

Profile ID	Depth (cm)	Moisture %	E.C. 1:5 dS/m	pH (H ₂ O)	pH (CaCl ₂)	Cl mg/kg	Total C%	Org. C %	Total N %	Exch. Cations Cmol (+)/kg			K Cmol (+)/kg	Total	C.E.C (NH ₄)	pH of Total	ESP	CO ₃ as CaCO ₃ %	Clay %	Silt %	Sand %	Fine sand %	Total %
										Ca Cmol (+)/kg	Mg Cmol (+)/kg	Na Cmol (+)/kg											
	35-45	4.23	0.15	7.7	6.9	34	0.6	0.6	-	5.80	11.8	4.15	1.30	23	24	8.5	17	>0.1	53	27	19	1	100
	85-95	3.47	0.61	9.0	8.4	415	1.1	0.1	-	4.64	10.5	4.99	1.24	21	19	8.5	26	8.1	36	35	22	9	102
	130-140	3.03	0.72	8.8	8.4	653	0.8	0.7	-	4.17	8.80	4.51	1.08	19	18	8.5	25	0.9	35	34	30	4	102
	160-170	2.16	0.63	8.8	8.4	629	0.8	0.6	-	3.48	7.85	3.38	0.85	16	14	8.5	23	1.6	26	37	30	8	100
	190-200	2.05	0.49	8.9	8.4	367	0.5	0.2	-	3.43	6.90	2.88	0.71	14	13	8.5	23	2.3	25	19	44	12	100
5C	0-8	1.24	0.37	6.2	6.2	47	1.2	1.1	0.15	5.88	1.41	0.12	1.11	9	9	7.0	1	-	13	25	48	16	101
	20-30	1.37	0.10	6.8	6.5	23	0.4	0.4	-	5.27	2.40	0.57	0.62	9	8	7.0	7	-	17	31	40	12	100
	35-45	3.92	0.21	7.6	6.9	59	0.7	0.7	-	6.42	7.54	4.05	1.98	20	23	8.5	18	0.1	46	23	27	5	101
	90-100	2.87	0.89	9.0	8.3	827	1.7	0.1	-	5.02	4.76	5.83	1.75	17	23	8.5	26	12.8	29	36	27	9	101
	150-160	2.36	0.74	9.1	8.3	664	2.4	0.1	-	4.87	5.97	4.61	1.11	17	15	8.5	30	18.2	33	19	27	22	101
	185-200	1.95	0.61	9.2	8.2	490	2.8	0.1	-	4.24	5.01	3.71	0.94	14	13	8.5	29	22.1	29	26	32	15	101
6E	0-8	2.21	0.18	6.8	6.6	44	2.0	2.0	0.22	13.6	2.95	0.22	2.01	19	16	7.0	1	-	17	29	43	13	102
	8-18	2.31	0.09	6.8	6.6	43	1.1	1.0	-	13.4	3.21	0.22	1.98	19	16	7.0	1	-	24	28	39	10	100
	35-45	3.14	0.06	7.4	6.9	24	0.5	0.5	-	15.7	4.56	0.66	1.55	22	17	7.0	4	<0.1	30	29	34	8	101
	110-120	2.66	0.61	9.4	8.5	198	1.6	0.1	-	3.87	5.39	6.68	1.80	18	15	8.5	44	12.2	26	36	30	9	101
	190-200	2.85	0.71	9.2	8.5	462	0.9	0.2	-	5.06	5.73	6.21	1.73	19	17	8.5	37	5.4	26	37	30	7	100
10F	0-8	2.20	0.22	7.8	7.6	72	2.5	2.0	0.22	15.3	1.32	0.14	0.59	17	18	8.5	1	3.9	13	26	47	16	102
	10-20	2.49	0.15	8.1	7.8	31	1.4	1.1	-	18.5	1.40	0.24	0.37	21	19	8.5	1	2.6	20	23	43	14	100
	30-40	1.96	0.20	8.3	7.9	54	5.8	0.8	-	12.2	1.92	0.37	0.26	15	12	8.5	3	40.5	31	24	24	21	100
	80-90	1.74	0.30	9.1	8.0	72	5.6	0.2	-	4.56	3.69	2.09	0.33	11	9	8.5	24	44.4	33	28	24	16	100

Appendix C – Physicochemical data of layers from selected profiles of the Midnorth study area

Profile ID	Depth (cm)	Moisture %	E.C. 1:5 dS/m	pH (H ₂ O)	pH (CaCl ₂)	Cl mg/kg	Total C%	Org. C %	Total N %	Exch. Cations Cmol (+)/kg			K Cmol (+)/kg	Total	C.E.C (NH ₄)	pH of Total	ESP	CO ₃ as CaCO ₃ %	Clay %	Silt %	Sand %	Fine sand %	Total %
										Ca Cmol (+)/kg	Mg Cmol (+)/kg	Na Cmol (+)/kg											
6B	0-8	2.44	0.17	8.0	7.7	44	2.5	2.1	0.23	17.7	1.80	0.17	0.59	20	20	8.5	1	2.9	14	29	47	11	101
	40-50	0.94	0.33	9.5	8.6	103	8.8	0.2	-	1.45	1.85	1.87	0.32	5	3	8.5	54	71.2	8	13	28	51	100
	60-70	0.42	0.35	9.6	8.6	170	5.4	0.2	-	0.77	1.40	1.51	0.25	4	2	8.5	81	42.5	5	26	60	10	100
	90-100	0.78	0.46	9.6	8.6	305	4.7	0.3	-	0.87	2.45	2.15	0.12	6	4	8.5	58	36.7	11	31	55	4	101
15G	0-6	1.79	0.21	8.1	7.8	76	3.0	2.3	0.32	13.0	1.92	0.42	0.62	16	13	8.5	3	5.7	12	41	43	6	102
	6-17	1.53	0.24	8.2	7.9	183	2.3	1.5	0.22	11.2	1.81	0.35	0.48	14	12	8.5	3	5.9	13	37	42	9	102
	35-40	0.90	0.93	8.8	8.1	1230	4.7	0.7	-	3.41	2.12	1.77	0.07	7	20	8.5	9	33.2	22	44	30	6	102
7F	0-10	0.95	0.11	5.9	5.4	48	0.8	0.7	0.07	3.89	1.46	0.31	0.36	6	8	7.0	4	-	11	17	48	24	99
	15-25	1.34	0.06	6.7	5.9	26	0.4	0.4	-	4.86	2.57	0.57	0.35	8	12	7.0	5	-	20	20	42	18	100
	25-34	1.00	0.06	7.1	6.3	24	0.2	0.2	-	2.81	2.28	0.61	1.02	7	22	7.0	3	-	15	20	42	24	100
	50-60	4.12	0.12	8.1	7.1	46	0.5	0.5	-	5.16	10.7	4.86	1.20	22	24	8.5	20	<0.1	53	11	25	12	101
	110-120	3.92	0.42	9.1	8.5	145	0.5	0.2	-	4.90	1.10	6.29	1.10	13	21	8.5	29	1.8	44	16	26	13	99
	185-195	4.46	0.65	9.1	8.4	376	0.3	0.1	-	5.05	1.50	8.40	1.50	16	27	8.5	31	2.0	51	9	24	13	98
4B	0-10	1.51	0.64	6.6	6.5	42	1.8	1.8	0.21	11.1	1.52	0.23	1.52	14	12	7.0	2	-	12	39	44	4	99
	25-35	3.10	0.06	7.1	6.6	24	0.5	0.5	-	13.2	1.83	0.29	1.83	17	17	7.0	2	-	34	32	31	1	98
	90-100	1.87	0.15	8.4	8.1	57	1.5	0.2	-	5.17	2.71	0.30	2.71	11	12	8.5	3	10.4	15	38	36	10	99
	190-200	3.88	0.22	8.8	8.3	32	0.2	0.1	-	4.42	1.16	2.25	1.16	9	4	8.5	25	1.5	40	24	31	4	99
2E	0-10	1.07	0.06	6.0	5.6	23	1.2	1.2	0.08	4.97	1.58	0.23	1.68	8	6	7.0	4	-	14	19	40	27	100
	70-80	1.98	0.07	7.5	6.6	27	0.3	0.3	-	4.46	0.46	1.89	0.46	7	7	8.5	26	<0.1	21	9	16	53	100
	190-200	3.74	0.45	9.2	8.4	135	1.3	0.1	-	5.02	2.45	6.32	2.45	16	5	8.5	39	9.9	45	11	27	14	98

Appendix D. Midnorth study area plot field data.

Differential GPS (MGA z54)		SITEID	Apparent electrical conductivity (EC _a) mS/m		Depth to clay (m)	Surface volume magnetic susceptibility (κ) x10 ⁻⁸ SI															
X	Y		EC _{av}	EC _{ah}		MS1	MS2	MS3	MS4	MS5	MS6	MS7	MS8	MS9	MS10	MS mean	Median	Std	Max	Min	Min Std
279268.1	6302133.1	1A1	10.0	30.0	19.0	283.0	202.0	226.0	208.0	171.0	187.0	182.0	122.0	195.0	245.0	202.1	198.5	43.5	283.0	122.0	180.3
279270.0	6302133.0	1A2	10.0	32.0	22.0	166.0	171.0	213.0	207.0	165.0	160.0	241.0	131.0	193.0	235.0	188.2	182.0	35.5	241.0	131.0	170.4
279272.2	6302132.9	1A3	17.0	32.0	24.0	266.0	229.0	229.0	272.0	248.0	225.0	236.0	218.0	194.0	261.0	237.8	232.5	24.1	272.0	194.0	225.7
279274.3	6302132.7	1A4	15.0	32.0	23.0	214.0	223.0	204.0	217.0	216.0	156.0	234.0	199.0	224.0	204.0	209.1	215.0	21.5	234.0	156.0	198.4
279276.3	6302132.6	1A5	14.0	35.0	23.0	188.0	176.0	162.0	232.0	196.0	184.0	146.0	140.0	138.0	199.0	176.1	180.0	30.0	232.0	138.0	161.1
279278.2	6302132.4	1A6	15.0	30.0	19.0	235.0	220.0	157.0	273.0	274.0	254.0	214.0	210.0	207.0	205.0	224.9	217.0	35.5	274.0	157.0	207.1
279268.3	6302131.2	1B1	14.0	37.0	23.0	208.0	153.0	168.0	182.0	168.0	246.0	264.0	240.0	193.0	172.0	199.4	187.5	38.4	264.0	153.0	180.2
279270.3	6302131.0	1B2	14.0	33.0	20.0	325.0	256.0	263.0	264.0	214.0	194.0	239.0	229.0	190.0	199.0	237.3	234.0	41.6	325.0	190.0	216.5
279272.2	6302130.8	1B3	15.0	34.0	16.0	231.0	244.0	171.0	233.0	219.0	217.0	192.0	226.0	188.0	175.0	209.6	218.0	26.0	244.0	171.0	196.6
279274.0	6302130.5	1B4	16.0	36.0	19.0	207.0	191.0	143.0	410.0	210.0	214.0	233.0	219.0	147.0	202.0	217.6	208.5	73.7	410.0	143.0	180.7
279276.0	6302130.5	1B5	15.0	36.0	17.0	247.0	224.0	247.0	239.0	167.0	224.0	216.0	236.0	159.0	240.0	219.9	230.0	31.7	247.0	159.0	204.0
279278.1	6302130.3	1B6	12.0	32.0	16.0	239.0	231.0	229.0	203.0	214.0	183.0	213.0	298.0	191.0	240.0	224.1	221.5	32.4	298.0	183.0	207.9
279268.1	6302129.1	1C1	15.0	34.0	25.0	172.0	17.0	162.0	187.0	163.0	169.0	212.0	214.0	198.0	213.0	170.7	179.5	57.9	214.0	17.0	141.8
279270.1	6302128.9	1C2	11.0	35.0	21.0	162.0	169.0	212.0	152.0	154.0	215.0	191.0	165.0	164.0	141.0	172.5	164.5	25.2	215.0	141.0	159.9
279272.0	6302128.9	1C3	15.0	33.0	22.0	263.0	250.0	239.0	249.0	221.0	214.0	269.0	277.0	232.0	224.0	243.8	244.0	21.4	277.0	214.0	233.1
279274.1	6302128.7	1C4	13.0	36.0	24.0	203.0	162.0	226.0	216.0	159.0	165.0	101.0	197.0	205.0	264.0	189.8	200.0	44.9	264.0	101.0	167.3
279276.1	6302128.6	1C5	13.0	35.0	22.0	221.0	207.0	274.0	347.0	249.0	203.0	186.0	163.0	220.0	244.0	231.4	220.5	51.7	347.0	163.0	205.6
279278.0	6302128.4	1C6	14.0	33.0	25.0	408.0	228.0	237.0	385.0	247.0	274.0	198.0	179.0	150.0	321.0	262.7	242.0	85.4	408.0	150.0	220.0
279268.2	6302127.1	1D1	17.0	35.0	25.0	178.0	196.0	211.0	210.0	233.0	210.0	209.0	184.0	214.0	188.0	203.3	209.5	16.6	233.0	178.0	195.0

Appendix D – Midnorth study area plot field data

Differential GPS (MGA z54)		SITEID	Apparent electrical conductivity (EC _a) mS/m		Depth to clay (m)	Surface volume magnetic susceptibility (κ) x10 ⁻⁸ SI															
X	Y		EC _{av}	EC _{ah}		MS1	MS2	MS3	MS4	MS5	MS6	MS7	MS8	MS9	MS10	MS mean	Median	Std	Max	Min	Min Std
279270.1	6302127.1	1D2	14.0	33.0	25.0	204.0	174.0	154.0	240.0	174.0	202.0	223.0	189.0	157.0	204.0	192.1	195.5	27.8	240.0	154.0	178.2
279272.2	6302126.8	1D3	15.0	35.0	26.0	194.0	213.0	234.0	208.0	230.0	154.0	191.0	197.0	209.0	252.0	208.2	208.5	27.2	252.0	154.0	194.6
279274.0	6302126.6	1D4	15.0	33.0	23.0	224.0	227.0	139.0	186.0	225.0	206.0	127.0	182.0	151.0	266.0	193.3	196.0	44.5	266.0	127.0	171.0
279276.0	6302126.4	1D5	13.0	31.0	24.0	212.0	192.0	202.0	157.0	164.0	183.0	241.0	226.0	269.0	143.0	198.9	197.0	39.4	269.0	143.0	179.2
279278.1	6302126.2	1D6	14.0	30.0	23.0	191.0	221.0	160.0	179.0	209.0	238.0	109.0	104.0	148.0	194.0	175.3	185.0	45.0	238.0	104.0	152.8
279268.1	6302125.3	1E1	14.0	34.0	26.0	182.0	202.0	166.0	182.0	200.0	347.0	182.0	174.0	168.0	197.0	200.0	182.0	53.2	347.0	166.0	173.4
279270.1	6302124.9	1E2	14.0	33.0	25.0	222.0	175.0	256.0	223.0	231.0	208.0	226.0	211.0	246.0	229.0	222.7	224.5	22.1	256.0	175.0	211.6
279272.1	6302124.6	1E3	17.0	33.0	24.0	125.0	183.0	15.0	223.0	207.0	209.0	194.0	216.0	294.0	257.0	192.3	208.0	76.4	294.0	15.0	154.1
279274.1	6302124.6	1E4	13.0	32.0	27.0	189.0	316.0	230.0	246.0	279.0	239.0	208.0	247.0	178.0	272.0	240.4	242.5	42.1	316.0	178.0	219.3
279276.2	6302124.3	1E5	13.0	31.0	33.0	231.0	193.0	157.0	219.0	205.0	256.0	233.0	202.0	171.0	186.0	205.3	203.5	30.2	256.0	157.0	190.2
279278.1	6302124.3	1E6	11.0	29.0	28.0	217.0	227.0	185.0	227.0	20.0	232.0	207.0	147.0	98.0	185.0	174.5	196.0	68.6	232.0	20.0	140.2
279267.9	6302123.2	1F1	14.0	32.0	27.0	220.0	230.0	223.0	250.0	231.0	253.0	215.0	151.0	215.0	222.0	221.0	222.5	27.9	253.0	151.0	207.0
279270.0	6302123.0	1F2	14.0	32.0	32.0	252.0	255.0	260.0	271.0	218.0	228.0	227.0	223.0	193.0	232.0	235.9	230.0	23.4	271.0	193.0	224.2
279271.9	6302122.8	1F3	14.0	31.0	32.0	170.0	186.0	197.0	216.0	205.0	246.0	211.0	208.0	228.0	237.0	210.4	209.5	23.0	246.0	170.0	198.9
279273.9	6302122.6	1F4	16.0	33.0	26.0	192.0	199.0	18.0	233.0	267.0	207.0	183.0	148.0	169.0	248.0	186.4	195.5	69.3	267.0	18.0	151.7
279275.8	6302122.4	1F5	13.0	32.0	35.0	213.0	222.0	218.0	311.0	218.0	235.0	216.0	234.0	222.0	251.0	234.0	222.0	29.4	311.0	213.0	219.3
279277.7	6302122.2	1F6	13.0	29.0	30.0	177.0	154.0	235.0	166.0	261.0	223.0	208.0	234.0	227.0	267.0	215.2	225.0	38.6	267.0	154.0	195.9
278847.6	6301862.5	2A1	4.0	24.0	20.0	134.0	243.0	276.0	182.0	223.0	329.0	221.0	228.0	245.0	184.0	226.5	225.5	53.7	329.0	134.0	199.6
278849.6	6301862.4	2A2	13.0	39.0	20.0	233.0	231.0	236.0	159.0	118.0	212.0	186.0	171.0	153.0	187.0	188.6	186.5	39.5	236.0	118.0	168.9
278851.6	6301862.2	2A3	23.0	43.0	13.0	211.0	245.0	246.0	245.0	319.0	212.0	287.0	246.0	232.0	218.0	246.1	245.0	33.9	319.0	211.0	229.1
278853.7	6301862.0	2A4	31.0	52.0	16.0	266.0	190.0	229.0	194.0	171.0	245.0	248.0	216.0	221.0	226.0	220.6	223.5	29.1	266.0	171.0	206.0

Appendix D – Midnorth study area plot field data

Differential GPS (MGA z54)		SITEID	Apparent electrical conductivity (EC _a) mS/m		Depth to clay (m)	Surface volume magnetic susceptibility (κ) x10 ⁻⁸ SI															
X	Y		EC _{av}	EC _{ah}		MS1	MS2	MS3	MS4	MS5	MS6	MS7	MS8	MS9	MS10	MS mean	Median	Std	Max	Min	Min Std
278855.6	6301861.9	2A5	38.0	51.0	13.0	264.0	194.0	248.0	320.0	429.0	197.0	167.0	199.0	174.0	527.0	271.9	223.5	120.3	527.0	167.0	211.7
278857.5	6301861.6	2A6	40.0	57.0	14.0	256.0	237.0	227.0	226.0	638.0	263.0	156.0	178.0	239.0	232.0	265.2	234.5	135.1	638.0	156.0	197.7
278847.5	6301860.4	2B1	1.0	28.0	17.0	189.0	179.0	216.0	233.0	196.0	239.0	162.0	221.0	203.0	297.0	213.5	209.5	37.9	297.0	162.0	194.6
278849.5	6301860.3	2B2	10.0	39.0	11.0	176.0	169.0	160.0	186.0	195.0	213.0	185.0	178.0	184.0	183.0	182.9	183.5	14.4	213.0	160.0	175.7
278851.4	6301860.1	2B3	20.0	40.0	12.0	252.0	266.0	258.0	271.0	258.0	261.0	271.0	213.0	283.0	217.0	255.0	259.5	22.8	283.0	213.0	243.6
278853.4	6301859.9	2B4	30.0	49.0	14.0	269.0	270.0	238.0	214.0	189.0	205.0	214.0	296.0	241.0	193.0	232.9	226.0	36.2	296.0	189.0	214.8
278855.5	6301859.8	2B5	37.0	51.0	19.0	231.0	283.0	247.0	224.0	241.0	262.0	257.0	249.0	281.0	253.0	252.8	251.0	19.2	283.0	224.0	243.2
278857.3	6301859.6	2B6	41.0	53.0	13.0	283.0	290.0	226.0	267.0	268.0	235.0	210.0	221.0	221.0	208.0	242.9	230.5	31.0	290.0	208.0	227.4
278847.1	6301858.5	2C1	1.0	28.0	11.0	222.0	157.0	215.0	181.0	245.0	277.0	95.0	163.0	193.0	245.0	199.3	204.0	53.1	277.0	95.0	172.8
278849.2	6301858.3	2C2	10.0	34.0	12.0	339.0	291.0	221.0	224.0	270.0	250.0	224.0	166.0	211.0	188.0	238.4	224.0	50.8	339.0	166.0	213.0
278851.1	6301858.5	2C3	18.0	39.0	12.0	289.0	245.0	246.0	272.0	305.0	289.0	184.0	239.0	199.0	311.0	257.9	259.0	43.2	311.0	184.0	236.3
278853.0	6301857.9	2C4	27.0	46.0	9.0	275.0	255.0	233.0	272.0	366.0	359.0	181.0	207.0	295.0	221.0	266.4	263.5	61.1	366.0	181.0	235.9
278854.9	6301857.6	2C5	33.0	48.0	12.0	225.0	269.0	255.0	275.0	218.0	197.0	217.0	259.0	276.0	239.0	243.0	247.0	27.8	276.0	197.0	229.1
278857.1	6301857.4	2C6	39.0	56.0	9.0	307.0	302.0	226.0	263.0	271.0	272.0	262.0	269.0	259.0	267.0	269.8	268.0	22.6	307.0	226.0	258.5
278847.1	6301856.6	2D1	1.0	24.0	9.0	254.0	171.0	184.0	171.0	186.0	170.0	245.0	208.0	308.0	249.0	214.6	197.0	47.1	308.0	170.0	191.0
278849.1	6301856.3	2D2	4.0	34.0	12.0	239.0	232.0	274.0	190.0	195.0	144.0	268.0	210.0	204.0	199.0	215.5	207.0	38.9	274.0	144.0	196.0
278851.1	6301856.1	2D3	18.0	41.0	15.0	254.0	196.0	234.0	276.0	203.0	226.0	283.0	233.0	253.0	225.0	238.3	233.5	28.5	283.0	196.0	224.1
278853.0	6301855.9	2D4	31.0	46.0	10.0	302.0	329.0	284.0	252.0	315.0	330.0	209.0	262.0	287.0	265.0	283.5	285.5	37.9	330.0	209.0	264.6
278855.1	6301855.7	2D5	32.0	47.0	10.0	336.0	373.0	264.0	280.0	229.0	243.0	281.0	252.0	242.0	251.0	275.1	258.0	45.8	373.0	229.0	252.2
278857.0	6301855.6	2D6	37.0	52.0	11.0	258.0	270.0	238.0	232.0	222.0	264.0	183.0	238.0	237.0	236.0	237.8	237.5	24.5	270.0	183.0	225.5
278847.0	6301854.5	2E1	1.0	23.0	8.0	276.0	286.0	231.0	276.0	118.0	209.0	267.0	285.0	251.0	259.0	245.8	263.0	51.1	286.0	118.0	220.2
278848.8	6301854.2	2E2	9.0	33.0	15.0	262.0	193.0	176.0	253.0	273.0	238.0	247.0	252.0	260.0	216.0	237.0	249.5	31.9	273.0	176.0	221.1

Appendix D – Midnorth study area plot field data

Differential GPS (MGA z54)		SITEID	Apparent electrical conductivity (EC _a) mS/m		Depth to clay (m)	Surface volume magnetic susceptibility (κ) x10 ⁻⁸ SI															
X	Y		EC _{av}	EC _{ah}		MS1	MS2	MS3	MS4	MS5	MS6	MS7	MS8	MS9	MS10	MS mean	Median	Std	Max	Min	Min Std
278851.0	6301853.9	2E3	16.0	41.0	11.0	238.0	250.0	258.0	321.0	252.0	256.0	436.0	404.0	216.0	244.0	287.5	254.0	75.1	436.0	216.0	250.0
278852.8	6301853.7	2E4	18.0	41.0	12.0	261.0	362.0	275.0	227.0	245.0	247.0	215.0	283.0	284.0	272.0	267.1	266.5	40.7	362.0	215.0	246.8
278854.9	6301853.5	2E5	19.0	38.0	9.0	219.0	245.0	325.0	297.0	218.0	212.0	261.0	228.0	214.0	254.0	247.3	236.5	38.2	325.0	212.0	228.2
278856.7	6301853.2	2E6	25.0	42.0	15.0	286.0	244.0	347.0	222.0	257.0	195.0	258.0	264.0	202.0	183.0	245.8	250.5	48.8	347.0	183.0	221.4
278846.6	6301852.2	2F1	2.0	25.0	10.0	200.0	224.0	219.0	265.0	195.0	183.0	225.0	235.0	227.0	197.0	217.0	221.5	24.0	265.0	183.0	205.0
278848.7	6301852.1	2F2	6.0	32.0	20.0	198.0	213.0	233.0	234.0	224.0	222.0	192.0	252.0	299.0	283.0	235.0	228.5	34.5	299.0	192.0	217.8
278850.6	6301851.8	2F3	8.0	31.0	12.0	272.0	224.0	188.0	221.0	255.0	210.0	267.0	255.0	258.0	261.0	241.1	255.0	28.2	272.0	188.0	227.0
278852.7	6301851.5	2F4	10.0	29.0	14.0	275.0	246.0	251.0	222.0	166.0	231.0	261.0	242.0	265.0	261.0	242.0	248.5	31.2	275.0	166.0	226.4
278854.6	6301851.3	2F5	16.0	32.0	9.0	218.0	195.0	247.0	252.0	238.0	216.0	206.0	223.0	246.0	279.0	232.0	230.5	25.0	279.0	195.0	219.5
278856.4	6301851.1	2F6	18.0	41.0	11.0	216.0	312.0	275.0	221.0	252.0	236.0	239.0	240.0	201.0	245.0	243.7	239.5	31.5	312.0	201.0	228.0

Appendix E. Midnorth study area plot laboratory data.

Profile and layer ID	EC 1:5 (dS/m)	Clay%	EC _{se} (dS/m)	Depth (m)	pH (w)	pH (ca)	Low Frequency mass magnetic susceptibility (χ) x10 ⁻⁸ SI	Low Frequency mass magnetic susceptibility (χ) x10 ⁻⁸ SI	Frequency dependency (χ)%	CaCO ₃ (%)	Average EC _{se} for profile (combined layers 1,2 and 3)
SPMT 1A2/1	0.09	23.64	0.86	0.06	6.71	5.60	646.30	587.30	9.13	1.2	0.58
SPMT 1A2/2	0.05	27.40	0.43	0.17	7.34	6.10	838.30	767.90	8.40	0.3	
SPMT 1A2/3	0.07	50.10	0.45	0.22	7.97	6.47	908.70	788.00	13.28	0.4	
SPMT 1A4/1	0.08	27.60	0.72	0.06	6.90	5.82	781.60	708.30	9.38	0.5	0.64
SPMT 1A4/2	0.06	23.01	0.52	0.17	7.61	6.29	780.30	723.60	7.27	0.1	
SPMT 1A4/3	0.12	56.41	0.68	0.23	7.82	6.39	965.50	826.40	14.41	0.7	
SPMT 1A6/1	0.07	29.35	0.56	0.00	7.11	5.99	800.10	726.30	9.22	0.9	0.47
SPMT 1A6/2	0.05	29.33	0.44	0.01	7.64	6.31	827.60	752.40	9.09	0.7	
SPMT 1A6/3	0.07	51.05	0.40	0.02	7.78	6.32	1009.00	876.20	13.16	0.5	
SPMT 1B1/1	0.08	26.31	0.72	0.06	6.60	5.51	790.80	722.50	8.64	0.2	0.58
SPMT 1B1/2	0.05	25.87	0.43	0.17	7.61	6.19	905.20	842.60	6.92	0.1	
SPMT 1B1/3	0.11	56.18	0.60	0.23	7.97	6.53	1173.00	1013.10	13.63	1.3	
SPMT 1B3/1	0.06	25.92	0.56	0.00	7.24	5.93	820.90	756.20	7.88	0.7	0.73

Appendix E – Midnorth study area plot laboratory data

Profile and layer ID	EC 1:5 (dS/m)	Clay%	EC _{se} (dS/m)	Depth (m)	pH (w)	pH (ca)	Low Frequency mass magnetic susceptibility (χ) x10 ⁻⁸ SI	Low Frequency mass magnetic susceptibility (χ) x10 ⁻⁸ SI	Frequency dependency (χ)%	CaCO ₃ (%)	Average EC _{se} for profile (combined layers 1,2 and 3)
SPMT 1B3/2	0.09	25.85	0.80	0.01	7.87	6.48	813.00	746.10	8.23	0.5	
SPMT 1B3/3	0.15	57.64	0.84	0.02	8.09	6.75	948.10	812.40	14.31	0.9	
SPMT 1B5/1	0.06	27.19	0.54	0.04	6.82	5.63	816.30	746.10	8.60	0.1	0.58
SPMT 1B5/2	0.07	24.05	0.67	0.13	7.98	6.62	372.90	341.30	8.47	0.3	
SPMT 1B5/3	0.10	63.21	0.53	0.17	7.88	6.48	967.90	822.00	15.07	2.4	
SPMT 1B6/1	0.08	27.98	0.66	0.04	7.05	5.94	818.80	752.10	8.15	1.1	0.57
SPMT 1B6/2	0.06	31.29	0.47	0.12	7.88	6.46	695.00	643.40	7.42	0.5	
SPMT 1B6/3	0.12	64.95	0.58	0.16	8.06	6.70	1113.30	951.80	14.51	1.3	
SPMT 1C2/1	0.07	25.48	0.60	0.05	6.76	5.55	868.10	798.30	8.04	0.5	0.56
SPMT 1C2/2	0.05	24.96	0.44	0.16	7.64	6.17	824.60	764.40	7.30	0.7	
SPMT 1C2/3	0.10	49.79	0.64	0.21	8.16	6.69	1078.00	944.30	12.40	1.2	
SPMT 1C4/1	0.06	26.18	0.55	0.06	7.05	5.86	885.40	819.40	7.45	0.8	0.57
SPMT 1C4/2	0.06	26.14	0.56	0.18	7.82	6.34	985.20	910.50	7.58	0.8	
SPMT 1C4/3	0.12	63.76	0.60	0.24	8.04	6.63	951.30	814.30	14.40	1.6	
SPMT 1D1/1	0.08	24.57	0.69	0.06	6.79	5.63	813.60	749.50	7.88	0.8	0.59

Appendix E – Midnorth study area plot laboratory data

Profile and layer ID	EC 1:5 (dS/m)	Clay%	EC _{se} (dS/m)	Depth (m)	pH (w)	pH (ca)	Low Frequency mass magnetic susceptibility (χ) x10 ⁻⁸ SI	Low Frequency mass magnetic susceptibility (χ) x10 ⁻⁸ SI	Frequency dependency (χ)%	CaCO ₃ (%)	Average EC _{se} for profile (combined layers 1,2 and 3)
SPMT 1D1/2	0.05	25.21	0.44	0.19	7.72	6.28	1020.90	951.80	6.77	1.0	
SPMT 1D1/3	0.11	49.95	0.65	0.25	8.03	6.58	962.40	846.00	12.09	0.9	
SPMT 1D3/1	0.06	25.81	0.51	0.07	6.80	5.61	903.40	845.40	6.42	0.1	0.53
SPMT 1D3/2	0.05	23.68	0.49	0.20	7.63	6.32	842.00	780.10	7.35	0.2	
SPMT 1D3/3	0.09	47.52	0.58	0.26	8.03	6.55	1071.60	947.30	11.60	0.0	
SPMT 1D5/1	0.05	25.23	0.45	0.06	7.05	5.85	896.60	828.80	7.56	0.0	0.50
SPMT 1D5/2	0.05	24.13	0.42	0.18	7.70	6.28	1053.00	982.20	6.72	0.0	
SPMT 1D5/3	0.12	58.21	0.64	0.24	7.98	6.64	1044.90	906.00	13.29	0.4	
SPMT 1E2/1	0.09	23.06	0.87	0.06	6.91	5.90	826.20	761.10	7.88	0.5	0.61
SPMT 1E2/2	0.05	24.87	0.46	0.19	7.64	6.33	886.00	824.70	6.92	0.4	
SPMT 1E2/3	0.09	53.52	0.52	0.25	7.86	6.41	886.90	778.20	12.26	0.5	
SPMT 1E4/1	0.05	24.58	0.49	0.07	6.84	5.68	833.00	765.00	8.16	0.4	0.48
SPMT 1E4/2	0.05	21.82	0.42	0.20	7.87	6.39	941.70	874.40	7.15	0.0	
SPMT 1E4/3	0.10	58.83	0.54	0.27	8.04	6.58	1056.20	909.50	13.89	0.0	
SPMT 1E6/1	0.06	24.38	0.51	0.07	6.88	5.73	884.10	814.40	7.88	0.4	0.47

Appendix E – Midnorth study area plot laboratory data

Profile and layer ID	EC 1:5 (dS/m)	Clay%	EC _{se} (dS/m)	Depth (m)	pH (w)	pH (ca)	Low Frequency mass magnetic susceptibility (χ) x10 ⁻⁸ SI	Low Frequency mass magnetic susceptibility (χ) x10 ⁻⁸ SI	Frequency dependency (χ)%	CaCO ₃ (%)	Average EC _{se} for profile (combined layers 1,2 and 3)
SPMT 1E6/2	0.05	24.90	0.42	0.21	7.77	6.39	911.30	848.20	6.92	0.0	
SPMT 1E6/3	0.08	47.34	0.48	0.28	8.04	6.46	966.80	855.50	11.51	0.4	
SPMT 1F1/1	0.08	22.02	0.74	0.07	6.82	5.66	933.70	863.10	7.56	0.7	0.52
SPMT 1F1/2	0.04	25.34	0.37	0.20	7.67	6.29	945.60	874.60	7.51	1.6	
SPMT 1F1/3	0.09	62.86	0.43	0.27	7.84	6.35	957.60	825.10	13.84	1.5	
SPMT 1F3/1	0.06	25.98	0.51	0.08	6.60	5.47	897.00	830.70	7.39	2.4	0.52
SPMT 1F3/2	0.05	23.26	0.46	0.24	7.87	6.47	846.20	784.50	7.29	3.8	
SPMT 1F3/3	0.09	42.43	0.59	0.32	8.06	6.43	863.40	769.50	10.88	4.3	
SPMT 1F5/1	0.06	23.95	0.54	0.09	6.97	5.83	915.30	842.90	7.91	2.4	0.49
SPMT 1F5/2	0.05	24.32	0.42	0.26	7.70	6.30	923.10	859.70	6.87	4.5	
SPMT 1F5/3	0.08	42.76	0.51	0.35	8.04	6.43	849.00	752.00	11.43	0.0	
SPMT 2A1/1	0.10	17.84	0.97	0.03	6.64	5.72	704.80	650.10	7.76	0.2	0.57
SPMT 2A1/2	0.06	38.01	0.42	0.10	6.77	5.67	739.00	656.00	11.23	0.6	
SPMT 2A1/3	0.06	57.48	0.33	0.13	7.24	6.10	804.50	680.70	15.39	3.3	
SPMT 2A4/1	0.11	16.89	1.10	0.04	6.76	5.62	921.10	860.70	6.56	0.0	0.80

Appendix E – Midnorth study area plot laboratory data

Profile and layer ID	EC 1:5 (dS/m)	Clay%	EC _{se} (dS/m)	Depth (m)	pH (w)	pH (ca)	Low Frequency mass magnetic susceptibility (χ) x10 ⁻⁸ SI	Low Frequency mass magnetic susceptibility (χ) x10 ⁻⁸ SI	Frequency dependency (χ)%	CaCO ₃ (%)	Average EC _{se} for profile (combined layers 1,2 and 3)
SPMT 2A4/2	0.07	24.04	0.63	0.12	7.02	5.66	642.00	584.40	8.97	0.3	
SPMT 2A4/3	0.14	65.97	0.68	0.16	7.73	6.48	814.10	689.50	15.31	1.0	
SPMT 2B2/1	0.14	15.72	1.49	0.03	6.95	5.87	707.30	653.90	7.55	0.2	0.82
SPMT 2B2/2	0.07	29.86	0.59	0.08	7.10	5.78	920.80	831.80	9.67	0.1	
SPMT 2B2/3	0.07	61.95	0.37	0.11	7.65	6.27	943.50	804.20	14.76	0.1	
SPMT 2B5/1	0.07	17.75	0.67	0.05	6.75	5.56	680.70	633.70	6.90	0.3	0.72
SPMT 2B5/2	0.07	19.47	0.64	0.14	7.34	6.03	943.00	880.70	6.61	0.0	
SPMT 2B5/3	0.09	20.16	0.85	0.19	7.64	6.27	677.80	623.80	7.97	0.0	
SPMT 2C3/1	0.12	20.08	1.17	0.03	6.67	5.67	805.20	751.20	6.71	0.6	0.75
SPMT 2C3/2	0.06	22.48	0.58	0.09	7.03	5.78	793.70	730.20	8.00	0.3	
SPMT 2C3/3	0.10	59.86	0.50	0.12	7.83	6.55	908.30	779.10	14.22	0.9	
SPMT 2C6/1	0.11	14.50	1.17	0.02	7.01	5.88	742.10	693.80	6.51	0.0	0.91
SPMT 2C6/2	0.08	16.94	0.83	0.07	7.14	5.88	788.20	731.50	7.19	0.0	
SPMT 2C6/3	0.10	41.87	0.71	0.09	7.53	6.15	893.10	785.30	12.07	0.3	
SPMT 2D1/1	0.13	19.20	1.24	0.02	6.67	5.81	774.70	717.80	7.34	0.3	0.77

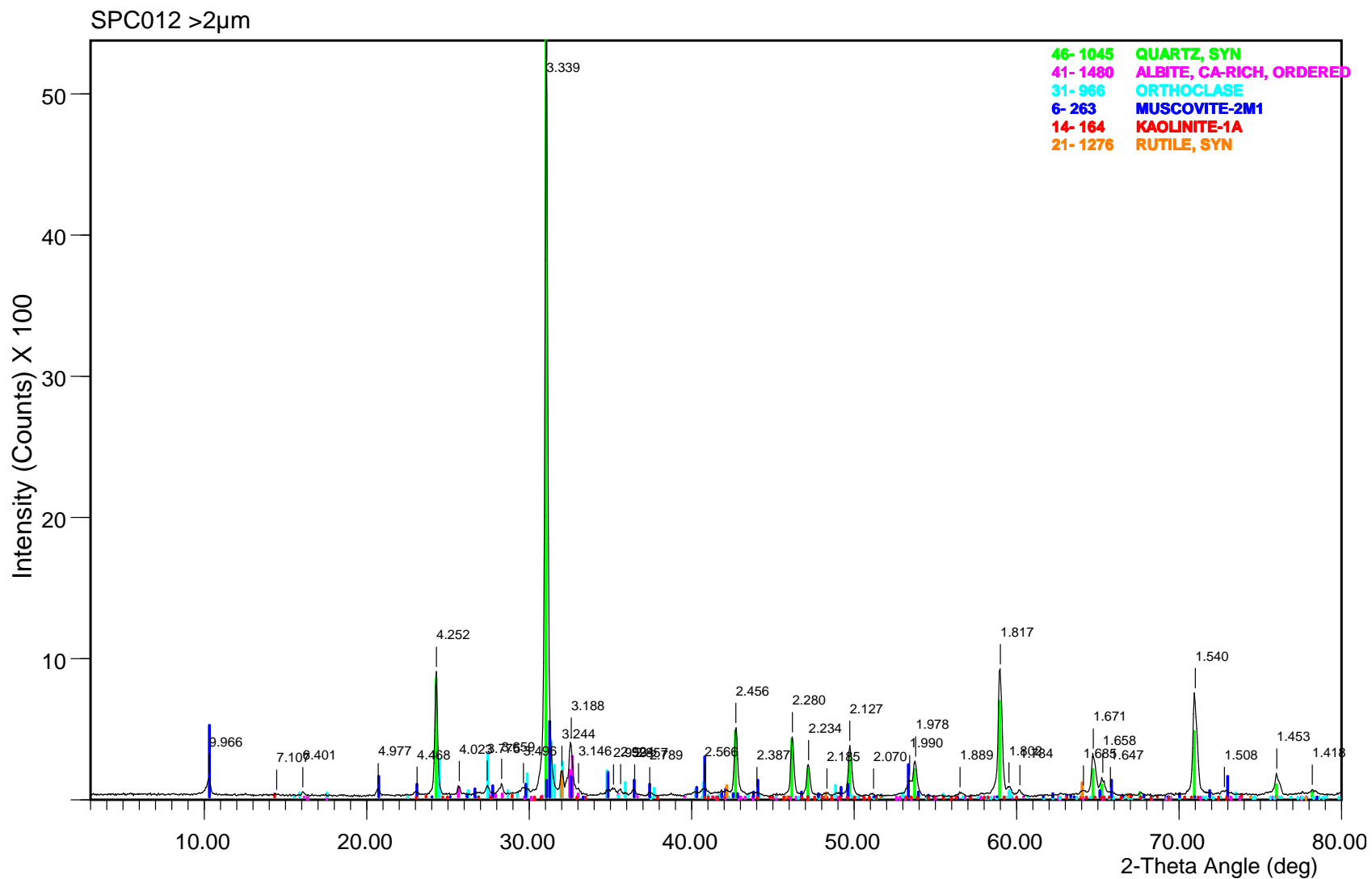
Appendix E – Midnorth study area plot laboratory data

Profile and layer ID	EC 1:5 (dS/m)	Clay%	EC _{se} (dS/m)	Depth (m)	pH (w)	pH (ca)	Low Frequency mass magnetic susceptibility (χ) x10 ⁻⁸ SI	Low Frequency mass magnetic susceptibility (χ) x10 ⁻⁸ SI	Frequency dependency (χ)%	CaCO ₃ (%)	Average EC _{se} for profile (combined layers 1,2 and 3)
SPMT 2D1/2	0.08	21.45	0.73	0.07	6.76	5.71	740.70	686.00	7.38	0.0	
SPMT 2D1/3	0.05	40.41	0.34	0.09	6.92	5.89	808.30	724.10	10.42	0.1	
SPMT 2D4/1	0.13	16.54	1.37	0.03	6.36	5.31	724.40	674.90	6.83	0.3	0.98
SPMT 2D4/2	0.08	22.70	0.73	0.08	6.96	5.62	732.00	671.10	8.32	0.4	
SPMT 2D4/3	0.16	61.52	0.83	0.10	7.84	6.62	918.60	785.30	14.51	1.1	
SPMT 2E2/1	0.10	19.95	0.95	0.04	6.35	5.33	789.10	731.20	7.34	0.3	0.63
SPMT 2E2/2	0.06	25.52	0.49	0.11	6.75	5.54	760.20	704.10	7.38	0.6	
SPMT 2E2/3	0.08	53.19	0.44	0.15	7.81	6.42	876.00	764.90	12.68	0.5	
SPMT 2E3/1	0.08	19.94	0.82	0.03	6.70	5.60	697.70	646.60	7.32	0.5	0.77
SPMT 2E3/2	0.07	25.16	0.62	0.08	7.42	6.03	704.40	650.70	7.62	0.2	
SPMT 2E3/3	0.17	62.51	0.87	0.11	8.02	6.81	934.40	805.40	13.81	0.2	
SPMT 2E4/1	0.12	17.35	1.18	0.03	6.72	5.72	860.00	805.00	6.40	0.0	0.98
SPMT 2E4/2	0.09	20.47	0.87	0.09	7.11	5.80	695.30	643.20	7.49	0.2	
SPMT 2E4/3	0.17	61.42	0.90	0.12	7.87	6.57	840.50	717.10	14.68	0.1	
SPMT 2F3/1	0.09	19.86	0.84	0.03	6.50	5.45	751.20	697.40	7.16	0.0	0.57

Appendix E – Midnorth study area plot laboratory data

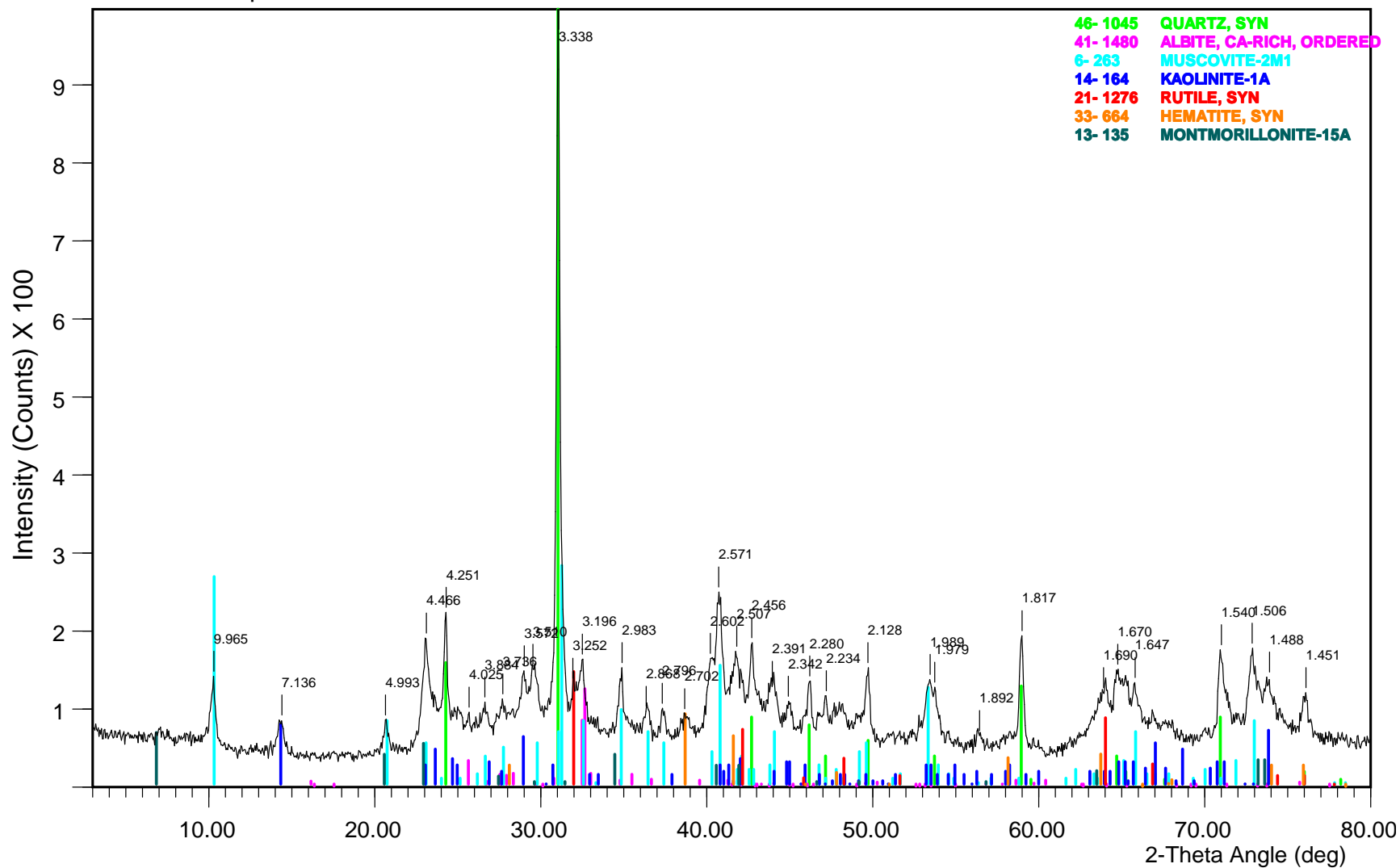
Profile and layer ID	EC 1:5 (dS/m)	Clay%	EC _{se} (dS/m)	Depth (m)	pH (w)	pH (ca)	Low Frequency mass magnetic susceptibility (χ) x10 ⁻⁸ SI	Low Frequency mass magnetic susceptibility (χ) x10 ⁻⁸ SI	Frequency dependency (χ)%	CaCO ₃ (%)	Average EC _{se} for profile (combined layers 1,2 and 3)
SPMT 2F3/2	0.06	22.64	0.51	0.09	6.77	5.66	878.60	813.70	7.39	0.7	
SPMT 2F3/3	0.06	46.00	0.37	0.12	7.36	6.10	844.80	747.40	11.53	0.0	
SPMT 2F6/1	0.09	18.70	0.87	0.03	6.94	5.92	798.20	747.60	6.34	0.6	0.77
SPMT 2F6/2	0.07	24.08	0.66	0.08	7.14	5.80	755.30	696.10	7.84	0.0	
SPMT 2F6/3	0.13	53.14	0.78	0.11	7.88	6.60	905.10	790.30	12.68	0.7	

Appendix F. Midnorth study area X-ray diffraction plots.



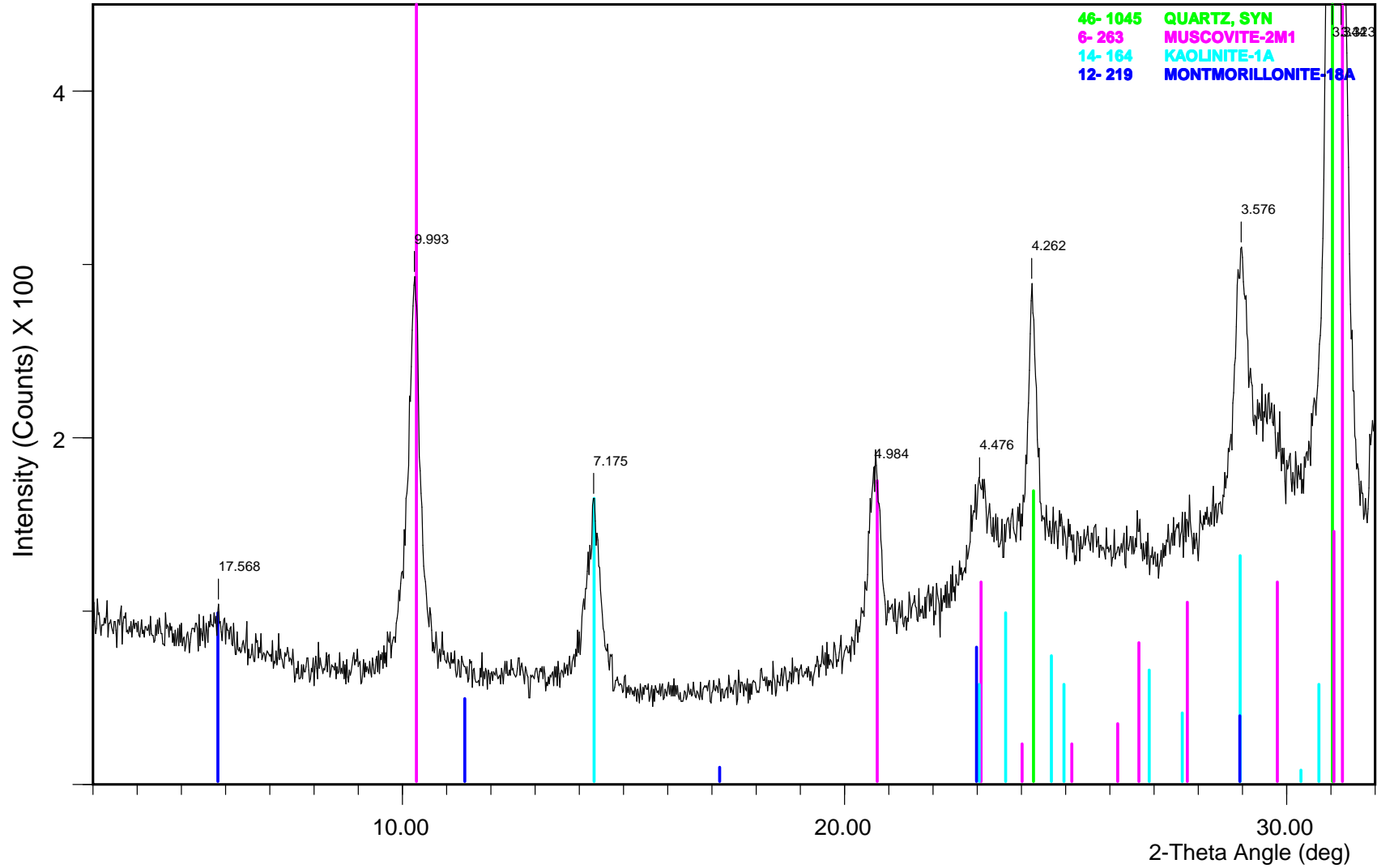
File Name: d:\xrddat-1\11204blk.201

SPC012 0.2-2µm

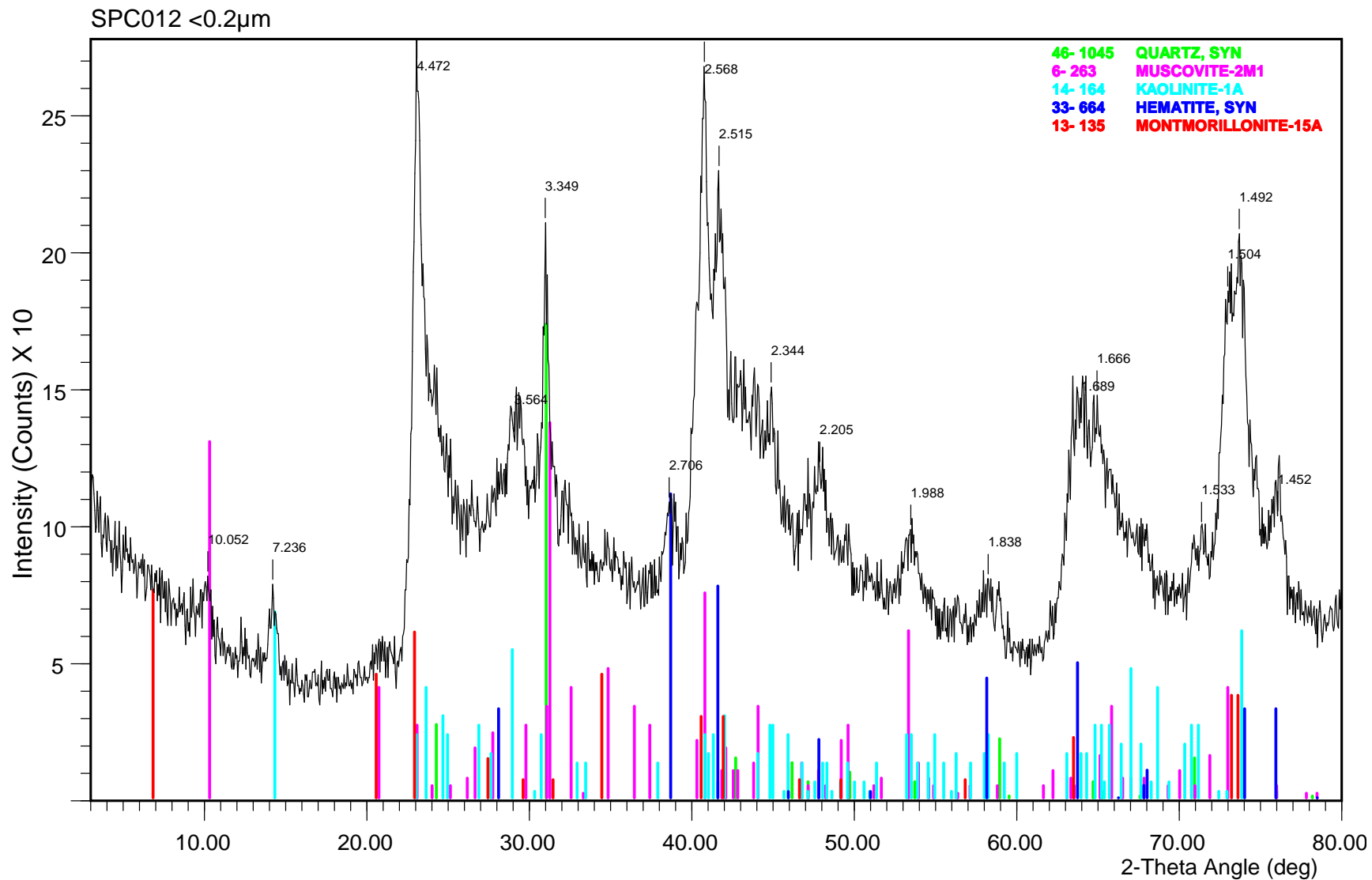


File Name: d:\xrddat~1\11205blk.202

SPC012 0.2-2µm Ca and glycerol

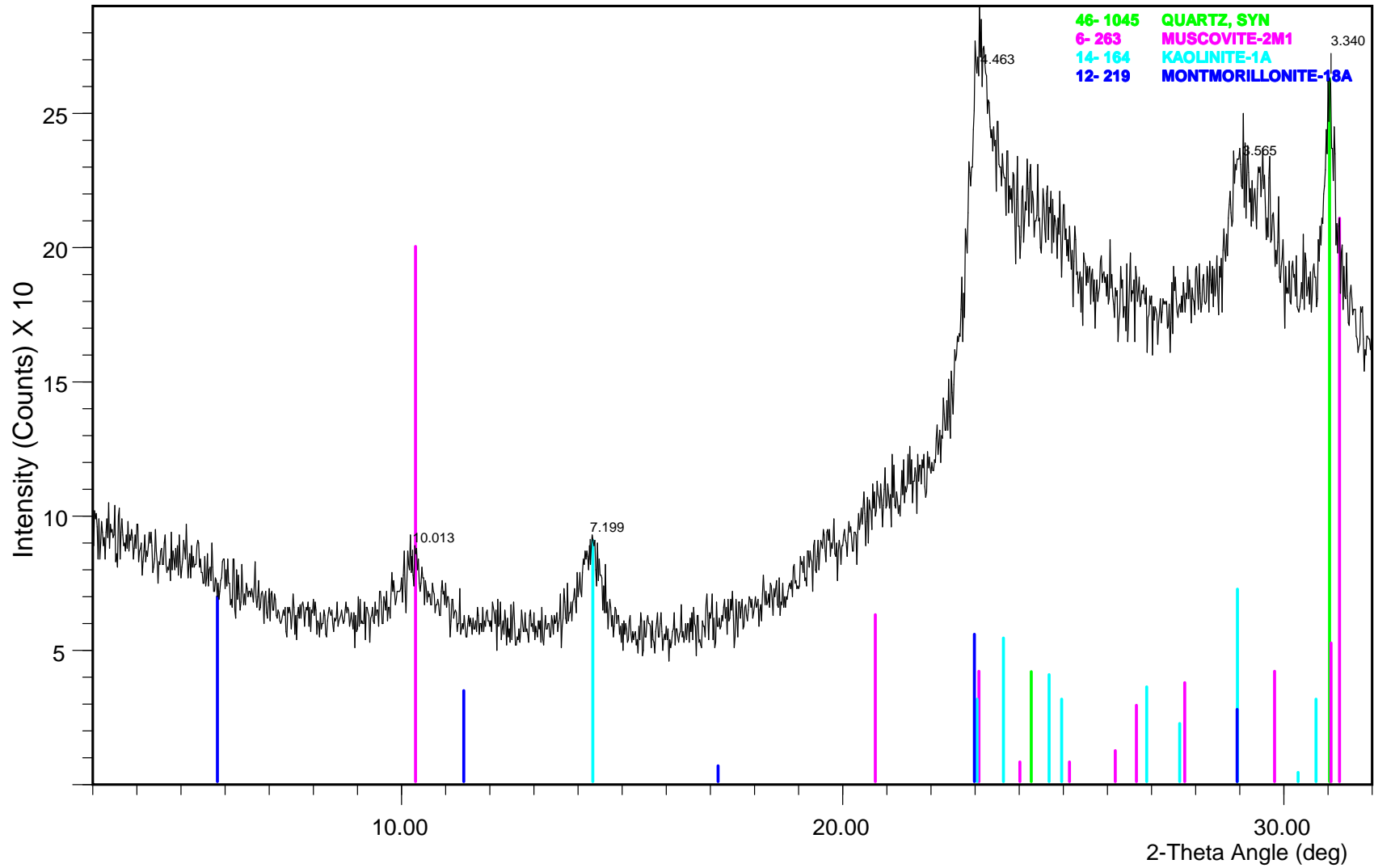


File Name: d:\xrddat~1\11205cgl.102

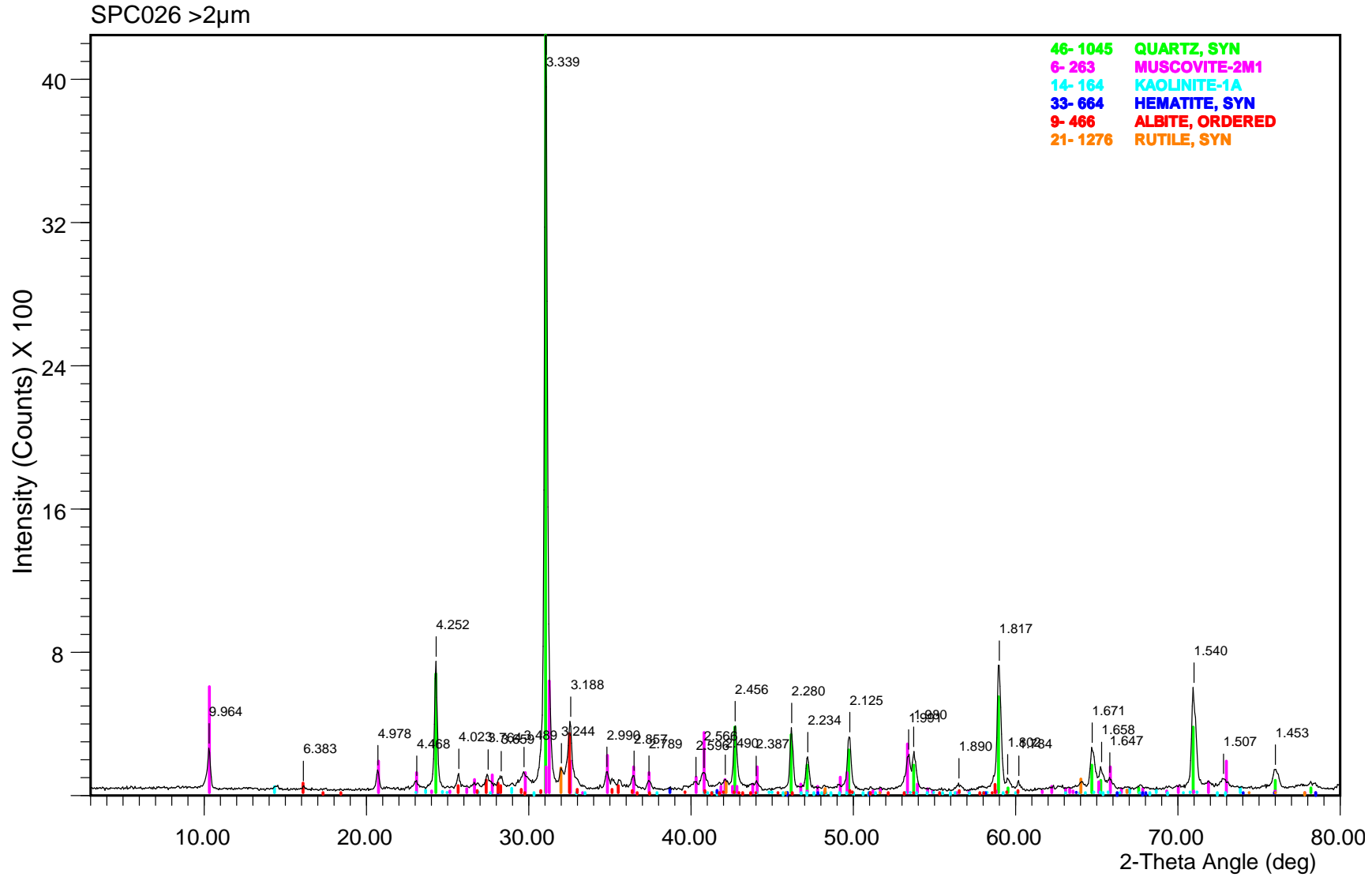


File Name: d:\xrddat~1\11206blk.203

SPC012 <0.2µm Ca and glycerol

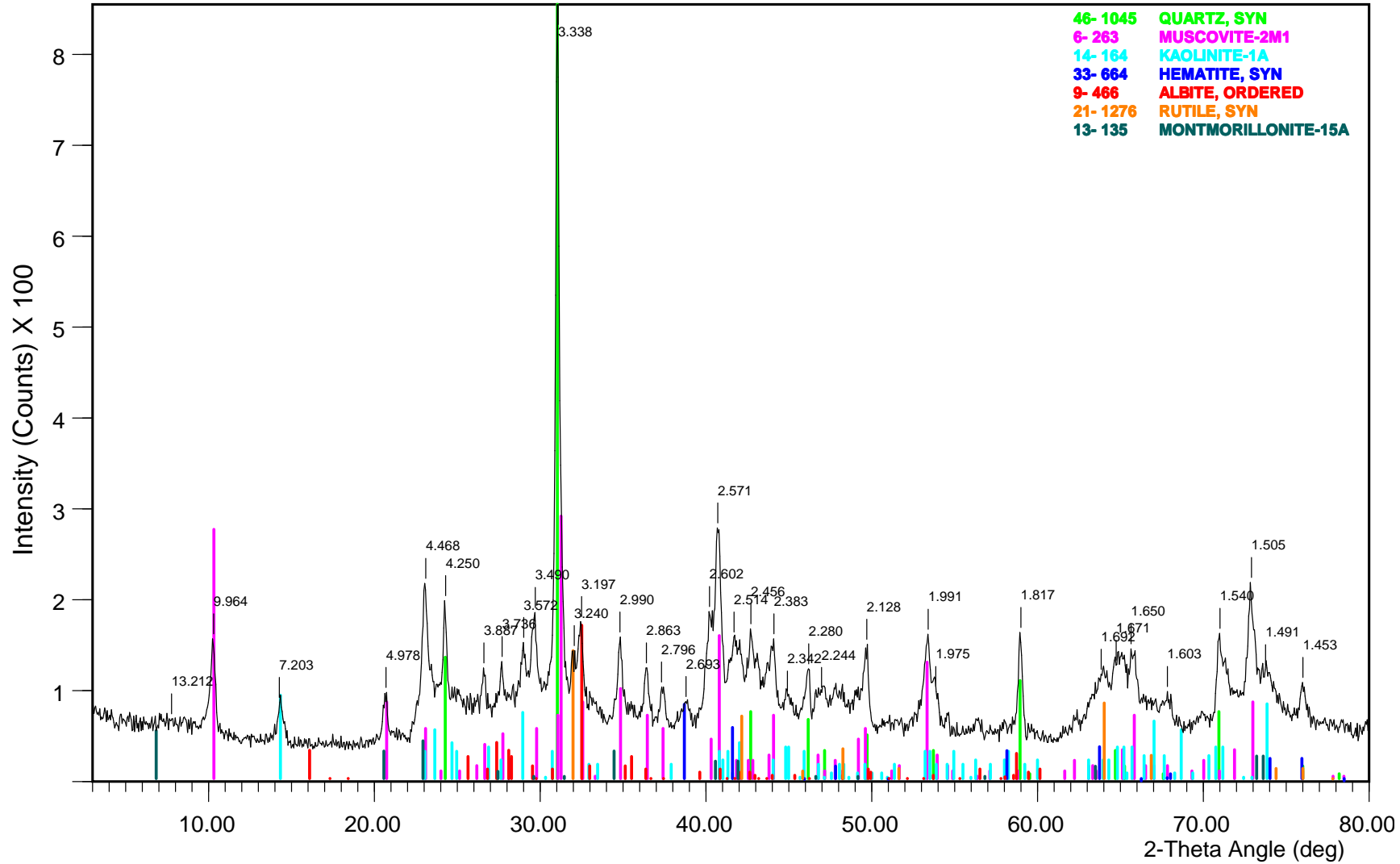


File Name: d:\xrddat~1\11206cgl.101

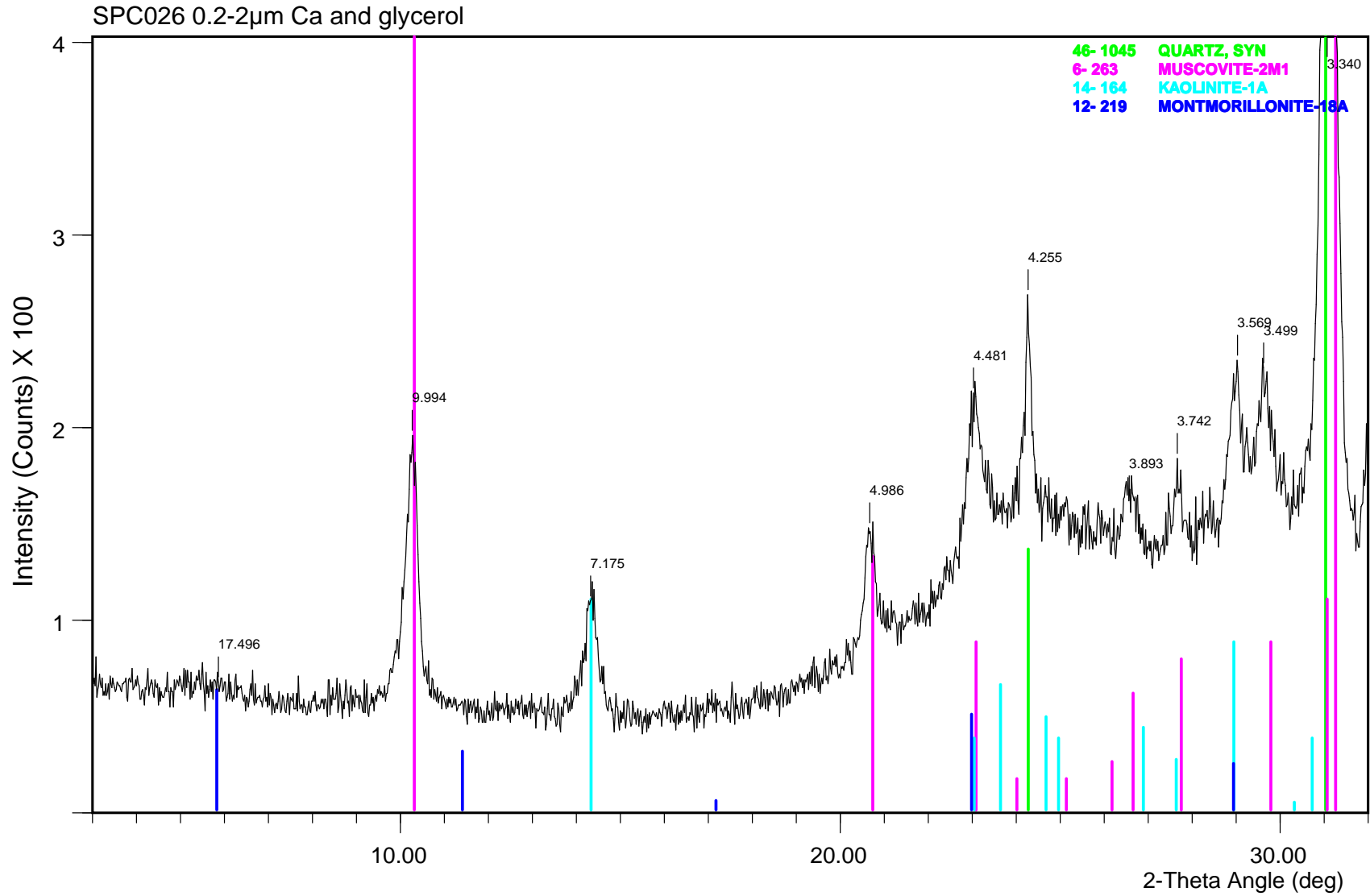


File Name: d:\xrddat~1\11207blk.204

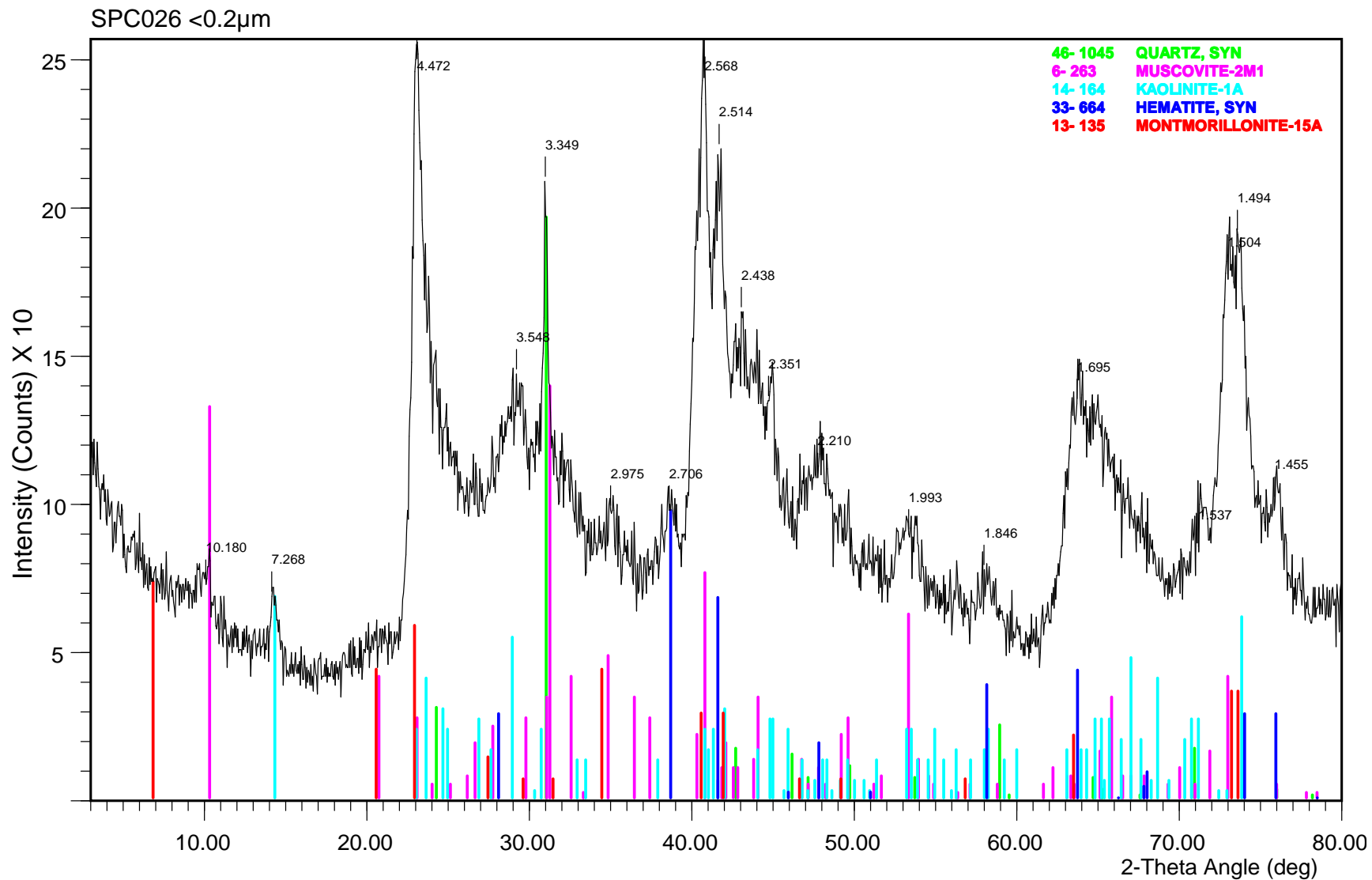
SPC026 0.2-2µm



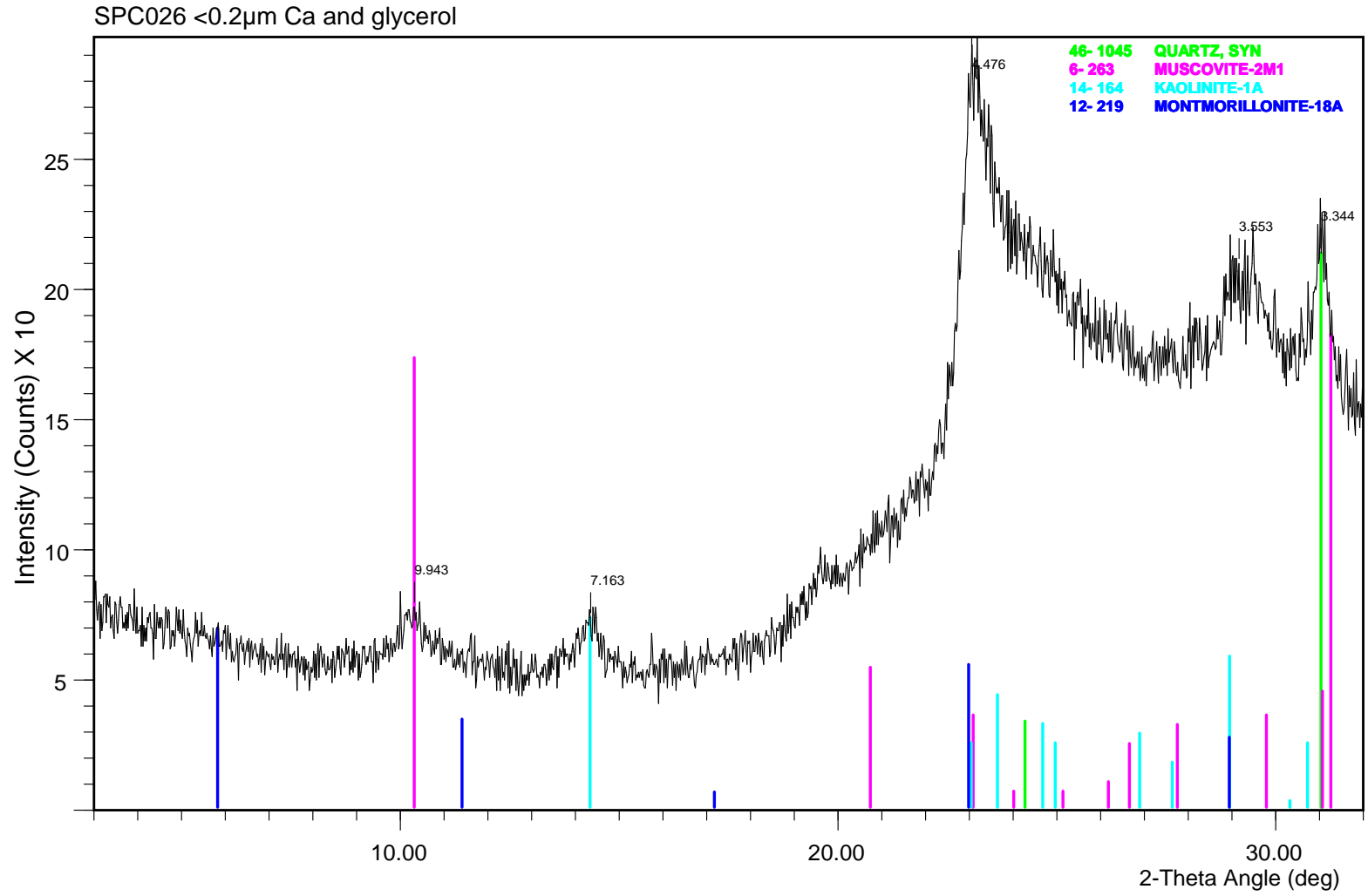
File Name: d:\xrddat~1\11208blk.205



File Name: d:\xrddat~1\11208cgl.104



File Name: d:\xrddat~1\11209blk.206



File Name: d:\xrddat-1\11209cgl.103

Appendix G. Mount Lofty Ranges magnetic susceptibility data.

Sample ID	Weight	Low frequency mass magnetic susceptibility (χ) $\times 10^{-8}$ SI	High frequency mass magnetic susceptibility (χ) $\times 10^{-8}$ SI	Frequency Dependency (%)
1/1	12.62	53	48.7	8.11
1/2	13.27	80	73.2	8.5
1/3	15.99	96.6	92.8	3.93
1/4	14.7	277.1	260	6.17
2/1	12.6	475.2	459.1	3.39
2/2	14.41	510.4	492.2	3.57
2/3	15.56	621.4	595.9	4.1
2/4	13.8	145.2	129	11.16
3/1	13.73	125.8	119.3	5.17
3/2	14.98	185.3	176.5	4.75
3/3	16.06	323.3	315.7	2.35
3/4	16.18	627.9	609.3	2.96
5/1	10.98	75.7	67.8	10.44
5/2	12.16	99.1	92.1	7.06
5/3	13.52	83.6	78.9	5.62
5/4	13	20.5	18.8	8.29
6/1	11.15	60.6	54.7	9.74
6/2	12.75	58.5	53.8	8.03
6/3	14.21	72.9	67.4	7.54
6/4	13.29	42.9	37.6	12.35
8/1	12.6	16.7	14.4	13.77
8/2	14.19	20.1	18.1	9.95
8/3	14.92	44.8	43.3	3.35
8/4	14.85	40.4	38.5	4.7
9/1	13.57	117.3	110.9	5.46
9/2	14.92	222.6	216.6	2.7
9/3	16.27	849.1	809.8	4.63

Sample ID	Weight	Low frequency mass magnetic susceptibility (χ) $\times 10^{-8}$ SI	High frequency mass magnetic susceptibility (χ) $\times 10^{-8}$ SI	Frequency Dependency (%)
9/4	14.66	68.1	66.9	1.76
10/1	12.84	280.3	270.3	3.57
10/2	12.89	292.9	274.5	6.28
10/3	13.6	557	515.5	7.45
10/4	13.88	41.8	36.2	13.4
11/1	11.01	40.4	37.5	7.18
11/2	12.78	57.1	51.3	10.16
11/3	14.23	55.4	49.9	9.93
11/4	15.46	18.9	16.9	10.58
12/1	13.33	240	231.8	3.42
12/2	13.36	152.6	145	4.98
12/3	15.97	190.1	180.2	5.21
12/4	13.65	77.2	73.4	4.92
14/1	13.83	121.3	112	7.67
14/2	13.99	187.7	176.5	5.97
14/3	14.9	210	197.9	5.76
14/4	14.75	127.2	112.7	11.4
15/1	12.37	38.4	36.8	4.17
15/2	13.12	43.7	41.5	5.03
15/3	14.43	60.6	56.7	6.44
15/4	13.92	27.5	22.7	17.45
18/1	11.4	75.5	70.8	6.23
18/2	12.96	107.2	103.3	3.64
18/3	14.6	197.8	191.1	3.39
18/4	13.3	31.9	29.7	6.9
20/1	11.93	326.6	312.4	4.35
20/2	11.75	308.6	294.7	4.5
20/3	14.54	284.8	270.4	5.06
20/4	15.26	84.5	75	11.24
25/1	12.26	37.3	34.8	6.7
25/2	13.26	28.7	26.2	8.71

Sample ID	Weight	Low frequency mass magnetic susceptibility (χ) x10 ⁻⁸ SI	High frequency mass magnetic susceptibility (χ) x10 ⁻⁸ SI	Frequency Dependency (%)
25/3	15.72	37.3	35.1	5.9
25/4	15.93	23.5	25.2	-7.23
26/1	12.08	33	30.5	7.58
26/2	13.61	39.3	36.2	7.89
26/3	16.82	136.9	133	2.85
26/4	14.97	35.3	32.1	9.07
27/1	12.47	24.2	24.2	0
27/2	13.23	21.8	20	8.26
27/3	15.13	23.8	21.6	9.24
27/4	16.48	14.7	14.2	3.4
28/1	13.75	201.1	195.5	2.78
28/2	15.93	482.3	470.7	2.41
28/3	17.77	824.9	808.8	1.95
28/4	15.78	182	178.5	1.92
29/1	13.28	14.4	13.9	3.47
29/2	14.27	18.6	16.9	9.14
29/3	15.7	23	22.7	1.3
29/4	15.84	165.6	162.2	2.05

Appendix H. Layer physicochemical properties of profiles grouped according to each salinity process model (i.e. Models 1a, 1b, 2a, 2b), featuring winter (W_) and summer (S_) salinity (EC_{se}, dS/m), clay content (%) and concentration of soluble salts (mg/kg⁻¹).

Model 1a

Profile ID	Layer ID	Depth range (m)	Winter EC _{se}	Summer EC _{se}	Clay %	W_Ca	S_Ca	W_K	S_K	W_Mg	S_Mg	W_Na	S_Na	W_P	S_P	W_Cl	S_Cl	W_S	S_S
001	L1	0 - 0.05	0.6	0.3	11.4	45.7	12.8	42.6	43.1	11.9	3.8	38.4	22.4	0.7	2.4	19.8	22.8	7.4	9.3
	L2	0.05 - 0.10	0.3	0.3	10.7	16.0	13.9	22.8	20.9	4.4	3.9	23.6	32.4	0.3	1.1	12.1	25.8	4.7	7.6
	L3	0.10 - 0.40	0.2	0.2	11.3	8.7	2.9	8.7	4.6	3.1	1.1	31.4	21.2	0.1	0.1	29.7	18.3	4.9	2.9
	L4	0.40 - 0.75	0.2	0.2	22.6	4.4	2.3	1.8	1.8	1.9	1.0	25.1	34.9	0.1	0.1	10.5	27.2	4.8	6.3
002	L1	0 - 0.05	0.6	0.6	17.1	30.2	30.3	68.0	59.8	7.7	8.5	34.0	45.8	0.8	2.6	26.6	62.0	8.6	10.4
	L2	0.05 - 0.10	0.3	0.1	13.4	17.5	4.9	31.9	18.1	6.2	1.8	26.2	19.8	0.5	0.9	26.9	19.1	5.0	4.9

Appendix H – Layer physicochemical properties of profiles grouped according to each salinity process model

Profile ID	Layer ID	Depth range (m)	Winter ECse	Summer ECse	Clay %	W_Ca	S_Ca	W_K	S_K	W_Mg	S_Mg	W_Na	S_Na	W_P	S_P	W_Cl	S_Cl	W_S	S_S
	L3	0.10 - 0.20	0.1	0.1	24.7	4.5	1.2	6.3	8.2	1.7	0.6	18.0	16.1	0.1	0.5	9.6	11.0	1.2	3.4
	L4	0.20 - 0.75	0.2	0.2	56.0	8.2	0.6	3.0	1.8	4.5	0.6	28.6	37.4	0.3	0.1	16.1	18.7	8.0	16.4
005	L1	0 - 0.05	2.8	0.6	15.0	212.9	39.1	25.8	14.8	106.0	18.0	43.0	55.1	1.9	3.5	37.3	36.3	25.6	13.1
	L2	0.05 - 0.10	0.5	0.5	16.9	54.8	40.0	6.1	4.3	22.5	17.5	21.4	37.4	0.4	1.5	12.1	62.4	9.2	11.5
	L3	0.10 - 0.40	0.2	0.2	19.2	15.0	4.0	4.8	0.1	8.8	3.6	35.7	28.8	0.3	0.6	25.1	17.6	6.5	6.0
	L4	0.40 - 0.75	0.4	0.3	34.2	3.3	1.8	0.5	0.7	6.0	2.0	77.5	71.6	0.3	0.3	50.7	54.3	8.5	9.4
006	L1	0 - 0.05	2.3	0.8	16.0	195.7	49.5	26.1	20.4	103.6	26.5	32.5	55.7	0.4	2.7	38.1	71.4	16.6	12.9
	L2	0.05 - 0.10	0.6	0.2	16.1	65.1	18.0	12.9	3.5	32.6	8.9	22.3	22.0	0.4	1.7	10.8	28.5	8.6	6.6
	L3	0.10 - 0.25	0.2	0.1	15.9	18.6	4.8	5.9	0.9	8.8	3.0	23.0	15.0	0.3	0.4	6.1	12.9	4.4	2.9
	L4	0.25 - 0.75	0.1	0.2	29.5	3.0	0.1	7.0	0.1	5.0	0.3	27.3	32.2	0.4	0.1	5.8	23.9	6.7	9.6
008	L1	0 - 0.05	1.2	0.4	8.0	34.1	19.1	61.4	55.4	14.7	6.5	31.0	26.4	1.5	2.4	56.1	27.8	21.7	13.4

Appendix H – Layer physicochemical properties of profiles grouped according to each salinity process model

Profile ID	Layer ID	Depth range (m)	Winter ECse	Summer ECse	Clay %	W_Ca	S_Ca	W_K	S_K	W_Mg	S_Mg	W_Na	S_Na	W_P	S_P	W_Cl	S_Cl	W_S	S_S
	L2	0.05 - 0.10	0.4	0.3	8.2	52.0	21.6	17.3	25.7	14.8	7.3	23.6	26.5	0.4	1.1	15.9	34.7	4.9	7.7
	L3	0.10 - 0.40	0.1	0.1	7.1	12.5	4.0	6.1	6.9	4.2	1.4	14.6	9.6	0.2	0.3	5.3	10.1	0.5	2.1
	L4	0.40 - 0.75	0.2	0.2	32.6	2.3	0.5	2.0	1.9	1.4	0.5	25.9	21.5	0.1	0.1	45.5	14.8	10.0	7.1
010	L1	0 - 0.05	0.5	0.9	17.2	41.2	73.4	50.9	53.8	13.0	19.1	40.8	46.5	0.8	1.1	35.0	67.3	9.4	10.0
	L2	0.05 - 0.10	0.4	0.3	20.7	32.0	18.9	18.3	7.3	8.8	6.8	24.0	27.2	0.8	0.9	10.9	21.5	6.5	7.4
	L3	0.10 - 0.54	0.2	0.2	32.1	9.3	1.7	3.5	0.1	4.8	1.6	25.6	26.6	0.1	0.1	15.7	16.5	1.4	6.4
	L4	0.54 - 0.75	0.2	0.2	57.7	0.5	1.7	0.5	0.1	2.2	1.7	22.9	29.4	0.1	0.1	9.9	20.1	7.7	12.2
012	L1	0 - 0.05	0.6	0.9	9.4	25.6	40.5	49.3	111.2	6.8	11.6	39.8	50.6	1.8	1.9	26.4	49.1	6.1	10.8
	L2	0.05 - 0.10	0.4	0.3	9.0	20.8	10.0	27.9	41.6	4.8	3.0	27.3	22.9	1.1	0.9	18.2	18.6	5.6	7.0
	L3	0.10 - 0.35	0.2	0.3	8.0	11.3	8.2	17.4	12.1	5.7	3.4	19.9	19.2	0.4	0.7	6.9	14.5	3.6	5.8
	L4	0.35 - 0.75	0.4	0.6	49.1	6.1	0.4	22.5	0.1	17.2	0.7	57.8	93.5	0.3	0.1	31.6	69.6	12.5	21.3

Appendix H – Layer physicochemical properties of profiles grouped according to each salinity process model

Profile ID	Layer ID	Depth range (m)	Winter ECse	Summer ECse	Clay %	W_Ca	S_Ca	W_K	S_K	W_Mg	S_Mg	W_Na	S_Na	W_P	S_P	W_Cl	S_Cl	W_S	S_S
014	L1	0 - 0.05	0.5	1.0	10.4	41.3	85.6	36.0	80.9	9.6	19.4	18.1	41.0	1.3	1.9	13.5	87.1	8.5	13.1
	L2	0.05 - 0.10	0.4	0.3	11.2	43.4	25.8	21.3	23.8	10.7	7.6	11.9	16.7	0.4	0.7	8.3	28.2	6.2	6.6
	L3	0.10 - 0.17	0.2	0.2	9.2	14.1	13.1	10.6	15.1	6.2	4.9	10.4	12.9	0.3	1.0	6.8	14.9	3.8	6.1
	L4	0.17 - 0.75	0.2	0.2	50.0	7.5	0.2	4.5	3.5	4.6	0.3	26.5	27.3	0.1	0.2	20.1	15.6	2.9	8.0
015	L1	0 - 0.05	1.2	1.5	12.0	59.3	103.6	72.2	138.6	20.6	34.8	46.2	73.1	7.1	7.1	48.9	92.9	15.1	19.6
	L2	0.05 - 0.10	0.6	0.6	14.5	37.8	41.8	41.8	45.4	12.2	13.4	25.6	30.5	1.6	1.4	13.1	34.5	7.6	8.9
	L3	0.10 - 0.15	0.2	0.2	14.2	16.4	6.7	25.5	13.0	5.7	3.3	18.2	23.8	0.5	0.4	26.2	19.2	5.8	4.2
	L4	0.15 - 0.75	0.3	0.4	32.9	12.1	2.8	27.7	6.0	14.4	2.8	44.1	58.4	0.5	0.5	15.7	51.3	5.7	11.3
025	L1	0 - 0.05	1.4	0.5	15.6	102.8	24.2	37.0	31.6	37.3	9.9	51.7	46.8	0.5	1.5	35.3	65.6	21.4	15.3
	L2	0.05 - 0.10	0.5	0.3	14.1	36.2	14.8	14.8	19.8	14.0	6.0	30.3	33.4	0.3	1.3	9.1	45.9	5.6	8.9
	L3	0.10 - 0.23	0.1	0.1	7.4	7.4	2.7	7.1	4.9	3.2	1.5	14.5	15.5	0.1	0.3	8.5	15.6	0.5	2.2

Appendix H – Layer physicochemical properties of profiles grouped according to each salinity process model

Profile ID	Layer ID	Depth range (m)	Winter ECse	Summer ECse	Clay %	W_Ca	S_Ca	W_K	S_K	W_Mg	S_Mg	W_Na	S_Na	W_P	S_P	W_Cl	S_Cl	W_S	S_S
	L4	0.23 - 0.74	0.1	0.2	18.3	0.5	0.1	1.8	0.1	1.9	0.2	21.2	24.0	0.3	0.1	8.0	17.4	2.7	3.2
026	L1	0 - 0.05	0.5	0.3	11.8	25.8	16.1	28.8	30.1	7.9	4.9	27.0	20.7	0.8	1.5	32.0	24.4	10.3	9.7
	L2	0.05 - 0.10	0.3	0.3	12.7	21.4	20.8	9.2	11.1	6.7	7.2	22.7	22.0	0.4	0.9	16.8	25.3	4.6	5.7
	L3	0.10 - 0.25	0.1	0.1	13.4	7.4	3.4	7.5	3.3	3.9	1.7	17.5	13.5	0.3	0.1	5.5	13.4	0.5	2.0
	L4	0.25 - 0.75	0.2	0.2	40.7	18.1	0.1	4.6	0.1	11.5	0.2	30.3	17.9	0.1	0.1	8.0	12.1	2.6	5.1
028	L1	0 - 0.05	0.5	1.0	7.8	24.8	86.9	29.7	20.5	11.1	23.3	34.0	71.4	0.3	1.5	29.1	85.4	5.5	10.2
	L2	0.05 - 0.10	0.1	0.2	16.0	5.8	14.6	8.3	5.5	1.9	4.3	13.6	18.3	0.3	0.6	8.0	18.4	3.0	5.2
	L3	0.10 - 0.50	0.1	0.0	4.7	2.1	1.3	3.9	0.8	1.7	0.8	10.1	7.9	0.2	0.4	5.1	9.1	0.5	1.6
	L4	0.50 - 0.75	0.2	0.3	52.3	3.5	0.2	0.1	0.1	5.8	0.5	36.6	40.6	0.4	0.1	16.5	21.2	11.7	15.8

Model 1b

Profile ID	Layer ID	Depth range (m)	Winter ECse	Summer ECse	CEC	Clay %	W_Ca	S_Ca	W_K	S_K	W_Mg	S_Mg	W_Na	S_Na	W_P	S_P	W_Cl	S_Cl	W_S	S_S
003	L1	0 - 0.05	0.8	1.1	8.8	9.2	47.2	68.2	52.3	60.1	12.5	21.2	48.2	54.1	2.1	1.7	24.2	42.2	8.1	8.4
	L2	0.05 - 0.10	0.4	1.0	5.3	9.8	20.4	62.8	28.9	57.0	5.5	19.4	36.5	47.1	0.9	1.0	10.4	30.6	5.9	7.0
	L3	0.10 - 0.45	0.2	0.4	2.2	7.7	5.5	18.9	16.7	39.2	3.5	6.9	30.4	39.0	0.6	1.4	11.6	26.0	3.9	5.1
	L4	0.45 - 0.75	0.4	1.2	6.6	19.8	35.1	0.5	10.8	2.1	31.0	0.6	95.5	157.6	0.2	0.1	36.2	106.5	5.4	52.2
009	L1	0 - 0.05	0.8	0.7	6.5	7.0	44.2	18.6	44.7	14.4	17.7	8.3	65.5	100.5	4.2	2.2	47.3	49.4	8.6	13.9
	L2	0.05 - 0.10	0.5	0.5	5.8	8.3	32.3	9.2	12.7	3.7	11.5	4.7	37.8	86.2	1.3	2.7	55.9	40.6	6.7	9.5
	L3	0.10 - 0.34	0.2	0.3	3.7	5.6	12.4	1.9	9.4	0.3	7.3	1.0	28.8	54.3	0.6	1.3	8.4	21.8	5.3	5.9
	L4	0.34 - 0.75	0.6	1.5	16.2	53.7	48.2	1.3	6.3	0.1	26.1	0.9	75.8	177.3	0.6	0.1	18.5	159.8	1.6	30.1

Model 2a

Profile ID	Layer ID	Depth range (m)	Winter ECse	Summer ECse	Clay %	W_Ca	S_Ca	W_K	S_K	W_Mg	S_Mg	W_Na	S_Na	W_P	S_P	W_Cl	S_Cl	W_S	S_S
020	L1	0 - 0.05	3.4	0.7	14.4	288.5	40.6	141.3	67.2	53.4	9.9	140.1	55.6	9.6	4.2	175.6	61.4	89.0	19.8
	L2	0.05 - 0.10	0.5	0.6	15.5	49.7	45.8	14.0	18.8	10.6	12.4	17.6	45.5	0.6	1.9	38.9	63.7	8.2	11.8
	L3	0.10 - 0.25	0.2	0.2	21.3	13.2	5.2	7.4	6.3	6.4	2.0	19.0	20.3	0.4	0.3	7.2	21.2	4.7	4.7
	L4	0.25 - 0.75	0.3	0.2	51.6	8.0	0.8	18.3	0.5	14.8	0.7	29.5	20.3	0.9	0.1	23.6	16.4	6.9	3.1

Model 2b

Profile ID	Layer ID	Depth range (m)	Winter ECse	Summer ECse	Clay %	W_Ca	S_Ca	W_K	S_K	W_Mg	S_Mg	W_Na	S_Na	W_P	S_P	W_Cl	S_Cl	W_S	S_S
011	L1	0 - 0.05	2.2	2.6	13.6	22.7	34.0	27.9	26.4	6.7	11.0	324.0	528.9	1.3	2.5	516.3	785.0	26.5	25.5
	L2	0.05 - 0.10	0.9	1.5	18.4	16.2	18.3	10.6	5.9	4.0	6.5	250.2	312.3	1.0	2.1	212.2	423.3	30.5	22.3
	L3	0.10 - 0.35	0.7	1.4	17.1	11.2	6.5	7.1	0.5	3.7	3.2	153.6	277.1	0.6	0.8	130.0	346.8	17.8	24.6
	L4	0.35 - 0.75	1.8	3.9	16.5	20.8	6.5	9.4	0.1	14.0	5.2	268.6	545.0	0.2	0.1	295.4	696.9	24.8	51.1
018	L1	0 - 0.05	1.8	1.8	14.3	204.6	77.7	16.4	83.2	44.0	23.2	118.6	203.3	2.1	5.9	77.5	256.8	56.7	99.0
	L2	0.05 - 0.10	0.8	0.8	17.2	59.0	28.6	6.5	4.7	18.8	9.7	73.5	130.7	0.5	1.9	20.3	131.8	32.3	30.7
	L3	0.10 - 0.25	0.5	0.6	14.1	6.0	5.0	17.1	3.6	12.4	3.3	77.5	132.7	0.5	1.3	30.9	134.2	12.2	16.3
	L4	0.25 - 0.75	2.4	3.5	38.8	30.5	2.0	14.7	2.5	40.4	3.0	473.1	756.2	0.1	0.3	470.2	953.9	54.9	98.1
027	L1	0 - 0.05	0.7	0.7	28.3	36.7	26.6	22.5	18.3	30.3	21.2	59.3	72.0	1.4	3.2	26.2	98.5	12.4	11.0

Appendix H – Layer physicochemical properties of profiles grouped according to each salinity process model

Profile ID	Layer ID	Depth range (m)	Winter ECse	Summer ECse	Clay %	W_Ca	S_Ca	W_K	S_K	W_Mg	S_Mg	W_Na	S_Na	W_P	S_P	W_Cl	S_Cl	W_S	S_S
	L2	0.05 - 0.10	0.4	0.3	31.3	22.8	10.3	16.6	3.4	20.6	6.9	45.3	41.2	1.1	2.3	12.0	31.6	8.4	6.4
	L3	0.10 - 0.27	0.2	0.7	14.4	8.8	4.9	8.8	0.8	10.2	5.8	35.7	92.6	0.7	0.5	17.4	118.9	2.9	3.3
	L4	0.27 - 0.75	0.9	3.3	29.3	28.3	4.8	9.2	2.3	37.3	7.0	140.9	449.6	0.1	0.2	76.0	593.1	7.1	35.1
029	L1	0 - 0.05	12.1	10.8	16.1	277.6	227.6	40.5	21.0	209.8	166.6	1250.0	1225.1	1.3	1.2	2450.0	2495.7	175.8	82.2
	L2	0.05 - 0.10	5.0	6.1	6.6	54.9	83.7	12.4	7.6	45.9	70.2	646.7	809.0	1.1	0.2	877.7	1385.8	72.1	53.5
	L3	0.10 - 0.62	3.7	5.6	10.6	18.6	58.2	19.1	8.1	21.2	46.6	433.4	654.4	0.6	0.1	627.1	1099.0	30.5	44.3
	L4	0.62 - 0.75	2.5	6.2	24.8	14.6	63.6	41.9	4.9	33.4	46.0	373.8	720.4	0.6	0.1	450.9	1216.8	35.5	50.6

